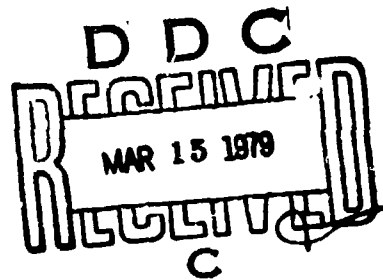


AFFDL-TR-78-150



LEVEL II

AD A0 65734

ELECTROMECHANICAL ACTUATION DEVELOPMENT

AiResearch Manufacturing Company of California
2525 W. 190th Street
Torrance, California 90509

December 1978

Final Report for Period February 1976 - September 1978

Approved for public release
Distribution unlimited

Prepared for
Air Force Flight Dynamics Laboratory
Air Force Systems Command
Wright-Patterson Air Force Base, Ohio 45433

79 03 13 026

DDC FILE COPY

NOTICE

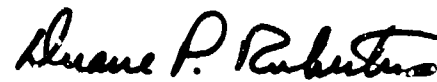
When Government drawings, specifications, or other data are used for any purpose other than in connection with a definitely related Government procurement operation, the United States Government thereby incurs no responsibility nor any obligation whatsoever; and the fact that the government may have formulated, furnished, or in any way supplied the said drawings, specifications, or other data, is not to be regarded by implication or otherwise as in any manner licensing the holder or any other person or corporation, or conveying any rights or permission to manufacture, use, or sell any patented invention that may in any way be related thereto.

This report has been reviewed by the Information Office (OI) and is releasable to the National Technical Information Service (NTIS). At NTIS, it will be available to the general public, including foreign nations.

This technical report has been reviewed and is approved for publication.

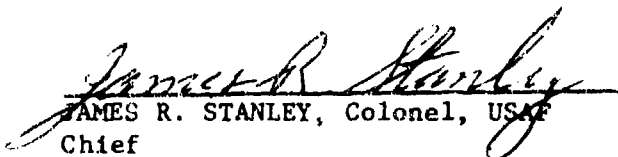


DANIEL K. BIRD
Program Manager



DUANE P. RUBERTUS, Acting Chief
Control Systems Development Branch
Flight Control Division

FOR THE COMMANDER



JAMES R. STANLEY, Colonel, USAF
Chief
Flight Control Division

"If your address has changed, if you wish to be removed from our mailing list, or if the addressee is no longer employed by your organization please notify AFFDL/FGL, W-PAFB, OH 45433 to help us maintain a current mailing list".

Copies of this report should not be returned unless return is required by security considerations, contractual obligations, or notice on a specific document.

UNCLASSIFIED

SECURITY CLASSIFICATION OF THIS PAGE (When Data Entered)

REPORT DOCUMENTATION PAGE		READ INSTRUCTIONS BEFORE COMPLETING FORM	
1. REPORT NUMBER AEDL-TR-78-1501	2. GOVT ACCESSION NO.	3. REPORT'S CATALOG NUMBER	
4. TITLE (and Subtitle) Electromechanical Actuation Development.		5. TYPE OF REPORT & PERIOD COVERED Final Report. Feb '76-Sep '78	
6. AUTHOR(s) Neal E. Wood, Robert A. Lewis		7. PERFORMING ORG. REPORT NUMBER 78-150674	
8. PERFORMING ORGANIZATION NAME AND ADDRESS AirResearch Manufacturing Company A Division of The Garrett Corporation 2525 W. 190th Street Torrance, California 90509		9. CONTRACT OR GRANT NUMBER(s) F33615-76-C-30439	
10. CONTROLLING OFFICE NAME AND ADDRESS Air Force Flight Dynamics Laboratory AFSC/AFWAL, United States Air Force Wright-Patterson AFB, Ohio 45433		11. REPORT DATE Dec 1978	
12. MONITORING AGENCY NAME & ADDRESS (if different from Controlling Office) 12517		13. NUMBER OF PAGES 410	
14. DISTRIBUTION STATEMENT (of this Report) Approved for public release, distribution unlimited.		15. SECURITY CLASS. (of this report) UNCLASSIFIED	
16. DISTRIBUTION STATEMENT (of the abstract entered in Block 20, if different from Report)		15a. DECLASSIFICATION/DOWNGRADING SCHEDULE	
17. SUPPLEMENTARY NOTES			
18. KEY WORDS (Continue on reverse side if necessary and identify by block number) Power-by-Wire Fly-by-Wire "Rare Earth" Samarium Cobalt Magnets Brushless DC Motor Permanent Magnet Rotor			
19. ABSTRACT (Continue on reverse side if necessary and identify by block number) Electromechanical actuation of primary flight control surfaces has been demonstrated by the development of an integrated rotary hinge-line dual-redundant actuation unit. The characteristics of the developed hardware closely correlate with the design predictions. A digital computer program was developed to simulate dynamic operation of the unit based upon the known equipment characteristics. The system simulation results showed that the electromechanical actuation unit			

DDC
RECEIVED
MAR 15 1979
REGULATED
C

DD FORM 1473 EDITION OF 1 NOV 65 IS OBSOLETE

UNCLASSIFIED

SECURITY CLASSIFICATION OF THIS PAGE (When Data Entered)

79 03 13 026

UNCLASSIFIED

SECURITY CLASSIFICATION OF THIS PAGE(When Data Entered)

can meet selected performance goals. Component compatibility, system function, performance capabilities, and redundant operation were demonstrated using the laboratory hardware and computerized simulation analyses.

ADDED TO FILE

WHS	Write Section	<input checked="" type="checkbox"/>
CSO	Staff Section	<input type="checkbox"/>
RECEIVED		
EX		
RECEIVED		
RECEIVED		

A

UNCLASSIFIED

SECURITY CLASSIFICATION OF THIS PAGE(When Data Entered)

PREFACE

This final report was prepared by AiResearch Manufacturing Company of California, a division of The Garrett Corporation, for the Air Force Flight Dynamics Laboratory, Wright Patterson Air Force Base, under Contract F33615-76-C-3043, Integrated Hinge (Rotary) Electromechanical Actuation Development. The technical effort was performed from February 16, 1976 to September 6, 1978 by the AiResearch Mechanical Power Systems Product Line, with Mr. Neal Wood as principal investigator. Mr. Daniel K. Bird (FGL), the Air Force technical monitor for the program, provided direction, technical support, and many hours of discussion on actuation principles and methods of presentation.

Although many individuals have made significant contributions to the organization and content of this report, the efforts of several key people merit special recognition. E.F. Echolds and K.C. Wong were responsible for the development of the electric powered servo motor; J. Ashmore, J. Cleek, and J. Yasuda were responsible for the electronic design and breadboard controller fabrication; and D. Bailey and J. White provided specialized technical support in the development of the computerized system simulation program and dynamic analysis of the system.

The following discussion, provided by Mr. Bird, briefly summarizes the relation of the work reported in this document to associated efforts, many of which were sponsored by the USAF Flight Dynamics Laboratory.

Two relatively new technologies are emerging for aircraft flight control systems: (1) fly-by-wire, a proven approach to signal transmission, and (2) power-by-wire, an approach to control surface actuation using electrical power. Electromechanical actuation is peculiarly able to incorporate these two advanced techniques to provide the flexibility and efficiency inherent in both fly-by-wire and power-by-wire. Electromechanical actuation carries the concept of the electromechanical direct drive control valve, made possible by fly-by-wire, one step further. The direct drive control valve eliminates one stage of hydraulic signal amplification. Electromechanical actuation eliminates both stages. If viewed from the power distribution side, electromechanical actuation carries the concept of the integrated actuator packages (IAP's) one step further. The IAP concept changes the conventional hydraulic power distribution system to an electrical system, but then converts electrical power to hydraulic power at the actuators. Electromechanical actuation uses electrical power directly and avoids the electrical-to-hydraulic power conversion penalty. Electromechanical actuation carries the inherent capability to convert a digital command to an analog force output within the actuation unit. If proved credible for primary flight control actuation, the electromechanical actuation concept has gone a long way towards removing the need to add hydraulic systems to future aircraft. This effort is dedicated to validating the credibility of electromechanical actuation for primary flight control with a unique, one-of-a-kind electromechanical actuation unit.

CONTENTS

<u>Section</u>	<u>Page</u>
1. SUMMARY	1
1.1 Electromechanical Actuator Features	1
1.2 Hardware Definition	2
1.3 Hardware Fabrication	3
1.4 Test Results	5
2. INTRODUCTION	7
2.1 Objectives	8
2.2 Scope	8
2.3 Program Review	9
3. HARDWARE DESCRIPTION	12
3.1 Electromechanical Actuation Unit Definition	12
3.1.1 Baseline Problem Statement	12
3.1.2 System Synthesis	13
3.1.3 Modes of Operation	16
3.2 Actuator	17
3.2.1 Motor	17
3.2.2 Gearing	31
3.3 Controller	39
3.3.1 Discussion of Approaches	39
3.3.2 Controller Operational Description	53
3.3.3 Controller Circuit Design	61
3.3.4 Projected Controller Sizing and Configuration	79
3.4 Position Feedback Transducer	82
3.4.1 Encoder Interface Configuration Modifications	83
3.4.2 Alternate Encoder Interface Arrangements	86
3.5 Dynamic Analysis and System Simulation	86
3.5.1 Approach to Simulation for Laboratory Hardware	86
3.5.2 Model Description for Laboratory Hardware	90
3.5.3 Correlation Control Synthesis for Laboratory Hardware	92
3.5.4 Data Correlation for Laboratory Demonstration Hardware	98
3.5.5 Control Synthesis for Baseline Problem Statement Load Inertia	102
3.5.6 Predicted Performance for Laboratory Hardware, Tachometer Servo Control	105
4. TEST EQUIPMENT	116
4.1 Special Test Equipment and Fixtures	116
4.1.1 Test Stand	116
4.1.2 Power Supply	123
4.2 Facilities	123

CONTENTS (Continued)

<u>Section</u>	<u>Page</u>
5. TESTING	124
5.1 Test Plan	124
5.2 Tests Performed	124
6. TEST RESULTS	127
6.1 Component Tests	127
6.1.1 Motor Performance	127
6.1.2 Encoder Receiving Inspection	142
6.1.3 Controller Checkout	142
6.1.4 Rotary Gearbox Performance	142
6.2 Electromechanical Actuation Unit Tests	149
6.2.1 Frequency Response	152
6.2.2 Dynamic Stiffness	155
6.2.3 Step Response	155
6.2.4 Position Resolution Hysteresis	162
6.2.5 Regeneration	170
6.2.6 Reliability Management Demonstration	170
6.2.7 Thermal Management	173
7. CONCLUSIONS AND RECOMMENDATIONS FOR FUTURE EFFORT	177
7.1 Conclusions	177
7.2 Recommendation For Future Effort	177
8. REFERENCES	181
<u>Appendix</u>	
A ELECTROMECHANICAL ACTUATION DEVELOPMENT DESIGN DATA PACKAGE	183
B ACTUATION UNIT PERFORMANCE SPECIFICATION	286
C SCREENING LOGIC DIAGRAM	299
D MOTOR TRADE STUDY	305
E MICROPROCESSOR CONTROLLER	310
F EQUIPMENT TEST PLAN	322
G EARLY TEST DATA FOR ELECTROMECHANICAL ACTUATION UNIT	346
H HARDWARE TEST DATA	383

ILLUSTRATIONS

<u>Figure</u>		<u>Page</u>
1.	Electromechanical Actuation Unit Block Diagram	2
2.	Dual Electromechanical Rotary Hingeline Actuator and Position Transducers	3
3.	Functional Interface Block Diagram for Electromechanical Actuation Unit	9
4.	Program Schedule	11
5.	Electromechanical Actuation Unit for Primary Flight Control (Shown Without Redundancy)	13
6.	System Model	15
7.	Primary Flight Control Hingeline Actuator	16
8.	Simplified Motor Model	18
9.	Machine Configuration	19
10.	Comparison of Magnet Materials	20
11.	Hingeline Actuator Motors	22
12.	Rare-Earth Permanent Magnet Motor Parts	22
13.	Techniques of Permanent Magnet Rotor Construction	27
14.	Variable Reluctance Rotor Position Sensor	29
15.	Motor Torque/Speed Curve	30
16.	Rotor Position Sensor Geometry	32
17.	Rotary Hingeline Actuation Unit Conceptual Design and Potential Structural Advantages	32
18.	Hingeline Actuator Gearing	34
19.	Hingeline Actuator Gearing Details	37
20.	Example of Motor Control	40
21.	Synchronized Commutation Control	41
22.	Voltage Control Using Fixed Frequency Pulse Width	42

ILLUSTRATIONS (Continued)

<u>Figure</u>		<u>Page</u>
23.	Generalized Torque Speed Curve	42
24.	Possible Operation of the Motor in a Typical Duty Cycle	43
25.	Switching Waveform	45
26.	Transistor Operating During Switching	46
27.	Typical Output Characteristics	47
28.	Rotor Position Sensor Output Waveforms	48
29.	Modulation Approach	49
30.	Hysteresis Switch Schematic	50
31.	Current Control with Hysteresis Switch	50
32.	Typical Current Source	51
33.	Back Emf and Current Relationship	52
34.	Voltage Sourced Drive Circuit	52
35.	Waveforms for Voltage Sourced, Modulated Drive Circuit	54
36.	System Block Diagram	55
37.	Controller Block Diagram	57
38.	Rotor Velocity Controlled by Stator Frequency	59
39.	Position Error and Compensation Amplifiers, Pulse-Width Modulators, and Direction Sense Circuitry	62
40.	Pulse-Width Modulation Idealized Timing Diagram	64
41.	Triangle Wave Generator	65
42.	Triangle Waveform	65
43.	Surface Position Decoding Circuitry	66
44.	Rotor Position Outputs	67
45.	Motor Rotor Position Detection Circuitry	68

ILLUSTRATIONS (Continued)

<u>Figure</u>		<u>Page</u>
46.	Sequence, Control, and Inhibit Logic	70
47.	Sequencer Timing Diagrams	71
48.	Driver Switches	73
49.	Typical Turnoff Locus	75
50.	Current Limit Circuitry	76
51.	Power Supply	77
52.	Tachometer Feedback Control Block Diagram	78
53.	Tachometer Control Circuitry	79
54.	Rotor Speed Detection Circuit	80
55.	Rotor Direction Detector	81
56.	Hingeline Actuation Encoders	83
57.	Optical Position Sensor Interface Parts	84
58.	Assembled 4.48:1 Gearbox for Increased Encoder Resolution	89
59.	Encoder Gearbox Component Breakdown	89
60.	Model Block Diagram	91
61.	Open-Loop Nichols Locus Diagram	94
62.	Initial Control Block Diagram	95
63.	Modified Nichols Locus Diagram	96
64.	Improved Control Block Diagram	97
65.	Frequency Response Comparison for One-Channel, No-Load, ± 1 deg Amplitude, Voltage Servo Control	100
66.	Frequency Response Comparison for 2-Channel, No-Load, ± 1 deg Amplitude, Voltage Servo Control	101
67.	Frequency Response Comparison for 2-Channel, No-Load, ± 1 deg Amplitude, Tachometer Feedback Servo Control	103

ILLUSTRATIONS (Continued)

<u>Figure</u>		<u>Page</u>
68.	Frequency Response for 2-Channel, Tachometer Feedback ± 1 deg Amplitude, 30-Percent Load	104
69.	Frequency Response for 2-Channel, Tachometer Feedback ± 1 deg Amplitude, 50-Percent Load	104
70.	Dynamic Stiffness, Tachometer Feedback	105
71.	Response to Gust Loads	106
72.	Control Block Diagram for Motor Tachometer Feedback	108
73.	Open Loop Nichols Locus Diagram	109
74.	Nichols Locus Diagram with Gain Adjustment	110
75.	Nichols Locus Diagram with Gain of 19950	111
76.	Final Nichols Locus Diagram	112
77.	Demonstration of Control Loop Using Tachometer Feedback (No Limit on Major Loops)	113
78.	Demonstration of Control Loop Using Tachometer Feedback (Limited Major Loop)	114
79.	Demonstration of Control Loop Using Tachometer Feedback (Limited Range of Minor Loop)	115
80.	Actuator Mounted in Test Stand	120
81.	Hydraulic Load System Setup	121
82.	Strain Gage Mounted on Output Arm	122
83.	Block Diagram of the Power Supply	123
84.	Test Flow Diagram	126
85.	Load Test and Short-Circuit Test Schematic	128
86.	Closeup of Generator Test Setup	129
87.	Generator Test Setup	130
88.	270-vdc Brushless Motor (M1) Generator Test, Ac Voltage	132

ILLUSTRATIONS (Continued)

<u>Figure</u>		<u>Page</u>
89.	270-vdc Brushless Motor (M1) Generator Test, Dc Voltage	132
90.	270-vdc Brushless Motor (M2) Generator Test, Ac Voltage	133
91.	270-vdc Brushless Motor (M2) Generator Test, Dc Voltage	133
92.	270-vdc Brushless Motor (M1) Test Data Correlation	134
93.	Commutating Reactance	135
94.	Flywheel Test Schematic Diagram	136
95.	270-vdc Brushless Motor/Voltage Source Drive Circuit Test (M1), Direction of Rotation: CW	138
96.	270-vdc Brushless Motor/Voltage Source Drive Circuit Test (M1), Direction of Rotation: CCW	138
97.	270-vdc Brushless Motor/Voltage Source Drive Circuit Test (M2), Direction of Rotation: CW	139
98.	270-vdc Brushless Motor/Voltage Source Drive Circuit Test (M2), Direction of Rotation: CCW	139
99.	Motor/Voltage Source Drive Circuit Test Schematic Diagram	140
100.	Dynamometer Test Setup	141
101.	270-vdc Brushless Motor/Voltage Source Drive Circuit Test, Direction of Rotation: CW	143
102.	270-vdc Brushless Motor/Voltage Source Drive Circuit Test, Direction of Rotation: CCW	143
103.	Setup for Static Stiffness and Backlash Gearbox Testing	145
104.	Backlash Measurement Method and Calculations	146
105.	Gearbox Stiffness	148
106.	Gearbox Efficiency for Both Channels	150
107.	Demonstration Test Hardware	151

ILLUSTRATIONS (Continued)

<u>Figure</u>		<u>Page</u>
108.	Frequency Response for the Digital Controller, +1 deg Amplitude	153
109.	Frequency Response for the Digital Controller, +2 deg Amplitude	154
110.	Frequency Response for Voltage Control Servo, No-Load, Dual-Channel +2-deg Amplitude	156
111.	Frequency Response for Voltage Control Servo, 11,250 in.-lb Load, Dual-Channel, +2 deg Amplitude	156
112.	Frequency Response for Voltage Control Servo, 15,080 in.-lb Load, Dual-Channel, +2 deg Amplitude	157
113.	Frequency Response for Tachometer Feedback Servo, Dual-Channel, No-Load, +1 deg Amplitude	157
114.	Frequency Response for Tachometer Feedback Servo, Dual-Channel, 8,630 in.-lb Load, +1 deg Amplitude	158
115.	Frequency Response for Tachometer Feedback Servo, Dual-Channel, 13,310 in.-lb Load, +1 deg Amplitude	158
116.	Frequency Response for Tachometer Feedback Servo, Single-Channel, No-Load, +2 deg Amplitude	159
117.	Frequency Response for Tachometer Feedback Servo, Dual-Channel, No-Load, +2 deg Amplitude	159
118.	Equipment Schematic for Dynamic Stiffness	160
119.	Response to Step Input Dual-Channel Operation	161
120.	Response to Step Input Single-Channel Operation, Microprocessor Controller	161
121.	Voltage Control Servo--Dual-Channel Step Response, 1 deg, No Load	163
122.	Voltage Control Servo--Dual-Channel Step Response, 5 deg, No Load	164
123.	Voltage Control Servo--Dual-Channel Step Response, 10 deg, No Load	165
124.	Dual-Channel Step Response with Tachometer Feedback, 1 deg, No Load	166

ILLUSTRATIONS (Continued)

<u>Figure</u>		<u>Page</u>
125.	Dual-Channel Step Response with Tachometer Feedback, 5 deg, No Load	167
126.	Dual-Channel Step Response with Tachometer Feedback, 10 deg, No Load	168
127.	Hysteresis Band Between Input Command and Control Surface Position, Early Hardware Configuration	169
128.	Hysteresis of Improved Actuation Unit, 0.08 Hz, 20 deg Peak-to-Peak Amplitude, Analog Servo Circuit, 0.022 deg Output Position Resolution	171
129.	Hingeline Actuator Reliability Management Demonstration	174
130.	Temperature Monitoring of Actuator	175
131.	Demonstration Hardware Developed	178
132.	Frequency Response Comparison for 2-Channel, No-Load, ± 1 deg Amplitude Voltage Servo Control	180

TABLES

<u>Table</u>		<u>Page</u>
1	Evolution of System Development	4
2	Test Results	6
3	Program Ground Rules and Performance Objectives	12
4	Design Summary, Electromechanical Actuation Unit	15
5	Motor Characteristics	30
6	Actuator Gear Ratios	34
7	Power Switch Tradeoffs	44
8	Specifications for Encoder	85
9	Simulation Constants and Nomenclature	93
10	Summary of Single-Channel Step Response Correlation	99
11	Summary of Dual-Channel Step Response Correlation	99
12	Summary of Dual-Channel Step Response Correlation	102
13	Tests Performed and Test Objectives	125
14	Actuator Static Stiffness Data	147
15	Actuation Unit Tests	152
16	Temperature Measurements Test 17	176
17	Summary of Performance Goals and Test Results	179

DEFINITION OF TERMS AND SYMBOLS

<u>Term</u>	<u>Definition</u>
Actuator	A subassembly of the electromechanical actuation unit that contains the motor and gearing.
Back iron	The magnetic conducting path located at the outer periphery of the stator used to transmit magnetic flux between poles.
Commutation	Control of the motor stator electromagnetic flux field to establish the polarity of applied voltage and magnitude of applied current to achieve the desired direction, velocity, and torque of the motor rotor.
Controller	The electronics portion of the electromechanical actuation unit that interfaces input power, command signal, and actuator position for servo control.
Duty cycle	The ratio of average-to-peak values, usually expressed in terms of power or current.
Efficiency	A ratio of power output to power input, P_0/P_i .
Electrical time constant	The stator winding inductance divided by the stator winding resistance. Expressed as τ , sec, it is numerically equal to 63.2 percent of the time required for the current to increase to the final value based on the step input change in applied voltage and the rotor locked.
EM	Electromechanical (actuator unit).
Feedback	The assembly which provides the servo circuits with information for closing the servo loop; the information could be position, torque output, rate output, or combinations, for example.
Fly-by-wire	Transmission of command signals from the aircraft flight control system to the EM actuation unit using electrical inputs, which could be either digital or analog in form.
Generator mode	The specific operation of the motor and controller, wherein the motor is driven by the torque applied to the output, and the motor responds to producing current and a voltage.
Mechanical time constant	The no-load velocity times the rotor inertia divided by the stall torque. Expressed as τ , sec; it is numerically equal to the time required for the speed to increase to 63.2 percent of the final value based upon a given step input voltage change.

DEFINITION OF TERMS AND SYMBOLS (Continued)

<u>Term</u>	<u>Definition</u>
Motor mode	The specific operation of the motor by applying controlled voltage and current to cause the motor rotor to rotate in the direction desired.
No-load	A condition at the (motor or actuator) output, wherein there are no aiding or opposing static or acceleration forces.
Power-by-wire	The technique of utilizing electric energy as the primary power source for flight control actuation.
Power switches	The component that is commanded to control high voltage and potentially high currents to the electric motor, providing power demand control of the motor output.
Plugging mode	The operation of the motor and controller under the following special conditions. (1) The motor is rotating in one direction and (2) the controller is providing voltage and current in an attempt to cause the motor to reverse direction. This condition is usually experienced for only short time periods during rapid acceleration/deceleration. (This is sometimes called reverse plugging.)
PWM	Pulse width modulation (PWM) is a method of controlling the applied motor current by adjusting the duty cycle of applied motor voltage.
Rotor	The mechanical rotating part of the motor, which can be either a permanent magnet or electromagnet design.
Servo circuits	The electronic circuits that interface the EM actuation unit with the aircraft flight control system, including the command input for control surface position, and provide the logic and command signals for the operation of the power switches.
Stall torque	Maximum output torque, lbf-in.
Stator	The stationary, outer part of the motor, which can be either electromagnetic or permanent magnet design.
Stiffness, dynamic	The resistance of the actuator system (actuator, motor, and controller) to applied loads at the output of the actuator. Dynamic stiffness is usually expressed as a function of the frequency of the applied load in units of lbf-in./radian.

DEFINITION OF TERMS AND SYMBOLS (Continued)

<u>Term</u>	<u>Definition</u>
Unit	Unit (electromechanical actuation) consisting of the electronic controller, actuator, and a feedback device.
PM	Permanent magnet.
A	Amplitude, radians.
B	Flux density, gauss.
f	Frequency, Hz.
G	Gear ratio (input speed/output speed).
I	Inertia, lbf-in.-sec.
L	Reactance, henries.
P	Power, watts.
Q	Electrical power dissipated as heat in the motor, watts.
S	Slope of torque, speed relationship, rad/sec/in.-lbf.
T	Torque, lbf-in.
$\dot{\theta}$	Velocity, rad/sec.
$\ddot{\theta}$	Acceleration, rad/sec.
τ	Time constant, sec.

1. SUMMARY

This final report presents the results of the design, development, and analysis of laboratory demonstration hardware for an electromechanical primary flight control surface actuation unit. Advances in the state-of-the-art make electromechanical actuation feasible. Significant developments in the technologies of magnet materials for motors, motor construction techniques, high-current capacity transistor switches for motor control, and digital microprocessors for servo and redundancy management have resulted in the development of an electromechanical actuation unit that is competitive with current hydraulic units.

1.1 ELECTROMECHANICAL ACTUATOR FEATURES

The electromechanical actuation unit developed provides dual redundancy in the electronic control, motor drive, and mechanical elements. Therefore, the unit provides fail-safe operation with reduced performance after any one component failure. Major actuation unit features are:

- (a) Closed-loop position servo circuits were implemented using both analog and digital techniques to demonstrate versatility to interface with various aircraft flight control systems. Microprocessor servo controls offer programmable current and voltage control of the motor. Optical, digital encoders were used to monitor control surface position and used in the servo feedback loop. Transistorized electric power switch circuits were designed and fabricated for motor torque-rate and commutation control.
- (b) Permanent-magnet, 270-vdc motors using brushless commutation and rare-earth cobalt magnets in the rotor assembly to achieve high acceleration and torque in minimum space and weight. Samarium cobalt and other high-energy, rare-earth-magnet materials are being used to reduce servo motor size and weight while maintaining high performance output. As a result, dc electric motors are competitive with hydraulic motors for primary flight control systems. The selection of 270-vdc power was made based upon rectification of a standard 115/200-v, 400-Hz aircraft power source (study program ground rule).
- (c) A rotary hingeline actuator which implements dual redundant drive channels using a velocity summing planetary differential and planetary gear stages to the rotary output. The rotary actuator gear ratio matches the torque and speed requirements of the control surface to the motor output. Improved materials and manufacturing processes make use of high-strength alloys to achieve smaller gears with superior backlash characteristics.

1.2 HARDWARE DEFINITION

The hardware developed was initially based upon a dual-channel electro-mechanical drive to a final hinge line geared output to a simulated control surface. In this arrangement (shown in Figure 1), complete separation of the two drive channels is maintained up to the output stages of gearing in the actuator. The arrangement shown is not the only arrangement which has merit. For example, redundancy could be implemented using force summing of two drives onto a single panel, or by using separate, nonredundant actuation systems operating onto split control surfaces. The selection of the particular optimum redundancy concept is a function of the total vehicle reliability philosophy, including determination of the criticality of the control surface, alternate control possibilities, and accepted reliability of the hardware elements.

Thus, the hardware arrangement developed for test is not the only configuration, but is representative for demonstrating actuation system considerations that may be useful to future development and aircraft actuation design programs.

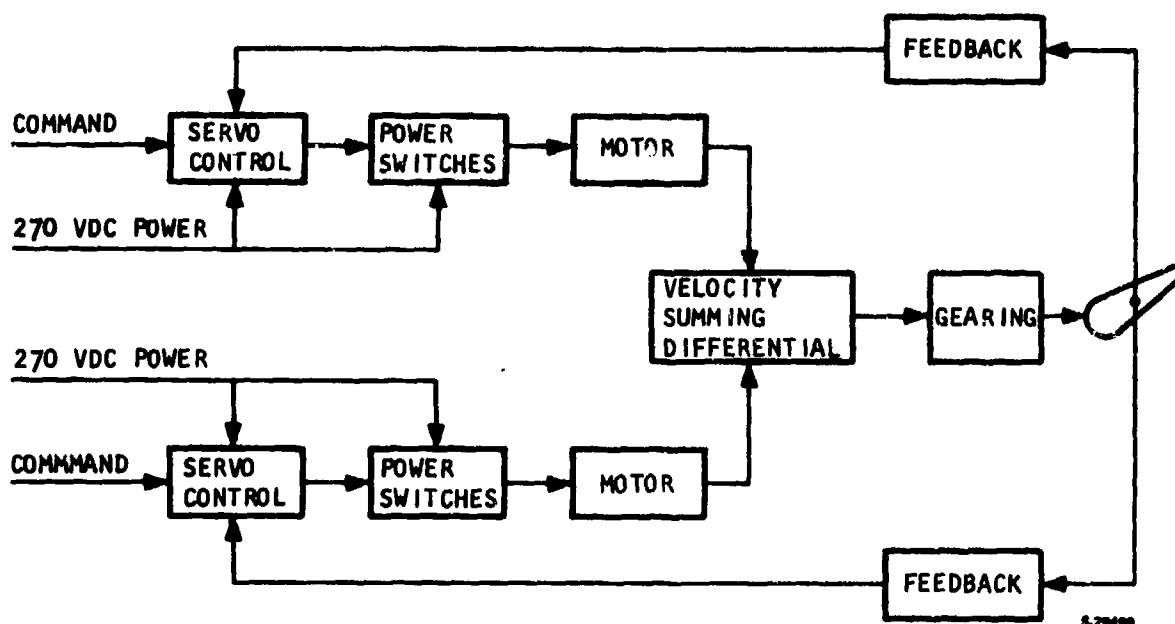
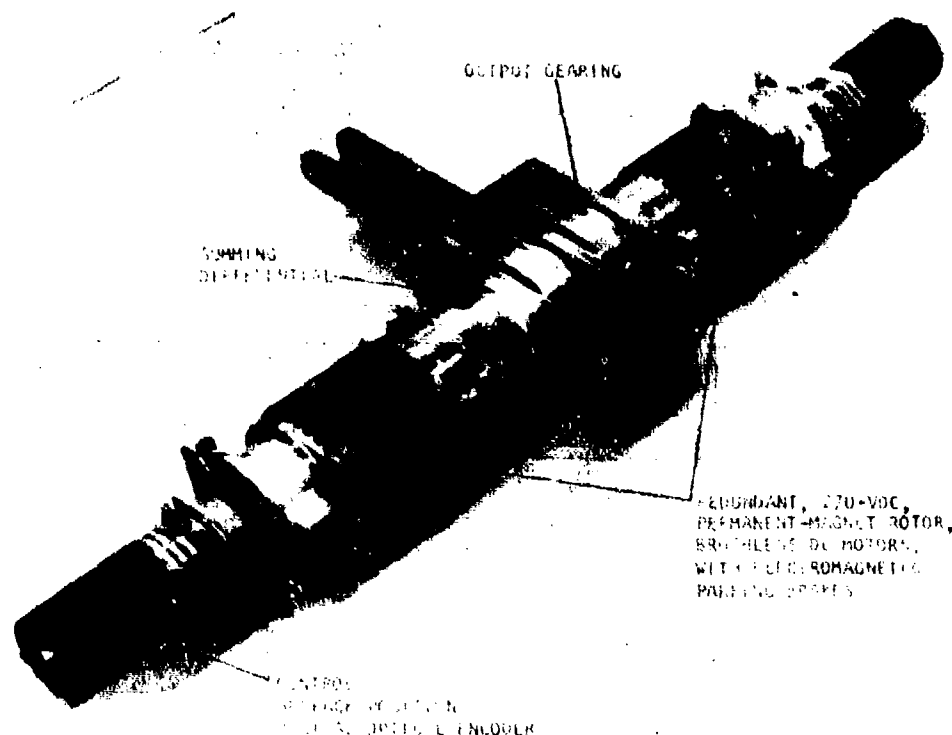


Figure 1. Electromechanical Actuation Unit Block Diagram

1.3 HARDWARE FABRICATION

The actuation unit was designed to be in a flight configuration to illustrate hingeline structural interface capability, thermal management considerations, and servo feedback mounting and design considerations. The fabricated actuator and purchased position transducers are shown in Figure 2. The position transducer is an optical encoder purchased from Renco Corporation. The motors were fabricated at AIResearch using permanent magnets in the rotor purchased from Varian. The gearing and housing were fabricated entirely by AIResearch.



78366-2

SPECIFICATIONS:

37,500 IN.-LB STALL TORQUE
80-DEG/SEC NO-LOAD RATE
4-HP OUTPUT
 3.75×10^6 LB-IN./RAD SPRING RATE
34.8 LB WEIGHT

F-27214

Figure 2. Dual Electromechanical Rotary Hingeline Actuator and Position Transducers

The controller hardware was fabricated as an engineering breadboard, with two separate, rack-mounted, servo circuits and power switch assemblies. The purpose was to provide maximum flexibility to incorporate design improvements and simulate functional interfaces without packaging and other special constraints. The microprocessor was purchased from Wave Mate, and the power switch

assembly was fabricated using Motorola MJE 10005 transistors. Although the initial hardware fabricated was based directly (without change) on the preliminary design prepared during the feasibility study, certain changes in the controller area were necessary as the development progressed. The evolution of the development effort is listed in Table 1, which shows that the configurations and general design approach for the power switch, motor, and gearing assemblies remained unchanged from the initial preliminary design definition through to the final configuration used for demonstration testing. This is not true for the servo controller circuits.

The initial hardware fabricated for the servo was a dual-channel microprocessor. Concurrently, the power switch assembly was being fabricated and developed using transistor bridges to interface with the motors. As the development program progressed, it became evident that the effort required for parallel developments of the high-power switching devices and the microprocessor were excessive. For example, because of difficulties in electrical and functional interfaces between the servo and power switch circuits, development problems in the servo area impacted development in the power switch assembly.

TABLE 1
EVOLUTION OF SYSTEM DEVELOPMENT

Component	Initial Design Approach	Original Hardware Configuration	First Modification	Second Modification	Final Configuration
Servo control	Microprocessor	2-channel microprocessor	2-channel analog	One analog channel and one microprocessor channel	1-channel analog
Power switch	Transistorized pulsewidth modulated bridge	2-channel transistorized pulsewidth modulated bridge	None	None	Same
Feedback	Digital, position feedback	2-channel, digital, optical, absolute position encoder	Single channel	None	Single channel
Motor	270-vdc, permanent-magnet rotor with brushless commutation	270-vdc, permanent-magnet rotor with brushless commutation	None	None	Same
Gearing	Planetary with summing differential	Planetary with summing differential	None	None	Same

An alternate program approach was planned in which the development of the switch assemblies would continue and simple analog servo circuits would be used to drive the total unit. This materially reduced the design, checkout, and interface resolution effort for the power switch assembly. Once the system was operating with the analog servo circuits, attention was again directed toward design modification and completion of the microprocessor servo configuration. One microprocessor servo circuit was integrated into the breadboard controller, replacing one of the analog servo circuits. Therefore, the actuation system was operated successfully with one analog servo circuit driving one of the channels, and one microprocessor servo circuit driving the second channel. The early system evaluation tests were run with the analog/microprocessor servo circuit configuration.

Based upon the results of the system simulation and performance prediction analysis, it was decided to modify the equipment to improve the performance demonstration capability. To accomplish the required hardware changes in reasonable time, a single servo circuit was designed and fabricated using analog techniques. The majority of the system test data presented in this report, and the correlation to test data with the system simulation analysis, is based upon the use of the single analog servo circuit in the controller operating both power switch driver circuits.

1.4 TEST RESULTS

Test data were collected at the component and the unit operating levels. The significant results of the tests are summarized as follows.

- Motor--The torque/speed relationship and the torque per amp were as predicted. The motor assembly showed a minimum of 18 percent thermal duty cycle capability.
- Gearbox--The efficiency of the gearing was 1 to 5 percent below the analytical prediction. The static stiffness was approximately 12 percent below the predicted value.
- Controller--Both microprocessor and analog servo circuits used in testing the two channel unit. Transistorized power switches proven capable of controlling peak currents up to 18 amp at 270 vdc.
- Actuation Unit--Output rate, frequency response, and step response meet performance goals and are predicted using computer simulation techniques.

The specific test results are summarized in Table 2.

TABLE 2
TEST RESULTS

Test	Actuation Goal	Test Result	Comment
Step response	No-load speed, 80 deg/sec	80 deg/sec	Rate demonstrated on square, triangle, and sinusoidal wave input.
Frequency response	Bandwidth of 4 to 12 Hz, 8 Hz nominal	8 Hz nominal	Under no-load conditions, an amplitude of ± 1 deg shows less than 3 dB amplitude degradation. Phase lag approximately 90 deg.
Thermal management	Duty cycle, 20 percent	18 percent continuous	Steady-state temperature, of 234°F occurred at 3 amp with control surface locked. Motor can operate at short term temperature up to 450°F.
Position resolution	0.5 percent of full stroke	<0.5 percent of ± 20 deg stroke	Full stroke was demonstrated.
Controller/actuator system tests	Operate mode	Controller operated as predicted	Capability of physical and functional interfaces demonstrated.
Reliability management demonstration	Simulate failure of one channel	One-channel operation allows reduced rate control with full torque output	Manually demonstrated; provisions for closed-loop shutdown were not implemented in the controller.
Static stiffness	3.75×10^6 in.-lb/rad	3.25×10^6 in.-lb/rad	Calculated dynamic stiffness of 2.6×10^6 in.-lb/rad at 8 Hz.
Regeneration	Demonstration	14 amp at 270 vdc	Demonstrated during reverse plugging operation.

2. INTRODUCTION

In this report, a 3-year program for design, development, and test of a demonstration electromechanical flight control actuation unit is described. The program was centered upon the new and continually evolving electrical, electromechanical, and electronic technologies now available to satisfy aircraft primary flight control actuation requirements. Each of these technologies contributes in a collective, synergistic manner to the credibility of electromechanical actuation for primary flight control, and includes the following:

- High-voltage dc power sources
- Dc servo motor design using high-performance, rare-earth-cobalt permanent magnets in the rotor assembly and brushless commutation to achieve fast response, minimum electrical losses as heat, long life, and flexibility in commutation sequencing and logic
- Programmable digital microprocessor servo control that can be adapted to various motor types and torque-speed requirements, and can accommodate primary flight control requirement variations for specific real-time aircraft operating characteristics
- Commercially available solid-state electric power switches that can switch currents of up to 600 amp at voltages ranging up to 300 v, and which allow exploitation of electronic commutation
- Geared, rotary, high-efficiency, hingeline control surface actuator configurations that may include drive redundancy provide structural weight savings through more uniform load distribution between aircraft structural elements

Synthesis and optimization of these technologies for specific flight control applications indicate that electromechanical actuation offers an alternative to hydraulic systems. The potential advantages of electromechanical actuation compared with hydraulic actuation are:

- Low Maintenance--No periodic maintenance scheduled for electromechanical systems. Hydraulic actuation systems require periodic line maintenance for replacement of filters, repair of leaks, and refill of fluid levels.
- Competitive Weight--Electromechanical systems (including power source and distribution) show a slight weight advantage. Hydraulic actuation systems are heavy. Interconnecting tubing, fittings, bulky housings, and fluids comprise a large percentage of "fixed" weight.

- Low Cost--Installation and operating costs reduced for electromechanical systems. Increased parts count for hydraulic tubing and fittings not only increases the cost of fabrication, but requires a spares inventory for maintenance support.
- Reduced Hazards--Electromechanical actuation is safe. Some hydraulic fluids are corrosive and flammable, and require special handling and adjacent structure materials.
- Simple Installation--Compared with hydraulic systems, wiring can be installed in the airframe in less time, thereby reducing initial assembly costs.

2.1 OBJECTIVES

The objective of the program is to demonstrate the feasibility of electro-mechanical techniques applied to a primary flight control surface actuation unit as a competitive alternate to hydraulic actuation. The electromechanical actuation unit incorporates the concepts of both fly-by-wire and power-by-wire, which are defined as follows:

Fly-by-Wire--Command signals are transmitted to the control surface actuators using only electrical techniques, as opposed to mechanical transmission.

Power-by-Wire--Flight control surface actuators are powered by electrical power, as opposed to hydraulic power.

One particular objective of the program is performance of tests and demonstrations to determine the actuation unit parameters, including frequency response, duty cycle, static and dynamic stiffness, and thermal characteristics, which can then be used to develop a performance prediction computer program. This program is used to evaluate unit performance capability over a wide range of typical operating conditions.

2.2 SCOPE

The actuation unit (based upon the preliminary design of Appendix A) was designed to illustrate realistic interface requirements with the aircraft, including structural attachments, thermal provisions, and dual-redundant control surface actuation. The electronic controller and transistor power switches are designed as laboratory brassboard items to maximize demonstration of capability and flexibility in actuating a simulated control surface. The operational flexibility may be in excess of the flexibility requirements of any one particular flight control application. The priorities of this development program did not allow an electronic packaging effort, which would be required to satisfy a particular application.

The scope of the program included the following:

- Development and test of brassboard hardware
- Power output to the control surface is 3 hp minimum

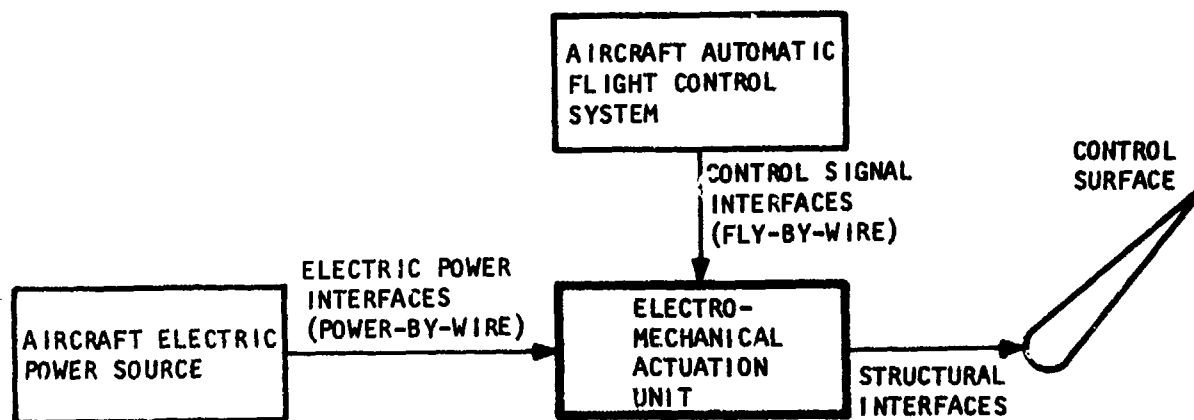
- Actuator configuration of hingeline design, with a 4-in.-maximum hingeline depth

The major design goals for the actuation unit design are listed below.

Stall hinge moment	37,575 in.-lb
No-load rate	80 deg/sec
Bandwidth	8 Hz at ± 1 deg amplitude
Stroke at output	± 30 deg minimum
Power source	115/200 vac, 400 Hz, 3-phase power

2.3 PROGRAM REVIEW

In 1975 AIREsearch was awarded a contract by the United States Air Force to study the feasibility of and conduct a preliminary design for a selected candidate electromechanical actuation unit for aircraft primary flight controls (Reference 1). In this one-year study program, the electric power, communication signals, and structural interfaces with the aircraft were defined (see Figure 3) and the technical tradeoffs to be considered in synthesizing an actuation unit for any one particular application were identified.

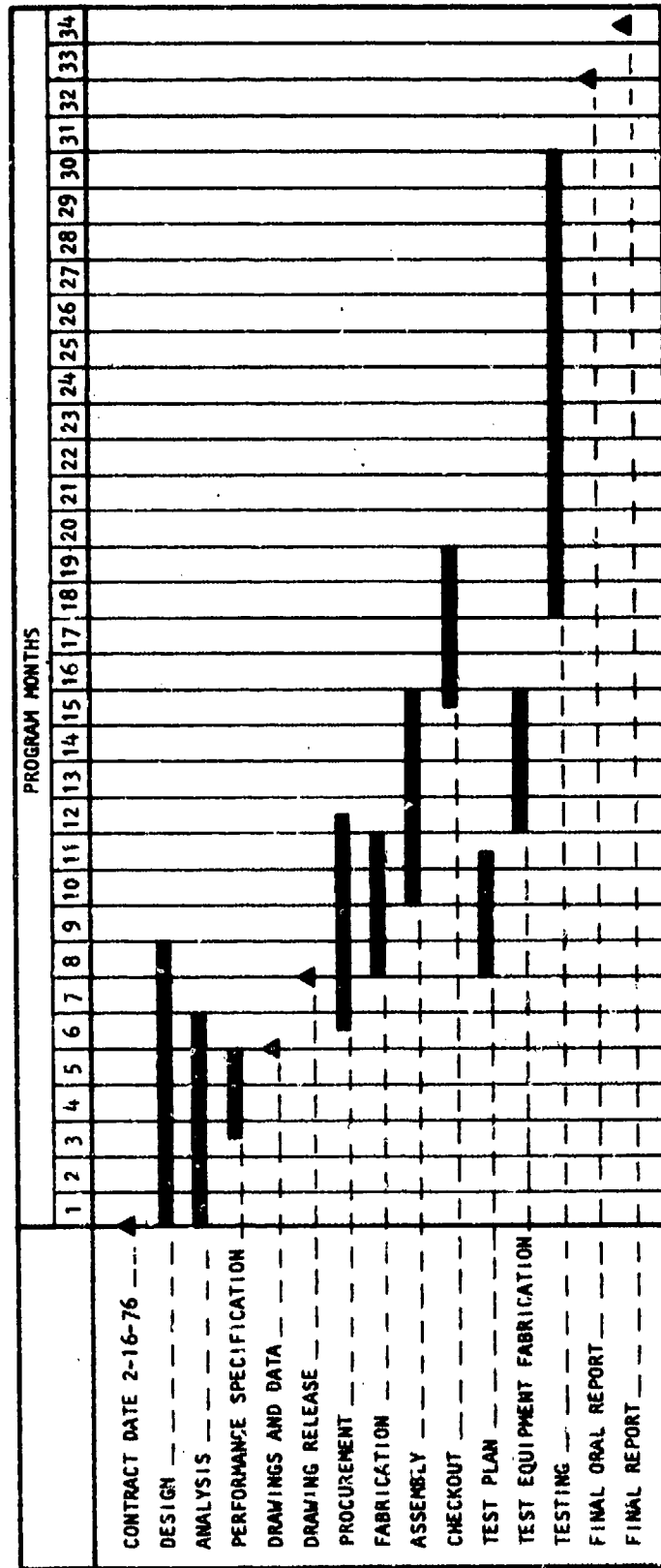


6-29400

Figure 3. Functional and Interface Block Diagram for Electromechanical Actuation Unit

Based upon the results of the feasibility study, a second contract was awarded to AIResearch to develop the demonstration hardware, which is the subject of this report. The schedule for this development program is presented in Figure 4. The major milestones are as follows.

<u>Activity</u>	<u>Months After Contract Go-Ahead</u>
Design complete	8
Procurement complete	11-1/2
Assembly complete	15
Test complete	30-1/2
Submittal of final report	34-1/2



3-25307-A

Figure 4. Program Schedule

3. HARDWARE DESCRIPTION

The electromechanical actuation demonstration hardware is described in this section. The hardware baseline problem statement is presented, including the rationale for hardware configuration and operating modes. Each of the actuation assemblies is described in detail; appropriate design analyses and supporting data for the hardware components are presented in appendixes.

3.1 ELECTROMECHANICAL ACTUATION UNIT DEFINITION

3.1.1 Baseline Problem Statement

A problem statement for actuation unit performance was generated for purposes of conducting the design of the actuator and controller. Appendix B (AiResearch Report No. 76-12942) presents a complete performance specification, which was used as a guide during the design of the demonstration unit. These performance characteristics were taken directly from the electromechanical feasibility study and preliminary design documented in Report AFFDL-TR-76-42 (Reference 1). Principal features of the problem statement are listed in Table 3.

TABLE 3

PROGRAM GROUND RULES AND PERFORMANCE OBJECTIVES

<u>Vehicle Application Interfaces</u>	
Structurally integrated, rotary hingeline actuator	
3 hp available at control surface, maximum	
115/200-vac, 3-phase power supply	
Redundancy, fail-safe (two-channel)	
<u>Actuation Goals</u>	
Stall hinge moment	37,575 in.-lbf
No-load rate	80 deg/sec
Bandwidth	4 to 12 Hz (8-Hz nom.) at ± 1 deg amplitude
Load inertia	45.6 lb-in.-sec ²
Duty cycle	Continuous operation at a minimum of 20 percent peak current (torque output)
Stroke	± 30 deg for demonstration

3.1.2 System Synthesis

The practical and efficient combination of power-by-wire and fly-by-wire technologies is the principal criterion for synthesis of the actuation system to meet the problem statement. The screening of various candidate concepts and the selection of the preferred approach was accomplished in the feasibility study (Reference 1). Appendix C presents the screening logic diagrams used to limit the scope of the study and that lead to the selection of an approach for preliminary design.

The functions to be performed by the electromechanical actuation unit include the following:

- (a) Respond to command signal inputs from the aircraft flight control system (fly-by-wire technology)
- (b) Operating from the aircraft electrical bus, provide electric current and voltage control to an electromechanical drive unit (power-by-wire)
- (c) Match and apply the rate and torque output of the drive unit to the aircraft control surface
- (d) Provide any necessary control surface parameter (such as position feedback) to stabilize and simplify the control surface response to command input signals

One method of implementing these simplified operational functions is shown in Figure 5. The three basic subsections of the electromechanical actuation unit are (1) controller, (2) actuator, and (3) feedback.

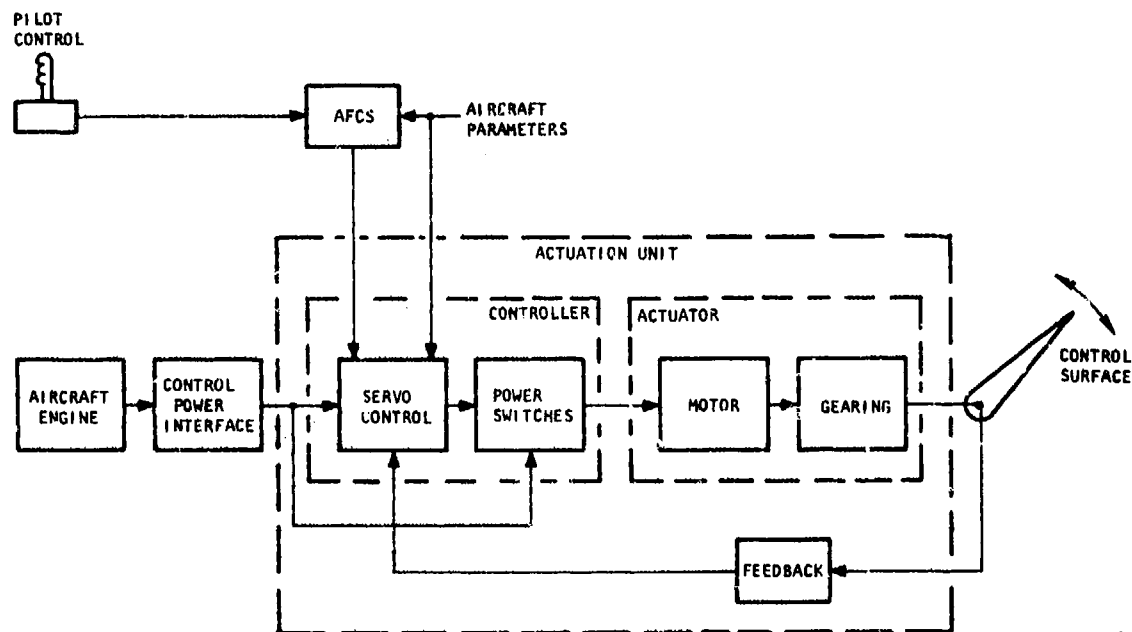


Figure 5. Electromechanical Actuation Unit for Primary Flight Control (Shown without Redundancy)

The controller has a signal processing section that serves as the servo control and is the interface with the aircraft flight control system. Input signals (fly-by-wire) can be either digital or analog in form, and could be electrical or optical in nature, for example. The baseline approach is to use a digital microprocessor, although analog servo circuits were also developed and tested in the demonstration program. The controller power switch responds to any logic and sequencing commands from the servo control, and is designed to handle high current and voltage levels (power-by-wire), as may be commanded to match control surface torque and rate demands. The power switch provides electric current at a voltage to the electric motor to produce mechanical torque. Transistors were selected as the switching devices because of fast switching time, current carrying capability, small size, and ease of actuation on and off (i.e., commutation) (References 2, 3).

Current applied to the motor produces torque. Evaluation and comparison of an ac induction motor and a permanent-magnet-rotor, brushless dc motor (for the same problem statement) showed the two motors to be closely matched; however, the dc motor showed the following advantages (Appendix D):

- Faster acceleration (reduced rotor inertia for the same rotor diameter)
- Higher overall average torque output based upon the same maximum operating temperatures (increased duty cycle because of better heat rejection characteristics)
- Lower weight (reduced length to provide same power output)

The selected dc motor was fabricated using a six-pole, rare-earth-cobalt magnet rotor configuration with brushless commutation of the three stator winding circuits using variable reluctance transducers for rotor position sensing.

The motor output torque and rate are matched to the control surface static and dynamic load requirements using a gear ratio. Planetary gearing was selected on the basis of weight, packaging volume, and high efficiency. The gear ratio can be selected based upon any one set or sets of requirements, including control surface maximum rate, stall torque, acceleration, and/or a running load at a specified rate (Reference 4).

The control surface motion (location) is then sensed and this feedback information is supplied to the servo circuit in the controller. The servo may be configured in various ways, depending upon the requirements of the vehicle and the specific control surface. The selected method for this demonstration program is closure of the servo loop using control surface position information from a digital encoder.

The final design for this demonstration hardware was based upon a dual-redundant, fail-safe performance concept. Figure 6 shows the system model, emphasizing the two separate electrical and mechanical drives to the control surface. (As described in para. 1.2, redundancy can also be accomplished using split control surfaces). The summing differential could be either a force or a velocity summing device. A velocity summing differential was selected because

It provides full torque at one-half rate after a failure in one drive channel. This approach requires that a parking brake be added to each input shaft of the differential to lock a failed drive channel. Although a force summing approach would not require this additional element, the decision for reliability management of a particular control surface must be made only after an in-depth evaluation of failure probability, criticality, probable failure mode, and the desirable mode of operation after a failure (Reference 5).

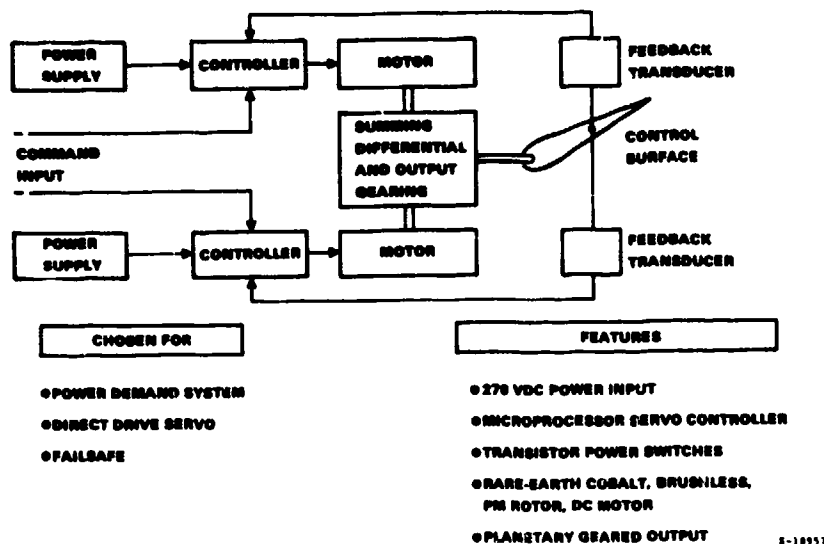


Figure 6. System Model

Based upon the baseline problem statement, the screening and selection of candidate component concepts, and the synthesis of components into a unit, the preferred electromechanical actuation unit configuration was selected (see Table 4). The special arrangement of the motor and gearing to achieve velocity summing of the motor inputs is shown in Figure 7. This actuator configuration was designed, fabricated, and tested during this development program.

TABLE 4

DESIGN SUMMARY, ELECTROMECHANICAL ACTUATION UNIT

Function	Approach	Rationale
Power source	115/200 vac, 400 Hz, rectified to 270 vdc	Weight, simplicity
Motor	Brushless dc, permanent-magnet rotor	Thermal design, response, efficiency, growth potential
Control	Digital microprocessor, transistor switches	Flexibility, monitoring, cost, growth potential
Actuator	Geared planetary	Stiffness, weight, redundancy
Redundancy	Dual-channel with mechanical velocity summing	Home safe capability with reduced rate

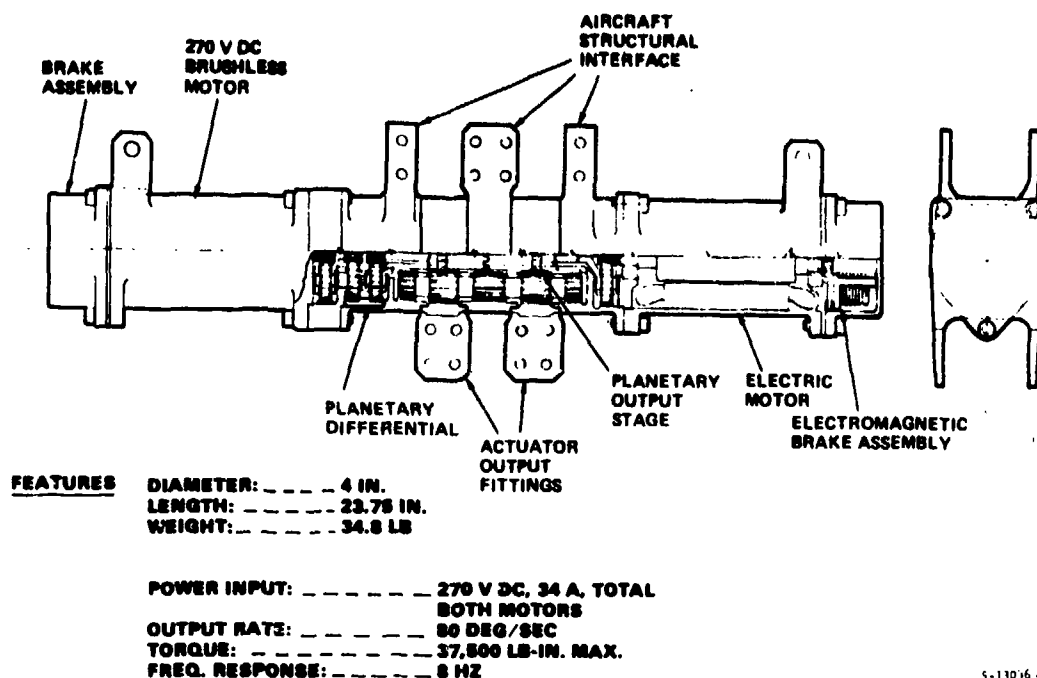


Figure 7. Primary Flight Control Hingeline Actuator

3.1.3 Modes of Operation

The design of the demonstration unit is based upon operation of both operating channels to achieve full performance. The two electromechanical drive channels operate together as a direct drive servoactuation unit. The operating modes are:

- Off
- Activate
- Operate
- Shutdown

Each mode is described below. Also described are failure monitoring and fail-safe operating provisions.

The off mode is characterized by removal of all electrical power and control signals from the system. The motor parking brakes will be spring-loaded into the on, or locked, condition. With power removed and the brakes locked, the control surface will be locked in its last position.

To activate the system, the main power supply is switched on. This also energizes the low-voltage power supply for the microprocessor, and activates the parking brakes off. Since all components are solid state, the unit does not require a warmup period.

For the operate mode, the servosystem input command is control surface position. This can be input manually or by use of a function generator. During operation, the two-channel unit may draw a maximum current of approximately 35 amp at 270 vdc for the total electrical input to both motors, controllers, and other electrical components. This maximum current condition will occur only when operating at full rated stall, or for short periods of time when providing maximum acceleration torque. Since the system is a power demand type, it requires power only in proportion to the torque and rate experienced at the control surface, as shown in the test data of Section 6.

Shutdown can be initiated at any time. Removal of the main power to both controller channels causes the simultaneous shutdown of the controllers and application of both motor parking brakes. This action causes the actuator to lock in its last position.

In the event of a power failure of the electrical bus supplying power to one of the drive channels, the brake in that drive channel will be spring-loaded to the locked, or on, condition. Spring-loading the brake to the on condition ensures the continued operation of the control surface at full torque and reduced rate.

3.2 ACTUATOR

The actuator consists of two motors operating into a velocity summing differential, the output of which drives a planetary geared output with structural attachments, all of which serves as a rotary hinge for the control surface. The gearing assembly serves as the structural mounting for the two redundant motors and as the structural interface between the control surface and mating aircraft structure (Reference 5). The main components of the actuator are (1) motor and (2) gearing. These are described in the following paragraphs.

3.2.1 Motor

The motor in an electromechanical actuation unit functions to convert electrical current and voltage to mechanical torque. The discussion of motors for the actuation unit is presented as follows:

Potential motor configurations and characteristics

Selected motor design

Motor fabrication

3.2.1.1 Potential Motor Configurations and Characteristics

A simplified representation of a 2-pole electric motor is shown in Figure 8. The magnetic fields may be formed using permanent magnets or electromagnets. The interaction of the magnetic fields produces torque in accordance with the expression (Reference 6):

$$T = KPLr F_R F_S \sin \delta \quad (1)$$

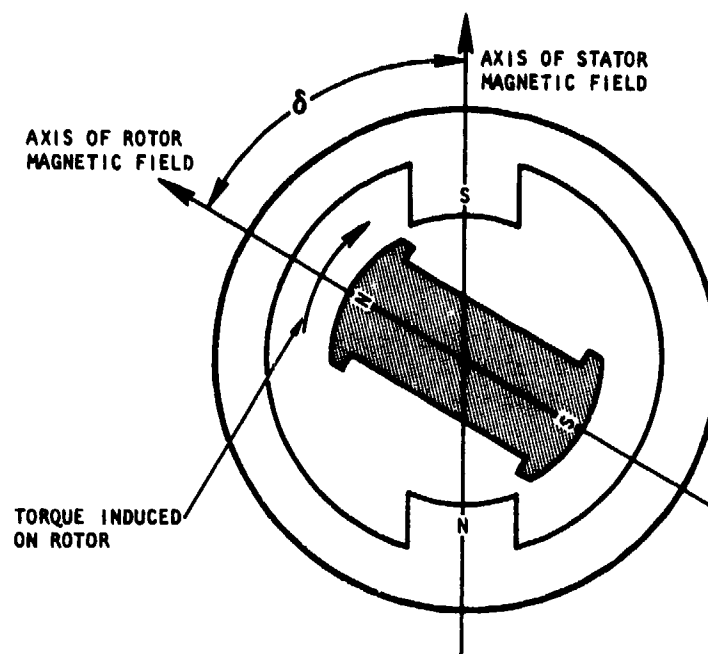


Figure 8. Simplified Motor Model

where

- T = torque
- K = constant of proportionality
- P = number of poles
- F_S = maximum stator MMF
- F_R = maximum rotor MMF
- L = rotor lengths
- r = rotor radius
- δ = angle between stator MMF and rotor MMF

For given values of F_S and F_R , the torque is maximum when the term $\sin \delta$ is equal to 1 (i.e., when $\delta = 90$ deg). The interacting magnetic fields may be developed using combinations of permanent magnets and electromagnets. Representative variations of wound and permanent-magnet motor types are shown in Figure 9.

The wound stator and rotor brush type machine is typical of state-of-the-art variable-speed commercial motors. The variable voltage applied to the rotor controls the output torque and rate. Electrical power dissipated as I^2R losses occurs in both the stator and rotor. The heating which occurs in the rotor is particularly difficult to transfer to the outer frame of the motor. Therefore, thermal management to limit temperature rise would be a major design limitation if this type of motor were used in a flight control application.

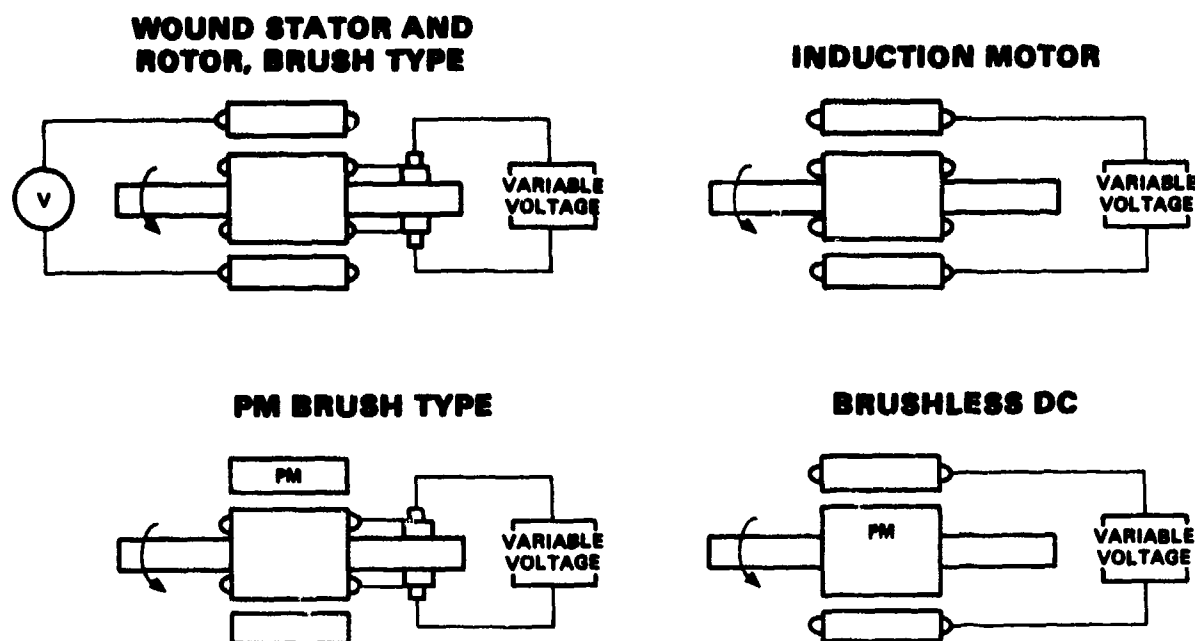


Figure 9. Machine Configuration

The PM brush-type motor is configured to replace the stator electromagnetic field with a fixed permanent magnet. All electrical losses occur in the wound rotor. Brushes are required for commutation of electric power to the proper rotor winding to control direction of rotation and torque. In both these latter configurations using wound rotors, the motor life may be limited by brush wear.

The induction motor and the brushless dc motor eliminate the practical limitations of brush life. The induction motor has been compared to a brushless dc motor, as described in Appendix D. The comparison is based on the criteria that fast response, low weight, and low electrical losses are important to a high-performance servo application. The comparison of induction and brushless dc motors (based upon the same problem statement) shows that the dc motor offers approximately a 16 percent improvement in acceleration capability, a 17 percent weight savings, and twice the operating duty cycle.

Electrical losses for the induction motor occur in both the stator and the rotor; therefore, both elements must be designed from a thermal viewpoint. Cooling of the induction motor is complicated because the available modes of heat transfer from the rotor to the stator and motor casing are limited. The brushless dc motor exhibits twice the duty cycle capability of the induction motor (References 1,7,8) because nearly all losses that occur are located in the stator windings. Electrical power dissipation as heat can be more readily transferred to the outer periphery of the dc motor. Here, the heat can be transferred from the motor by forced or natural convection, radiation, and conduction to the structure.

A power servo must be evaluated using a combination of criteria such as peak power, slew rate, stall torque, acceleration, and duty cycle. The power servo will usually be designed using acceleration, power, and duty cycle as the principal requirements. High acceleration is achieved by a machine that exhibits a low rotor inertia and a high output torque. Therefore, a useful figure of merit for comparison of power servo motors is the value of $(\text{torque})^2$ divided by inertia, i.e., $\frac{T_m^2}{J_m}$ (Reference 9). The ratio can be maximized using the brushless dc motor configuration and high-performance, rare-earth cobalt permanent magnets in the rotor.

The $(\text{torque})^2$ -to-inertia ratio using the improved magnet materials is increased compared to wound rotor designs. The magnetic flux available per unit magnetic cross-section is continually increasing as technological advances occur. Magnet materials are compared in Figure 10 (References 10, 11, and 12). Until 1973, only Alnico and Ferrite materials were readily available on a commercial basis. In 1974, the first samarium-cobalt (Sm-Co) material was available with a BH product of 15×10^6 G \cdot O. Sm-Co material with a BH product rating of 23×10^6 was available in 1977, and in 1978, small commercial quantities of material with a product rating of 30×10^6 were available.

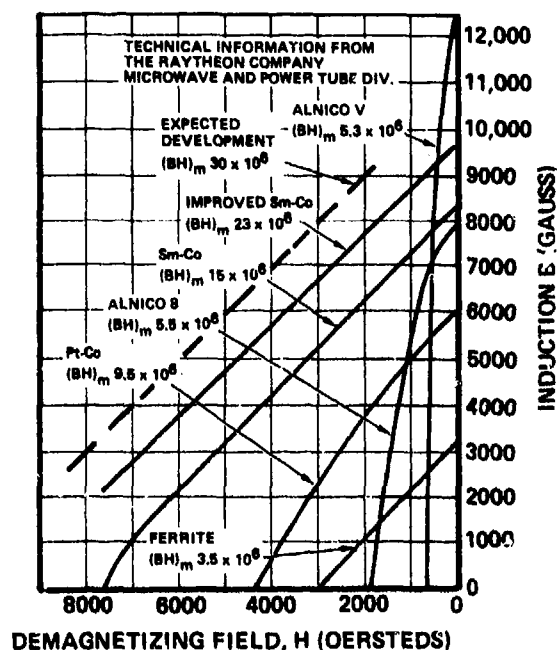


Figure 10. Comparison of Magnet Materials

Equation 1 shows that the motor torque is a direct function of the rotor magnetic vector. The newer Sm-Co magnet materials provide increased rotor magnetic flux, and therefore provide increased torque output with the same rotor geometry and inertia. Conversely, if rotor magnetic flux is held constant, the new magnetic materials allow the rotor to be made smaller, thus reducing the rotor inertia. For both cases, the acceleration capability of the motor is improved because the ratio of (torque)²-to-inertia is increased (References 13, 14, 15, and 16).

The motor selected for fabrication is a reversible, brushless, dc, rare-earth-cobalt permanent-magnet design comprising a permanent-magnet rotor and wound stator. This approach was selected because it offers the following advantages for power servo applications.

- Improved thermal management
 - (a) Minimum rotor heating
 - (b) Increased conductor area in the stator, lower copper losses, higher overall efficiency
 - (c) Wider stator teeth - lower iron loss, higher air gap flux
- Brushless commutation for long life, flexible phasing of commutation
- Improved motor geometry, improved winding size and distribution

3.2.1.2 Selected Motor Design

The motor assembly contains a separately excited dc brake and shaft position sensor. This direct-drive servomotor design provides exceptional performance, low-weight, and high efficiency. The location of the motor assemblies on the hingeline actuator and the motor parts are shown in Figures 11 and 12. The motor outline is shown in Drawing 515018, and the motor assembly is presented in Drawing P515018.

3.2.1.2.1 Motor Assembly Components

3.2.1.2.1.1 Rotor

The assembled permanent-magnet rotor, consisting of high-energy-density, samarium cobalt magnets, allows high-speed operation with low inertia. The magnets in the rotor are arranged in a tangential orientation as shown in Figure 13. The six-pole rotor configuration is relatively simple to fabricate and the tangential arrangement results in less magnet material required compared to the radial orientation (also shown in Figure 13). Motors with 2 or 4 poles would be simpler to construct using the radial design.

The tangential magnet orientation allows a minimum rotor diameter consistent with an acceptable magnet length-to-width ratio. This geometry permits optimum utilization of the samarium cobalt material by condensing the flux from two magnets into the pole piece, which directs the flux into the air gap between the stator and the rotor. Rotor inertia of the motor is 9.94×10^{-4} in.-lb-sec².

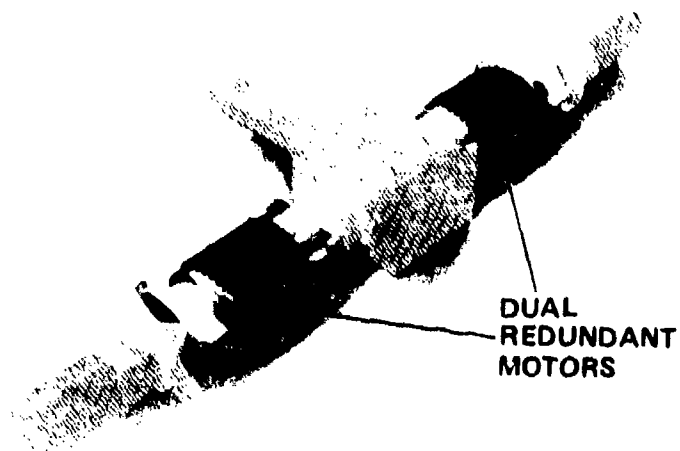
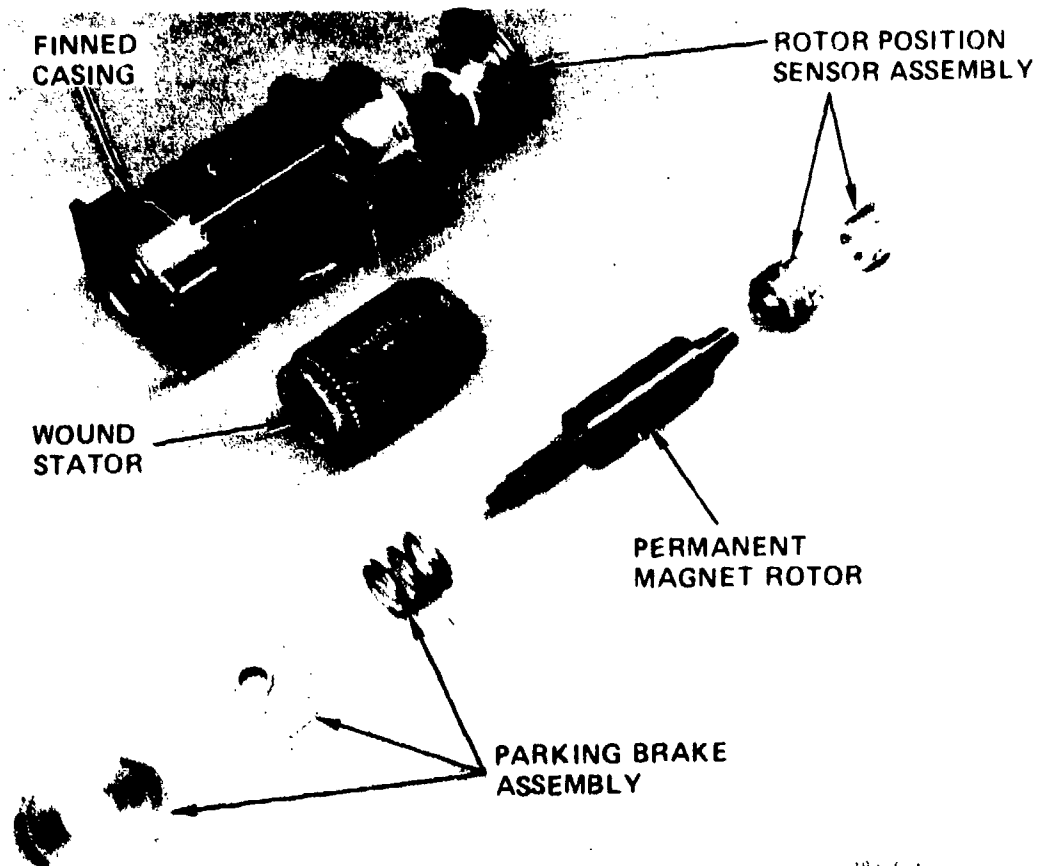
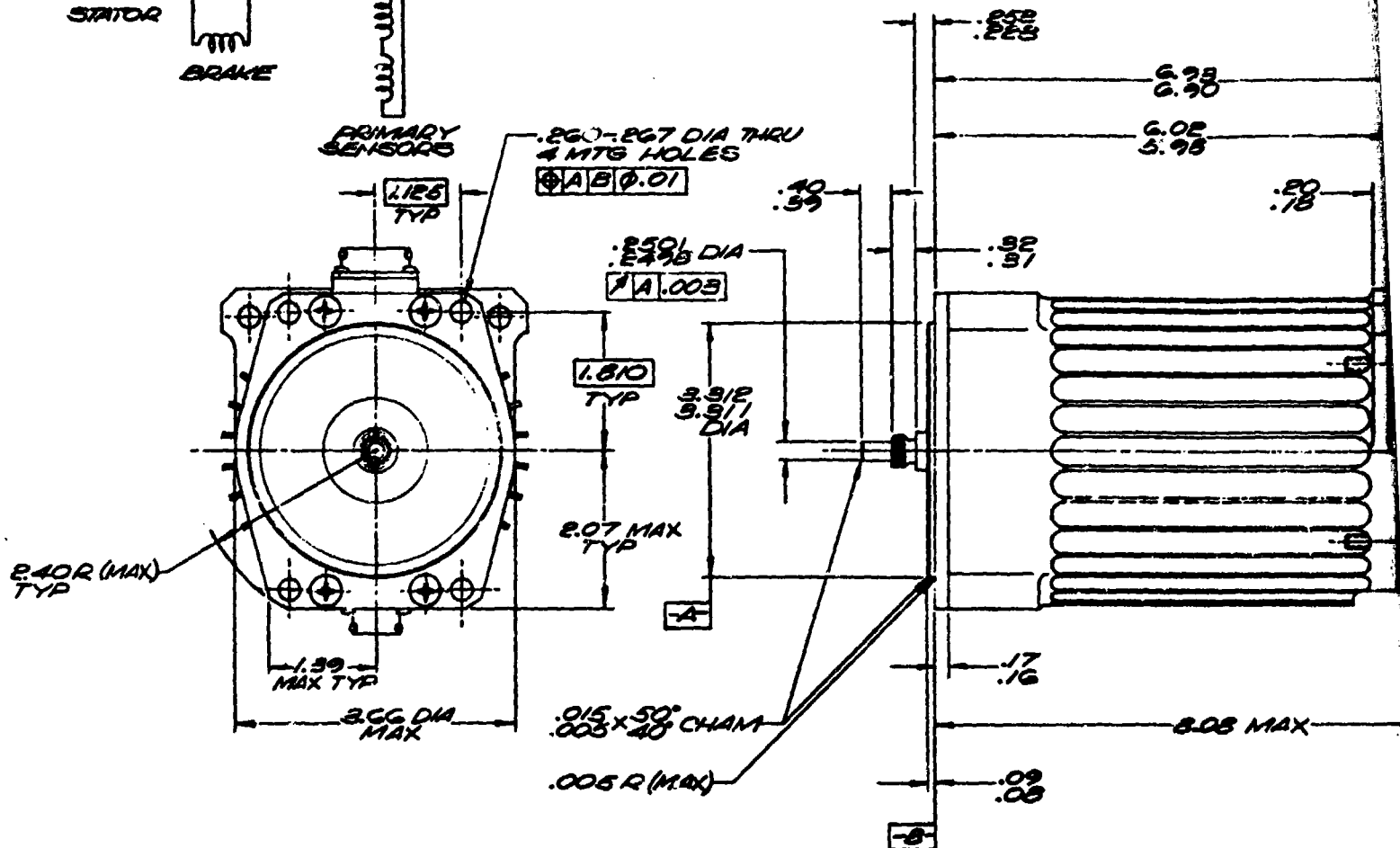


Figure 11. Hingeline Actuator Motors



78306-1 1 2/78

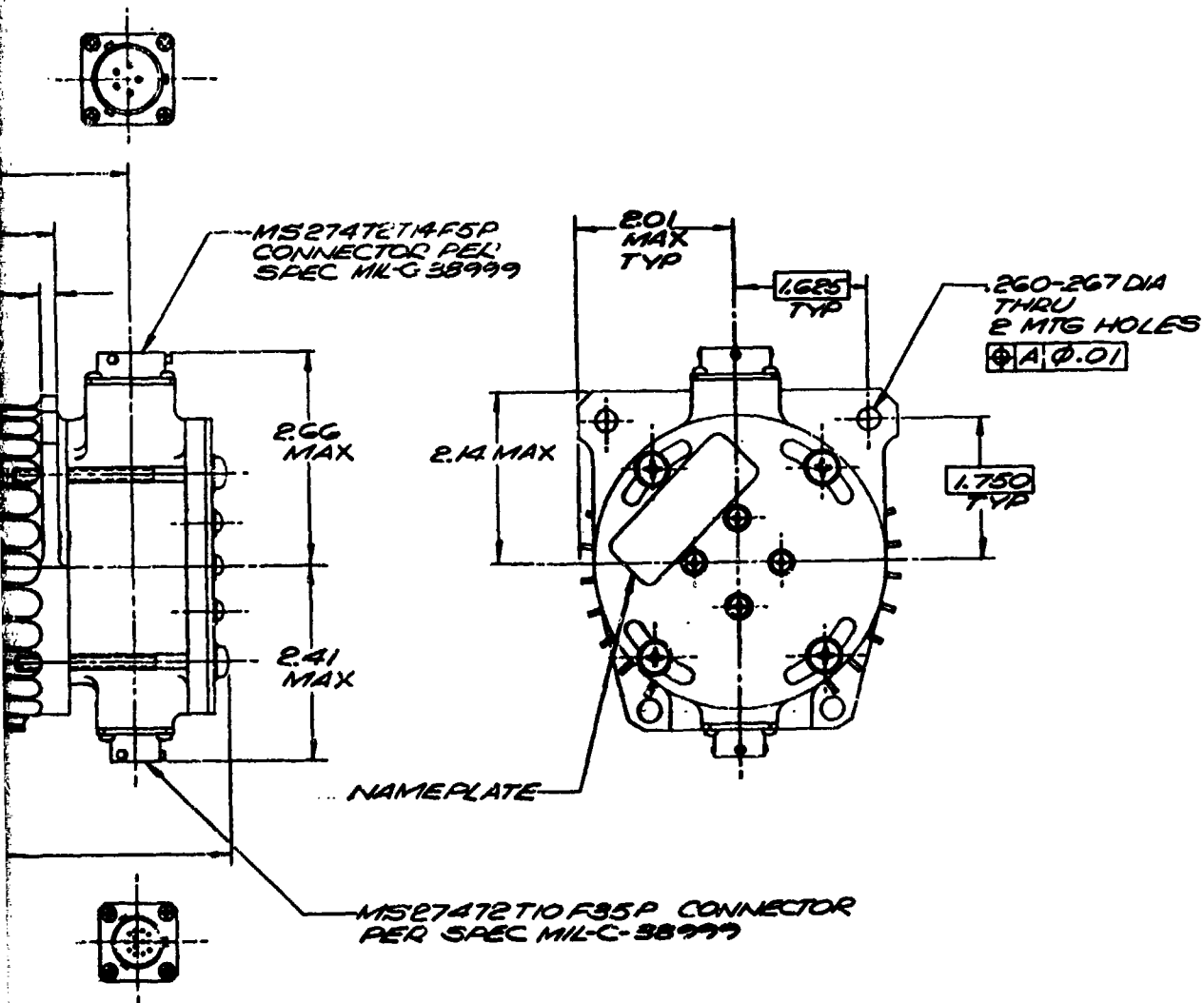
Figure 12. Rare-Earth Permanent Magnet Motor Parts



EXTERNAL INVOLUTE SPLINE DATA	
ANSI B92.1-1970 PILET ROOT S/D 1/2" FIT	
NUMBER OF TEETH	15
PITCH	.25796
PRESSURE ANGLE	30°
BASE DIAMETER	.824739 REF
PITCH DIAMETER	.873000 REF
MAJOR DIAMETER	.991-.996
FORM DIAMETER	.960
MINOR DIAMETER	.918 MIN
CIRCULAR TOOTH THICKNESS	
MAX EFFECTIVE	.0327
MIN ACTUAL	.0302
MIN MEASUREMENT OVER PINS .930 REF	
PIN DIAMETER	.0400

2. MOTOR SPECIFICATIONS:
RATING: 2.4 HP, 3000 RPM, 265 VOLTS,
9.0 AMPS
DUTY CYCLE: 50% AT 1/2 LOAD, 1/2 SPEED
OPERATING TEMP: LABORATORY AMBIENT
ROTATION LOOKING AT SHAFT END: CCW
UNIT IS PROVIDED WITH MAGNETIC BRAKE
1. DIMENSIONS FOR INSTALLATION PURPOSES
NOTES: UNLESS OTHERWISE SPECIFIED

REVISIONS			
REV	DATE	DESCRIPTION	APPROVED



515018-1-1	515018-1
PART NO.	ASSEMBLY NO.

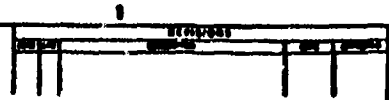
23

TS,
FEED
VENT
NEW
PAKE
ROSES ONLY
D

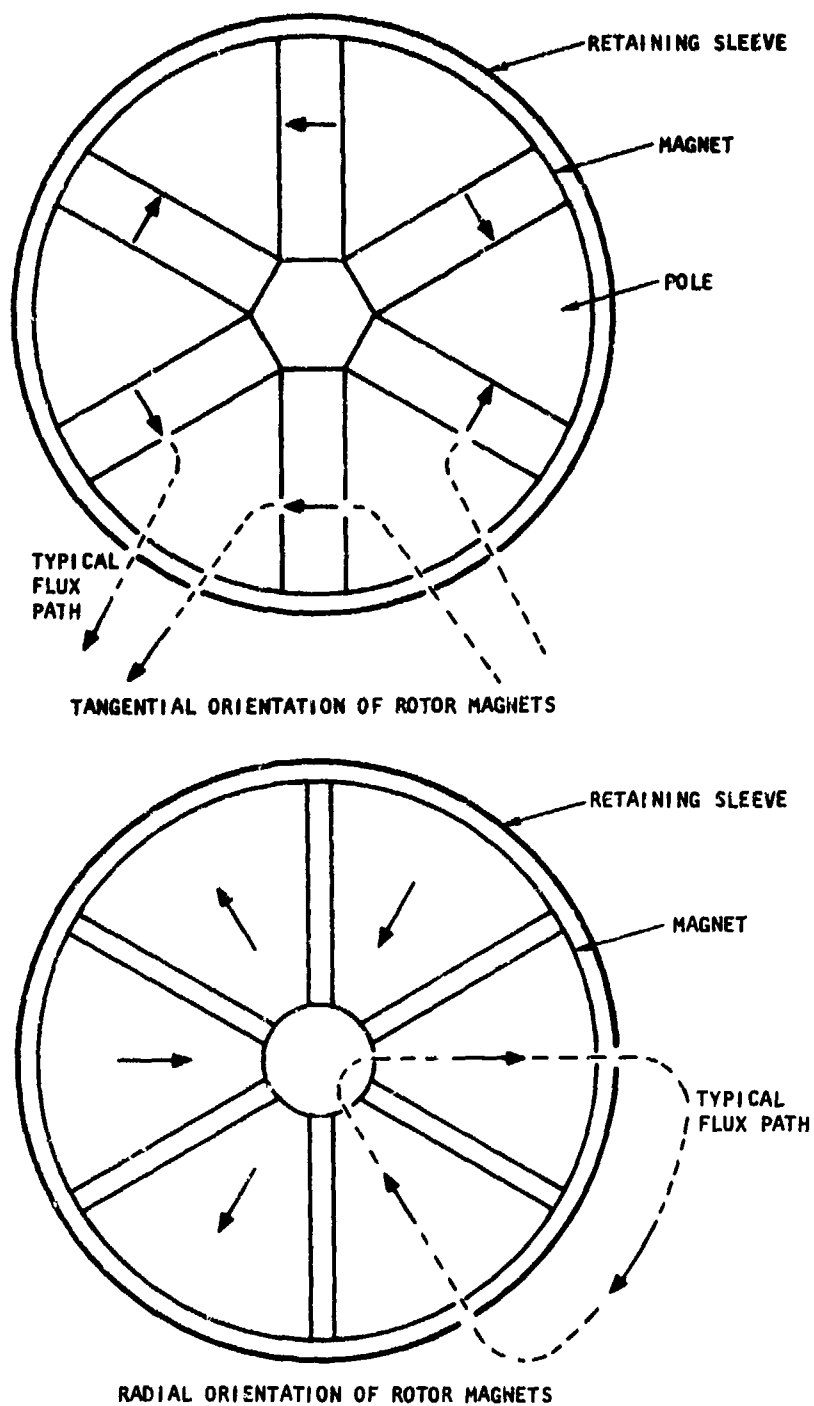
PART NO		REVISED		AMERICAN MANUFACTURING COMPANY OF CALIFORNIA A DIVISION OF THE FINEST CORPORATION TORRANCE, CALIFORNIA	
515018-1-1 PART NO.		515018-1 ASSEMBLY NO.		MOTOR OUTLINE, DIRECT CURRENT, BRUSHLESS	
515018-1-1 PART NO.		515018-1 ASSEMBLY NO.		D 70210 515018	
515018-1-1 PART NO.		515018-1 ASSEMBLY NO.		SCALE 1/1	
515018-1-1 PART NO.		515018-1 ASSEMBLY NO.		SHEET 1 OF 1	

2





ITEM NO	DESCRIPTION	MATERIAL
1	SHAFT	STEEL 1018
2	ROD	STEEL 1018
3	WASHER	STEEL 1018
4	WASHER	STEEL 1018
5	WASHER	STEEL 1018
6	WASHER	STEEL 1018
7	WASHER	STEEL 1018
8	WASHER	STEEL 1018
9	WASHER	STEEL 1018
10	WASHER	STEEL 1018
11	WASHER	STEEL 1018
12	WASHER	STEEL 1018
13	WASHER	STEEL 1018
14	WASHER	STEEL 1018
15	WASHER	STEEL 1018
16	WASHER	STEEL 1018
17	WASHER	STEEL 1018
18	WASHER	STEEL 1018
19	WASHER	STEEL 1018
20	WASHER	STEEL 1018
21	WASHER	STEEL 1018
22	WASHER	STEEL 1018
23	WASHER	STEEL 1018
24	WASHER	STEEL 1018
25	WASHER	STEEL 1018
26	WASHER	STEEL 1018
27	WASHER	STEEL 1018
28	WASHER	STEEL 1018
29	WASHER	STEEL 1018
30	WASHER	STEEL 1018
31	WASHER	STEEL 1018
32	WASHER	STEEL 1018
33	WASHER	STEEL 1018
34	WASHER	STEEL 1018
35	WASHER	STEEL 1018
36	WASHER	STEEL 1018
37	WASHER	STEEL 1018
38	WASHER	STEEL 1018
39	WASHER	STEEL 1018
40	WASHER	STEEL 1018
41	WASHER	STEEL 1018
42	WASHER	STEEL 1018
43	WASHER	STEEL 1018
44	WASHER	STEEL 1018
45	WASHER	STEEL 1018
46	WASHER	STEEL 1018
47	WASHER	STEEL 1018
48	WASHER	STEEL 1018
49	WASHER	STEEL 1018
50	WASHER	STEEL 1018
51	WASHER	STEEL 1018
52	WASHER	STEEL 1018
53	WASHER	STEEL 1018
54	WASHER	STEEL 1018
55	WASHER	STEEL 1018
56	WASHER	STEEL 1018
57	WASHER	STEEL 1018
58	WASHER	STEEL 1018
59	WASHER	STEEL 1018
60	WASHER	STEEL 1018
61	WASHER	STEEL 1018
62	WASHER	STEEL 1018
63	WASHER	STEEL 1018
64	WASHER	STEEL 1018
65	WASHER	STEEL 1018
66	WASHER	STEEL 1018
67	WASHER	STEEL 1018
68	WASHER	STEEL 1018
69	WASHER	STEEL 1018
70	WASHER	STEEL 1018
71	WASHER	STEEL 1018
72	WASHER	STEEL 1018
73	WASHER	STEEL 1018
74	WASHER	STEEL 1018
75	WASHER	STEEL 1018
76	WASHER	STEEL 1018
77	WASHER	STEEL 1018
78	WASHER	STEEL 1018
79	WASHER	STEEL 1018
80	WASHER	STEEL 1018
81	WASHER	STEEL 1018
82	WASHER	STEEL 1018
83	WASHER	STEEL 1018
84	WASHER	STEEL 1018
85	WASHER	STEEL 1018
86	WASHER	STEEL 1018
87	WASHER	STEEL 1018
88	WASHER	STEEL 1018
89	WASHER	STEEL 1018
90	WASHER	STEEL 1018
91	WASHER	STEEL 1018
92	WASHER	STEEL 1018
93	WASHER	STEEL 1018
94	WASHER	STEEL 1018
95	WASHER	STEEL 1018
96	WASHER	STEEL 1018
97	WASHER	STEEL 1018
98	WASHER	STEEL 1018
99	WASHER	STEEL 1018
100	WASHER	STEEL 1018



8-20402

Figure 13. Techniques of Permanent Magnet Rotor Construction

3.2.1.2.1.2 Stator

The stator windings are designed with a large copper cross-section to provide low electrical losses (I^2R), high current, and high torque capabilities. Improved thermal control of the motor is a result of winding locations in the stator. Heating that occurs in the windings can be more easily transferred to the finned motor housing.

The stator is wound using 6 turns per coil of 4 strands of No. 24 wire arranged in a 3-phase "Y" configuration. The winding and stator characteristics are presented in para. 3.2.1.2.2.

3.2.1.2.1.3 Rotor Position Sensor

The motor assembly includes a rotor shaft position sensor. Commutation (putting current in the proper direction through the stator windings) is accomplished by using variable reluctance pickups. Six "C" core sensors are aligned on opposite sides of a windowed shutter 60 deg apart. The shutter is connected directly to the rotating shaft of the motor, with the angular position of the slots established relative to the rotor poles. An oscillator drives the primary side of the coils. As the shutter rotates, the voltage induced on the opposite coil varies according to the presence or absence of the shutter material in the sensor gap. This rotor position logic is input to the controller switching network. The sensor schematic is shown in Figure 14.

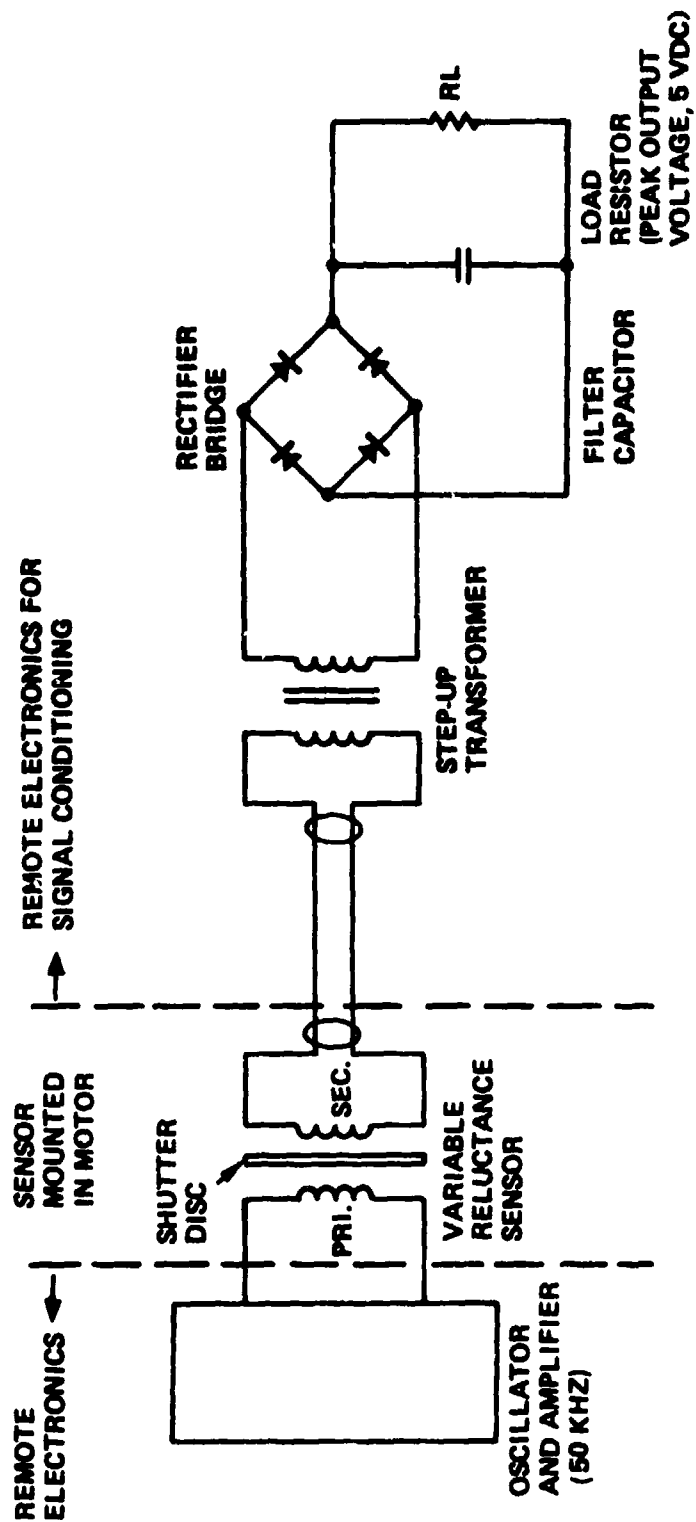
3.2.1.2.1.4 Parking Brake

A parking brake is included as a part of the motor. Its only design purpose within the present configuration is to lock a failed drive channel. Without this lock, the operating motor could back-drive the failed motor through the high-efficiency differential gearing.

The parking brake is a two-surface disc brake actuated by an electromagnetic coil. When the brake coil is not excited, the 50-lb brake spring clamps the brake disc between the two nonrotating brake surfaces. When the brake coil is energized, the brake armature pulls in against the spring, thus leaving a clearance air gap for the brake disc. The rotor assembly then is free to rotate. The brake coil requires approximately 1000 amp-turns to pull in. The excitation current this represents results in coil losses. This results in heating on a continuous excitation basis. Therefore, after pull-in, the coil current should be modulated by the controller to approximately 25 percent of its pull-in value, the holding ampere turns required being significantly lower than the pull-in value because there is no gap in the brake magnetic circuit after pull-in.

3.2.1.2.2 Steady-State Motor Performance

The predicted torque speed curve for the motor operating at 265 vdc is shown in Figure 15. The motor has a peak power output corresponding to a maximum speed and current limit of hp (approximately 6 kw). Table 5 shows the motor characteristics.



S-98079-B

Figure 14. Variable Reluctance Rotor Position Sensor

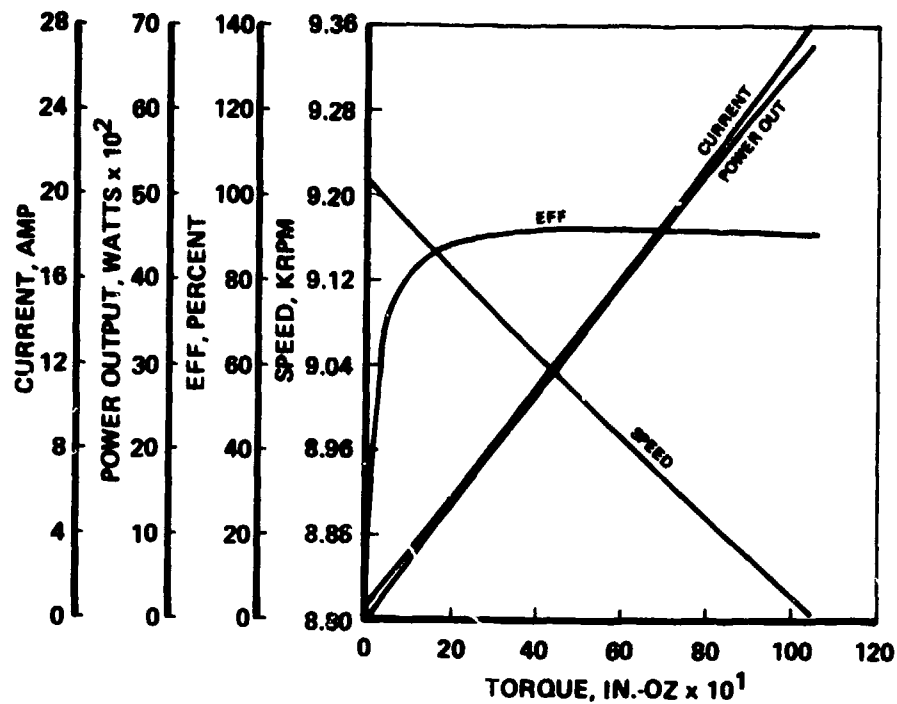


Figure 15. Motor Torque/Speed Curve

TABLE 5

MOTOR CHARACTERISTICS

Rated voltage	265 vdc
No-load speed	9200 rpm
Torque per amp	35 ozf-in./amp
Stator resistance (68°F)	0.74 ohm (line to line)
Rotor inertia	9.95×10^{-4} lbf-in.-sec ²
Time constants	0.002 sec, electrical 0.015 sec, mechanical
Back EMF	28.7 v/100 rpm
Brake voltage	270 vdc
Brake torque	75 lbf-in. (minimum)
Weight	9.65 lb

3.2.1.3 Fabrication

The motor was fabricated using a magnet material rated at 18×10^6 G-Oe. Currently, magnet material rated at 23×10^6 G-Oe is commercially available, and 30×10^6 G-Oe may be available in the foreseeable future. Using the new materials would result in performance improvements. The motor assembly is shown in Drawing No. 515018. The motor performed according to design, as shown by test results included in Section 6.

As the units were fabricated, two areas were identified that required minor rework. First, the stator slot width was too small to allow easy winding of the stator. The stamped stator laminations also were found to be rough, with the potential for damage to the wire insulation. Rework consisted of machining the slot openings to provide additional space for inserting the windings and to smooth the surface prior to winding.

Secondly, the installation of the rotor position sensors was found to be critical. The following three areas were of principal concern:

- (a) The "C" cores must be oriented so that the gap length of both the primary and secondary are arranged parallel with the rotor axis.
- (b) The gap distance between the primary and secondary must be uniform for each sensor pair, and as small as is practical.
- (c) The physical length of the "C" cores must be considered when determining the shutter slot length so that output signals truly represent rotor pole position.

The solutions to these development concerns are given in Figure 16 and para. 3.3.1.3.2.2. Because only two motors were fabricated for this demonstration program, no manufacturing tooling was available. Tooling would be necessary in the assembly of these sensors for a production program.

3.2.2 Gearing

The actuator gearbox design was based upon program ground rules representative of future aircraft actuation system requirements. The following list of parameters form the basis of the gearbox design:

- Rotary hingeline design
- 4 in. depth
- 37,575 in.-lb maximum hinge moment torque
- 80 deg/sec no-load rate

Figure 17 illustrates the conceptual design and shows potential structural advantages of the electromechanical hingeline design over conventional hydraulic subsystems. From this basis, actuator concepts were evaluated in terms of weight, volume, stiffness, and life. Appendix A, electromechanical actuation development design data package, presents drawings, sketches, trade studies, and analyses of the actuator gearbox design concepts.

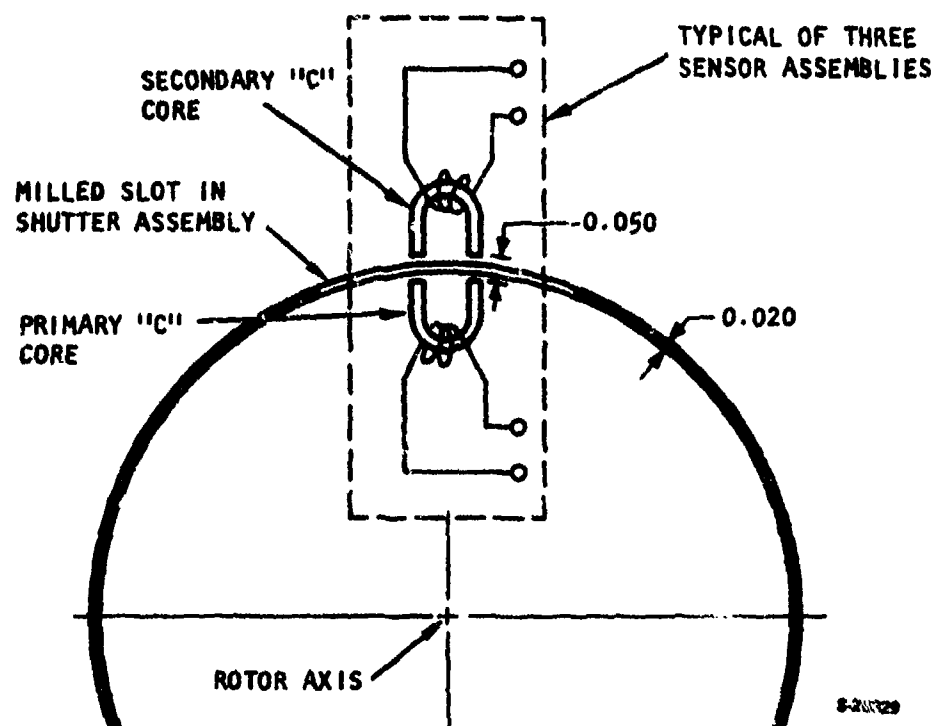


Figure 16. Rotor Position Sensor Geometry

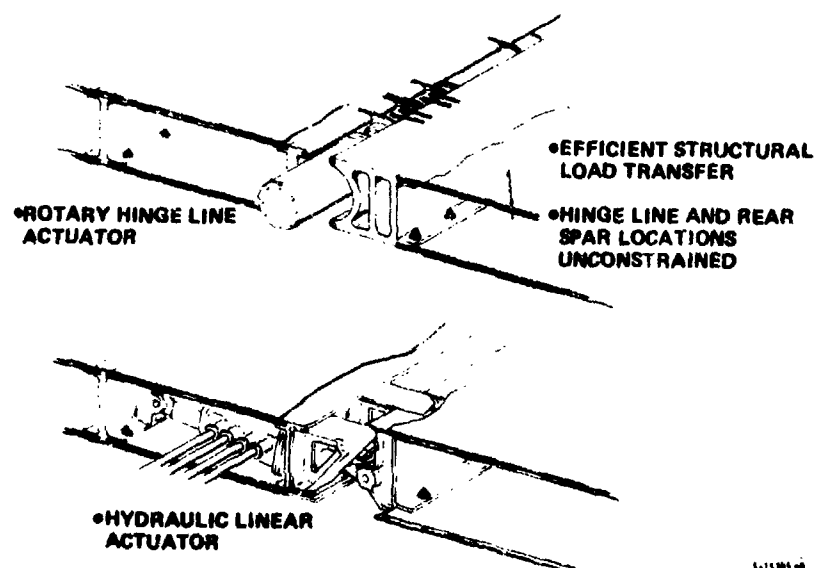


Figure 17. Rotary Hingeline Actuation Unit Conceptual Design and Potential Structural Advantages

An outline drawing of the gearbox is shown in Drawing 2022192. Dual redundant motors operate into the velocity summing differential, followed by the two stages of simple planetary reduction. The output of the second stage operates into the compound planetary gearset, which consists of two identical load sharing slices. The gear ratios for each stage are listed in Table 6.

Considering cost, manufacturing, and simplicity, the planet gears in the differential and the two planetary stages are identical. The associated sun gears also are identical, as are the ring gears for these assemblies. The differential uses three planet gears in each half, and the first stage planetary gear set uses three planets. Because of the higher loads reflected to the second-stage planet gearset, four planet gears are used. The compound planet output stages use six planet gears in each slice to achieve life and torque capability.

The gearbox portion of the actuator, attached to the test stand interfacing structure, is emphasized in Figure 18. Figure 19 shows an exploded view of the manufactured parts comprising the reduction gearing of the hingeline actuator assembly.

3.2.2.1 Stress Considerations

The stress analyses for the output ring gear back iron, mounting lugs, and the input shaft torsional shear stresses were based on the following conditions:

Life-- 10^5 cycles

Load--Linearly increasing with position from null

Travel-- ± 30 deg

Fatigue Life--Load equivalent = $6 \sqrt{\frac{1}{N_1}} N (\text{LOAD})^6$

The conservative calculation of ring gear back iron stress (46,782 psi) could be increased easily to approximately 65,000 psi and not affect the actuator fatigue life. The mounting lug web thickness is 0.16 in. to maintain a positive margin of safety at ultimate load. The input shaft shear stress level is quite adequate, with a 0.060-in. wall thickness.

3.2.2.2 Inertia

Acceleration of the system for a given motor torque is a function of the load torque, and the inertias of the control surface, gearing, and the motor rotor. The effective load inertia, J_L , reflected to the motor is $J_L + (GR)^2$, where GR is the overall gear ratio. The inertia of the actuator gearing is found to have a minor impact upon effective motor inertia. The effect of the distributed inertia was evaluated for three cases: (1) both motors operating, (2) the right-hand motor operating with the left-hand motor fixed, and (3) the left-hand motor operating with the right-hand motor fixed. Detailed calculations of these three cases are presented in Appendix A. The analysis shows the gearing and load inertias result in approximately 16 to 34 percent increase in the effective motor rotor inertia, depending on the drive train or combination of drive trains operating.

TABLE 6
ACTUATOR GEAR RATIOS

Gear Stage	Stage Gear Ratio	
	Two Motors Operating	Either Motor Operating
Differential	2.187:1	4.375:1
Final stage	4.375:1	4.375:1
Second stage	4.375:1	4.375:1
Compound output	14.47:1	14.47:1
Total (all stages)	605.72:1	1211.44:1

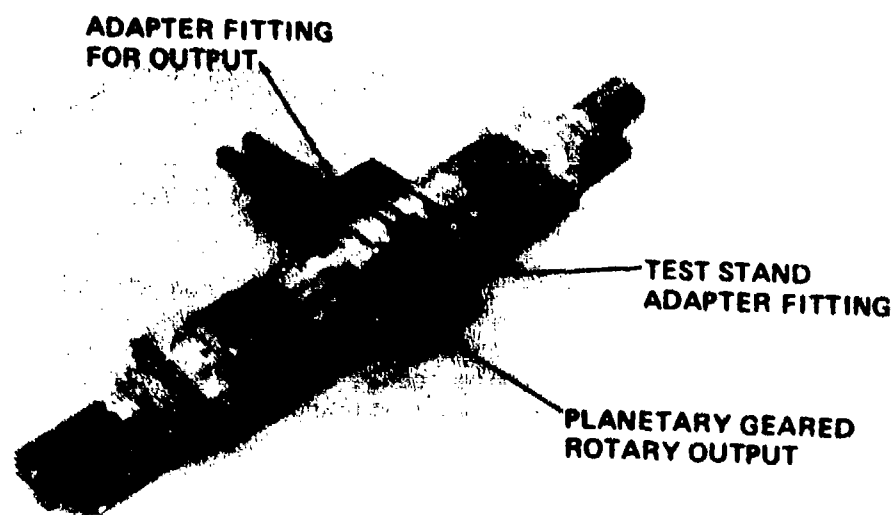
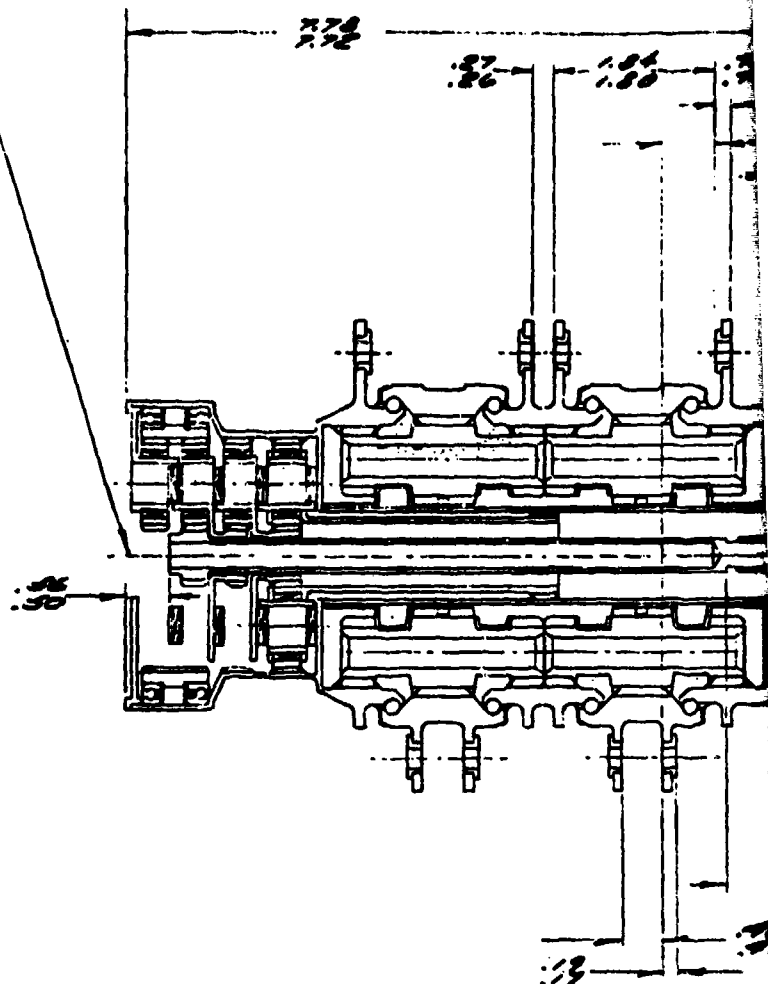
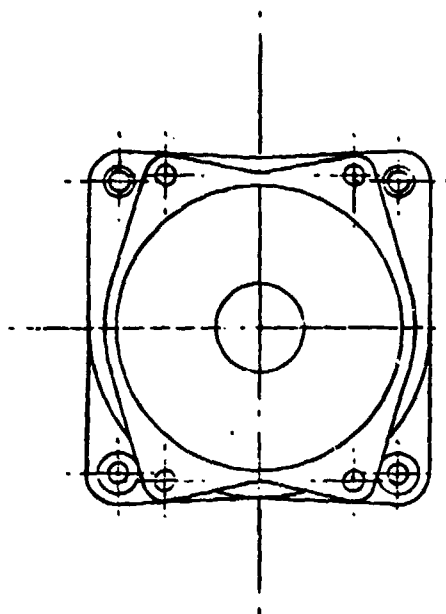
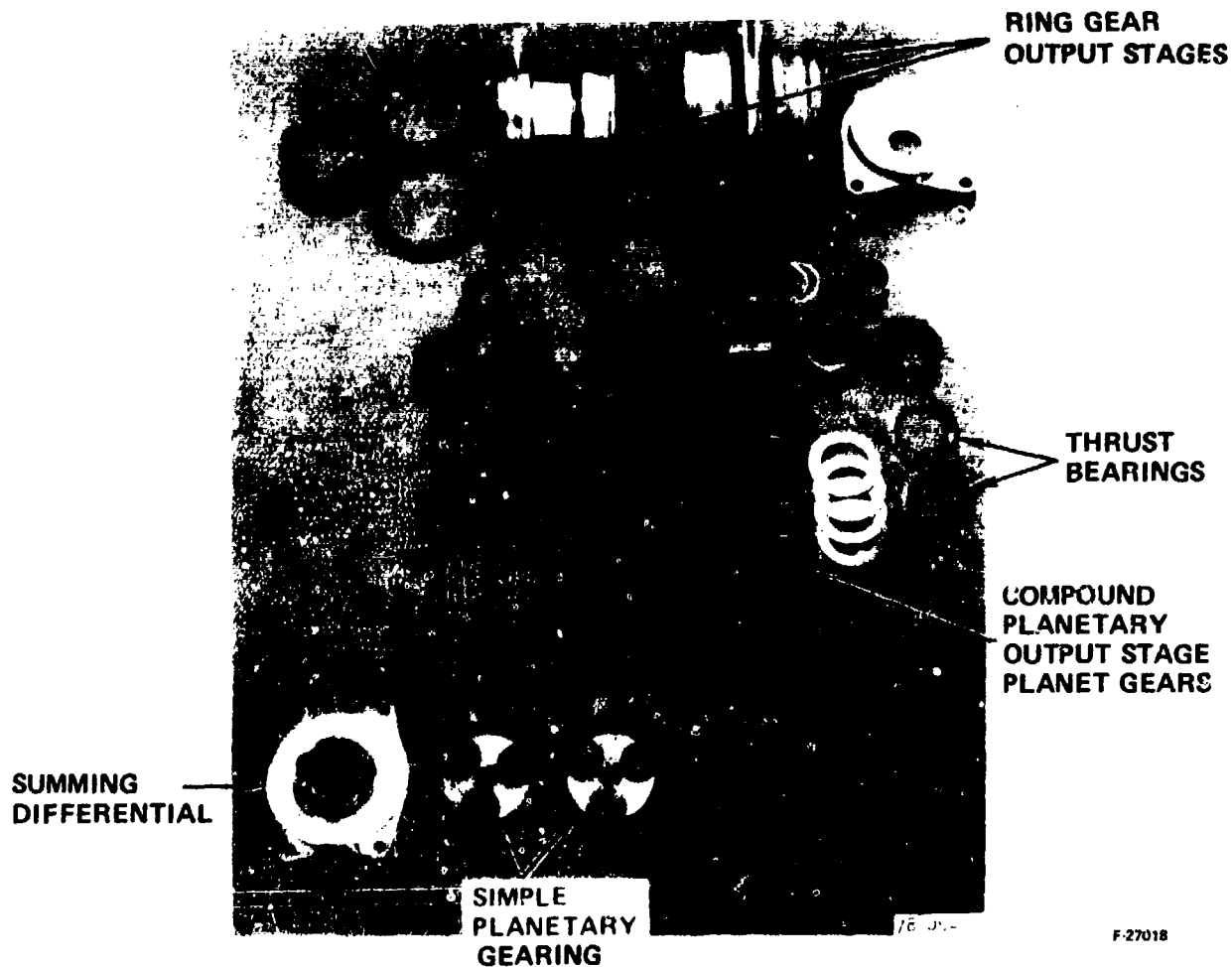


Figure 18. Hingeline Actuator Gearing

GEARING PART DRIVE
25 T 32P 20°
FULL DEPTH INVOLUTE



2. GEAR RATIO: 62.42:1 EFFICIENCY: 93%
3. ULTIMATE STATIC LOAD 75000 IN.-LB
4. LIMIT STATIC LOAD 50,000 IN.-LB
5. MAX OPERATING LOAD 37,500 IN.-LB
NOTES: UNLESS OTHERWISE SPECIFIED



F-27018

Figure 19. Hingeline Actuator Gearing Details

3.2.2.3 Gear Ratio Selection

The actuator gear ratio selection involved several gear train analyses to achieve optimum efficiency and weight. An analysis of the system from a performance standpoint indicates that the desired total gear ratio with two motors operating is 637:1 (see Appendix A). The gear ratio recommended in Appendix A, however, was 627:1 based upon the availability of existing tooling. This adjustment was judged satisfactory because the difference between the 637:1 and 627:1 ratios is only 1.5 percent, which is well within the design tolerance for other factors in gear ratio selection, such as efficiency, motor torque, and load torque (Reference 4). At the time of actual manufacture of the gears, the availability of tooling dictated a change in the gear ratio to 605:1. This results in an actuator no-load speed decrease of 5 percent and torque increase of 5 percent, which are well within the design allowances of the motor (see Reference 4).

3.2.2.4 Materials

The environmentally sealed gearbox is a high-efficiency design rated at 83 percent. The output gear material is the new alloy HP-9-4-30, which provides ease of fabrication, high fatigue strength, and stability after heat treatment. All other gears are conventional carburizing grade AISI 9310. The gearbox assembly is shown in Drawing No. 2022194. The assembly was fabricated according to print, without major rework. Demonstration test results presented in Section 6 show that the predicted performance correlated well with test data.

3.2.2.5 Potential for Improvement

The current gearbox was developed to prove a concept and not to produce an optimal configuration for any specific application. It is self-evident that additional development and future production configurations will provide the justification for improved performance (from 83 percent to approximately 85 percent efficiency) and weight reduction (approximately 10 percent) while simultaneously reducing costs.

3.2.2.5.1 Fabrication

The current design contains three internal gears produced by the shaping process. A configuration change to permit broaching is indicated, provided lead time/schedule conflicts are not present. The output planet configuration contains 12 output planets. These are conventionally constructed by the hobbing process, which requires clearance between gears for hob runout. Three setups are required. Gear-to-gear indexing is required for assembly and extreme indexing accuracy is required to secure load sharing. However, manufacturing limitations with the method employed restrict the tooth-to-tooth positioning accuracy to ± 2.5 minutes of arc. When the tolerances are adverse, it is not uncommon to induce loads during assembly which approach in magnitude the externally applied operational loads. This disadvantage may be overcome by a multi-piece planet construction subsequently joined by such means as brazing, welding, hot isostatic process, etc. Indexing accuracy would be accomplished by suitable jigs or fixtures repeatably capable of holding accuracies in the vicinity of ± 5 seconds of arc.

Future designs suitable for quantity production will consider the use of such processes as powder metallurgy, investment casting, and forgings. Implementation of these techniques may offer substantial cost and weight savings.

3.2.2.5.2 Weight

Pending a formal analysis of processes and materials, implementation of quantity production techniques could potentially reduce the weight of the gearbox by 7 percent. It is further anticipated that the use of nonintegral diametral pitch tooling (the readily available 20 pitch is employed in the test specimen) plus performance of an in-depth finite element analysis should produce at least an additional 5 percent reduction in weight.

3.2.2.5.3 Efficiency

An efficiency gain of 1.8 percent may result from the use of nonintegral diametral pitch tooling. Other gains could occur from ball-bearing utilization throughout; however, the return would be insignificant compared to the adverse impact upon cost, size, and weight.

3.2.2.5.4 Other Hingeline Applications

Rudder and other hingeline applications that require the hingeline axis to be substantially vertical rather than horizontal will require means to ensure lubrication of dynamic components. An unsophisticated gear pump, pilot pump, or even screw pump should be quite adequate. It may also be necessary to provide an end face (carbon) seal to retain lubricant in the lower-most end of the actuator.

3.3 CONTROLLER

The controller for the electromechanical actuation unit consists of the servo and power switch assemblies, which are the two major functional elements (as shown in Figure 5). The design of the controller and motor in the actuator are highly interdependent, as highlighted in Appendix C, which compares various electromechanical drive approaches.

For the reasons presented in Appendix C, the selected motor-controller configuration is a pulse-width-modulated, transistorized power bridge controlled by a microprocessor servo circuit and a brushless dc, permanent-magnet motor.

In Section 1 and para. 3.1, the development of the baseline servo circuits using a microprocessor is described. In Appendix E, the design approach, circuit details, and development history of this approach are presented. Analog servo circuits also were developed for the controller. The analog servo design offered greater developmental flexibility (compared to the microprocessor) for this engineering development since modifications in the servo characteristics could be made by single component substitutions, rather than reprogramming, and software changes.

Therefore, the controller discussion presented in this section includes the development of the two separate analog servo controller approaches. Because of the motor/controller interface, specific discussions of the dc brushless motor are also included, where required.

3.3.1 Discussion of Approaches

The selected design approach for control of the brushless dc motor is presented below.

3.3.1.1 Motor Rotor Rotation

The brushless dc permanent magnet machine consists of a rotating magnet assembly and a wound stator. In order to rotate the rotor, a rotating magnetic field in the stator must be produced that is synchronous with the rotor. This

rotating magnetic field is produced by switching currents in the stator winding in sequence to produce the necessary magnetic flux changes in the stator (see para. 3.2.1 and Figure 8). The production of a stator electromagnetic field is discussed below.

The simple two-pole configuration in Figure 20 shows that when switches A and B are closed, current flows left to right. When C and D are closed, current flows from right to left. If the switch pair closures are now synchronized to rotor position (Figure 21), it is possible to make the stator flux follow that of the rotor to produce motion and torque.

By this example, two important requirements of the control electronics are established: (1) the requirement to switch current into the stator windings at the rotor frequency, and (2) the requirement to control the power switch firing as a function of instantaneous rotor position.

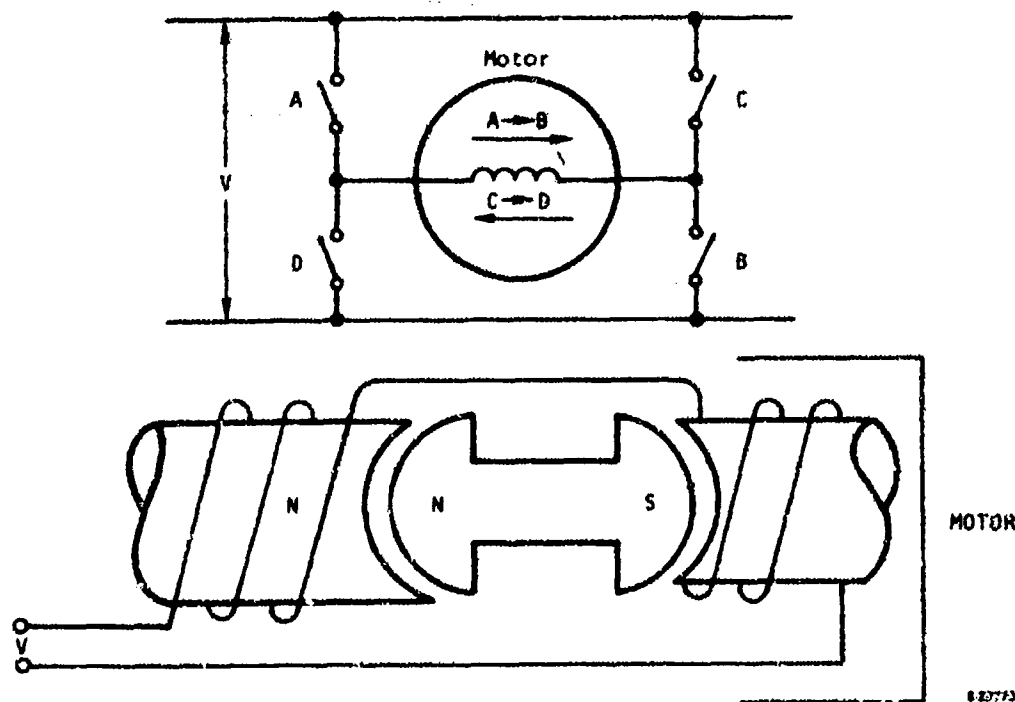


Figure 20. Example of Motor Control

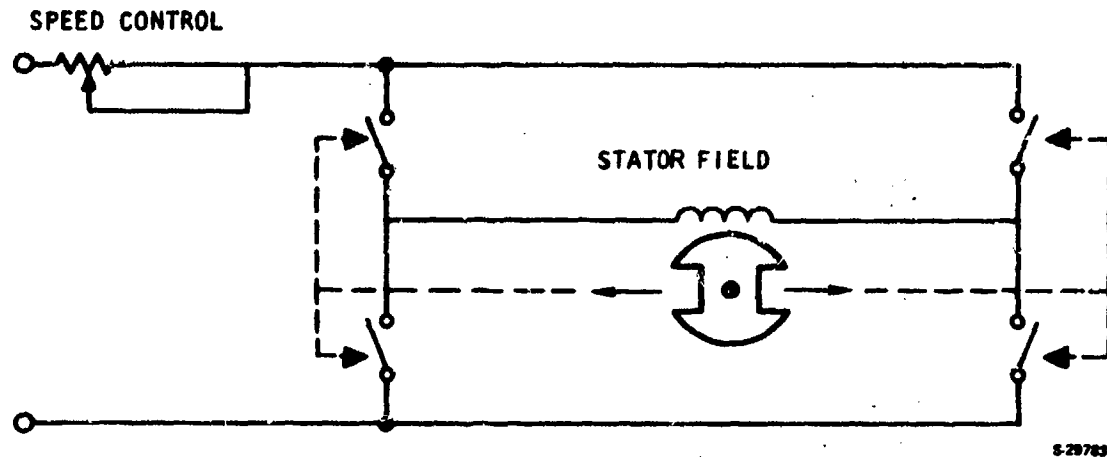


Figure 21. Synchronized Commutation Control

3.3.1.2 Speed Control

To control motor speed, it is necessary to control the voltage and current transferred into the motor windings. For instance, a simple method of control could be a rheostat in the main power line to adjust the motor current (see Figure 21). In order to control current in the most efficient manner, a pulse width modulation (PWM) scheme is utilized. Figure 22 illustrates this concept.

It can be seen that as the pulse width (voltage) is increased, the average value of current is also increased for the same motor speed.

The motor increases speed by increasing the applied voltage to the stator windings. Increased winding voltage results in increased current, which in turn results in increased torque, which accelerates the rotor to a new speed. Since the rotor position sensor is also synchronized with the rotor, the excitation of the stator is always synchronized and the machine runs in a similar manner to a motor with a mechanical commutator (References 17 18).

The typical permanent-magnet motor speed torque relationship is shown in Figure 23.

Figure 23 shows that speed and current are typically and approximately linear with torque. The torque speed relationship also is defined for one specific voltage applied to the motor. Therefore, a variety of operating conditions is available for operation of the servo actuator using PWM control. Figure 24 shows the possible operation of the motor in a typical duty cycle.

First, for example, the motor may be required to hold against a nonmoving load corresponding to T_1 (or point A). The current I_1 to produce the torque T_1 to balance the load is a direct function of the applied voltage V_1 , i.e., there is no back emf. Assuming that the holding torque increases to T_2 , the motor current must also increase. This is accomplished by increasing the average applied PWM voltage to V_2 thus increasing the current to I_2 . At this point, the motor is still stationary and there is no back emf to be considered.

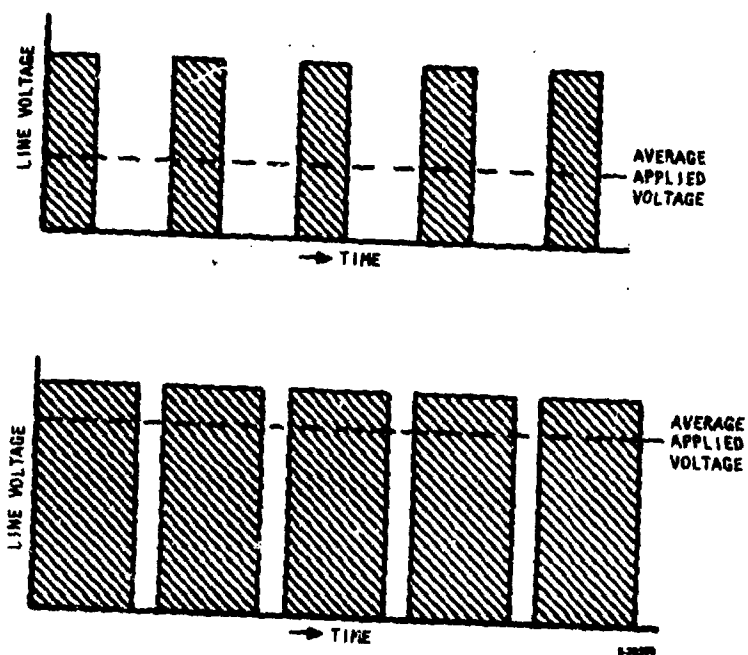


Figure 22. Voltage Control Using Fixed Frequency Pulse Width Modulation

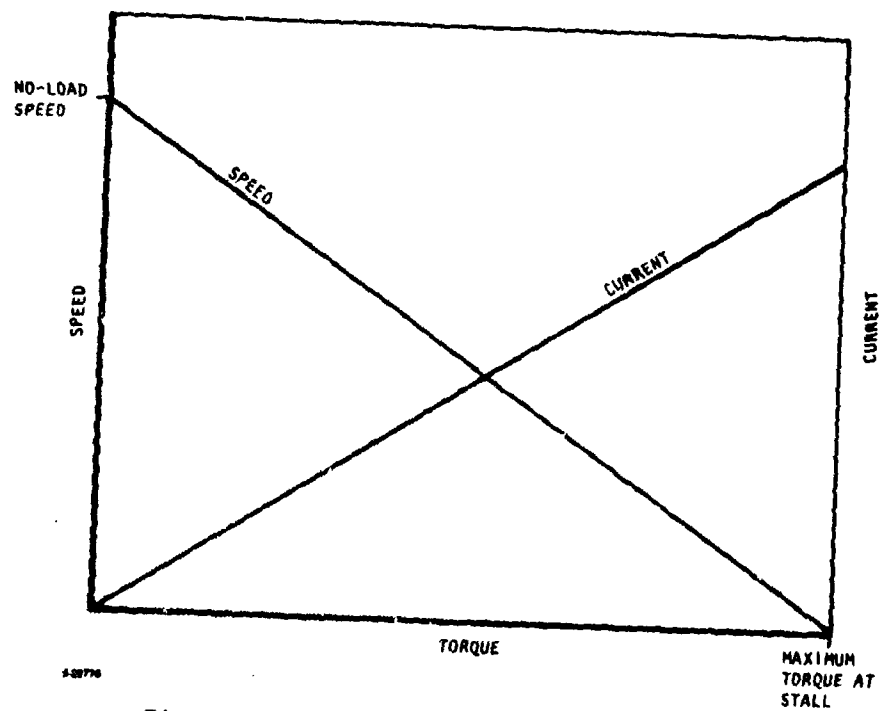


Figure 23. Generalized Torque Speed Curve

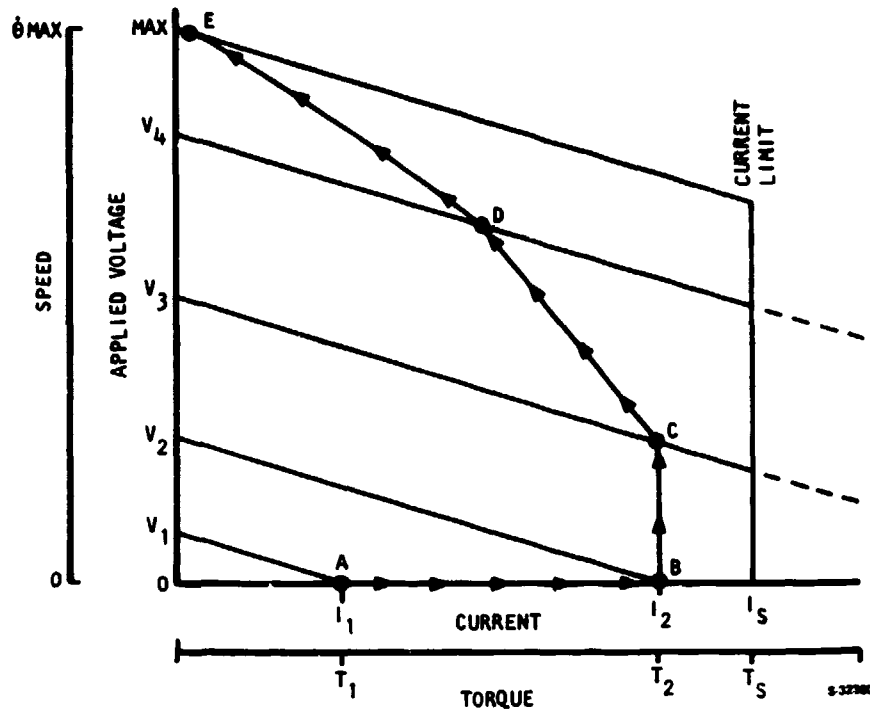


Figure 24. Possible Operation of the Motor in a Typical Duty Cycle

If the control surface must move with a velocity corresponding to point C, and torque equal to T_2 , the applied voltage must be increased from V_2 to V_3 to compensate for the back emf of the motor as its speed increases. The current flow through the motor for both points B and C are the same, corresponding to the same output torque, (neglecting the acceleration torque requirements of the rotor).

If the speed of the control surface must increase and the torque reduces to correspond to point D, the applied voltage to the motor must be increased to voltage level V_4 .

The back emf is increased and the current flow is reduced, corresponding to the reduced torque output.

Finally, at point E the motor is operating at no-load and maximum speed, as defined by the maximum available voltage. The current is nearly zero because no useful torque is being produced by the motor--only torque to overcome losses (Reference 19).

3.3.1.3 Control Scheme

The functions of the control scheme include (1) current switching, (2) rotor position sensing, and (3) modulation technique. These are discussed below.

3.3.1.3.1 Current Switching

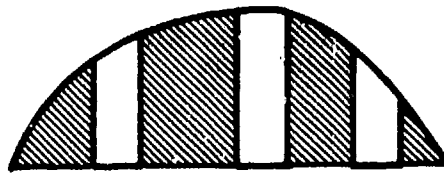
Current switching can be achieved by solid-state devices. The choices in high-power devices are limited to transistors or silicon controlled rectifiers (SCR's). The tradeoffs involved in the selection of these devices are listed in Table 7.

TABLE 7
POWER SWITCH TRADEOFFS

Silicon Controlled Rectifier
Requires commutation to turn off
High forward conduction loss
Junction temperature derates to 125°C
Slow switching speeds
Can work at high voltage and currents
Cheaper than transistors
Transistors
Limited in voltage (approximately 500 v)
Second breakdown characteristic requires careful consideration
Suitable for switching up to 100 amp (single devices)
More expensive than SCR's
Simple switch control circuit
Fast switching speed

3.3.1.3.1.1 Silicon Controlled Rectifier (SCR)

The SCR has been the traditional choice for power inverters, but has some inherent characteristics which result in added complexity to the circuitry. The main problem involves turning off the device. The anode-to-cathode voltage must be reversed. If it is necessary to modulate a waveform at periods other than the zero crossing (Figure 25), some additional circuitry is required to reverse-bias the SCR. The additional circuitry is called the commutation circuit.



8-29780

Figure 25. Switching Waveform

It is possible to self-commutate the SCR's when driving a permanent magnet machine by utilizing the back emf waveform to commutate the power switches. However, when the machine is at standstill and no back emf is available, forced commutation of the SCR's is required.

High frequency operation of SCR's is limited by their turnoff times. A good quality 100 amp Inverter SCR would have a turnoff time ranging from 15 to 30 μ sec. This compares with 1 to 5 μ sec for transistors of similar current ratings.

Other areas in which the SCR is limited are the junction temperatures, which are normally derated to 125°C, and higher forward conduction loss.

Advantages of the SCR's include the ability to work at high operating voltages (1200 to 1500 v) and their inexpensive cost.

3.3.1.3.1.2 Transistors

Transistors overcome one of the SCR disadvantages in that they do not require special commutation circuitry to turn them off when conducting current. They also have a considerably faster turnoff time (1 to 5 μ sec), which enables them to be utilized in higher frequency switching applications.

Since the power transistors are used in a switched mode, the power losses are divided into two categories: (1) forward conduction losses and (2) switching losses. The forward conduction losses are losses associated with the transistor when it is turned on and saturated ($V_{CE SAT}$). The switching losses are those losses associated with the transistor when it is changing state from off to on. During the period when current is rising and voltage is falling, the instantaneous product of voltage and current is the transient power that must be dissipated by the device, as shown in Figure 26.

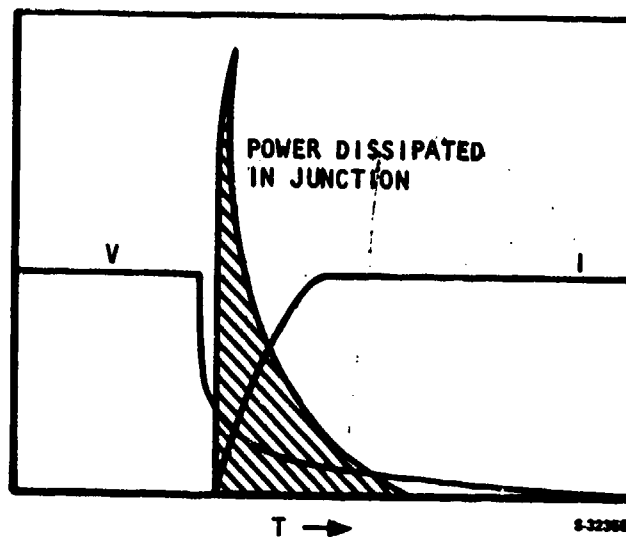


Figure 26. Transistor Operating During Switching

Since this high transient power pulse occurs in approximately 5 μ sec, the inherent design of the silicon wafer must be such that it absorbs this power transient.

This transient behavior is an inherent weakness in available transistors. A great deal of testing and analysis of vendor parts is required before reliable high power switching is achieved.

There are circuit techniques to change the phase relationship between the transient voltages and currents to control or eliminate the transient power pulses. These techniques require the use of inductors and capacitors to form turnon and turnoff snubber networks.

3.3.1.3.2 Rotor Position Sensing

The alternate schemes for rotor position sensing that were evaluated include (1) hall effect probes, (2) photo transistors, and (3) electromagnetic.

3.3.1.3.2.1 Hall Effect Probes

The hall effect probe involves a hall crystal being placed in a magnetic field, excited with a dc potential in one plane. This dc potential is proportional to the magnetic field, and is produced in the plane at 90 deg to the excited plane. Typical output characteristics are ± 50 mv superimposed on a dc level of 5 v (Figure 27).

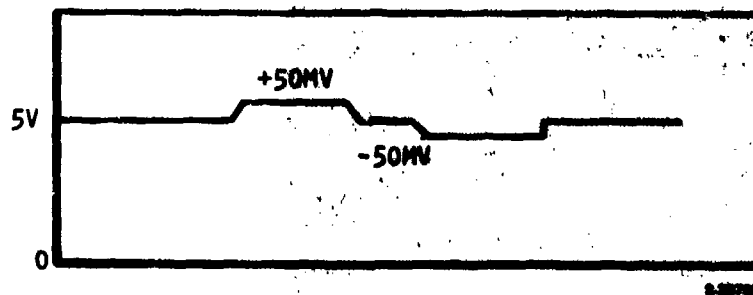


Figure 27. Typical Output Characteristics

The problems with the application of these devices is reliable operation at high temperature. The very low output signal and fringing effects produce a ramping edge to the waveforms.

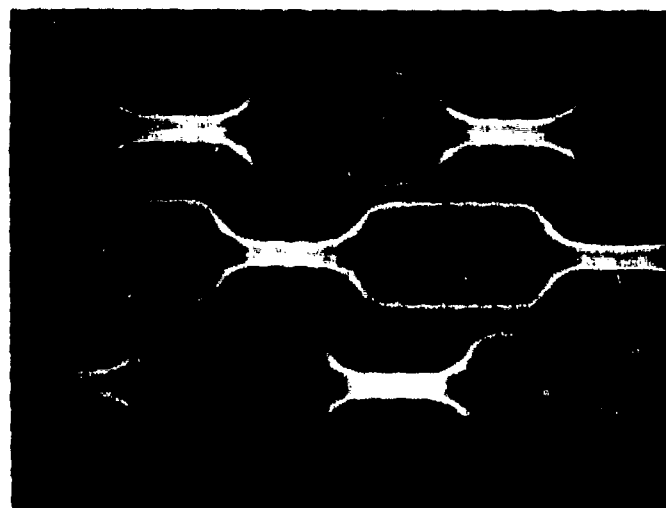
3.3.1.3.2.2 Photo Transistors

Photo transistors are used with a light source and shutter mechanism. When the shutter is open, light impinges on a photo diode, which in turn conducts and switches a transistor. These devices have low gain and will not operate in the high ambient temperatures that could be generated within the motor frame.

3.3.1.3.2.3 Electromagnetic Sensor

The electromagnetic sensor consists of a magnetic circuit that can be interrupted by a shutter manufactured with a ferromagnetic material. The magnet is excited with a high-frequency magnetizing current. Through transformer action, an output alternating voltage is obtained. As the shutter rotates, the reluctance of the magnetic circuit is changed, and hence the output transformed voltage is modulated. This modulated voltage envelope is demodulated and dc pulses formed that are representative of rotor position.

This type of sensor is most suited to the application because it can reliably operate in the motor temperature environment. However, there are some problems with this type of sensor. The main problem involves fringing effects on the shutter, which causes ramping of the modulated envelope. (See para. 3.2.1.3). Figure 28 shows the typical outputs from the sensor windings for three-phase operation. Since the modulated envelope takes approximately 0.5 msec to rise to its full value, any logic circuitry that senses level changes may switch at random points on the leading and trailing edges of the waveform. This fact results in mismatch of the drive pulses so that each pulse is not exactly 120 deg in duration. The effect of nonsymmetrical waveforms on the machine is the introduction of harmonics, resulting in lower efficiency and greater losses.



1 V/CM
1 MSEC/CM
MOTOR #2

F-28023

Figure 28. Rotor Position Sensor Output Waveforms

3.3.1.3.3 Modulation Scheme

A variety of modulation schemes is available to control motor winding current. These schemes include (1) fixed-frequency, variable duty cycle and (2) variable-frequency, variable duty cycle.

3.3.1.3.3.1 Fixed Frequency

The fixed-frequency, variable duty cycle method controls current by controlling the pulse width as a function of current demand.

In Figure 29, speed error command is compared to a fixed-frequency triangle wave. When speed error exceeds the triangle oscillator input, the comparator switches to form the pulse train that drives the load.

This pulse train now has a duty cycle which has a linear relationship with speed error.

Load current is measured by a shunt and compared to a predetermined current limit in the current limit amplifier. When the current limit is exceeded, the PWM pulse train is interrupted to modulate the current at a lower duty cycle. This circuitry is explained in detail in para. 3.3.3.

3.3.1.3.3.2 Variable Frequency

The variable-frequency, variable duty cycle circuit utilizes a hysteresis switch to control current, as shown in Figure 30.

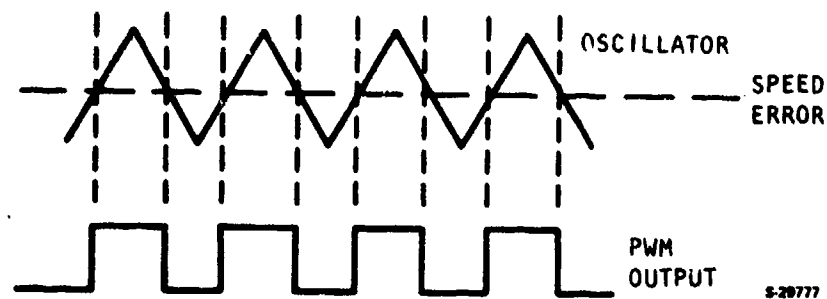
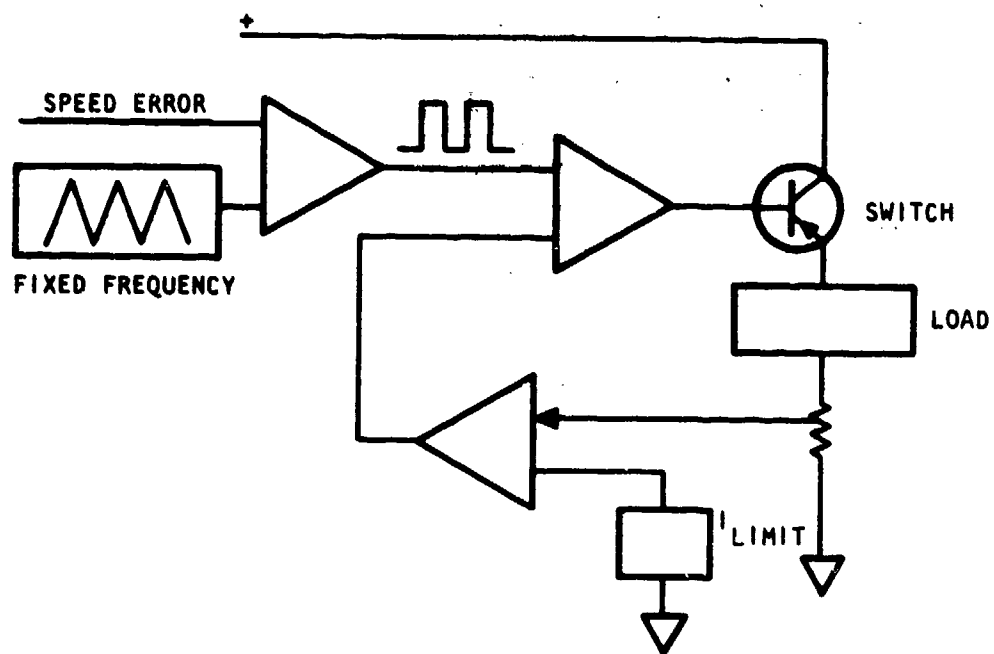


Figure 29. Modulation Approach

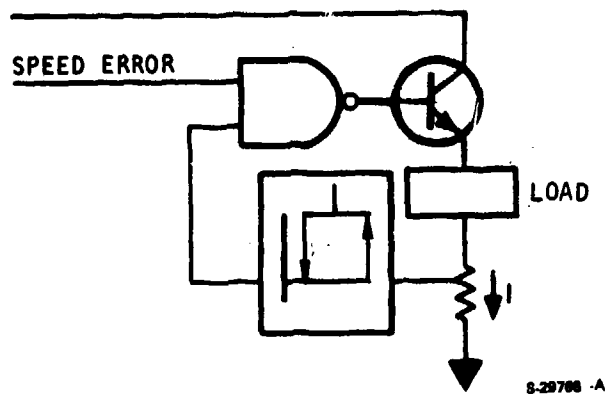


Figure 30. Hysteresis Switch Schematic

When there is a speed error present, the power switch is on and current flows in the load until the upper current limit is reached. The hysteresis switch then turns off the power switch and the current starts to decay in the load. When the current reaches the lower point on the hysteresis switch, the power switch is again turned on, as shown in Figure 31.

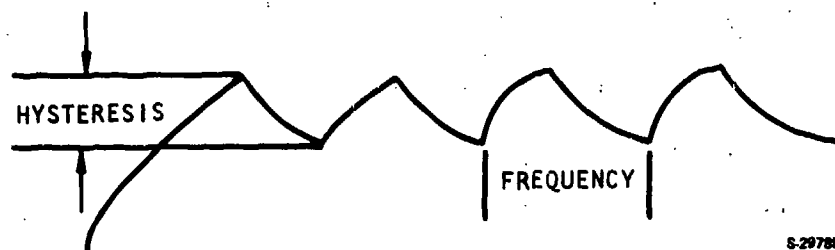


Figure 31. Current Control With Hysteresis Switch

Since at low speeds the applied voltage is high and the back emf is low, the rate of current rise is high, which produces a high-frequency modulation. At high speeds, the back emf approaches the magnitude of the applied voltage and thus the rate of rise of current is lower, resulting in a lower modulation frequency. This method of control was not selected due to the nonlinear gain characteristics.

3.3.1.4 Voltage vs Current Source Drive

The permanent magnet machine has certain characteristics that require consideration when matching the drive circuit with the machine. The most predominant characteristic is that a rotating machine produces a back emf that opposes the applied voltage to the machine terminals. Hence, the voltage available to force current through the windings is the applied voltage minus the back emf. This relationship becomes particularly important when the attempt is made to get high load torque at high speed.

The most suitable driver configuration for the application is the current sourced driver circuit shown in Figure 32.

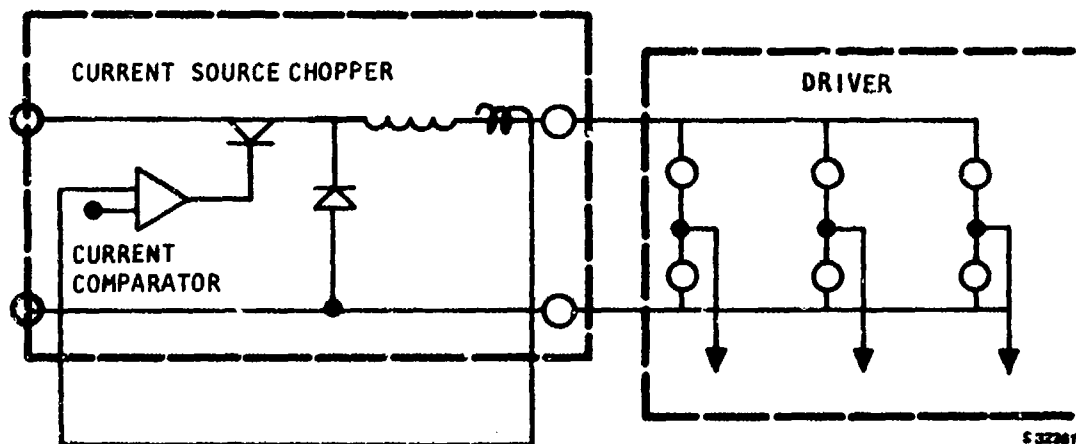


Figure 32. Typical Current Source

The current source is formed by the chopper transistor and choke (inductor). Current is fed back from the current sensor and the transistor modulated to set the current at the required value.

The relationship between the machine back emf and motor current is shown in Figure 33. The current waveform has a square wave shape, and the current wave shape is flat topped. This is a result of the current source ability to force the required current into the machine winding regardless of the back emf. This characteristic is most desirable because the average current magnitude is proportional to output torque.

The disadvantages of this particular approach are (1) it requires a choke for the current source chopper, which could result in a weight penalty (particularly in an aircraft system), and (2) power can only flow one way (i.e., from the source to the load).

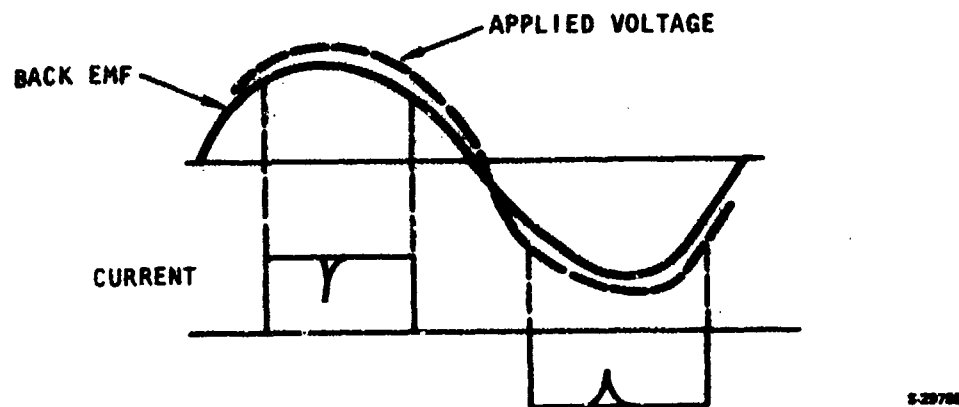


Figure 33. Back Emf and Current Relationship

The voltage sourced drive circuit, as shown in Figure 30, is not suitable for driving the low impedance machine because the stiff voltage source will cause very large currents to flow in the machine windings when the back emf is low compared to the line voltage. Therefore, a variation of the voltage sourced drive circuit that controls the winding current is utilized.

An essential variation of the voltage sourced driver, as shown in Figure 34, is a modulated driver operated from a voltage source. In this approach, when any pair of switches in the driver are energized, the positive switch is energized for the complete coil conduction period, and the negative switch is

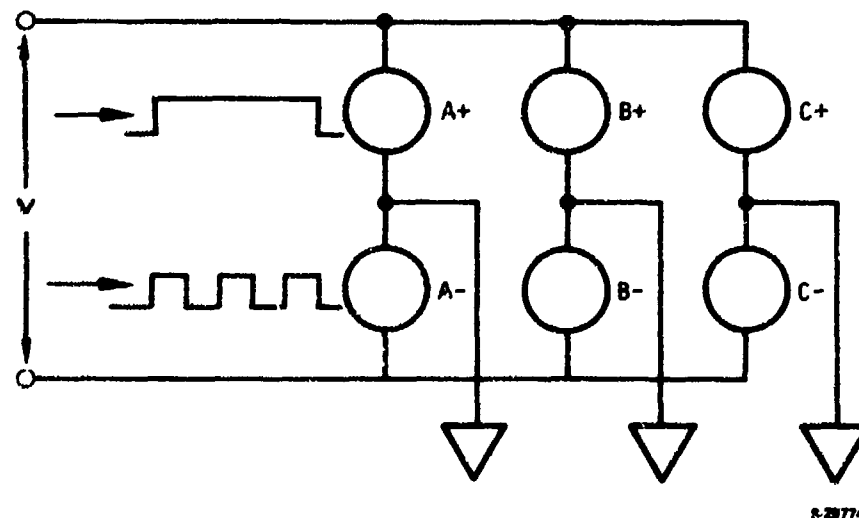


Figure 34. Voltage Sourced Drive Circuit

modulated to set an average current in the machine winding. This configuration has the advantage that it can return power to the source and also may be operated in plug and regenerate modes without any additional power devices. The chopper action of the negative switches sets the current by control of the pulse width of a PWM current regulator. A typical example of the waveforms is presented in Figure 35.

3.3.2 Controller Operational Description

The controller provides proper drive signals to the dc brushless motors for position control of the actuator output. The controller comprises the command signal conditioning, forward loop gain, feedback transducer signal conditioning, and two channels of drive electronics. During the normal mode of operation, both channels are designed to be activated and both motors are operating. If one drive channel fails, its motor will be braked, allowing servo operation on the motor to continue under reduced performance. Each drive channel receives its input from a common PWM, as shown in Figure 36. Power for the actuator is derived from a rectified 270-vdc source. Figure 37 shows the typical operation of a single-channel controller.

3.3.2.1 Forward and Feedback Loops

Each drive channel shares the same forward loop gain, dynamics, and feedback path. Controller position command signal input conditioning is provided by a differential amplifier, allowing position command signals to be sent single-ended or differentially. Forward loop gain and dynamic compensation are provided by an analog amplifier. An output clamp on the forward loop gain and compensation amplifier prevent amplifier saturation.

Control surface position feedback is provided by an optical position encoder (see para. 3.4). The output of the position encoder is in a 12-bit digital format representing 360-deg revolution of the encoder shaft. A 4.48-to-1 gear is used between the output position and the position encoder, allowing for 270-deg encoder shaft movement for a 60-deg movement of the output. This provides greater bit/degree position resolution. Output from the position encoder is in a gray code format. This gray code format must be changed to binary coded format before the coded position information can be utilized. A gray code to binary logic converter performs this function. The binary coded output from the gray-to-binary logic converter is applied to a 12-bit, digital-to-analog (D/A) converter. The D/A converter changes the digitally coded position information to an analog voltage. A low-pass filter with $\tau_{DA} = 1.5$ msec is used on the output of the D/A to smooth out the discrete level transitions as encoder position varies. The filter dynamics do not play a significant roll in the loop dynamics. The D/A filter output is then fed into an analog lead-lag feedback compensation amplifier, where $\tau_1 = 0.02$ and $\tau_2 = 0.01$. The signal from this lead-lag compensation amplifier is then introduced into the forward loop, thus closing the feedback loop.

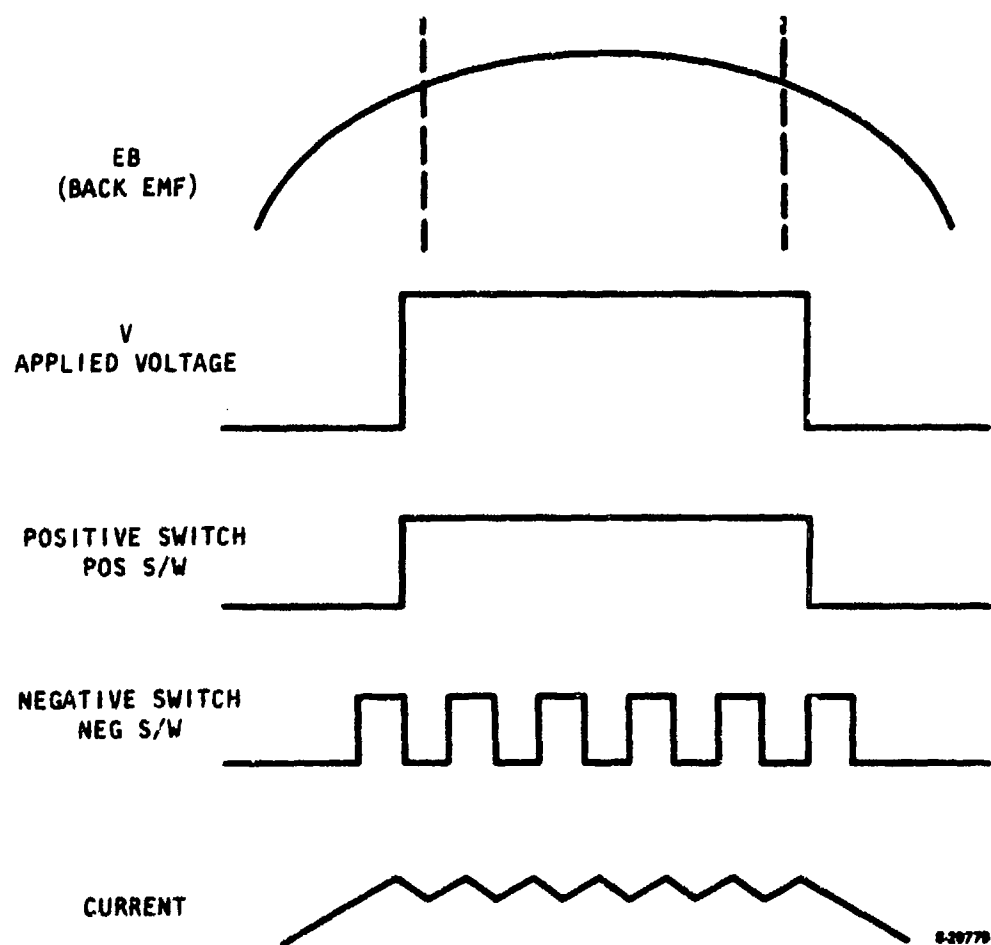


Figure 35. Waveforms for Voltage Sourced, Modulated Drive Circuit

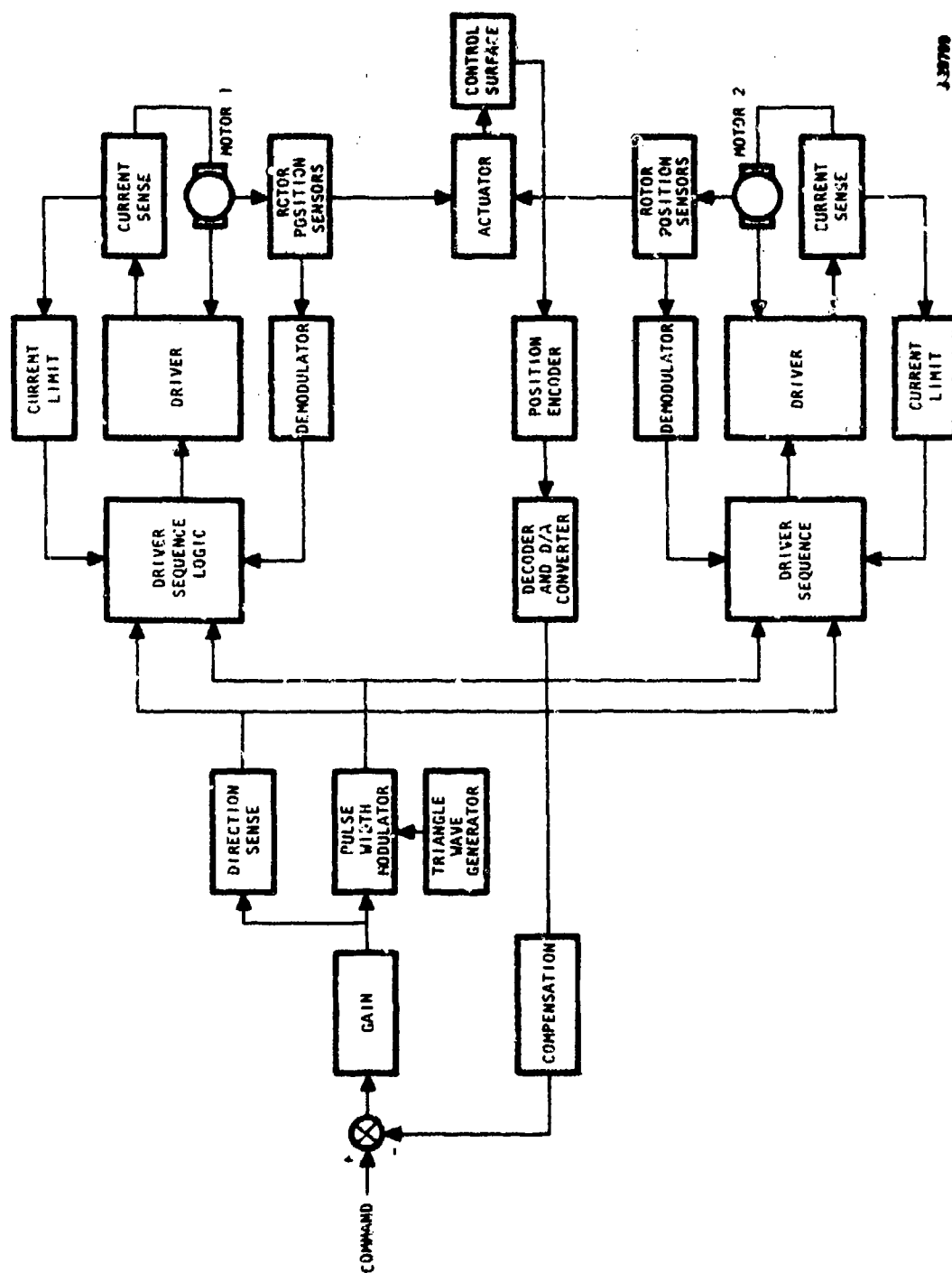


Figure 36. System Block Diagram

3.3.2.2 Pulse-Width Modulator and Sequence Logic

Dc output from the forward loop gain and compensation amplifier commands motor speed. The pulse-width modulator, sequence logic, and control logic translate the forward loop amplifier dc output to the 3-phase excitation required by the motor.

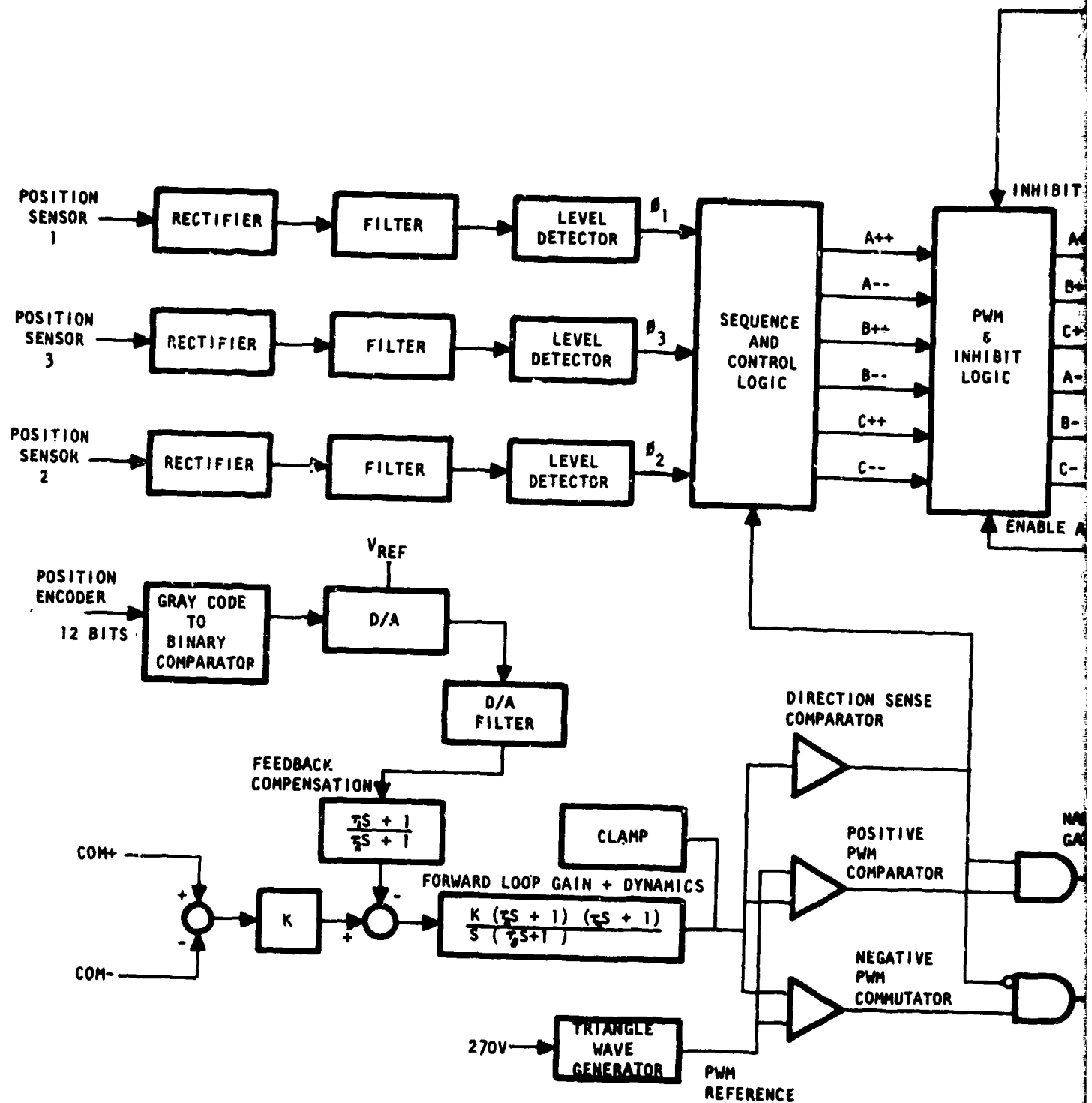
Rotor rotation results from the torque developed by the stator rotating field vector acting upon the permanent-magnet field vector of the rotor (see Figure 8). To produce the rotating stator field vector, the stator coils must be excited in the proper sequential order and polarity. The sequence and control logic performs this function, and requires some input to determine where the rotor position is before proper stator coil excitation can be commanded. Rotor position information is produced by three position sensors built into the motor. Rotor speed is dependent upon the stator magnetic field vector rotation speed because the rotor is moving at the same rotational velocity as the stator field vector.

Stator field rotational velocity is dependent upon the 3-phase frequency input, which is dependent upon rotor speed through the rotor position sensors. The process of motor speed control is as follows:

- (a) Frequency and sequencing of stator coil excitation is dependent upon rotor position information.
- (b) Rotor position information is dependent upon torque induced in the rotor by the frequency and average 3-phase voltage applied to the stator coils.
- (c) Since the frequency of coil excitation is derived from rotor position (as noted in (a) above), the speed of the rotor is only dependent upon the average 3-phase excitation voltage applied to the stator coils.

A pulse-width modulator (PWM) is used to control the average voltage to the motor. The PWM chops the input voltage at 3 kHz, which is substantially higher than the 480-Hz, 3-phase motor frequency. By controlling the duty cycle of 3 kHz PWM operating at the higher frequency, the average voltage the motor sees is controlled, as shown in Figure 38.

The PWM consists of three voltage level detectors, logic gates, and a triangle wave generator operating at 3 kHz. The clockwise/counter clockwise (CW/CCW) direction is sensed by a polarity sensor that indicates whether the forward loop amplifier is commanding clockwise motor rotation (positive output) or counter-clockwise rotation (negative output). The direction sensor output, which is in a discrete form, is used by the sequence and control logic for proper sequencing of driver switches and is also used for selecting the PWM comparator to be used.



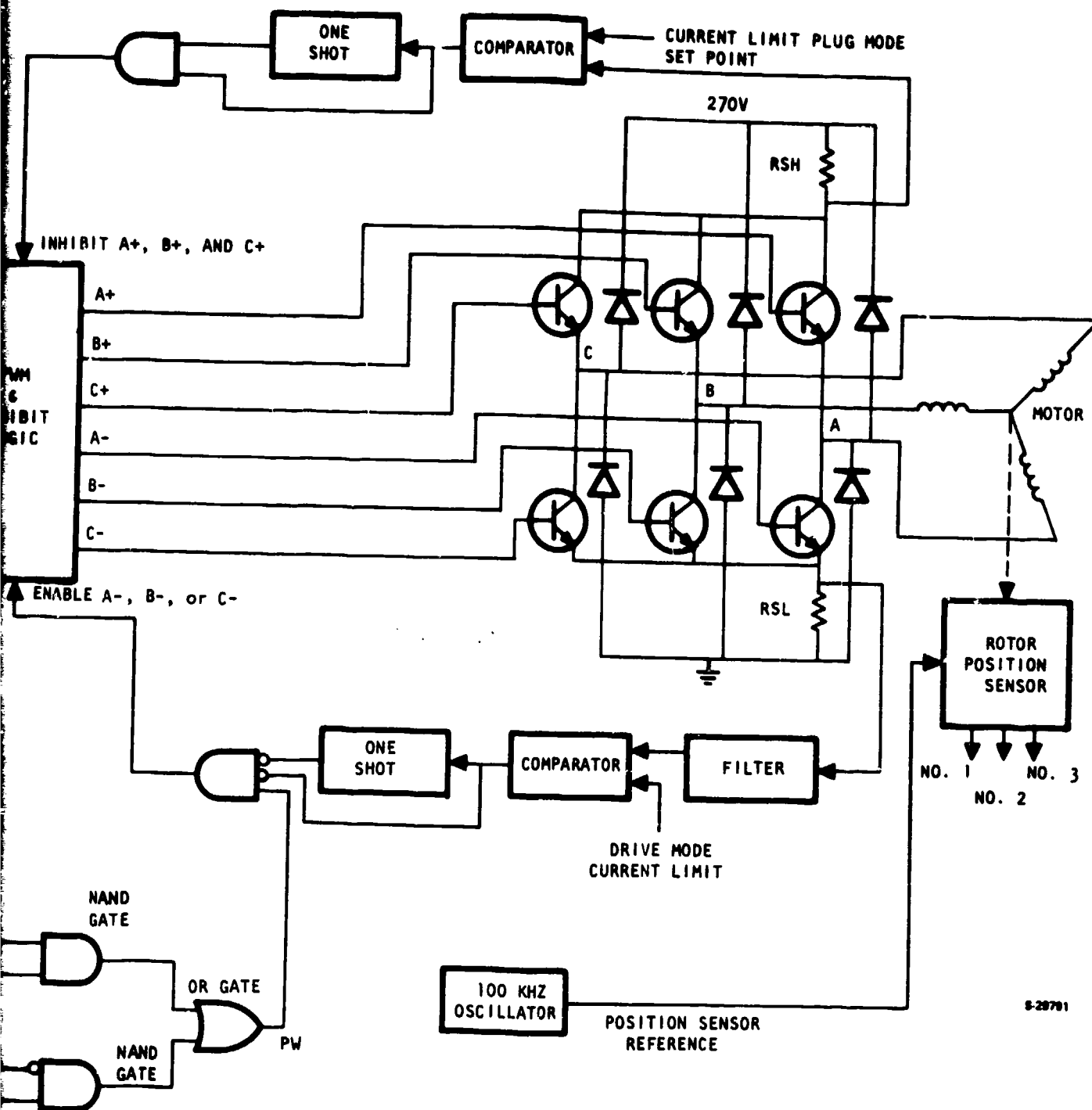
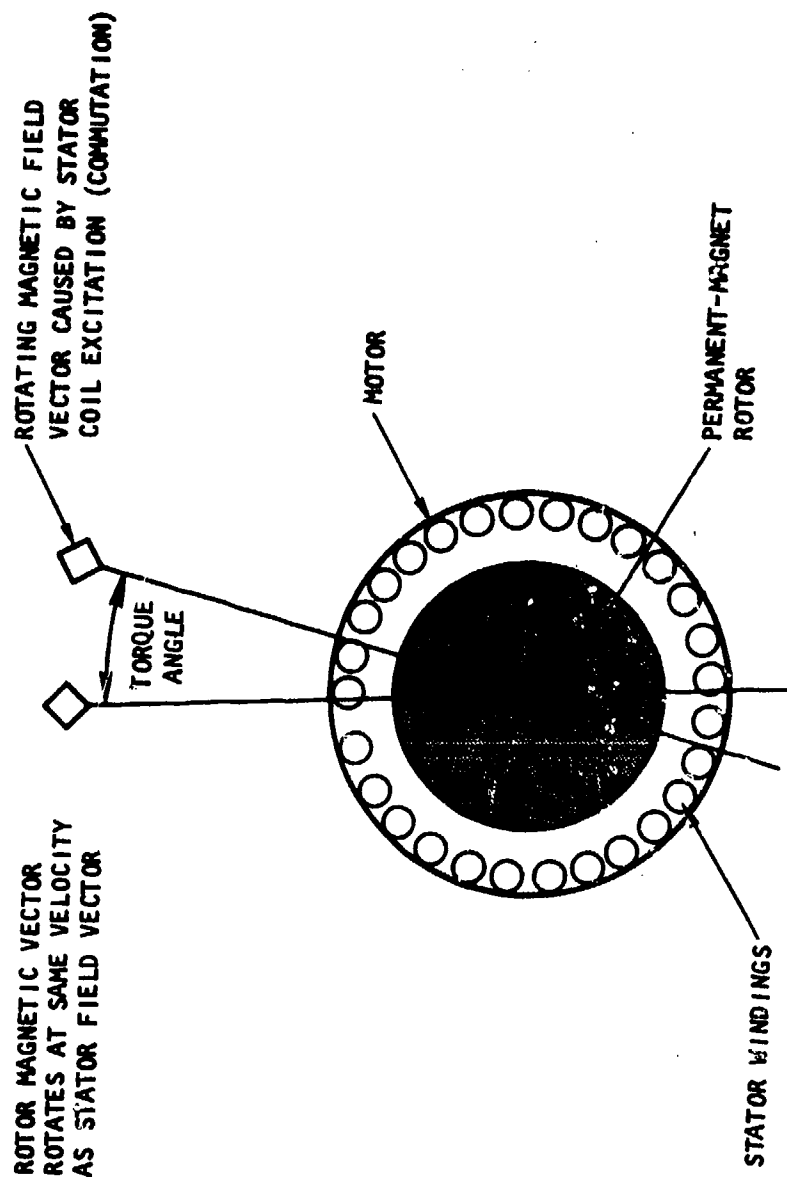


Figure 37. Controller Block Diagram



8-38781

Figure 38. Rotor Velocity Controlled by Stator Frequency

The need for a pulse-width-modulated signal with a duty cycle proportional to the output magnitude of the forward loop amplifier to achieve motor speed control is accomplished by comparing the voltage level of the forward loop amplifier to a 3-kHz triangle wave. The comparator output is switched, depending on which voltage level is higher. Two pulse-width comparators are needed for positive or negative (clockwise or counter-clockwise) output commands from the forward loop amplifier. The direction sensor selects which PWM comparator output is to be used by controlling two NAND gates. The NAND gate outputs are "OR'd" together to produce a PWM control signal for clockwise or counter-clockwise motor rotation.

3.3.2.3 Pulse-Width Modulation Logic and Rotor Position Sensors

The pulse-width modulator logic uses a modulated pulse train from the PWM comparators to control the output of the sequence and control logic. The PWM comparator controls the sequence and control logic outputs to achieve the pulse width modulation of actuator input voltage. The rotor position sensors, as discussed above, are variable reluctance transformers, the primary of which is excited with a 50-kHz sine wave. Between the primary and the secondary (within the motor), a slotted squirrel cage functions as the transformer core. Output from the transformer secondary is rectified and filtered to provide a dc output. As the slotted squirrel cage rotates past the transformer, the average ac output from the secondary changes in magnitude due to the change in reluctance of the transformer core. This change in ac output magnitude causes the dc voltage level of the filter to change. Filter output is then fed into a level detector. The discrete output of the level detector changes state when the filter dc voltage level changes, thus changing the sequence logic output. The position sensors and squirrel cage are located within the motor such that proper level changes are provided at the instant the stator coil excitation sequence should be changed.

3.3.2.4 Power Drivers and Current Limits

Six high-voltage transistors and six flyback diodes are provided in the power driver stage. The transistors buffer the control signals from the PWM and inhibit logic to control the excitation of the stator coils. The flyback diodes provide current paths for the dissipation of stator coil inductive energy.

During the first few milliseconds of motor excitation, large currents flow because the back emf of the motor has not built up. If no limit on this start-up current existed, destruction of the driver transistors and excessive motor heating would result. A drive mode current limit is used to shut off the power transistors before motor currents reach destructively high values. In operation, a low valued (1-ohm) sense resistor is used to change the current to a voltage output, and a low-pass filter on the output of the sense resistor is used to filter out unwanted noise. The output of the sense resistor filter is then applied to a comparator, which compares sensed resistor voltage, and indicates current to a setpoint voltage. When the resistor voltage exceeds the set point, the comparator changes state and provides an inhibit signal. The inhibit signal shuts off the drivers and allows the motor current to decay through the flyback diodes. After a selected time period, the drivers are then enabled. In this way, startup current is limited.

Another current limit is needed to prevent power driver destruction when the motor is operated in the plug reverse condition. The plug reverse condition corresponds to the situation when the drivers command the motor to operate in the opposite direction from which it is rotating. When this condition occurs, the motor "looks like" a generator to the power drivers, which causes currents to add and flow within the power driver back to the power source through the flyback diodes and power transistors. The plug mode current limit limits the amount of current flowing back into the 270-v power supply, preventing destruction of the drive transistors. Plug mode current operation is the same as drive mode current limit operation.

3.3.3 Controller Circuit Design

The detailed circuits designed for the demonstration unit include both microprocessor and analog servo assemblies. Both servo types were used to drive the transistorized power switch modules. The microprocessor controller development is described in Appendix E. The details of the analog servo circuitry and the modified power switch modules are described below. These circuits include the following.

Servo circuits for voltage feedback configuration

- Control circuitry
- Surface position sensing
- Rotor position detectors
- Sequence control and inhibit logic

Power switch

- Driver switches
- Current limit
- Power supplies

Servo circuits for tachometer feedback configuration

- Tachometer feedback control loop
- Rotor speed detection

3.3.3.1 Control Circuitry

The schematic for the control circuitry is shown in Figure 39. The control circuitry consists of the command buffer, position error, loop dynamic compensation, pulse width modulators, and error direction detectors. Amplifier U1 combines the functions of buffering the command input, summing the command and feedback position signals to produce a position error, and providing dynamic compensation for the position feedback signal. Amplifier U2 integrates the position error and provides the additional dynamic compensation required for position loop stability. The zener diodes VR1 and VR2 provide a clamp for the integrator to limit the range of the integrator to correspond to the range of the pulse-width modulator.

Pulse-width modulation is accomplished by comparators U3 and U4. The pulse width is generated for positive errors by comparing the error voltage with a 3-kHz triangle wave, which is offset so that the bottom tip of the waveform is at zero. When the error is greater than the triangle wave, the output is energized, which applies the line voltage to the motor. When the error is less than the triangle, the line voltage is turned off. For negative

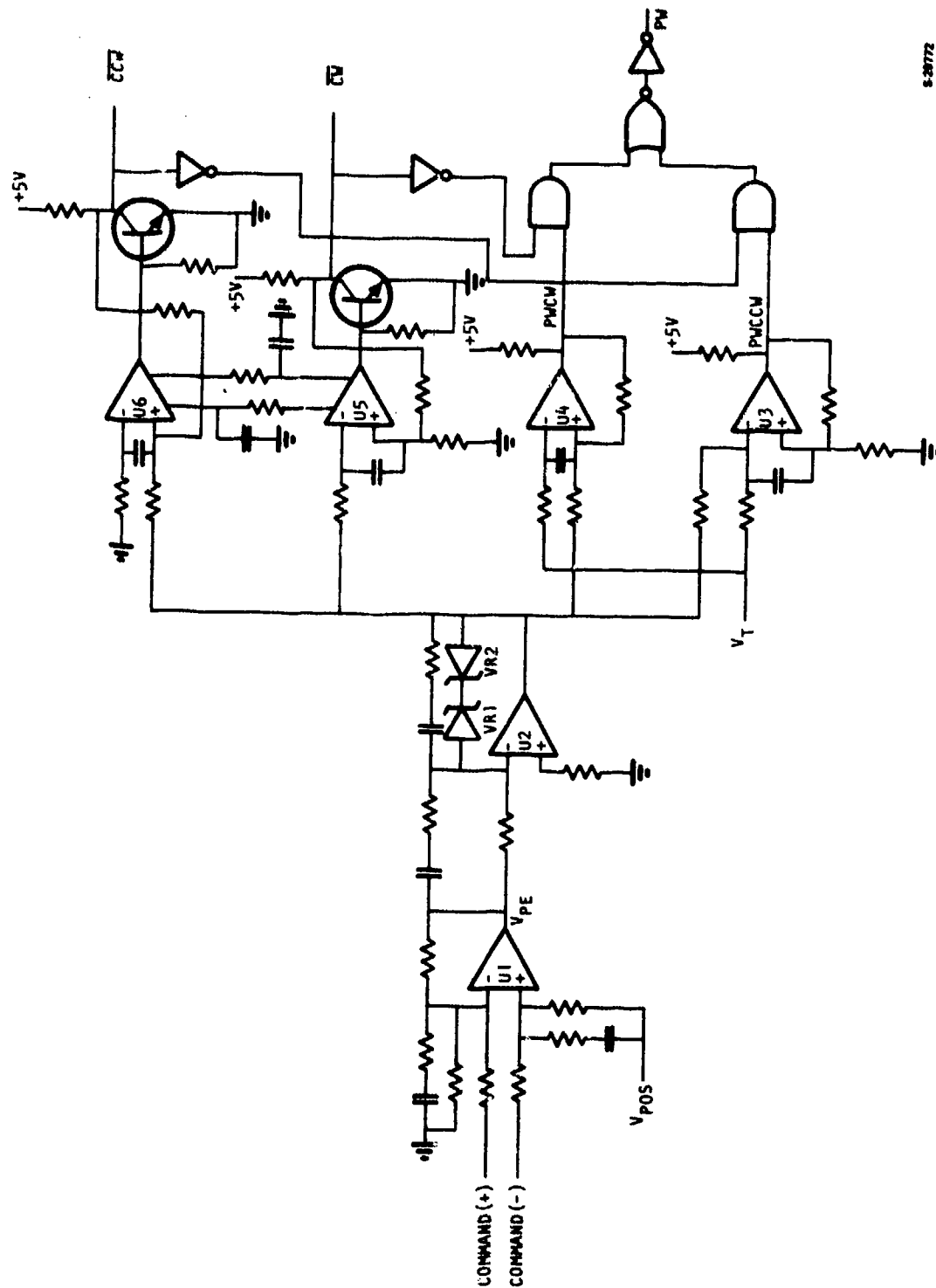


Figure 39. Position Error and Compensation Amplifiers, Pulse-Width Modulators, and Direction Sense Circuitry

errors, the error is added to the triangle wave and the sum is compared with zero, which produces the same pulse widths as for positive errors. The pulse width produced is proportional to the error voltage, as shown in Figure 40. The average motor voltage is therefore the V_{line} times duty cycle, where duty cycle = t/T , t = pulse width, and T = period of the triangle wave. This means that the gain of the pulse-width modulator is a direct function of the line voltage. To eliminate this and keep a constant gain, the line voltage is monitored and used as the reference for the triangle wave. The triangle wave is, therefore, amplitude-modulated as a function of line voltage. For a given error voltage, the pulse width is increased or decreased in the inverse proportion to line fluctuations, assuring a fixed motor voltage and gain.

The schematics of the triangle wave generator and its resulting waveform are shown in Figures 41 and 42. Comparators U5 and U6 are used to detect the motor drive direction. The two detectors are cross-coupled with a 10-sec delay between turnoff of one and turnon of the other. This ensures that the drive transistors for one direction have time to turn off before the transistors for the other direction are turned on; this prevents transistors in series across the 270-vdc line from being on at the same time, thus ensuring that they are not damaged.

3.3.3.2 Surface Position Sensing

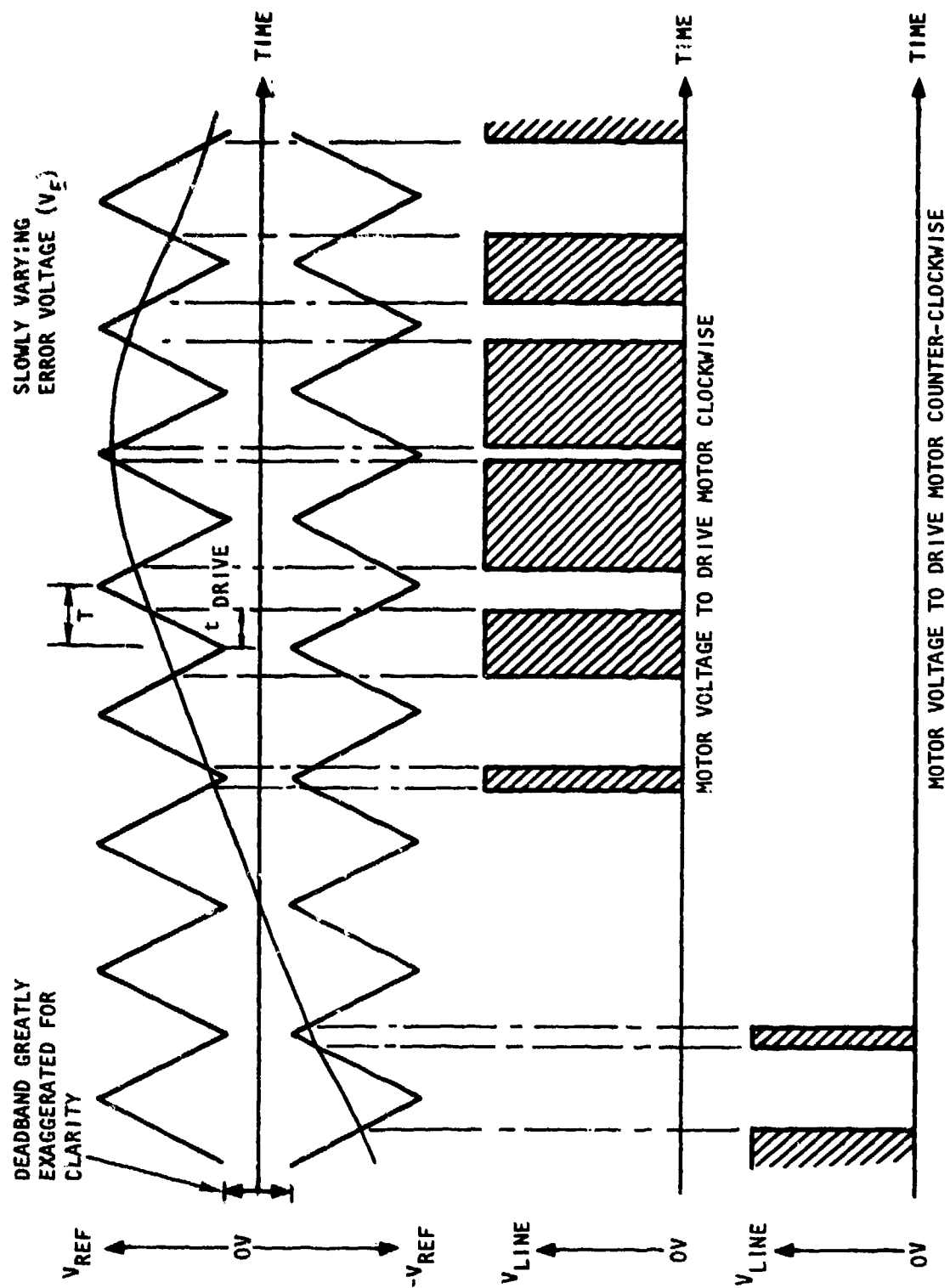
The control surface position is sensed by a 12-bit digital rotary shaft encoder. The encoder output is in a digital gray code and must be decoded to binary format by a cascaded series of exclusive or gates. The decoded binary number is then converted to an analog voltage level by an analog-to-digital converter that is offset to provide bipolar output corresponding to positive and negative surface positions. A filter is included in the output buffer to smooth the bit-to-bit transitions of the converter. A schematic is shown in Figure 43.

The precision 10-v reference is used for the D/A conversion, which gives an output scaling of 0.2489 v/deg. The 12-bit encoder gives two discrete states for 80.36 deg of travel, which provides a resolution of 0.0196 deg.

3.3.3.3 Rotor Position Detectors

To synchronize the stator voltage with the rotor for efficient torque transfer, the position of the rotor must be known. To sense this position, three position sensors are mounted in the motor frame at 40-deg intervals. These sensors are transformers with a mechanical shutter mounted on the motor shaft that varies the coupling between the primary and secondary. This change in coupling varies the amplitude of the voltage in the sensor secondary. A diagram of the idealized position outputs is shown in Figure 44.

The position detection circuitry is shown in Figure 45. There are three identical detector circuits. The primaries of the sensors are driven with a 50-kHz, 18-v peak-to-peak square wave. This frequency is generated by timer U1, which is connected as a square-wave oscillator; the frequency is amplified to the proper level by Q1 and Q2. The sensor output is demodulated by U2 and U3, which amplify and full-wave-rectify the signal. The signal is then filtered and level-detected to eliminate the 50-kHz reference frequency and give the position output.



S-78017-8

Figure 40. Pulse-Width-Modulation Idealized Timing Diagram

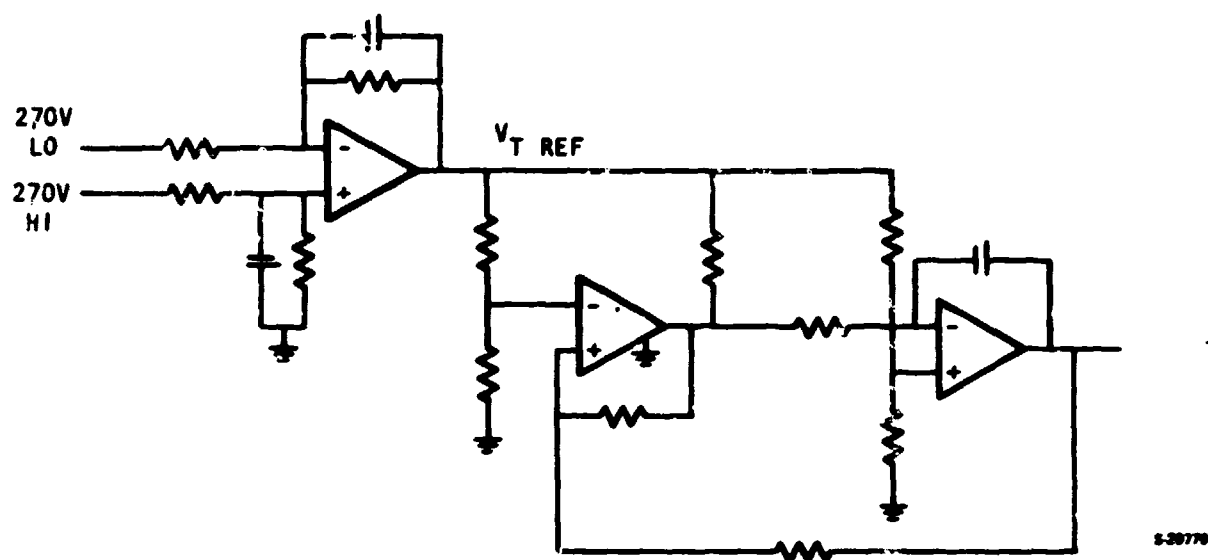


Figure 41. Triangle Wave Generator

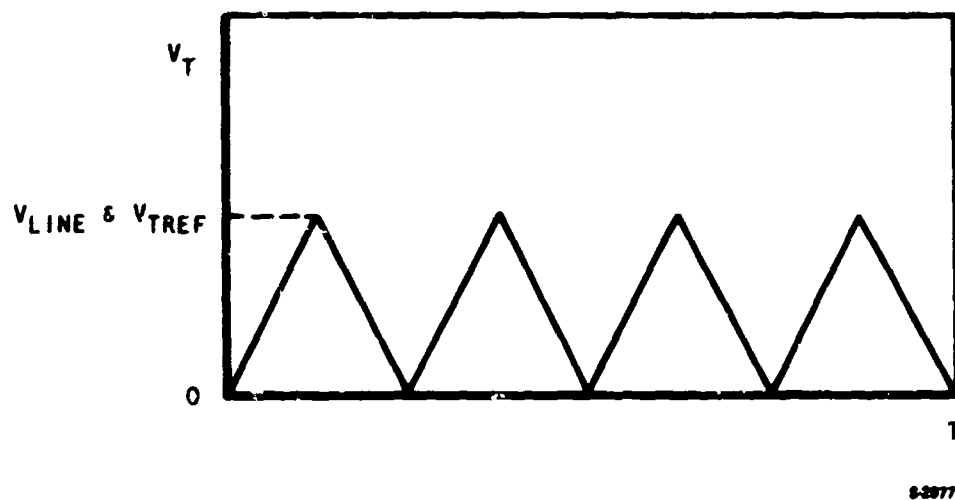


Figure 42. Triangle Waveform

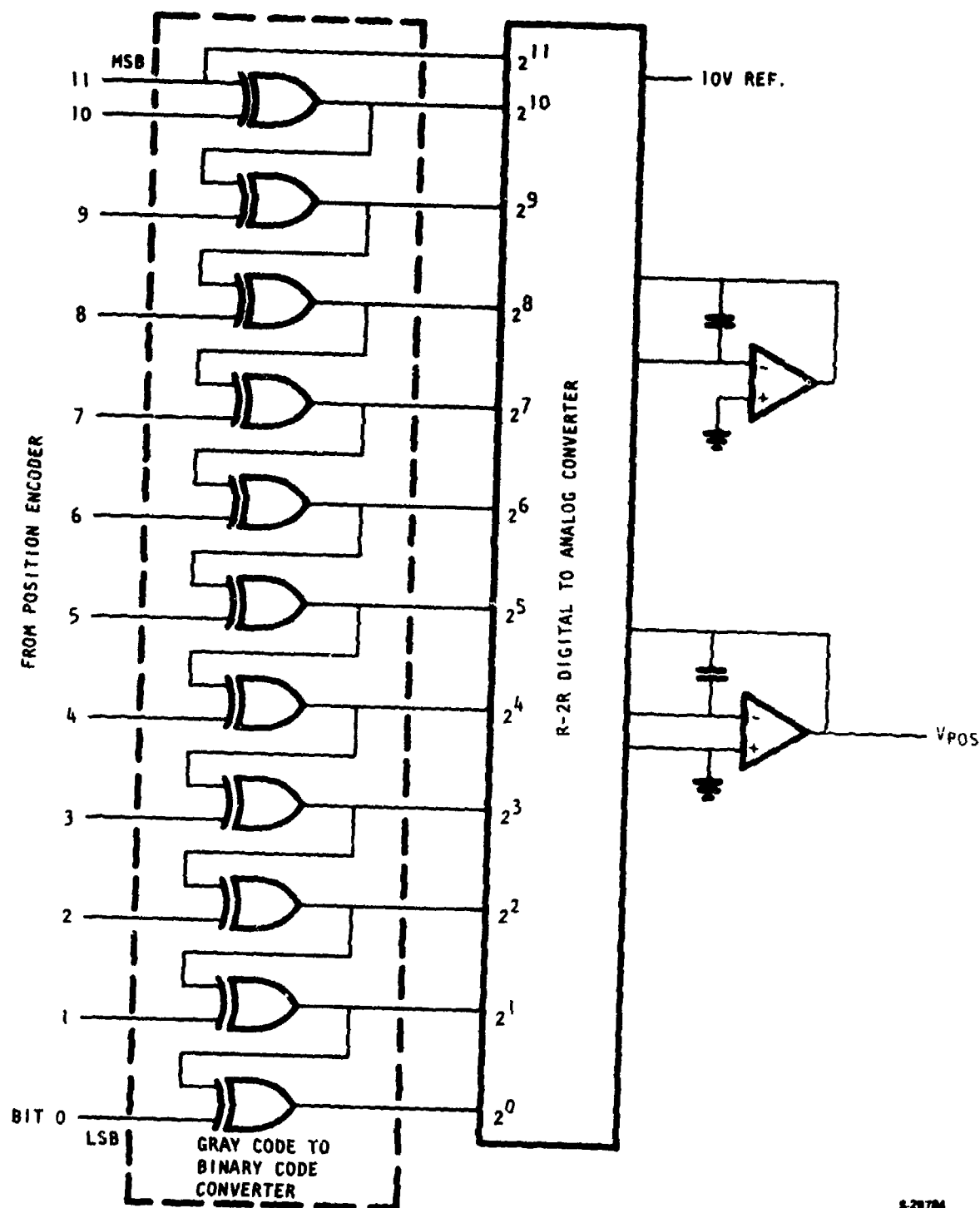
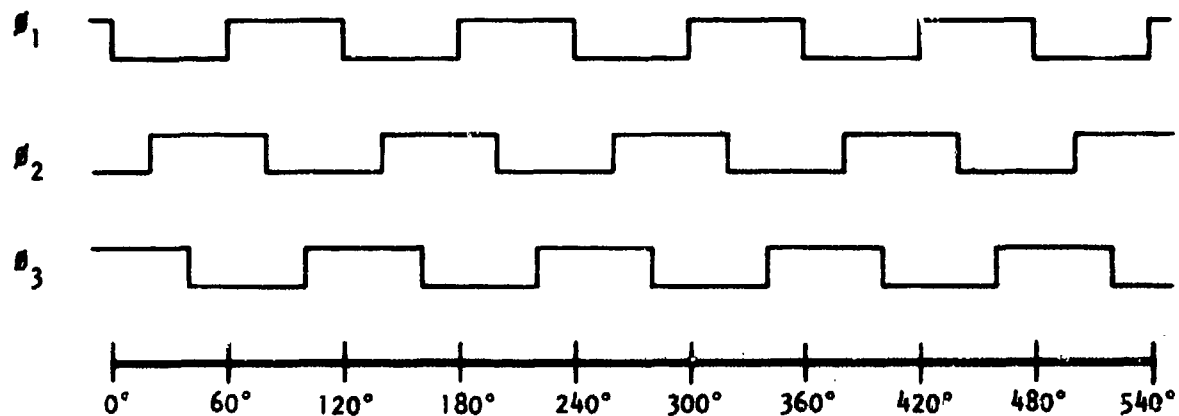
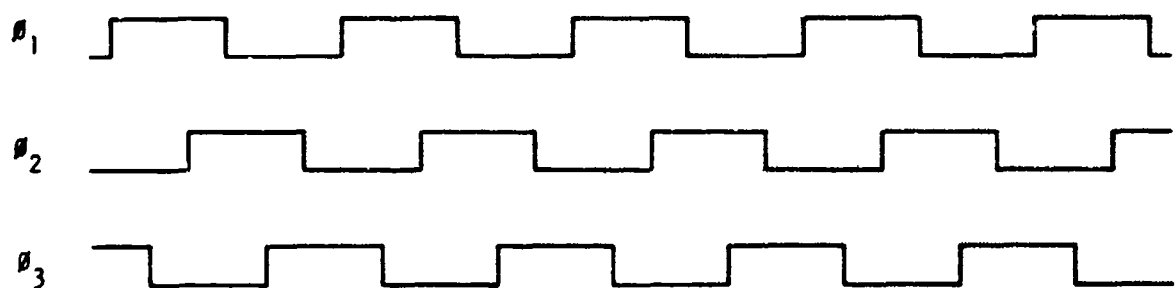


Figure 43. Surface Position Decoding Circuitry

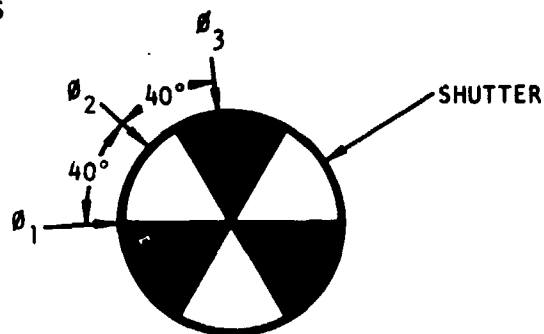
COUNTER CLOCKWISE



CLOCKWISE

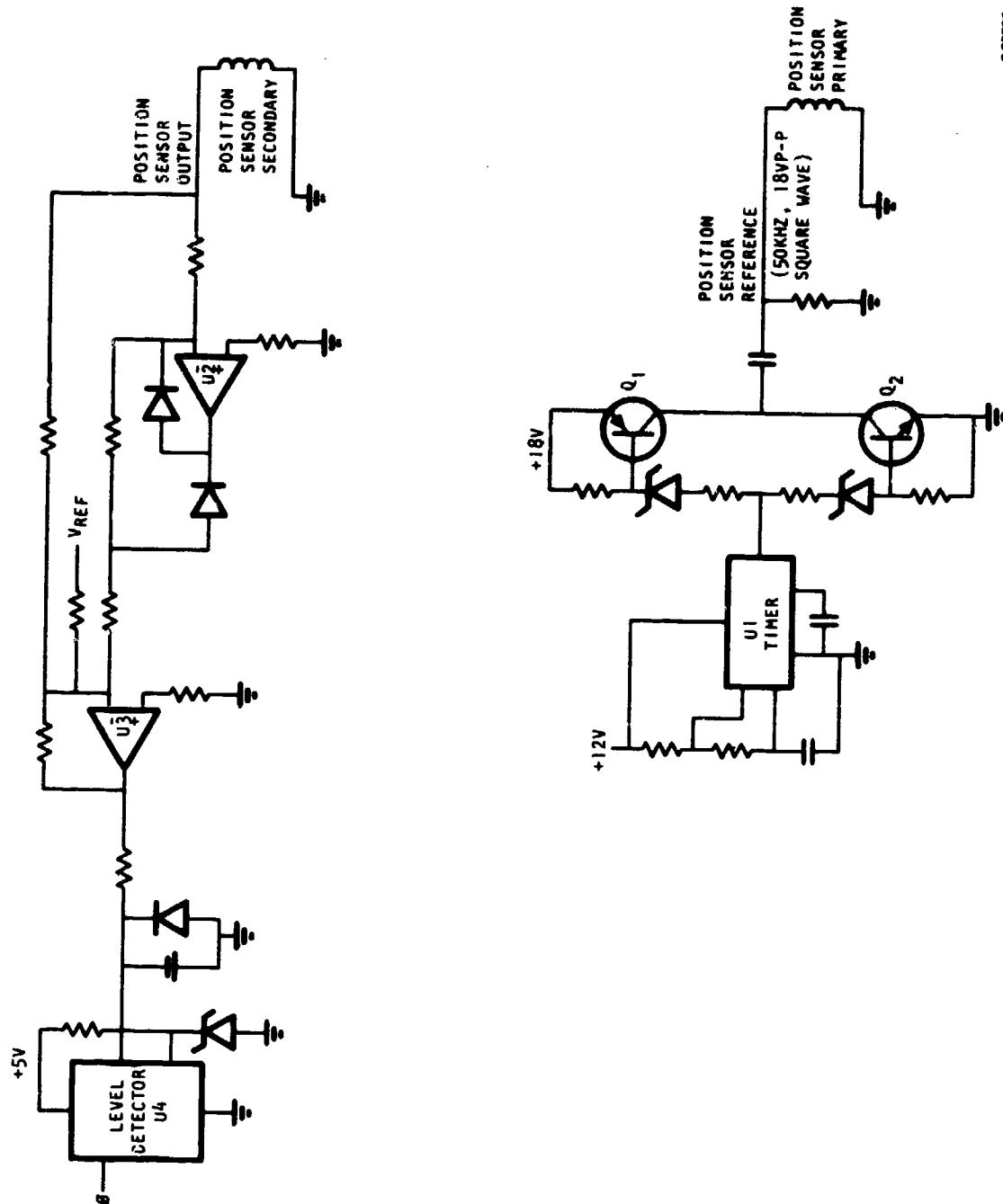


POSITION
SENSORS



8-28788

Figure 44. Rotor Position Outputs



8-28787

Figure 45. Motor Rotor Position Detection Circuitry

3.3.3.4 Sequence, Control, and Inhibit Logic

The schematic of the drive logic is shown in Figure 46. The drive logic sets the sequence in which the driver transistors are turned on as a function of the rotor position (as indicated by θ_1 , θ_2 , and θ_3) and the commanded direction signals CW and CCW. The upper switches, indicated by a +, are turned on as a function of direction and rotor position, whereas the lower switches, indicated by a -, are modulated as a function of the pulse-width modulation signal. The logic equations for the switches are as follows:

Upper switches

$$A + = (\bar{\theta}_1 \cdot \theta_3 \cdot CW + \theta_1 \cdot \bar{\theta}_3 \cdot CCW) \cdot \overline{INHIBIT} \cdot \overline{AM}$$

$$B + = (\theta_2 \cdot \bar{\theta}_3 \cdot CW + \bar{\theta}_2 \cdot \theta_3 \cdot CCW) \cdot \overline{INHIBIT} \cdot \overline{BM}$$

$$C + = (\theta_1 \cdot \bar{\theta}_2 \cdot CW + \bar{\theta}_1 \cdot \theta_2 \cdot CCW) \cdot \overline{INHIBIT} \cdot \overline{CM}$$

Lower switches

$$A - = (\theta_1 \cdot \bar{\theta}_3 \cdot CW + \bar{\theta}_1 \cdot \theta_3 \cdot CCW) \cdot ENABLE \cdot \overline{AP}$$

$$B - = (\bar{\theta}_2 \cdot \theta_3 \cdot CW + \theta_2 \cdot \bar{\theta}_3 \cdot CCW) \cdot ENABLE \cdot \overline{BP}$$

$$C - = (\bar{\theta}_1 \cdot \theta_2 \cdot CW + \theta_1 \cdot \bar{\theta}_2 \cdot CCW) \cdot ENABLE \cdot \overline{CP}$$

where: $\overline{INHIBIT} = \overline{CLH} \cdot \overline{DELH}$

CLH = plug current limit

DELH = plug 140 sec delay

ENABLE = PW · \overline{CLL} · \overline{DELL}

PW = pulse width modulation

CLL = lower current limit

DELL = lower 140 sec delay

Timing diagrams of the drive logic are shown in Figure 47.

The AP, BP, CP, AM, BM, and CM signals are used to ensure that two of the switches (for example, A+ and A-) are never enabled at the same time. This condition would cause a short across the line, which would damage the transistors.

3.3.3.5 Driver Switches

The schematic of the driver switches is shown in Figure 48. The operation of a switch (for example, switch A+) is typical for all of the power switches. When logic signal A+ is high, optical coupler Q₃ is off, which makes

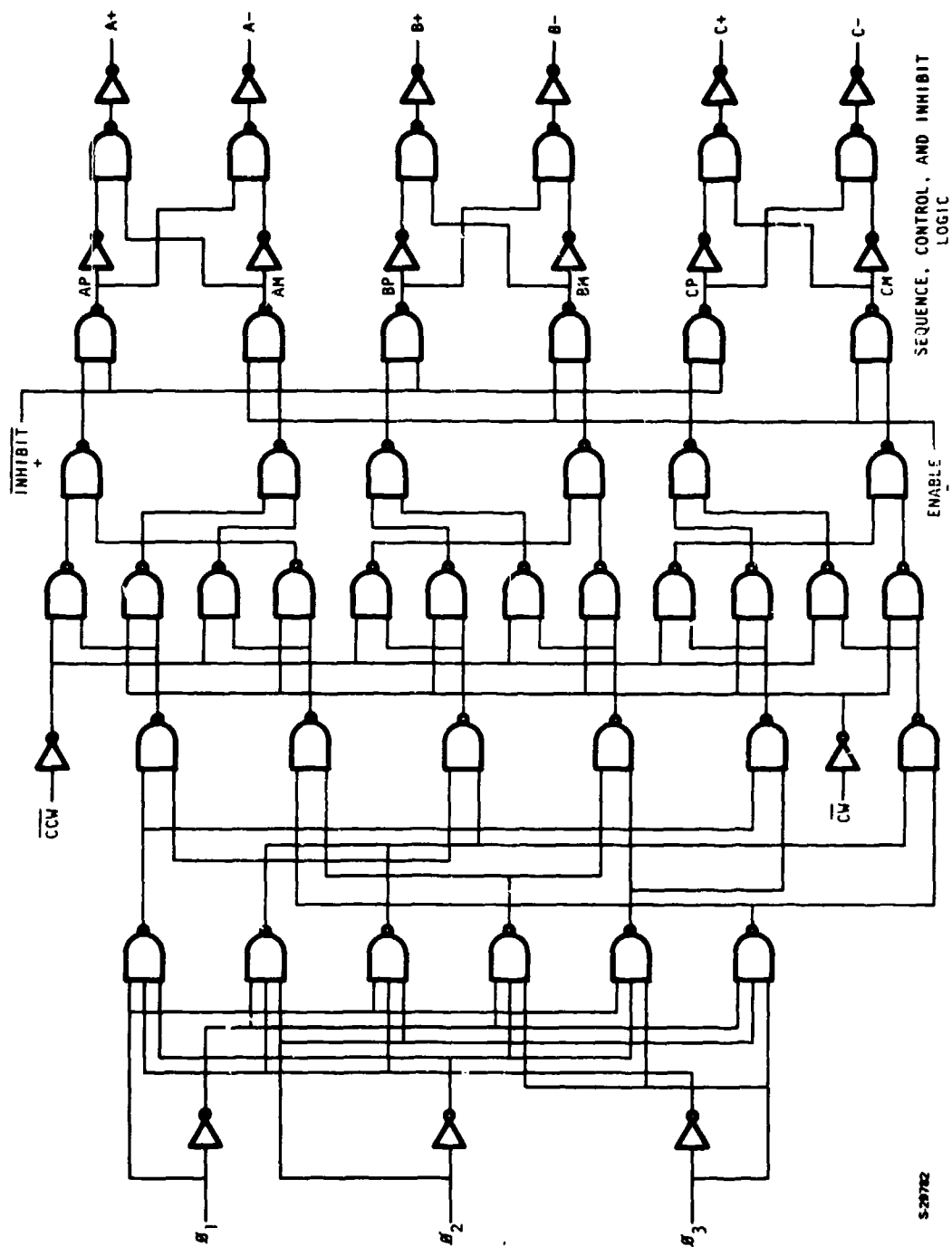
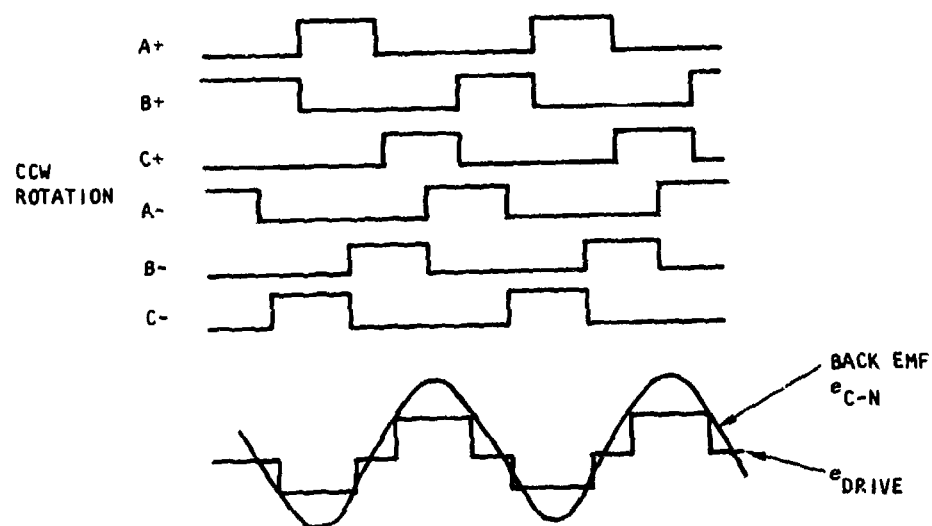
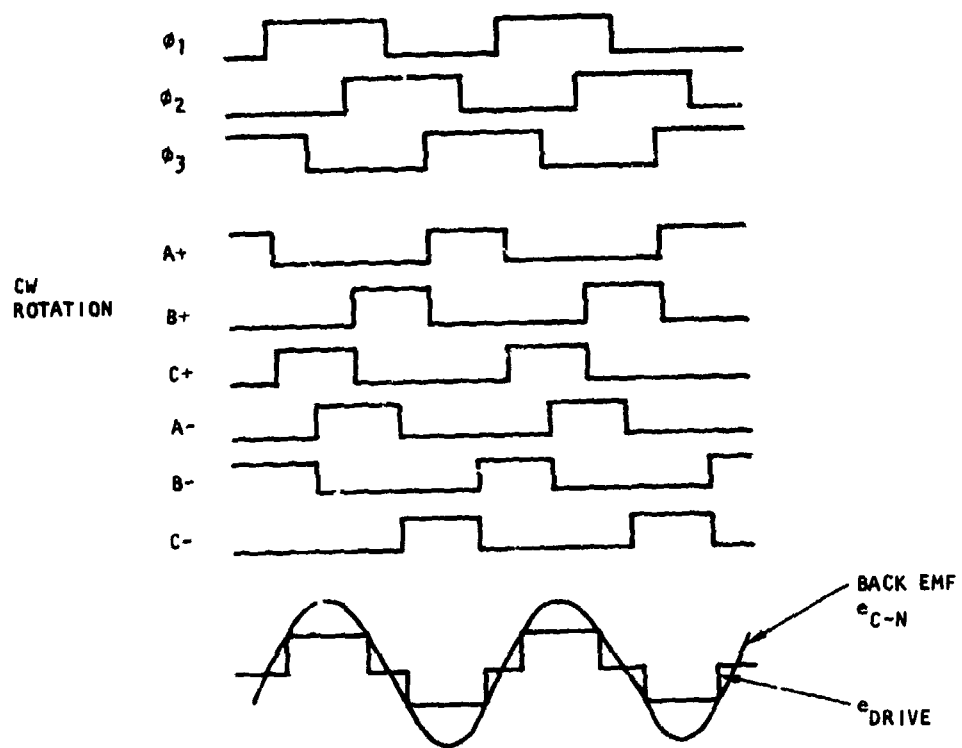


Figure 46. Sequence, Control, and Inhibit Logic



S-29748

Figure 47. Sequencer Timing Diagrams

the level detector output low. This turns on Q_1 and energizes switch $A+$, causing current to flow in one leg of the motor. When logic signal $A+$ goes low, optical coupler Q_3 is energized, which forces the level detector output high. This turns off Q_1 and turns on Q_2 , which pulls current out of the base of switch $A+$, thus turning it off. Since the motor has inductance, the current cannot be interrupted; the voltages go low and forward bias diode $CRA-$, giving a path for the motor current.

The bias for the power switches is obtained from a floating power supply PSA , which is referenced to the motor terminal A . The optical couplers isolate the logic signals from the 270-v power.

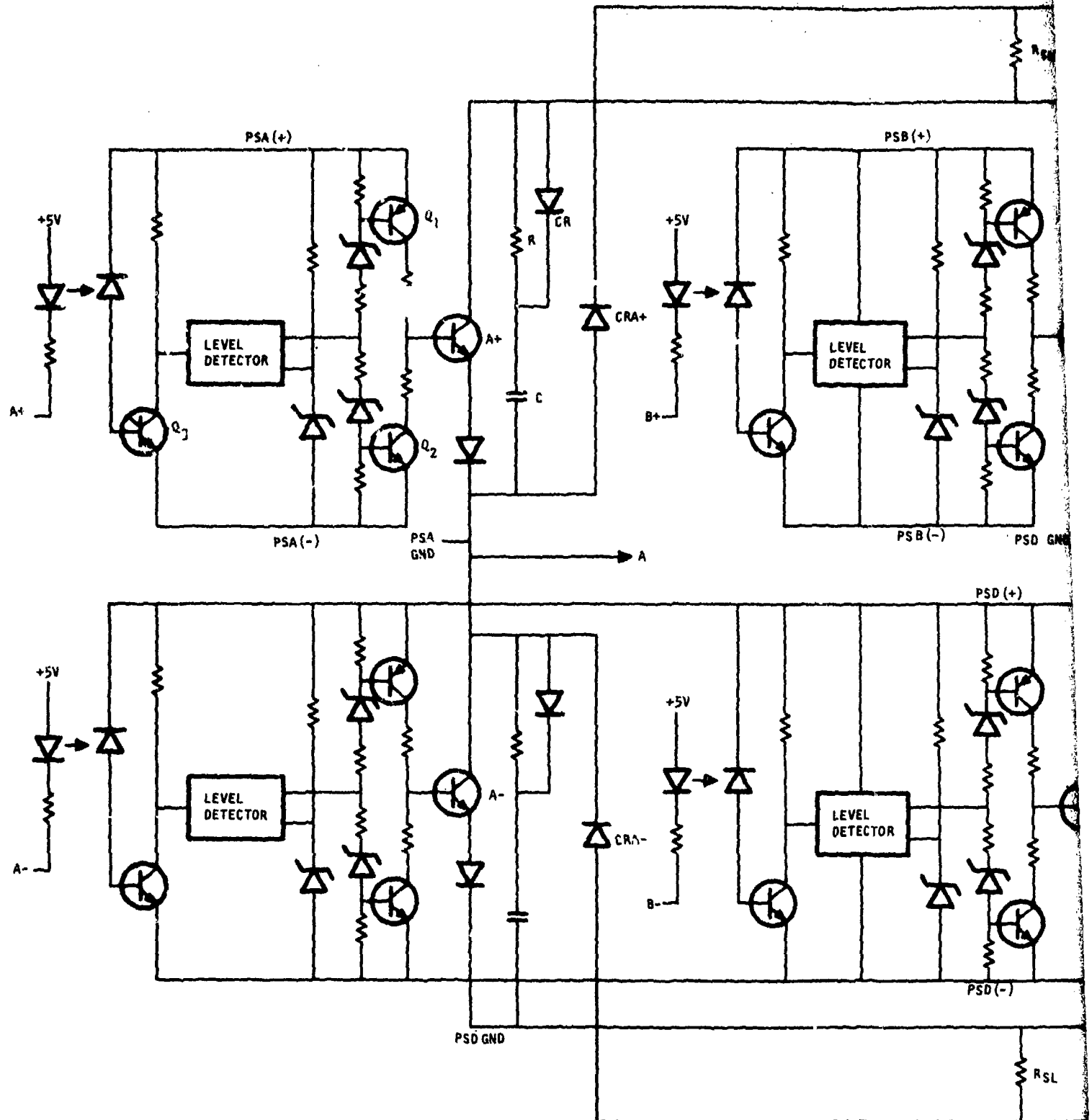
The network R , C , and CR is a snubber network to shape the transistor current-voltage turnoff locus. Without the snubber, when the transistor turns off with an inductive load, current continues to flow in the transistor until the flyback diode starts to conduct, which means it has full line voltage across it and full current at the same time. This produces a very high power spike in the transistor that can cause damage or failure. With the snubber, capacitor C charges through the diode CR when the voltage across the transistor increases, therefore sharing the current with the transistor. A typical curve of this operation is shown in Figure 49.

3.3.3.6 Current Limit

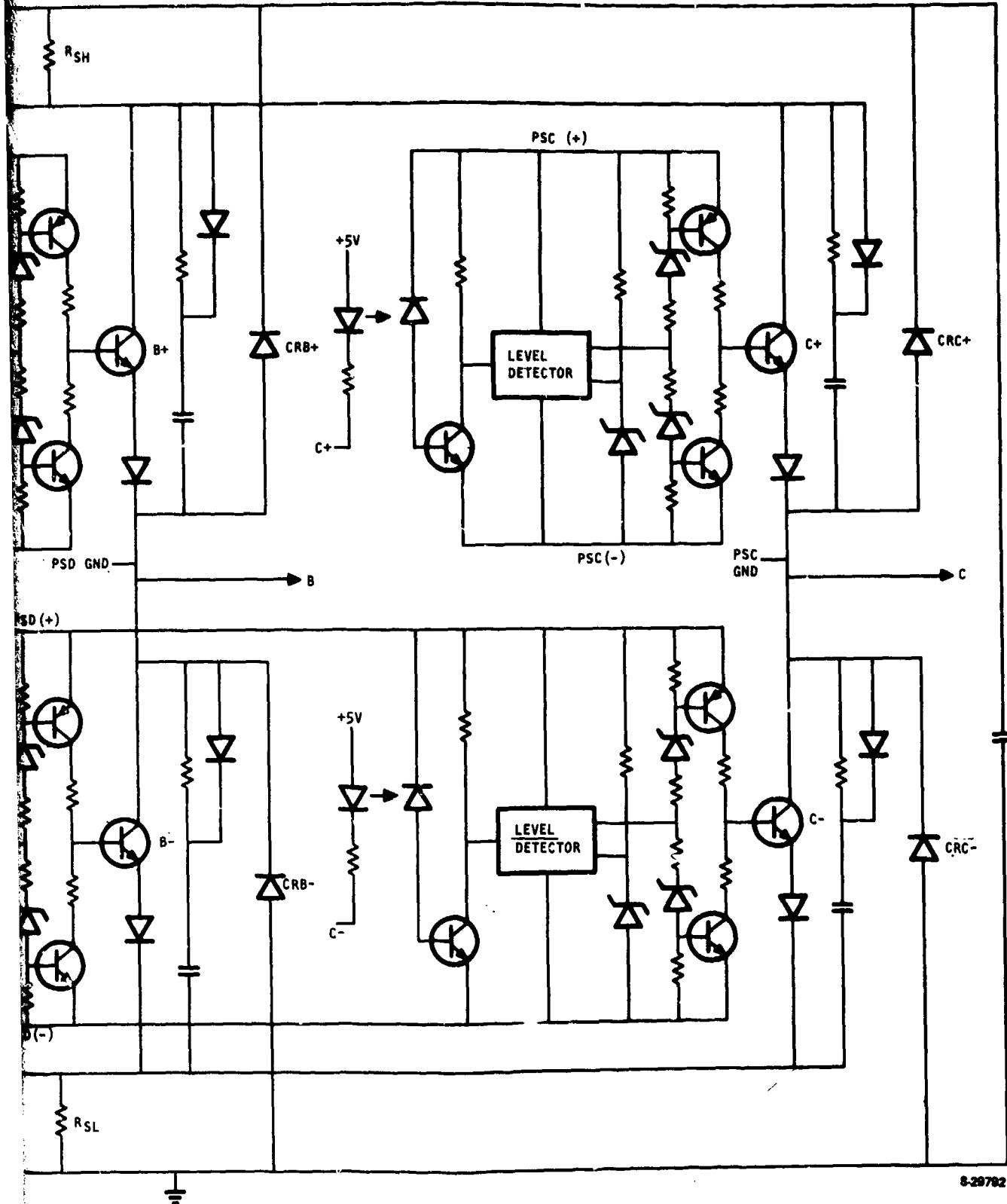
The current limit circuitry is shown in Figure 50. There are two current limits for controlling motor and transistor currents. The primary function of the lower limit is to limit the motor torque and power in normal operation. The upper limit is used in the plugging mode of operation when the motor is rotating in one direction and the inverter is driving in the other. This condition occurs during braking and reversing. Under these conditions, the back emf and the applied voltage both cause current to flow in the same direction and can cause high currents. This upper limit is primarily to protect the transistors from possible damage.

For normal operation with one upper and one lower switch on (for example $A+$ and $B-$), the current flow is from the line through R_{SH} , switch $A+$, motor windings $A - B$, switch $B - R_{SL}$, and into ground. The voltage across R_{SH} and R_{SL} is proportional to motor current. When the motor current reaches the limit level of 16 amp, U_2 goes low, which starts one shot U_3 and forces the $ENABLE$ low; this turns off the $B-$ switch. Due to the motor inductive flyback, the current path is now changed to the line, R_{SH} , switch $A+$, motor winding $A - B$, diode $CRB+$, and back to the line. In this condition, the current loop does not include the line, so no current is taken out of the supply. The current in the motor decays in this condition. Since no current flows in R_{SL} , U_2 returns high. The $ENABLE$ remains low until the one-shot period of 140 μsec is over; the $ENABLE$ then returns high, depending on the level of PW . Switch $B-$ is again turned on and current increases in the motor until it reaches the current limit, and the sequence repeats.

In the plugging mode, the current rapidly rises in the motor due to the addition of the back emf and the applied voltage. The lower limit is first reached and the operation is as described above. Due to the back emf, the



270 VDC



8-29782

Figure 48. Driver Switches

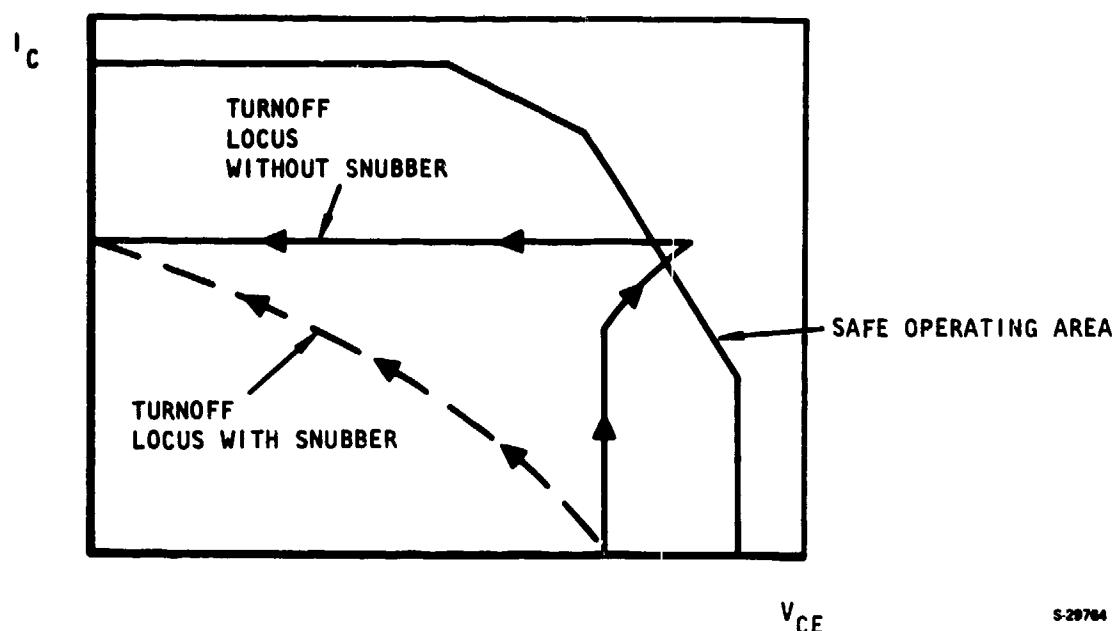


Figure 49. Typical Turnoff Locus

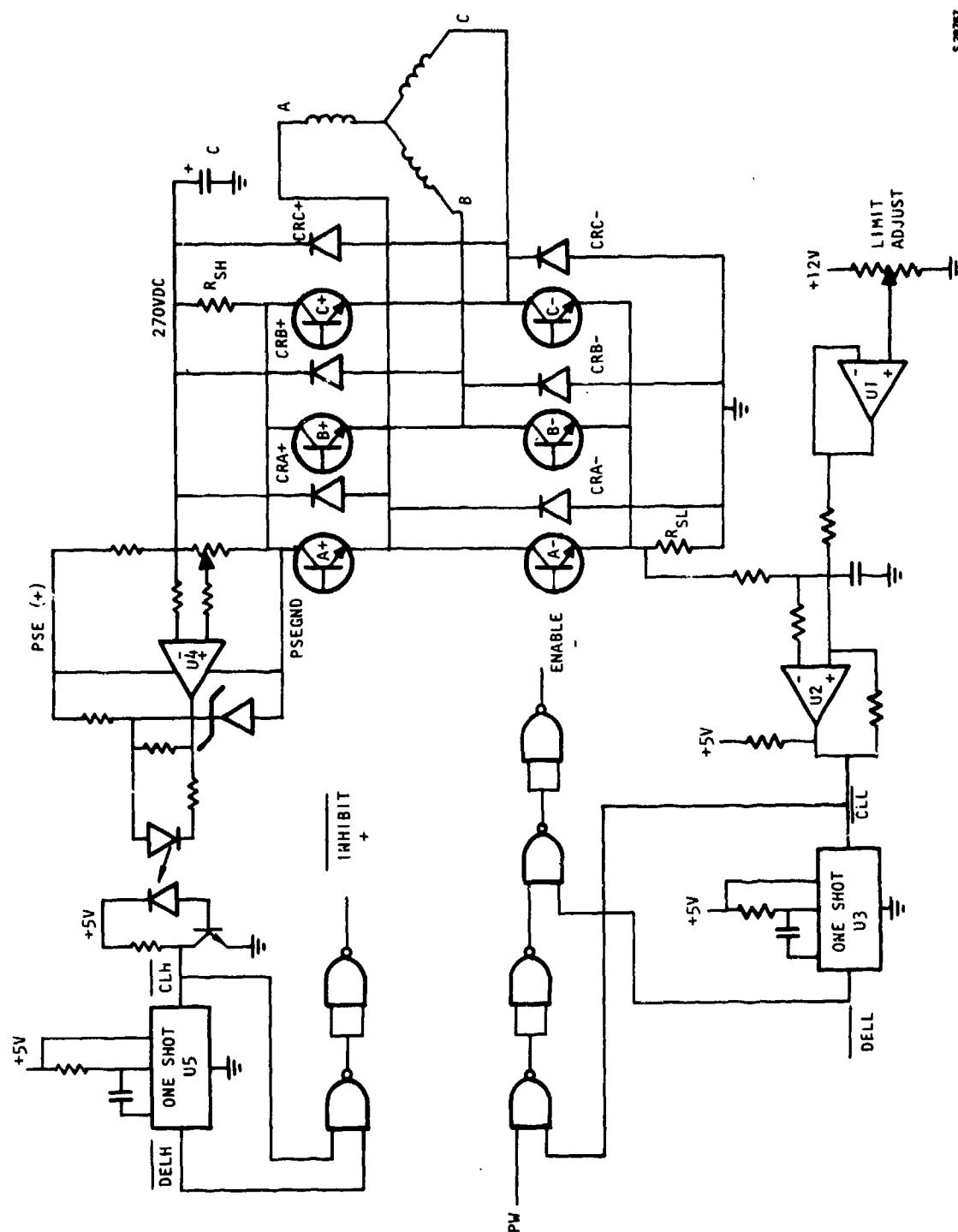
current continues to rise until the upper limit of 18 amp is reached. At this time, U4 goes low, starting one shot U5 and forcing INHIBIT low, thus turning off A+. The current path is now from ground, diode CRA-, motor winding A - B, diode CRB+, and into capacitor C to ground. Since current cannot flow back into the supply, the capacitor is charged with the current. In this condition the motor current decays. The INHIBIT is held low until the one-shot period of 140 μ sec ends, when it again goes high, turning on A+. The current again increases, repeating the process until the motor speed is reduced to a point where the back EMF and the applied voltage will not drive the limit current.

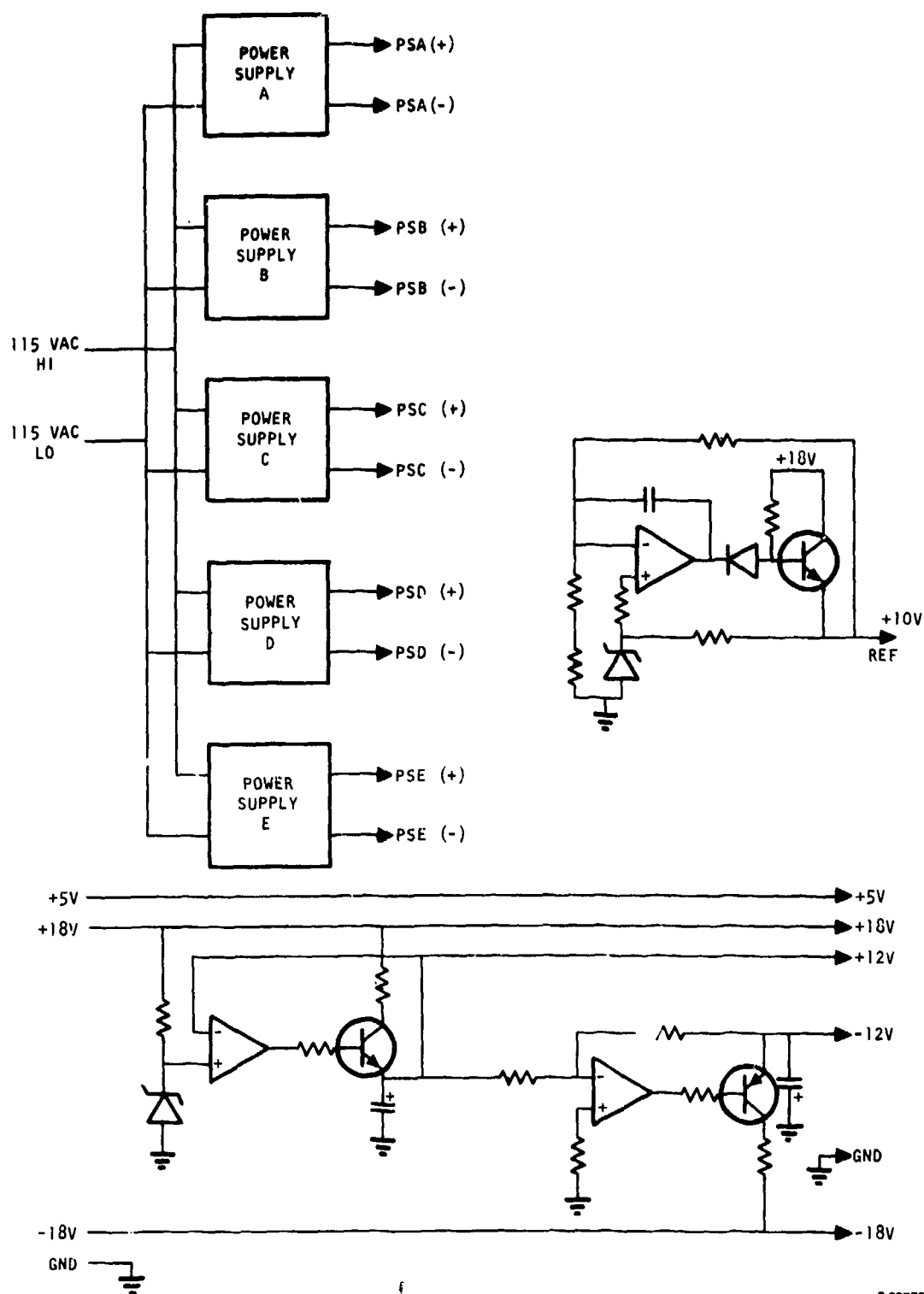
3.3.3.7 Power Supply

The power supplies are shown in Figure 51. Power supplies A, B, C, D, and E are commercial, and are used to bias the power switches and provide a floating supply for the upper current limit circuitry. A precision 10-v reference is created for the D/A converter reference and for other circuits in the system. The +12 v and -12 v supplies are derived from the +18 v and -18 v supplies for use as references and as supplies for lower voltage circuits.

3.3.3.8 Tachometer Feedback Control Loop

For additional dynamic compensation of the position control loop, the speed of the motor rotor is sensed and used as a secondary control loop. A block diagram of this control is shown in Figure 52. The control loop electronics have been changed to accommodate this addition and the circuitry





S-29773

Figure 51. Power Supply

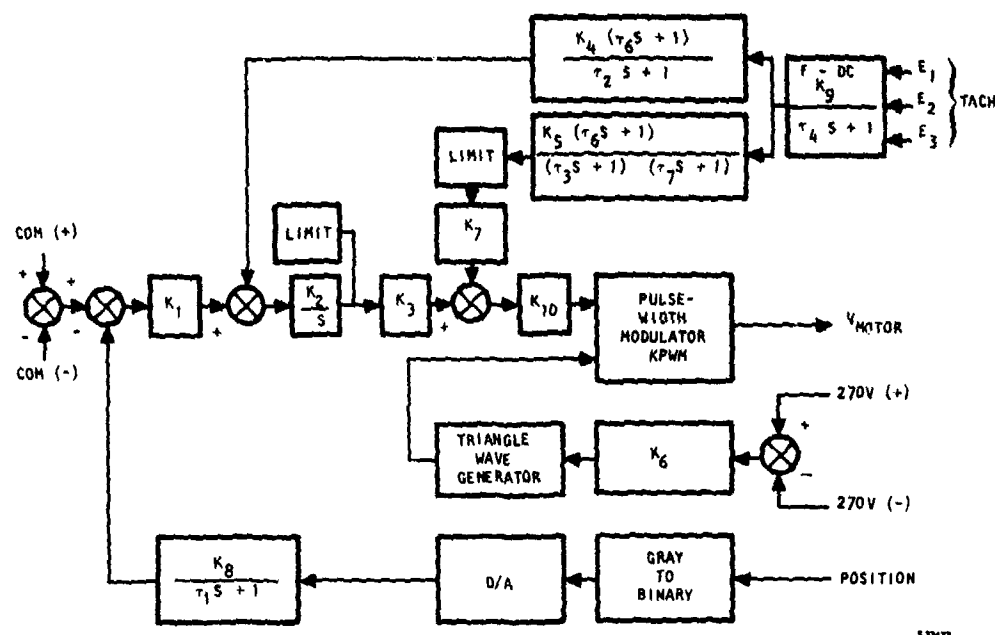


Figure 52. Tachometer Feedback Control Block Diagram

associated with rotor speed and direction detection have been added. The pulse-width modulators, sequence control logic, current limiting, drive switches, rotor position, and fin position circuitry are the same as previously described.

The schematic of the control loop circuitry is shown in Figure 53. Amplifier U1 sums the command input, fin position, and rotor speed, and provides an error output. This error is integrated by U2. Zener diodes VR1 and VR2 limit the output to prevent integrator windup. U3 sums an additional speed input with the integrator to provide a voltage signal that is compared with the triangle wave in the pulse-width modulator.

Amplifier U4 and U5 provide speed signal scaling and phase compensation required for loop stability. Zener diodes VR3 and VR4 limit the authority of the secondary speed loop.

3.3.3.9 Rotor Speed Detection

To determine the rotor speed, a tachometer winding was added in parallel with each of the three motor windings. This provides a 3-phase sine wave signal with the amplitude proportional to the rotor speed.

The schematic of the speed detection circuitry is shown in Figure 54. The 3-phase speed signal is converted to dc by a precision full-wave rectifier circuit, U1 through U6, which does not have the voltage losses due to diodes that are usually associated with rectifier circuits. This gives a signal that

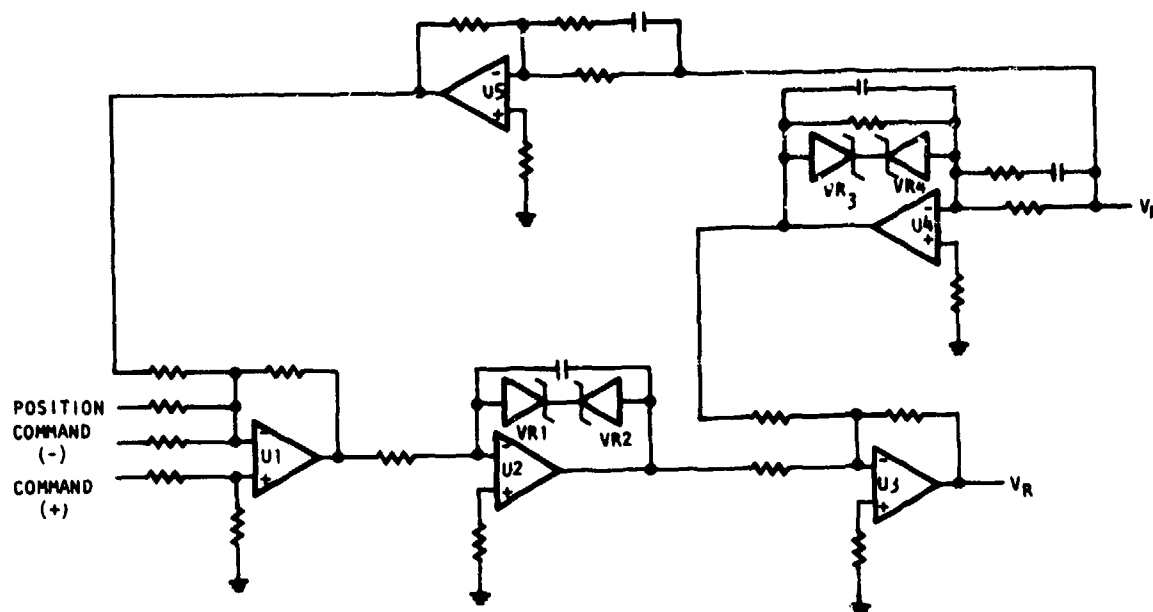


Figure 53. Tachometer Control Circuitry

is continuous from zero to full amplitude. Because this signal has the same sign for both directions of rotation, the signal must be inverted for the reverse direction. This is accomplished by amplifier U7 and transistor Q1. When Q1 is off, the sign of U7 is positive. When Q1 is on, the sign is negative. Q1's state is determined by the rotor direction detection circuit.

The schematic diagram for the motor rotor direction circuit is shown in Figure 55. The direction of rotation is sensed by the output of the three rotor position detectors: θ_1 , θ_2 , and θ_3 . On each transition of these outputs, a pulse is generated. At this time the previous state of rotor position, which has been stored in flip-flops 1 and 2, is compared with the present state and a direction is determined. A transition occurs every 60 deg of electrical cycle and there are 3 electrical cycles for each complete rotation; therefore, a direction change can be determined within 20 deg of rotation.

3.3.4 Projected Controller Sizing and Configuration

The scope of the development program was limited to the fabrication of breadboard electronics. The effort required to package the servo and power switch circuits into a representative aircraft installation was not included and would be largely dependent upon factors such as the following.

- Environment
 - Thermal
 - Vibration

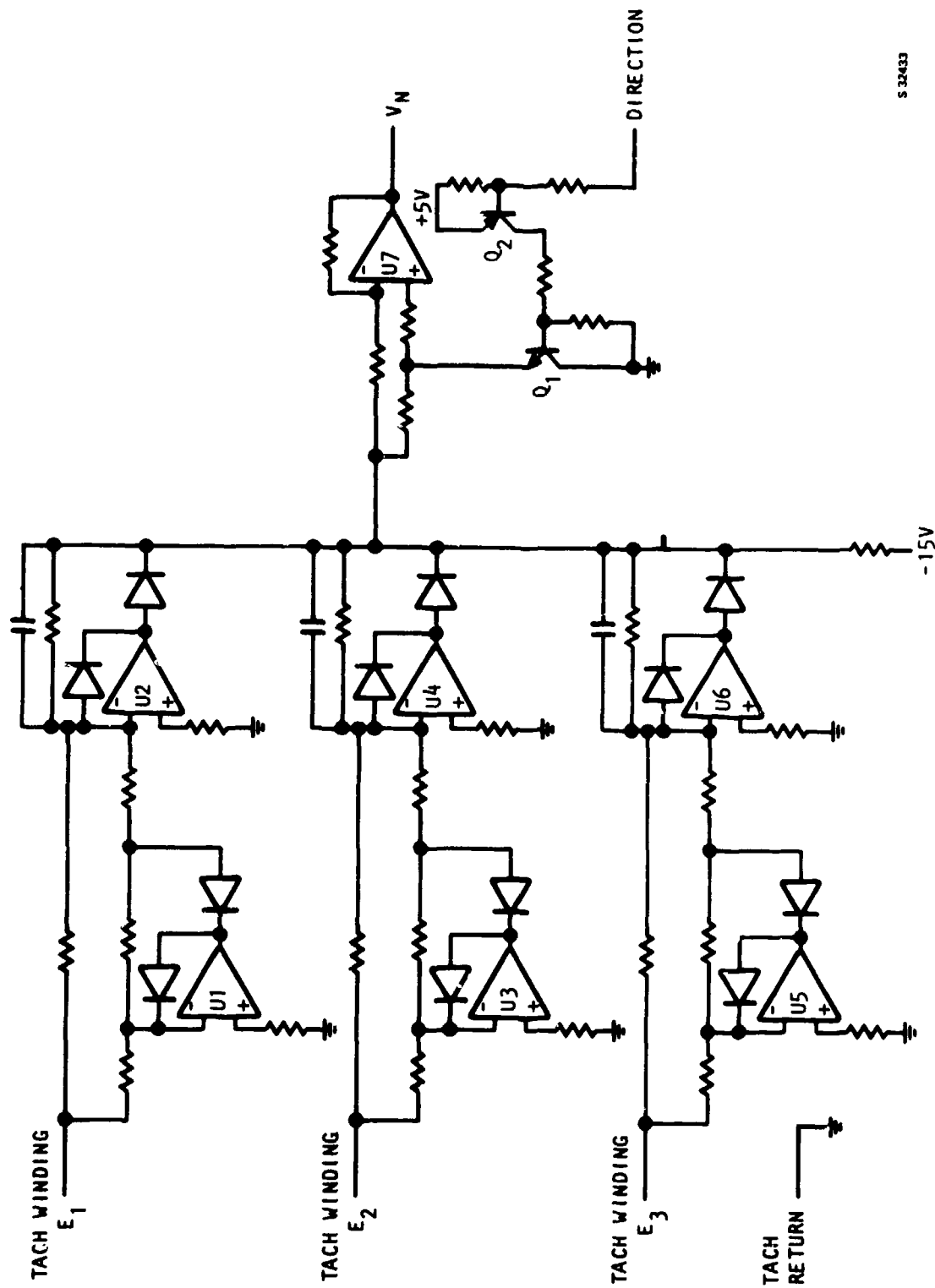
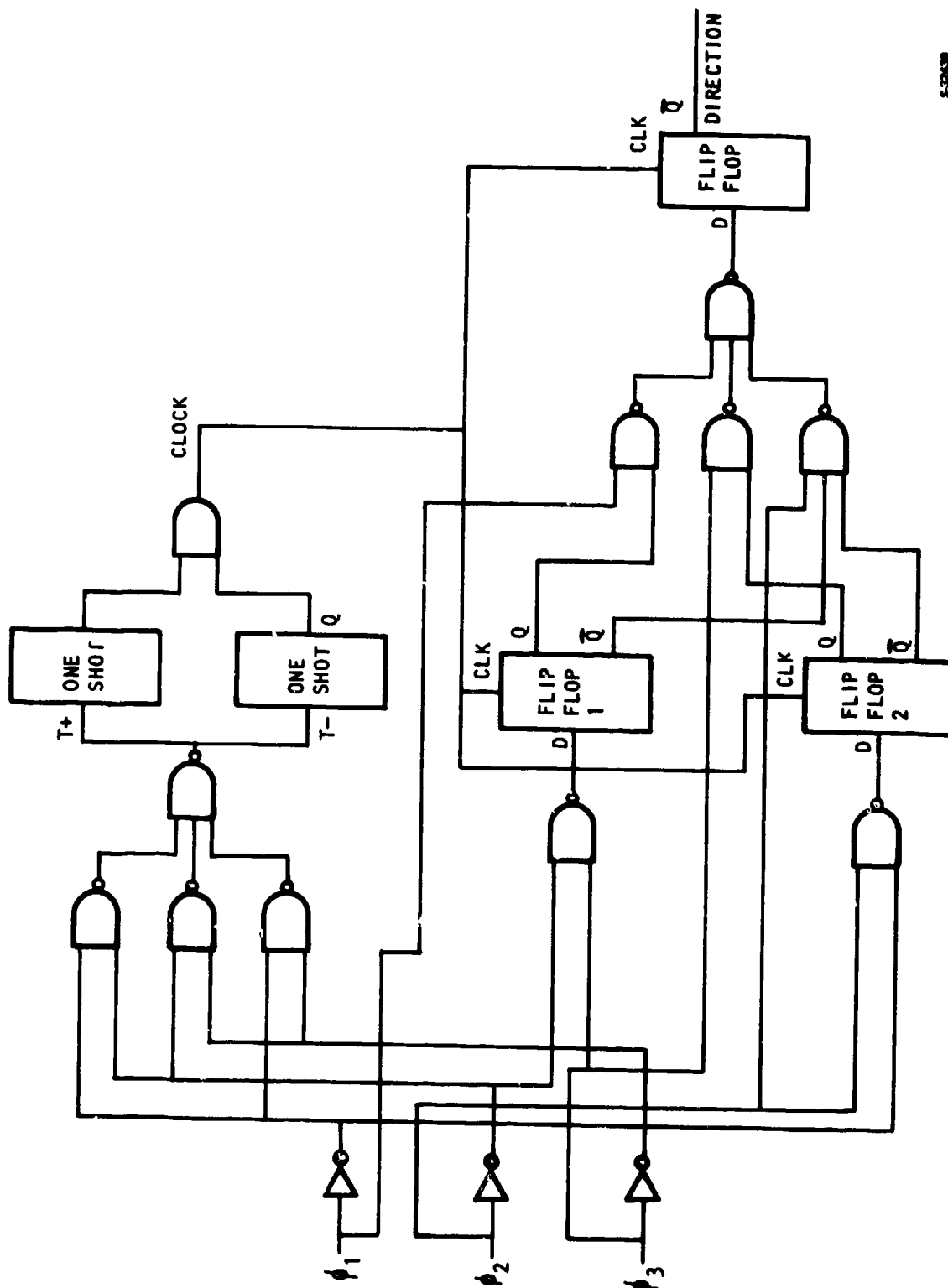


Figure 54. Rotor Speed Detection Circuit



5-20438

Figure 55. Rotor Direction Detector

- Location

- Single controller for each actuator located at the actuator
- Single controller for each actuator located at some central location
- Split controller package where the servocircuits may be located in a central location, and the power switch located at the actuator

Clearly, the specific size and weight of the controller is a direct function of the particular design approach for the location of the controller. An estimate was made, however, for the size and weight of a controller that may be representative of a generalized application. For a single-channel controller operating a single 270-vdc brushless-motor-driven actuator, the major characteristics of the controller are as follows.

- Weight, 5 lb
- Size, 150 cu in.

These weight and volume allocations include the servocircuits, power switch circuits, and provision for EMI filtering.

3.4 POSITION FEEDBACK TRANSDUCER

The actuator output position was designed to be monitored by two independent position transducers; this arrangement is shown in Figure 6 at the beginning of this section. The transducer provides control surface position information to the controller for servo loop closure. Each transducer is dedicated to a single drive channel. The transducer selected for the demonstration hardware was a digital, optical, absolute-position rotary encoder. This selection was made for the following reasons:

- Resolution of 0.1 deg of rotation
- Digital output to interface with digital microprocessor controller
- Absolute position output (as opposed to incremental output) to provide positive reference for position loop closure, even after power failures
- Rotary configuration to interface with rotary hingeline actuator configuration

A different problem statement may dictate a different transducer selection. For example, if an analog servo circuit is optimum, then a rotary potentiometer may be a more suitable match because digital-to-analog conversion would not be necessary.

The position of the encoders related to the actuator assembly, which are located close to the end of the actuator but not physically attached to it, is shown in Figure 56. As shown in Figure 2 (Section 1 of the report), the

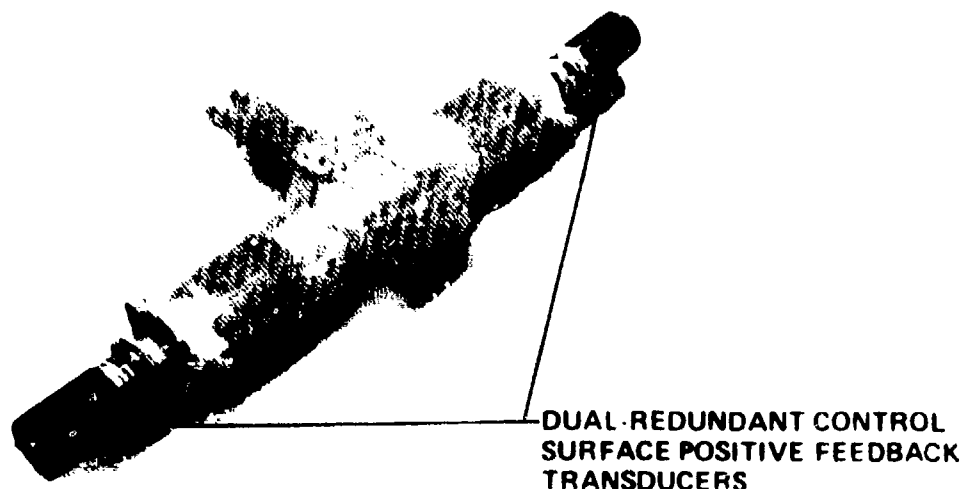


Figure 56. Hingeline Actuator Encoders

position transducers directly sense the position of the simulated control surface compared to the structural frame of the actuator support. A breakdown of position transducer parts is presented in Figure 57. The bearing and hinge point assembly serves to prevent shear loads from the test fixture being transmitted directly to the transducer shaft. The only load seen at the transducer is the rotational torque required to move the sensor assembly. The mounting flange allows the encoder to be rotated with respect to the control surface. This adjustment established a null, or zero, reference for the servo loop.

The optical encoder units were purchased from Renco Corporation, Goleta, California under PN 25AE-12GC-7A3-C3. General specifications for the encoder are presented in Table 8.

3.4.1 Encoder Interface Configuration Modifications

Operation of the actuation unit is based upon two separate servo circuits, power switches, and motors operating into the geared differential for velocity summing to the control surface. Both servo systems use the position of the control surface (based on output of the digital encoders) for closure of the servo loop. To assure stable operation, both encoders must provide nearly identical data to the separate servo loops. This requires that the encoders move in a coordinated fashion (i.e., that the support structure and simulated control surface exhibit high flexural and torsional stiffness).

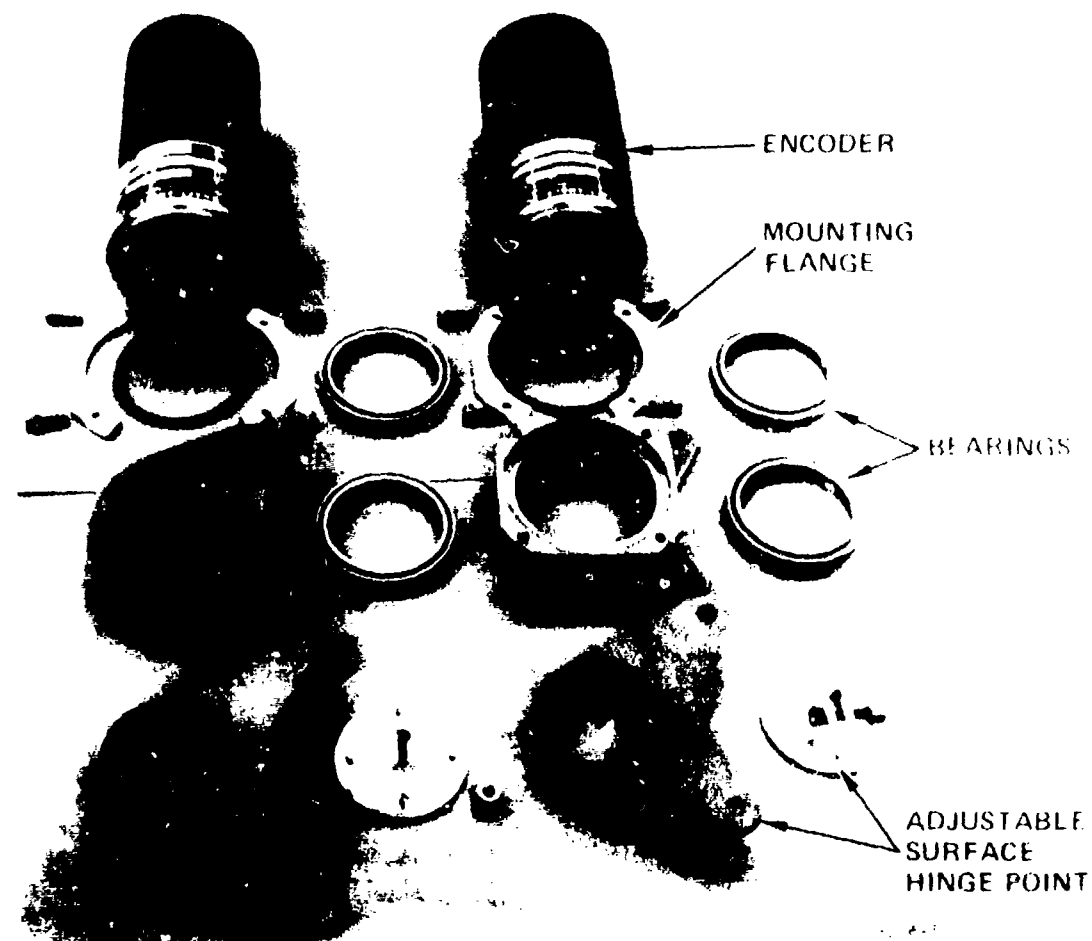


Figure 57. Optical Position Sensor Interface Parts

Early development testing and structural interface evaluation showed that the two encoders were not tracking each other because the load stand, structure, and control surface are not infinitely rigid. As a result, the two servo loops were attempting to close the position error based upon different position feedback information. The hardware was modified to eliminate one of the encoders and provide the position feedback information to both servo controllers from a single encoder. This eliminated the ambiguity of feedback position data, with minimum hardware modification.

The results of system analysis presented in para. 3.5 showed that increased position resolution was required. Therefore, the digital encoder was connected to the control surface using a gear head with a ratio of 4.48:1. This gear ratio causes the encoder to rotate 4.48 deg for each degree of control surface travel, and therefore provides digital resolution equal to $\frac{0.0879 \text{ deg}}{4.48}$, or 0.0196

deg. The 4.48:1 gear ratio comprises two identical spur gear sets. The spur gears are spring-loaded, antibacklash type to eliminate gear freeplay.

TABLE 6
SPECIFICATIONS FOR ENCODER

MECHANICAL	
Parameter	Units
Weight	18 oz
Torque without shaft seal	0.05 oz-in. starting maximum 0.05 oz-in. running maximum
Torque with shaft seal	0.9 oz-in. starting maximum 0.7 oz-in. running maximum
Axial shaft loading	1 lb
Radial shaft loading	0.5 lb applied approximately 1/8 in. from bearing
Moment of Inertia	29 gm-cm ²
Maximum slew speed without shaft seal	7500 rpm
Maximum slew speed with shaft seal	500 rpm
Materials	Cover: black anodized aluminum Front housing: iridized aluminum
ELECTRICAL	
Supply voltage	5 vdc ± 5 percent standard 6 vdc ± 5 percent optional
Supply current	400 ma plus 10 ma per channel
Pull-up resistor	1K Ω standard Open collector optional (No pullup)
OUTPUT DATA	
Resolution*	Up to 2 ¹³
Code	Natural binary or gray code
Accuracy	$\pm 1/2$ bit
LOGIC LEVELS	
Standard	Logic 1 = vcc Logic 0 = 0 v
Optional	Logic 1 = 0 v Logic 0 = vcc
Output amplitude	TTL compatible
Direction of rotation to produce an increasing count (viewing shaft end)	
Standard	Counterclockwise
Optional	Clockwise
ENVIRONMENTAL	
Operating temperature	0° to 50°C
Relative humidity	0 to 80 percent without condensation
Shock	50 g's for μ +1 msec
Vibration	Up to 2000 cps maximum
Sand, dust, and oil	Nondetrimental with shaft seal

*Implemented in control to provide 0.0879 degree resolution.

An assembly drawing of the modified encoder interface gearbox assembly is shown in Drawing 2046585. The drawing includes a parts list and designates vendor-supplied items. The encoder interface assembly is mounted on the test stand in the identical manner as the previous assembly. Figure 58 illustrates the encoder assembly disconnected from the test stand, and Figure 59 shows the components of the encoder interface assembly.

3.4.2 Alternate Encoder Interface Arrangements

High reliability is a primary consideration of the electromechanical actuation unit. Although only one encoder was used in this demonstration program for servo loop closure, redundancy could be achieved in at least two other ways. First, two separate transducers could be mounted back-to-back at the same point on the control surface in order to eliminate structural deflections between the two sensors. Although this arrangement can provide two separate feedback signals, both of which should be nearly identical, the close proximity of one to the other is undesirable when considering aircraft survivability due to battle damage, for example.

Second, a separate transducer located a distance from the first can be operated in a redundant standby mode. This standby transducer could be mounted as shown in Figure 56. In the event of a failure, the standby encoder could be activated through a fault-isolation/fault-detection network. Although this approach provides the separation of redundant elements, which is essential, the activation of the standby unit requires active logic and switching, and therefore, complexity. The method of implementation then becomes an important consideration in the reliability failure modes, effects, and overall reliability philosophy.

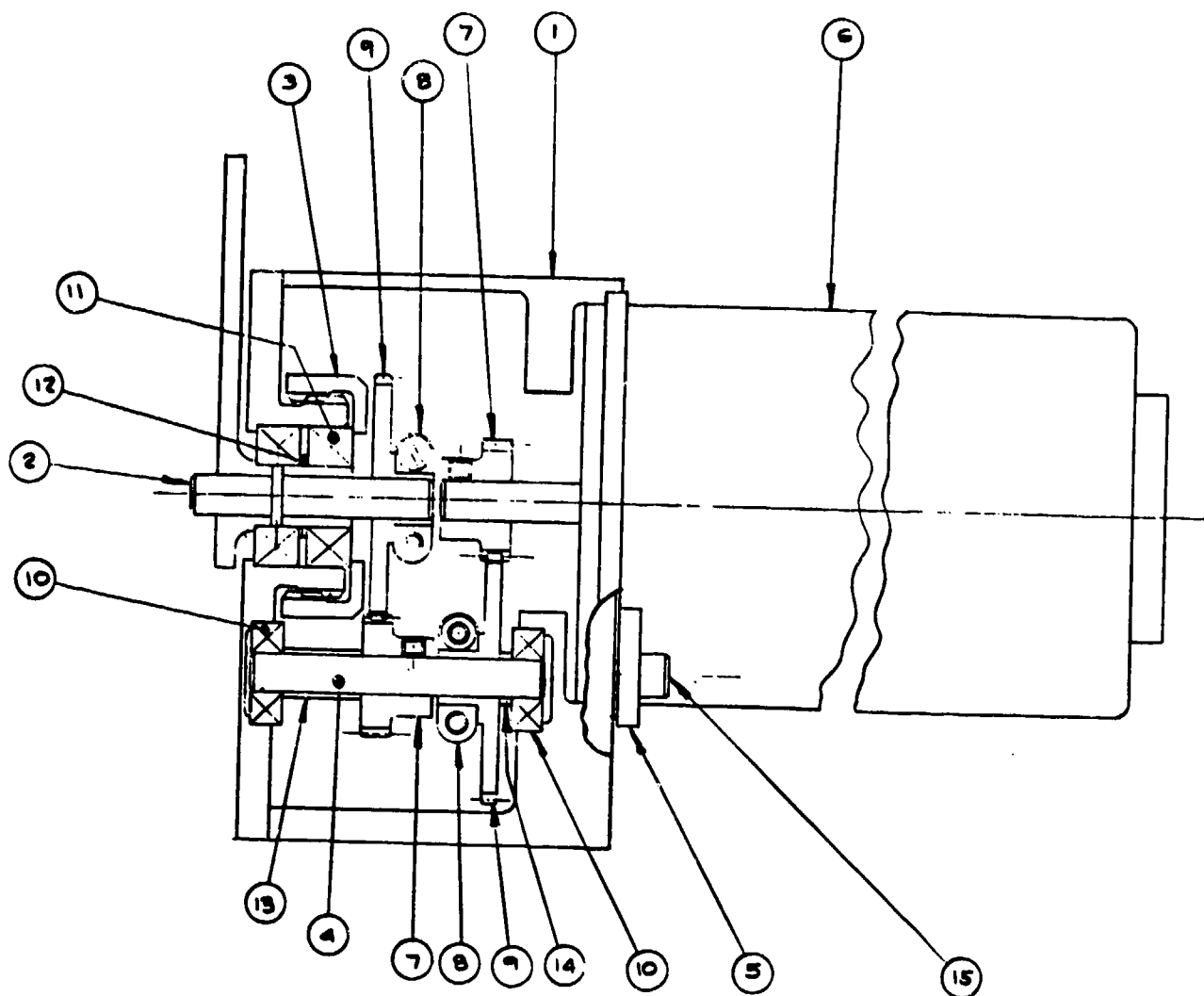
3.5 DYNAMIC ANALYSIS AND SYSTEM SIMULATION

The performance of the electromechanical actuation unit was predicted in Reference 1 using analog simulation techniques. To support the development of the demonstration hardware and to determine the specific control servo characteristics, a digital computer program was developed. The program contains simulation of the controller, actuator, power source, and load, and was used as a tool to evaluate (1) predicted performance, (2) operating sensitivity to selected component characteristics, and (3) suitability of candidate control laws to satisfy unit operating goals.

The following paragraphs briefly describe the AIResearch developed computer program, discuss the correlation of analytical prediction to test results, and present optimized control law configurations for typical flight control system requirements.

3.5.1 Approach to Simulation for Laboratory Hardware

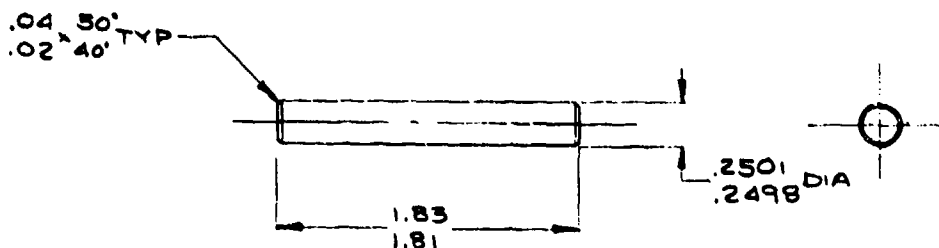
The key to simulation of the electromechanical actuation unit performance is development of the proper plant. Analysis of the plant simulations, including both static and dynamic performance, assures control components that are properly defined. The use of digital simulation techniques allows resolution of performance problems prior to hardware development, significantly reducing



- 3 MFD BY RENCO CORP. GOLETA
 2 MFD BY PIC DESIGN CORP.
 VAN NUYS, CALIFORNIA
 1 MFD BY NEW DEPARTURE. BRISTOL
 CONN

NOTES: UNLESS OTHERWISE SPECIFIED

PAGE NO		2046585		BY	REV	1	
REVISIONS							
TIME	LTR	DESCRIPTION			DATE	APPROVED	R.



DETAIL OF ITEM 4 (2046395-3)
SCALE: 2/1

[illegible]

GOLETA, CAL.

CORP.

BRISTOL.

IFIED

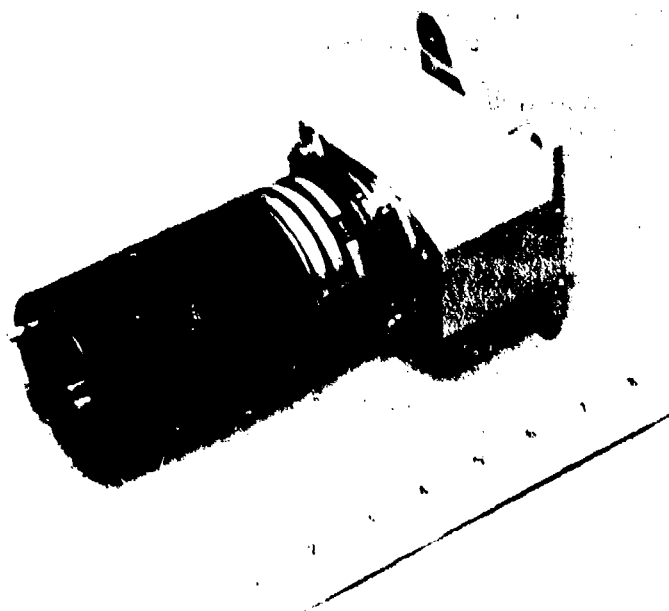


Figure 58. Assembled 4.48:1 Gearbox for Increased Encoder Resolution

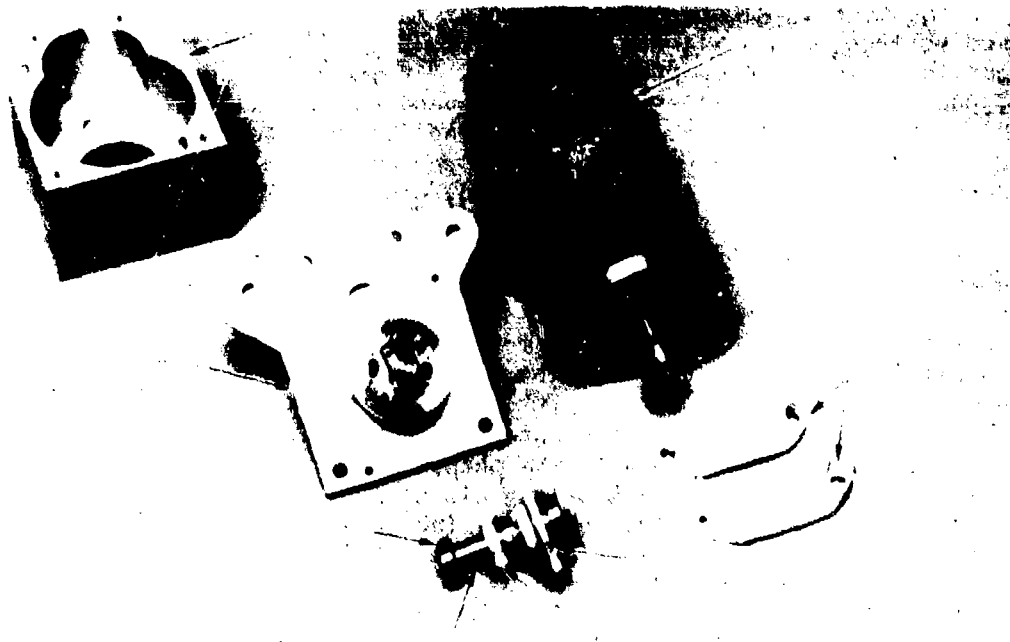


Figure 59. Encoder Gearbox Component Breakdown

F-27990

overall development costs by limiting the required testing to support the plant-control integration development phase.

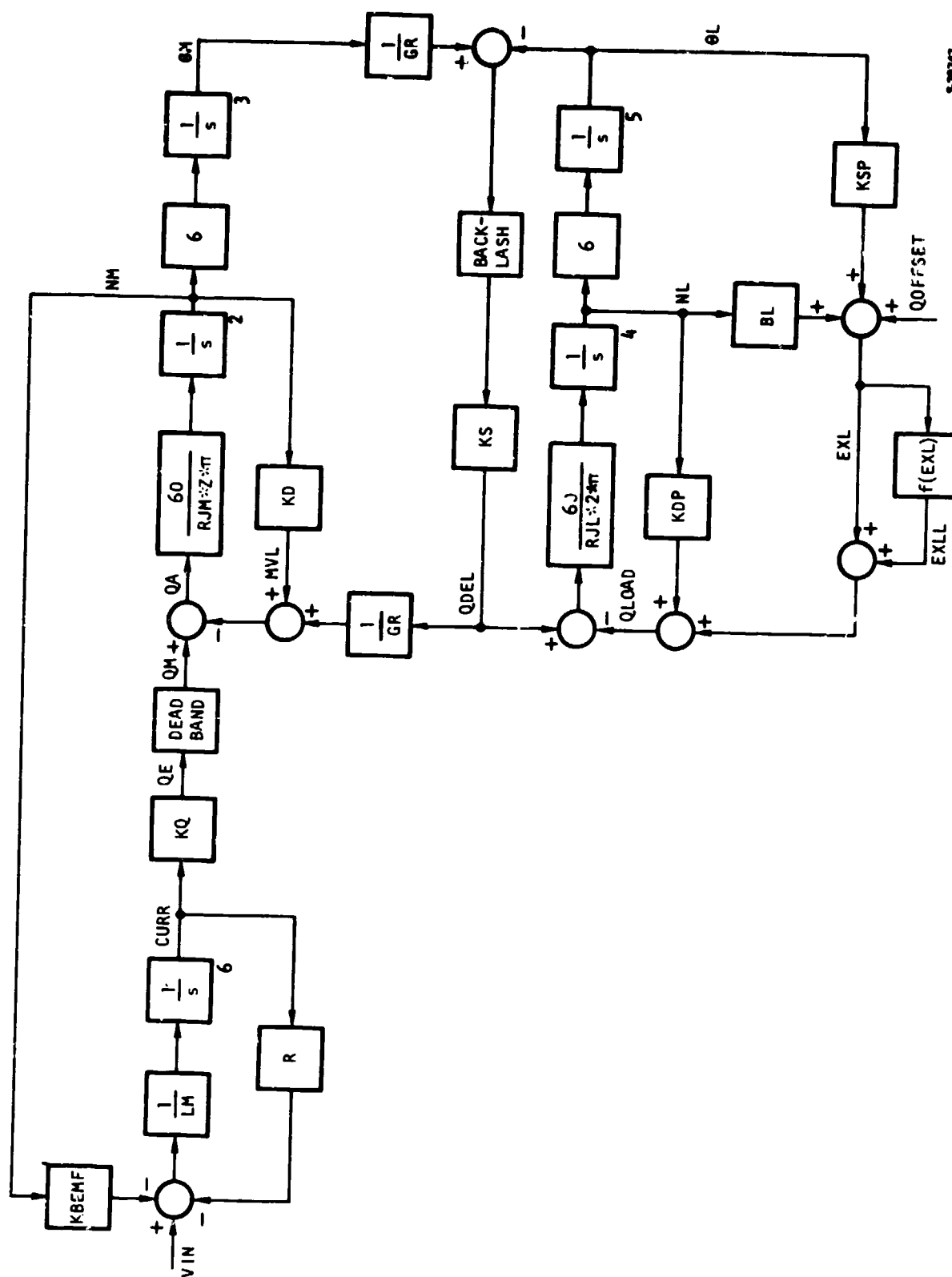
The procedure employed for control synthesis is to develop a linear model of the plant. From this model it is possible to generate (1) open-loop harmonic response in the form of computer-plotted Bode characteristics, (2) Nichols loci, and (3) Nyquist loci. The controller is then added to the simulation and developed until satisfactory bandwidth, stability, and resonance ratios are achieved. At this point control algorithms with nonlinearities added are incorporated into the simulation. System performance is evaluated by observing the response to step and sinusoidal inputs as well as to load disturbances. Necessary refinements are then made to offset adverse effects caused by the added nonlinearities. In some cases, an alternate control scheme may be required. When hardware becomes available, the model performance is checked against the experimental results. Changes may be required in either the model, hardware, or both until correlation has been achieved. If the model is found faulty, additional control work may be required to produce satisfactory performance. The developed model is then particularly useful for evaluating anticipated hardware component changes and in the prediction of hardware performance when operating at loads and conditions other than those originally specified.

3.5.2 Model Description for Laboratory Hardware

The digital simulation program contains several options which provide flexibility necessary for the modeling of a variety of controller-motor-gearing configurations. Figure 60 shows the elements of this program that have been used in the model. Algebraic summation of the voltages involved (i.e., the applied voltage, back emf, and IR drop) produces the inductive term that, upon integration, yields motor current (CURR). In the model of the demonstration unit, additional logic is included to prevent current flow in a direction opposing the PWM control voltage. Deadband is incorporated in the model by using finite levels of electrical torque and motor speed that are required before mechanical torque (QM) is produced, and as a result, rotor breakaway.

The torque available for acceleration of the motor rotor (QA) is derived by subtracting a motor viscous loss torque (MVL) and the torque delivered to the gearbox (QDEL), referred to the motor from QM. Unit conversion and consideration of the motor inertia (RJM) produces motor speed (NM) after integration of the acceleration rate. An additional integration provides motor shaft angle (QM).

The motor shaft angle, after referral to the output shaft through the gear ratio (GR), is then compared with the output shaft angle (θ_L). The difference in angle is transmitted via a backlash discontinuity to the overall system spring constant. Twist of the spring is indicative of the torque being delivered to the gearbox (QDEL). The load torque (QLOAD) consists of the sum of the external load(s) applied to the gearbox and the internal gearbox losses. The external loads take three forms. An aerodynamic load is simulated by a grounded spring with rate KSP, so that the load is proportional to output shaft angle. A viscous load that is proportional to speed (with the magnitude dependent on the value of BL) simulates the load that has been applied to the hingeline system in the laboratory. A constant load can be imposed by assigning a value to



S-25747

Figure 60. Model Block Diagram

QOFFSET. Losses within the gearbox are composed of two types: (1) the viscous form, which is dependent on load speed (NL) and damping coefficient (KDP), and (2) loss EXLL, which is dependent on the level of the combined external loads (EXL). The EXLL loss includes a dry friction offset term. Logic is included in the model so that EXLL always opposes rotation of the output shaft. However, if the system is at rest and an external load is applied, no torque appears at QLOAD until the offset term has been exceeded; thereafter, as would occur when the load is driving the motor actuator, the EXLL losses are subtracted from the external load.

Subtraction of QLOAD from QDEL yields the torque available for acceleration of the load. The rate of acceleration of the load shaft is obtained from the acceleration torque and the load inertia (RJL) with appropriate conversion constants to obtain output shaft speed (NL) in rpm after integration. A second integration provides the output shaft angle (θ L).

The variables, constants, and units are summarized in Table 9.

3.5.3 Correlation Control Synthesis for Laboratory Hardware

As the initial step in the control synthesis, the actuator and load were modeled using the linear digital program. The elements modeled were the same as depicted in Figure 60, with the nonlinearities eliminated. The load inertia had a value of 2.55 in.-lb-sec² to simulate the demonstration fixture, compared to the specification value of 46.6. This approach assured direct correlation between the test data from the laboratory evaluation and the analytical predictions of performance.

The open-loop Nichols locus shown in Figure 61 was then generated with a gain of 40 db added to conveniently locate the locus within the range of the plotter coordinates.

The initial position control was then synthesized, and is shown in block diagram form in Figure 62. The forward loop contains an integrator to ensure steady-state accuracy, while the strong lead term provides a form of proportional plus integral control. The short lag in the forward loop is intended to filter out noise emanating from the encoder position sensor. As shown by the Nichols locus in Figure 63, an additional lead-lag in the feedback causes a peak in the phase shift at about 70 rad/sec and maintains a bandwidth in excess of the required 8 Hz. The integrator gain was set by making the locus tangent to the 2.3 db contour, thus establishing a resonance ratio of about 1.3.

The foregoing control was then incorporated into the nonlinear motor model and evaluated by stepping the input command to the controller. A stable limit cycle at a frequency of 13 Hz was present. To counter this condition, an additional compensating network (as shown on Figure 64) was incorporated in the forward loop. A time constant ratio of three was selected, with the absolute values determined so that maximum phase occurs at 13 Hz. At the same time, the forward loop gain was adjusted to offset the effect of the lead-lag network. This configuration proved to be stable under all conditions evaluated and has been incorporated into the breadboard controllers.

TABLE 9

SIMULATION CONSTANTS AND NOMENCLATURE

Term	Definition
BACKLASH	± 0.045 deg
BL	Load damping coefficient, in.-lbf/deg
CURR	Motor current, amp, range ± 16
DEADBAND	in.-lbf, 2.3 and rpm, 10
EXL	Total external load torque, in.-lbf
EXLL	Load losses, in.-lbf, $EXLL = 0.0000119 (EXL)^2 + 1223$
GR	Gearbox speed ratio, 1254:1
KBEMF	Motor back emf, v/rpm, 0.028342
KD	Motor damping coefficient, in.-lbf/rpm, 0.0001476
KDP	Load damping coefficient, in.-lbf/rpm, 232.1
KQ	Motor torque-current constant, in.-lbf/amp, 2.3
KSP	Ground spring, in.-lbf/deg, 1252.5 at 100 percent load
KS	Overall spring rate, in.-lbf/deg, 56,723
LM	Motor inductance, henry, 0.00155
MVL	Motor viscous damping torque, in.-lbf
NM	Motor shaft speed, rpm
QA	Motor shaft acceleration torque, in.-lbf
QDEL	Torque delivered to gearbox, in.-lbf
QE	Motor electrical torque, in.-lb:
QLOAD	Overall gearbox load torque, in.-lbf
QOFFSET	Constant external load torque, in.-lbf
RJL	Load inertia, in.-lbf-sec ² , 2.55
RJM	Motor inertia, in.-lbf-sec ² , 0.0012651
s	Integration symbol
θ_L	Output shaft angle, deg
θ_M	Motor shaft angle, deg
VIN	Motor input voltage, v, range ± 270

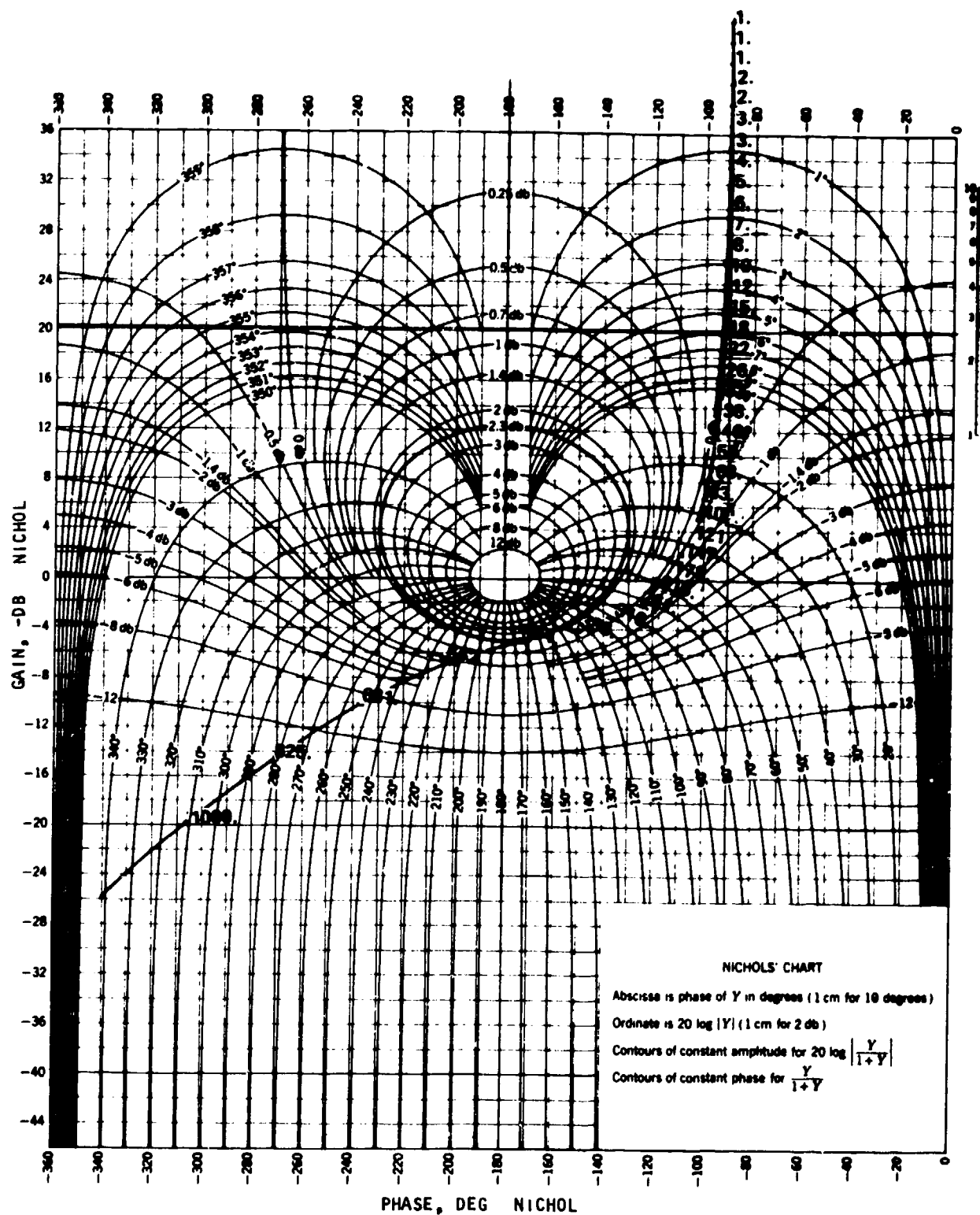
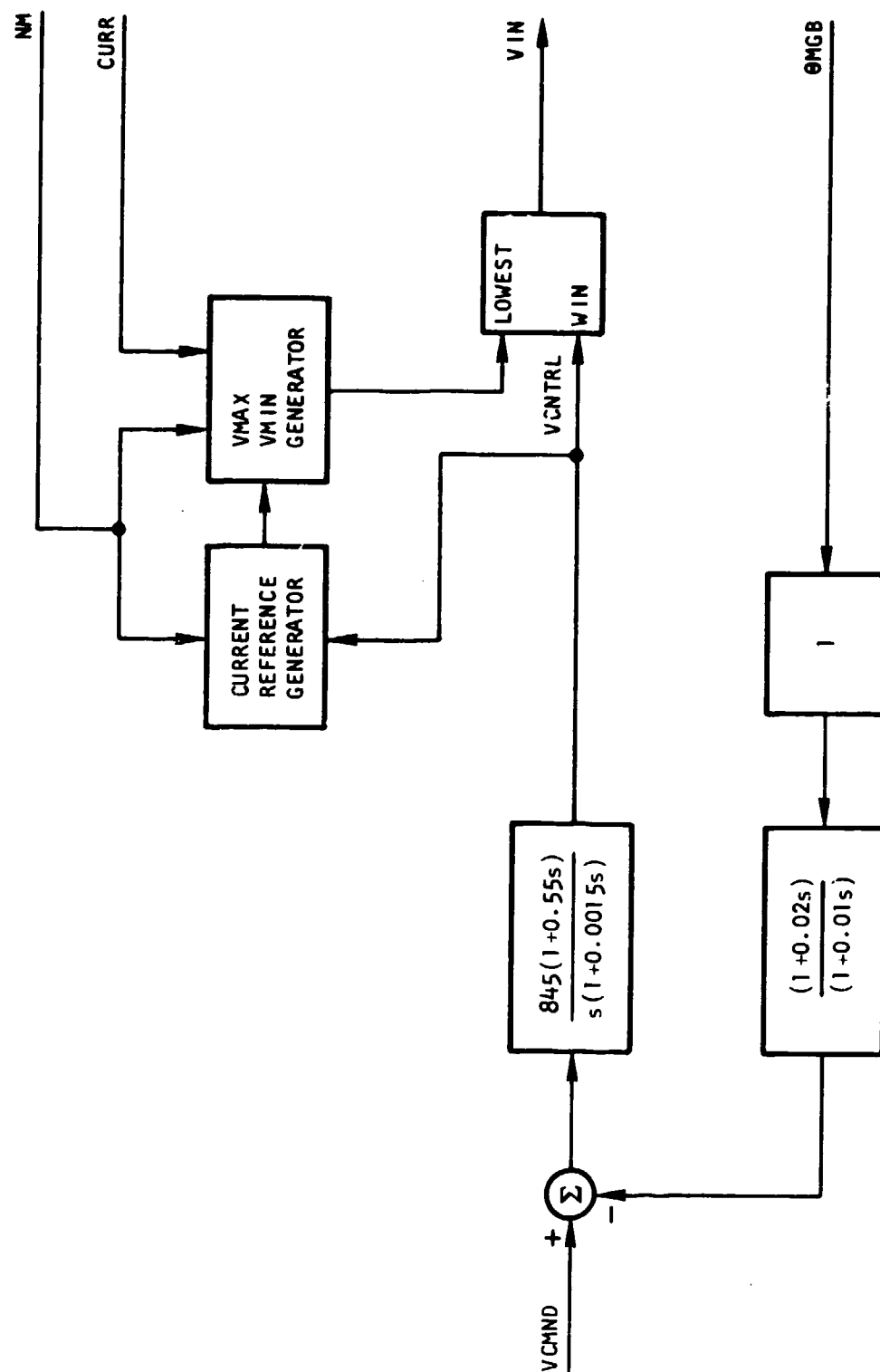


Figure 61. Open-Loop Nichols Locus Diagram



2-39746

Figure 62. Initial Control Block Diagram

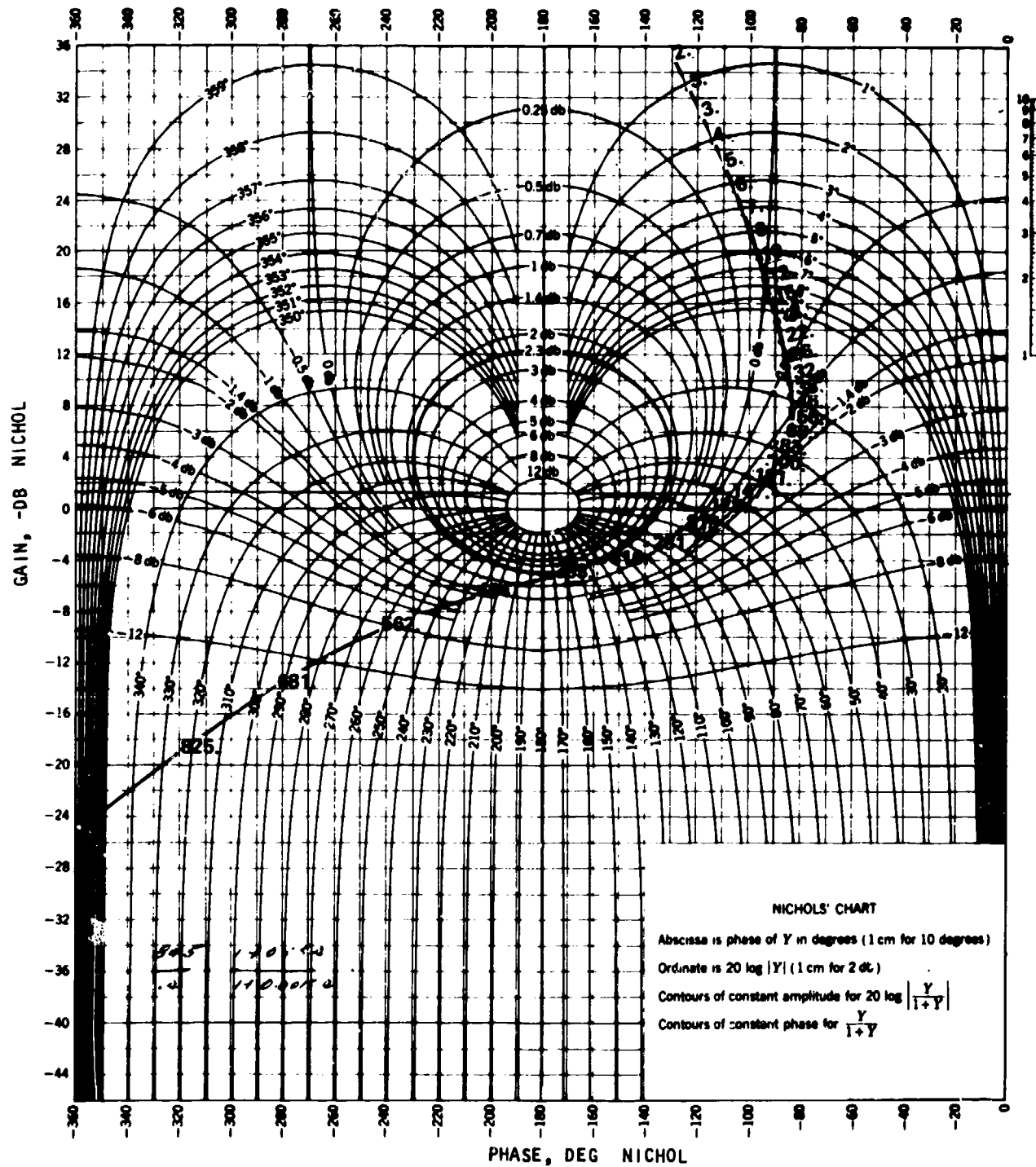
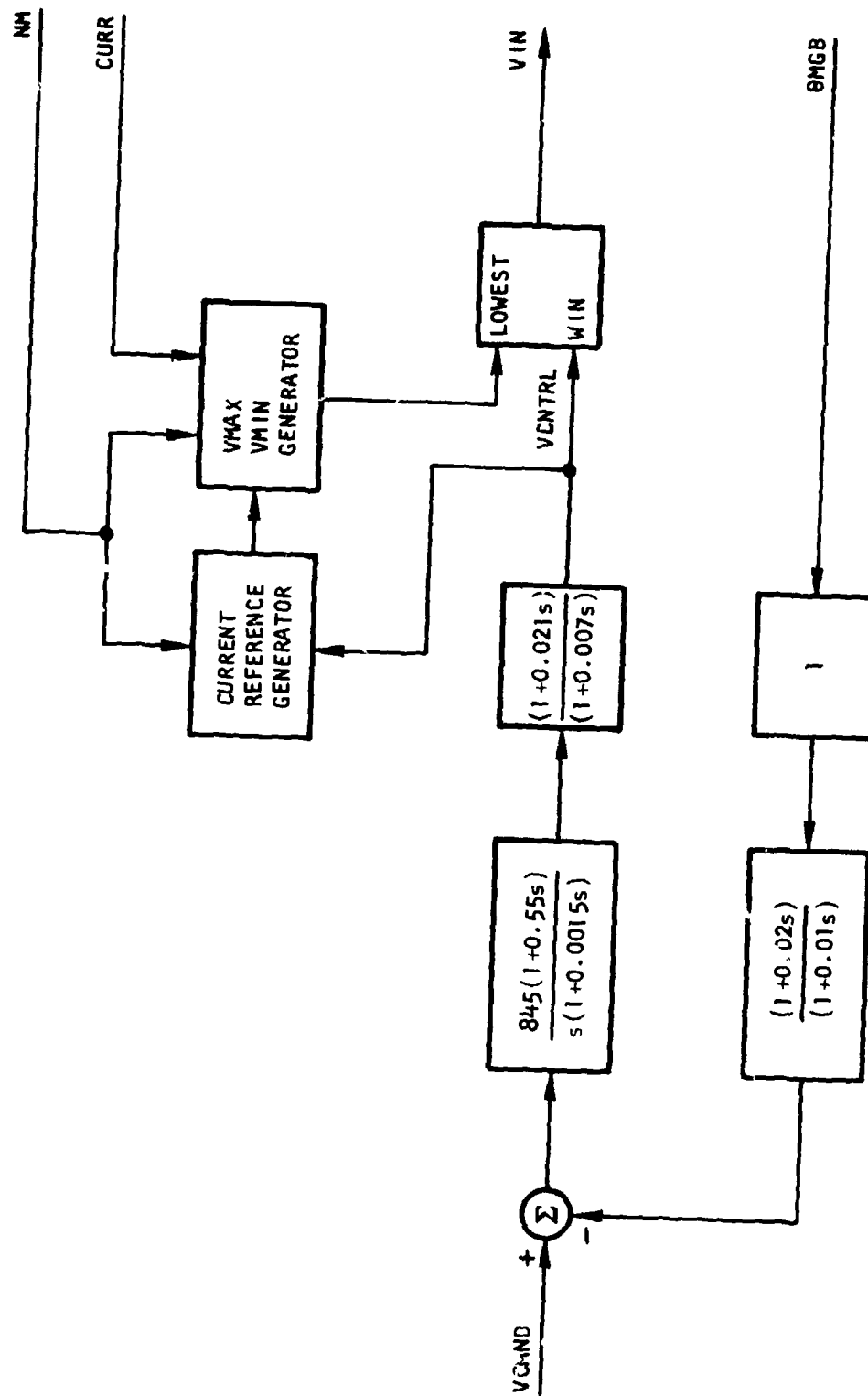


Figure 63. Modified Nichols Locus Diagram



S-29746

Figure 64. Improved Control Block Diagram

The simulation includes modeling the motor current control. During the normal motoring mode, the current reference is constant when the motor speed is higher than 4150 rpm. At lower speeds, the reference is a function of actual speed. However, logic is included to preclude current flow in a direction opposing the PWM control voltage (VCNTRL). Other logic establishes a different set of current limits when the motor rotational sense is opposite to that of VCNTRL. In all cases, current control is obtained by calculating the motor voltage that will prevent the current from exceeding the prevailing reference. The actual motor voltage is the lower, in an absolute sense, of the position control voltage (VCNTRL) or the current limit voltage (VMAX or VMIN).

The following paragraph (3.5.4) presents the results of correlation of the developed analytical simulation model to the test results using the laboratory electromechanical actuation hardware unit.

3.5.4 Data Correlation for Laboratory Demonstration Hardware

To verify the motor-actuator-control model, a comparable set of transients was run using the demonstration hardware for comparison with the results of the analytical model. Both single-channel and dual-channel no-load operation was employed for all transients as described in Appendix F. Input command steps were made with amplitudes of 1, 5, and 10 deg. Harmonic response was evaluated with sinusoid commands with 2-deg peak-to-peak amplitude and at frequencies of 0.5, 1.0, 2.0, 4.0, 6.0, 8.0, and 10.0 Hz. The results of step response tests recorded on an oscillograph are compared with the corresponding analytical model results.

The results of the step command runs, using the voltage servo control, are summarized in Table 10 and shown in Appendix G. The time to reach the command position, the percent overshoot, and the settling time (to within 1 percent of the commanded position) are listed. The data for time to reach the commanded position agree well, which indicates that the model is valid with respect to the motor-actuator. However, the model exhibits considerably greater overshoot and longer settling times, which are two related parameters. This difference is believed to be due to the presence of an additional lead term with a value of approximately 0.020 sec in the feedback loop of the hardware.

The frequency response results for both the hardware and the model are shown in Bode plot form in Figure 65. The test results were obtained by the use of a harmonic analyzer in which the fundamental of the output wave is separated using Fourier techniques and then compared with the input on an amplitude ratio and phase shift basis. The phase shift in the model results was derived by noting the shift at the zero crossover, while the amplitude ratio was based on the maximum amplitude observed. Agreement exists between the two sets of results, although the bandwidth obtained experimentally is somewhat narrower. This is believed to be due to a combination of the effects of the additional lead term in the hardware and to the use of the fundamental amplitude versus the actual wave shape peak.

Similar data were collected and compared for dual-channel operation using the voltage servo control. The step response summary is shown in Table 11. The correlation of analysis with the test data shows good agreement. These data were taken at a no-load condition at the actuator output. Figure 66

TABLE 10

SUMMARY OF SINGLE-CHANNEL STEP RESPONSE CORRELATION
(Based on Voltage Servo Control)

Parameter	Computer Simulation			Laboratory Demonstration Hardware		
	1 deg	5 deg	10 deg	1 deg	5 deg	10 deg
Time to reach the command position, sec	0.098	0.160	0.282	0.1	0.15	0.3
Percent overshoot	6.0	9.5	5.0	5.0	7.0	3.5
Settling time, sec	>1.0	0.716	0.800	-	-0.8	0.7

TABLE 11

SUMMARY OF DUAL-CHANNEL STEP RESPONSE CORRELATION
(Based on Voltage Servo Control)

Parameter	Computer Simulation			Laboratory Demonstration Hardware		
	1 deg	5 deg	10 deg	1 deg	5 deg	10 deg
Time to reach the command position, sec	0.11	0.1	0.16	0.13	0.11	0.16
Percent overshoot	5.0	9.0	9.0	4.0	8.0	6.0
Settling time, sec	>1.0	>1.0	>1.0	--	>1.0	>1.0

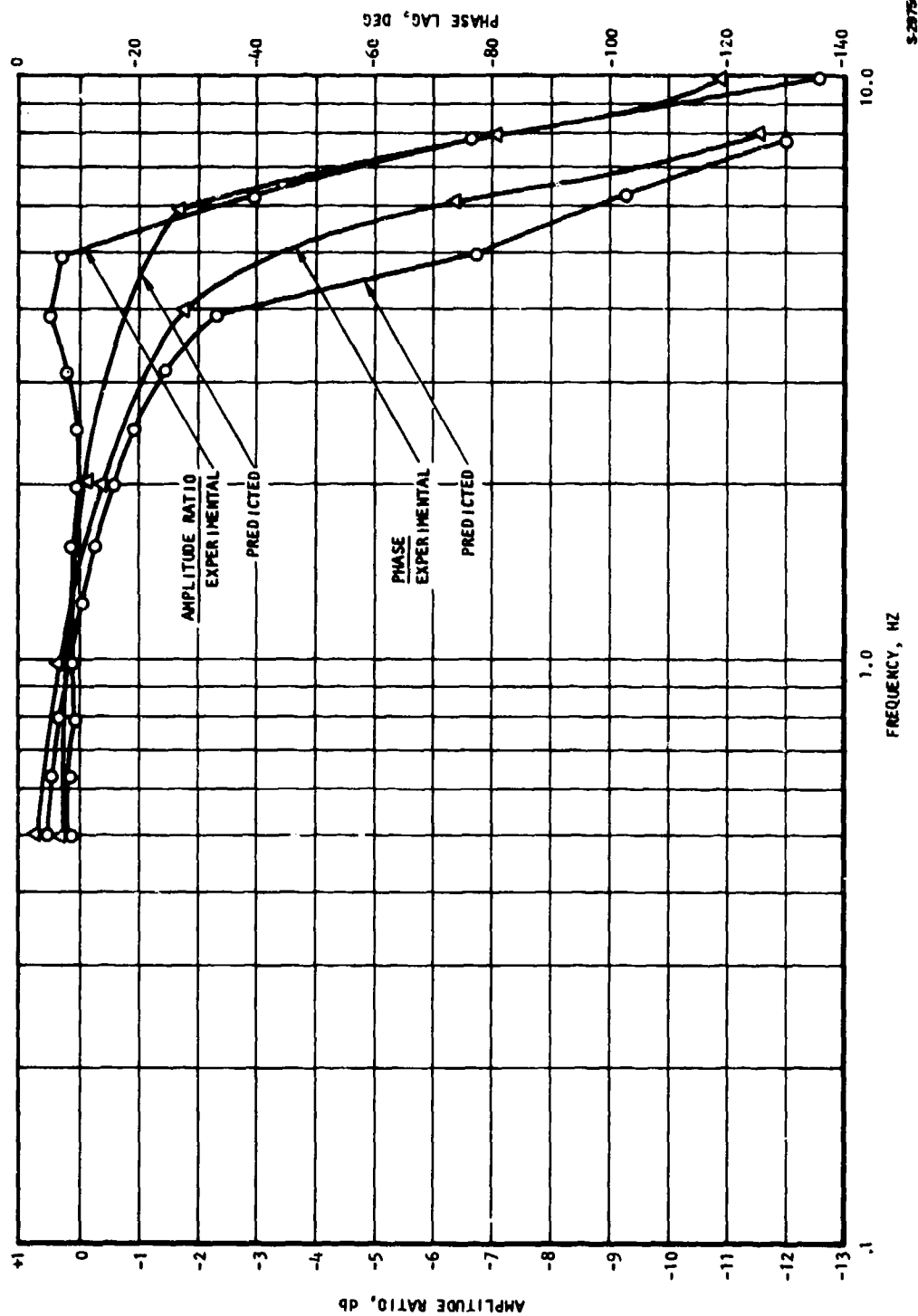


Figure 65. Frequency Response Comparison for One-Channel, No Load, ± 1 Deg Amplitude, Voltage Servo Control

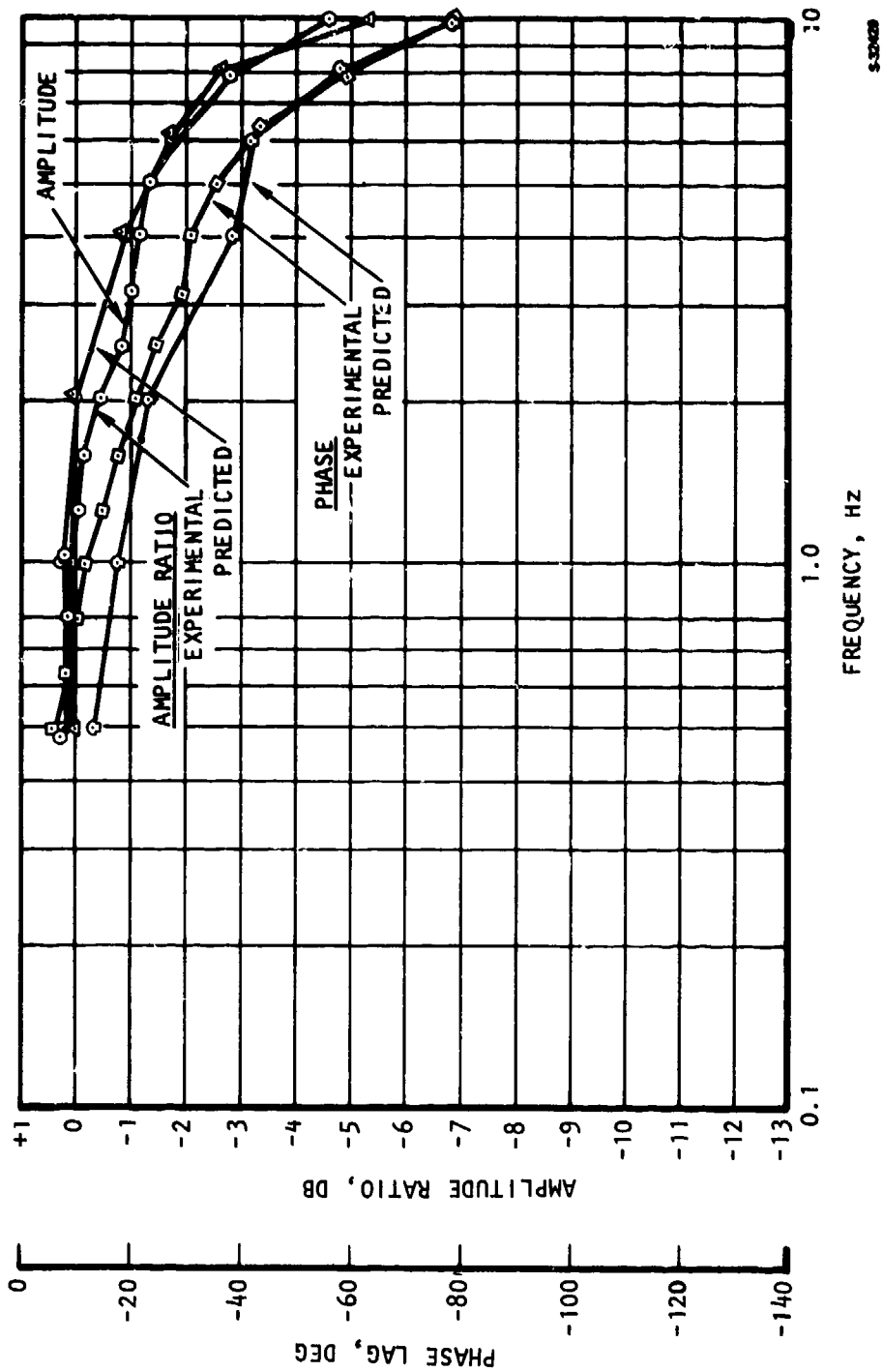


Figure 66. Frequency Response Comparison for 2-Channel, No-load, ± 1 Deg Amplitude Voltage Servo Control

shows the Bode plot comparison of the two-channel operation, based on ± 1 deg amplitude, and no-load at the actuator output. Again, correlation of test and analytical results shows good agreement.

The analytical model was modified to simulate a servo control configuration including tachometer feedback (refer to Section 3.3). This modification was made to correspond to the servo hardware changes. Table 12 presents the comparison of predicted step response to the actual step response using the modified tachometer feedback control. Figure 67 presents the comparisons of the frequency response Bode plots obtained from the analysis and from the operation of the demonstration hardware.

The conclusion is that an analytical model has been developed that has sufficient versatility and accuracy to be of value in predicting performance of electromechanical actuation hardware.

TABLE 12

SUMMARY OF DUAL-CHANNEL STEP RESPONSE CORRELATION
(Based on Tachometer Feedback Servo Control)

Parameter	Computer Simulation			Laboratory Demonstration Hardware		
	1 deg	5 deg	10 deg	1 deg	5 deg	10 deg
Time to reach the command position, sec	0.08	0.1	0.154	0.08	0.11	0.16
Percent overshoot	3.1	10	8.1	5.0	7.0	6.0
Settling time, sec	0.27	0.23	0.28	0.18	0.16	0.23

3.5.5 PREDICTED PERFORMANCE FOR LABORATORY HARDWARE, TACHOMETER SERVO CONTROL

To complete the performance prediction for the 2-channel, tachometer feedback servo configuration, Figures 68 and 69 show the Bode plots for the 30 and 50 percent loaded conditions. The loads are defined as 30 percent of maximum load (where maximum load is 37,575 in.-lb) at a deflection angle of 30 deg. The load is modeled as a linear spring with a constant of 375.7 in.-lb/deg. Similarly, the load for the 50-percent case, (Figure 69) is a linear spring with a constant of 626.3 in.-lb/deg.

Dynamic stiffness of the actuator has also been evaluated analytically for the laboratory hardware. Figure 70 presents the predicted results of exciting the output with a sinusoidal load and monitoring the response of the system. During this time the controller is active and is responding to an input command representing a fixed, null position. The figure also shows the predicted and actual static stiffness values for comparison with the dynamic stiffness.

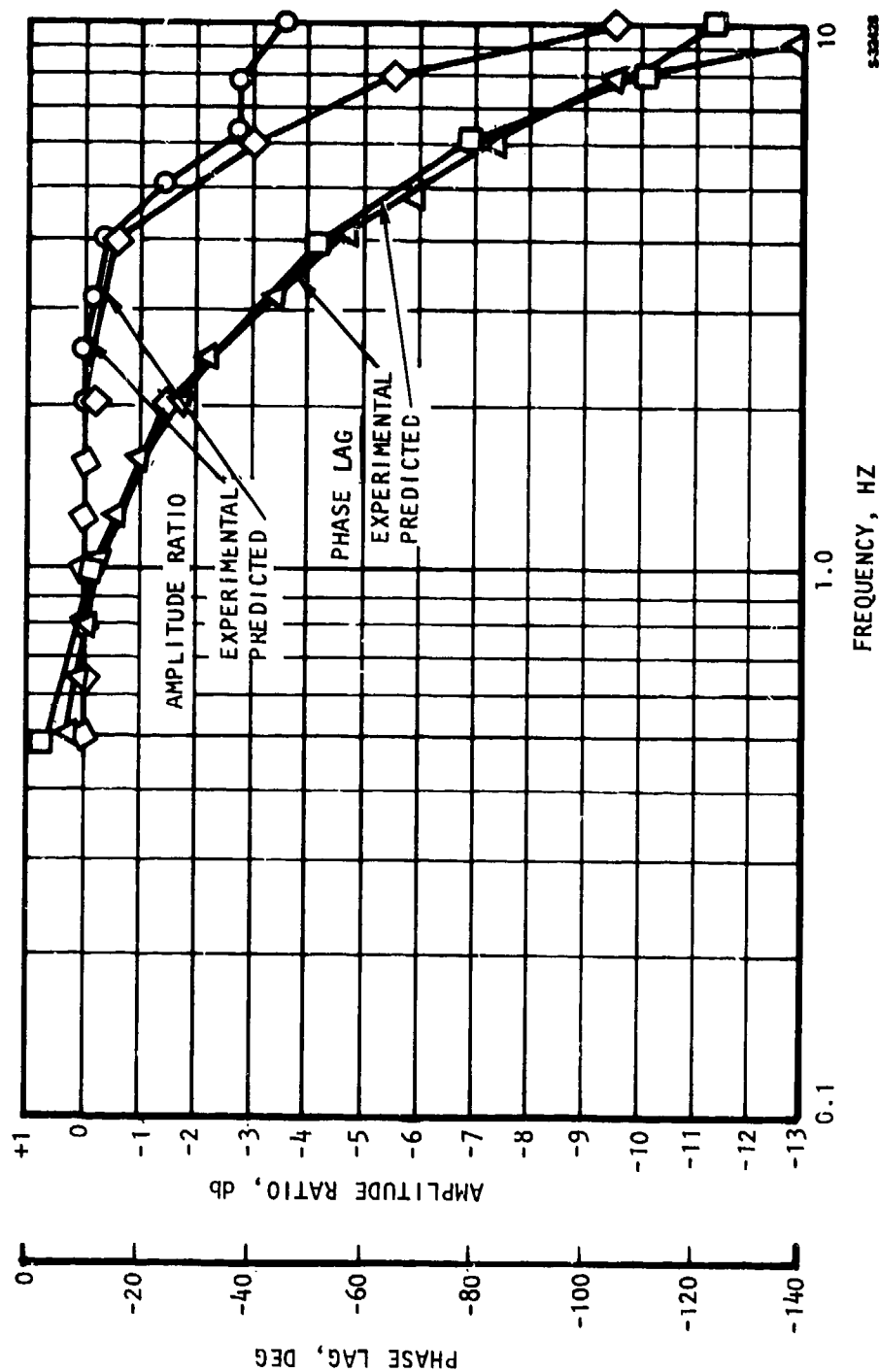


Figure 67. Frequency Response Comparison for 2-Channel, No-Load, +1 deg Amplitude, Tachometer Feedback Servo Control

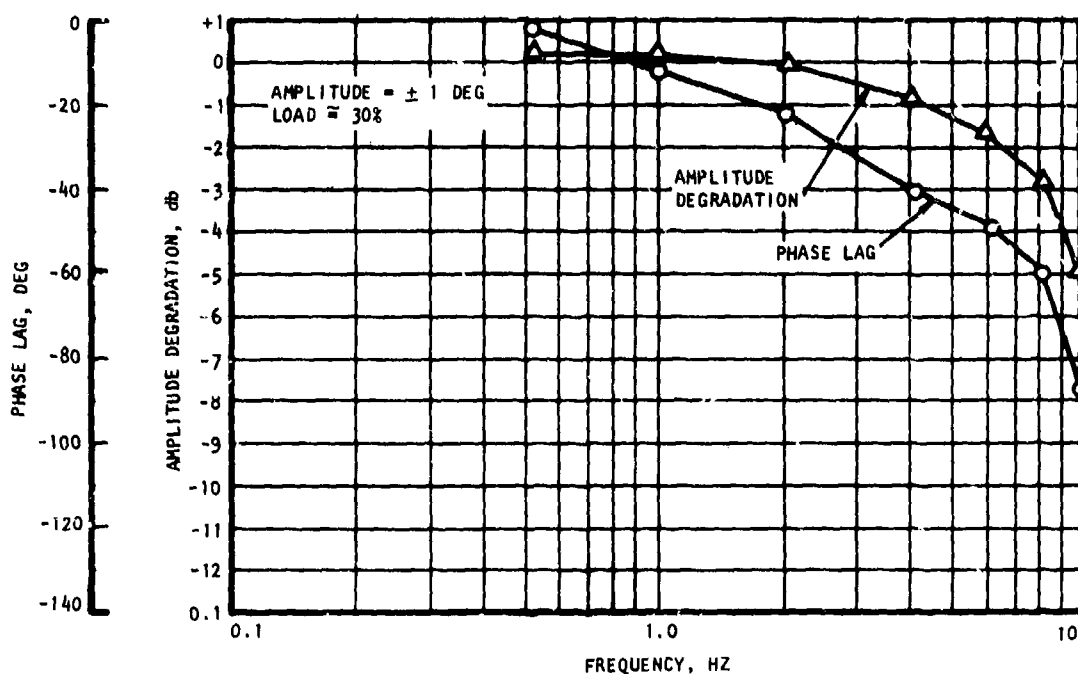


Figure 68. Frequency Response for 2-Channel, Tachometer Feedback ± 1 Deg Amplitude, 30-Percent Load

8-32426

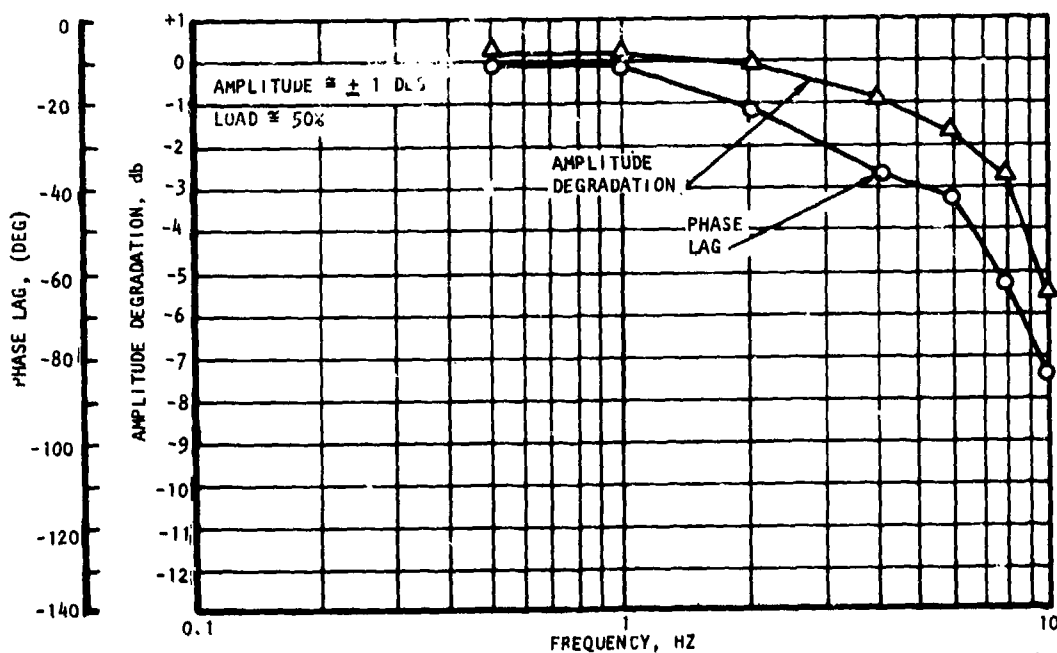
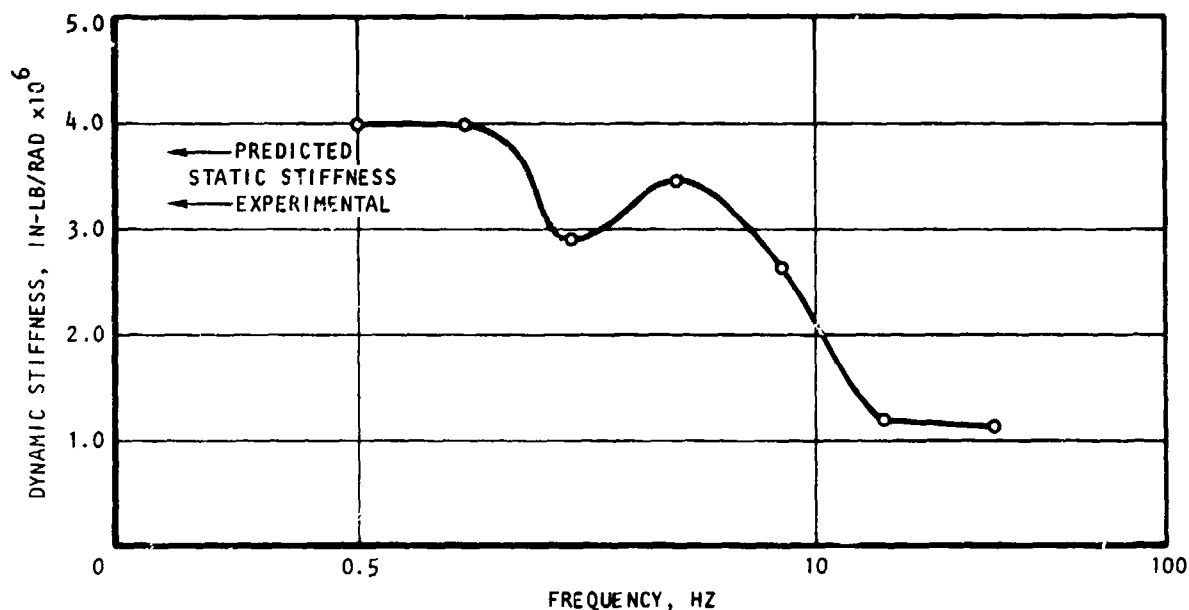


Figure 69. Frequency Response for 2-Channel, Tachometer Feedback ± 1 Deg Amplitude, 50-Percent Load

8-32427



S 32426

Figure 70. Dynamic Stiffness, Tachometer Feedback

Figure 71 shows the results of prediction of the actuation unit when subjected to gust loads. A 50-percent steady-state aerodynamic load is assumed.

The figure shows that a position pulse load (an additional 10 percent) is applied for 10 msec, and the response of the system is stable. Then a negative pulse load is applied, and again the system is shown to react to the load in a stable manner.

3.5.6 Control Synthesis for Baseline Problem Statement Load Inertia

The laboratory demonstration hardware and test stand (as fabricated) resulted in an effective load inertia of 2.55 in.-lbf-sec². The baseline problem statement includes a control surface inertia of 46.6 in.-lbf-sec², or approximately 20 times the inertia of the laboratory test stand. The parameters of the tachometer feedback servo control then were re-evaluated to better match the increased load inertia.

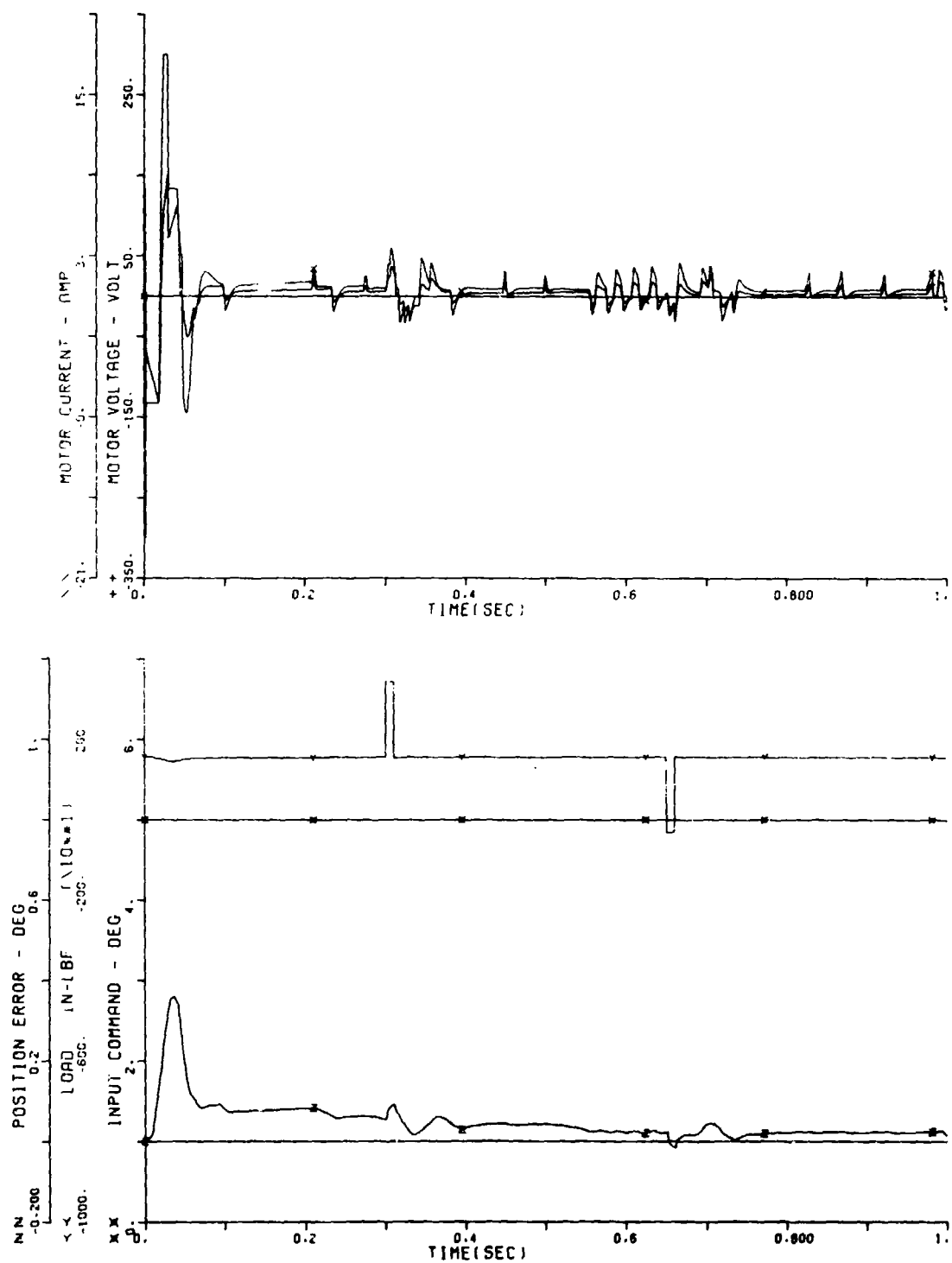
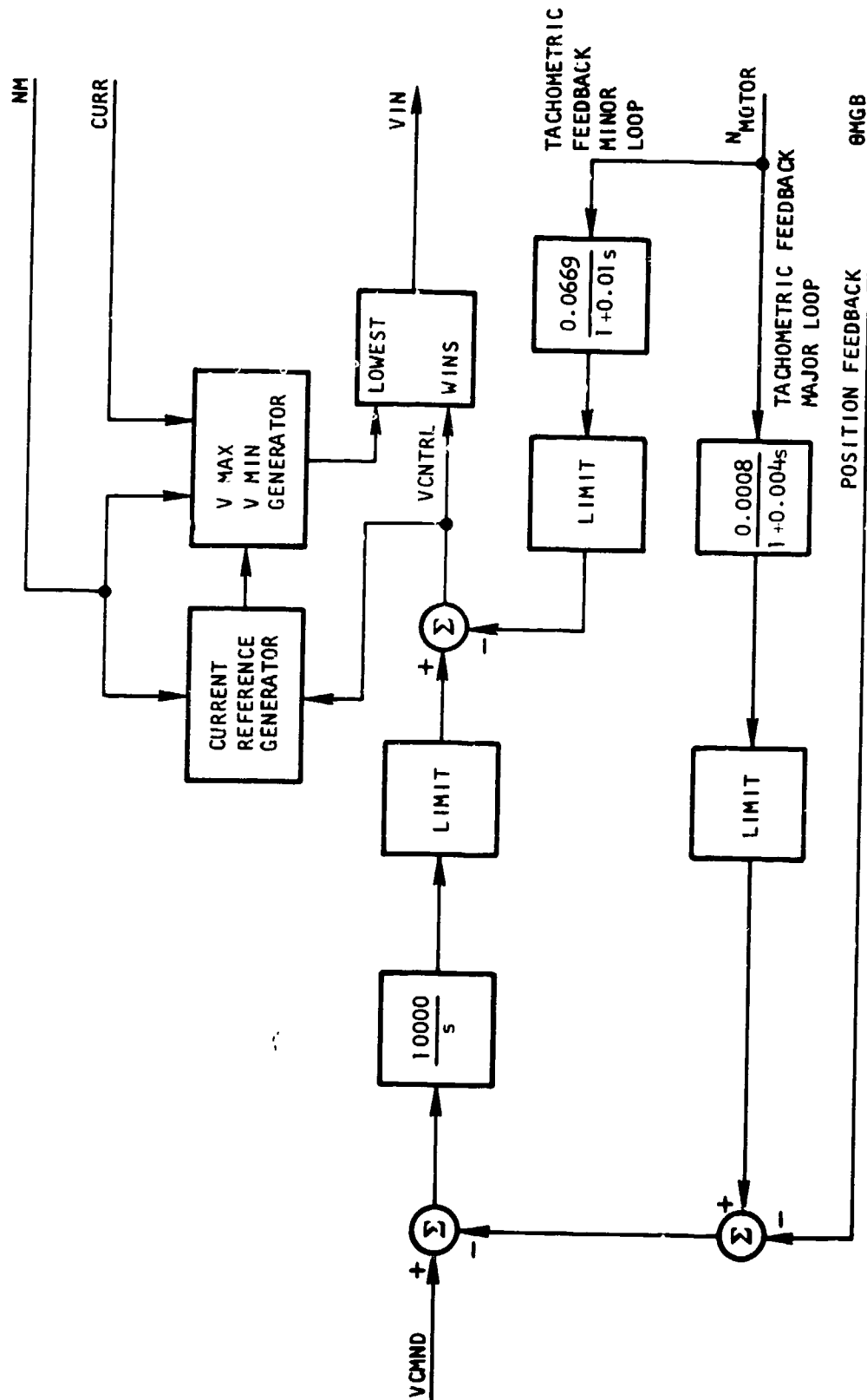


Figure 71. Response to Gust Loads

A block diagram of this control arrangement is shown on Figure 72. Tachometric feedback included in a minor control loop permits rolling off the response of the motor so that the influence of high-frequency disturbances is attenuated. Tachometric feedback in the major loop readily permits adjustment of damping and of the system natural frequency.

The linear model of the unit, with load inertia set at the specification value of 46.6 in.-lbf-sec², in conjunction with Nichols charts, was again employed as the basic synthesizing tool. Figure 73 shows the open-loop transfer locus for the motor speed minor loop. A single lag with the pole at 100 rad/sec was included in the minor loop feedback; after gain adjustment, the minor loop transfer locus was reshaped to that shown in Figure 74. The open-loop transfer locus for the major loop, with the minor loop closed and with an integrator only having a gain of 19950 as the control, was then generated and is shown in Figure 75. The final step was to include a lag in the major loop feedback path (time constant = 0.004) and to readjust the integrator gain. The resulting characteristic is shown in Figure 76.

Further investigation of the tachometric feedback control concept was conducted on the nonlinear motor-actuator model. Initially, limits were not imposed on the magnitude of the tachometer feedback in either the minor or major loop. As shown in Figure 77, the large magnitude of the major loop tachometer feedback, in equivalent output shaft angle, results in stair-case type operation in response to an input step command. By limiting the major loop tachometer feedback, the percentage of overshoot can be controlled to any desired value under a given set of operating conditions. An example in which two channels are operating under no load conditions, with the overshoot in response to a step command limited to about 3 percent, is shown on Figure 78. Further improvement in the response characteristics of the system can be realized by limiting the range over which the minor loop tachometer feedback is active. This has the effect of permitting acceleration to occur at the maximum possible rate once the saturation range has been reached. An example of the performance with the major loop range restricted to ± 1.8 deg and the minor loop to ± 100 v is shown on Figure 79. Again, the operation is two-channel with 100-percent aerodynamic (or linear spring) load imposed.



TACH FEEDBACK
CONTROL HINGELINE

Figure 72. Control Block Diagram for Motor Tachometer Feedback

S-29744-A

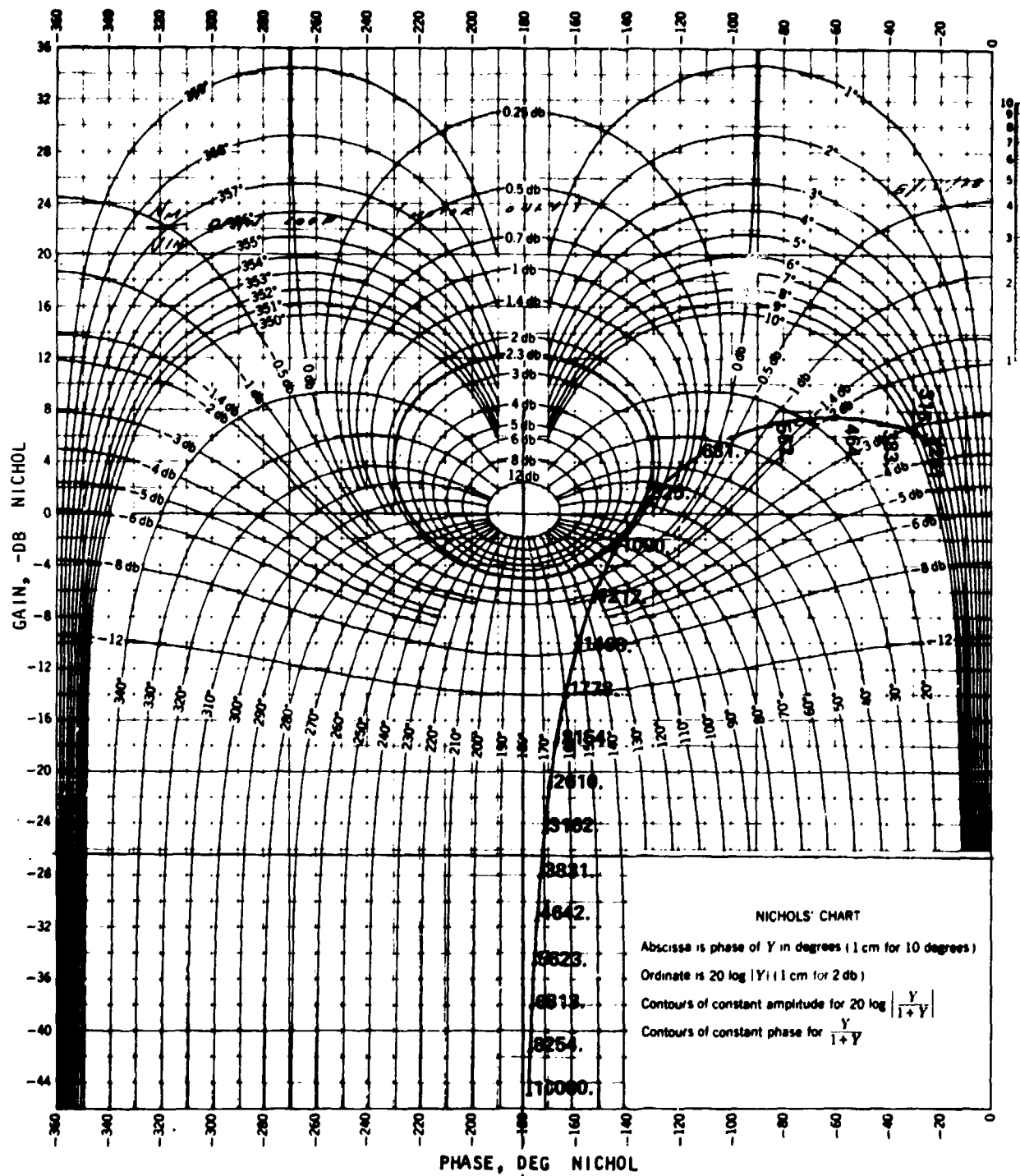


Figure 73. Open Loop Nichols Locus Diagram

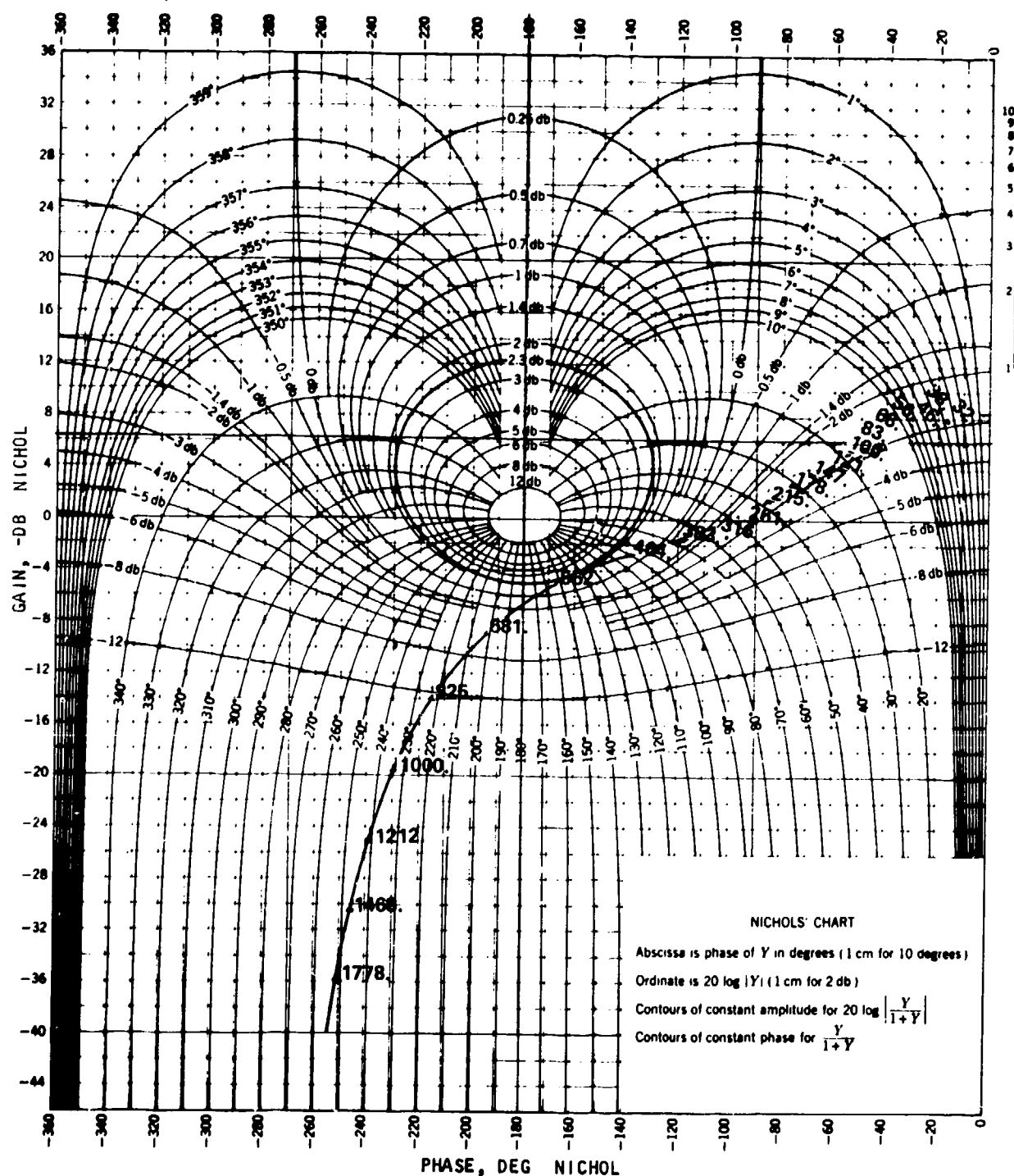


Figure 74. Nichols Locus Diagram with Gain Adjustment

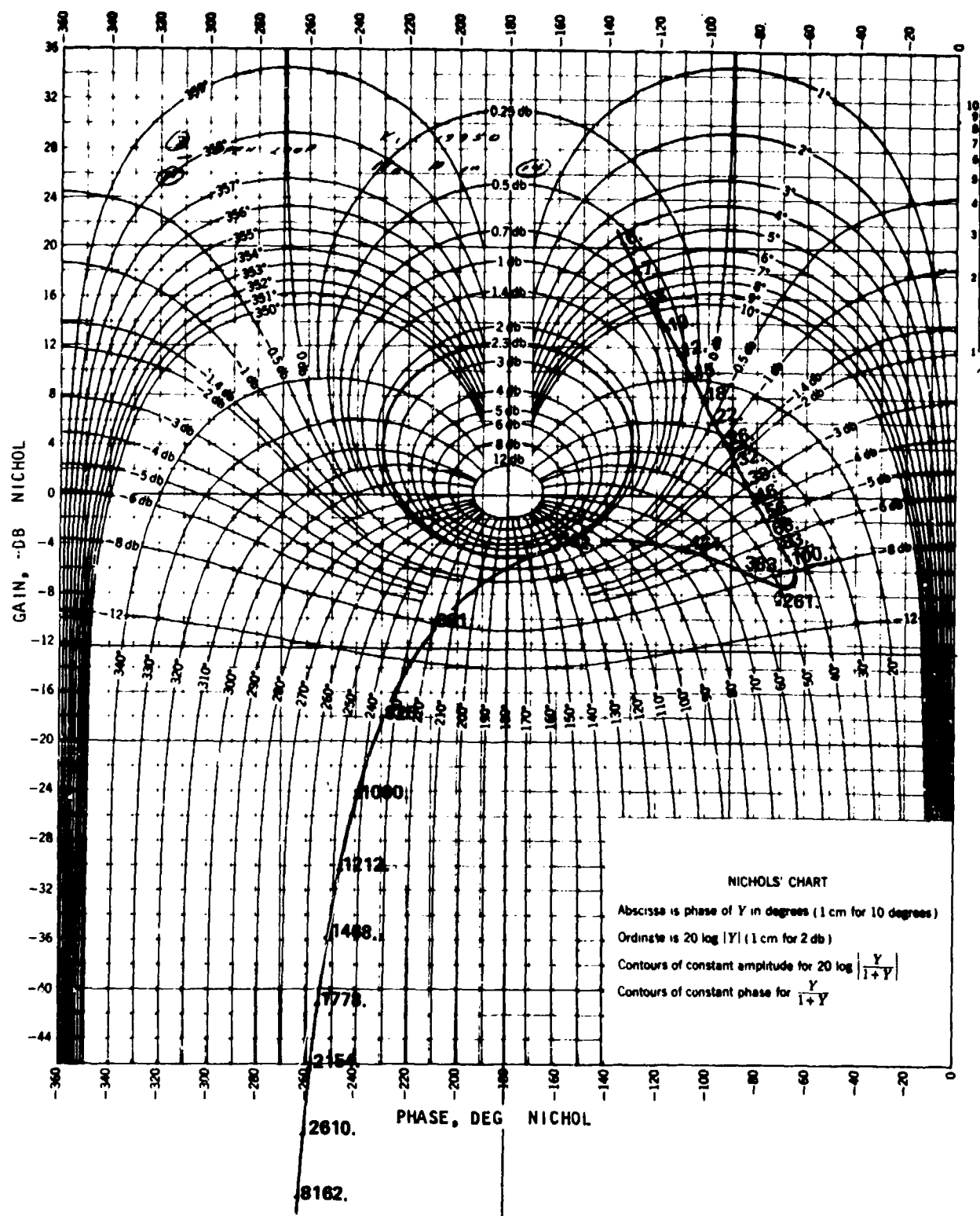


Figure 75. Nichols Locus Diagram with Gain of 19950

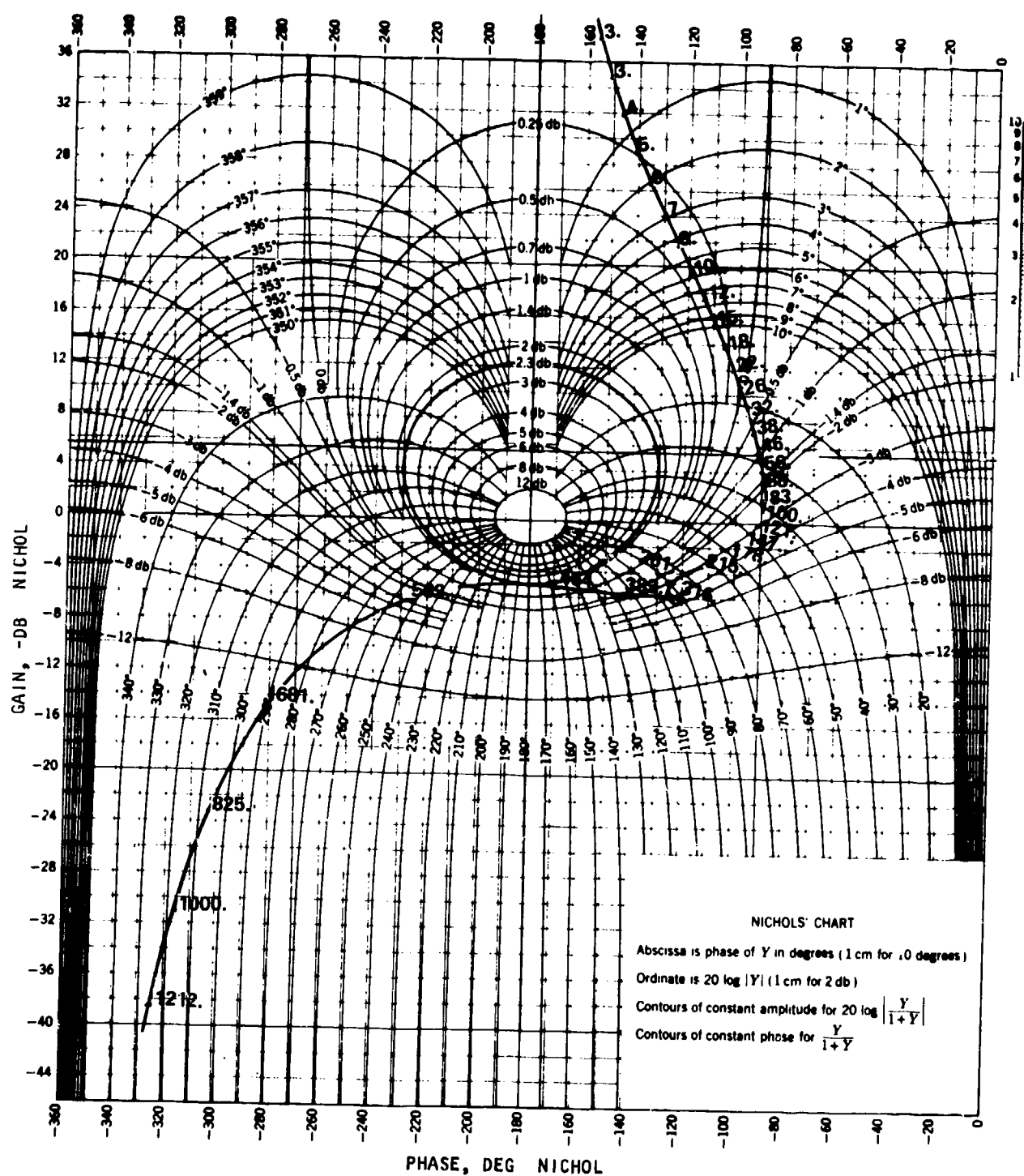
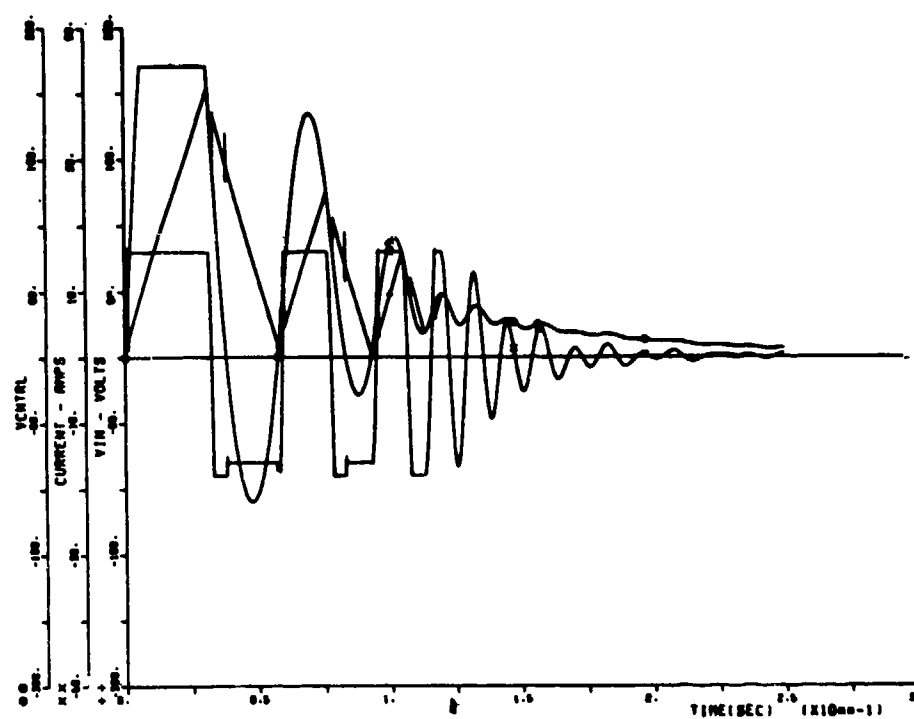


Figure 76. Final Nichols Locus Diagram



CONTROL WITH TACH FEEDBACK

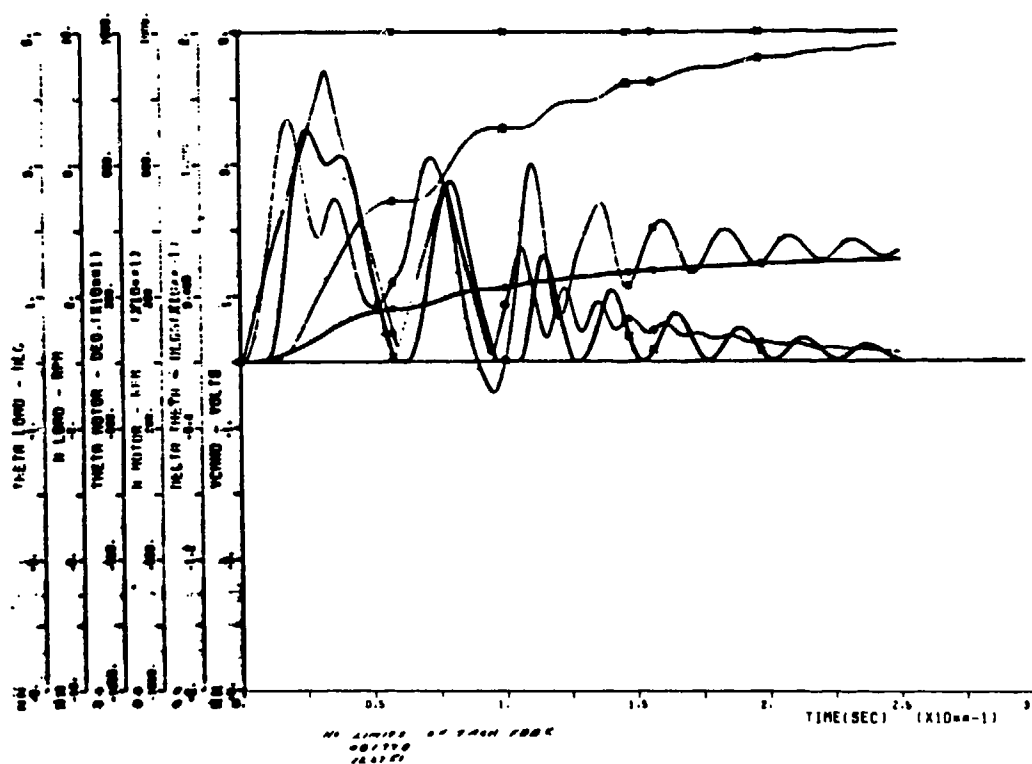


Figure 77: Demonstration of Control Loop Using Tachometer Feedback
(No Limit on Major Loops)

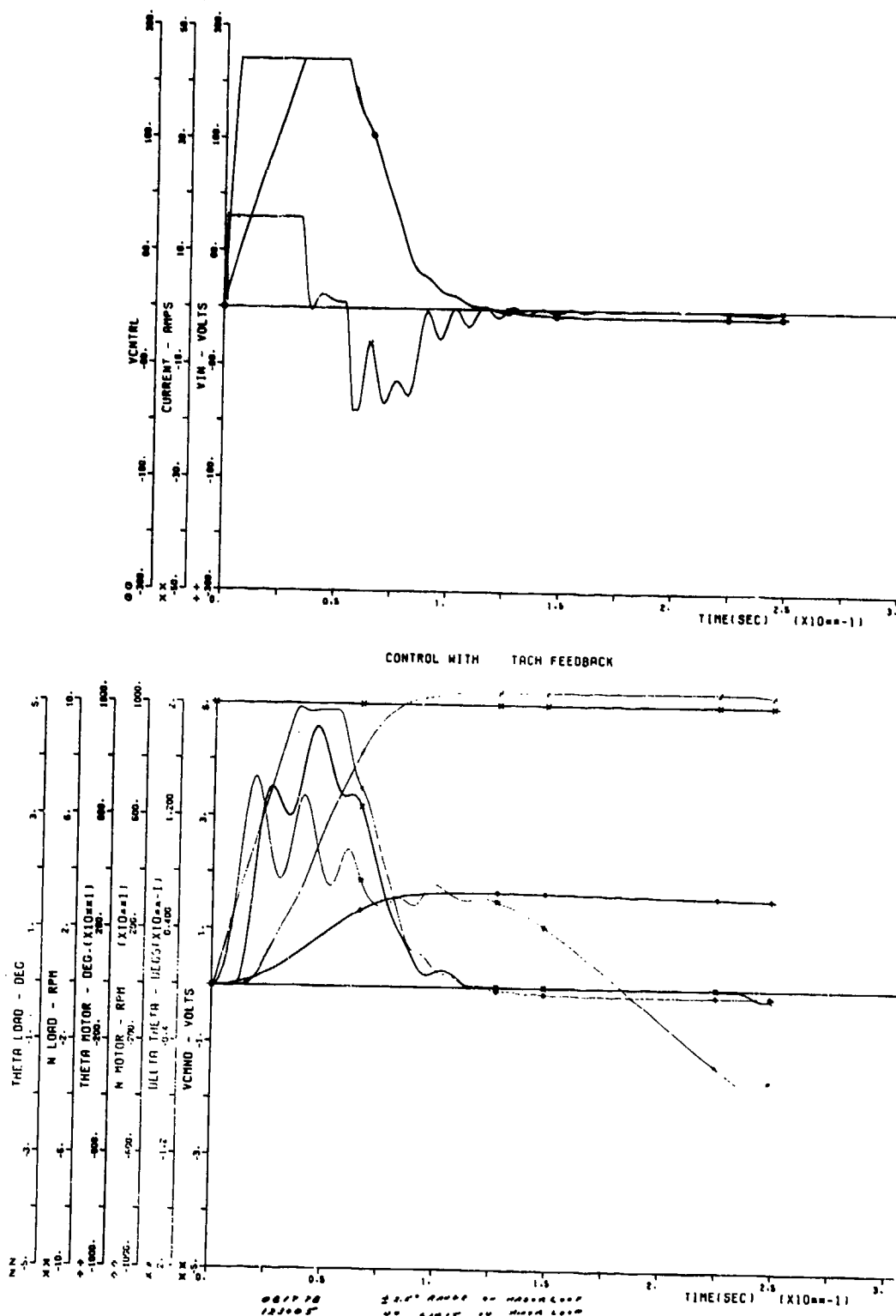


Figure 78. Demonstration of Control Loop Using Tachometer Feedback (Limited Major Loop)

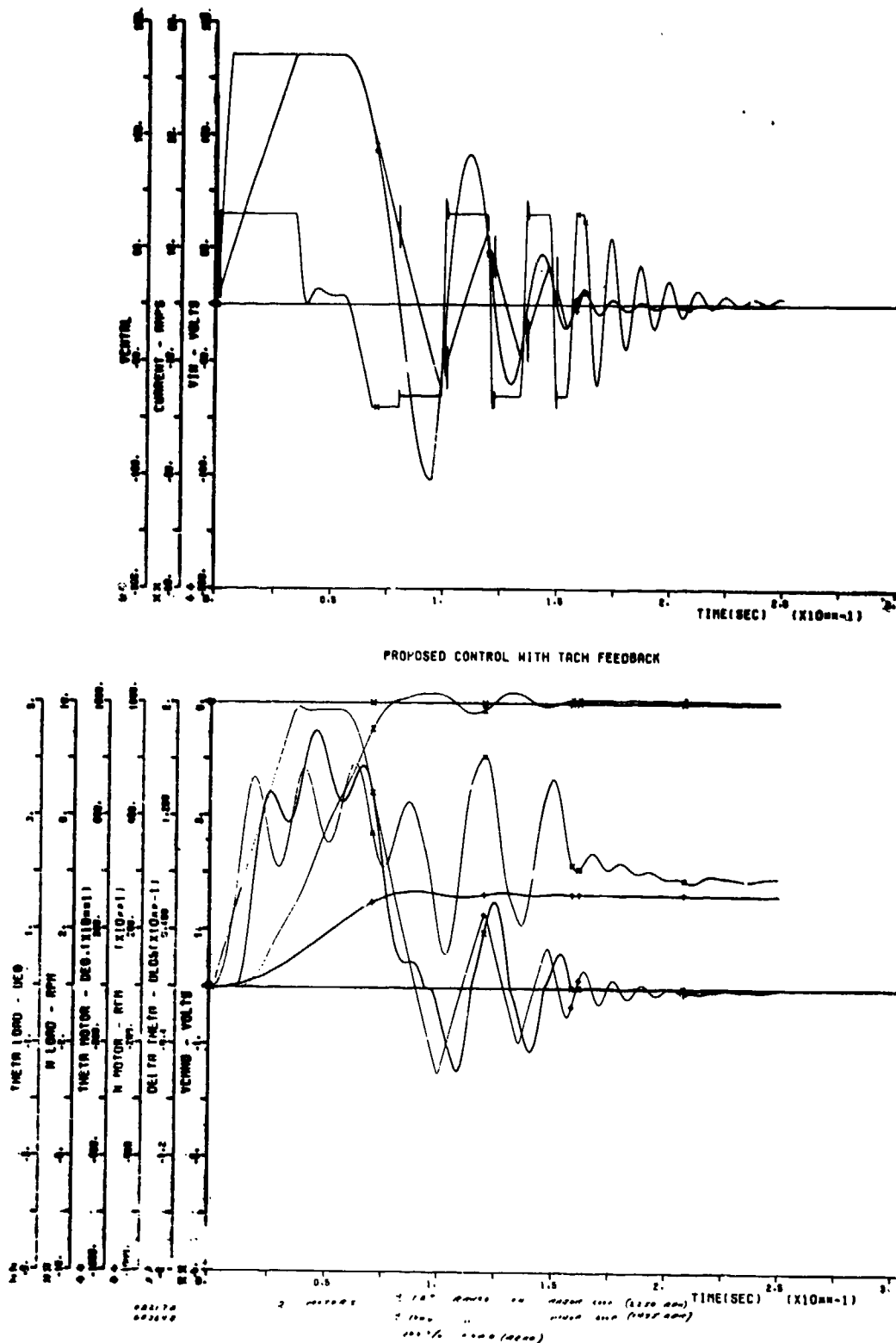


Figure 79. Demonstration of Control Loop Using Tachometer Feedback (Limited Range of Minor Loop)

4. TEST EQUIPMENT

4.1 SPECIAL TEST EQUIPMENT AND FIXTURES

The hingeline actuation laboratory demonstration unit was tested using a test stand to support the actuator and to simulate the aircraft structural interfaces. The test stand also included a device to provide a variable load on the actuator. An electric supply was set up to provide 270-vdc power to the controller and the motor. These test and support hardware items are described below.

4.1.1 Test Stand

The test stand was designed to interface with the actuator assembly in a manner similar to an aircraft installation. The test stand drawing (LSK 14850) shows the arrangement as designed. The test stand provides for mounting of the two position feedback encoders at the extreme ends of the simulated control interface.

The output of the actuator mates to a 10-in.-long arm, which allows interface with the hydraulic load cylinder and includes a strain gage for monitoring the actuator torque output.

The arrangement of the actuator fitted to the test stand is shown in Figure 80, which also shows the safety stroke limit switches used to limit the control surface excursion for safety purposes (the actuator does not have mechanical stroke limit stops).

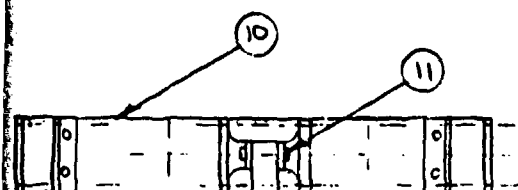
The actuator is loaded using the hydraulic cylinder. The output load is varied by throttling the fluid flow from and to the cylinder. The fluid reservoir, valves, and gages used to control and monitor the hydraulic fluid flow are shown in Figure 81. The load is monitored using the strain gage on the output arm and the hydraulic fluid pressure gages. These values are then correlated to the measured value of motor current to determine losses and overall efficiency of the actuation unit.

The hydraulic load stand also is used to conduct dynamic stiffness tests. A hydraulic pump provides power to the hydraulic cylinder. Flow to the cylinder is controlled by a servovalve. As the load frequency is varied from 0.5 to 10 Hz, the stiffness of the actuation system is monitored using the optical digital position feedback transducer.

The early testing of component compatibility showed that the two position encoders were not providing the same position information to the two servo circuits. The two encoders were located at opposite ends of the simulated control surface. Even at relatively modest loads (less than 10 percent of

REVISIONS

LTR	DESCRIPTION	DATE	APPROVED



SIMULATED AIRFOIL
REMOVED FROM
THIS VIEW

9

SHEET 2 OF 2 FOR PARTS LIST

NOMENCLATURE OR DESCRIPTION

SYM

PARTS LIST

CONTRACT NO



AIRRESEARCH MANUFACTURING COMPANY OF CALIFORNIA
A DIVISION OF THE BARRETT CORPORATION
TORRANCE, CALIFORNIA

BLACK & S7

FIXTURE, LOAD
FBW ACTUATOR

SIZE

CODE IDENT NO

DWG NO

C

70210


LSK 14850

SCALE

SHEET

OF

QTY	ITEM	DESCRIPTION
	12	LSK 14983 ELEVON, SIMULATED
1	11	3/4 DIA PIN (HYDROLINE C-9004-3)
1	10	LSK 14981 MOUNT-SIMULATED SPAR
1	9	LSK 14982 BRACKET, CLEVIS
1	8	FEMALE EYE (HYDROLINE C-9304)
2	7	3X3X3/8 ANGLE 20 IN LG STEEL
1	6	HYD. CYL. (HYDROLINE N2UD 12" STROKE)
1	5	12X3 CHANNEL 30#/FT. 41 IN LG STEEL
1	4	LSK 14980 ARM-MOMENT
1	3	12X3 CHANNEL 30#/FT. 44 IN. LG. STEEL
1	2	LSK 14849 MOUNT-STATIONARY
8	1	1/2-13UNC X 1 3/4 LG BOLT-SOCKET HEAD

 AEROSPACE MANUFACTURING COMPANY OF CALIFORNIA A DIVISION OF THE GARRETT CORPORATION TORRANCE, CALIFORNIA	SIZE A	CODE IDENT NO 70210	DWG NO LSK 14850
	SCALE	REV	SHEET 2 OF 2

FORM 2347-4 (1-74)

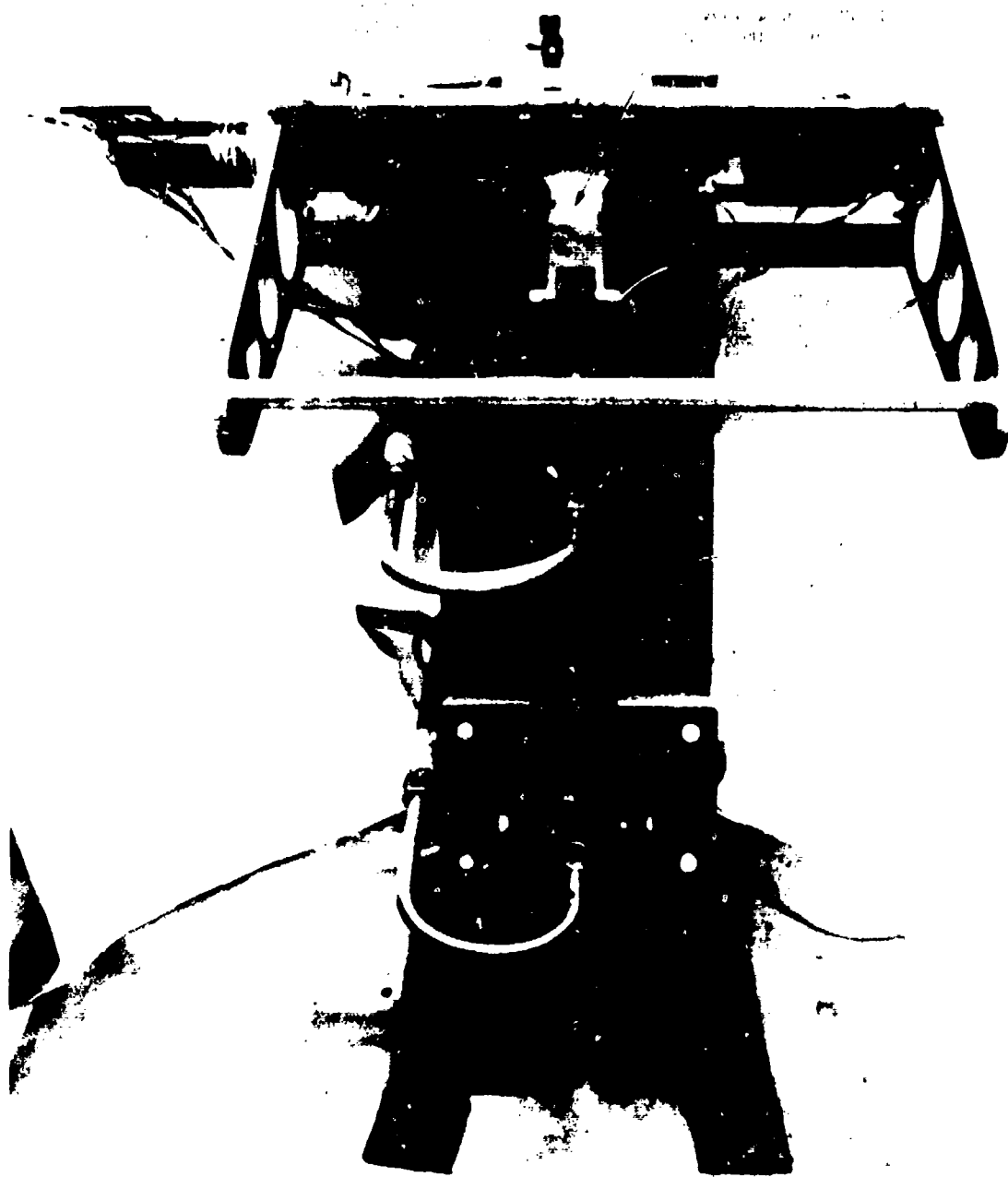


Figure 80. Actuator Mounted in Test Stand

F-26980

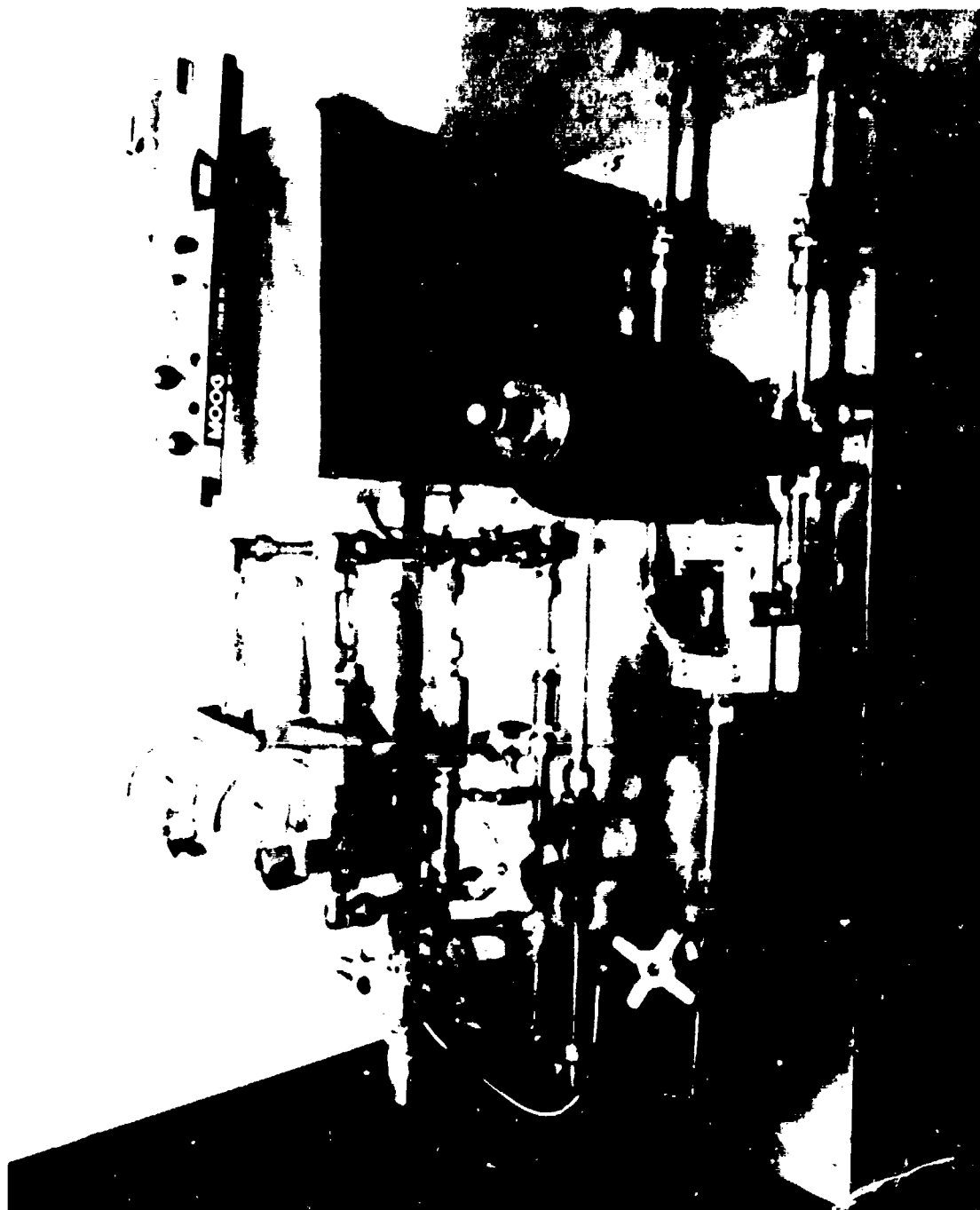


Figure 81. Hydraulic Load System Setup

stall torque), the positions sensed by the two encoders were not equal. It was determined that the simulated structure of the control surface had sufficient flexibility, especially when under load, that the two encoders would not track properly. Solutions to this problem are discussed in para. 3.4.2 of this report. In summary, the solutions are as follows.

- Use only one encoder to provide position feedback information to both servo circuits.
- Use two encoders physically attached to each other with a structure that has exceptionally high stiffness.

As shown in Figure 82, the first solution was implemented (one encoder to provide position data to both servo circuits).

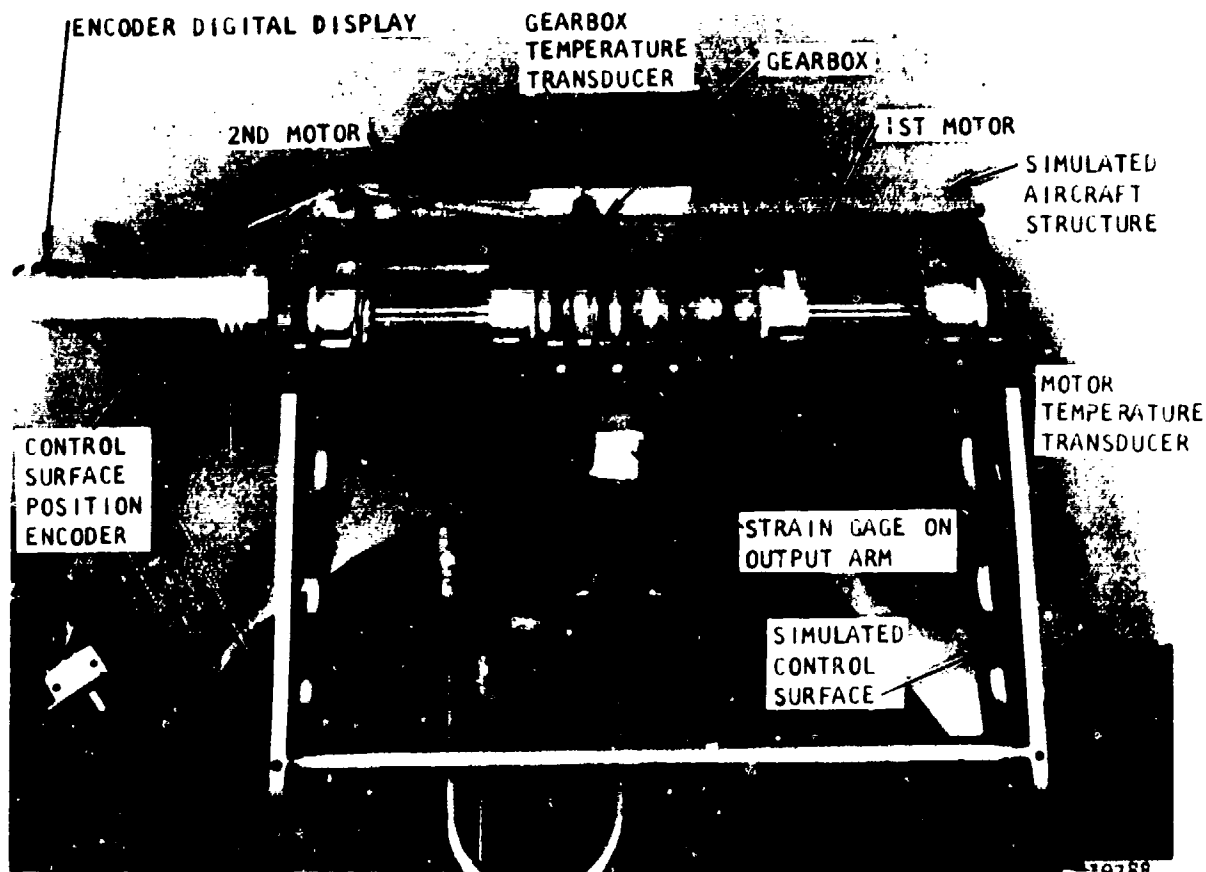
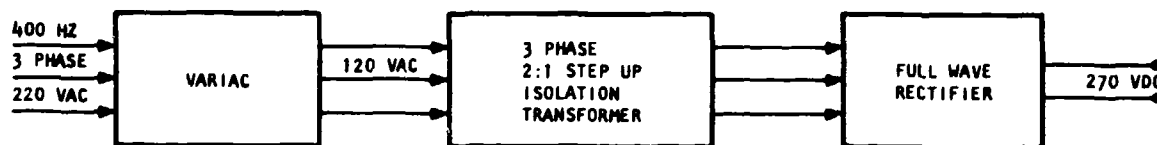


Figure 82. Strain Gage Mounted on Output Arm

4.1.2 Power Supply

The electrical power distribution system comprises a primary power source; a 3-phase stepup isolation transformer, and a full-wave rectifier. The power supply converts the primary power source to 270-vdc power, which is used to drive the dc permanent-magnet motors. A functional block diagram of the power supply is shown in Figure 83. The schematic diagram and a technical discussion of the power supply is contained in para. 3.3.3.

The dc voltage output of the power supply is sensitive to the output demand. Variations as high as 20 percent were observed under loaded conditions. Although this fluctuation is a large one, frequency response and performance requirements were met. The performance of the unit would be improved however, if a power source were used that did not exhibit the voltage variation as a function of power demand. A reduction in the power supply voltage reduces the maximum actuator output rate.



620011

Figure 83. Block Diagram of the Power Supply

4.2 FACILITIES

AiResearch Manufacturing Company of California provided all engineering and testing facilities required for the rotary hingeline actuation unit test program.

5. TESTING

5.1 TEST PLAN

The test plan for the rotary hingeline actuation unit was designed to demonstrate the capabilities of electromechanical actuation units for primary flight controls. The test plan is presented in Appendix F. Results of the tests are contained in Section 6. The test program was organized to determine component and unit operating characteristics in a controlled environment.

The first component testing began in March 1977 and final unit tests were completed in September 1978.

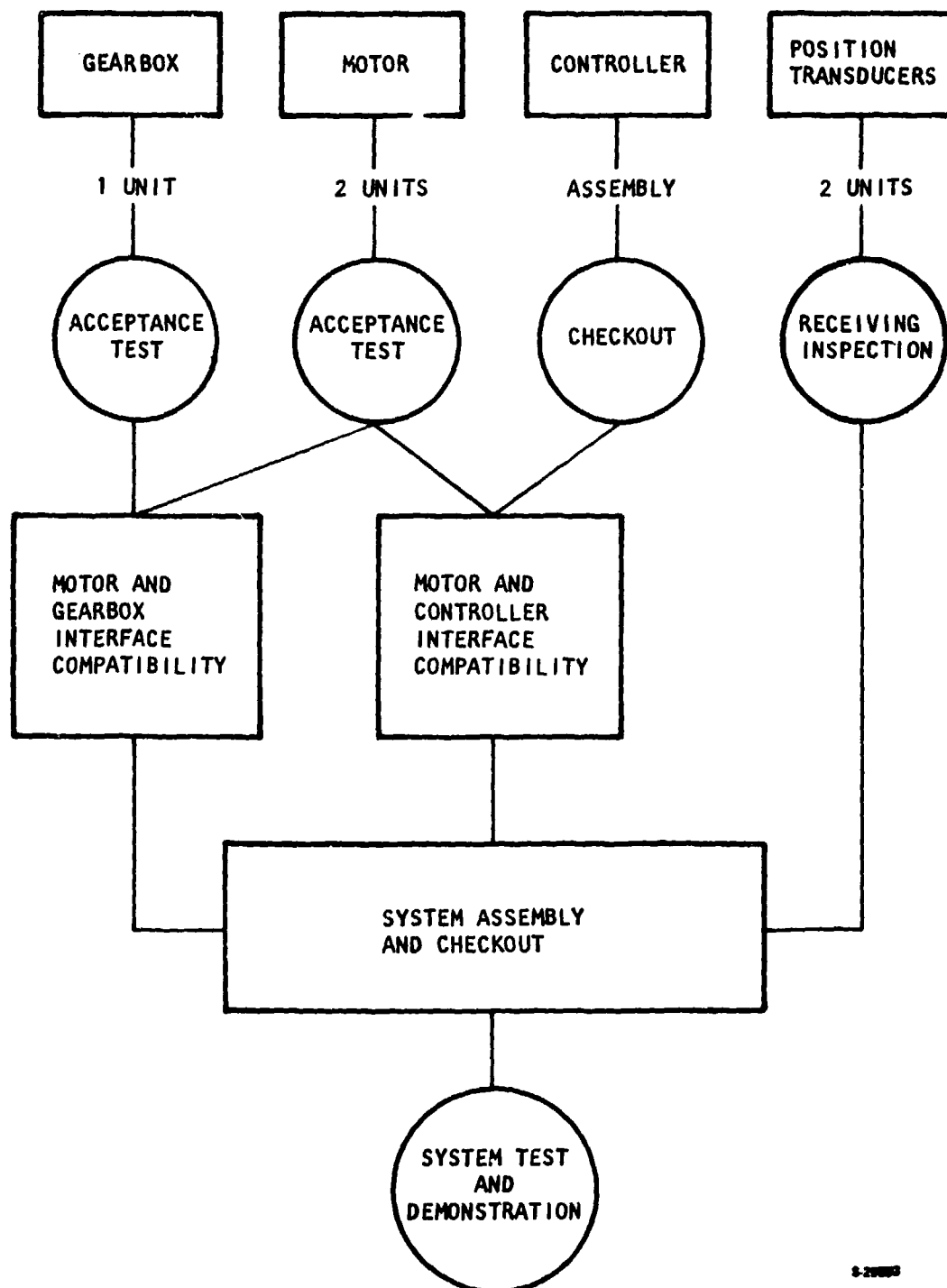
5.2 TESTS PERFORMED

The test program was divided into three areas: (1) component tests, (2) assembly tests, and (3) unit operating tests. Table 13 lists tests performed in each area and the objective of the individual tests. These tests were performed in accordance with the test flow diagram shown in Figure 84.

TABLE 13
TESTS PERFORMED AND TEST OBJECTIVES

Test	Objective
Component	
Motor acceptance	Verify performance and critical design parameters
Encoder receiving inspection	Verify form and function of vendor part
Controller checkout	Verify operation of input-output circuits, servoloop, and switch modules
Rotating gearbox acceptance	Determine functional characteristics of gearbox
Assembly	
Motor and gearbox capability	Verify interface and functional compatibility
Motor and controller compatibility	Verify drive circuits for motor control
EM: signature*	Define signature of EMI conducted and susceptibility to conducted EMI
Static stiffness	Demonstrate spring rate of the actuator
System	
Frequency response	Determine the amplitude ratio and phase angle vs frequency
Dynamic stiffness	Demonstrate the dynamic stability when subjected to fluctuating external loads
Step response	Determine quality of transient response to step inputs
Position resolution*	Determine hysteresis band
Power efficiency*	Determine the energy input vs output relationship
Regeneration	Determine the operating characteristics as a generator when back-driven
Continuous running servo demonstration*	Determine the regeneration effectiveness with the control surface locked
Reliability management	Demonstrate redundancy
Thermal management	Evaluate thermal characteristics during duty cycle loads

*Denotes a test that was not conducted, or that was attempted but did not result in significant data being generated.



8-29885

Figure 84. Test Flow Diagram

6. TEST RESULTS

This section contains the results of tests performed on the rotary hingeline actuation demonstration unit. Testing was conducted in accordance with the Equipment Test Plan, AIResearch Document No. 76-13276, Rev. 1, January 1977; this plan is reproduced in Appendix F. Detail test results are presented for each component (i.e., motor, actuator), and for the actuation unit operating with a microprocessor and with analog servo controllers.

6.1 COMPONENT TESTS

The component tests conducted in this program are:

- Motor performance
- Encoder receiving inspection
- Controller checkout
- Rotary gearbox performance

The results of these tests are presented in this section in the order listed above.

6.1.1 Motor Performance

Performance of the two brushless dc motors was evaluated by the following techniques.

- Operation of the Motors as Generators--To determine power capability, no-load voltage, and short-circuit capability.
- Operation as a Motor Driving a Flywheel--To determine acceleration capability.
- Operation as a Motor into a Dynamometer--To determine current, torque, and speed relationships.

Each of these tests is described in detail in the following paragraphs.

6.1.1.1 Motor Operated as a Generator

Unlike a brush-type dc motor, a brushless dc motor needs a commutating controller to drive it. Therefore, evaluation of performance characteristics of the motor could be complicated by the interaction of the controller/motor

combination. The testing can be simplified, and the motor characteristics can be determined directly by operating the motor as a generator. This allows determination of the motor voltage constant (volts/rpm) by no-load test and motor power capability by load test. The motor speed-torque relationship also can be obtained from generator voltage regulation. Because the brushless motor was originally designed as a generator (refer to Appendix A), it is very useful to verify such generator parameters as short circuit current and commutating reactance. Three basic tests were performed: (1) load test, (2) short circuit test, and (3) commutating reactance test.

6.1.1.1.1 Test Setup

A schematic diagram of the generator test setup is shown in Figure 85. The motor is connected as a generator to a variable-speed prime mover using adapters fabricated for this test. The electrical output was rectified and connected to a purely resistive load bank. The test setup included a shorting switch used to interconnect the three phases of the generator output (see Figure 85). Photographs of the generator test setup are presented in Figures 86 and 87, which show the adapters and the arrangement of the instrumentation.

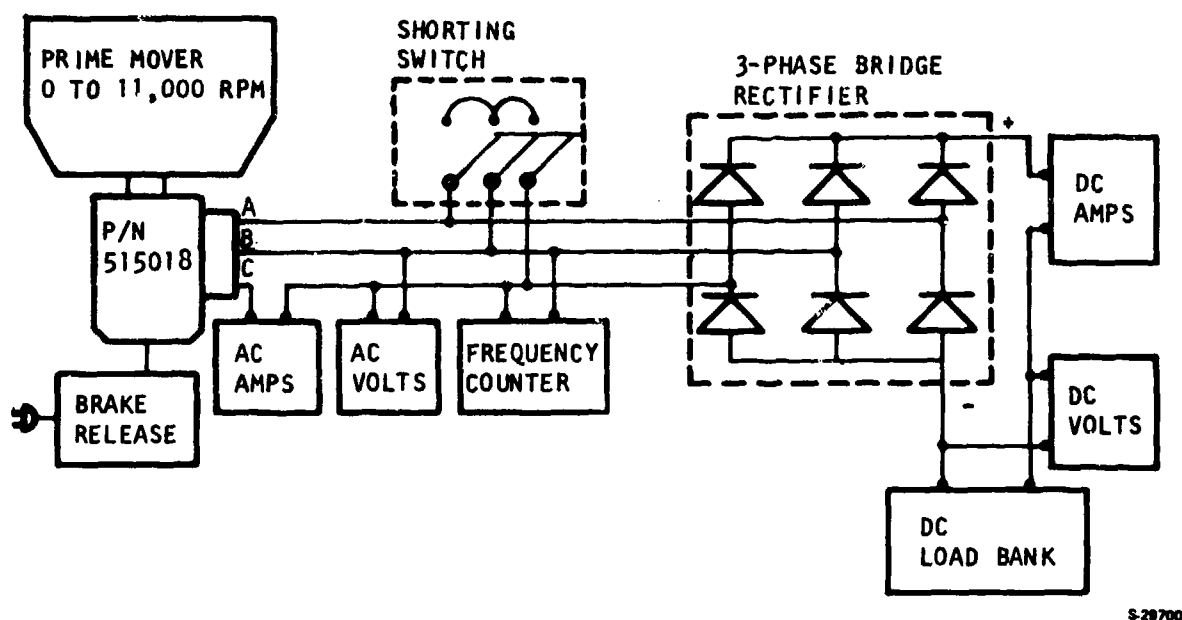
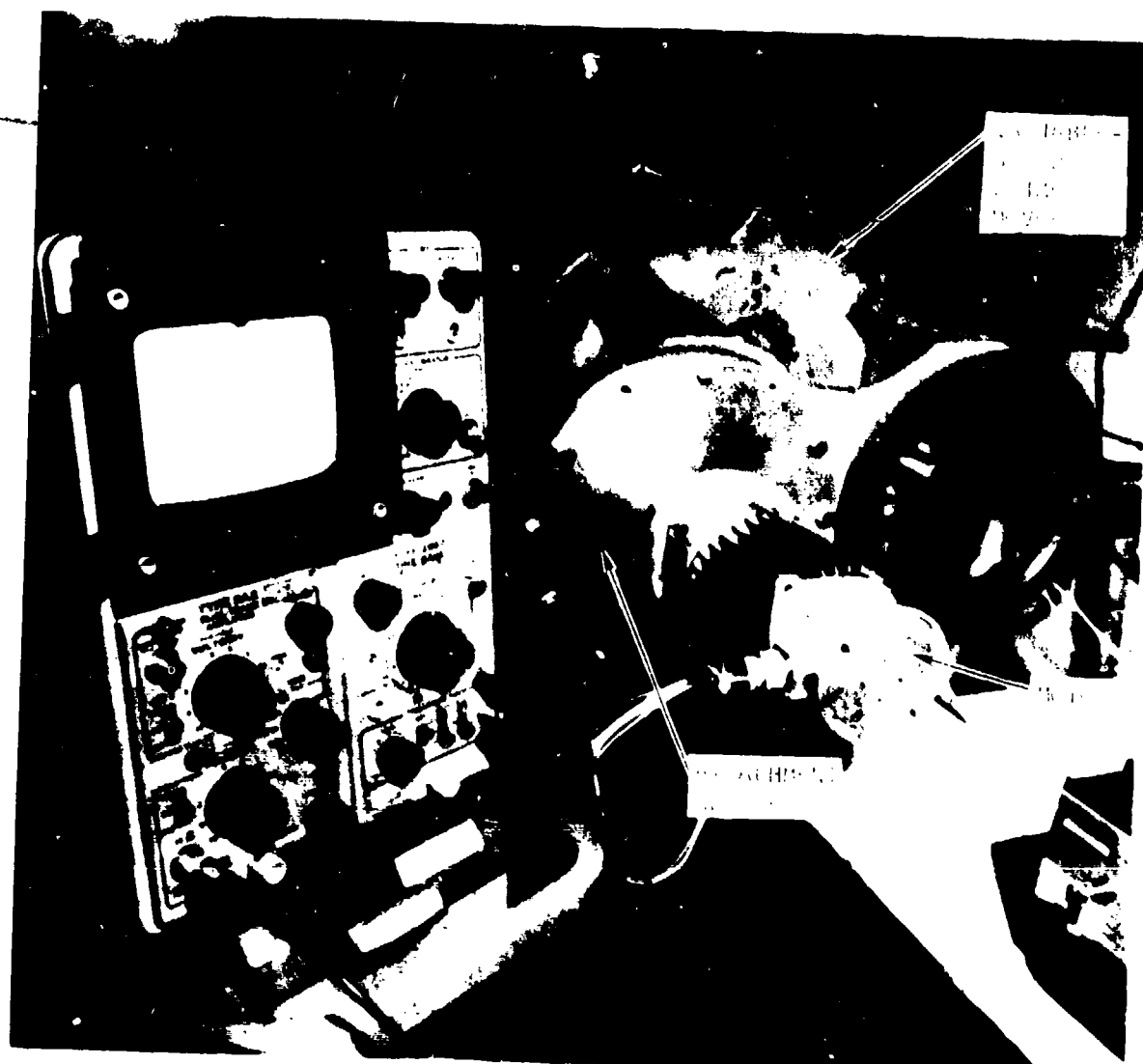


Figure 85. Load Test and Short-Circuit Test Schematic

6.1.1.1.2 Procedure

The procedures for performing the load test are as listed below.

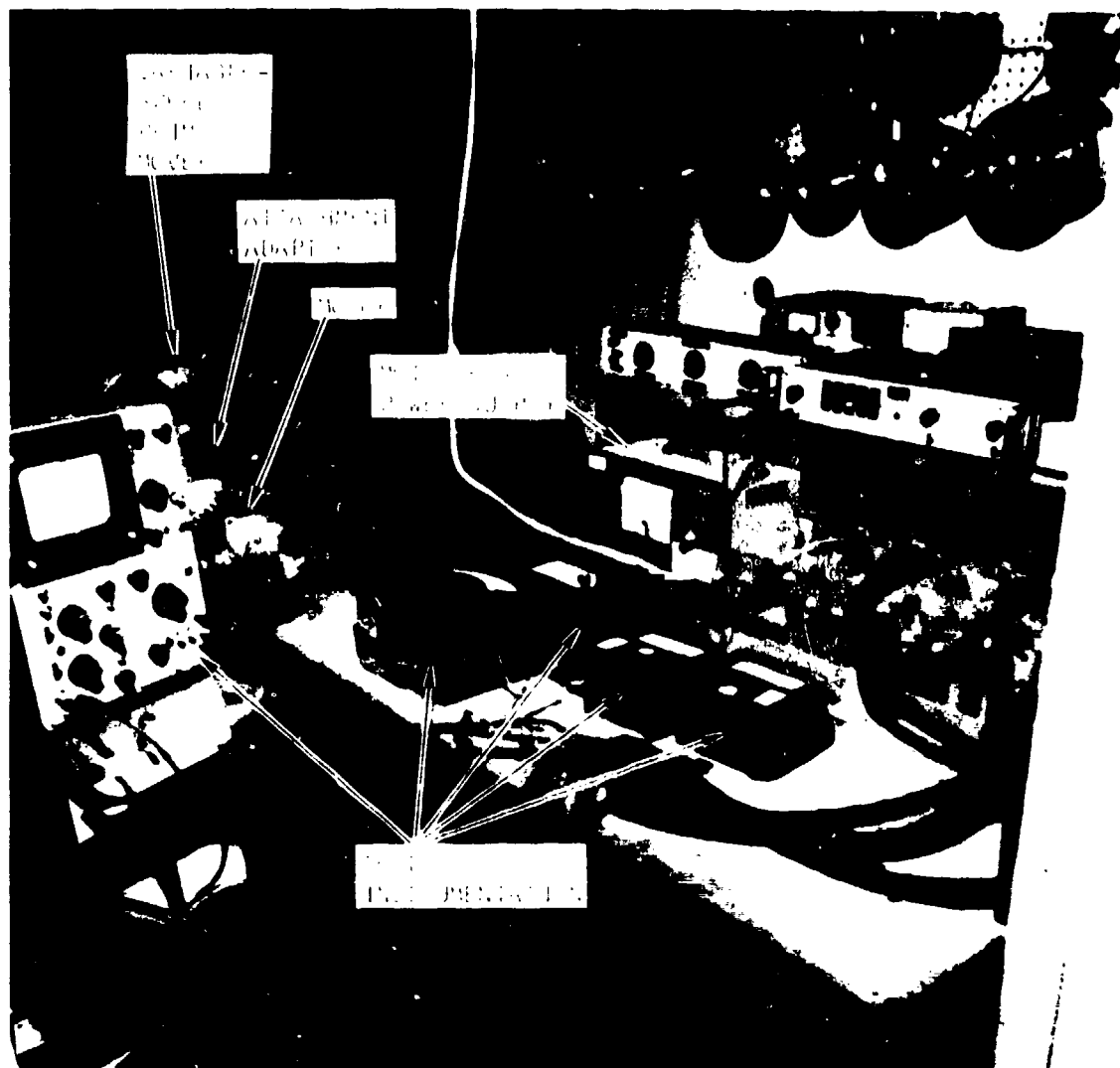
Step 1--Mount motor No. 1 onto the variable-speed drive.



80222-1

F-28018

Figure 56. Closeup of Generator Test Setup



80222-2

F-28017

Figure 87. Generator Test Setup

Step 2--Set up instruments for the test according to the schematic shown in Figure 85.

Step 3--Drive the motor at 6000 rpm and adjust the load to provide five different amperage outputs between 0 and 20 amp dc. Record shaft speed, dc volts, dc amperes, ac line-to-line volts, and ac amperes.

Step 4--Repeat Step 3 for 8000 rpm and 10,000 rpm.

Step 5--Repeat Steps 1 through 4 for motor No. 2.

For the short-circuit test, the motor was run at 8000 rpm and the 3-phase generator output shorted by closing the shorting switch momentarily. The phase current was read and recorded.

The commutating reactance test was performed using the following procedures.

Step 1--Replace the load bank with the choke provided for this test.

Step 2--Run the motor at 10,000 rpm.

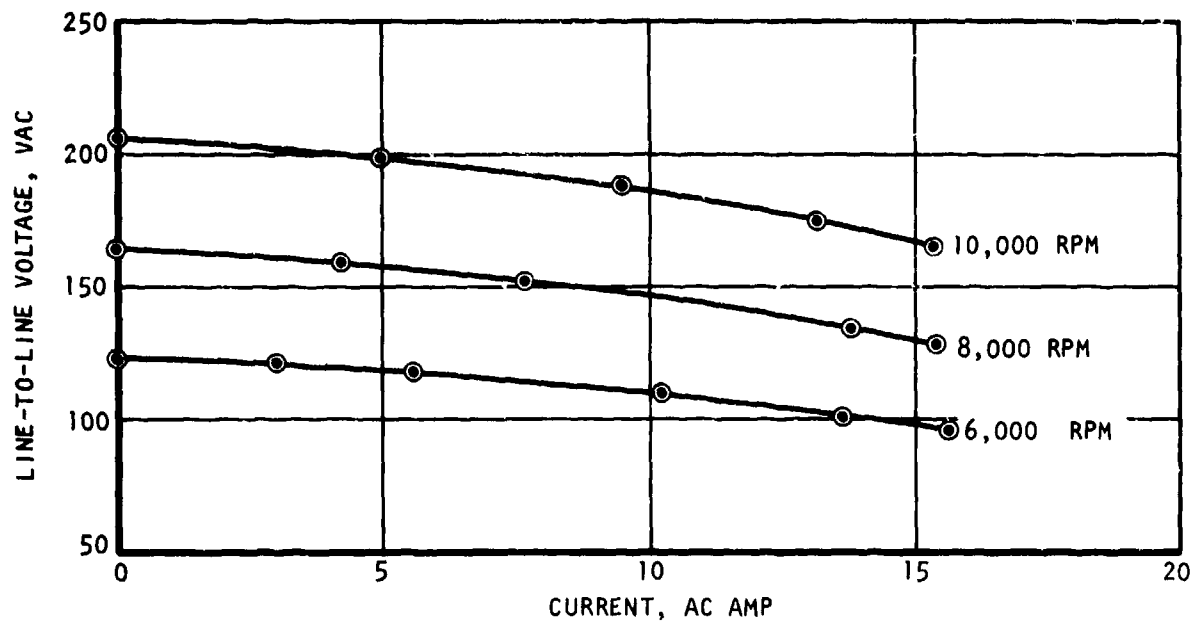
Step 3--Take a picture of the line-to-line voltage waveform on an oscilloscope.

6.1.1.1.3 Discussion of Results

The load test results are plotted in Figures 88 through 91 for both motors. As shown, the relationship between no-load voltage and speed is the same as predicted for the motors. The ac voltage regulation of the motor operated as a generator is 0.23, and the dc voltage regulation is 0.29, which is higher than the predicted value. The voltage regulation compares the reduction in voltage occurring between no-load and the rated load points. The 0.23 voltage regulation for the ac case, for example, shows that as the output load is increased from zero to full-rated current, the output voltage reduces a factor of 0.23 from the initial no-load value.

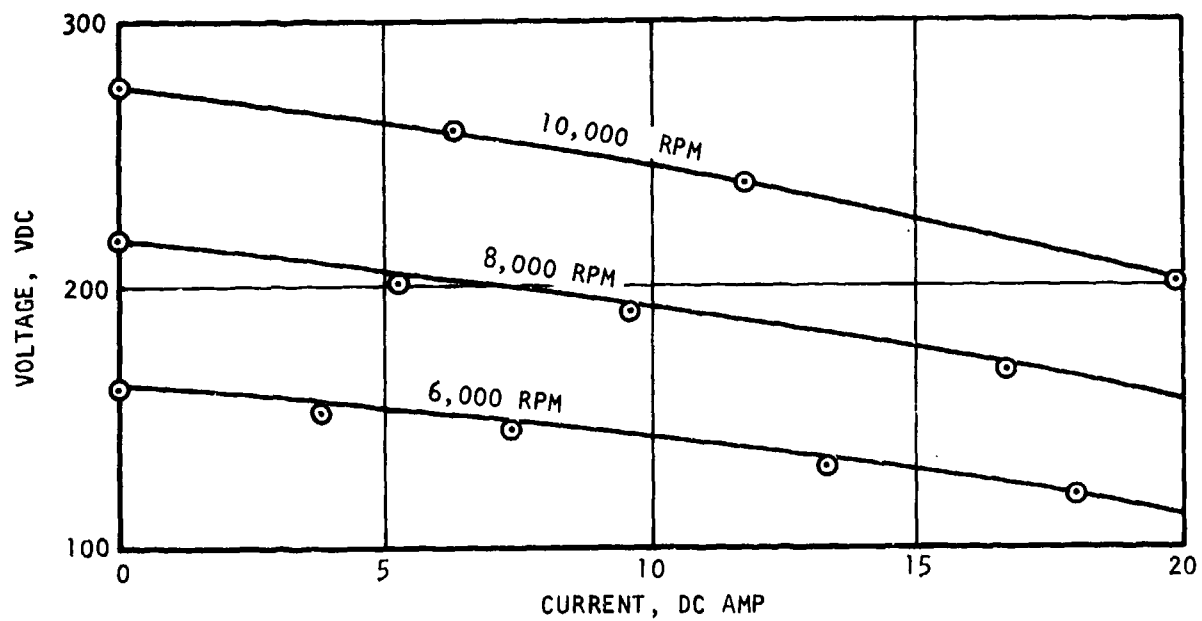
The test results and the computer predicted performance of the motor run as a generator are compared in Figure 92. The commutating reactance of the motor was calculated from the waveform picture of line-to-line voltage to a 3-phase bridge rectifier, the output of which was coupled to an inductive load.

The voltage waveform and the calculations for computing commutating reactance are shown in Figure 93.



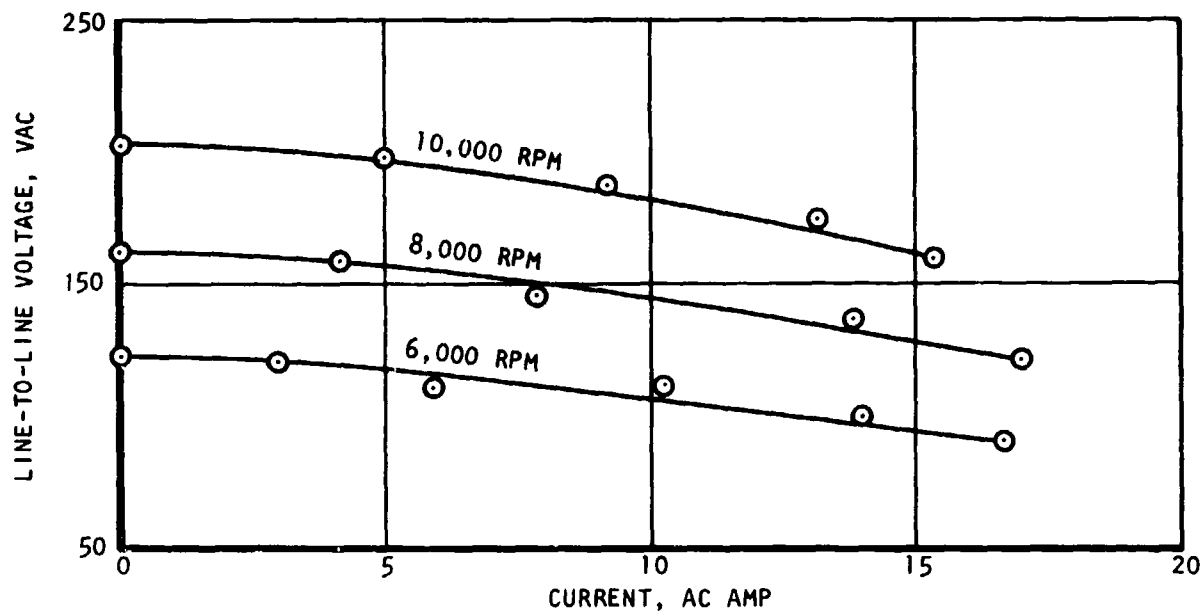
S-29687

Figure 88. 270-vdc Brushless Motor (M1)
Generator Test, Ac Voltage



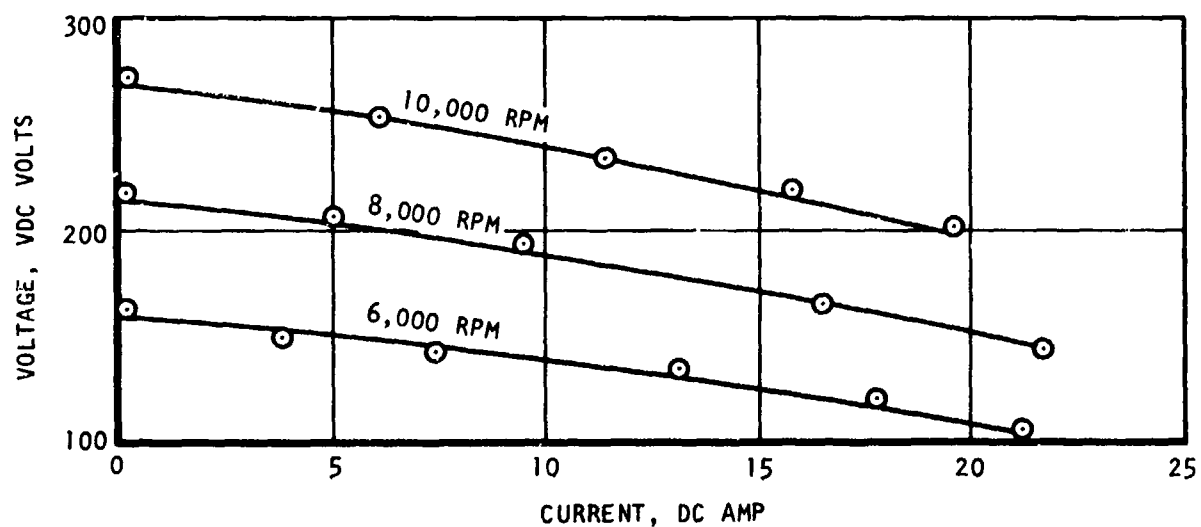
S-29691

Figure 89. 270-vdc Brushless Motor (M1)
Generator Test, Dc Voltage



S-29093

Figure 90. 270-vdc Brushless Motor (M2)
Generator Test, Ac Voltage



S-29096

Figure 91. 270-vdc Brushless Motor (M2)
Generator Test, Dc Voltage

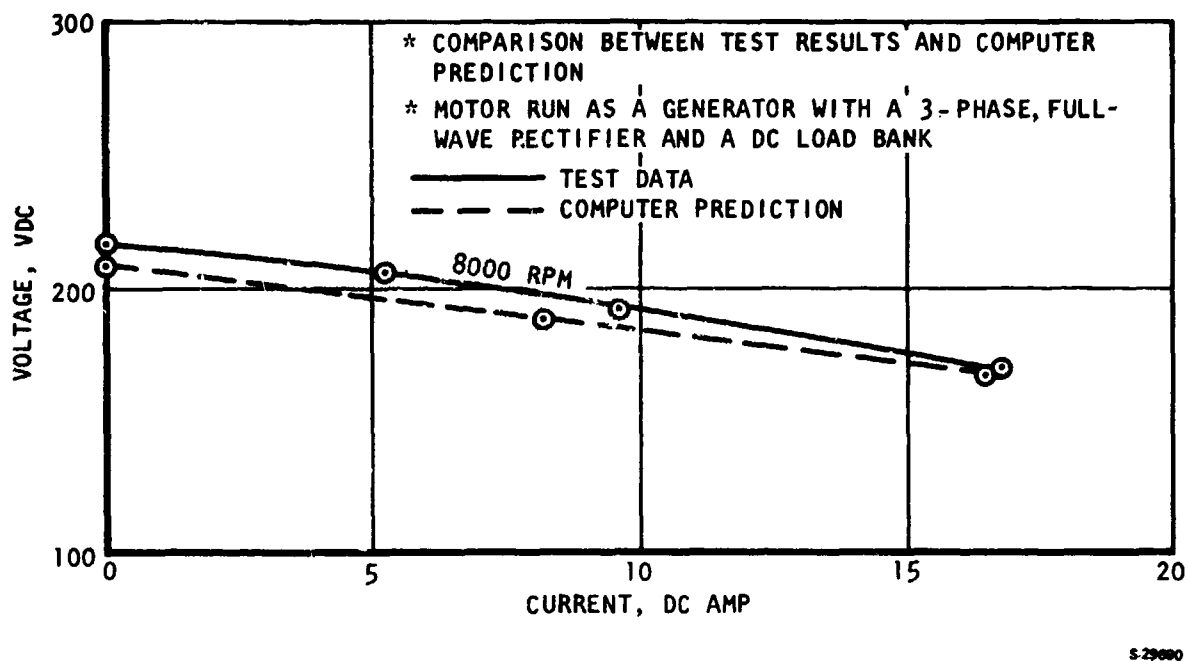


Figure 92. 270-vdc Brushless Motor (M1) Test Data Correlation

Commutating Reactance and Inductance

$$I_{DC} = 19 \text{ amp (Dc current)}$$

$$V_{LLO} = 204 \text{ V}_{RMS} \text{ (Line-to-line voltage)}$$

$$V_{LNO} = \frac{204}{1.732} = 117.8 \text{ V}_{RMS} \text{ (Line-to-neutral voltage)}$$

$$T_{180} = 4.1 \text{ cm/2} = 2.05 \text{ cm (Half-cycle time base)}$$

$$T_u = 0.6 \text{ cm (Commutating time, used with } T_{180} \text{ as dimensionless ratio)}$$

$$U = \frac{0.6}{2.05} \times 180 = 52.6 \text{ deg (Commutating angle)}$$

$$\begin{aligned} U &= 52.6 \cong \cos^{-1} (1 - I_{DC} * X_{COM} / \sqrt{1.5} / V_{LNO}) \\ &= \cos^{-1} (1 - 19 * X_{COM} / \sqrt{1.5} / 117.8) \\ &= \cos^{-1} (1 - 0.1317 X_{COM}) \end{aligned}$$

$$X_{COM} = \frac{1 - \cos(52.6)}{0.1317} = 2.98 \text{ ohm (Commutating reactance)}$$

$$L_{COM} = \frac{2.98}{2\pi \times 500} = 0.95 \text{ mh/ph (Commutating inductance)}$$



F-28022

Figure 93. Commutating Reactance

The results obtained by shorting the 3 phases of the generator output are as follows:

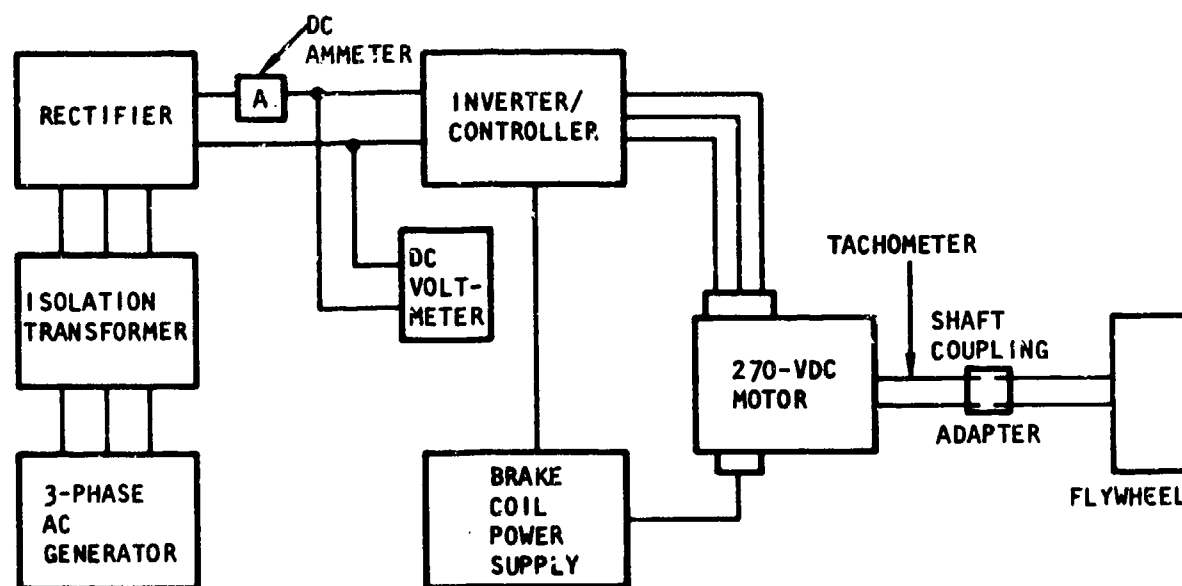
<u>Frequency, Hz</u>	<u>Speed, rpm</u>	<u>Short-Circuit Current, dc amp</u>
133	2660	30.0
250	5000	31.5
300	6000	31.7
400	8000	31.9

6.1.1.2 Flywheel Acceleration

The objective of this test was to obtain the motor performance map by recording the motor speed, torque, voltage and current while accelerating an inertial load.

6.1.1.2.1 Test Setup

The test setup consisted of the motor mounted to the flywheel test stand using an existing shaft coupling adapter that directly connects the motor shaft to the flywheel shaft. A schematic diagram of the test setup is shown in Figure 94.



S-29701

Figure 94. Flywheel Test Schematic Diagram

An oscillograph was used to measure motor speed, torque, current, and voltage. A strain gage and tachometer pickup are incorporated in the flywheel test fixture, therefore the torque and speed could be measured directly.

The test was performed on both motors in both directions.

6.1.1.2.2 Procedure

The procedures used to conduct the motor performance test are as follows:

Step 1--Set up an oscillograph to record speed, torque, voltage, and current.

Step 2--Mount motor No. 1 onto the flywheel test stand using the shaft coupling made for this test to couple the motor shaft to the flywheel shaft.

Step 3--Connect the motor, controller power, and power supplies according to Figure 94.

Step 4--Energize the brake coil to release the brake.

Step 5--Set motor power supply at 100 vdc.

Step 6--Turn on the controller to run the motor and record motor speed, torque, voltage, and current on the oscillograph.

Step 7--Repeat above steps to run motor in the other direction of rotation.

Step 8--Repeat above steps for motor No. 2.

6.1.1.2.3 Discussion of Results

Since an isolation transformer was included between the alternator and the rectifier in the power supply, a substantial voltage drop occurred at current limit. Therefore, the performance curves obtained for both motors were limited by the available test equipment.

The performance curves for both motors running at both directions of rotation are presented in Figures 95 through 98. As shown, the no-load speed and torque/amp data are as predicted, while the speed at high torques is low because of the reduced input voltage caused by the isolation transformer voltage drop.

6.1.1.3 Dynamometer

The objective of this test was to (1) obtain the motor torque-speed relationship, (2) verify the back emf constant (volts/rpm), and (3) verify the torque constant (torque/amp).

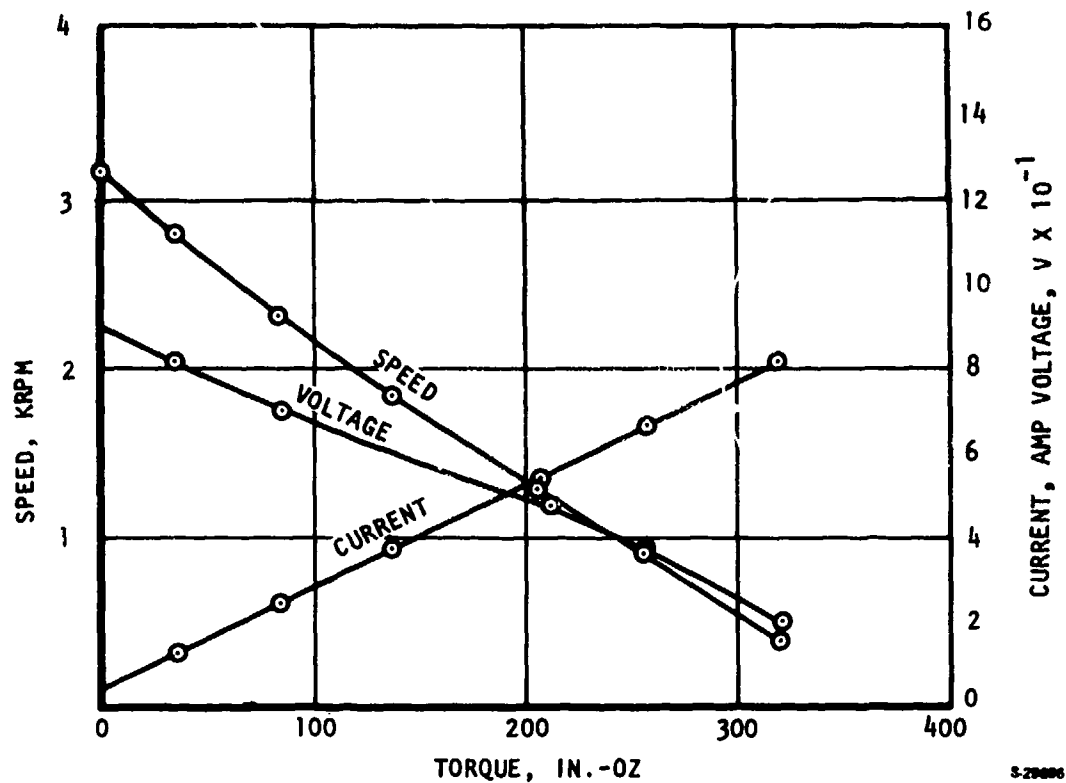


Figure 95. 270-vdc Brushless Motor/Voltage Source Drive Circuit Test (M1), Direction of Rotation: CW

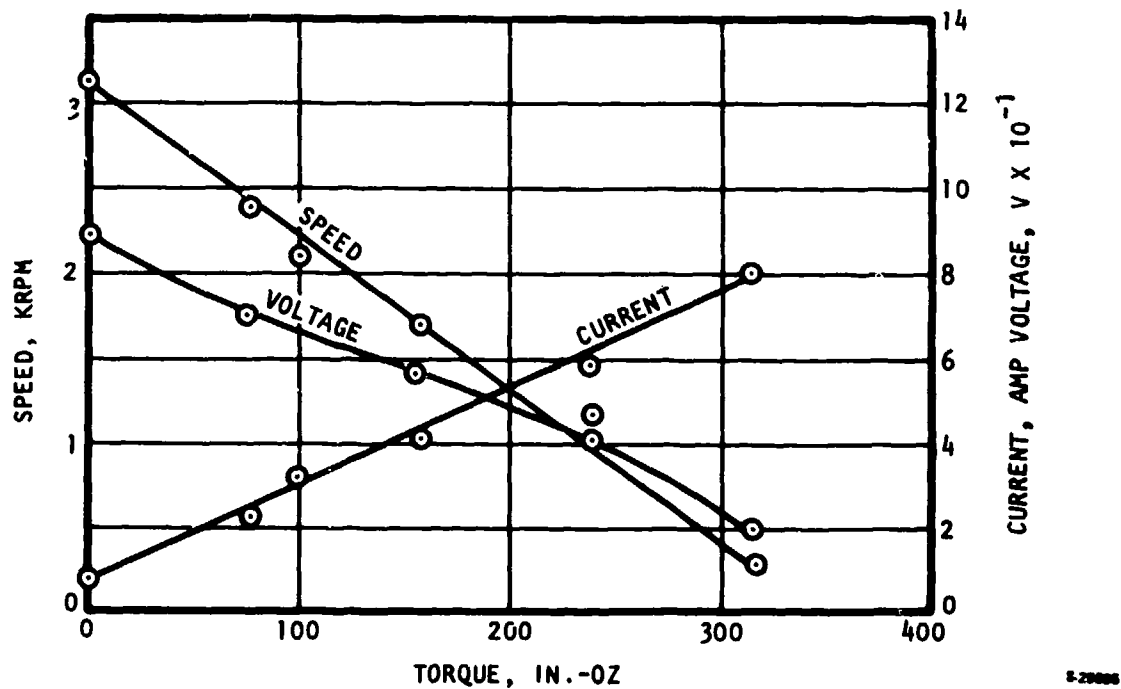
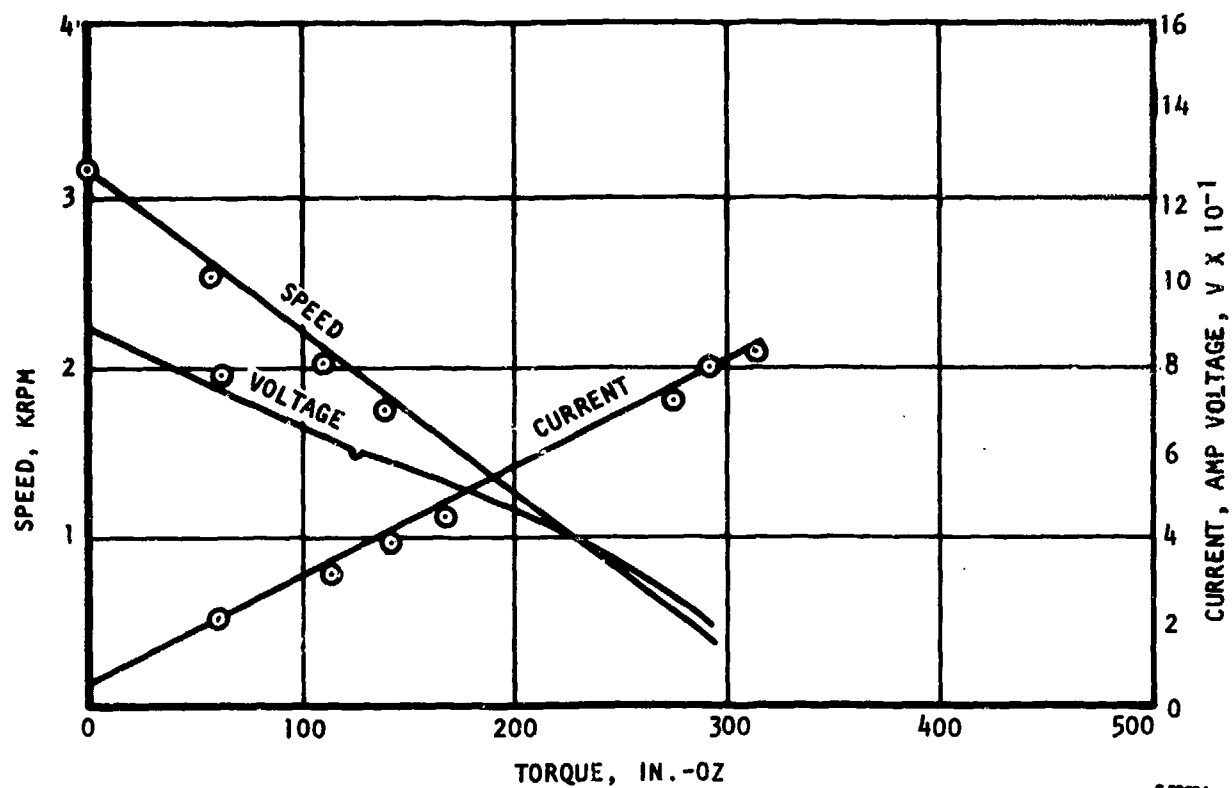
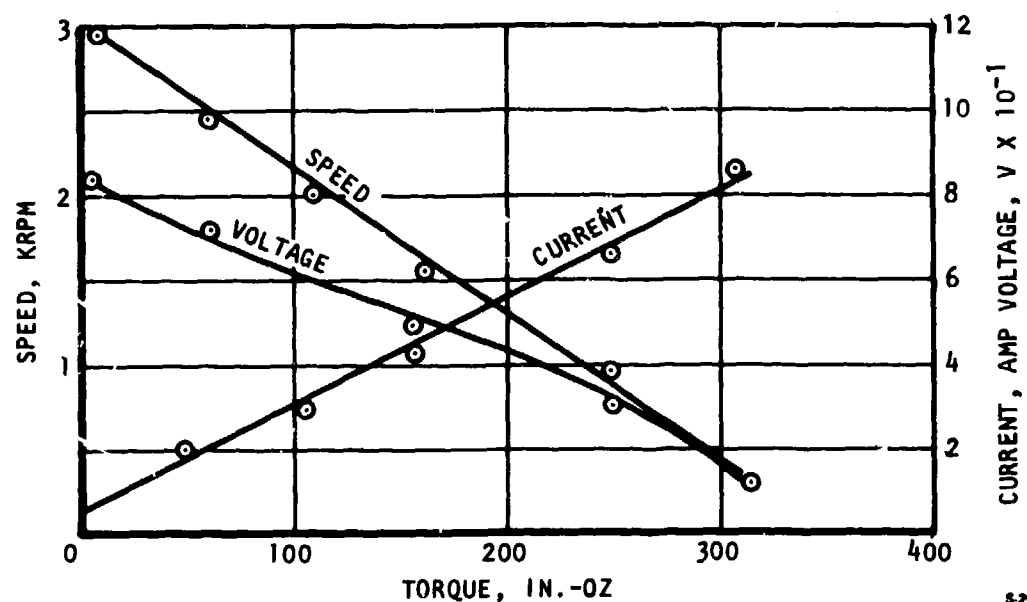


Figure 96. 270-vdc Brushless Motor/Voltage Source Drive Circuit Test (M1), Direction of Rotation: CCW



S-29604

Figure 97. 270-vdc Brushless Motor/Voltage Source Drive Circuit Test (M2), Direction of Rotation: CW



S-29602

Figure 98. 270-vdc Brushless Motor/Voltage Source Drive Circuit Test (M2), Direction of Rotation: CCW

6.1.1.3.1 Test Setup

The dynamometer test setup is shown schematically in Figure 99. Adapters were fabricated to attach the motor to the dynamometer and achieve proper alignment. The test setup is shown in Figure 100.

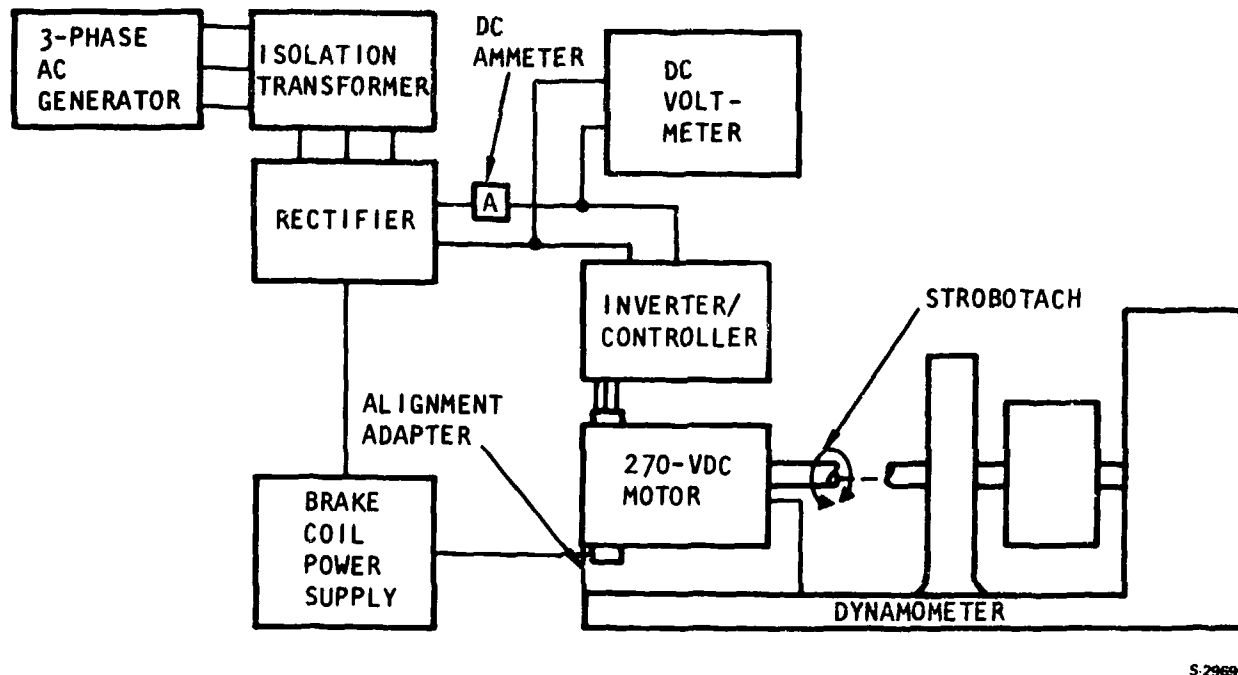


Figure 99. Motor/Voltage Source Drive Circuit Test Schematic Diagram

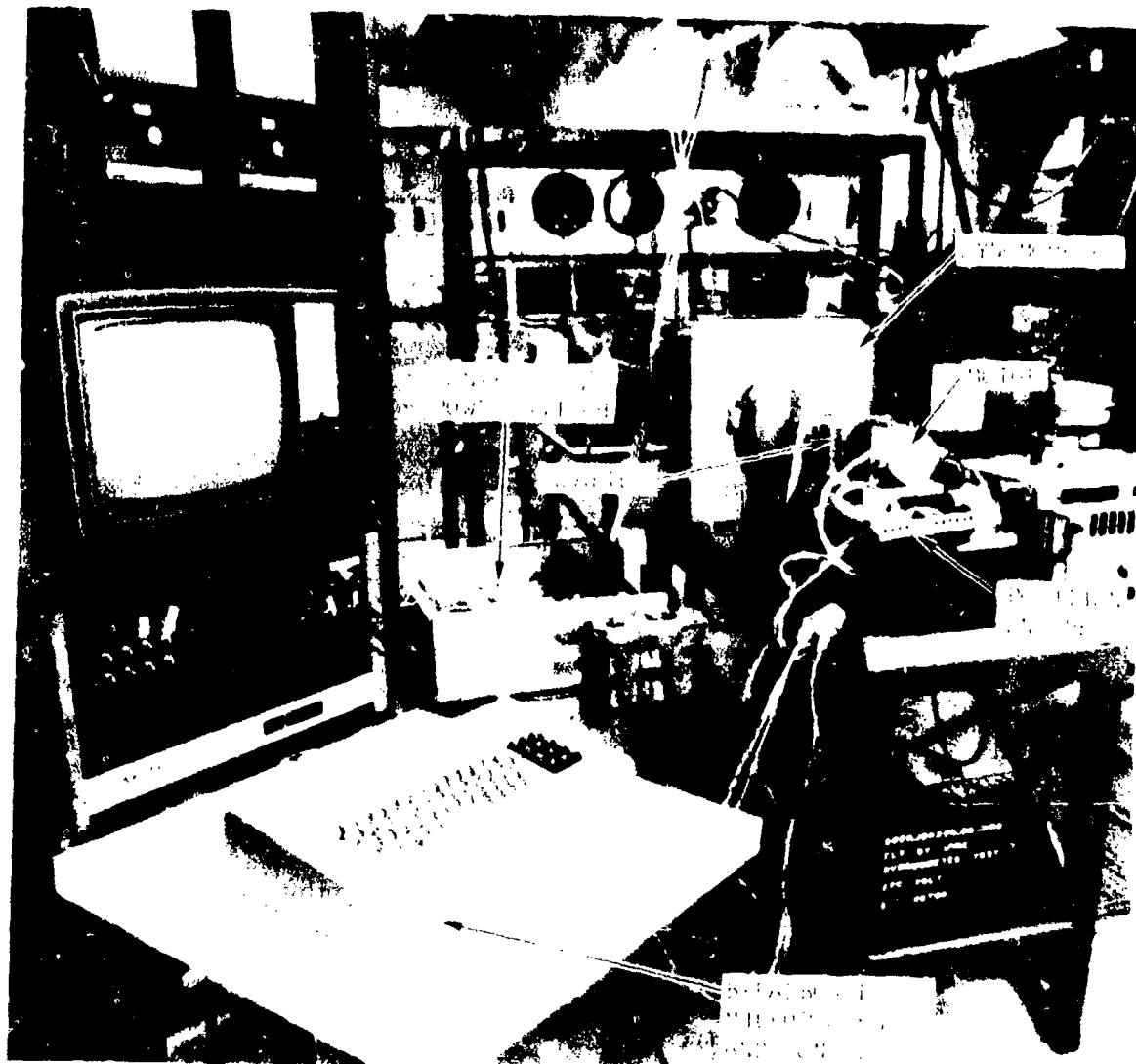
6.1.1.3.2 Procedure

The procedures used for dynamometer testing are as follows.

Step 1--Adapt the test motor to a dynamometer with 800 in.-oz capability.

Step 2--Drive the motor from the inverter/controller with a dc input voltage of 270 v.

Step 3--Read and record voltage, current, speed, and torque simultaneously for five different load points up to the current limit.



80255-1

F-28019

Figure 100. Dynamometer Test Setup

6.1.1.3.3 Discussion of Results

The back emf constant (volts/rpm) and torque constant (torque/ampere) obtained from the test data correlated well with the design value. Because of the current limiting designed into the inverter, the motor current was limited at about 7 amp. The test results are plotted in Figures 101 and 102. Since the inherent characteristic of the chopper inverter causes it to behave like a dc transformer, the motor torque/ampere at current limit is higher than the theoretical value, while the motor speed at that torque is lower than expected; thus, the loss in speed is compensated by the gain in torque (i.e., no loss in power output).

6.1.2 Encoder Receiving Inspection

The encoders are vendor-supplied parts manufactured by RENCO Corporation, Goleta, California. The part was within manufacturer specifications for both form and function. Because the parts were used in a development program under engineering control, no formal receiving inspection was performed. Proper operation of the unit, including physical interfacing, was verified by installation into the breadboard, and performing engineering checkout and functional performance tests.

6.1.3 Controller Checkout

Checkout of the controller for the electromechanical rotary hingeline actuation unit was completed in the laboratory under engineering direction, as part of the electrical interface evolution and resolution. Para. 3.3 contains the discussion of the controller design approach and features. The test verified the operation of the input-output circuits, servoloop, and switch modules. Para. 3.5, dynamic simulation and analysis, shows the correlation of test data to the predicted performance. The control law used in the servo hardware was determined using the digital computer design program. The results of simulation analysis illustrate the ability to analytically predict the operation of electromechanical actuation units.

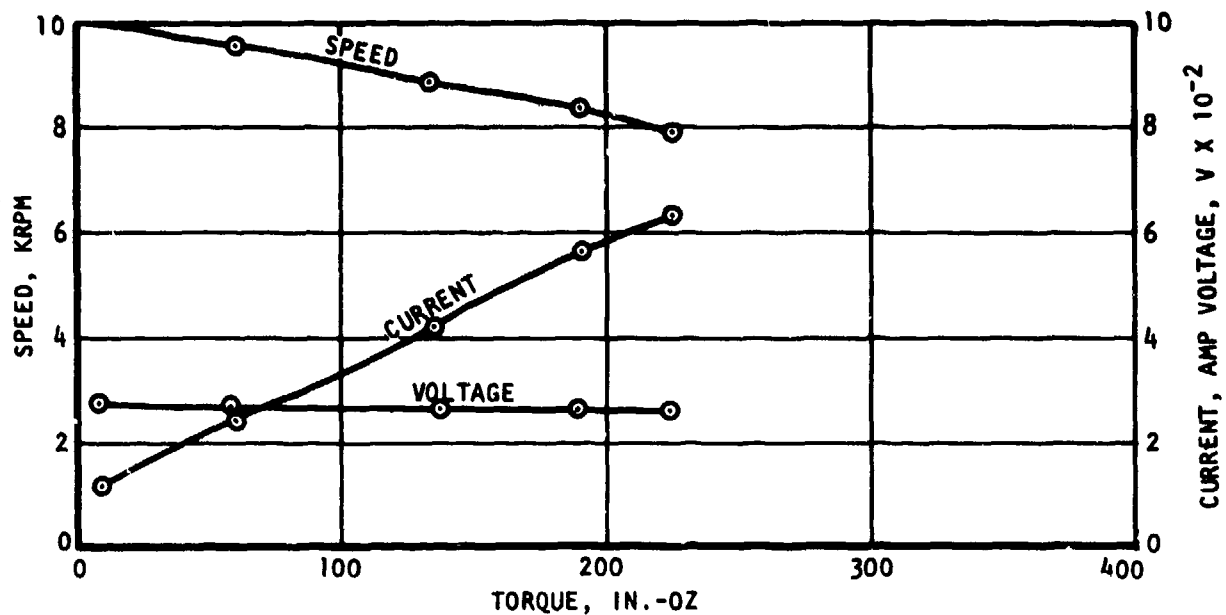
Final design of the power drive circuits involved considerable effort, as discussed in Sections 3 and 7. The present system performs as predicted.

6.1.4 Rotary Gearbox Performance

The gearbox, consisting of the velocity summing differential and the output gearing, was evaluated to determine the backlash, static stiffness, and torque efficiencies. These values were then used in the performance analysis and simulation program to develop the required servo control law.

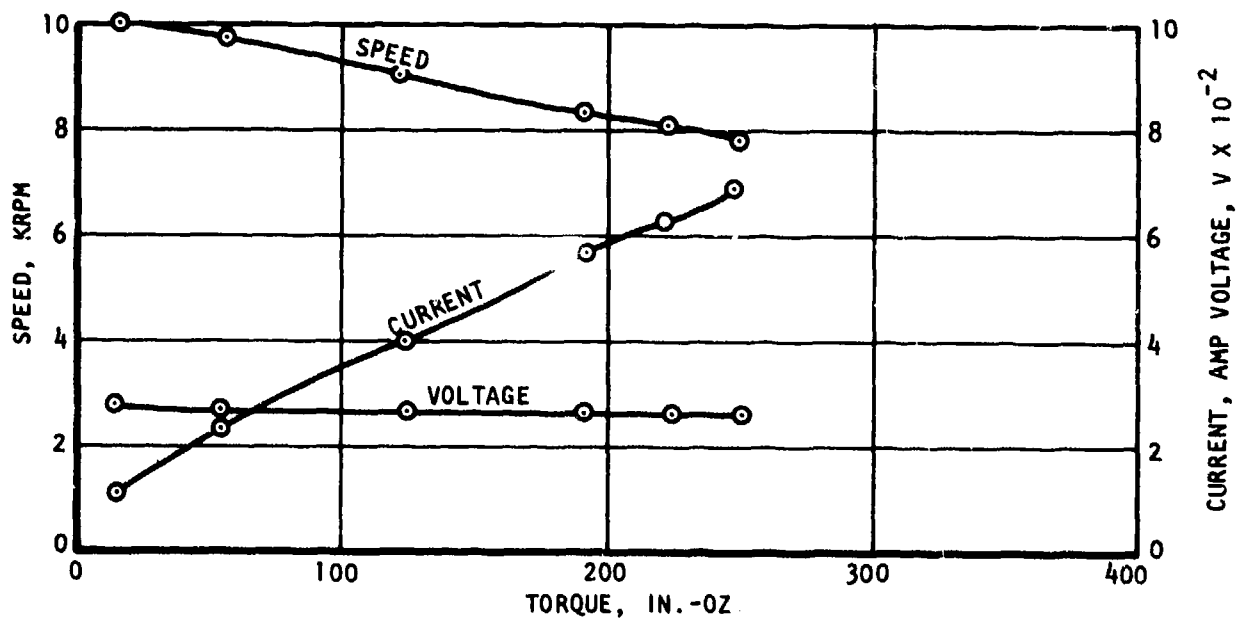
6.1.4.1 Static Stiffness and Backlash

The objective of this test was to determine the spring rate and free play of the actuator gearing.



5-79000

Figure 101. 270-vdc Brushless Motor/Voltage Source Drive Circuit Test, Direction of Rotation: CW



5-79000

Figure 102. 270-vdc Brushless Motor/Voltage Source Drive Circuit Test, Direction of Rotation: CCW

6.1.4.1.1 Test Setup

A schematic drawing of the static stiffness and backlash test setup is shown in Figure 103. For purposes of this test, the motors and the encoder were removed from the actuator. The motor input gears were held stationary by welding dummy motor shafts to attachment plates and bolting the plates to the motor mounts. The setup contains the actuator gearbox installed in the test stand, a pneumatic load cylinder, a load cell, and a dial indicator. A load cell, connected between the 10-in. actuator output arm and the load cylinder, directly measured the load in pounds; a digital readout was attached to the output of the load cell for data collection. The dial indicator was placed on top of the gearbox between the fixed and movable sides of the gearbox.

6.1.4.1.2 Procedure

The actuator backlash was determined by using the test setup shown in Figure 103 and the following procedures.

Step 1--Set the actuator to null position.

Step 2--Apply a positive (upward) load of 5 lb to the actuator output arm.

Step 3--Zero the dial indicator.

Step 4--Apply a negative (downward) load of 5 lb to the actuator output arm.

Step 5--Measure and record the total deflection.

Step 6--Repeat steps 2 through 5 to check results.

In the actuator status stiffness test, the same test setup was used, and the following procedures were performed.

Step 1--Set the actuator to the null position.

Step 2--Apply a positive (upward) load of 5 lb to the actuator output arm.

Step 3--Zero the dial indicator.

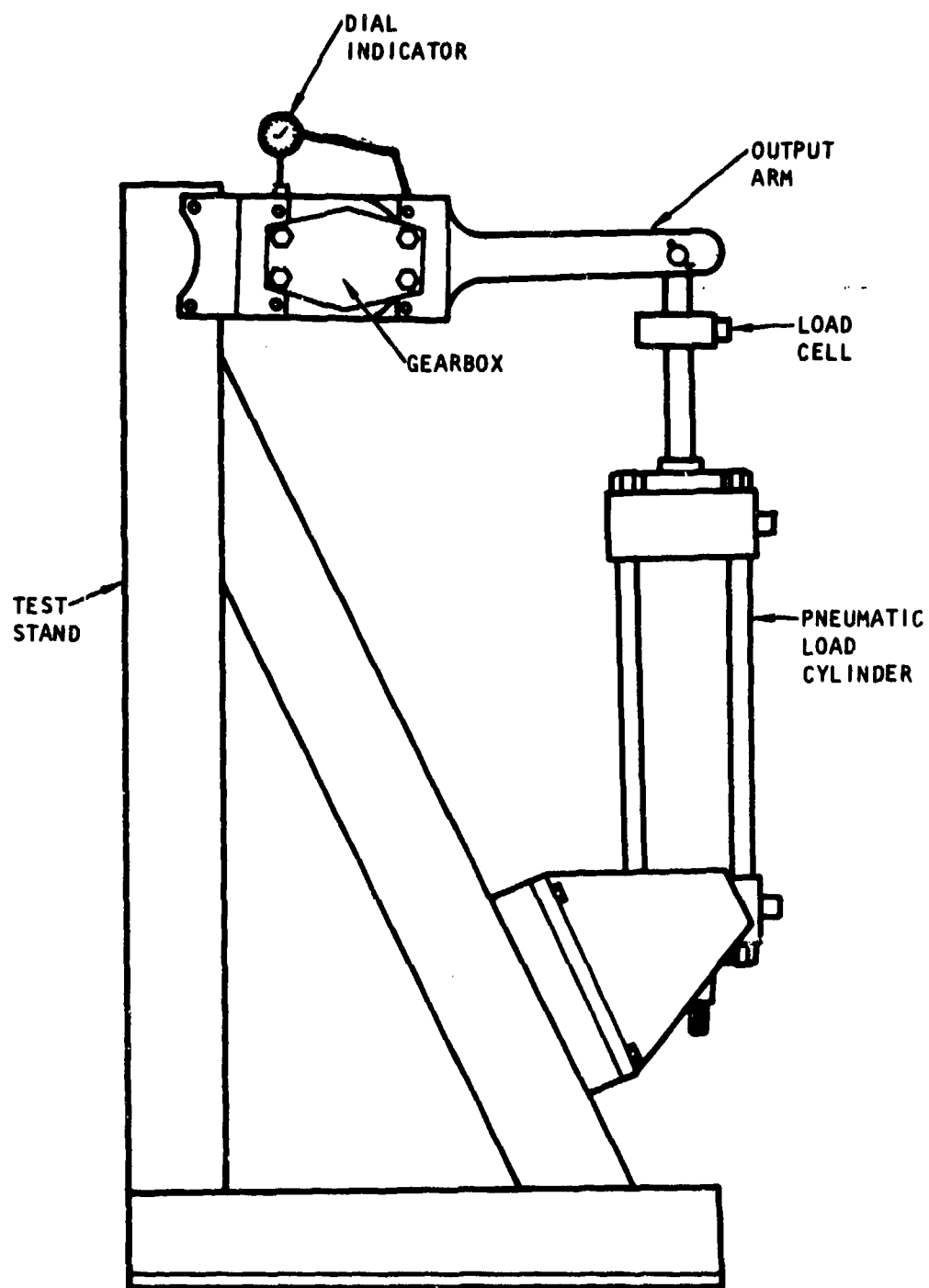
Step 4--Apply positive loads of 10, 25, 50, 75, 100, 200, 300, 400, 500, 750, 1000, 1250, 1500, and 2000 lb to the actuator output arm.

Step 5--Measure and record the deflection at each load.

Step 6--Repeat steps 2 through 5, applying negative loads instead of positive loads.

Step 7--Move the dial indicator to measure actuator and fixture stiffness (i.e., place the dial indicator between the pin centerline and the movable end of the fixture).

Step 8--Repeat steps 2 through 6.

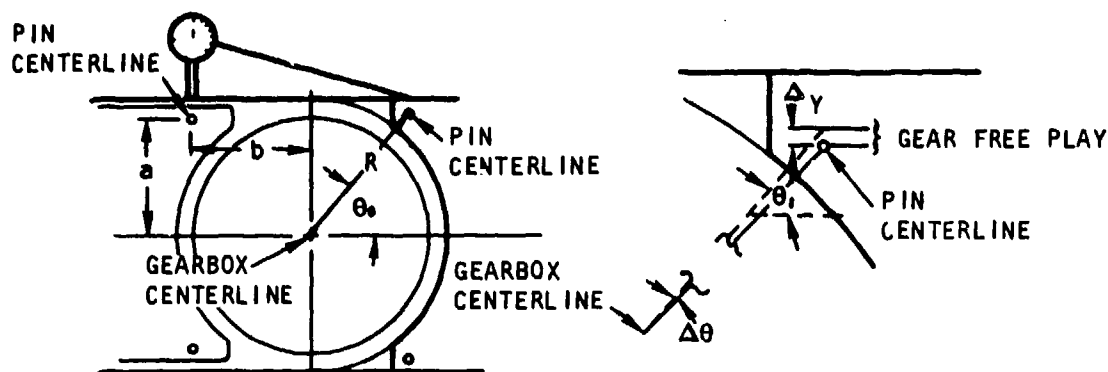


S-29703

Figure 103. Setup for Static Stiffness and Backlash Gearbox Testing

6.1.4.1.3 Discussion of Results

The backlash (free play) of the actuator gearbox is 0.0983 deg. The method used to measure the free play of the gears and calculations used to obtain the backlash are shown in Figure 104.



$$R(\ln) = \sqrt{a^2 + b^2} = \sqrt{(1.625)^2 + (1.75)^2} = 2.3881$$

$$\sin \theta_0 = \frac{a}{R} = \frac{1.625}{2.3881} = 0.68045 \Rightarrow \theta_0 = 42.8789 \text{ deg}$$

$$\sin \theta_1 = \frac{a + \Delta y}{y} = \frac{1.625 + 0.003}{2.3881} = 0.68171 \Rightarrow \theta_1 = 42.9772 \text{ deg}$$

$$\Delta \theta = \theta_1 - \theta_0 = 42.9772 - 42.8789 = 0.0983 \text{ deg}$$

S-28702

Figure 104. Backlash Measurement Method and Calculations

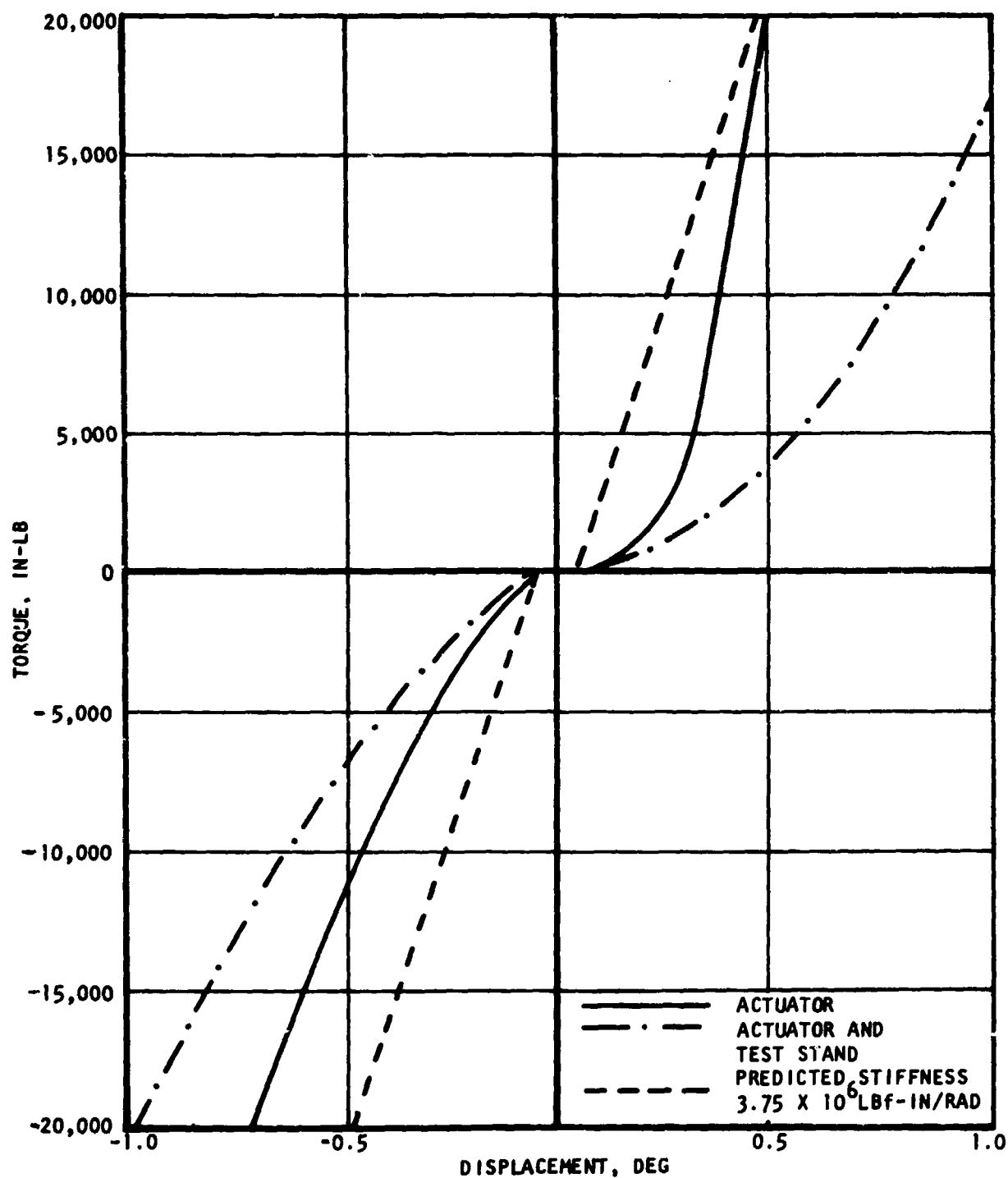
The results of the stiffness test are listed in Table 14 and shown graphically in Figure 105. The predicted spring rate (3.75×10^6 in.-lbf/rad) of the actuator is also shown in Figure 105.

Parametric data representing typical flight control requirements were used to predict the backlash and spring rate. The following compare the predicted values to the test results.

<u>Characteristic</u>	<u>Predicted Value</u>	<u>Test Results</u>
Backlash	0.25 deg	0.0983 deg
Spring rate	3.75×10^6 lbf-in./rad	3.269×10^6 lbf-in./rad (average)

TABLE 14
ACTUATOR STATIC STIFFNESS DATA

Actuator Only				Actuator and Test Fixture			
Upward Load, lb	Deflection, in.	Downward Load, lb	Deflection, in.	Upward Load, lb	Deflection, in.	Downward Load, lb	Deflection, in.
0	0.0	0	0.0	0	0.0	0	0.0
+10	0.0	-10	0.0006	+10	0.0005	-10	0.0008
+25	0.0003	-25	0.0011	+25	0.0007	-25	0.0012
+50	0.0022	-50	0.0014	+50	0.0024	-50	0.0018
+75	0.0030	-75	0.0018	+75	0.0035	-75	0.0023
+100	0.0034	-100	0.0022	+100	0.0042	-100	0.0034
+200	0.0055	-200	0.0037	+200	0.0074	-200	0.0052
+300	0.0064	-300	0.0047	+300	0.0098	-300	0.0076
+400	0.0072	-400	0.0057	+400	0.0128	-400	0.0094
+500	0.0078	-500	0.0069	+500	0.0146	-500	0.0110
+750	0.0088	-750	0.0094	+750	0.0186	-750	0.0151
+1000	0.0097	-1000	0.0119	+1000	0.0218	-1000	0.0184
+1250	0.0108	-1250	0.0141	+1250	0.0244	-1250	0.0213
+1500	0.0115	-1500	0.0163	+1500	0.0273	-1500	0.0240
+2000	0.0135	-2000	0.0200	+2000	0.0318	-2000	0.0293



S-20007

Figure 105. Gearbox Stiffness

The slight difference in upward stiffness compared to downward stiffness may be a result of one or more of the following considerations:

- Gear phasing
- Manufacturing difference in gear slices

6.1.4.2 Efficiency

The objective of this test was to determine the torque efficiency of the gearing.

6.1.4.2.1 Test Setup

The setup for this test is similar to that shown in Figure 101.

6.1.4.2.2 Procedure

The efficiency data were obtained by measuring the input torque and the output force as measured using the load cell at the end of the 10-in. arm. The output torque then could be calculated. The torque multiplication factor is 1211:1 for single-ended drive (i.e., one motor).

6.1.4.2.3 Discussion of Results

Gearbox efficiency for both channels is shown in Figure 106. The efficiency is low at low input torque values because of the relatively constant losses in the gearing due to viscous drag and stiction. The efficiency begins to reduce slightly at high input torque due to the additional friction caused by elastic deformation of the gearing. The values of efficiency shown (approximately 75 to 82 percent) compare well with the predicted performance of 83 percent (Appendix A).

6.2 ELECTROMECHANICAL ACTUATION UNIT TESTS

The tests and evaluation of the complete actuation unit operating as a dual-channel, redundant assembly, and in certain instances as a single-channel assembly, are summarized below. During setup for the actuation unit tests, physical compatibility was established as well as resolution of functional interfaces. The motors and gearbox interfaced without hardware modification. Extensive development effort was required (as discussed in para. 3.3 and Appendix E) to establish compatible current limits, rate, and torque limits between the motor, power switch, and servo circuits.

As the unit underwent design improvements during the checkout and early development phase, the controller servo circuits were modified from the baseline microprocessor to the analog configuration. The test data presented therefore include the data from the unit when (1) operating with microprocessor servo circuits and (2) when the servo circuits were both analog. The actuator, test stand, and breadboard controller are shown in Figure 107. The tests conducted on the unit are listed in Table 15.

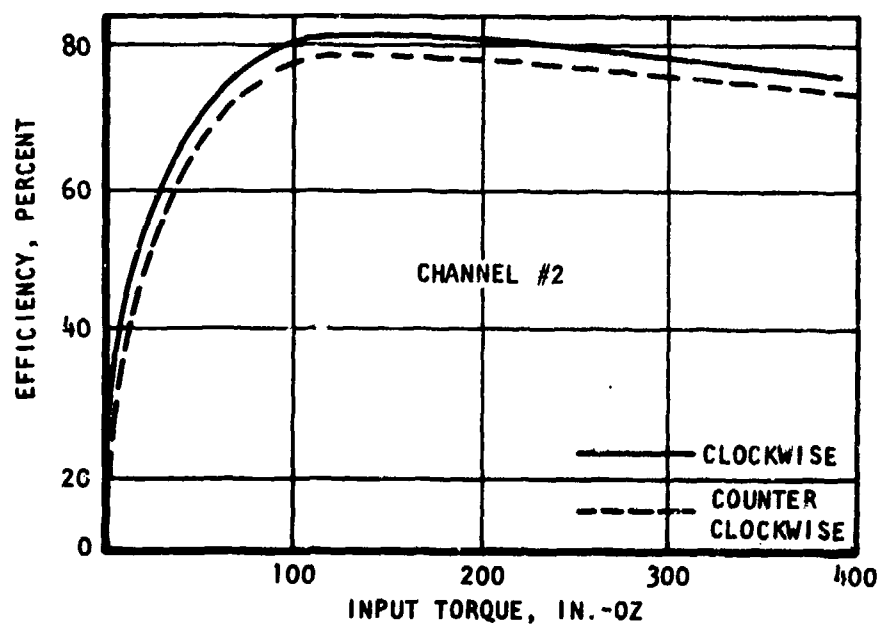
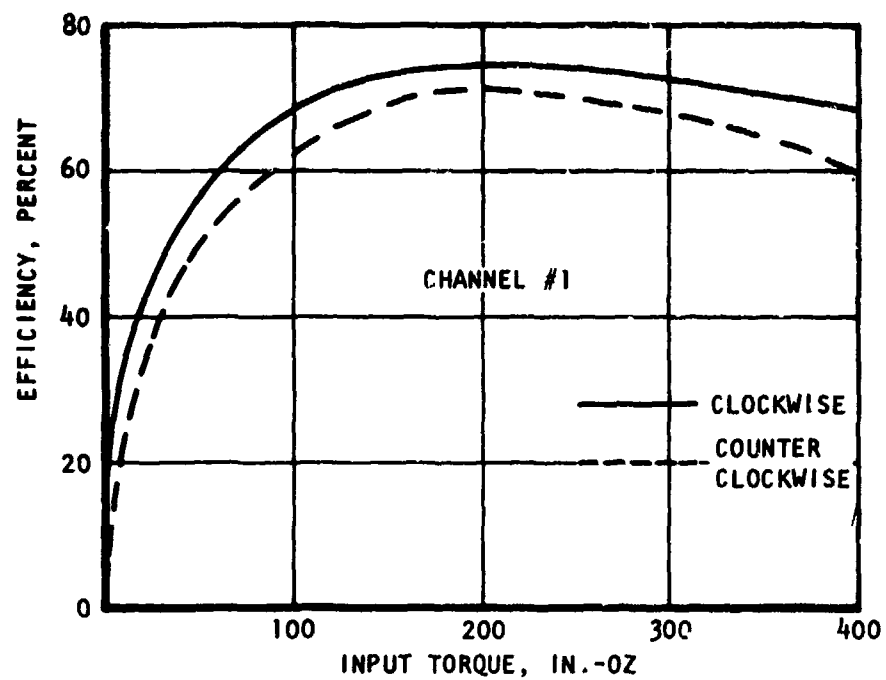
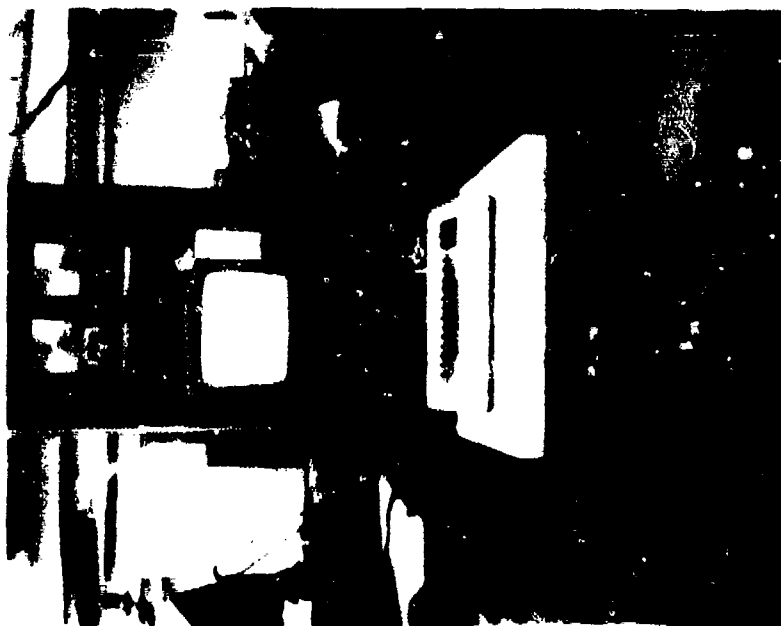


Figure 106. Gearbox Efficiency for Both Channels



ELECTROMECHANICAL ACTUATOR
ON TEST STAND

F-28021



BRASSBOARD MICROPROCESSOR CONTROLLER
AND POWER INVERTER ASSEMBLY

Figure 107. Demonstration Test Hardware

TABLE 15
ACTUATION UNIT TESTS

Test Conducted	Paragraph Reference No.	Servo Configuration	
		Microprocessor	Analog Servo Circuits
Frequency response	6.2.1	Yes	Yes
Dynamic stiffness	6.2.2	Yes*	No
Step response	6.2.3	Yes	Yes
Position resolution/hysteresis	6.2.4	Yes	Yes
Regeneration	6.2.5	Yes	No
Reliability management demonstration	6.2.6	Yes	No
Thermal management	6.2.7	Yes	No

*Data were gathered, but found to be inconclusive.

6.2.1 Frequency Response

The objective of the frequency response tests was (1) to determine the amplitude ratio between input command and output position as a function of input frequency and (2) to evaluate phase lag between input and output.

6.2.1.1 Procedure

The frequency response test began with the actuation unit being turned on. The input sine wave command was adjusted to correspond to ± 1 deg position signal. The output position was determined from the digital optical encoder. These two signals were recorded by an oscillograph. The input signal sine wave frequency was varied in steps from 0.5 to 10 Hz. Appendix H shows representative oscillograph traces of the data taken.

6.2.1.2 Discussion of Results

Figures 108 and 109 show the results of tests performed using the early digital microprocessor controller. The curves for both ± 1 and ± 2 deg input amplitudes show reasonable correlation with the required 8-Hz bandwidth goal (i.e., the amplitude degraded less than 3 db at 8 Hz). Both curves, however,

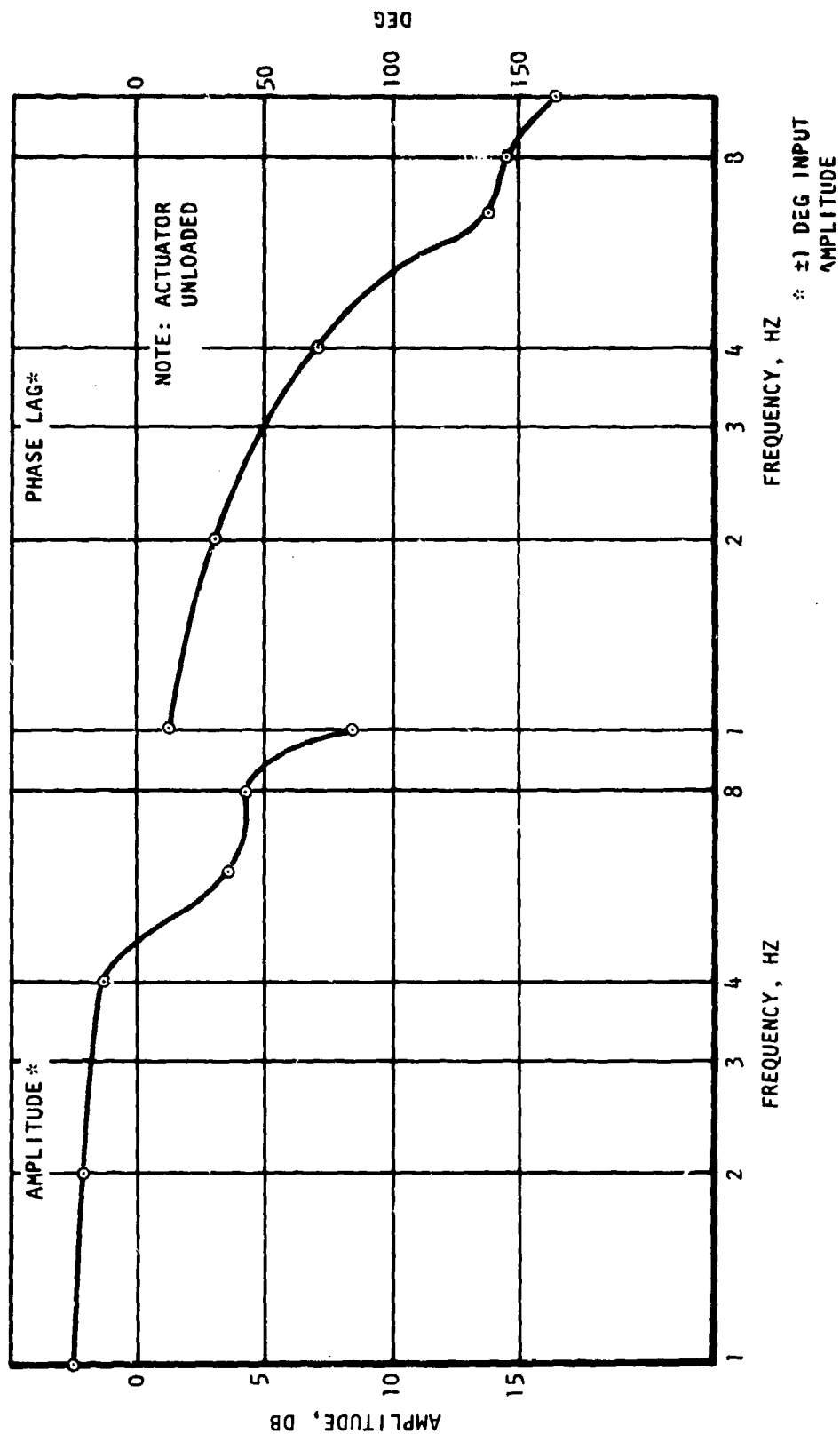


Figure 108. Frequency Response for the Digital Controller, ± 1 Deg Amplitude

5-20788

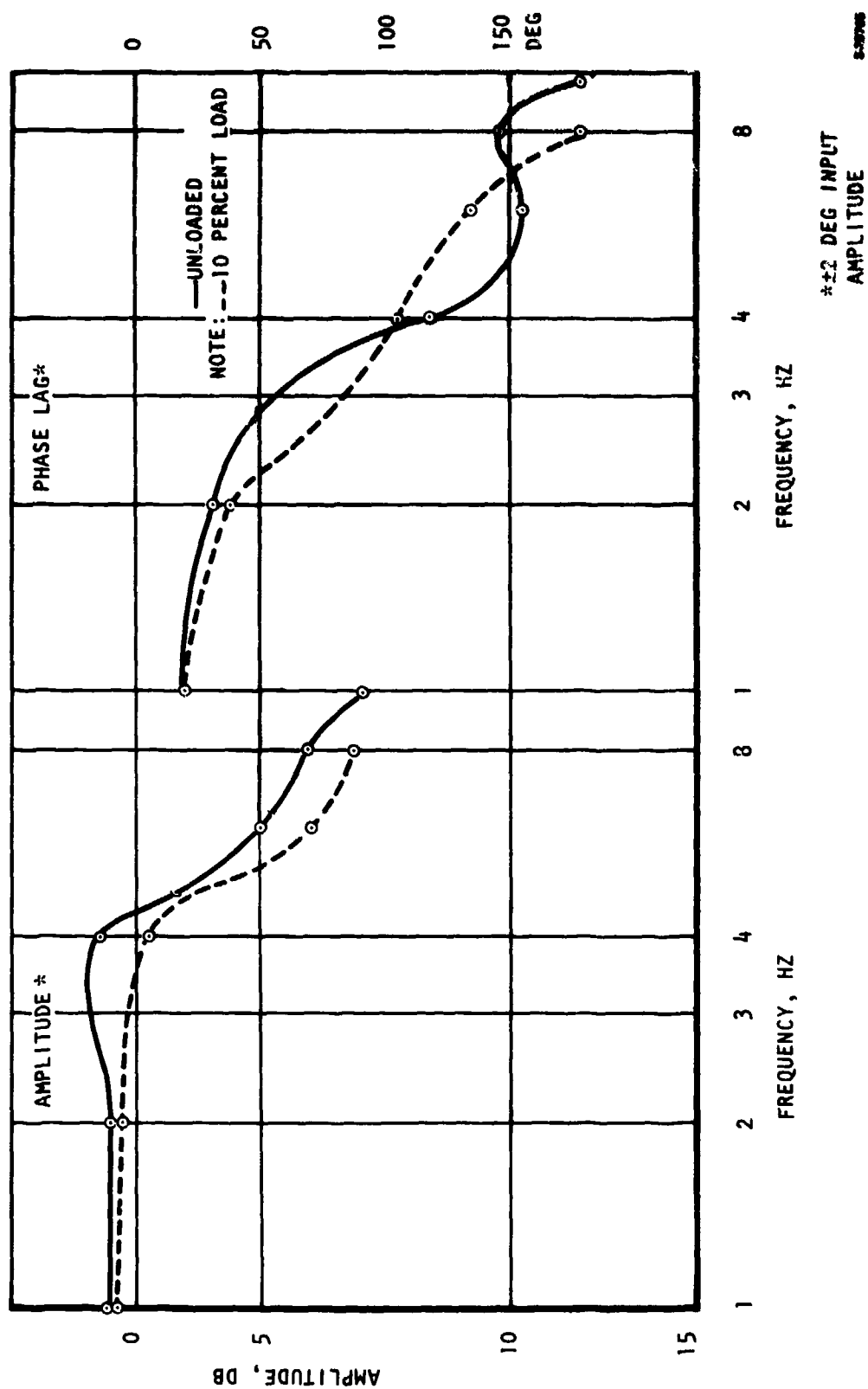


Figure 109. Frequency Response for the Digital Controller, +2 Deg Amplitude

show the phase lag to be approximately 150 deg at 8 Hz. This compares unfavorably with the goal of only a 90 deg phase lag at 8 Hz.

As discussed in para. 3.3, two analog servo circuits were fabricated and tested. The analog configurations of the servo controller were equipped with more desirable control laws than the digital servo. Figures 110 through 117 show the frequency response characteristics for combinations of servo configuration, load, amplitude and number of operating channels. The oscillograph traces used to calculate phase lag and frequency response are shown in Appendix H. The tests were performed at laboratory ambient temperatures. The correlation with the performance goals is high. Additional frequency response Bode plots are contained in para. 3.5 along with the comparison to the analytical prediction of performance.

6.2.2 Dynamic Stiffness

The objective of the dynamic stiffness test was to show the dynamic stability of the actuation unit when it is subjected to fluctuating loads of various frequencies applied to the simulated control surface.

6.2.2.1 Test Procedure

A hydraulic-powered load stand was connected to the load cylinder on the actuation unit test stand. Hydraulic fluid was controlled to the load cylinder to cause a quasi-sine wave load at the actuator output (as shown in Figure 118).

The signal generator provided the control signal to the servo valve to cause fluid to enter the load cylinder. The frequency of the signal generator was varied from 1 to 15 Hz. The load cell was used to determine the applied load at each frequency. The controller was active, and the input command signal was set to a null (or center) control surface position. Data taken on the oscillograph included the applied load and output position.

6.2.2.2 Discussion of Results

Data taken during early development testing (microprocessor controller) showed dynamic stiffness of approximately 15,000 to 20,000 in.-lb/deg over the frequency range of 1 to 10 Hz. Because of difficulties in clearing air from the hydraulic load stand, the results of tests could not be repeated, and are not included here. Analytical prediction of dynamic stiffness (refer to para. 3.5) shows approximately 95,000 in.-lb/deg at a frequency of 8 Hz with the tachometer feedback configuration of the analog servo control.

6.2.3 Step Response

The objective of the step response test is to determine the quality of response to step input, and specifically acceleration, no-load rate, overshoot, and limit cycling, if any.

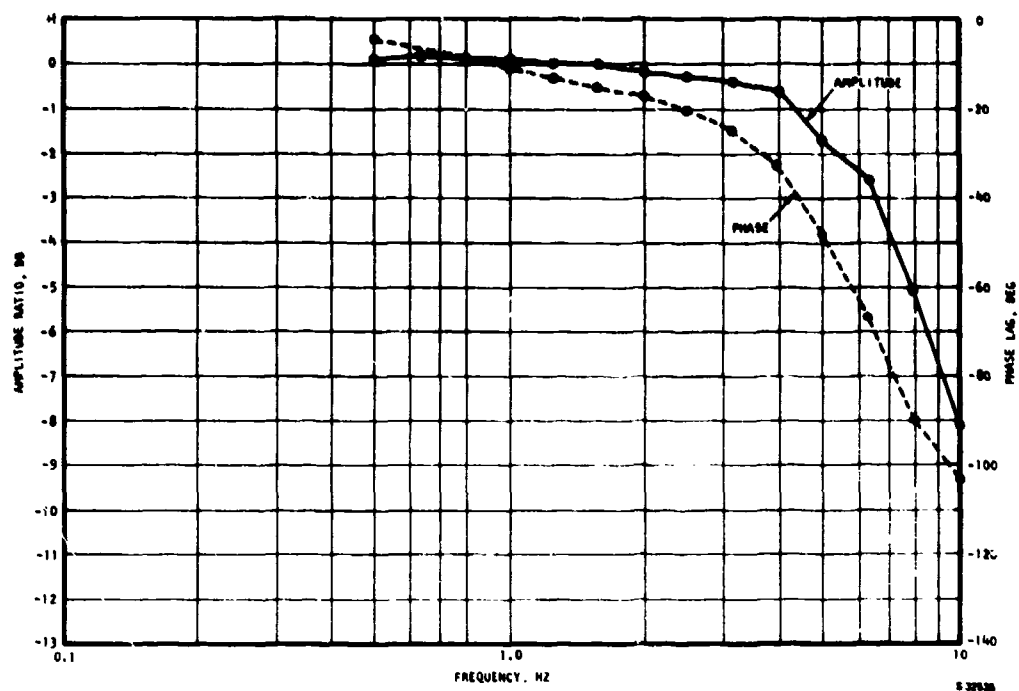


Figure 110. Frequency Response for Voltage Control Servo, No-Load, Dual-Channel ± 2 deg Amplitude

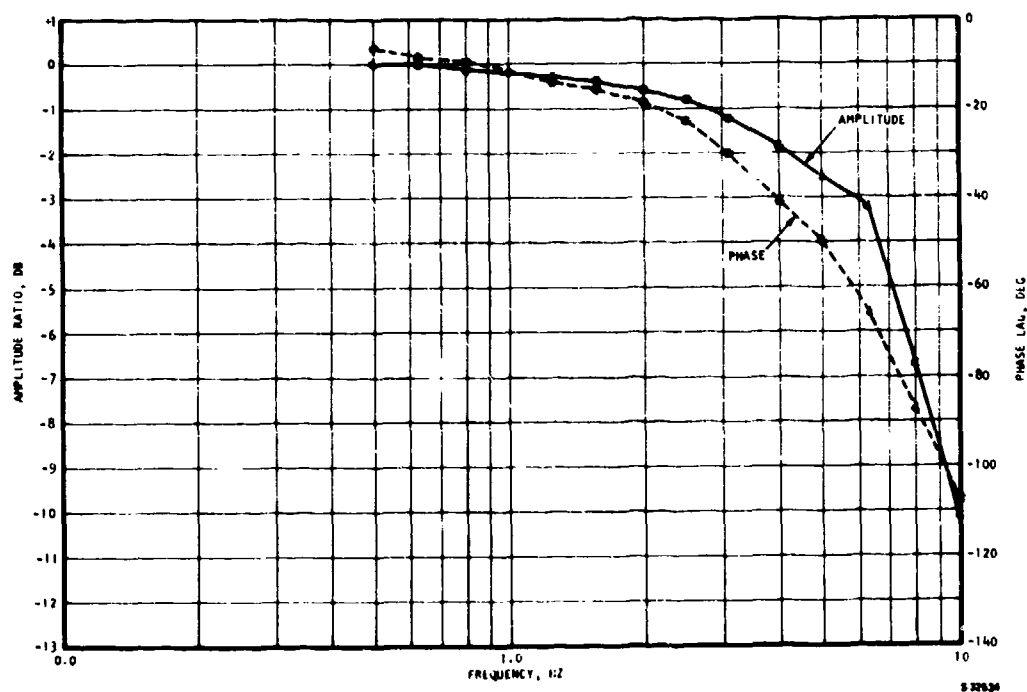


Figure 111. Frequency Response for Voltage Control Servo, 11,250 in.-lb Load, Dual-Channel ± 2 deg Amplitude

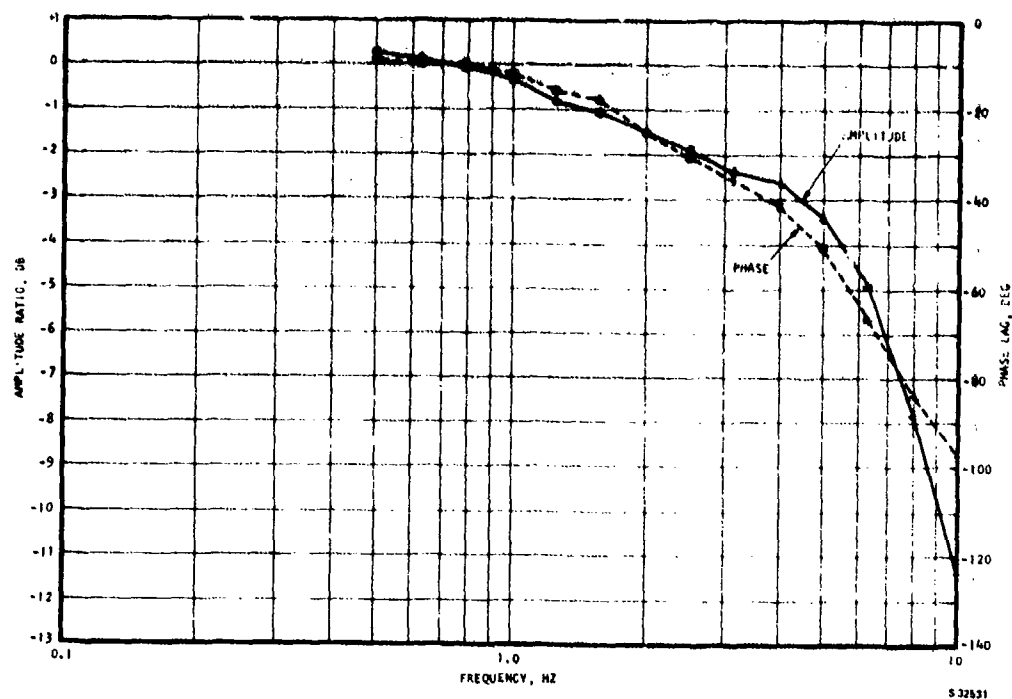


Figure 112. Frequency Response for Voltage Control Servo, 15,080 in.-lb Load, Dual-Channel, ± 2 deg Amplitude

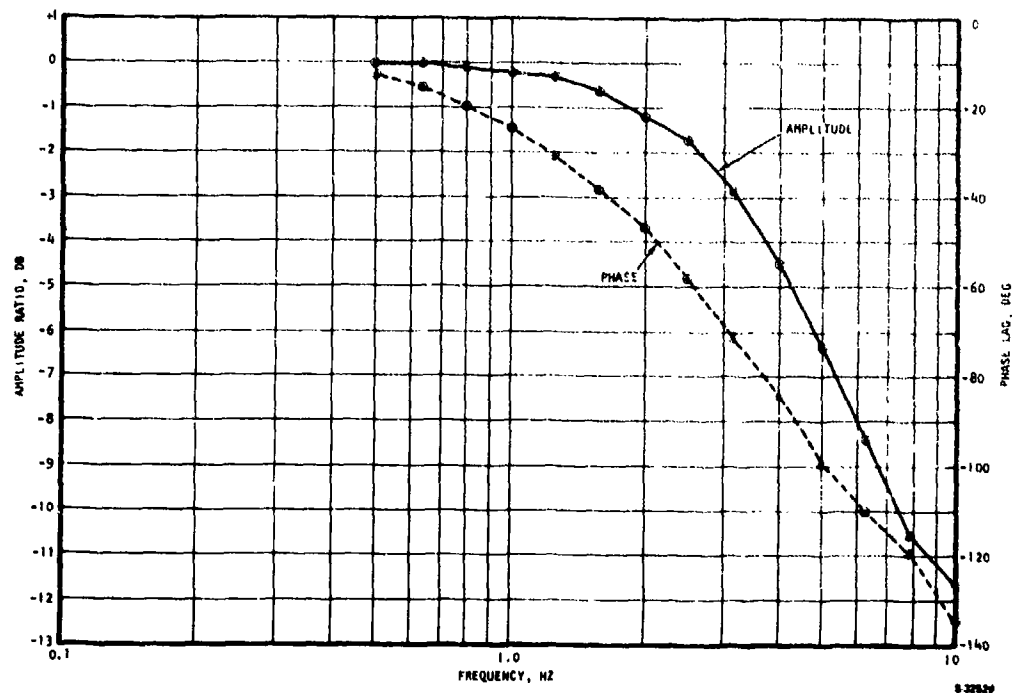


Figure 113. Frequency Response for Tachometer Feedback Servo, Dual Channel, No-Load, ± 1 deg Amplitude

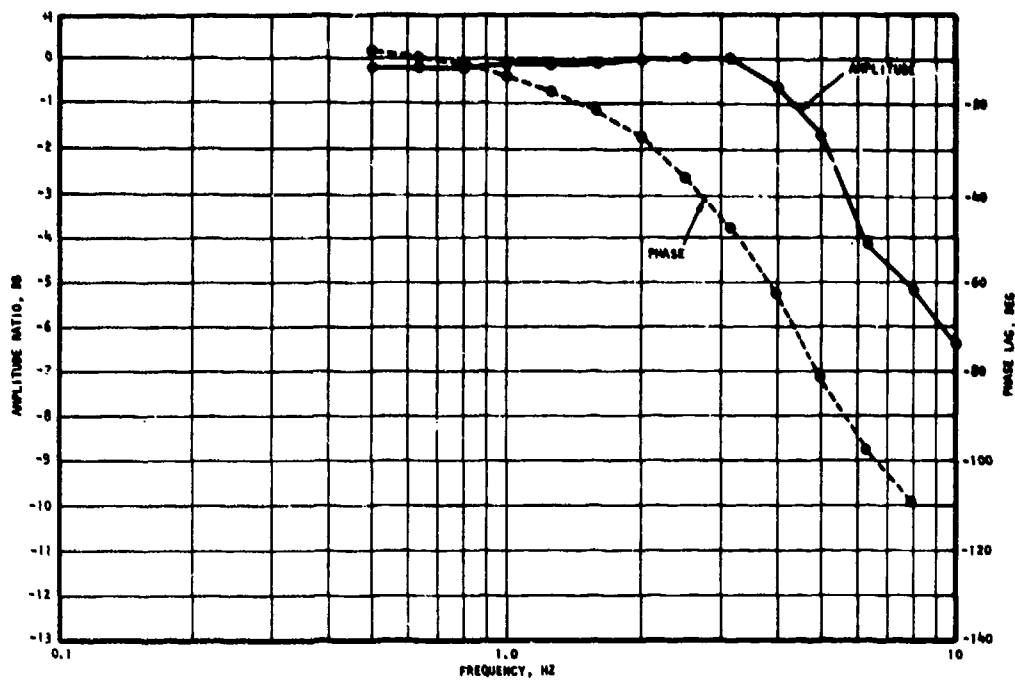


Figure 114. Frequency Response for Tachometer Feedback Servo, Dual-Channel, 8,630 in.-lb Load, ± 1 deg Amplitude

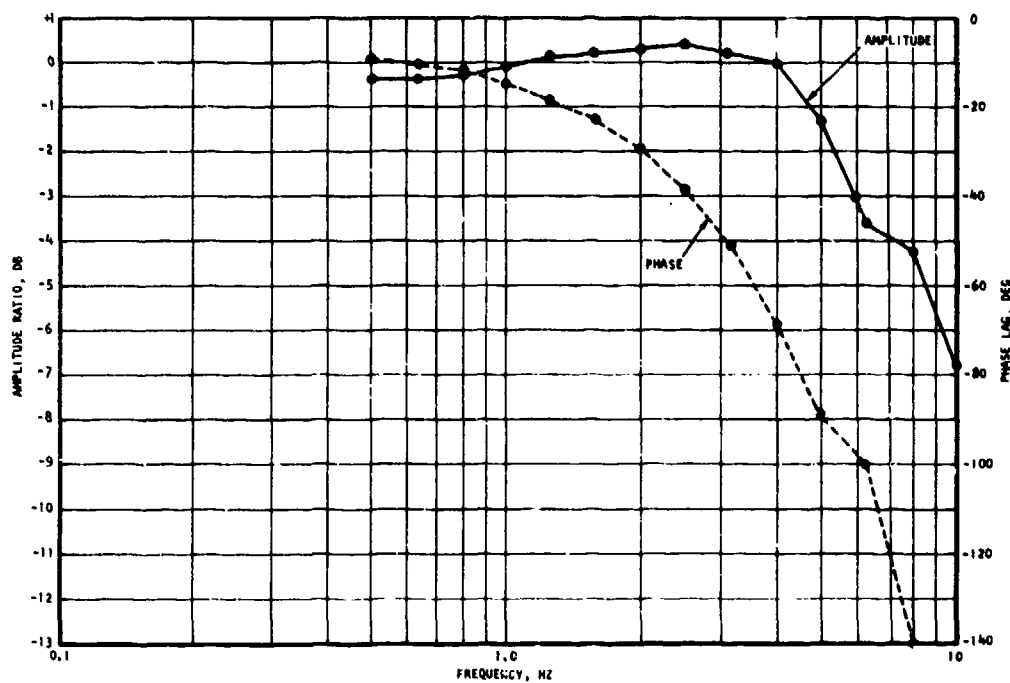


Figure 115. Frequency Response for Tachometer Feedback Servo, Dual-Channel 13,310 in.-lb Load, ± 1 deg Amplitude

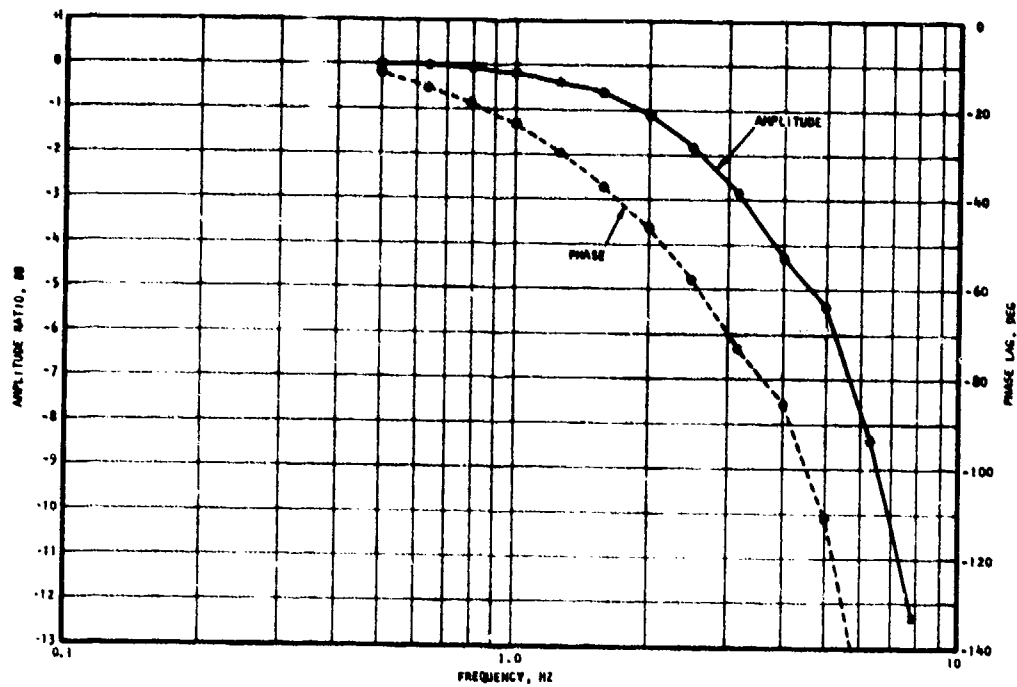


Figure 116. Frequency Response for Tachometer Feedback Servo, Single-Channel, No-Load, ± 2 deg Amplitude

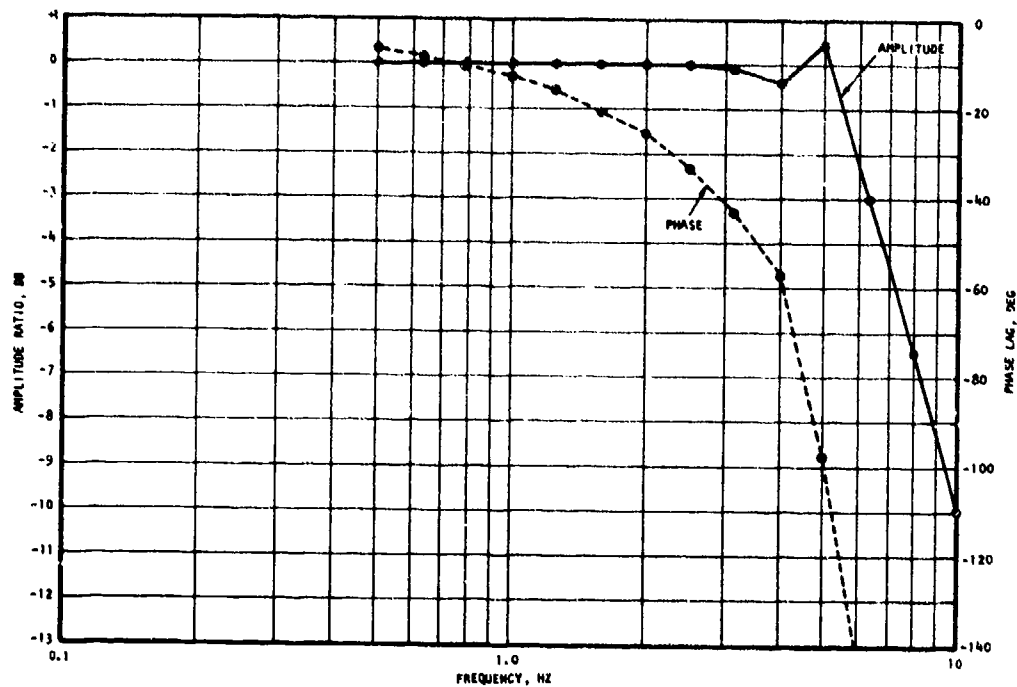


Figure 117. Frequency Response for Tachometer Feedback Servo, Dual-Channel, No-Load, ± 2 deg Amplitude

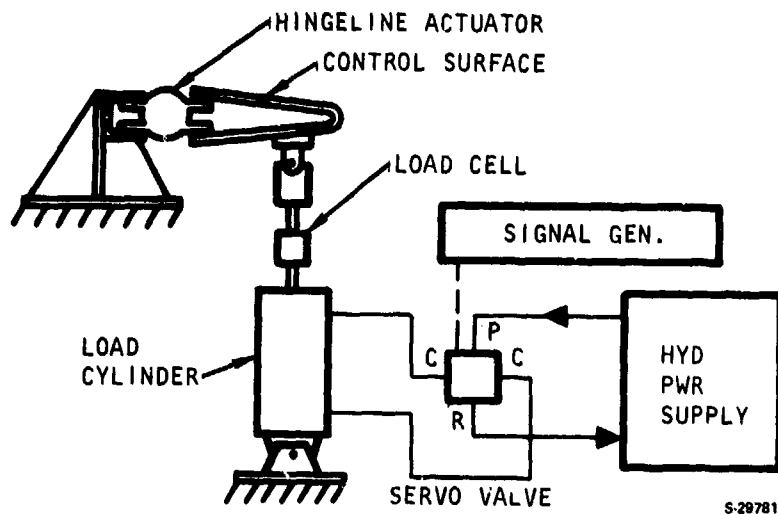


Figure 118. Equipment Schematic for Dynamic Stiffness

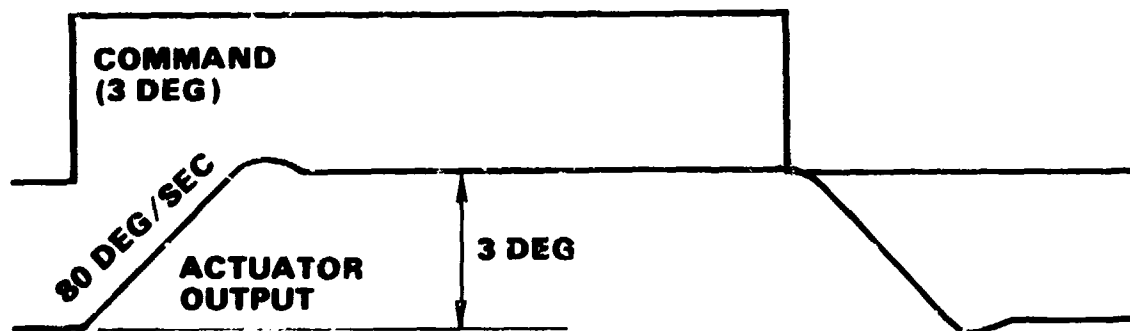
6.2.3.1 Test Procedure

The actuation unit was operated using a square wave generator for the input command signal. The amplitude of the command signal was adjusted to provide output position changes of 1, 3, 5, and 10 deg. Data were recorded using an oscillograph, and included input command, output position, motor current, and load, if any.

6.2.3.2 Discussion of Results

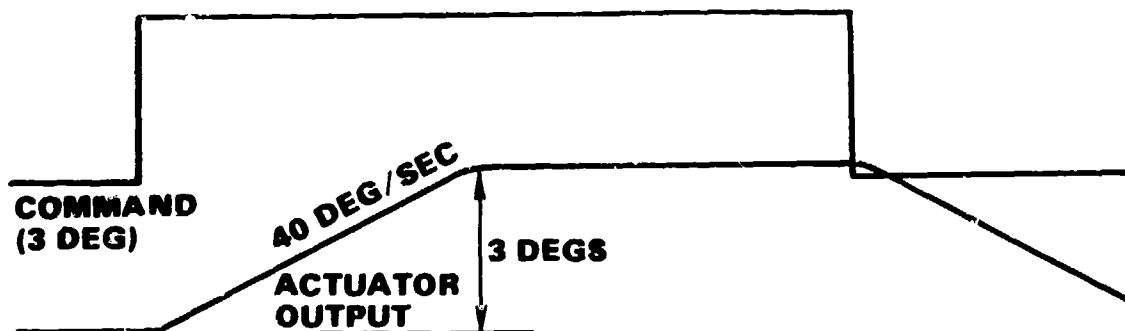
6.2.3.2.1 Step Response for Early Microprocessor Controller

The actuation unit response to 3-deg step input commands is shown in Figures 119 and 120. Figure 119 shows an 80 deg/sec rate for dual-channel operation, and Figure 120 shows a 40 deg/sec rate for single-channel operation. A representative sample of raw data compiled for the step response test is contained in Appendix H.



S 24404

Figure 119. Response to Step Input Dual-Channel Operation



S 24405

Figure 120. Response to Step Input Single Channel Operation, Microprocessor Controller

Acceleration and velocity of the control surface were evaluated as part of this test. The results are summarized below:

<u>Input Waveform</u>	<u>Load</u>	<u>Velocity</u>		<u>Acceleration (Max.)</u>
		<u>Min.</u>	<u>Max.</u>	
Square wave	20 percent	76*	77	3080 deg/sec ²
Square wave	35 percent	57**	80	3200 deg/sec ²

*Power supply voltage varied between 221 and 270 vdc.

**Power supply voltage varied between 168 and 270 vdc.

6.2.3.2.2 Step Response for Analog Servo Controllers

Improved performance of the actuation unit was achieved with both the control and tachometer feedback servo configurations as shown in the step response data of Figures 121 through 126 for step commands of 1, 5, and 10 deg. The overshoot is reduced compared to earlier test results. The slew rate is approximately 80 deg/sec, which corresponds to two-channel operation for all data shown. Comparison of the actual step response with the analytical prediction is presented in para. 3.5.

6.2.4 Position Resolution/Hysteresis

The objective of the position resolution/hysteresis test is to evaluate the hysteresis band between the input command position and the output response.

6.2.4.1 Procedure

The actuation unit was energized and a low frequency (0.1-Hz) triangle wave was applied as an input command. The amplitude of the input was scaled to yield an amplitude in excess of 20 deg. Data taken with an oscillograph include input command and output position.

6.2.4.2 Discussion of Results

The results of early testing of the unit using the microprocessor control are shown in Figure 127. These data were collected for a total deflection of +23 deg. Results of this test indicated that resolution was an area for potential improvement during subsequent design and development activities. As a result, the resolution of the output position was increased by the addition of the 4.48:1 gear head between the optical position encoder and the control surface. This increased the resolution capability from 0.0879 to 0.0196 deg. Para. 3.4 describes the development modification. This addition, as well as concurrent improvements in the threshold and gain characteristics of the analog servo circuits, resulted in substantially reduced hysteresis. The performance of the improved actuation unit is shown in Figure 128.

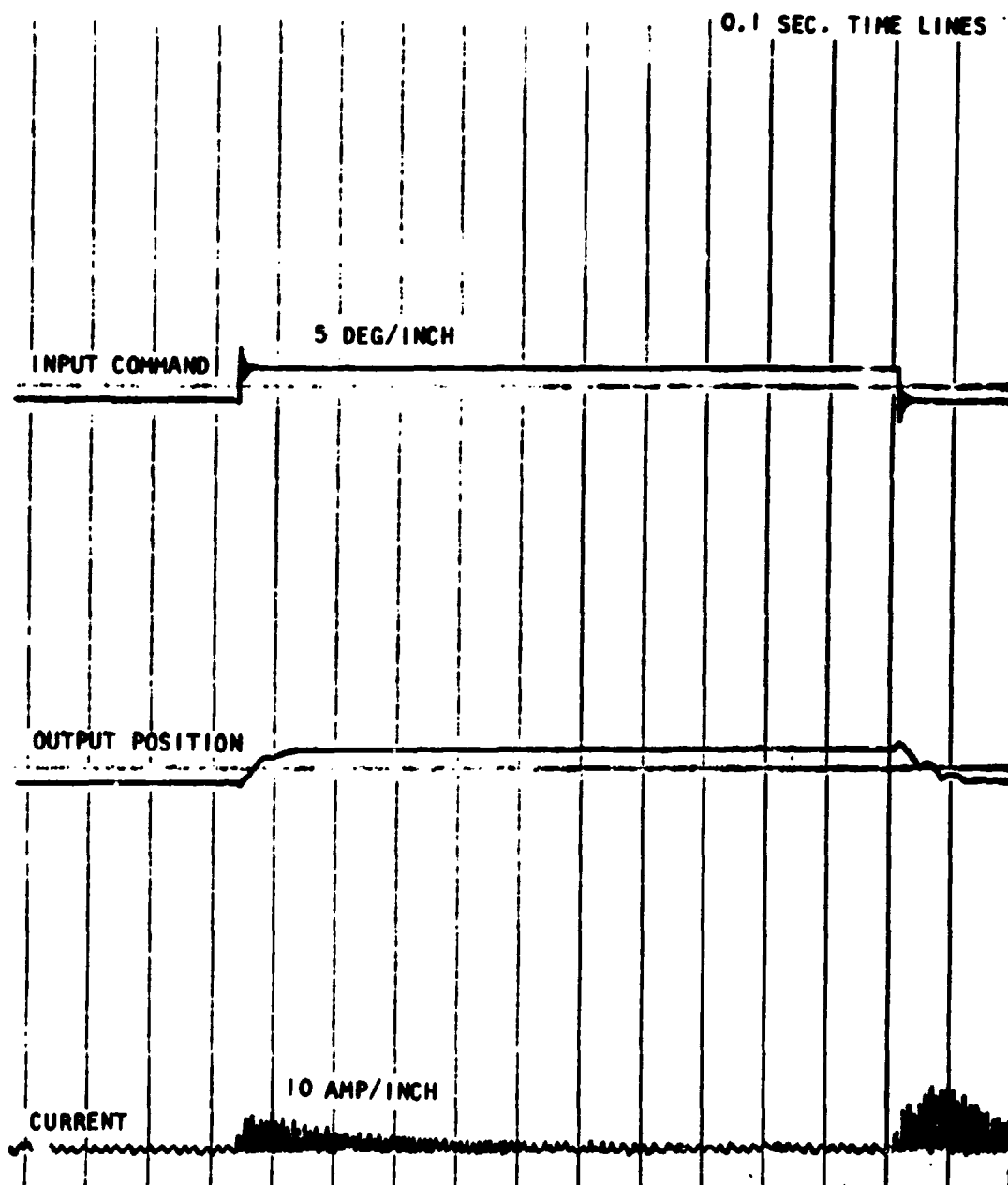


Figure 121. Voltage Control Servo--Dual-Channel Step Response,
1 deg, No Load

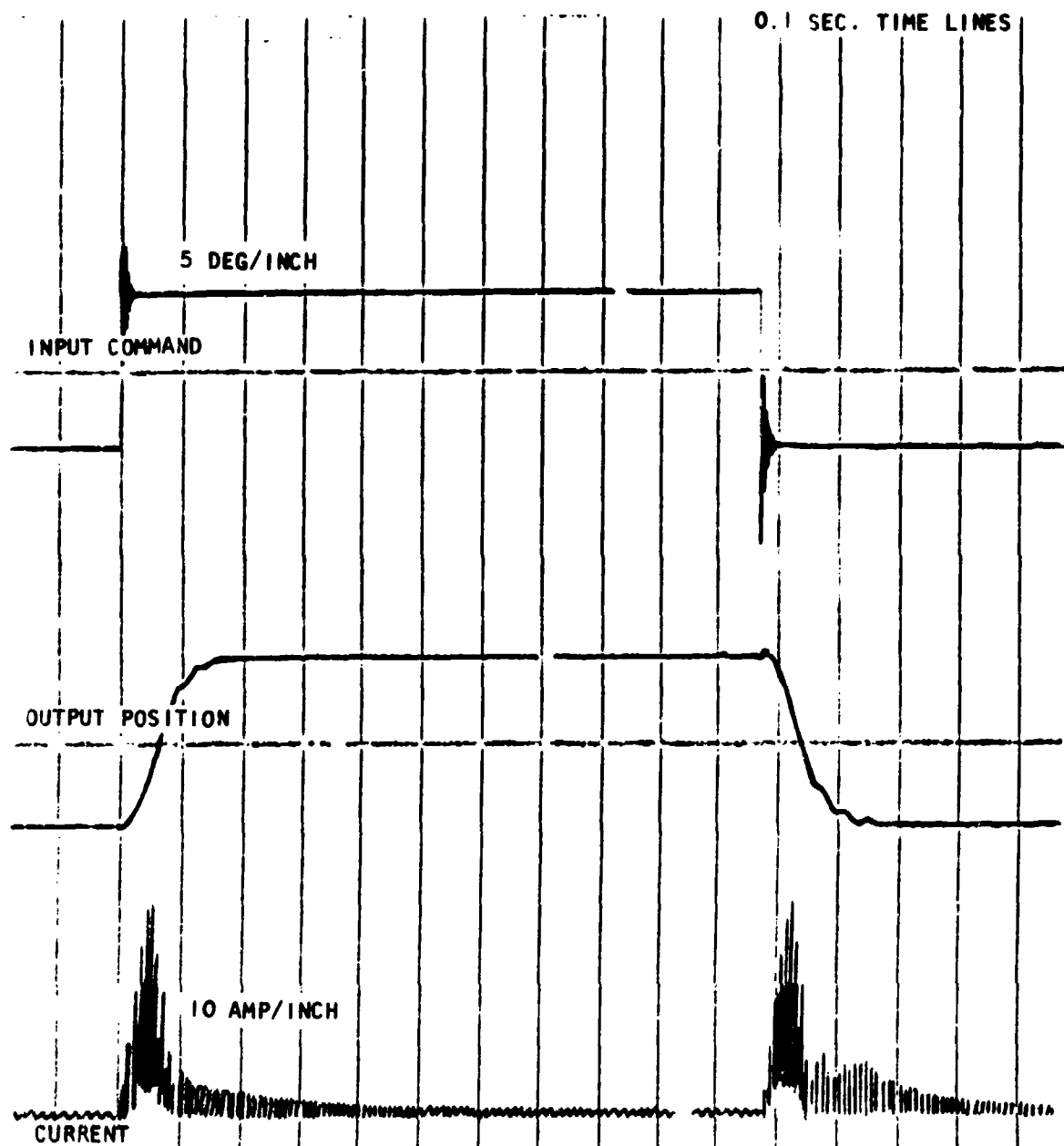


Figure 122. Voltage Control Servo--Dual-Channel Step Response, 5 deg, No Load

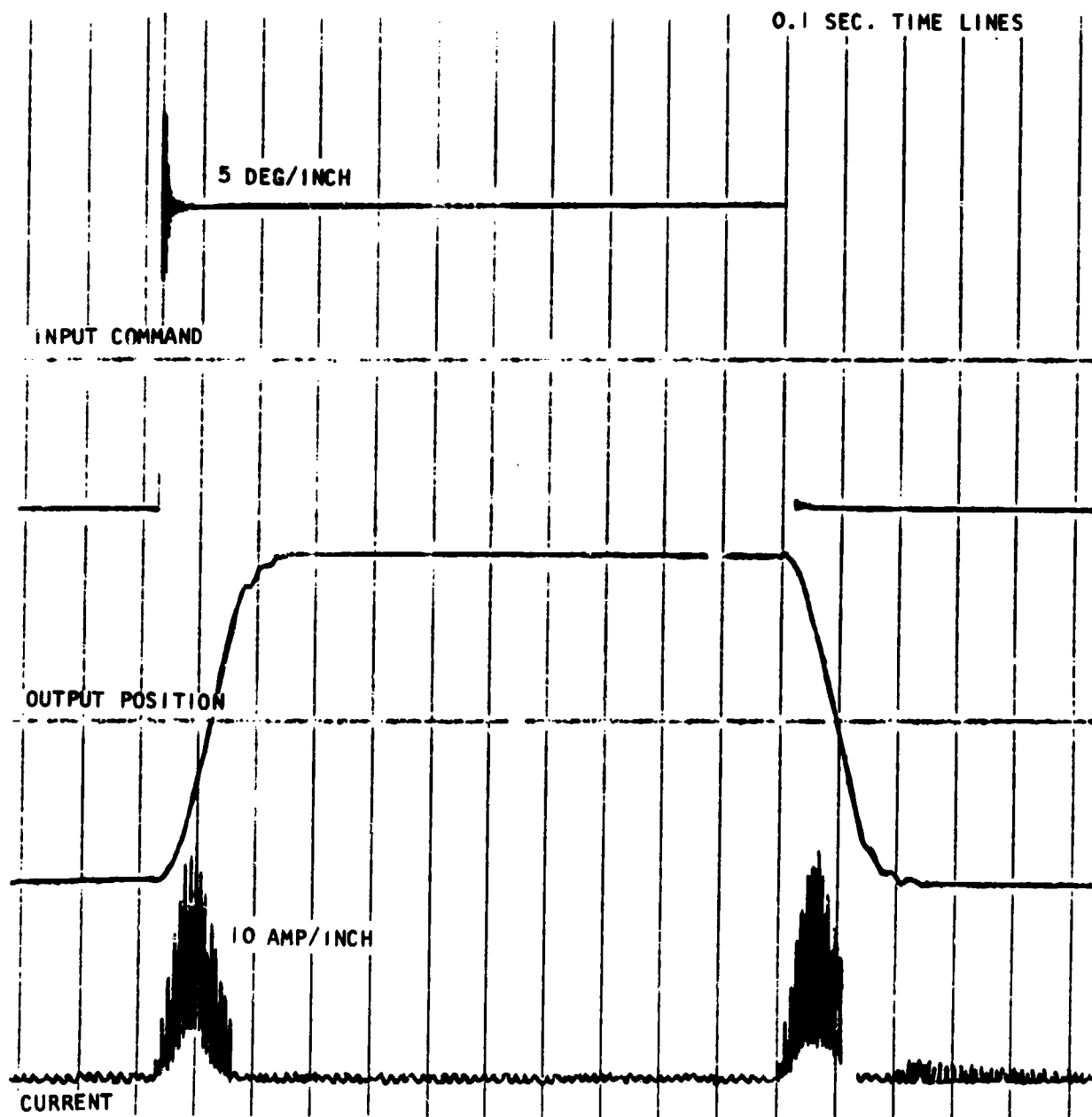


Figure 123. Voltage Control Servo--Dual-Channel Step Response,
10 deg, No Load

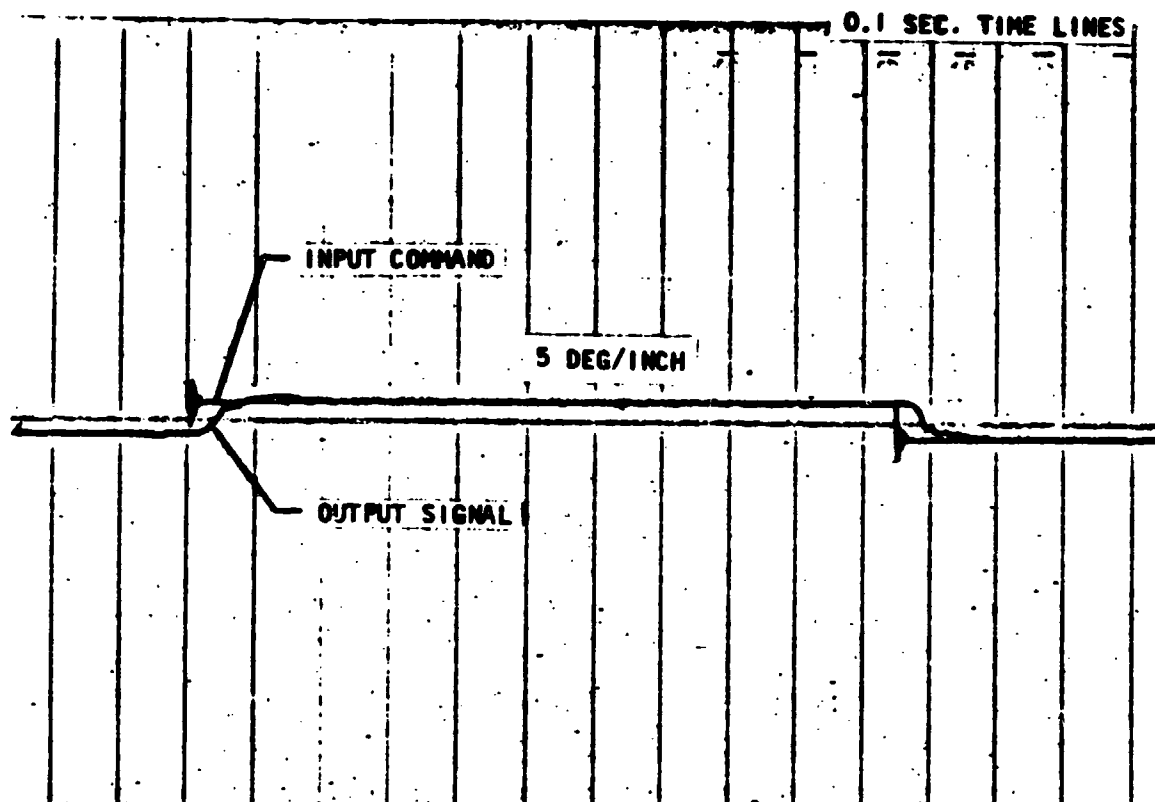


Figure 124. Dual-Channel Step Response with Tachometer Feedback, 1 deg, No Load

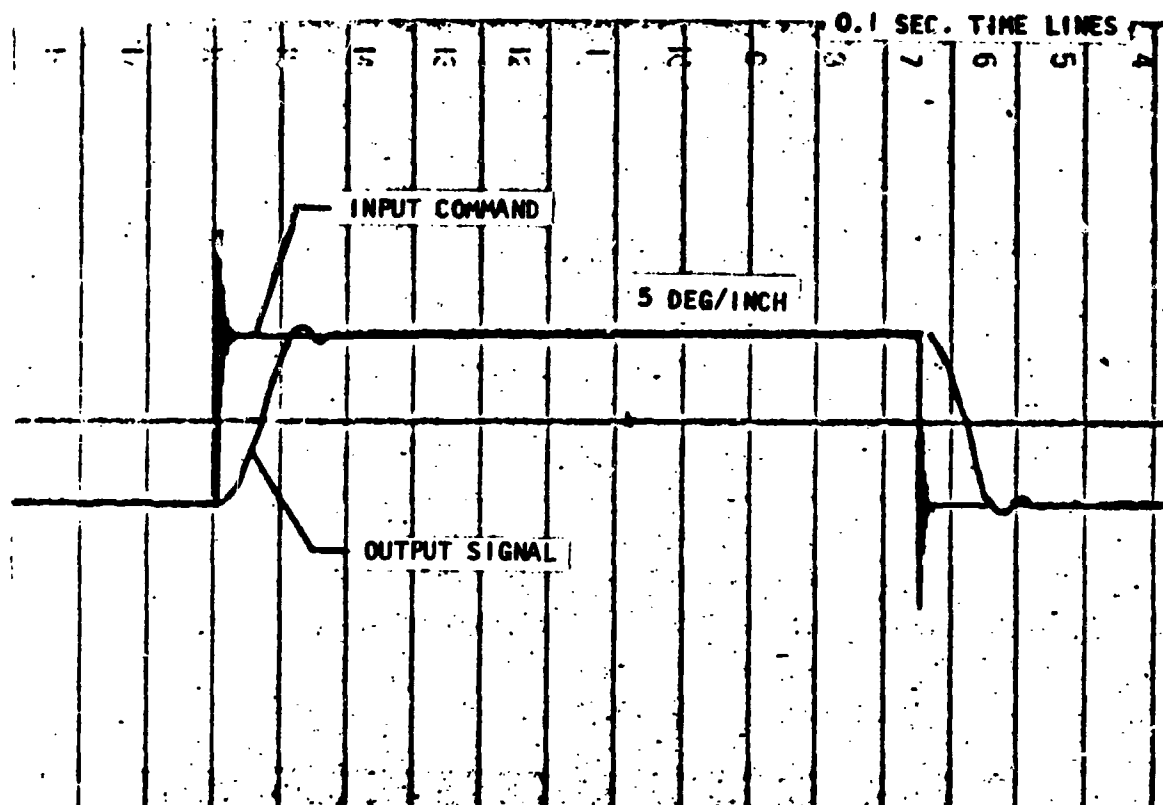


Figure 125. Dual-Channel Step Response with Tachometer Feedback, 5 deg, No Load

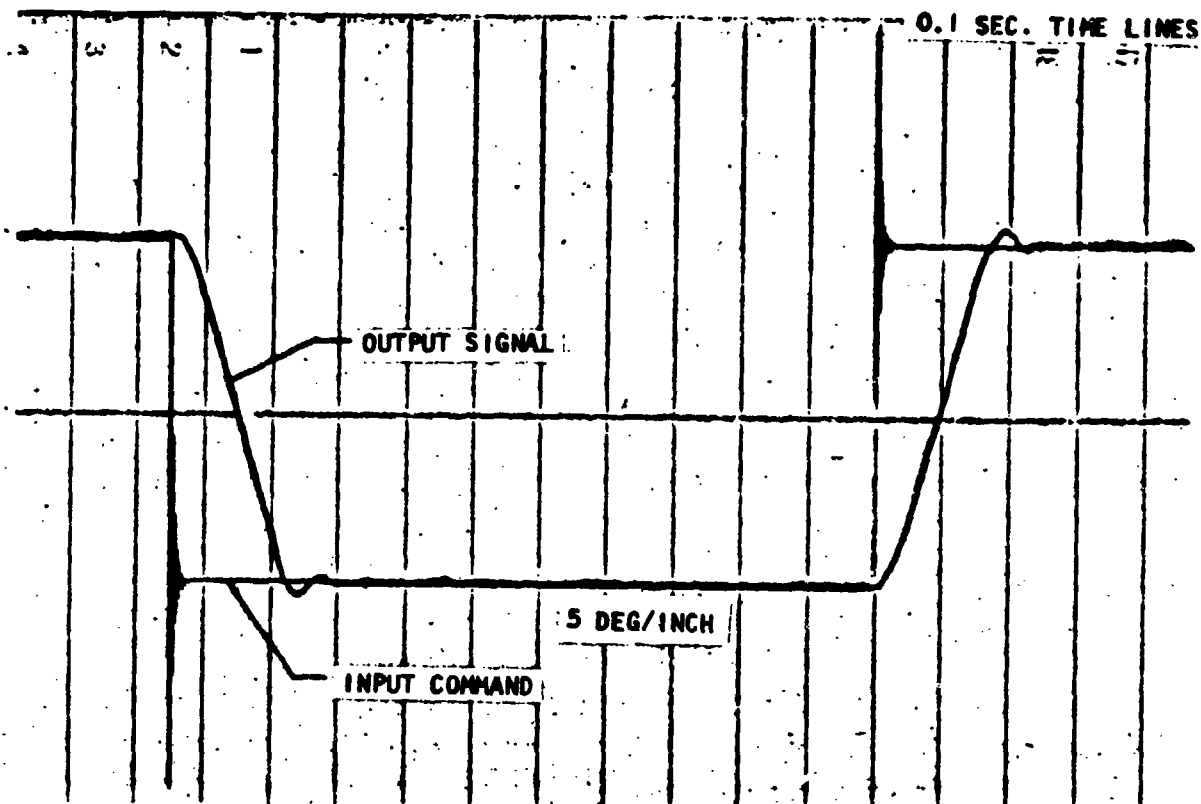


Figure 126. Dual-Channel Step Response with Tachometer Feedback,
10 deg, No Load

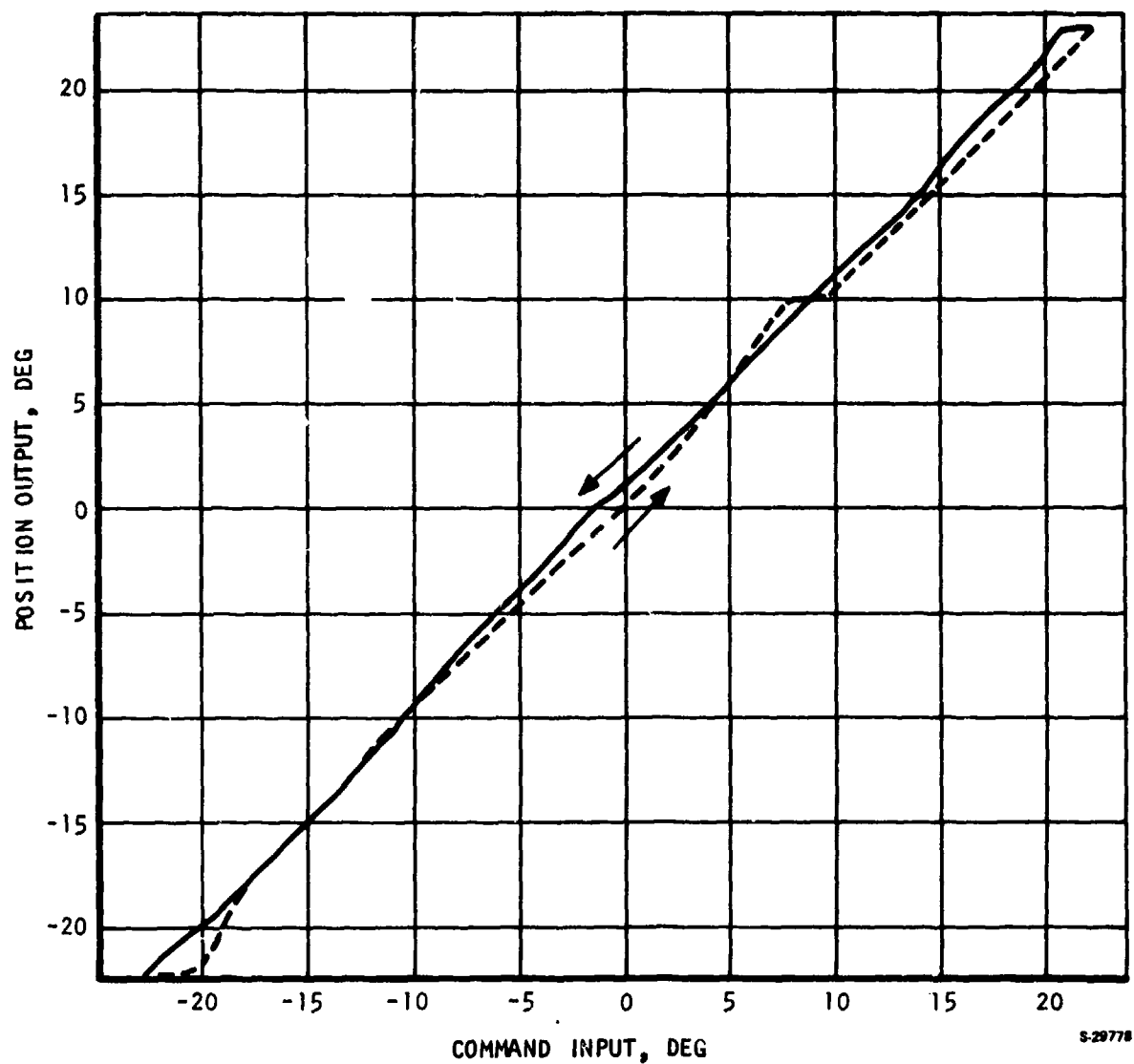


Figure 127. Hysteresis Band Between Input Command and Control Surface Position, Early Hardware Configuration

6.2.5 Regeneration

The regeneration test objective was to show that the electromechanical actuation concept is capable of conserving total energy, and also that it is capable of providing power to the electrical bus when the unit is operating in conjunction with either an aiding or opposing load depending upon the deceleration rate commanded.

6.2.5.1 Procedure

The unit was operated using the microprocessor servo control in a normal servo mode at a no-load condition. The inertia of the test stand load cylinder was the only significant load. The input signal to the control was a sine wave at approximately 4 Hz.

6.2.5.2 Discussion of Results

When the control surface nears the stroke limit at the 4-Hz test condition, the motors are operated in the plug reverse mode to provide maximum deceleration (as discussed in para. 3.3 of Section 3). During this interval of deceleration, the motors are operating as generators. Thus, the mechanical power is converted to electrical power and can be used by other systems if appropriate circuit provisions exist in the power switch.

Tests performed on the microprocessor servo controller showed that the peak current available for regeneration to the electrical bus was 14 amp at a 270-vdc bus voltage. This compares to 17 amp, which is the maximum current limit for the forward direction. As described in Reference 1, the power available for regeneration is a function of magnitude and direction of the hinge moment, frequency, and amplitude. The test shows that energy savings are possible, and that circuitry is available to implement this feature.

6.2.6 Reliability Management Demonstration

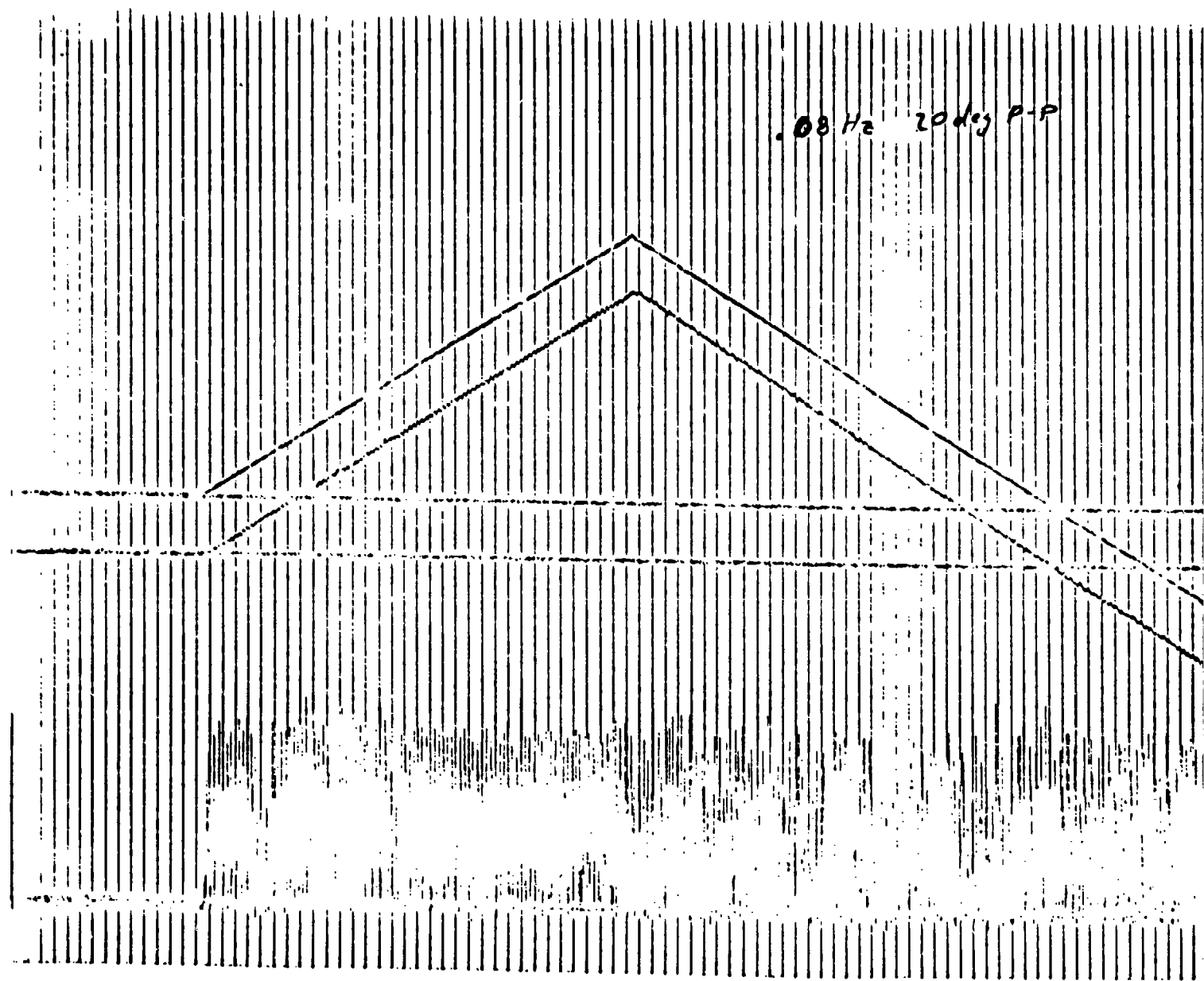
The test objective is to evaluate the effect upon system operation and performance when a failure in one of the dual channels is simulated.

6.2.6.1 Procedure

During the reliability management demonstration, the unit is operated at one of several frequencies between 1 and 10 Hz. The oscillograph is turned on to show data such as voltage, output position, input command, and motor current. The power is then removed from one channel. As described in Section 3 of this report (operating modes), loss of electric power to one channel requires the application of the electromagnetic motor brake and subsequent locking of that drive channel.

6.2.6.2 Discussion of Results

These tests were run using the microprocessor controller configuration.



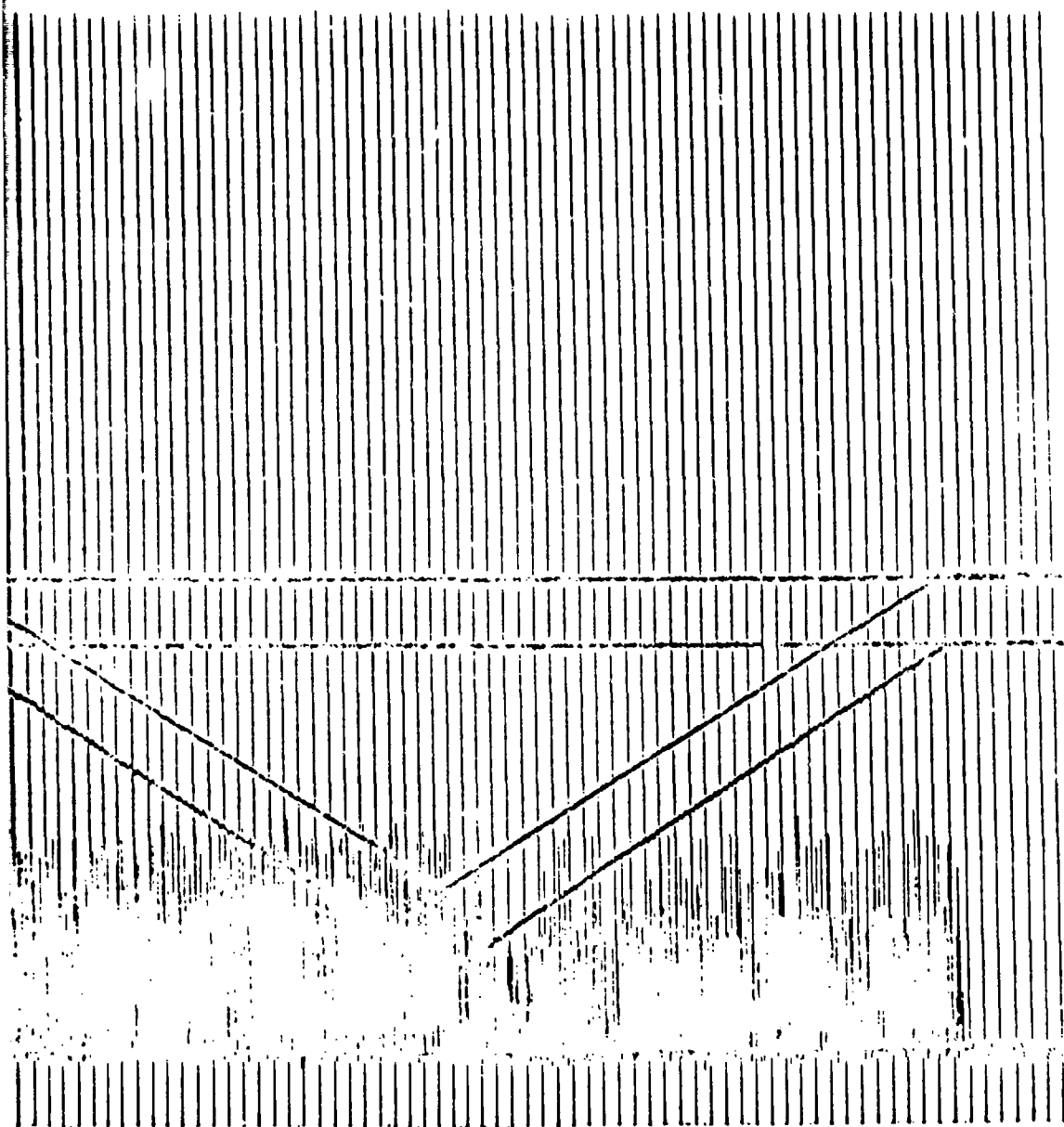


Figure 128. Hysteresis of Improved Actuation Unit,
0.08 Hz, 20 deg Peak-to-Peak Amplitude,
Analog Servo Circuit, 0.022 deg Output
Position Resolution

Each of the data traces shows the line voltage falling from 270 vdc in a rather slow manner, which is due to the large capacitors used in the motor power switch circuits (discussed in para. 3.4 of Section 3).

Figure 129 shows the frequency response of the system before and after manual simulation of failure of one of the servoloops. The response is reduced, but is sufficient for minimum control.

6.2.7 Thermal Management

The objective of the thermal management test is to evaluate the thermal characteristics of the motor and gearbox during simulated duty cycle loading.

6.2.7.1 Procedure

The unit was operated in laboratory ambient conditions without any form of active or forced cooling of the motor, gearbox, or test stand. The unit was operated at several load conditions for a sufficient period of time, which resulted in the attainment of thermal equilibrium.

Figure 130 shows the location of the thermocouple for the motor and the gearbox. A thermocouple also was located on 1 of the 12 power transistors in the power switch assemblies.

6.2.7.2 Discussion of Results

Results of this test are presented in Table 16. The results show that the motor case temperature of 234°F was reached with a 3-amp load current in 15 min. Normal duty cycle operation (20 percent) would correspond to an average current of approximately 3 amp.

The brake coil heating alone resulted in a temperature rise of 26°F. This increase can be reduced by the technique of modulating the brake coil power after pull-in. Holding the brake in the "off" position requires approximately 10 percent of the current (ampere turns) required to actuate the brake.

It is expected that the motor temperature (which was monitored using a thermocouple) could be allowed to increase to 450°F without damage to the motor. However, the temperature monitored at any particular point on the motor is also a function of the heating rate occurring in the stator windings.

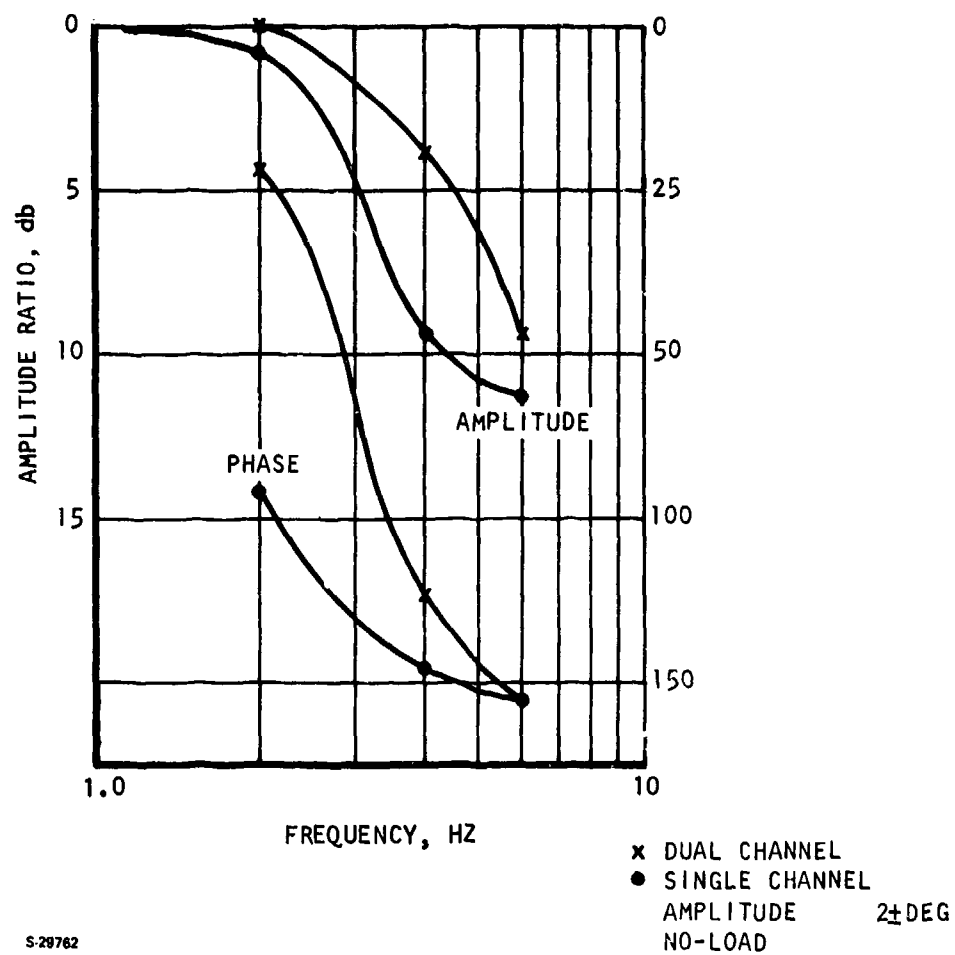
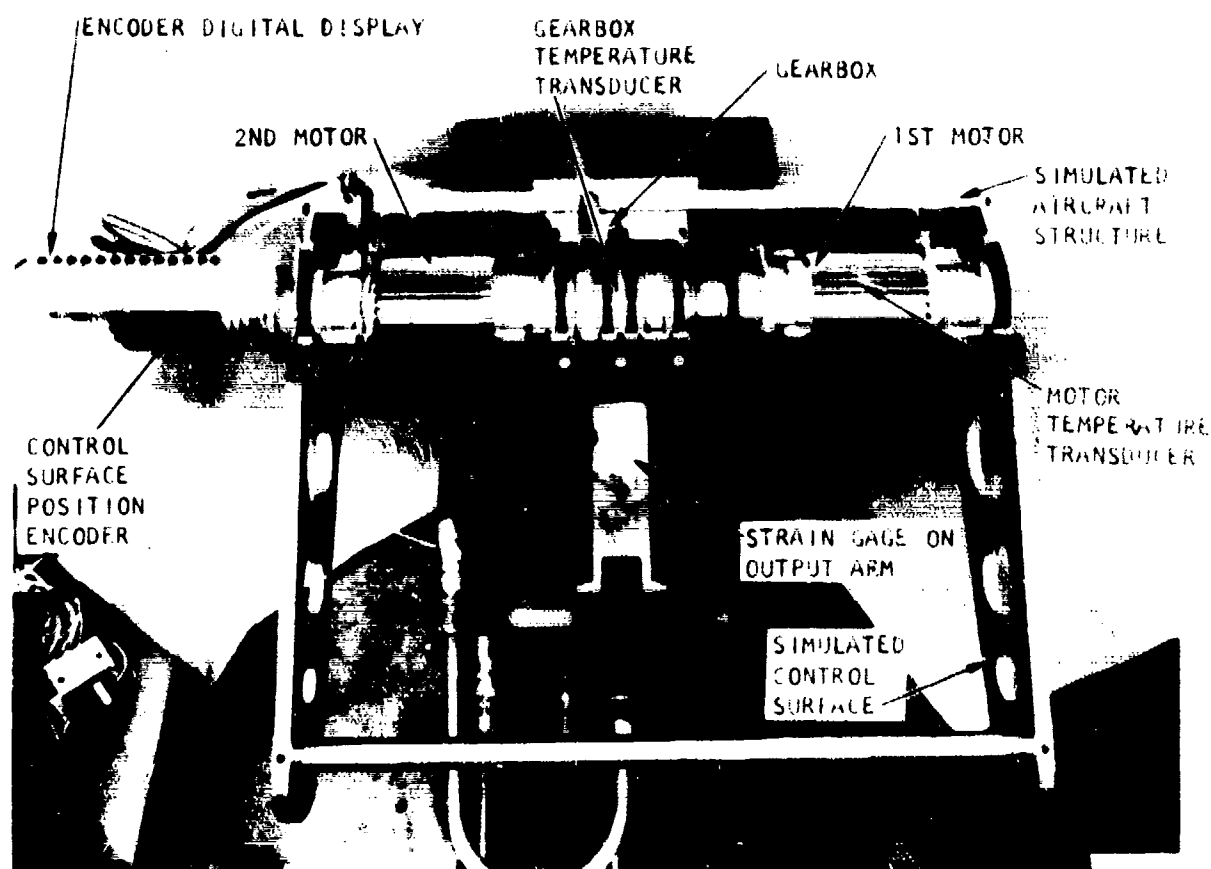


Figure 129. Hingeline Actuator Reliability Management Demonstration



F 26889 A

Figure 130. Temperature Monitoring of Actuator

TABLE 16
TEMPERATURE MEASUREMENTS
TEST 17

Condition	Temperature, °F		
	Motor	Gearbox	Power Transistor
Initial and ambient	72	72	72
Brake coil energized	98	72	72
Brake and 1-amp load on motor (30 min.)	160	104	90
Brake and 3-amp load on motor (15 min.)	234	126	102

7. CONCLUSIONS AND RECOMMENDATIONS FOR FUTURE EFFORT

Under contract from WPAFB, AIResearch Manufacturing Company of California designed, developed, and tested a rotary hingeline actuation unit for laboratory demonstration purposes. Photographs of the electromechanical power-by-wire actuation unit are shown in Figure 131.

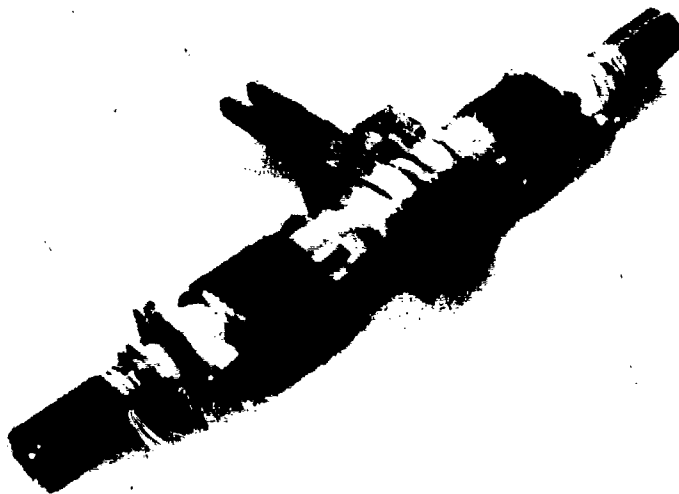
7.1 CONCLUSIONS

1. The feasibility of developing an integrated hingeline electromechanical actuation unit, with redundancy, has been demonstrated.
2. Technology exists in the areas of actuators, motors, and controllers that can be directly applied to primary flight control actuation requirements.
3. The performance objectives of the program compared to demonstrated test results are summarized in Table 17.

7.2 RECOMMENDATIONS FOR FUTURE EFFORT

The expanding and improving technologies employed in this development activity are 3-years old. Significant improvements in some technologies have occurred during the development period and can be expected to improve further. These new areas should be explored as follows.

1. Design, fabricate and test a 270-vdc servo motor using the improved magnet material, i.e., $26 \text{ to } 30 \times 10^6$ Ge-0 energy product. The potential impact of this improvement is to increase the acceleration capability of the motor and/or reduce the motor size and weight.
2. The concept of an integrated hinge electromechanical actuation unit emphasizes the need to evaluate actuator diameter and length changes in terms of performance and thermal capability variations.
3. The brakes in the present hardware are used to implement redundancy after a failure. Future designs should explore means of reducing the steady-state current draw and to use the brakes as a static load-holding device.
4. The technique of force summing of redundant drives should be considered, compared to the velocity summing approach used in this design.
5. Consider the use of optical sensors for motor rotor position sensing. This approach will simplify commutation input logic for an all-digital control, and will provide improved rotor position resolution.



ELECTROMECHANICAL ACTUATOR FOR PRIMARY FLIGHT CONTROL



F-27083

REDUNDANT MICROPROCESSOR SERVOCONTROL BREADBOARD

Figure 131. Demonstration Hardware Developed

TABLE 17

SUMMARY OF PERFORMANCE GOALS AND TEST RESULTS

Characteristics	Value	
	Specified*	Test Results
Output stroke	± 30 deg	± 30 deg
Output velocity (no-load)	80 deg/sec	80 deg/sec
Output torque (stall)	37,575 in.-lb	--**
Hysteresis	<0.5 percent full stroke	0.5 percent
Frequency response	4 to 12 Hz 90 deg phase lag	8 Hz 90 deg phase lag
Bandwidth	8 Hz	8 Hz
Position null	<0.5 deg	0.5 deg

*AIResearch Document No. 76-12942, performance specification for Electromechanical Flight Control Actuation System; see Appendix B.

**Not tested.

6. In the present design for a ± 1 deg amplitude, acceleration limiting occurs between 6 and 8 Hz. Use of higher current power switch transistors should increase the bandwidth of the servoloop. The implementation of higher current levels requires the availability of solid-state switch devices (i.e., transistors or SCR's) that have adequate design margin for reliability derating to satisfy thermal and other environmental requirements. New solid-state devices exist and must be studied to determine application benefits.

7. Testing should be conducted on the actuator motors while operating in ambient temperatures ranging from -65° to 250°F . The results of tests will be used to expand the engineering data base for future applications studies. The results will be correlated with computer prediction program runs to verify actuation simulation analyses techniques.

8. The selection of a microprocessor should be re-examined based upon the recent availability of devices offering higher data processing rates and increased memory logic capability. This continuing improvement can be expected to minimize "real-time" computation limitations and concurrently increase the logic capacity to develop an adaptive servo unit that can effectively communicate with digital flight control aircraft systems.

8. REFERENCES

1. Electromechanical Actuation Feasibility Study, AirResearch Manufacturing Company, Report 75-12153, Air Force Contract F33615-75-C-3055, Report AFFDL-TR-76-42.
2. Bird, Daniel, "Electromechanical Flight Control Actuation Update," SAE Paper 780582 presented at SAE Committee A-6 Technical Symposium, Cherry Hill, New Jersey, April 12, 1978.
3. Bird, Daniel, "Electromechanical Flight Control Actuation," SAE Paper 771004, presented at SAE Aerospace Meeting, Los Angeles, California, Nov. 17, 1977.
4. Johnson, Tom, "Primary Flight Control Actuation with Electric Motors," Proceedings of the IEEE 1977 National Aerospace and Electronics Conference (NAECON), Dayton, Ohio, May 1977.
5. Helsey, C. W., Jr, "Power-By-Wire for Aircraft - The All-Electric Airplane," SAE Paper 771006, presented at SAE Aerospace Meeting, Los Angeles, California, Nov. 17, 1977.
6. Fitzgerald, A. E. and Charles Kingsley, Electric Machinery, 1952.
7. Sawyer, B., and J. T. Edge, "Design of Samarium Cobalt Brushless DC Motor for Electromechanical Actuator Applications," Proceedings of the IEEE 1977 National Aerospace and Electronics Conference (NAECON), Dayton, Ohio, May 1977.
8. Wood, Neal E., "Advances in Primary Flight Control Actuation Using Electromechanical Technology," Proceedings of the IEEE 1977 National Aerospace Conference (NAECON), Dayton, Ohio, May 1977.
9. Herdeg, D. F., H. W. Proctor, W. B. Spring, and G. C. Newton, Jr., Electromagnetic Harmonic Drive Low Inertia Servo Actuator, ASD-TDR-63-466 Contract AF33(657)-7731, United Shoe Machinery Corp., Beverly, Mass., December 1963.
10. Parker, R. J., "Rare Earth Permanent Magnets and Energy Conversion Processes," Proceedings of the IEEE 1977 National Aerospace and Electronics Conference (NAECON), Dayton, Ohio, May 1977.
11. Brown, J. M., "Rare Earth Magnets - A New Trend in Dc Motors", Control Engineering, October 1975.

12. Parker, Rolling J. and Robert J. Strudders, Permanent Magnets and Their Application, 1962.
13. Sawyer, Bert, Barrett, A., et.al, Electromechanical Flight Control Actuator, Final Report, NASA Contract NAS9-14952, January 1978.
14. Electromechanical Flight Control Actuator, Delco Electronics, NASA Contract NAS 9-14331.
15. Brown, James, "Rare Earth Magnets - a New Trend In D.C. Motors," Control Engineering, October 1975.
16. Vcight, A. A., "Electrical Flight Control Systems - Applicable Now," Proceedings of the IEEE 1977 National Aerospace and Electronics Conference (NAECON), Dayton, Ohio, May 1977.
17. Inagaki, J., Kuniyoshi, M., and S. Tadakuma, "Commutators Get The Brushoff," IEEE Spectrum, June 1973, pp 52 to 58.
18. "Machine Design," Electrical and Electronics 1978 Reference Issue, Vol. 50.
19. Grau, Richard, Feasibility Investigation for Advanced Flight Control Actuation Systems; All Electric Concepts (AFCAS AE), McDonnell Douglas Electronics Company, NADC Report 76160-30.

APPENDIX A

ELECTROMECHANICAL ACTUATION DEVELOPMENT
DESIGN DATA PACKAGE
(PARTIAL REVISION OF 76-12943)

INTRODUCTION

The data contained herein includes drawings, sketches, trade studies, and analyses of the electromechanical actuator being designed for laboratory demonstration purposes.

The actuator assembly is designed to illustrate realistic interface requirements with the aircraft including structural attachments, thermal provisions, and dual redundant control surface actuation. The electronic controller, including the transistor power switches are designed as laboratory brass board items. Brass board equipment will be designed to maximize demonstration of capability and flexibility of actuating a simulated control surface. This equipment includes features of operational flexibility useful in demonstrating capability of electromechanical actuation systems which may be in excess of the flexibility requirements of any one particular flight control application.

The data presented in support of the design is organized as follows:

- Drawing list
- Full size outline drawing
- Overall schematic and system model
- System design considerations
- Component studies and design
- Listing of long lead items for procurement

DRAWING LIST

The following is a list of the major drawings of the actuation unit:

Actuator outline 2022194

Actuator cross-section 2022192

Motor cross-section 515018

Control surface position transducer 2022196

FULL SIZE OUTLINE DRAWING

The outline drawing of the actuator assembly is shown on AIResearch drawing 2022194. The actuator consists of the following elements:

- Geared mechanical output
- Gear differential
- 2 brushless dc motors, with rotor position transducers
- 2 parking brakes, one for each motor
- 2 control surface position feedback transducers.

The characteristics of the actuator are listed below:

Overall length, in.	23.75
Maximum hingeline depth, in.	4.0
Weight, lb	34.8
Volume, in ³	298

OVERALL SCHEMATIC - SYSTEM MODEL

The overall system schematic is shown in Figure A-1. The actuation system consists of two entirely independent drive channels operating into a combining gear box to supply controlled torque at a rate to the control surface. Each drive channel consists of the microprocessor servo controller, transistor power switching for the motor and brake, motor, motor rotor position transducer, and parking brake. Each drive channel is operated from the 270 VDC bus. The inputs to the servo controller are as follows:

- Control surface position
- Surface rate limit (a fraction of maximum)
- Surface torque limit (a fraction of maximum)
- Commutation angle
- Fault simulation

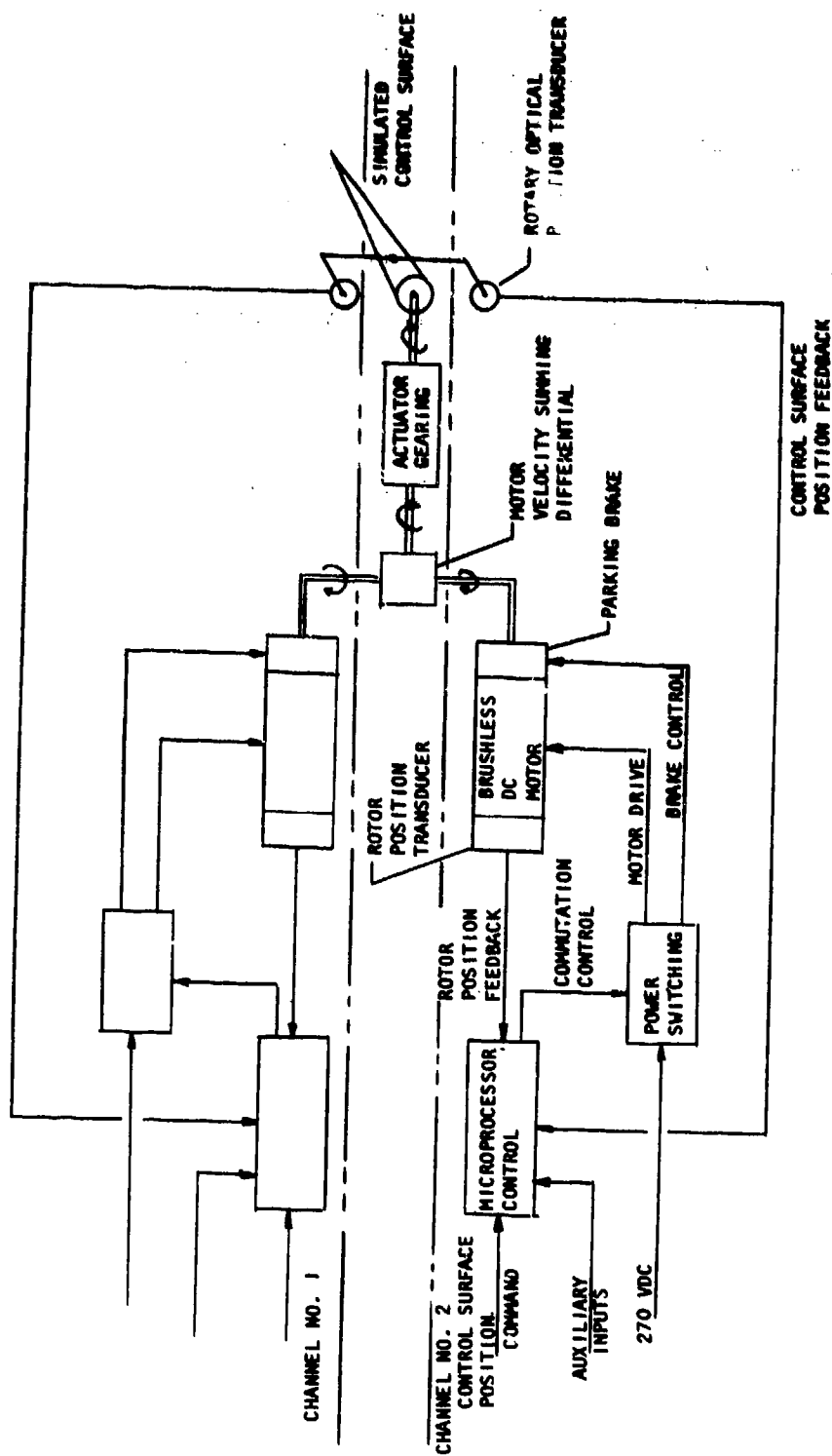


Figure A-1. Overall Actuation Unit Schematic

SYSTEM DESIGN CONSIDERATIONS

The design of the electromechanical flight control actuation system is based upon program ground rules, review and interpretation of operational requirements, and utility of the hardware for demonstration. This section presents the system considerations of major significance in the design of the actuation concept, and illustrates the impact the results of system design has upon component requirements.

The data is organized as follows:

- Program ground rules and performance objectives

- Modes of operation

- Gear ratio selection

- Gearing trade offs

- Sensitivity analysis

- Arrangement of assembly

- Inertia calculations

- Thermal studies

- Performance specification

PROGRAM GROUND RULES AND PERFORMANCE OBJECTIVES

Vehicle Application Interfaces

- Structurally integrated, rotary, hingeline actuator
- 3 HP available at control surface, maximum
- 115/200 VAC 3-phase power supply
- 4 in maximum hingeline depth
- Redundancy - failsafe

Actuation Requirements

- | | |
|----------------------|--|
| • Stall hinge moment | 37,575 in.-lb |
| • No-load rate | 80 deg/sec |
| • Bandwidth | 4 to 12 Hz (8 Hz nom.) |
| • Load inertia | 46.6 lb-in.-sec ² |
| • Duty cycle | Continuous operation at 20 percent peak power (minimum). |
| • Stroke | 60 deg. for demonstration, ($\pm 30^\circ$) |

MODES OF OPERATION

The design of the demonstration unit is characterized by versatility. Two operational modes are possible. First, the two motors operate together as a direct drive servo actuator. In this mode, the motors are driven as parallel power channels, the outputs are mechanically summed to provide the torque and rate required at the control surface. Second, the two motors and gearing operate as a differential serve. One motor operates as a motor and the other as a generator. The motors rotate continuously at the same speed but in opposite directions. No output rotation is realized since the differential mechanically sums the equal but opposite inputs to zero. An output rate is achieved by changing the speed of either the motor or the generator.

Direct Drive Servo

The direct drive servo approach was the baseline concept detailed in the study (Phase I). The operating modes for this concept are:

1. Off
2. Activate
3. Operate
4. Shutdown
5. Failure.

Each mode is described below:

1. Off

The off mode is defined by removal of all electrical power and control signals from the unit. The actuator brakes will be spring loaded into the "on" or locked, condition. With power removed, and the brakes locked, the control surface will be locked in its last position.

2. Activate

To activate the system, the main power supply is switched on. This also energizes the low voltage power supply for the microprocessor. Since all components are solid state, the unit does not require a warm up period.

3. Operate

The primary servo system input command is control surface position. This can be input manually or by use of a function generator, either sine wave or other. Operation can also be demonstrated showing torque and rate limiting, and variation in the commutation angle. During operation, the unit will draw a maximum current of approximately 35 amps at 270 VDC, for the total electrical input to both motors, controllers and other electrical components. This maximum current condition will only occur when operating at stall, or for short periods of time when providing maximum acceleration torque.

4. Shutdown

Shutdown can be initiated at any time. Removal of the main power causes the simultaneous shutdown of the microprocessor and application of both motor brakes. This action causes the actuator to lock in its last position.

5. Failure

The servo loop in each drive channel is monitored to determine that the loop is being closed.

The failsafe operating criteria requires that minimum control be available after any one failure. The implementation of this failsafe provision includes dual, parallel drive channels. Each channel must be monitored to determine that operation is satisfactory. As a means of showing redundancy management techniques, and to illustrate fault detection and isolation, the system has the following features.

First, each servo loop is monitored to determine that the loop is being closed. Second, loss of electrical power to a redundant channel, automatically places that channel in a failsafe mode.

Servo loop error signal will be monitored. If the error is excessive for a determined period of time, it will be assumed that the servo loop is not being closed, and the controller, power switching and associated motor will be shut down. Simultaneously, the power to the parking brake will be removed and the brake will lock. The actuator will then continue to operate on the remaining drive channel. The rate at the output will be reduced to 40 deg/sec maximum, but the maximum output torque will be unchanged.

In the event of a power failure on the electrical bus to one of the drive channels, the brake will be spring loaded to the locked or "on" condition. Spring loading the brake to the on condition of failures assures the continued operation of the control surface at full torque and reduced rate.

GEAR RATIO SELECTION

The selected gear ratio is 627:1 based upon availability of tooling to produce gearing of high efficiency.

The following page presents a calculation of the gear ratio taking into account the gearing efficiency, inertia of the motor rotor, gearing and load. The use of the 627:1 ratio compared to the calculated value results in the following:

Motor no-load speed decrease	-	2 percent
Motor torque increase	-	2 percent

These variations are entirely within the design allowances of the motor.

DETERMINE ACTUATOR GEAR RATIO

Given data:	Stall Torque	37.575 in.-lb
	Rate	80 deg/sec
	*Acceleration	44.2 rad/sec ²
	Load inertia	46.6 lbf-in.-sec ²
	**Rotor inertia	2.51 x 10 ⁻³ lbf-in.-sec ²

$$\text{Rate } \dot{\theta} = 80 \text{ deg/sec} \times .01745 \text{ rad/deg} = 1.396 \text{ rad/sec}$$

$$\text{Load inertia torque } (\tau_{IL}) = \text{Load inertia} \times \ddot{\theta} = 46.6 \text{ lbf-in.-sec}^2 \times 44.2 \text{ rad/sec}^2 = 2059.7 \text{ lbf-in.}$$

$$\begin{aligned} \text{Gear ratio} &= \sqrt{\frac{\text{Stall torque} - \text{load inertia torque}}{\text{Rotor inertia} \times \text{acceleration} \times \text{efficiency}}} \\ &= \sqrt{\frac{37,575 - 2059.7}{2.51 \times 10^{-3} \times 44.2 \times .83}} = 637 \end{aligned}$$

*Based on $\ddot{\theta} = A(2\pi f)^2$ where A = amplitude in rads.

A = ± 1.0 deg = ± 0.0175 rad. from Specification No. 76-12942

f = 8, required frequency response

$$\begin{aligned} \text{THEN: } \ddot{\theta} &= 0.0175 \times (2\pi \times 8)^2 \\ &= 44.2 \text{ rad/sec}^2 \end{aligned}$$

**includes reflected inertia of gear box.

$$I_m = 1.077 \times 10^{-3} \text{ lbf-in.-sec}^2 \text{ (1 motor)}$$

$$I_{GB} - 2 \text{ motors} = 0.355 \times 10^{-3} \text{ (total gear box)}$$

GEARING TRADE-OFFS

The actuator gear ratio selection involved several gear train analyses to achieve an optimum actuator efficiency commensurate with motor power level and total weight. Previous report, 75-12153, indicated an overall actuator efficiency of 90 percent. To achieve a high efficiency (88.6) requires six simple spur gear stages. The result is a long, heavy actuator with the output stage concentrated over a small area. The compound output planet gear stage was desired since it could distribute the load over a larger area. An IBM gear train analysis revealed a 90 percent compound stage was possible, as shown on the following computer printout sheets. Using the best compound output stage, and knowing the required output rate, it then was possible to size the motor speed, power and initial actuator gear train stages. A sample analysis of the selected gear ratio was presented earlier. This analysis indicates an overall gear ratio of 637:1 based on dynamic considerations. The mechanical gear ratio is 627.42:1. The power to the motor can be adjusted slightly to achieve the desired dynamic performance, if necessary.

All of the gears in the demonstrator actuator must be configured on available gear tooling since the program schedule does not allow time for fabricating new cutters and hobs. A lead time of some 44 to 52 weeks is needed for new gear tooling.

Recent stress analysis has shown that increased pressure angles will produce a stronger root form capable of higher fatigue life. The current output stage is 20 degrees pressure angle based on available tooling.

Table A-1 titled "Compound Gear Trade-off Study" presents a study of different compound gear sets which were evaluated to determine a suitable ratio for the WPAFB Fly-By-Wire Actuator. This study was made for 22.5 degree pressure angle cutters. The study revealed that the differential ratio had to be kept low if a high efficiency was to be achieved. Case 11 would be a good choice since it has high forward and reverse efficiency, at a low weight, a low differential ratio and a good allowable torque level. A second choice would be Case 5 which gives a slightly higher differential ratio with a slight reduction in allowable torque.

Column 10 and 11 show what can be done when optimizing for weight or volume. Case 1, Column 10 reveals the highest torque per pound of compound gear set of the eleven gear ratios studied. However, Case 1 turns out to be the highest total weight and near the lowest efficiency. In a like manner, Case 1, Column 11 reveals the highest torque per unit volume.

TABLE A-1
COMPOUND GEAR TRADEOFF STUDY

	1	2	3	4	5	6	7	8	9	10	11	12	13	14
Case	Number of Planets /D.P.	Gear Ratio (Neg.)	Fwd Eff / Rev Eff	Fwd M.A.	Face X (L)	Root X (Ø)	L/D % LD ²	Ball Pk Weight (lb)	Torque for 76.6 ksi	Tq/Lb 76.6 ksi	Tq/Ld ² 76.6 ksi	Planet Tooth Count	Remarks	Difference Ratio (Positive)
1 ^s	6/13.25	50.33	.717/.621	36.1	3.326	4.808	.692/76.89	12.76	40,440	3170	526	14/13		14.00
2 ^s	6/24.15	50.33	.716/.618	36.0	1.790	2.629	.681/12.37	2.06	6,352	3080	514	14/13		14.00
3 ^s	6/20.20	13.13	.908/.902	11.92	2.688	4.195	.641/47.30	6.78	19,300	2845	408	19/13	Max Load Cap. w/90% Eff.	4.08
4 ^s	5/20.20	18.07	.895/.886	16.17	2.649	3.694	.717/36.15	5.20	13,700	2635	379	18/13	Compromise M.A. w/90% Eff.	4.83
5 ^s	5/24.24	19.13	.911/.905	17.43	2.212	4.083	.542/36.87	5.47	10,950	2000	297	25/18	Max M.A. & Eff. (Hi Tooth Count)	4.83
6	6/20.20	16.25	.892/.867	14.50	2.657	4.195	.638/47.07	6.78	19,300	2845	410	19/14	Derivative of Case 3	4.98
7	6/20.20	20.92	.869/.839	18.18	2.625	4.195	.626/46.20	6.78	19,300	2845	418	19/15	Der. of Case 3	6.33
8	6/20.20	28.72	.834/.791	23.95	2.596	4.195	.619/45.68	6.78	19,300	2845	423	19/16	Der. of Case 3	8.59
9	6/20.20	44.31	.776/.695	34.38	2.567	4.195	.612/45.17	6.78	19,300	2845	427	19/17	Der. of Case 3	13.09
10	6/20.20	91.08	.628/.407	57.20	2.535	4.195	.604/44.61	6.78	19,300	2845	433	19/18	Der. of Case 3	26.60
11	6/22.22	14.73	.907/.900	13.36	2.414	3.880	.622/36.34	5.43	14,500	2670	398	20/14		4.37

NOTES:

1. Stress = 76.6 ksi at Noted Load
2. All values are for one slice
3. Face = Van Landt "Allowable"
4. All Cutters 22.5° P.A.
5. All stresses "Optimized"

DISCUSSION OF COMPOUND PLANETARY GEARING

In the study of the WPAFB Fly-By-Wire Actuator Design, it became readily apparent that the output compound planetary gear ratio had a decided affect on the overall gear train efficiency and directly affected the motor sizing. This discussion will be limited to the output compound stage gearing covering the influential parameters and the stress relationship of the Fly-By-Wire Actuator to an existing production fighter aircraft control surface actuator.

In the proposed actuator, the paramount objectives are:

Maximum efficiency; high stiffness/unit weight ratio
and a high load capacity/unit weight ratio.

Aside from windage and bearing losses, efficiency is generally a function of the interaction of number of gear teeth, operating pressure angle, and coefficient of friction. It is the coefficient of friction which make an absolute assessment of efficiency impossible. For example, depending on pitch line velocity, frictional coefficient may vary $\pm 25\%$ at constant lubricant viscosity. A sixfold change in viscosity may produce $\pm 15\%$ frictional effect. Loading is another variable which may produce $\pm 100\%$ frictional change when the load varies $\pm 60\%$. For a single internal mesh with nominally 99% efficiency, the cumulative effect of the above produce an efficiency range of 99.3 - 97.6. With application to the Fly-By-Wire actuator containing two internal meshes and one external mesh output stage, efficiency can be expected to vary $\pm 3.6\%$ for the above operational parameters. The limited viscosity change is only available by means of constant temperature supplied by an external lubricant. In the aircraft, greater extreme viscosity changes are anticipated because of the variation of external environment and self induced heating on an integrally lubricated device.

The foregoing indicates, in a gross manner, the major obstacles which lie in the path of quantitatively defining mechanical efficiencies. Means are available to establish trends and although the results cannot be considered optimal, they are conservative and the technique employed provides a manageable entry to the problem. Restricting the discussion to the compound differential, and noting for the usual construction

$$\begin{aligned}\mu &= .05 \text{ (coefficient of friction)} \\ \phi &= 25^\circ \text{ (operating pressure angle, and equal addenda)}^{(1)} \\ C &= \frac{1}{1 + .423 \left(\frac{1}{AP} + \frac{1}{BP} - \frac{1}{A} - \frac{1}{B} \right) (m-1)}\end{aligned}$$

(1) Designing Compound Epicyclic Gear Trains
W.A. Tuplin, Machine Design, April 1957

where A = teeth in moving ring gear

B = teeth in fixed ring gear

AP = teeth in planet mating with A

BP = " " " " " B

$$m = \text{gear ratio} = \frac{1}{1 - \frac{B \times AP}{BP \times A}}$$

By inspection it is evident that maximum efficiency occurs through minimum number of gear teeth, minimum difference in gear teeth, and minimum gear ratio, or combination of these.

There are, in addition, some constraints common to planetary gear systems which need be observed and which restrict choice of gear teeth to finite limits.

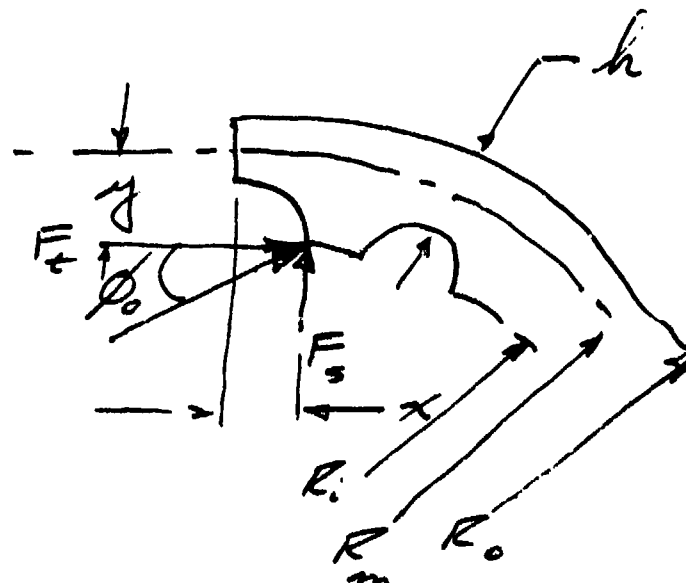
- Dephasing (i.e., the number of planets must have no common multiple with the ring or sun gear)
- Equal spacing (for the planets to be equally spaced $\frac{A + S}{N} = \text{integer}$)

where S = teeth in sun gear

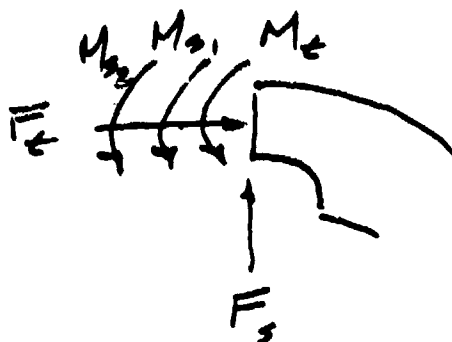
N = number of planets.

Additionally, physical restraints based on present practice impose further limits upon gear tooth choice. For example, a production gearbox similar to that under consideration is Part Number 2021656. This unit is qualified for aircraft control service. Analysis and strain gage measurements are readily available. It is proposed, therefore, to extrapolate the major physical dimensions from that unit to the current one on the basis of equivalent stress.

Ring gear loading is represented by:



Performing the indicated transferral to neutral axis and least section:



where:

$$M_t = F_t y$$

$$M_{s1} = \frac{F_s R_m}{2} \left(\frac{1}{\theta} - \cot \theta \right)$$

$$\theta = \frac{360}{2N}$$

N = number of planets

$$M_{s2} = F_s X$$

The maximum normal stress is compressive and has the value:

$$\sigma_A = \frac{K_1 (M_t + M_{s1} + M_{s2}) h/2}{I} + \frac{K_2 F_t}{A}$$

where: K_1 and K_2 = stress concentration factors

I = area moment of inertia

A = area

$$F_t = \frac{T}{NR_1}$$

$$F_s = F_t \tan \theta_0$$

$$I = \frac{1}{12} bh^3$$

$$A = bh$$

where: b = ring gear effective width

θ_0 = operating pressure angle

Letting $N = 6$, $\theta_0 = 25^\circ$ and making the indicated substitutions:

$$M_{s_1} = 6.9 \times 10^{-3} \frac{TR_m}{R_1}$$

$$M_{s_2} = .078 \frac{T_x}{R_1}$$

$$M_t = \frac{T_m}{6R_1}$$

and,

$$\sigma_A = \frac{TC}{R_1 bh}$$

$$C = \frac{6K_1}{h} (6.9 \times 10^{-3} R_m + .078x + .167y) + .167K_2$$

To check the validity of this describing function, a comparison with actual measurement is presented. Production unit 2021656 was strain gage instrumented which yielded a stress to applied torque relationship

$$\sigma_A = 7.67T$$

This unit had the proportions

$$R_m = 1.69, h = .285, b = .93$$

$$R_1 = 1.43, y = .26, x = .031$$

$$K_1 = K_2 = 2.2$$

Inserting these values in the derived function results in

$$C = 3.03$$

$$\text{and, } \sigma_A = 7.99T$$

It is claimed that the discrepancy is due to mounting lug influence, numerical value of stress concentration, or both. Justification is felt, therefore, to force the describing equation to conform to measurements so that, finally:

$$\sigma_A = \frac{.96 TC}{R_1 bh}$$

From the design standpoint and also in order to examine the potential for stress based gear limitations, it is preferable to have the describing function in terms which are available from the usual problem statement torque, outside diameter, length, gear teeth quantity and diametral pitch.

$$R_m = R_o - \frac{h}{2}$$

$$R_i = \frac{A}{2P}$$

$$y = R_m - R_i = R_o - \frac{h}{2} - \frac{A}{2P}$$

$$R_o = \frac{D_o}{2}$$

$$x = \frac{1}{2P}$$

Letting $h = .078$ and $b = \frac{15}{P}$ (the proportions of the 2021656 baseline unit)

$$\text{and } K_1 = K_2 = 2.2$$

$$C = 14 + \frac{6.6}{D_o P} - \frac{14.2A}{D_o P}$$

and

$$\sigma_A = \frac{1.67 TP (14D_o P + 6.6 - 14.2A)}{AD_o^2}$$

The planet stress, σ_{AP} , is

$$\frac{F_t P}{bJ}$$

where J = geometry factor ($= .45$ in the usual construction)

Substituting previously derived terms

$$\sigma_{AP} = \frac{.049 TP^3}{A}$$

Customarily, the problem statement will contain loading-cyclic requirements, which, when analyzed on the basis of cumulative damage, define a fixed relation of σ_A/σ_{AP} . The baseline unit for example is intended for use in a fighter aircraft flap application. It was found for balanced fatigue to let $\sigma_{AP} = .8 \sigma_A$

Using this relation and noting

$$D_o = \frac{1.185 (A + 3.6)}{P}, A \text{ has a single value of 87 teeth for which}$$

$P = 26.85$, a non-available form.

For the Fly-By-Wire Actuator, use of existing tooling is indicated, which restricts the possible diametral pitches to 24, 20, 17.5, 16.333, and 16. Some potential configurations appropriate to these pitches are shown in the Table A-2, together with their associated differential gear ratios, efficiencies and stress levels under two load conditions 200% structural margin and 130%. To furnish some basis of comparison for the latter, the baseline unit is rated for limit load of 70,000 in-lb/2 segments or $.27 \times 10^6$ psi, σ_A .

By inspection, the 24 pitch is a clear choice on an efficiency basis, however, the stress levels indicate 4 segments would be required. There is little to choose between the 17.5, 16.33, and 16 pitch configurations. An examination was also performed with a view to obtaining a better σ_A/σ_{AP} balance, by letting D_o vary. The results are shown in Table A-2. No gear teeth combinations could be found for 16.333 and 16 which satisfies phasing and equal spacing constraints ($AP \geq 13$). Although the stress picture improves, efficiency suffers.

From these considerations, the 20 pitch maximum efficiency configuration is recommended. This assumes that a structural margin of 130% is acceptable.

The desired total ratio with two motors operating is 637:1 from performance consideration.

The differential carrier speed due to one motor is

$$N_{C1} = \frac{N_{m1}}{\frac{A}{S} (1 + \frac{S}{A})} = \frac{N_m}{1 + \frac{A}{S}}$$

The differential carrier speed due to the other motor is

$$N_{C2} = \frac{N_{m2}}{1 + \frac{A}{S}}$$

The total differential carrier speed is then

$$N_C = N_{C1} + N_{C2} = \frac{2N_m}{1 + \frac{A}{S}}$$

It is anticipated that the overall ratio can be obtained by means of three identical simple planets and the output stage. The output speed is then

$$N_O = \frac{2 N_m}{(1 + \frac{A}{S})^3 \text{ mgf}}$$

TABLE A-2

DIAMETRICAL PITCHES

A. MAXIMIZED EFFICIENCY CONFIGURATIONS

P	A Max	AP	S	B	BP	m	e	D _o
24	77	23	31	59	13	2.81	0.935	3.98
20	63	18	27	58	13	3.64	0.900	3.95
17.5	55	16	23	35	13	4.61	0.876	3.97
16.33	51	15	21	44	15	7.29	0.805	3.96
16	50	14	22	42	14	10.0	0.726	3.97
	$\theta_A \times 10^6$ @T = 75,000		$\theta_A \times 10^6$ @T = 50,000		$\theta_{AP} \times 10^6$ @T = 75,000		$\theta_{AP} \times 10^6$ @T = 50,000	
P								
24	.29		0.19		0.33		0.22	
20	.27		0.18		0.24		0.16	
17.5	.24		0.16		0.18		0.12	
16.33	.23		0.15		0.16		0.11	
16	.23		0.15		0.15		0.10	

B. BALANCED STRESS CONFIGURATIONS

P	A	AP	S	B	BP	m	e	D _o
24	61	16	29	48	16	4.69	.877	3.19
20	55	16	23	49	16	9.17	.770	3.47
17.5	51	15	21	45	15	8.50	.775	3.70
16.33	48	No solution						
16	48	No solution						
	$\theta_A \times 10^6$ @T = 75,000		$\theta_A \times 10^6$ @T = 50,000		$\theta_{AP} \times 10^6$ @T = 75,000		$\theta_{AP} \times 10^6$ @T = 50,000	
P								
24	.50		.33		.44		.29	
20	.36		.24		.27		.18	
17.5	.29		.19		.20		.13	
16.33								
16								

The overall ratio is then

$$\frac{N_m}{N_o} = 637.0 = \frac{(1 + \frac{A}{S})^3}{2} \text{ mgf}$$

If $\text{mgf} = 12.12:1$, the ideal simple planet ratio is then 4.641:1. However, simultaneously satisfying equal spacing and load carrying requirements indicate 32 diametral pitch with $A = 85$ and $S = 23$. The overall ratio is thus 627.42. The overall efficiency is $.90 \times .98^4 = .83$.

The selected output stage compound planetary gear train computer solution is present in IBM print out sheet, Figure A-2. The print out sheets are based on the same compound ratio gear analyzed at three different operating pressure angles. AiResearch has chosen the 20 degree operating pressure angle for the WPAB Fly-By-Wire Actuator as having the best combination of efficiency (90.2%), torque per pound (3866.9) and total weight (6.455).

COMPOUND PLANETARY GEAR-SET, RING(A) IS FIXED FOR FIRST RATIO

MUE 0.1020 BEARING MUE 0.0040
ESP= 0.17577 EAF= 0.00211 EBF= 0.11181

NO. PLANETS= 6 AP-BP= 5 A-B= 5 DEL= 0

NS AP A BP B RATIO EFF FND
27 16 63 13 58 15.4667 0.90333
-19.4667 0.90333

DIAM. PITCH, CUTTER RING(B)
PRESS ANGLE, CUTTER 19.999
FACE WIDTH, NET 20.00
J-FACTOR (PLANET) 0.1440 0.0400
HERTZ-STRESS FACTOR 0.40129 0.45442 2.14376 2.70168

GEAR RATIO= 15.4667
MAX OPER TORQ, LB-IN= 7500.00
LIMIT TORQUE, LB-IN= 25000.00
BACK TORQUE, LB-IN= 37500.00
"BALL-PARK" WEIGHT, LBS= 8.463
MAX OPER TORQ LB-IN= 6942.46
MAX OPER INPUT LB-IN= 537.54

AREA FORMULAS ARE USED TO CALCULATE MAX OPER TORQ STRESSES.
GOOD CORRELATION IS OBTAINED USING FINITE ELEMENT PROGRAM "ANGSYS".
LIMIT AND BACK TORQUE STRESSES ARE DERATED TO ACCOUNT FOR
ADDITIONAL LOAD SHARING DUE TO DEFLECTIONS AT THE HIGHER TORQUES.

SUN M(V) SUN B(V) MUE-STD
10.048 34.678 13.982
37.352 12.982

CENTER GEAR IS RING(A)

MAX RING ROOT DIAZ 3.4069
MAX PLANET MEAN DIAZ 0.9302
MIN PLANET ROOT DIAZ 0.5750

*** HERTZ STRESS, KSI ***

NS AP BP
216.7 146.4 104.8
347.9 212.8 245.8
338.5 242.4 304.4

DELTA 0.0000 0.0000

RELATIVE-ROTATION RATIO OF PLANET TO OUTPUT =10.20000

16.1/1.35 3066.9

SIMPLE PLANETARY
RATIO EFF FND
3.33333 0.97981

DEPTH MAX SHEAR
AP BP

.0073 .0057

W-FACD 0.4300
RATIO 1.00000
1.07502

DIFF
RATIOS
0.60000
-3.60000

Figure A-2. Computerized Gear Analysis

THIS PAGE IS BEST QUALITY PHOTOGRAPH
FROM COPY FURNISHED TO DDC

GEAR-SET OPTIMIZATION PROGRAM

INITIAL INPUT DATA

DIAM. PITCH, CUTTER 19.999
PRESS ANGLE, CUTTER 20.00
NO. TEETH IN GEAR 18.000
NO. TEETH IN PINION 27.000
MIN CENTER DISTANCE 1.1999
THERMAL DIFF FACTOR 1.00070
TOLERANCE DP 482.1705
DECEHUM DP OF PINION 19.999
MELIX ANGLE= 0.0
PRE-FINISH= 0.0

CALCULATED DATA

DEL'D' TOL 0.0621
GD TOL 0.0036
ADDEI/OP 1.0000
DEDEI/OP 1.2654
CUTTER RT/OP 0.2774
MIN DEDEH/OP 1.2100
GEAR
PINION
0.0421
0.0040
1.0000
1.2654
0.2774
1.2100

SUM DEL D'S= 3.02610 TIGHT PA+V= 27.2399 MAX CDE 1.1929 DFL CT= 0.00183 OPER PA= 27.5802 BACKLASH= 0.00002/ 0.00179
DEL PIN MP 1.28732 0.44738 0.43506 0.06 MAX DEL BIP 0.00070 1.51040 0.02397 1.59040 MIN RDS EFF FAC MIN TIP N/2/1 MIN RDS
SRA= 0.4057 0.8831 ± TIF DIA= 1.3412 0.16000 0.37002 2.00000 2.00000
NO. TEETH, INTERNAL= 63. MATE(6)= 18. DEL CT= 0.00005 IDOL= 0.0046 MIN 0.1020 BACKLASH= 0.00007/ 0.00005
DEL INT TIGHT PA MP 1.36136 J-MATE MIN ID TIP DIM RDI MIN RDI TOL D+P MIN EFF FAC MIN EFF SET EFF FOR 24
4.78751 27.59091 0.47976 3.25000 0.68300 3.46370 0.01170 0.10310 0.07070 2.00000 0.00000 0.00000
SRA = 0.5473 0.8787 ± TIFD TIFD= 3.4432 FIL R= 0.0173 J-INT= 0.0000 INTRIN 2.0000

Figure A-2. Continued

THIS PAGE IS BEST QUALITY PRACTICABLE
FROM COPY SUBMITTED TO DDA

GEAR-SET OPTIMIZATION PROGRAM

INITIAL INPUT DATA

DIAM. PITCH, CUTTER 19.999
PRESS ANGLE, CUTTER 20.00
NO. TEETH IN GEAR 13.000
NO. TEETH IN PINION 36.000
MIN CENTER DISTANCE 1.8796
THERMAL DIFF FACTOR 1.00000
TOLERANCE DP 482.1785
DEDENDUM DP OF PINION 19.999
PRE-FINISH 0.0
HELIX ANGLE 0.0
DUMMY

CALCULATED DATA

DEL'D' TOL 0.0621
OD TOL 0.0036
ADDENOP 1.0000
DEDENOP 1.2654
CUTTER RTOP 0.2774
MIN DEENOP 1.2100
GEAR PINION
0.0621 0.0421
0.0036 0.0046
1.0000 1.0000
1.2654 1.2654
0.2774 0.2774
1.2100 1.2100

SUM DEL D'S 4.96780 MAX CD 1.8016

TIGHT PAVE 27.3046 DEL CTE 0.00100 OPER PA 27.5022 BACKLASH 0.00230/ 0.00000
DEL PIN MP 1.32533 0.40758 0.50577 0.80100 -0.19227 3.16850 0.82510 0.57210 0.16302 0.32318 3.23967 9.90000
SRA 0.4067 0.6210 = TIF DIA 2.9814 MIN RDS EFF FAC MIN TIP HEN-Y SUM SRA'S
WLS 1.16036

NO. TEETH, INTERNAL= 58.

MATE(6)= 13.

DEL CTE 0.00005

IDTOL= 0.0046

WLS 0.1020

BACKLASH 0.00437/ 0.00005

DEL INT TIGHT PA MP

J-MATE MIN ID TIP DIN ROI MIN ROI TOL D-V MIN EFF FAC MIN EFF SPT FOR SRA

0.43042 2.9770 0.63081 3.19420 0.81170 0.10050 0.10053 2.70478 0.00000 0.47881

TIFD= 3.1726

FIL R= 0.0170

J-INT= 0.6377

INDEX 4.1997

SRA = 0.4503

0.6181 = TIFD

TIFD= 3.1726

FIL R= 0.0170

J-INT= 0.6377

INDEX 4.1997

***** INTERNAL MESH CD= 1.1929/ 1.1909

Figure A-2. Continued

COMPOUND PLANETARY GEAR-SET, RING(A) IS FIXED FOR FIRST RATIO

ME= 0.1020 BEARING ME 0.0040
ESF= 0.16008 EAF= 0.07070 EBF= 0.10853

NO. PLANETS= 6 AP-BP= 5 A-B= 5 DEL= 0

NS AP A BP B RATIO EFF FWD
27 18 63 13 58 15.4667 0.90835
-14.4667 0.90201

SIMPLE PLANETARY
RATIO EFF FWD
3.33333 0.90111
-3.33333

SUN (HIV) SUM (HIV) MAXIMUM
18.940 34.600 14.049
37.338 13.059

DIAM. PITCH, CUTTER
PRESS ANGLE, CUTTER
FACE WIDTH, NET
J-FACTOR (PLANET)
HERTZ-STRESS FACTOR

SUN RING(A) RING(B)
19.999 19.999
20.00 20.00
0.1490 0.0400
0.43586 0.47976
2.88375 2.06412

CENTER GEAR IS RING(A)

MAX RING ROOT DIA= 3.4744
MAX PLANET MEAN DIA= 0.9412
MIN PLANET ROOT DIA= 0.5721

GEAR RATIO= 15.4667
MAX OPER TORQ, LB-IN= 7500.00
LIMIT TORQUE, LB-IN= 25000.00
BACK TB(RING), LB-IN= 37500.00
"BALL-PARK" WEIGHT, LBS= 6.932
MAX OPER TOFIX LB-IN= 6966.16
MAX OPER INPUT LB-IN= 533.84

*** TENSILE STRESS, KSI ***

NS AP BP
42.0 36.6 36.6
121.7 105.8 105.8
149.4 160.0 158.6

*** HERTZ STRESS, KSI ***

NS AP BP
203.9 142.4 180.8
282.5 205.8 239.2
309.0 280.8 316.2

DEPTH MAX STRESS
AP BP
.0076 .0004
STRESS 0.0000
MAXIMUM 1.0000
1.0000

MT= 131.81 737.12 862.03

RELATIVE-ROTATION RATIO OF PLANET TO OUTPUT = 14.00000

AGMA FORMULAS ARE USED TO CALCULATE MAX OPER TORQ STRESSES.
GOOD CORRELATION IS OBTAINED USING FINITE ELEMENT PROGRAM "ANSYS".
LIMIT AND BACK TORQUE STRESSES ARE DERATED TO ACCOUNT FOR
ADDITIONAL LOAD SHARING DUE TO DEFLECTIONS AT THE HIGHER TORQUES.

TOL/AB= 3466.4

*** VELAN ***

Figure A-2. Continued

ACTUATOR GEARING EFFICIENCY SENSITIVITY ANALYSIS

The selection of gearing for the rotary actuator includes the considerations of weight, volume and efficiency. As described in the discussion of the gearing arrangement, as efficiency is reduced, the weight and volume also increase. The effect of reduced efficiency, however, is an increase in the required gear ratio, motor speed, motor output torque, and motor current. As motor current (torque) increases, the selection available solid state transistor switches becomes limited. It is, therefore, desirable to understand the relationship between the efficiency of the gearbox, characteristics of the gearbox, motor sizing, and power switching limitations, before selection of a particular gearing efficiency. The actuator gearing efficiency analysis is as follows.

For a given control surface problem statement, the gear ratio is determined by

$$G = \left[\frac{T}{I \ddot{\theta} \eta} \right]^{1/2} \quad (A-1)$$

G = gear ratio

T = output acceleration torque, lbf-in.

I = motor inertia, lbf-in.-sec²

$\ddot{\theta}$ = output acceleration, rad/sec²

η = gearing efficiency

and for the given stall torque, inertia torque, motor rotor inertia, and output acceleration requirement:

$$G \propto \left[\frac{1}{\eta} \right]^{1/2} \quad (A-2)$$

In comparing the impact upon G of variations in η

$$\frac{G}{G_o} \propto \left[\frac{\eta_o}{\eta} \right]^{1/2} \quad (A-3)$$

or

$$G \propto G_o \left[\frac{\eta_o}{\eta} \right]^{1/2} \quad (A-4)$$

Therefore as efficiency decreases from η_o to η , the gear ratio increases from G_o to G according to the square root of the inverse of the efficiency ratio. As the gear ratio changes with η , the motor no-load speed must change.

$$\dot{\theta}_m = \dot{\theta}_s \times G \quad (A-5)$$

$\dot{\theta}_m$ = motor no-load speed, rad/sec

$\dot{\theta}_s$ = surface maximum rate, rad/sec

G = gear ratio

Since for a particular problem, $\dot{\theta}_s$ is fixed:

$$\dot{\theta}_m \propto G \quad (A-6)$$

$$\frac{\dot{\theta}_m}{\dot{\theta}_{mo}} \propto \frac{G}{G_o} \quad (A-7)$$

Substituting equation A-3 into Equation A-7

$$\frac{\dot{\theta}_m}{\dot{\theta}_{mo}} \propto \left[\frac{\eta_o}{\eta} \right]^{1/2} K \quad (A-8)$$

and

$$\dot{\theta}_m \propto \dot{\theta}_{mo} \left[\frac{\eta_o}{\eta} \right]^{1/2} \quad (A-9)$$

As before, when η decreases, the motor no-load speed increases to maintain the same maximum output rate, and acceleration. The motor speed must increase by the square root of the inverse efficiency ratio.

The torque supplied by the motor for a given output is a function of the gear ratio, as follows:

$$T_m = \frac{T_s}{G \times \eta} \quad (A-10)$$

T_s = Maximum torque at surface, lbf-in.

T_m = Maximum torque at motor for opposing load, lbf-in.

G = Gear ratio

η = Gear efficiency

For a given problem T_s is fixed, and therefore:

$$\frac{T_m}{T_{mo}} \propto \frac{G_o \times \eta_o}{G \times \eta} \quad (A-11)$$

Substituting Equation A-3 into Equation A-11

$$\frac{T_m}{T_{mo}} \propto \left[\frac{\eta}{\eta_o} \right]^{1/2} \times \frac{\eta_o}{\eta} \quad (A-12)$$

and

$$T_m \propto T_{mo} \left[\frac{\eta_o}{\eta} \right]^{1/2} \quad (A-13)$$

Once again, as efficiency decreases, the required motor torque increases by the square root of the inverse efficiency ratio.

Current requirements may be expressed in relationship to the torque produced and the motor no-load speed as follows:

$$T/A = \frac{K}{\dot{\theta}_m} \quad (A-14)$$

T = Motor torque, lbf-in.

A = Motor current, amps

$\dot{\theta}_m$ = Motor no-load speed, rad/sec

Equation A-10 may be rearranged as follows:

$$A \propto \dot{\theta}_m T \quad (\text{A-15})$$

and

$$\frac{A}{A_o} \propto \frac{\dot{\theta}_m}{\dot{\theta}_{mo}} \frac{T}{T_o} \quad (\text{A-16})$$

using Equations A-8 and A-13 in Equation A-16

$$\frac{A}{A_o} \propto \left(\frac{\eta_o}{\eta} \right)^{1/2} \times \left[\frac{\eta_o}{\eta} \right]^{1/2} \quad (\text{A-17})$$

therefore

$$\frac{A}{A_o} \propto \frac{\eta_o}{\eta} \quad (\text{A-18})$$

and current is proportional to the inverse efficiency ratio.

For a variation in gearing efficiency ranging from +20 to -20 percent from a nominal value, the values of G , $\dot{\theta}_m$ and T_m vary from +10 to -10 percent, approximately; while current, A , varies from +20 to -20 percent, as shown in Figures A-3 and A-4.

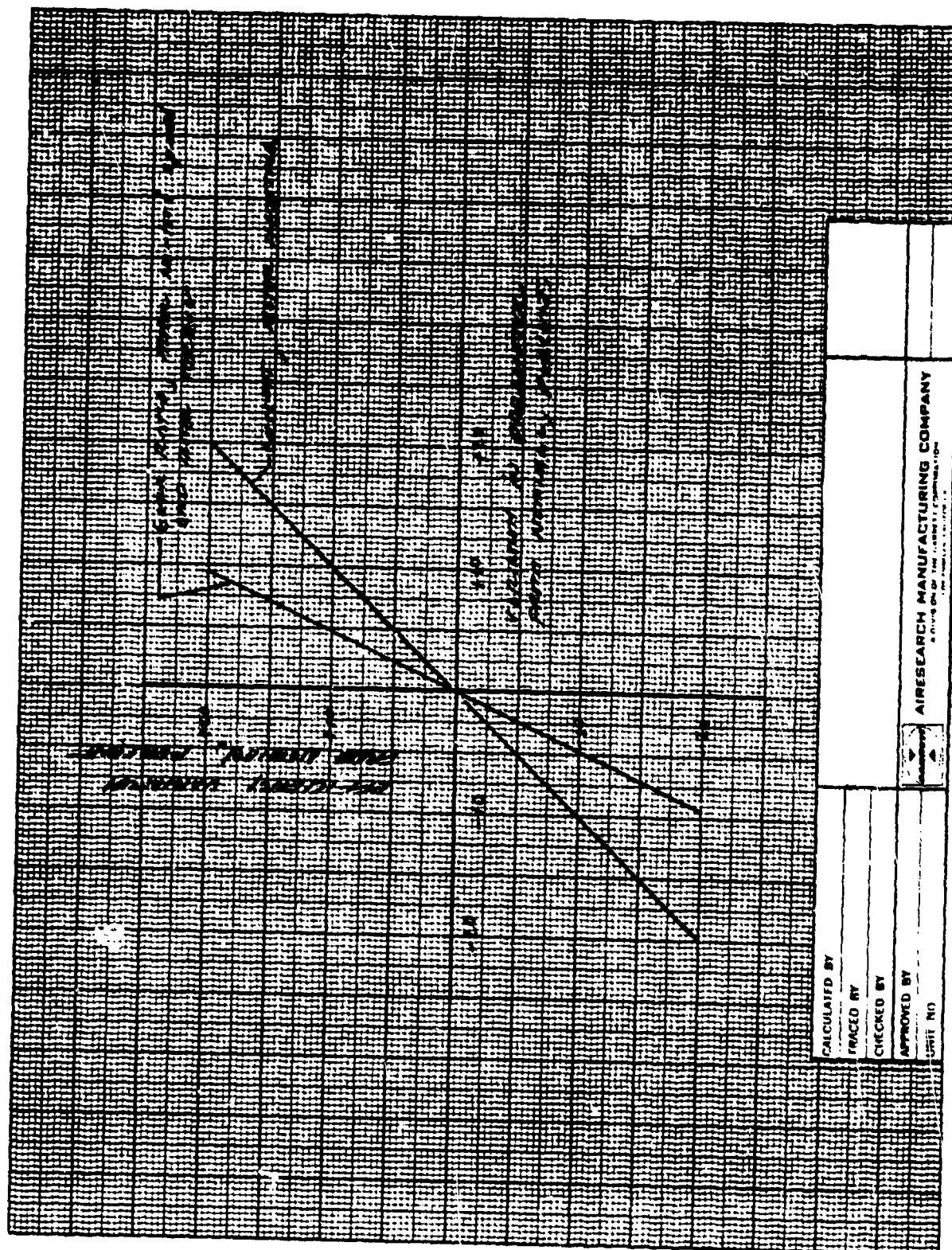


Figure A-3. Gearing Sensitivity

Heating in a motor is related to

$$W = A^2 R$$

(A-19)

W = Motor Heating, watts

A = Current, amps

R = Resistance, ohms

Motor no-load speed is related to resistance as follows:

As speed is increased by a factor of 2

Resistance is decreased by a factor of 4

Comparing motor heating for two cases

$$\frac{W}{W_o} \propto \frac{A^2}{A_o^2} \frac{R}{R_o}$$

(A-20)

Equation A-16 shows

$$\frac{A}{A_o} \propto \frac{\dot{\theta}}{\dot{\theta}_o} \frac{T}{T_o}$$

and Equation A-13 shows

$$T \propto T_o \left(\frac{\eta_o}{\eta} \right)^{1/2}$$

Substituting Equation A-13 into A-16

$$\frac{A}{A_o} \propto \frac{\dot{\theta}}{\dot{\theta}_o} \left(\frac{\eta_o}{\eta} \right)^{1/2}$$

(A-21)

and substituting A-21 into A-20

$$\frac{W}{W_o} \propto \left[\frac{\dot{\theta}}{\dot{\theta}_o} \left(\frac{\eta_o}{\eta} \right)^{1/2} \right]^2 \frac{R}{R_o}$$

(A-22)

Simplifying

$$\frac{W}{W_o} \propto \left(\frac{\dot{\theta}}{\dot{\theta}_o} \right)^2 \frac{\eta_o}{\eta} \frac{R}{R_o}$$

(A-23)

when

$$\frac{\theta}{\theta_o} = 2$$

$$\frac{R}{R_o} = 1/4$$

therefore

$$\frac{W}{W_o} \propto (2)^2 \times \frac{\eta_o}{\eta} \frac{1}{4}$$

$$\propto 4 \times \frac{\eta_o}{\eta} \frac{1}{4} = \frac{\eta_o}{\eta}$$

and the heating occurring in the motor is in proportion to the additional work required to compensate for reduced gearing efficiency.

ARRANGEMENT OF THE ASSEMBLY

The arrangement of the mechanical elements are presented in Figure A-5. The redundant motors operate into the velocity summing differential, followed by the two stages of simple planetary reduction. The output of the second stage operates into the compound planetary gear set, consisting of two identical load sharing slices. The gear ratios for each stage are presented in Table A-3.

TABLE A-3
ACTUATOR GEAR RATIO

GEAR STAGE	STAGE GEAR RATIO	
	Two Motors Operating	Either of One Motor Operating
Differential	2.35	4.7
1st Stage	4.7	4.7
2nd Stage	4.7	4.7
Compound Output	12.1	12.1

Considering cost, manufacturing, and simplicity, the planet gears in the differential and the two planetary stages are identical. Similarly, the associated sun gears are identical, as are the ring gears for these assemblies.

The differential uses 3 planet gears in each half, and the first stage planetary gear set uses 3 planets. Because of the higher loads reflected to the second stage planet gear set, 4 planet gears are used. The compound planet output stages uses 6 planet gears in each slice to achieve life and torque capability.

Operation of the differential gearing is shown in Figure A-6. Three cases are presented, (1) both motor operating (normal mode), (2) right hand input operating, and (3) left hand input operating. The last two cases represent operation of the differential to provide reduced rate capability in the event of failure of either of the drive channels.

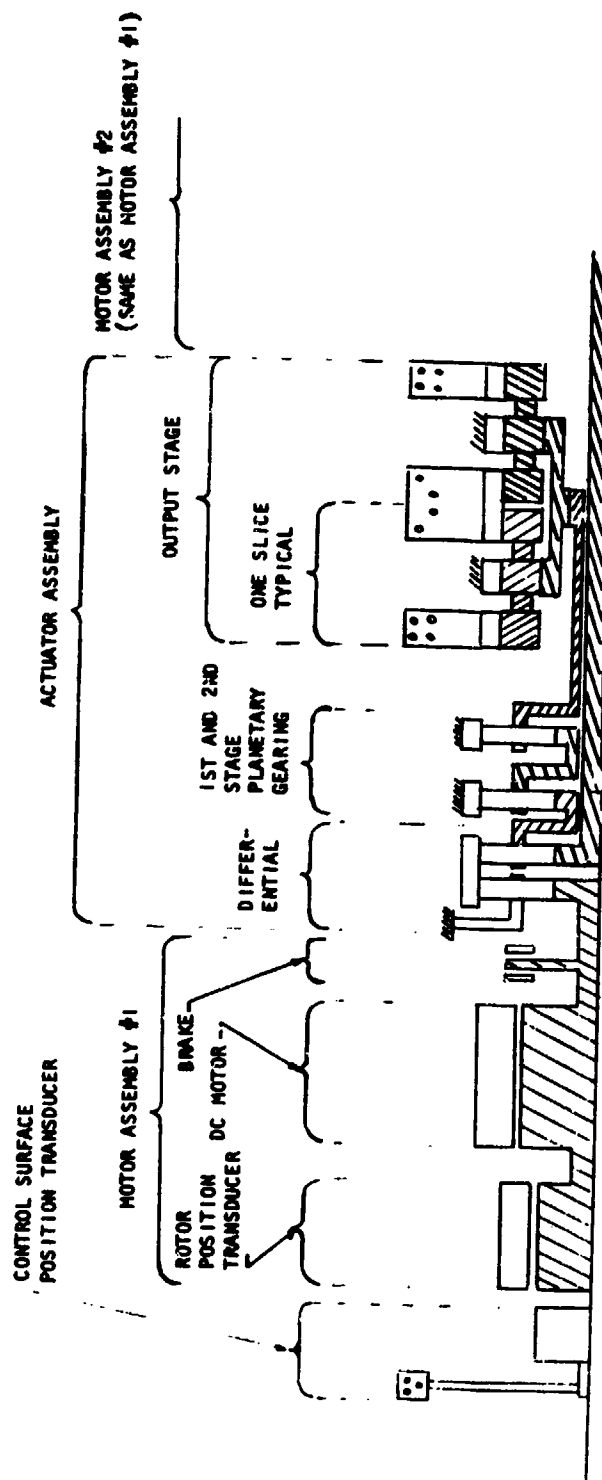


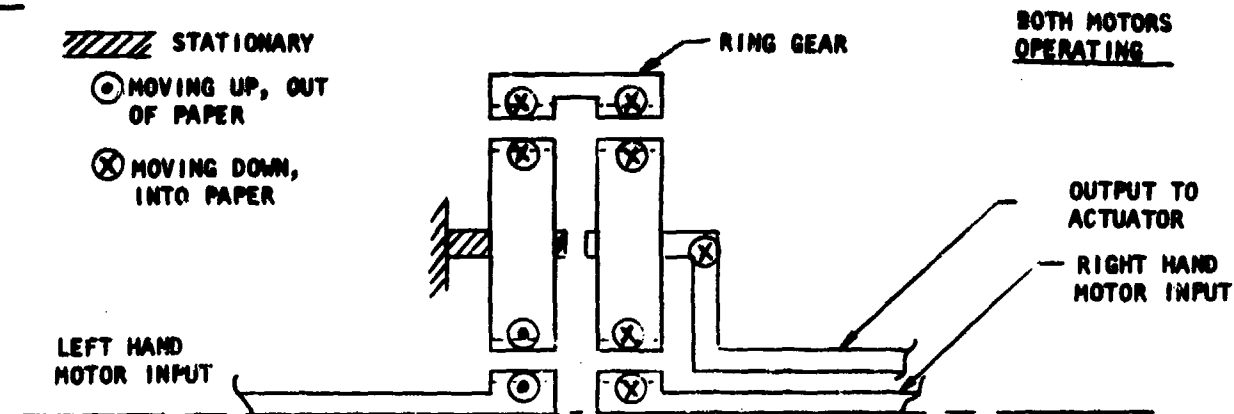
Figure A-5. Actuator Mechanical Arrangement

KEY

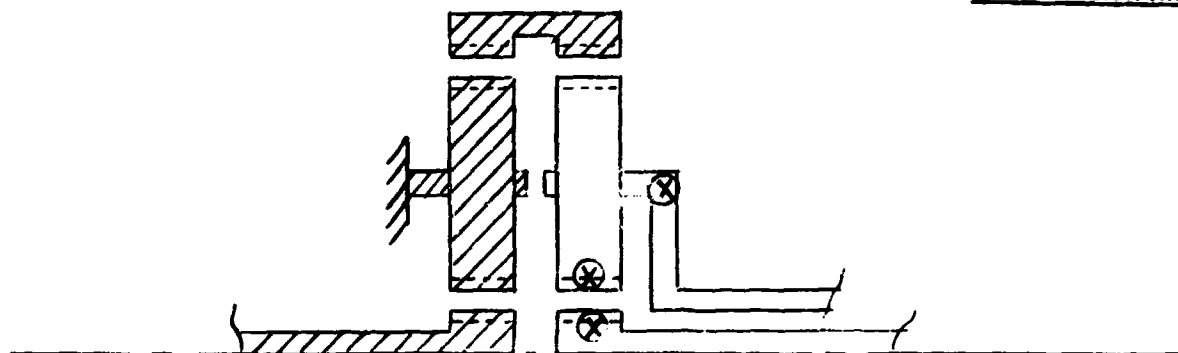
STATIONARY

MOVING UP, OUT
OF PAPER

MOVING DOWN,
INTO PAPER



RIGHT HAND
MOTOR OPERATING



LEFT HAND
MOTOR OPERATING

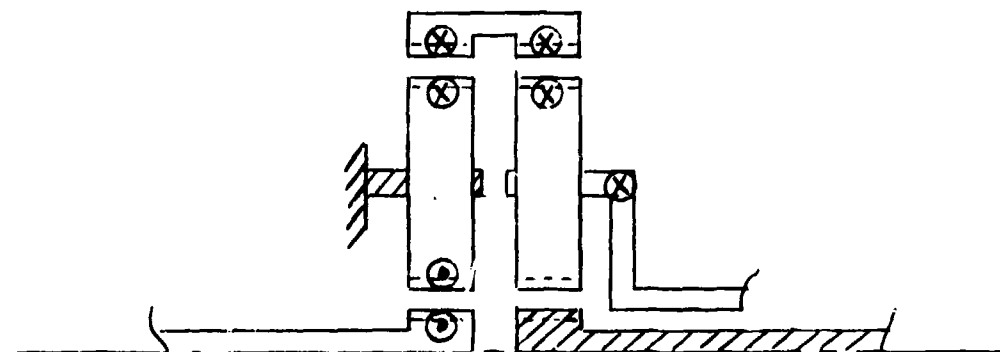


Figure A-6. Operation of Differential Gearing

INERTIA CALCULATIONS

This section presents detailed calculations of system inertia evaluated at the motor. The effective load inertia ($46.6 \text{ lbf-in-sec}^2$) reflected to the motor is $46.6 \div G^2$. The gear ratio, G is approximately 627:1, and therefore the load inertia, seen at the motor is only $119 \times 10^{-6} \text{ lbf-in-sec}^2$. In a similar way, the inertia of the actuator gearing is found to have a minor impact upon effective motor inertia. As shown by the calculations, the gearing and load result in approximately a 16 to 34 percent increase in motor rotor inertia, depending upon the drive train or combination of drive trains operating.

The calculations are presented for the reflected inertia for 3 cases. These are: (1) Both motors operating, (2) right hand motor operating and left hand motor fixed, and (3) left hand motor operating with the right hand motor fixed.

Inertia Calculations, Actuator Gearbox

Inertia of simple rotating bodies.

Solid disc Mass = M
 Radius = R

About its own axis.

$$I = 1/2 MR^2$$

Most all of the elements are considered to be:

Hollow cylinder Mass = M
 Radius = R

About its own axis.

$$I = MR^2$$

The mass of each rotating element is determined from the detailed weight calculations shown on Table A-4. The radius of each element is determined from the actuator cross section Drawing No. 2022192.

The gear ratio of each stage and each element is determined from the gear tooth count shown on the drawing of Figure A-7. This figure also correlates the item drawing number of Table A-4 to the cross section element of Figure A-7.

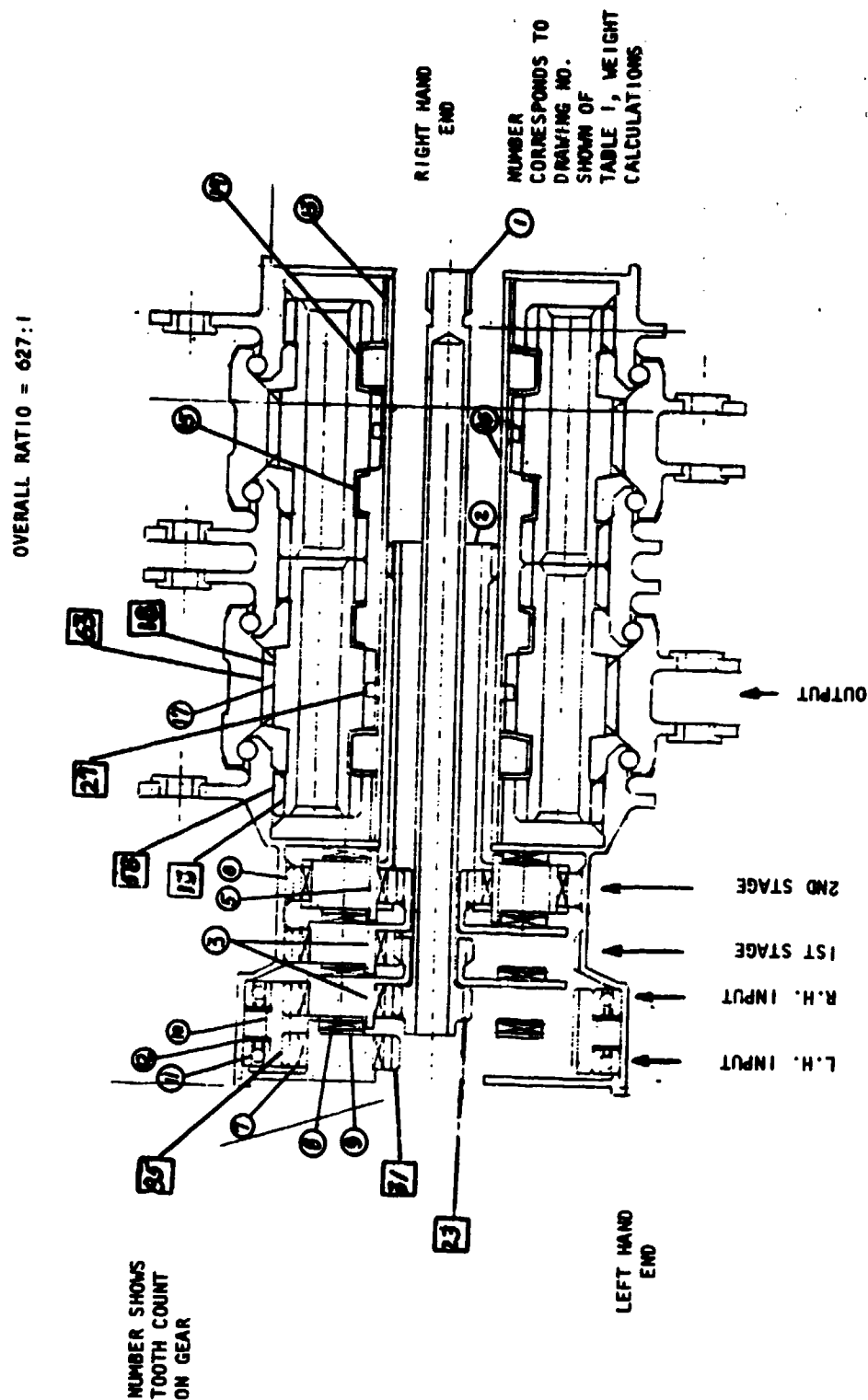
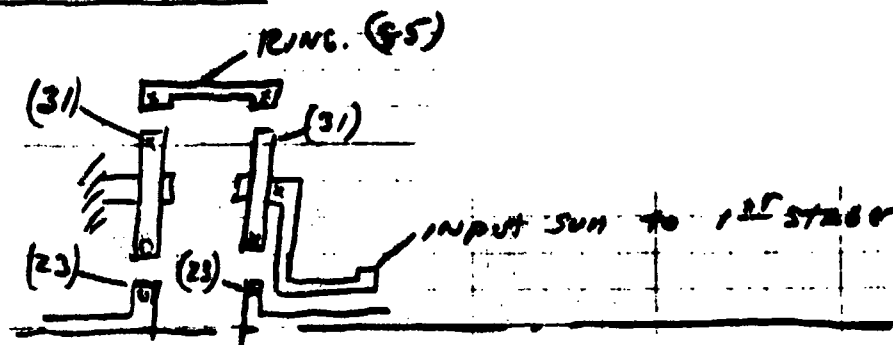


Figure A-7. Actuator Cross-Section Used for Inertia Calculations

Tables A-5 through A-7 present the detailed inertia calculation for each actuator gear element.

Angular Velocity Ratio



1. L. H. Input (R. H. Input Fixed or not Fixed)

Gear about own axis

$$\frac{31}{23} = 1.35$$

Ring about actuator axis (own axis)

$$\frac{85}{23} = 3.7$$

2. R. H. Input (L. H. Input Fixed)

Gear about actuator axis

$$\frac{85}{23} + 1 = 4.7$$

Gear about own axis

$$\frac{85}{31} - 1 = 1.74$$

3. R. H. Input (L. H. Input not Fixed)

Gear about actuator axis

$$4.7/2 = 2.35$$

Gear about own axis

$$1.74 \times 2 = 3.48$$

The output of the differential is

4.7 for either of one motor operating

2.35 for both motors (normal operation)

First Stage

Gear about own axis

$$\left(\frac{85}{31} - 1\right) 4.7 = 8.19 \quad 1 \text{ motor}$$

$$\left(\frac{85}{31} - 1\right) 2.35 = 4.09 \quad 2 \text{ motors}$$

Gear about actuator axis (second stage input)

$$\left(\frac{85}{23} + 1\right) 4.7 = 22.05 \quad 1 \text{ motor}$$

$$11.02 \quad 2 \text{ motors}$$

Second Stage

Gear about own axis

$$\left(\frac{85}{31} - 1\right) 22.05 = 38.41 \quad 1 \text{ motor}$$

$$19.2 \quad 2 \text{ motors}$$

Gear about actuator axis (C.P. stage input)

$$\left(\frac{85}{23} + 1\right) 22.05 = 103.54 \quad 1 \text{ motor}$$

$$51.77 \quad 2 \text{ motors}$$

Output Stage (Approximate)

Gear about own axis

$$\left(\frac{58}{13} - 1\right) 103.54 = 358.41 \quad 1 \text{ motor}$$

$$179.2 \quad 2 \text{ motors}$$

Gear about actuator axis

$$\left(\frac{58}{27} + 1\right) 103.54 = 325.96 \quad 1 \text{ motor}$$

$$162.98 \quad 2 \text{ motors}$$

TABLE A-5
TWO MOTORS OPERATING

Name	Item No.	Qty	R., In.	(W) Weight lb	Inertia, lb-in.-sec ²		Gear Ratio, I	Reflected Inertia $I/(I)^2$, lb-in.-sec ²
					$\frac{1}{2} \frac{W}{g} R^2$	$\frac{W}{g} R^2$		
A.H. Input								
Shaft	1	1	0.1875	0.14		13×10^{-6}	1	13×10^{-6}
Gear	6	3	0.47	0.075		43	3.48	3.55
		3	0.88	0.075		150	2.35	27.16
Bearing	7	3	0.88	0.048		96	2.35	17.38
							S-	61.09
L.H. Input								
Gear	6	3	0.47	0.075		43×10^{-6}	1.35	23.6
Bearing	7	3	0.31	0.048		12	1.35	6.58
Gear	10	1	1.44	0.31		1665	3.7	121.6
Bearing	11	2	1.56	0.14		883	3.7	64.5
Spacer	12	2	1.63	0.03		206	3.7	15.05
							S-	231.33
Combined								
Carrier	3	1	0.88	0.085		171×10^{-6}	2.35	30.9
Bearing	8	1	0.88	0.04		80	2.35	14.5
Spacer	9	1	0.88	0.024		48	2.35	8.7
							S-	54.1
1st Gear								
Gear	6	3	0.47	0.075		43×10^{-6}	4.09	2.57
		3	0.88	0.075		150	11.02	1.24
Bearing	7	3	0.88	0.048		96	11.02	0.8
Carrier	3	1	0.88	0.085		171	11.02	1.41
Bearing	8	1	0.88	0.04		80	11.02	0.7
Spacer	9	1	0.88	0.024		48	11.02	0.4
							S-	7.12
2nd Stage								
Gear	6	4	0.47	0.1		57×10^{-6}	18.2	0.15
		4	0.88	0.1		201	51.77	0.07
Bearing	7	4	0.88	0.064		128	51.77	0.05
Pin	5	4	0.56	0.06		49	51.77	0.02
Carrier	2	1	0.44	0.28		140	51.77	0.05
Bearing	8	1	0.88	0.04		80	51.77	0.03
Spacer	9	1	0.88	0.024		48	51.77	0.02
							S-	0.39
Output								
Shaft	16	1	0.53	0.27		196×10^{-6}	51.77	0.07×10^{-6}
Spacer	13	2	0.63	0.05		51	51.77	0.02
Ring	14	2	0.75	0.09		131	51.77	0.05
Ring	15	2	0.81	0.06		102	51.77	0.04
Gear	17	12	0.38	2.68		1003	179.2	0.03
		12	1.125	2.68		8787	169.9	0.33
							S-	0.54
Load						46.6	T-	354.57×10^{-6}
							627	119×10^{-6}
							GT-	473.57×10^{-6}
Rotor Inertia of two motors = 2150×10^{-6} lb-in.-sec ²								
Percent increase caused by gear box and load								
$\frac{2150 + 474}{2150} = 1.22 = 22 \text{ percent}$								

TABLE A-6

LEFT MOTOR OPERATING, RIGHT MOTOR FIXED

Name	Item No.	Qty	R., In.	(W) Weight, lb	Inertia, lb-in-sec ²		Gear Ratio, i	Reflected Inertia, 1/(i) ² , lb-in.-sec ²
					$\frac{1}{2} \frac{W}{g} R^2$	$\frac{W}{g} R^2$		
<u>R.H. Input</u> <u>Fixed</u>								00x10 ⁻⁶
<u>L.H. Input</u> Same as Table A-4								231.33
<u>Combined</u>								
Carrier	3					171x10 ⁻⁶	4.7	7.74
Bearing	8					80	4.7	3.62
Spacer	9					48	4.7	2.17
								<u>13.53</u>
<u>1st Stage</u> Table A-4 (divide results by 4)								1.78
<u>2nd Stage</u> Table A-4 (divide results by 4)								0.1
<u>Output</u> Table A-4 (divide results by 4)								<u>0.54</u>
							Subtotal	247.28
							Load	<u>119</u>
							Total	366.3
<p>Rotor inertia of one motor 1077x10⁻⁶ lb-in-sec²</p> <p>Percent increase caused by gear box and load</p> $\frac{1077 + 366}{1077} = 1.34 \approx 34 \text{ percent}$								

TABLE A-7

RIGHT MOTOR OPERATING, LEFT MOTOR FIXED

Name	Item No.	Qty	R., In.	(W) Weight, lb	Inertia, lb-in-sec ²		Gear Ratio, 1	Reflected Inertia, 1/(1) ² , lb-in.-sec ²
					$\frac{1}{2} \frac{W}{g} R^2$	$\frac{W}{g} R^2$		
<u>R.H. Input</u>								
Shaft	1						1	13×10^{-6}
Gear	6					43	1.74	14.2
						150	4.7	6.79
Bearing	7					96	4.7	4.35
								<u>38.34</u>
<u>L.H. Input</u>								
Fixed								00×10^{-6}
<u>Combined</u>								
Table A-5								13.53
<u>1st Stage</u>								
Table A-5								1.78
<u>2nd Stage</u>								
Table A-5								0.1
<u>Output</u>								
Table A-5								0.54
Act. total								<u>54.29</u>
Load								<u>119</u>
Grand total								<u>173.29</u>
<p>Motor rotor inertia; one motor 1077 lb-in-sec²</p> <p>Percent Increase caused by gear box and load</p> $\frac{1077 + 173.3}{1077} = 1.16 \approx 16 \text{ percent}$								

THERMAL ANALYSIS.

A thermal analysis was performed on the Fly-By-Wire actuator consisting of two motors and a gearbox. The purpose of the analysis was to determine the maximum temperatures of critical parts such as

1. Stator winding (400°F allowed)
2. Rotor magnet (350°F allowed)
3. Brake coil (400°F allowed)
4. Gearbox housing
5. Gear cluster consisting of gears and shafts

The ambient and structure temperature considered was 80°F. Heat transfer from the actuator was by natural convection, conduction through the lugs on the motor and gearbox housings, and radiation. To obtain maximum cooling by radiation, the external surfaces of the actuator were assumed to be painted black.

The actuator was analyzed using AIResearch Thermal Analyzer Computer Program H0298.

To facilitate the analysis, a steady state operating condition corresponding to one-half load and 50 percent duty cycle was examined. For this case the power loss breakdown for one-half of the actuator is:

<u>Power Source</u>	<u>Peak Power</u> (Watts)	<u>Power Used in</u> <u>Analysis</u> (Watts)
Stator copper	73-15	36.58
Stray losses	7.5	3.75
Stator teeth	14.6	7.30
Back iron	10.8	5.4
Brake coil	7.7 at 400°F 4.4 at 68°F	7.7 at 400°F 4.4 at 68°F
Gearbox	151.8	75.9
Rotor surface	3.0	1.5
Ball bearings (2 per motor)	--	4 each

The copper loss is given at 400°F and the computer program adjusts the copper loss as a function of the predicted temperature.

Figure A-8 shows the thermal model of the actuator motor. Included in this model are 0.5 inch high fins on the motor housing. These fins were added after it became apparent in the early thermal analysis that cooling of the stator winding would not be sufficient with the original motor design. There are 27 aluminum fins and each fin is 0.0625 inch thick, 0.5 inch high, and 4.35 inch long.

Figure A-9 shows a simplified model at one-half of the gearbox. As modeled, two heat sources are used. One gear (node 76) closest to the motor-to-gearbox interface dissipates 5.1 percent of the gearbox losses. The other heat source (node 77) dissipates the remaining 94.9 percent and this heat is rejected to the air within the gearbox and to the adjacent housing by conduction. Because of the simplified approach, the temperatures obtained for node 76 and 77 will be average values.

The stator windings are shown in Figure A-10. Because of the closeness of winding nodes 31 and 32 to the gearbox, these windings will have the highest stator copper temperatures. Convection cooling of these end turn windings were considered.

The rotor thermal model is in Figure A-11. The end view includes the damper ring, Sa-Co permanent magnet, iron core, and hexagon shaft.

The results for the one-half load, 50 percent duty cycle, are shown in the computer print out sheets presented in Figure A-12. The maximum temperatures of interest are:

- | | |
|-----------------------------|-------|
| 1. Stator winding (node 31) | 249°F |
| 2. Rotor magnet (node 61) | 261°F |
| 3. Brake coil (node 81) | 313°F |
| 4. Gear housing (node 68) | 330°F |
| 5. Gear cluster (node 77) | 387°F |

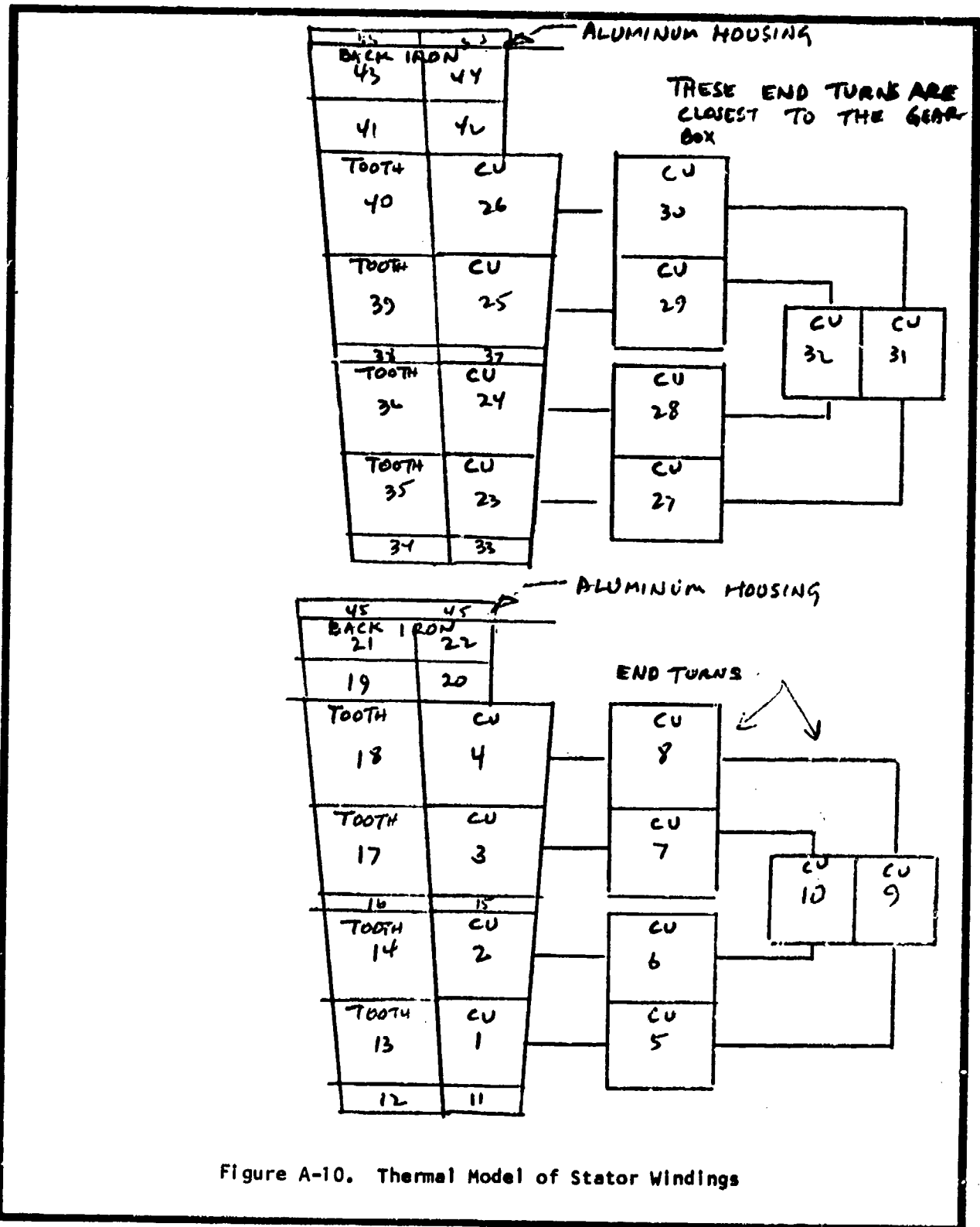
These temperatures satisfactorily meet the criterias previously specified. Additional analysis will be required to predict temperature at duty cycles above 50%.



Figure A-8. Actuator Motor Thermal Model

AFFDL-TR-78-150

CALC. NO. _____ SHEET NO. _____
MODEL NO. _____
CHECKED BY _____



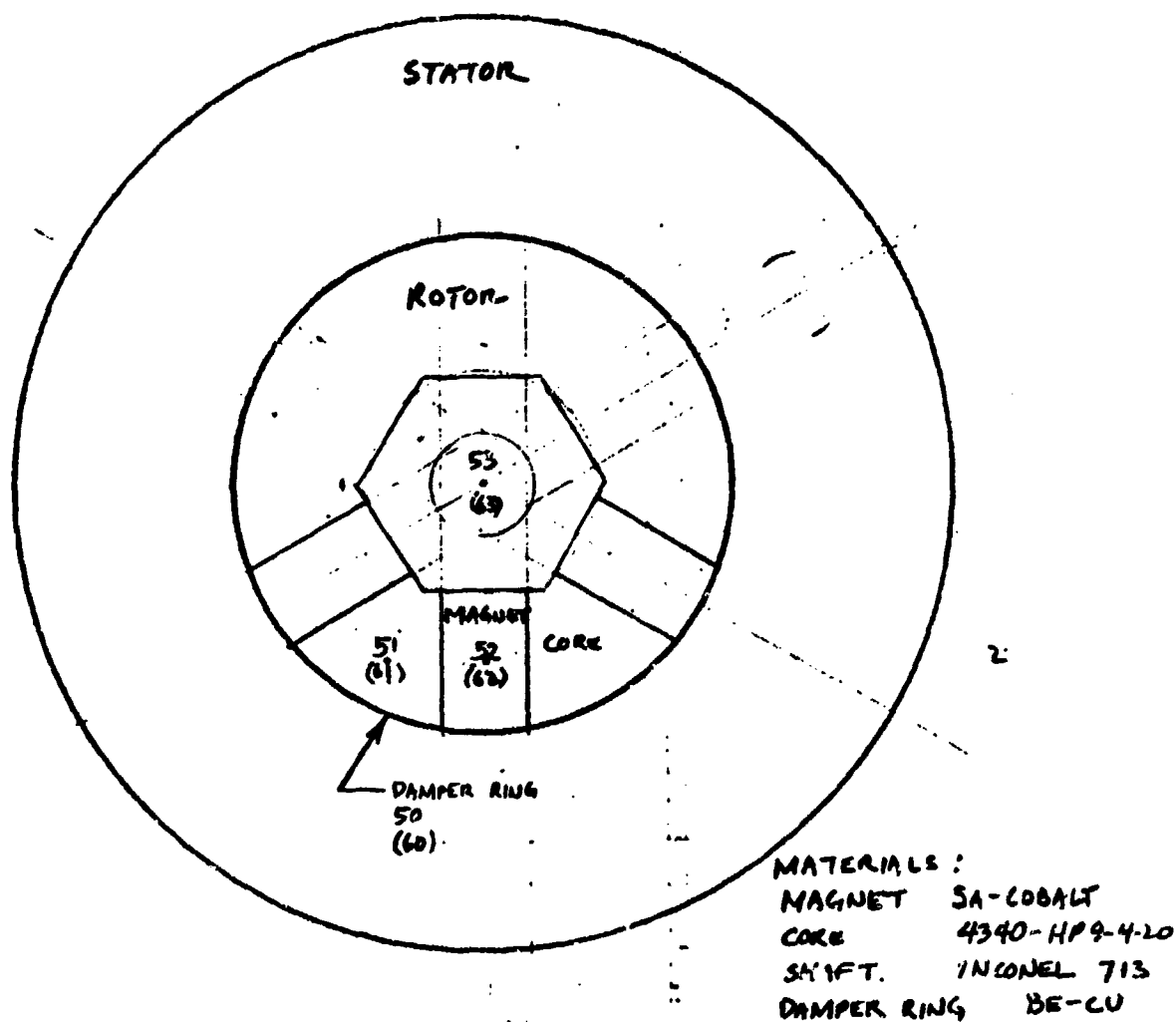


Figure A-11. Thermal Model of Rotor

SCALE 2:1

STEADY STATE SOLUTION

NO. OF ITER. = 26 ITER. = .3725

ACCEL = .0100

NODE NO.	TEMP.	HEAT IN.	WDOV	CPN	KN	TEMP.
1	244.79	2.7004	.063747	.0910	200.00000	118.21
2	244.45	2.7007	.062953	.0910	200.00000	118.24
3	244.37	2.7004	.062575	.0910	200.00000	117.97
4	242.41	2.6982	.062362	.0910	200.00000	116.99
5	246.13	.9807	.021977	.0910	200.00000	118.95
6	246.04	.9814	.021977	.0910	200.00000	118.24
7	246.44	.9811	.021977	.0910	200.00000	118.12
8	245.40	.9797	.021977	.0910	200.00000	118.54
9	246.09	.9811	.020572	.0910	200.00000	118.93
10	246.47	.9811	.020572	.0910	200.00000	118.93
11	244.53	.9800	.001031	.1200	.11000	118.06
12	243.59	.9800	.027966	.1200	15.36359	117.54
13	243.34	.9825	.141302	.1200	15.36359	117.42
14	242.50	.9825	.103007	.1200	15.36359	116.93
15	244.54	.9800	.000400	.1200	.11000	118.06
16	241.86	.9800	.001446	.1200	15.36359	116.58
17	241.32	.9825	.005110	.1200	15.36359	116.29
18	239.94	.9825	.074181	.1200	15.36359	115.51
19	238.32	.9817	.069902	.1200	15.36359	114.61
20	238.05	1.8190	.150110	.1200	15.36359	114.46
21	237.54	.9305	.069902	.1200	15.36359	114.20
22	237.51	1.8700	.157426	.1200	15.36359	114.16
23	246.74	2.7139	.063747	.0910	200.00000	119.31
24	246.75	2.7139	.062953	.0910	200.00000	119.29
25	246.36	2.7124	.062575	.0910	200.00000	119.04
26	245.14	2.7074	.062362	.0910	200.00000	118.40
27	246.93	.9845	.021977	.0910	200.00000	120.51
28	248.75	.9843	.021977	.0910	200.00000	120.40
29	248.01	.9841	.021977	.0910	200.00000	120.32
30	249.51	.9839	.021977	.0910	200.00000	120.27
31	249.15	.9820	.020572	.0910	200.00000	120.62
32	249.02	.9814	.020572	.0910	200.00000	120.55
33	246.37	.9800	.001031	.1200	.11000	119.04
34	245.07	.9800	.027966	.1200	15.36359	118.81
35	245.74	.9825	.141302	.1200	15.36359	118.75
36	245.19	.9825	.103007	.1200	15.36359	118.43
37	246.52	.9800	.000400	.1200	.11000	119.14
38	244.74	.9800	.001446	.1200	15.36359	118.18
39	244.34	.9825	.005110	.1200	15.36359	117.97
40	243.41	.9825	.074181	.1200	15.36359	117.44
41	242.25	.9807	.069902	.1200	15.36359	116.79
42	242.04	1.8190	.150110	.1200	15.36359	116.69
43	241.71	.9305	.069902	.1200	15.36359	116.49
44	241.86	1.8700	.157426	.1200	15.36359	116.46
45	235.55	.9800	.114366	.2100	100.00000	113.07
46	247.50	.1407	.000000	.2400	.01000	119.71
47	253.26	.9800	.071148	.2100	100.00000	111.80
48	212.67	.9800	.148862	.2100	100.00000	100.36
49	233.44	4.0000	.015565	.1100	8.00000	111.90
50	253.08	1.5000	.021314	.0910	65.00000	122.81
51	253.50	.9800	.251626	.1100	22.00000	123.04
52	253.48	.9800	.257400	.1000	4.05000	123.03
53	253.33	.9800	.127736	.1100	7.20000	122.43
54	235.04	.9800	.079475	.1100	7.20000	112.34
55	240.16	.9800	.114366	.2100	100.00000	115.03
56	241.41	.9800	.293372	.2100	100.00000	116.33

Figure A-12. Computerized Thermal Analysis

THIS PAGE IS BEST QUALITY PRACTICABLE
FROM COPY FURNISHED TO DDC

67	298.07	.0000	.675352	.1100	25.00000	146.69
68	305.14	4.0000	.031479	.1100	5.00000	151.73
69	261.43	.0475	.000000	.2400	.01000	127.45
70	261.35	1.5070	.021318	.0910	65.00000	127.40
71	261.05	.0000	.251826	.1100	22.00000	127.24
72	261.00	.0000	.257400	.1000	4.85000	127.26
73	261.57	.0000	.127738	.1100	7.20000	127.53
74	302.13	.0000	.113577	.1100	7.20000	150.06
75	331.12	.0000	.020322	.1100	7.20000	166.16
76	332.00	.0000	.013916	.1100	25.00000	166.90
77	297.53	.0000	.172956	.1100	25.00000	147.51
78	329.63	.0000	1.868848	.1100	25.00000	165.34
79	234.65	.0000	.024492	.1100	25.00000	112.57
80	229.92	.0105	.000000	.2400	.01000	109.98
81	292.03	1.5545	.000000	.2400	.01000	144.45
82	353.79	.0258	.000000	.2400	.01000	170.76
83	80.00	.0000	-1.000000	.2400	.01000	26.65
84	202.32	.0000	.058782	.1100	25.00000	96.61
85	219.19	.0000	.042336	.2100	100.00000	103.90
86	335.77	1.4920	.911200	.1100	25.00000	168.75
87	307.11	72.0100	5.062584	.1100	25.00000	197.27
88	203.33	.0000	.051548	.2100	100.00000	95.17
89	301.48	.0000	.017040	.1100	25.00000	149.68
90	299.59	.0000	.187376	.1100	25.00000	148.54
91	312.50	6.8308	.355588	.0910	.30300	155.82
92	300.55	.0000	.195108	.1100	25.00000	149.18
93	302.54	.0000	.071852	.1100	25.00000	150.29
94	307.41	1.3615	.000000	.2400	.02000	143.22
95	233.77	.0000	.188162	.2100	100.00000	112.08
96	239.23	.0000	.152478	.2100	100.00000	115.11
97	193.69	.0000	.009800	.2100	100.00000	89.82
98	251.54	.0000	.084200	.1100	25.00000	121.96
99	235.98	.0000	.029400	.2100	100.00000	113.24
00	80.00	.0000	-1.000000	1.0000	1.00000	26.65

Figure A-12. Continued

PERFORMANCE SPECIFICATION

The preliminary performance specification is presented in Appendix B of this report.

COMPONENTS

The following pages present the design approach to each of the major components of the actuation system. The descriptions are organized as follows:

Controller
Actuator
Motor
Surface position transducer

CONTROLLER

A sketch of the hardware arrangement of the controller is shown in Figure A-13. The CRT, keyboard, tape cassette, and the microprocessor monitor enable the program entry, debugging, editing, and display functions. These hardware components will be purchased parts. A description of the unit, produced by Wave Mate, is contained in Figure A-14.

The controller inputs on the front panel include commutation angle, velocity limit, torque limit, regeneration and position commands. The analog status monitors for both controllers 1 and 2 are motor speed, average voltage, average current and actuator position. The inverter chassis houses the transistor switches and the current limit loop circuits as well as the sensor and parking brake interface circuits.

The block diagram of Figure A-15 shows the functional characteristic of one channel of the motor controller. Hardware partitioning of controllers 1 and 2 is shown in Figure A-16.

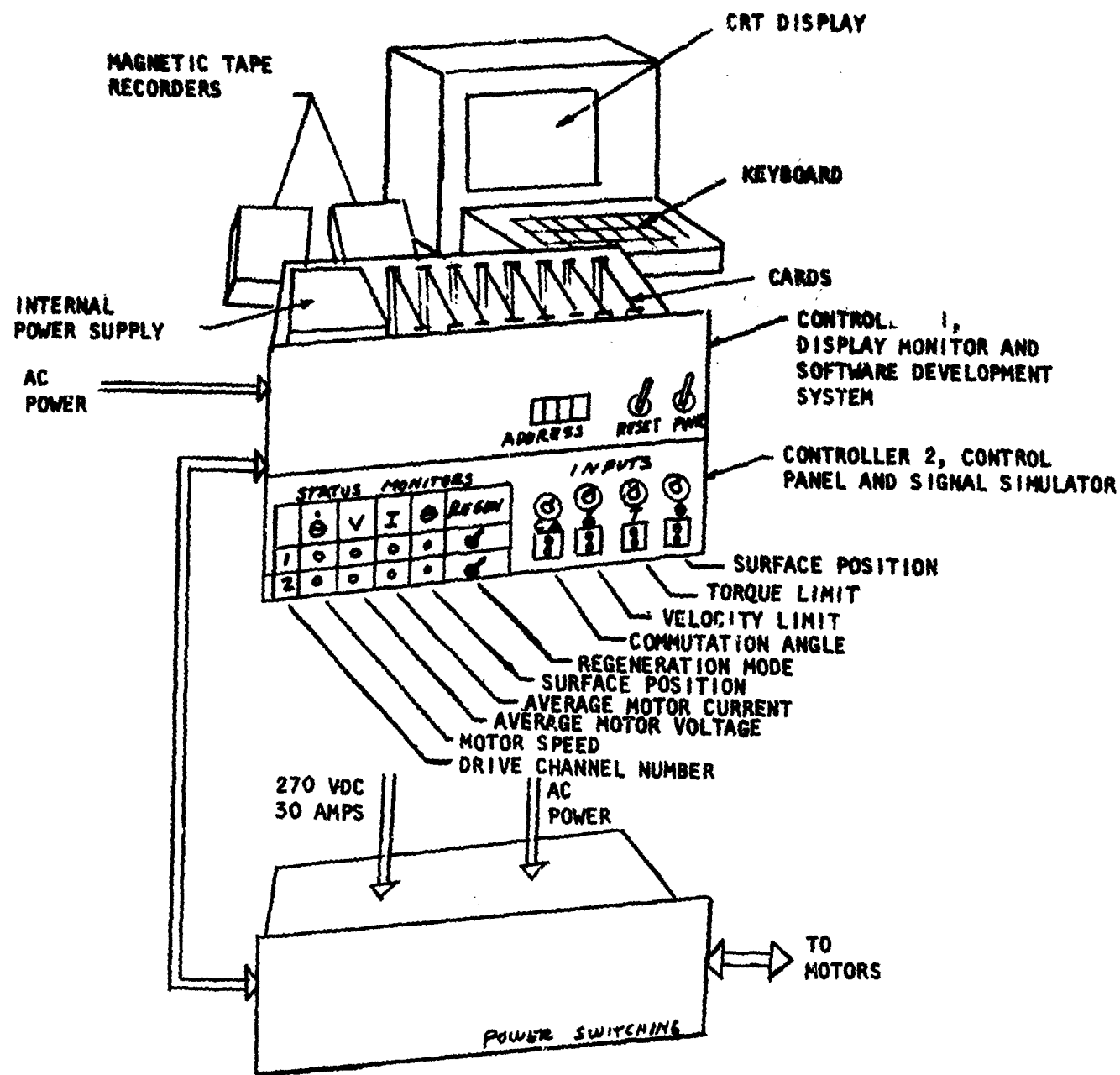
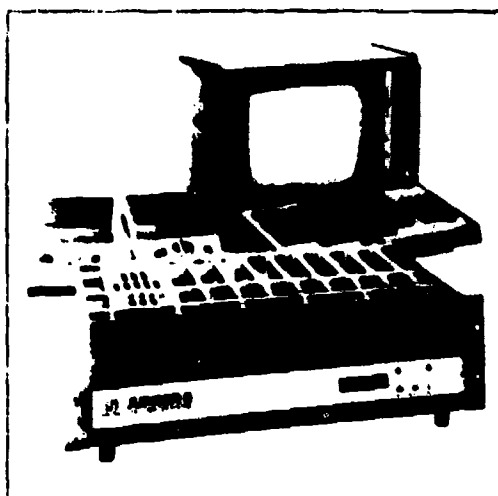


Figure A-13. Sketch of Controller and Power Switching Hardware Components

[illegible]

- The highest quality parts money can buy to insure reliability and value
- Low power Schottky TTL designs for high speed, less heat and longer life.
- CMOS used wherever possible to reduce power requirements
- Extensive LSI use for compactness in size and low power consumption.
- All parts 100% tested for dependability.
- Complete documentation for all functions, parts and design
- Easily adaptable and expandable design.
- The result of 4 years of intensive research, engineering

- **Direct Priority Device** vectoring for fast real-time response.
- **Priority Chained Direct Memory Access.**
- **Single cycle DMA Request** for minimum CPU interference.
- **Block DMA Request** for maximum throughput (1 MB/s).
- **Hardware Dynamic Memory refresh** output.
- **9-module capability** per module cage.

- 2KB standard system monitor in ROM for higher capability without killing the system.
- 3KB ROM monitor module capability for future expansion.
- No wasted user space with 128 byte write protected monitor RAM
- Full terminal control of all programs with a Single Instruction Execute.
- Fingertip debugging with Read or Write Address Breakpoint

- Addressing to 64KB for expansion ease
 - 7 addressing modes for fast memory access
 - 72 variable length instructions for efficient memory use
 - Stack processing instructions for temporary storage
 - 2 microsecond instruction time for ultra-speed execution
3. **Universal Bus**
- Universal bus structure for easy I/O or memory expansion
 - Asynchronous data transfers for high speed expansion
 - Simple design for ultimate interfacing efficiency
 - 7 vectored interrupt levels for easy I/O control

- Dual rack-mount or tabletop module cage that eliminates one-way options
- Easily expanded hot-on cage
- Quiet, fanless convection cooling
- No wiring required with etched PC backplane motherboard
- Short-proof pin/socket buss connectors
- Gold plated headers/sockets for the best connection
- Easy-to-maintain Plug-in Modules
- Card Ejector Retainer for simplicity in removal and installation

Figure A-14. Wave Mate Specification Sheets

240

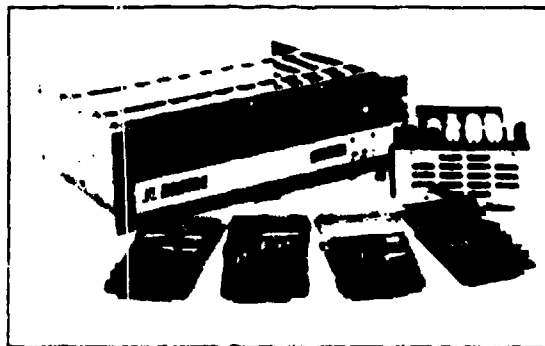
- Low Mean Time To Repair with sockets for every IC and more reliability as well as more flexibility
- Easy connections with on-card flat cable connectors.
- No more broken wires with Strain-Relieved I/O cable connectors.
- All cables furnished for your convenience.

MODULE PACKAGING

- Reduced engineering time, easy custom interfaces with universal wire wrap cards.
- Compact (4-1/2 x 7") card size for modular designs and short interconnections.
- On-card IC power regulator for reduced system noise.
- Large heat sinks for regulators that give cool, high power output.
- Up to 4 voltages available for each socket (± 5 , ± 12) for freedom of design.
- Can accommodate any IC from 8 to 40 pins.
- Room for up to 32 18-pin IC's on each module for tremendous functional capability.
- Low noise, efficient high-frequency bypassing.
- High efficiency tantalum low-frequency bypassing.
- Noise-reducing ground-clip construction.
- Ground Plane on each card for total noise reduction.
- Etched power busses for noise elimination.

POWER SUPPLY

- Easily tested, maintained Modular Plug-In power supply.
- AC line filter for low line interference.
- 5 voltage outputs for adaptability to many logic forms.
- Ferro-Resonant preregulator for reliable power with less regulator heat.
- Safe, detachable AC line plug.



KIT FEATURES

- Economy and learning value.
- Quality hand wrapping and unwrapping tools included.
- All wire supplied, precut, pre-stripped and color coded.
- All cables furnished, preassembled and fully tested.
- All IC's included: processed and tested so your kit works the very first time.
- Simple X/Y coordinate, sorted, level wiring.
- All tools provided except soldering iron and wire cutters.
- Readable, precise assembly manual with lots of illustrations so nothing is guesswork.

8KB DYNAMIC MEMORY

- 8KB on one module. High system utilization.
- Low power, high speed dynamic operation.
- Flexible addressing selection.
- Write Protect Jumpers for system development.
- Fully buffered with low fan-in requirements.

RS-232-C SERIAL INTERFACE

- Stable crystal controlled frequency that needs no adjustment.
- 16-selectable baud rates for flexibility.
- Easily handled 15-ft. cable to standard 25-pin connector.
- Request To Send/Clear To Send mode for system flexibility.

FRONT PANEL MODULE

- Smoke-tinted plexiglass panel for beauty, durability.
- 4 hex digits of address display that's easy to read.
- Hardware single-instruction step for diagnosis aid.
- System reset button.
- Monitor Interrupt Switch to control errant programs.
- Plugs into CPU module saving buss space.
- Clean, efficient, no-gadget design for economy, simplicity.

DOCUMENTATION

- Trouble-shooting manual for each module.
- Chain wire list, alphabetically sorted for easy debugging.
- Cross-reference list that's alphabetically sorted.
- Complete parts list.
- Full assembly illustrations.
- Detailed logic diagrams.
- Operational theory manual for each module.
- Examples for programming and operation.
- Interface design manual.
- Motorola programming handbook.
- Motorola M6800 Hardware handbook.
- Textbook on "BASIC".
- Text-Editor operation instructions.
- System monitor manual.

Figure A-14. Continued

F-28000

EPROM (2708 type) programmer card for quick program changes.
 2K static RAM cards with dual read ports giving constant access to refresh
 1024 character TV terminal for low-cost video display.*
 Writable character set.*
 ASCII keyboard interface.*
 Light pen for fast information exchange.*
 Dual read/write audio cassette interface with motor controls.*
 32-line parallel I/O interface card.
 16-line parallel I/O interface card.
 Buss extender card.
 Dual floppy disk controller interface.*
 RS232-C serial data interface.
 Dual RS232-C interface (on single card).
 8K dynamic RAM memory module.
 System parity checking memory card.*
 Modern module.*
 Low-cost hex terminal.*
 Custom interface support capability.
 Memory map card.*
 Driver software on all supplied devices.

*Soon to be available.

SOFTWARE - MONITOR

2KB (ROM) monitor with expandable RAM for more functions.
 Interrupt Driven I/O for high speed systems.
 Requires no user-RAM space.
 Sets Read or Write breakpoint in user program.
 Search Under Mask that also helps in debugging.
 Access to all user registers and status.
 Reads bootstrap binaries.
 Writes bootstrap binaries.

- Changes memory.
- Tests programs for illegal instructions - a great debugging aid.
- Trace programs for problem locating.
- Display programs in opcode format.
- Display text in ASCII format.
- Display data in single or dual byte hexadecimal.
- System calls are handled by monitor.
- Services I/O requests for programs.

SOFTWARE - ASSEMBLER

- Motorola® compatible assembler.
- 2 passes.
- Extra extensions to standard Motorola® assembler.
- Only needs an 8KB system to RUN (includes all symbol space).

SOFTWARE - EDITOR

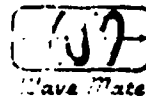
- Powerful "big machine" type text editor.
- Easy handling of single character editing.
- Fast text string editing.
- 1-line programming of commands with conditional branches for complex editing.
- Only requires an 8KB system to RUN (includes 1-page buffer).

SOFTWARE - BASIC

- Easiest-to-learn high level language.
- Space-saving deletable compiler at runtime.
- String handling capability.
- Random number generation.

USER GROUP

- Software exchange.
- Exchange of ideas.
- Newsletter formulation.



WAVE MATE 1015 WEST 190TH STREET/GARDENA, CALIFORNIA 90248/(213) 329-8941

F-28001

Figure A-14. Continued

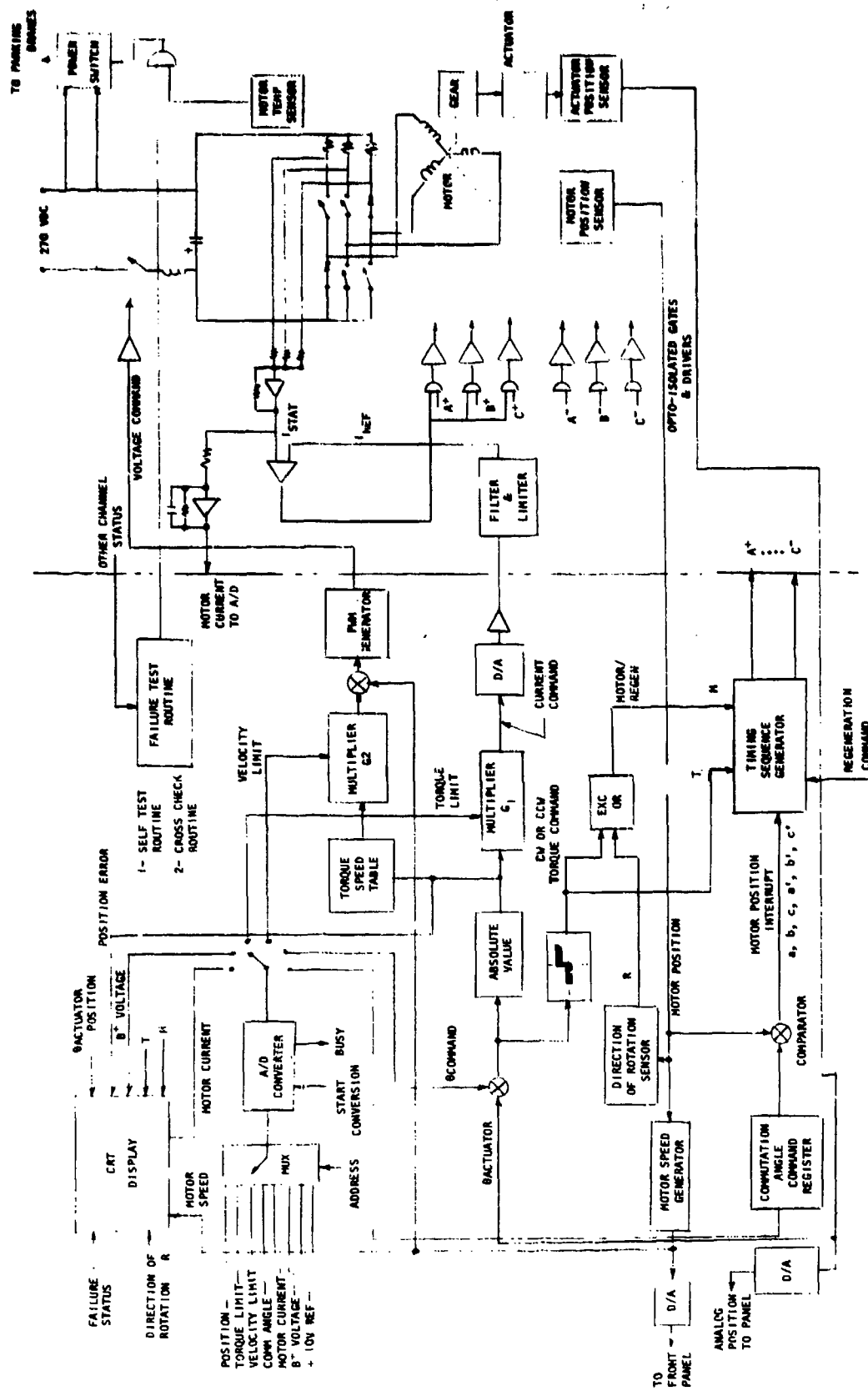


Figure A-15. Motor Controller Signal Gen, Display & Controller Block Diagram

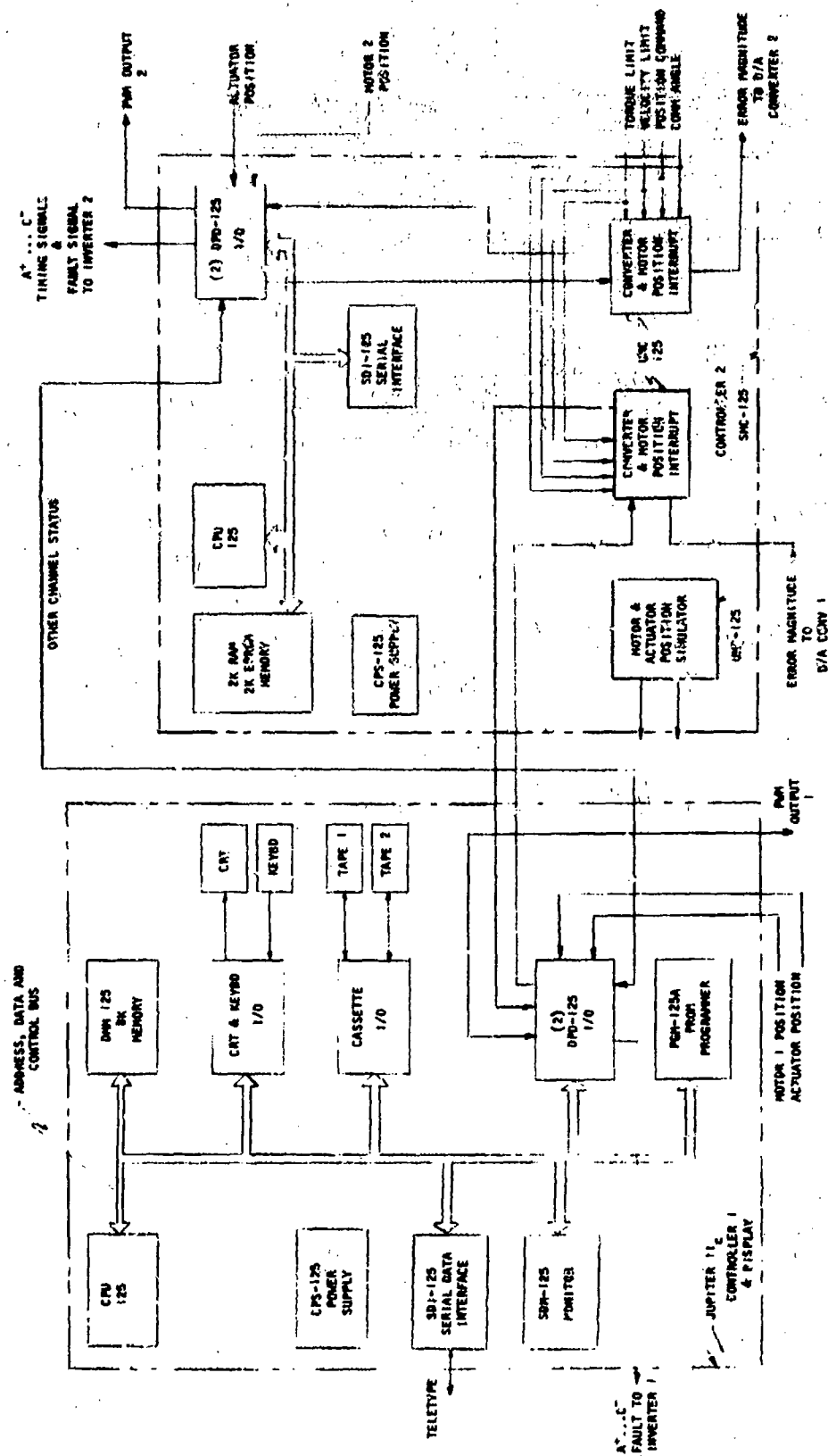


Figure A-16. Functional Block Diagram Motor Controller (1 Channel Only)

TORQUE SPEED CHARACTERIZATION

Some of the torque speed curves which are implemented are shown in Figure A-17. Program control will allow the selection of Curves 1, 2, or 3. The velocity limit and torque limit controls on the front panel will enable gain modification of the torque speed curves.

The torque of the brushless dc motor is proportional to the armature current and the speed is proportional to the voltage. The control system forces the motor current to be proportional to the position error and adjust the motor voltage (through the PWM generator) by using the data from the torque-speed table to obtain Curves 1, 2, or 3.

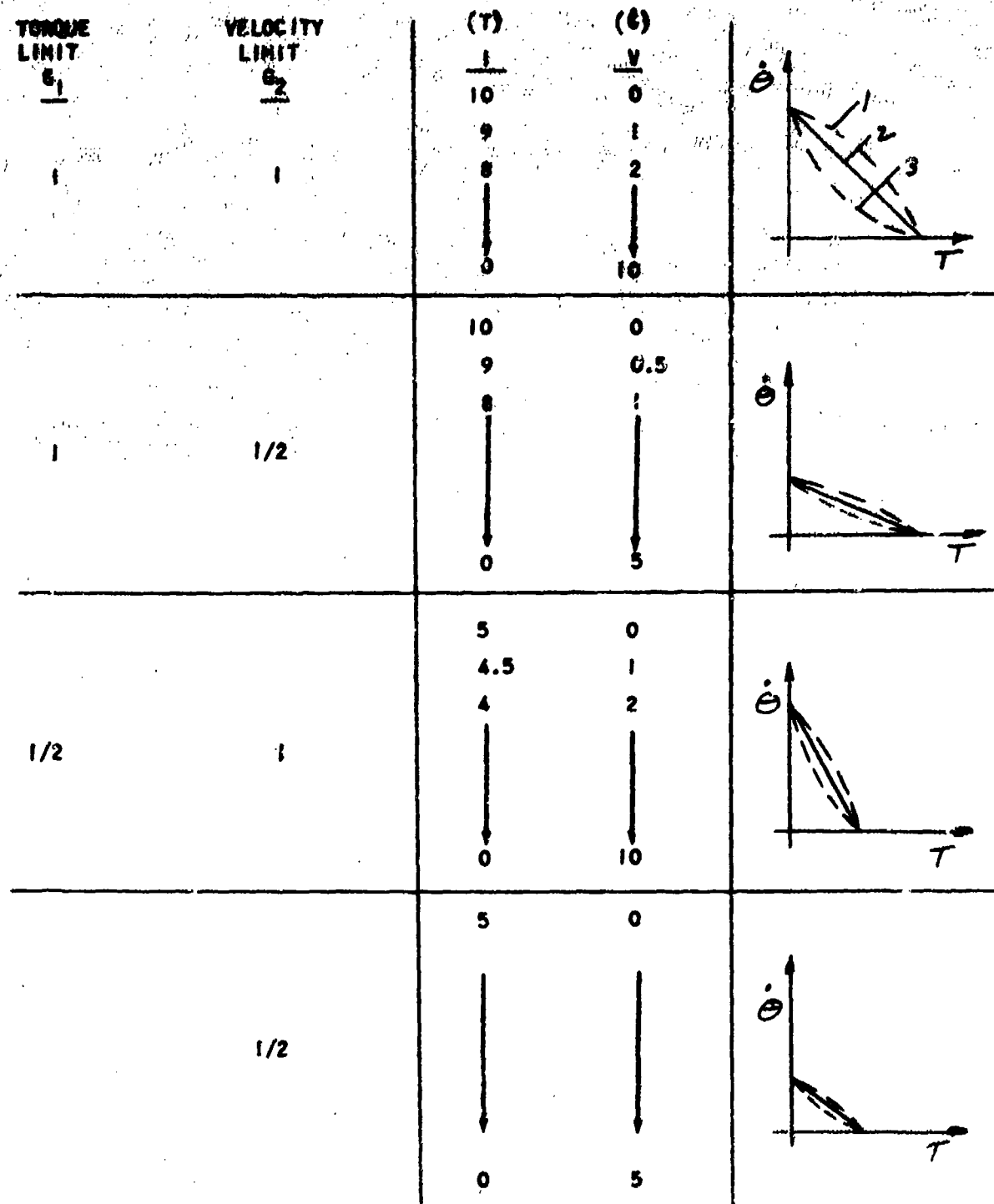


Figure A-17. Torque Speed Curves

COMMUTATION ANGLE CONTROL

The controller will be capable of adjusting the commutation angle to demonstrate capability and versatility, and to evaluate the importance of a controller commutation angle. The implementation of commutation angle control is shown in Figure A-18.

The commutation angle control allows the imaginary brush axis of the brushless dc motor to be shifted $\pm \alpha$ degrees from the null position. The null position occurs when the axis of the magnetic field established by the stator current is displayed 90° from the axis of the air gap flux field.

Prior to activating the system, the commutation angle command register is set to α . When the motor position corresponds to α , an interrupt signal is generated to initiate the timing sequence. The next interrupt is generated when the motor position corresponds to $\alpha + 60$ degrees. The interrupt cycle continues and the commutation angle register is cleared to α at 360 degrees.

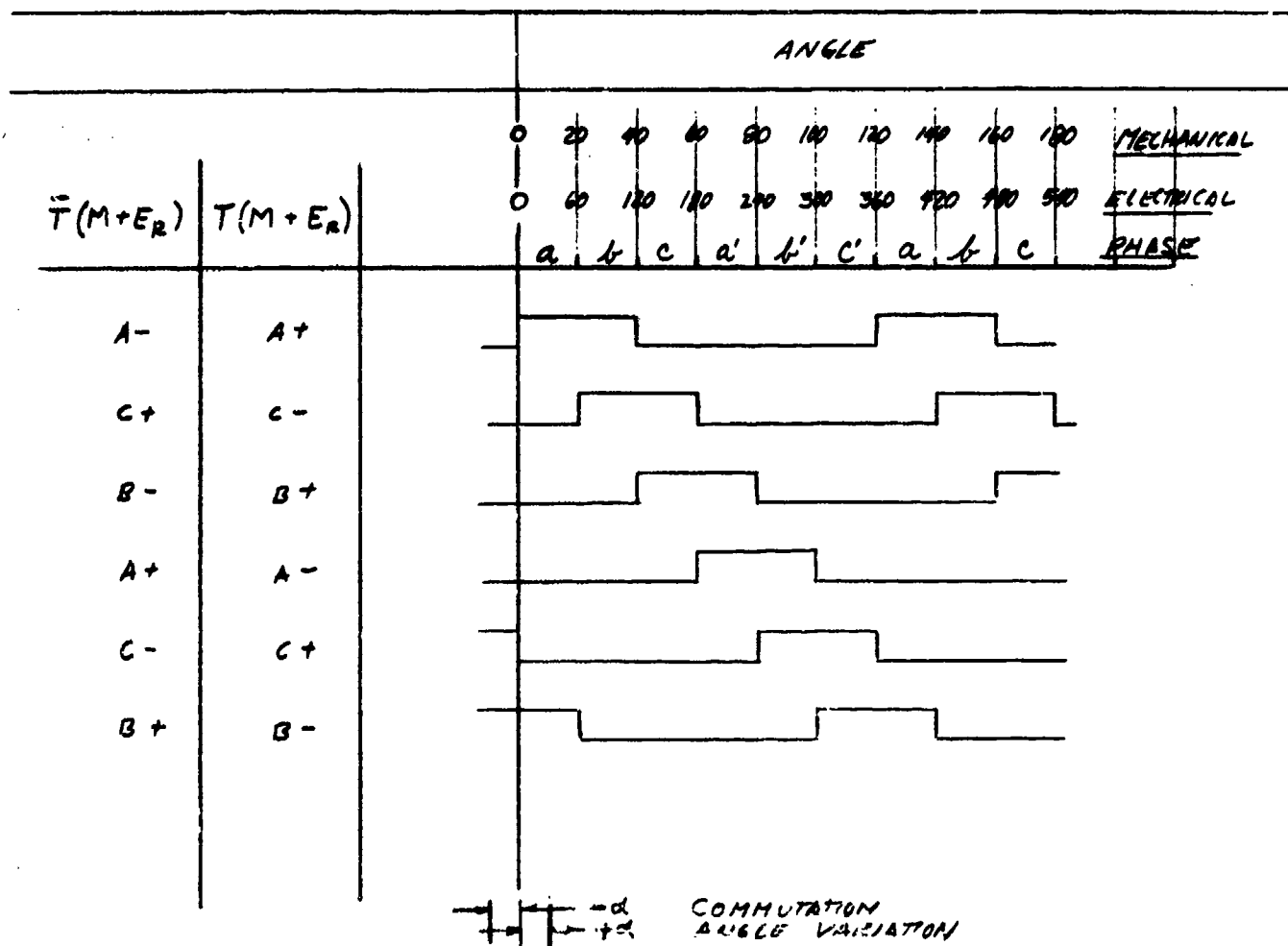


Figure A-18. Commutation Angle Wave Forms

THE CURRENT LIMIT APPROACH

The technique for current limiting is shown in Figure A-19. Definition of the terms used on the figure include the following.

I_{STATOR} is the instantaneous stator current

I_{REF} is the reference current derived from the position error signal

I_{LIMIT} is the max value of the reference current

I_{LINE} is the line current

I_{STATOR} is compared with I_{REF} . When I_{STATOR} exceeds I_{REF} , the line current I_{LINE} is turned off. Since I_{LIMIT} is the maximum value of the reference current, the maximum value of the stator current is established by I_{LIMIT} .

Current limit will be programmed as a function of output speed, and also as a function of time, as specified by paragraph 3.3.1.2.1 of the performance Specification, 76-12942 Rev. 1.

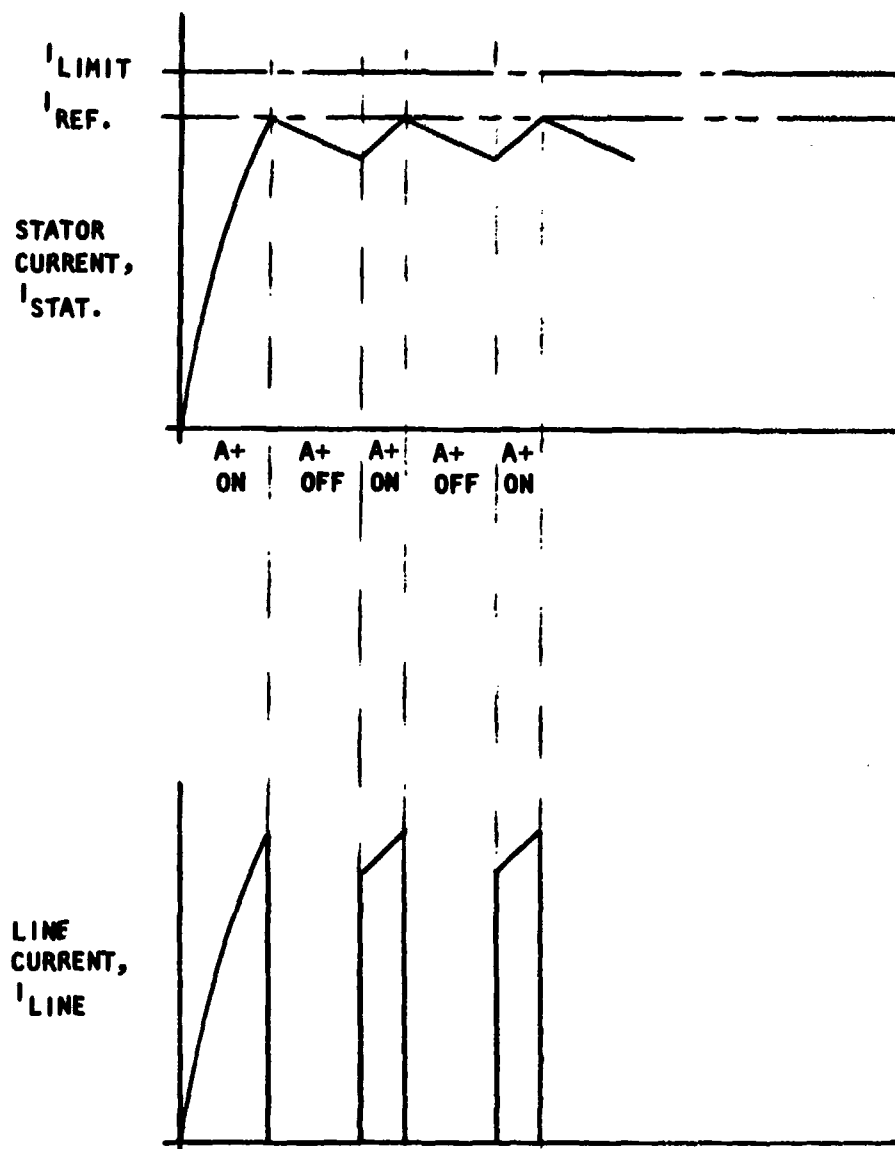


Figure A-19. Current Wave Forms

REGENERATION

The regenerative mode occurs when the motor revolves in the opposite direction to the commanded torque. The logic equations which control the switch are:

$$A+ = [(a' + b') \bar{T} + (a + b) T] M$$

$$B- = (M + E_r) [(a + b) \bar{T} + (a' + b') T],$$

$$B+ = [(a + c') \bar{T} + (a' + c) T] M$$

$$B- = (M + E_r) [(a' + c) \bar{T} + (a + c') T]$$

$$C+ = [(b + c) \bar{T} + (b' + c') T] M$$

$$C- = (M + E_r) [(b' + c') \bar{T} + (b + c) T]$$

and the regenerative condition is implemented when $M = \text{false}$ and $E_r = \text{true}$.

TRANSISTOR POWER SWITCHING

A candidate transistor power switching circuit to be investigated is shown in Figure A-20. The circuit consists of optical coupled isolators, darlington transistors, and forward and reverse base current drive features. Cost trade-off, circuit efficiency, switching speed, and power transistor gain characteristics will continue to be studied.

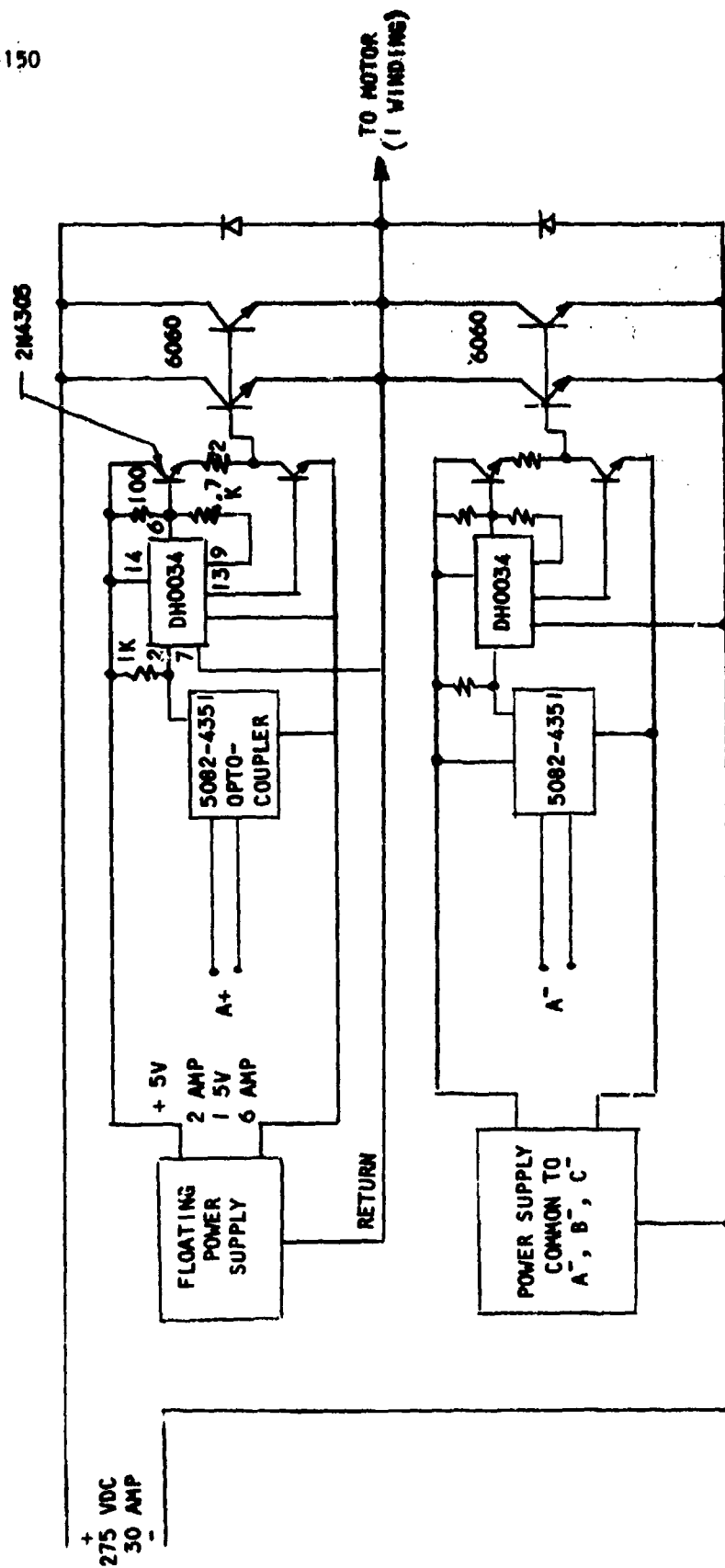


Figure A-20. Transistor Power Switches

CONTROLLER LOGIC AND FLOW

Controller logic diagram is shown in Figure A-21, and the functional logic flow diagram in Figure A-22. Data Sets 1 and 2 are stored in memory. When the motor position interrupt command occurs, the position code is first read. The torque and motor or regenerate commands are next examined. Data from memory location 1 or 2 is then moved to the timing sequence generator.

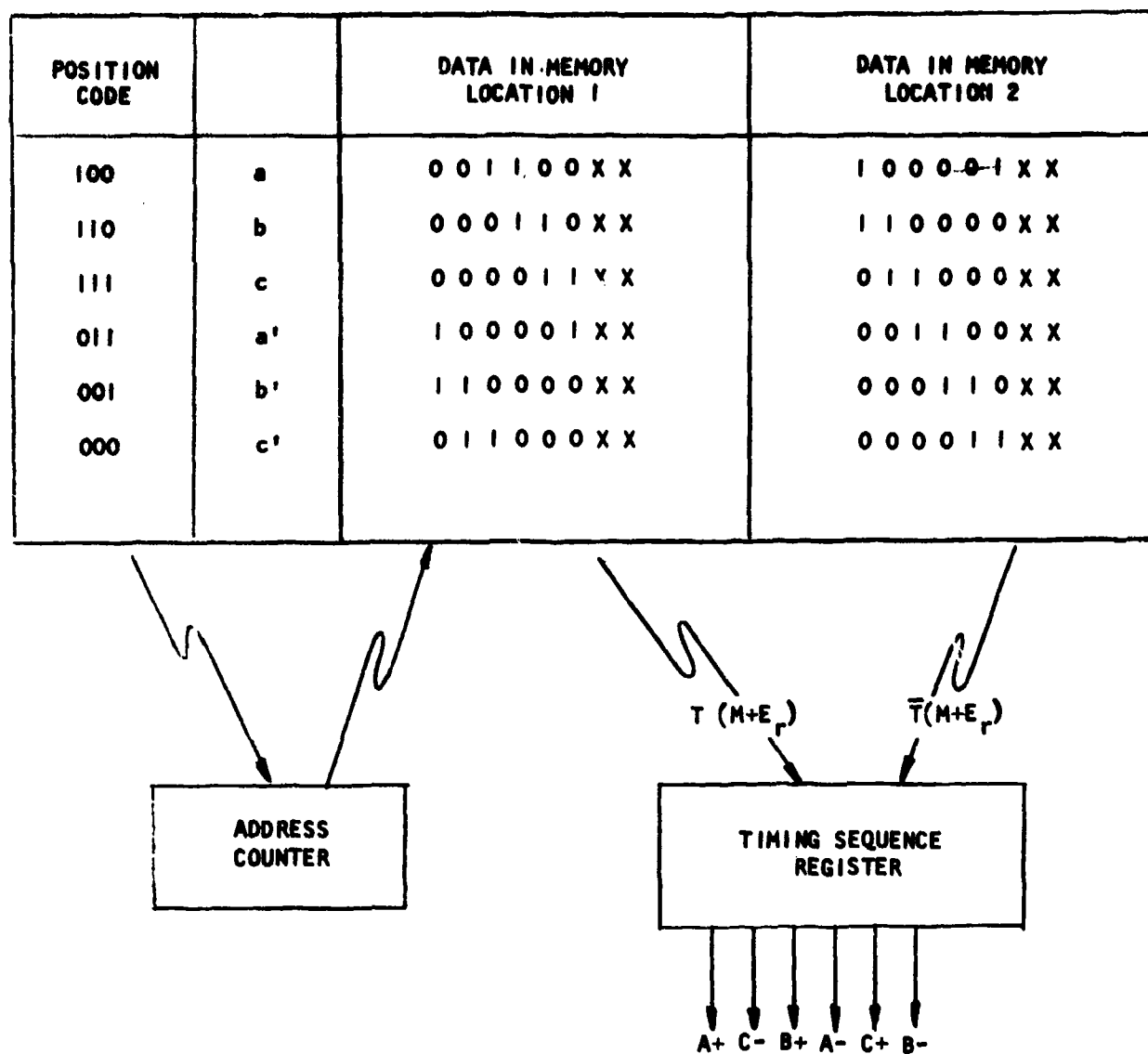


Figure A-21. Controller Logic

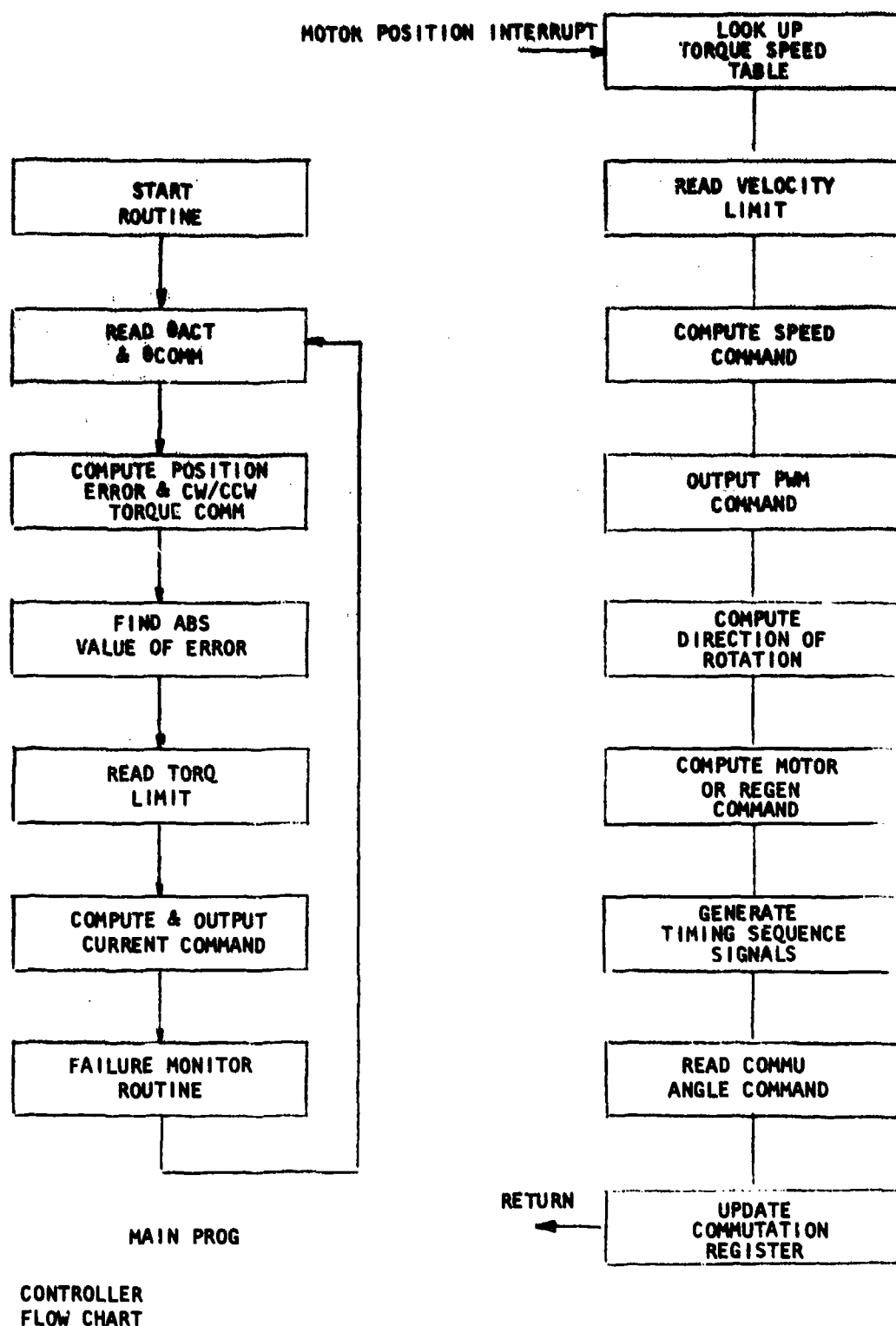


Figure A-22. Controller Flow Chart

REDUNDANCY MANAGEMENT

Redundancy management will consist mainly of differential braking command coordination. The status of the other channel will be continuously monitored. If the other channel is braking, self-braking is inhibited.

Self test will consist of internal power supply and position error monitors. Both B+ (for the logic circuits) and the dc reference will be monitored. If the voltage levels are not within the allowable tolerances, self braking commands will be initiated. The position error will be checked when the velocity is zero. Self braking commands will also be initiated if the position error exceeds the allowable tolerance.

ACTUATOR

The actuator cross section is shown in Drawing No. 2022192. This section presents the detailed weight analysis of the actuator, the stress analysis of the structure, and includes the effect of fatigue life. Detailed stress analysis of the gears has been presented earlier in this document.

Weight Calculation

Detailed analyses of the actuator and motor weight are presented in Table A-8. A summary of total actuator system weight is shown below:

Actuator		12.7
Motor, including parking brake and rotor position transducer	2 X 9.65	19.3
Control surface position transducer	2 X 1.4	2.8
TOTAL		34.8

Actuator Stress Considerations

A stress analysis was prepared of three significant areas, output ring gear back iron, mounting lugs and the input shaft torsional shear stress. This analysis is included in the pages which follow:

The conservative ring gear back iron stress of 46,782 psi could easily be increased to around 65,000 psi and not affect the actuator fatigue life. This will be studied as a weight reduction item prior to detail drawing release.

The mounting lugs originally were designed with a web thickness of 0.10 inches. However, as this analysis shows, the web thickness had to be increased to 0.16 inches to maintain a positive margin of safety at ultimate load. The input shaft shear stress level is quite adequate with a 0.060 wall.

The details of the stress calculations are presented in Table A-9.

TABLE A-8
WEIGHT CALCULATION SHEET

FORM #128

TABLE A-8
WEIGHT CALCULATION SHEET

DRAWING NO.	DESCRIPTION	MAT'L	CAGE	NO. REQ	CALCULATIONS	WEIGHT	STMT. 6	
①	SHAFT	572		1	$(\pi \times 3.32 \times 5.60) \times (572 \times 3.14159) \times (36 \times 10^{-6} \times 0.4 \times 0.5)$ $\times (1.67 \times 10^3) \times (0.062 \times 10^3) \times (1.08 \times 10^3) \times (2.83)$.14		
②	CARRIER			1	$(\pi \times 3.64 \times 3.12) \times (572 \times 3.14159) \times (36 \times 10^{-6} \times 0.4 \times 0.5)$ $\times (1.67 \times 10^3) \times (0.062 \times 10^3) \times (1.08 \times 10^3) \times (2.83)$			
③	CARRIER			2	$(\pi \times 3.64 \times 3.12) \times (572 \times 3.14159) \times (36 \times 10^{-6} \times 0.4 \times 0.5)$ $\times (1.67 \times 10^3) \times (0.062 \times 10^3) \times (1.08 \times 10^3) \times (2.83)$.28		
④	CARRIER - END			1	$(\pi \times 3.64 \times 3.12) \times (572 \times 3.14159) \times (36 \times 10^{-6} \times 0.4 \times 0.5)$ $\times (1.67 \times 10^3) \times (0.062 \times 10^3) \times (1.08 \times 10^3) \times (2.83)$.17		
⑤	PIN			4	$(\pi \times 3.64 \times 3.12) \times (572 \times 3.14159) \times (36 \times 10^{-6} \times 0.4 \times 0.5)$ $\times (1.67 \times 10^3) \times (0.062 \times 10^3) \times (1.08 \times 10^3) \times (2.83)$.35		
⑥	BEAR			13	$(\pi \times 3.64 \times 3.12) \times (572 \times 3.14159) \times (36 \times 10^{-6} \times 0.4 \times 0.5)$ $\times (1.67 \times 10^3) \times (0.062 \times 10^3) \times (1.08 \times 10^3) \times (2.83)$.31		
⑦	BEARING			4	$(\pi \times 3.64 \times 3.12) \times (572 \times 3.14159) \times (36 \times 10^{-6} \times 0.4 \times 0.5)$ $\times (1.67 \times 10^3) \times (0.062 \times 10^3) \times (1.08 \times 10^3) \times (2.83)$.16		
⑧	BEARING - THROUST			5	$(\pi \times 3.64 \times 3.12) \times (572 \times 3.14159) \times (36 \times 10^{-6} \times 0.4 \times 0.5)$ $\times (1.67 \times 10^3) \times (0.062 \times 10^3) \times (1.08 \times 10^3) \times (2.83)$.12		
⑨	SPACER			1	$(\pi \times 3.64 \times 3.12) \times (572 \times 3.14159) \times (36 \times 10^{-6} \times 0.4 \times 0.5)$ $\times (1.67 \times 10^3) \times (0.062 \times 10^3) \times (1.08 \times 10^3) \times (2.83)$.31		
⑩	GEAR			2	$(\pi \times 3.64 \times 3.12) \times (572 \times 3.14159) \times (36 \times 10^{-6} \times 0.4 \times 0.5)$ $\times (1.67 \times 10^3) \times (0.062 \times 10^3) \times (1.08 \times 10^3) \times (2.83)$.30		
⑪	GEAR			3	$(\pi \times 3.64 \times 3.12) \times (572 \times 3.14159) \times (36 \times 10^{-6} \times 0.4 \times 0.5)$ $\times (1.67 \times 10^3) \times (0.062 \times 10^3) \times (1.08 \times 10^3) \times (2.83)$.03		
⑫	SPACER			1	$(\pi \times 3.64 \times 3.12) \times (572 \times 3.14159) \times (36 \times 10^{-6} \times 0.4 \times 0.5)$ $\times (1.67 \times 10^3) \times (0.062 \times 10^3) \times (1.08 \times 10^3) \times (2.83)$.05		
⑬	RING			2	$(\pi \times 3.64 \times 3.12) \times (572 \times 3.14159) \times (36 \times 10^{-6} \times 0.4 \times 0.5)$ $\times (1.67 \times 10^3) \times (0.062 \times 10^3) \times (1.08 \times 10^3) \times (2.83)$.04		
⑭	RING			2	$(\pi \times 3.64 \times 3.12) \times (572 \times 3.14159) \times (36 \times 10^{-6} \times 0.4 \times 0.5)$ $\times (1.67 \times 10^3) \times (0.062 \times 10^3) \times (1.08 \times 10^3) \times (2.83)$.04		
⑮	SHAFT - GEAR			1	$(\pi \times 3.64 \times 3.12) \times (572 \times 3.14159) \times (36 \times 10^{-6} \times 0.4 \times 0.5)$ $\times (1.67 \times 10^3) \times (0.062 \times 10^3) \times (1.08 \times 10^3) \times (2.83)$.27		
⑯	GEAR			12	$(\pi \times 3.64 \times 3.12) \times (572 \times 3.14159) \times (36 \times 10^{-6} \times 0.4 \times 0.5)$ $\times (1.67 \times 10^3) \times (0.062 \times 10^3) \times (1.08 \times 10^3) \times (2.83)$	2.68		
DATE	7-9-76	CUSTOMER	WRIGHT	APPLICATION	TOTAL WEIGHT - DRY			LBS.
PROJ. ENGR.		TITLE	GEARBOX		TOTAL WEIGHT - WET			LBS.
CALC. BY	0. GIERERO				NEXT ASSY.			PAGE 1 OF 2
					CHANGES			DWG. NO. 2022192

**THIS PAGE IS BEST QUALITY PRACTICABLE
FROM COPY FURNISHED TO DDC**

TABLE A-8 (Continued)
WEIGHT CALCULATION SHEET

[illegible]

TABLE A-9
ACTUATOR STRESS CALCULATION

WPAFB FATIGUE LIFE

$$\text{LIFE} = 10^5 \text{ CYCLES}$$

LOAD = LINEAR WITH POSITION
(RUDDER, AILERON, ETC)

$$\text{TRAVEL} = \pm 30^\circ$$

for fatigue life,

$$\text{LOAD}_{\text{equiv}} = \sqrt[6]{\frac{1}{\sum N_i} \sum N_i (\text{LOAD})^6}$$

An actuator gearing, planet (carrier) moves 4.64 rws around output ring when ring is moved 1 rev, so with 6 planets, that gives 27.84 contacts on any given output ring tooth per output ring revolution. Conversely, on planet, each tooth makes 16.24 contacts per output ring revolution.

On each cycle, load is identical and

$$\text{LOAD} = K \phi \text{ where } \phi \text{ is travel}$$

$$\text{so } \sum N (\text{LOAD})^6 = \int (K \phi)^6 d\phi = \frac{1}{7} K^6 \phi^7 \Big|_0^{\phi_{\text{MAX}}}$$

but $K \phi_{\text{MAX}} = \text{design load, so}$

$$\text{LOAD}_{\text{equiv}} = \sqrt[6]{\frac{1}{7} (\text{LOAD}_{\text{peak}})^6} = 72.3 \% \text{ LOAD}_{\text{peak}}$$

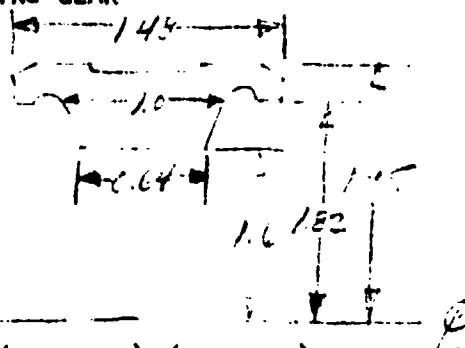
TABLE A-9 (continued)

WPAFB STRESS ANALYSIS (2022192)

Areas of interest:

- 1 Output ring gear
- 2 Mounting lugs
- 3 Input shaft torsional loads

1 OUTPUT RING GEAR



THIS PAGE IS BEST QUALITY PRACTICABLE
FROM COPY FURNISHED TO /DQ

$$\text{Area, } A = \left(\frac{1.6+0.64}{2} \right) (1.82-1.6) + \left(\frac{1.95-1.82}{2} \right) (1.48-0.2)$$

$$= 0.1804 + 0.1664 = 0.3468 \text{ in}^2$$

$$\text{CG Radius, } R_{CG} = \left[0.1804 \times \left(\frac{1.82+1.6}{2} \right) + 0.1664 \times \left(\frac{1.95+1.82}{2} \right) \right] / 0.3468$$

$$= 1.794 \text{ in}$$

$$\text{Thickness (max)} = 1.95 - 1.60 = 0.35 \text{ in}$$

$$\sigma_{\text{equiv}} = \frac{1.4311 \sigma_{\text{MAX}}}{1 - (2.31 \times 10^{-6}) \sigma_{\text{MAX}}}$$

from test data YF-16 LERA
(equivalent fully-reversed stress)

TABLE A-9 (continued)

$$\sigma_{\text{MAX}} = \sigma_{\text{MAX TEST}} \frac{\left(\frac{R_{\text{CG}}}{A}\right)_{\text{Test}}}{\left(\frac{R_{\text{CG}}}{A}\right)_{\text{WPAFB}}} = 3.278 \frac{1.6775 \times 0.4578}{1.794 \times 0.3468}$$

$$\sigma_{\text{MAX}} = 4.046 \text{ PSI/IN-LB TENSILE RELATION}$$

$$\sigma_{\text{MAX}} = \sigma_{\text{MAX TEST}} \frac{\left(\frac{R_{\text{CG}}}{t^2}\right)_{\text{Test}}}{\left(\frac{R_{\text{CG}}}{t^2}\right)_{\text{WPAFB}}} = 3.278 \frac{1.6775 \times 0.291^2}{1.794 \times 0.352^2}$$

$$\sigma_{\text{MAX}} = 2.119 \text{ PSI/IN-LB BENDING RELATION}$$

use $\frac{\sigma_{\text{normal}}}{\sigma_{\text{bending}}} = 0.158$, then combining stresses,

$$\sigma_{\text{MAX}} = (4.046 - 2.119) 0.158 + 2.119 = 2.423 \text{ PSI/IN.-LB}$$

$$\text{then } \sigma_{\text{equiv}} = \frac{1.4311 \times 2.243\tau}{1 - 2.231 \times 10^{-6} \times 2.243\tau} = \frac{3.21\tau}{1 - 5.0 \times 10^{-6} \tau}$$

letting $\sigma_{\text{endurance}} = 65,000 \text{ psi}$, then the value of τ below which there is no damage is

$$\tau = 18387 \text{ lb-in. torque}$$

damage
threshold

and full-load condition is (2 actuator slices)

$$\tau = \tau_{\text{IN}} = 1190 \times 608.7 \times 0.83 = 601,213 \text{ in-oz}$$

$$= 37,576 \text{ in-lb}$$

so, on each slice,

$$\tau_{\text{max}} = 18,788 \text{ lb-in}$$

and from the endurance calcs for a triangular load,

$$\tau_{\text{equiv}} = 0.723 \times \tau_{\text{max}} = 13,584 \text{ lb-in}$$

TABLE A-9 (continued)

using nos. from fatigue load calcs, calculate number of contacts on any given ring gear tooth,

$$N = 10^5 \text{ cycles} \times 60^\circ \text{ travel one-way} \times 2 \text{ ways} \times \frac{1 \text{ rev}}{360^\circ} \times 27.84 \frac{\text{contacts}}{\text{rev}}$$

$$= 9.28 \times 10^5 \text{ contacts}$$

and for life at $\tau_{\text{equiv}} = 13,584 \text{ lb-in.}$

$$\sigma_{\text{equiv}} = \frac{3.21 \times 13,584}{1.5 \times 10^{-6} \times 13,584} = 46,782 \text{ psi}$$

so since $\sigma_{\text{equiv}} < \sigma_{\text{endurance}}$, actuator ring gear has essentially infinite life.

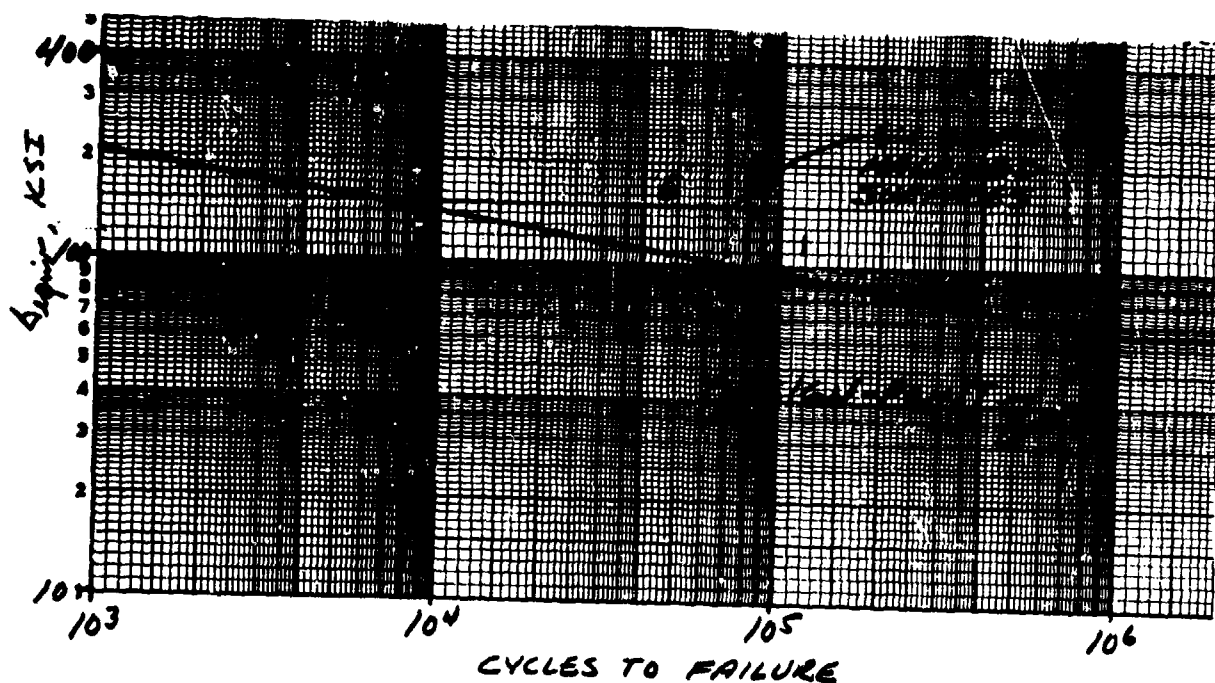
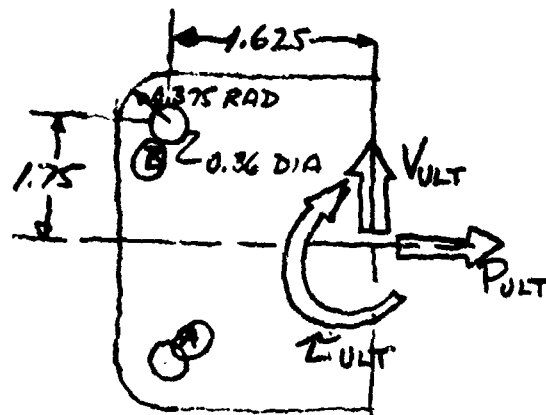


TABLE A-9 (continued)

2 MOUNTING LUGS

Mounting and output lugs are identical relative to actuator \mathcal{C}



$$T_{ULT} = 1.5 T_{MAX} = 28,182 \text{ LB-IN}$$

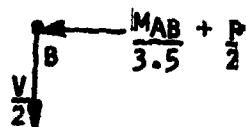
$$V_{ULT} = 1.5 V_{MAX} = 1500 \text{ LB}$$

$$P_{ULT} = 1.5 P_{MAX} = 1500 \text{ LB}$$

lug thickness = 0.32
(0.16 at 2 places)

$$\text{equivalent moment lever arm} = \frac{T}{V} = \frac{28,182}{22500} = 1.25 \text{ in}$$

$$M_{AB} = \left(V \times \frac{T}{V} + 1.625 \right) = 64,745 \text{ lb-in.}$$

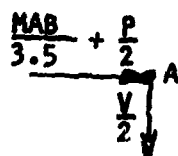


+ at lug B,

$$\text{total force} = \sqrt{\left(\frac{V}{2} \right)^2 + \left(\frac{M_{AB}}{3.5} + \frac{P}{2} \right)^2}$$

$$= \sqrt{(750)^2 + (18,499 + 750)^2}$$

$$= \underline{\underline{19,264 \text{ lbs}}}$$

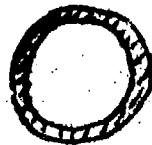


$$\text{in bearing, } \sigma = F/A = 19,264 / 0.36 \times 0.32 = 167,222$$

$$\text{margin of safety} = \frac{174,000}{167,222} - 1 = 4.05\%$$

TABLE A-9 (Continued)

3 INPUT SHAFT TORSION



0.400

0.2810

$$J = \frac{\pi}{32} (D_o^4 - D_i^4) = 1.9098 \times 10^{-3} \text{ in}^4$$

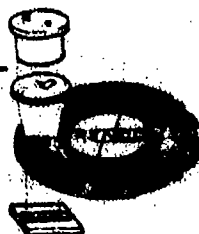
$$\tau_{MAX} = \tau_{INPUT} = 1190 \text{ in-oz}$$

$$\text{SHEAR} = \frac{\tau r_o}{J} = \frac{\frac{1190}{16} \times 0.2}{1.9098 \times 10^{-3}} = 7789 \text{ psi}$$

SURFACE POSITION TRANSDUCER

The actuation system consists of two independent control surface transducers. Each transducer is dedicated to an electromechanical drive channel. Drawing 2022196 shows the outline of the unit. It serves as an additional hinge point for the control surface, and provides the digital information for control surface position.

Data sheets for the unit are presented in Figure A-23. The designated manufacturers part number is 25AE-12GC-7A3-C3. It is manufactured by RENCO Corporation, Goleta, California.



RENCO CORPORATION

SANTA BARBARA BRANCH PARK
 26 COMCHAM DRIVE, P.O. BOX 124
 SANTA BARBARA, CALIF. 93101
 PHONE: (805) 964-1125 FAX: (805) 964-1100

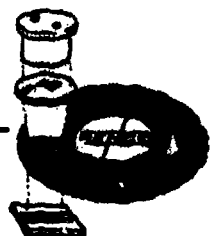
**SPECIFICATION A72365
 ABSOLUTE POSITION ENCODER**

**BASIC
 MODEL NUMBER
 25AE-NB
 25AE-GC**

A72365 PAGE 1 OF 6

REV		DATE		PREPARED BY	<i>[Signature]</i>	DATE	11/2/77
REV	A Eo 2040	DATE	17 DEC 75	CHECKED BY	<i>[Signature]</i>	DATE	11/2/77
REV	A Eo 2040	DATE	11/2/77	APPROVED BY	<i>[Signature]</i>	DATE	"

Figure A-23. Specification A72365

**SPECIFICATIONS****1.0 MECHANICAL**

- | | |
|--|--|
| 1.1 WEIGHT: | 18 OZ. |
| 1.2 TORQUE WITHOUT SHAFT SEAL: | .05 OZ-IN STARTING MAX
.05 OZ-IN RUNNING MAX |
| 1.3 TORQUE WITH SHAFT SEAL: | .9 OZ-IN STARTING MAX
.7 OZ-IN RUNNING MAX |
| 1.4 AXIAL SHAFT LOADING: | 1 LB. |
| 1.5 RADIAL SHAFT LOADING: | .5 LB. APPLIED APPROXIMATELY
1/8" FROM BEARING |
| 1.6 MOMENT OF INERTIA: | 29 GM-CM ² |
| 1.7 MAX SLEW SPEED WITHOUT SHAFT SEAL: | 7500 RPM |
| 1.8 MAX SLEW SPEED WITH SHAFT SEAL: | 500 RPM |
| 1.9 MATERIALS: | COVER - BLACK ANODIZED
ALUMINUM
FRONT HOUSING - IRIDITED
ALUMINUM |

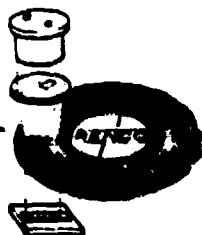
2.0 ELECTRICAL:

- | | |
|-----------------------|--|
| 2.1 SUPPLY VOLTAGE: | 5 VDC ±5% STANDARD
6 VDC ±5% OPTIONAL |
| 2.2 SUPPLY CURRENT: | 400 MA PLUS 10 MA PER CHANNEL |
| 2.3 PULL-UP RESISTOR: | 1KΩ STANDARD
OPEN COLLECTOR OPTIONAL
(NO PULLUP) |

3.0 OUTPUT DATA

- | | |
|----------------|--------------------------------|
| 3.1 RESOLUTION | UP TO 2 ¹³ |
| 3.2 CODE: | NATURAL BINARY OR
GRAY CODE |
| 3.3 ACCURACY: | ± 1/2 BIT |

Figure A-23. Continued



3.3 LOGIC LEVELS:

STANDARD:

LOGIC 1 = VCC

LOGIC 0 = 0 V

OPTIONAL:

LOGIC 1 = 0 V

LOGIC 0 = VCC

3.4 OUTPUT AMPLITUDE: TTL COMPATIBLE

3.5 DIRECTION OF ROTATION TO PRODUCE AN INCREASING COUNT (VIEWING SHAFT END):

3.5.1 COUNTER CLOCKWISE STANDARD

3.5.2 CLOCKWISE OPTIONAL

4.0 ENVIRONMENTAL:

4.1 OPERATING TEMPERATURE: 0°C TO 50°C

4.2 RELATIVE HUMIDITY: 0 TO 80% WITHOUT CONDENSATION

4.3 SHOCK: 50 G'S FOR $\mu \pm 1$ MILLISECOND

4.4 VIBRATION: UP TO 2000 CPS MAX

4.5 SAND, DUST AND OIL: NON-DETRIMENTAL WITH SHAFT SEAL

Figure A-23. Continued

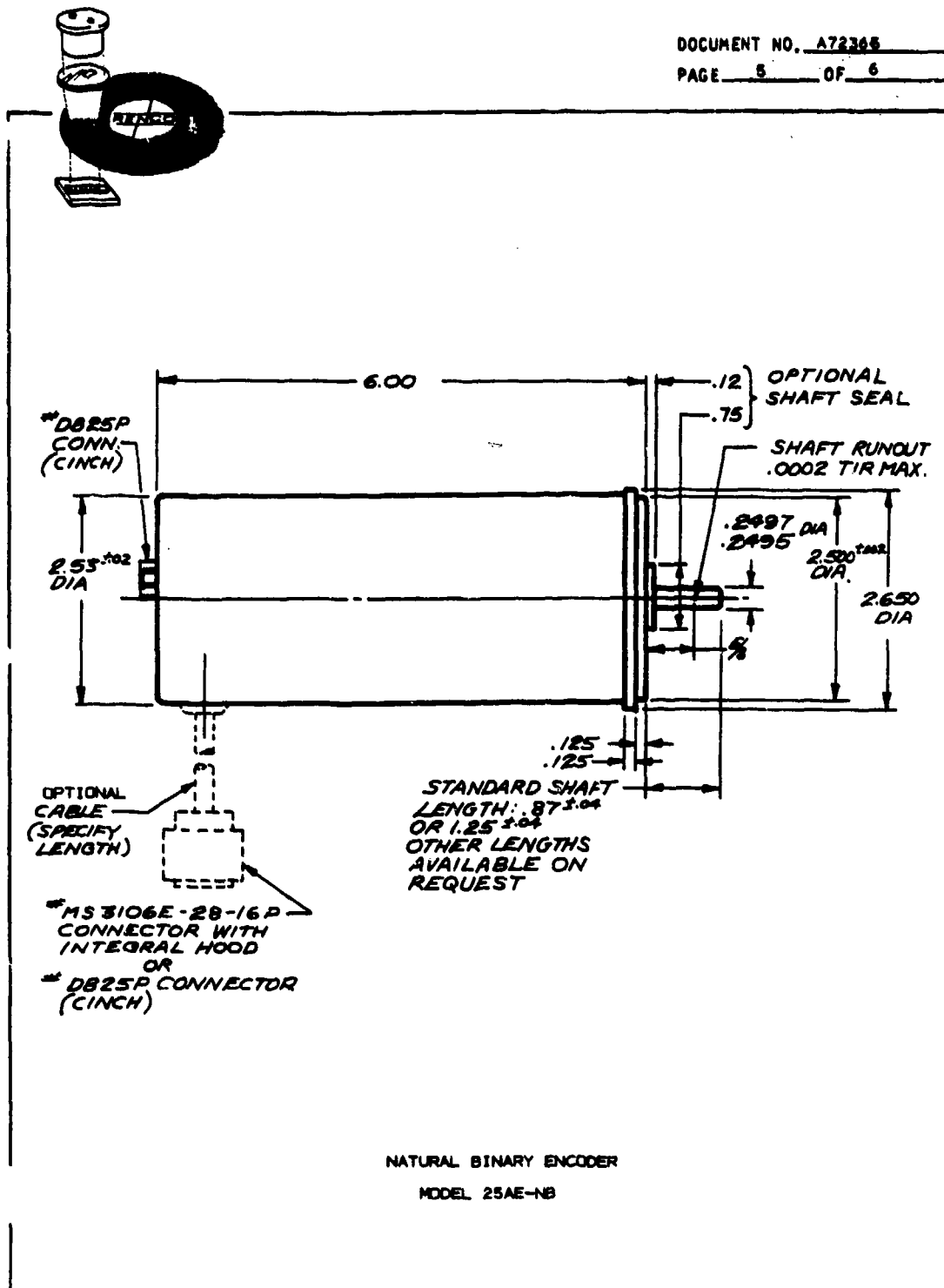


Figure A-23. Continued

DOCUMENT NO. A72365

PAGE 6 OF 6

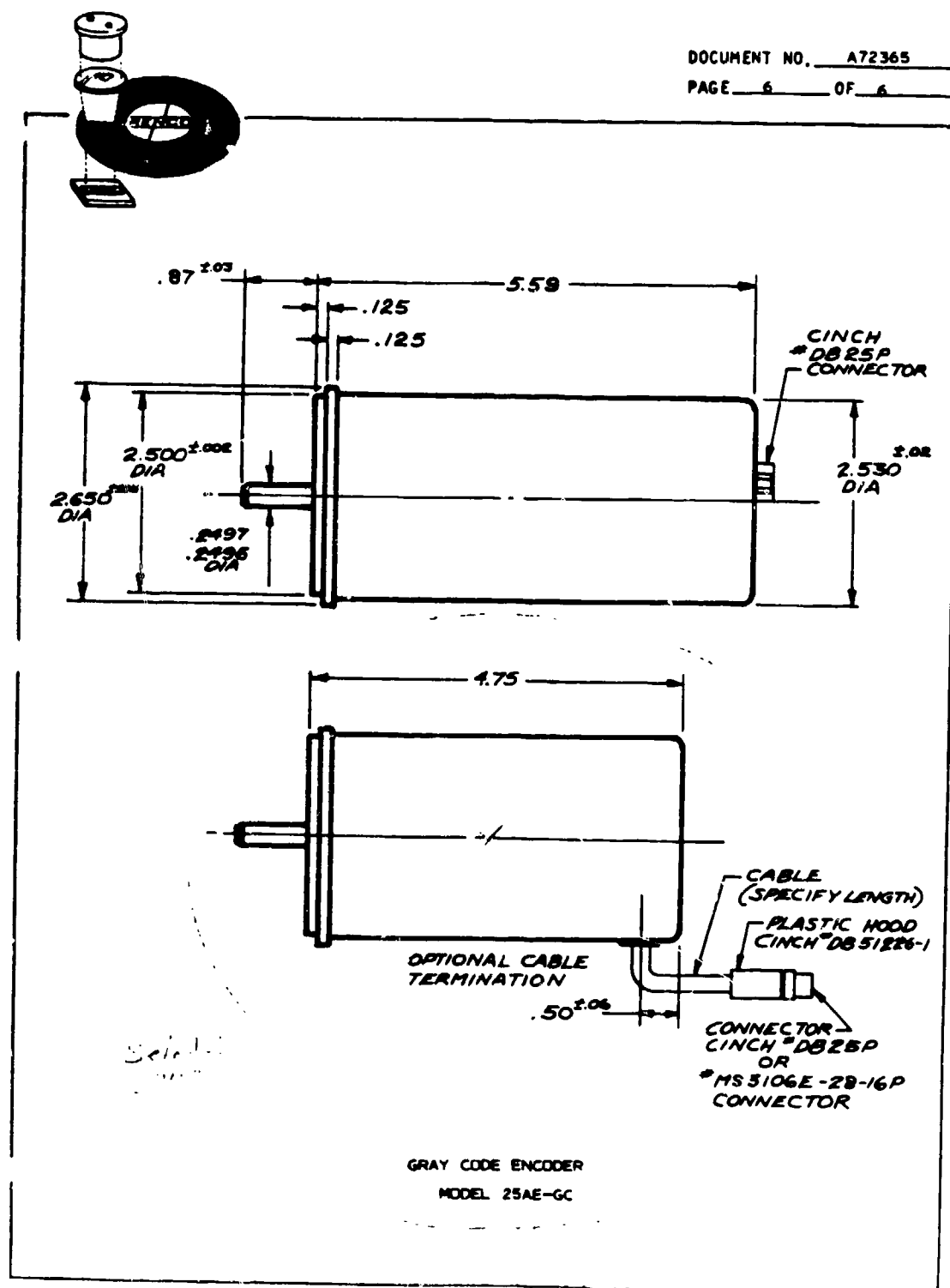


Figure A-23. Continued

MOTOR

Weight

Detailed weight calculations for the motor and brake assembly are presented in Table A-10. The cross section drawing for the assembly is shown in Drawing No. P515018.

Performance

Figure A-24 shows the torque speed curve for the motor resulting from this design.

The motor is a brushless dc samarium-cobalt permanent magnet configuration. In order to meet the system load, rate and acceleration requirements in an optimum design, a number of versions were evaluated in a computer performance program.

The main design criteria considered were, (1) low inertia, (2) acceptable sub-transient reactance, (3) thermal acceptability in the load, duty and environment specified.

The low inertia was achieved by designing for a minimum rotor diameter consistent with an acceptable length to diameter ratio and magnet geometry. The rotor is constructed with the magnets in a tangential orientation with the flux collected in the pole pieces and directed into the air gap. This geometry permits optimum utilization of the samarium-cobalt magnet material.

The sub-transient reactance of the motor was limited to 0.3 per unit in the design. This reactance relates to the electrical time constant of the motor and has a second order effect on the commutation of the unit. It represents a compromise between the motor size and the electrical time constant. The motor parameters varied to achieve this limit within the previously described inertia constraint were the number of stator slots and stator slot geometry.

The computer program calculated the losses for the selected motor configuration. A thermal model of one motor and half the actuator was made. The predicted temperature levels are compatible with the insulation materials used in the motor and the copper and magnet temperature assumed in the computer design.

TABLE A-10 WEIGHT CALCULATION SHEET							
DRAWING NO.	DESCRIPTION	MAT'L	QAGE	NO. REQ	CALCULATIONS	WEIGHT	STATUS
1	ROTOR ASSEMBLY			1			
	SHAFT 1 NUT	17-7 PH		1	$(.002178) \times (.126132) = (.000274) \times (.190232) = (.000052)$		
					$(.000052) \times (.126132) = (.000007)$		
					$(.000007) \times (.190232) = (.000001)$		
					$(.000001) \times (.126132) = (.000000)$.57	
	MAGNET	TAMARIN COBALT		6	$(.000007) \times (.190232) = (.000001)$.49	
	POLE	STL		6	$(.000007) \times (.190232) = (.000001)$.35	
	RETAINER	BERYLUM COPPER		1	$(.000007) \times (.190232) = (.000001)$.05	
	SLEEVE			1	$(.000007) \times (.190232) = (.000001)$.04	
2	STATOR ASSEMBLY						
	INDUCTIONS	STL		AR	$(.000007) \times (.190232) = (.000001)$	2.57	
	WINDING	COPPER		AR	$(.000007) \times (.190232) = (.000001)$.87	
3	DISC	ALUM		1	$(.000007) \times (.190232) = (.000001)$		
					$(.000007) \times (.190232) = (.000001)$.05	
4	ARMATURE	STL		1	$(.000007) \times (.190232) = (.000001)$.35	
5	SPRING	"		1	$(.000007) \times (.190232) = (.000001)$.05	
6	SPACER	"		1	$(.000007) \times (.190232) = (.000001)$.71	
7	BEARING	"		2	$(.000007) \times (.190232) = (.000001)$.12	
8	RETAINER	"		1	$(.000007) \times (.190232) = (.000001)$.32	
9	CARRIER	CAS		1	$(.000007) \times (.190232) = (.000001)$.33	
10	COMBUSTOR	ALUM		1	$(.000007) \times (.190232) = (.000001)$		
					$(.000007) \times (.190232) = (.000001)$.03	
11	CARRIER (SECONDARY)	ALUM		1	$(.000007) \times (.190232) = (.000001)$.07	
12	ROTOR POSITION SENSOR	"		1	$(.000007) \times (.190232) = (.000001)$.04	
DATE	7-14-76	CUSTOMER WEIGHT	APPLICATION	TOTAL WEIGHT - DRY			LBS.
PROJ. ENGR.		PATERSON	BY WIRE	TOTAL WEIGHT - WET			LBS.
CALC. BY	C. GUERRERO	TITLE	APPROX. BRUSHLESS P.C.	NEXT ASSY.			PAGE 1 OF 2
				CHANGES			DWG. NO. 515018-1-1

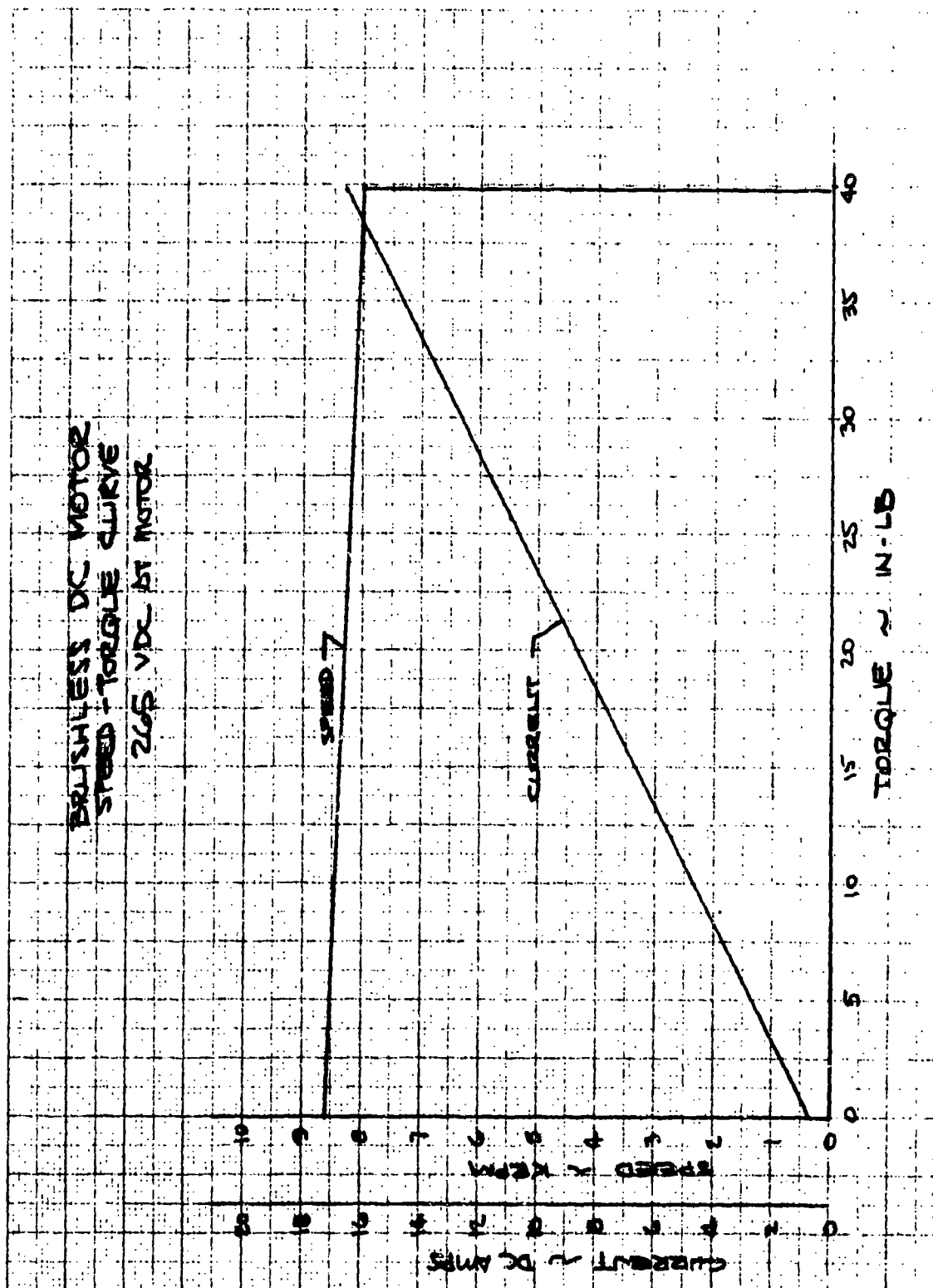


Figure A-24. Motor Performance

Motor Electromagnetic Design

The studies of this motor were conducted using BIGMAG, a Garrett Corporation computer program. Print out for the motor is shown in Figure A-25. A definition of all input and output words is not presented, but any information, definitions, or clarifications are available on request. Most of the words have been selected to be either mnemonic, literal, or a symbol standard in electrical machine design practice so that anyone with background in electrical machinery and an understanding of the proposed PM concept can comprehend the data.

The BIGMAG program iteratively solves the magnetic circuit represented in elemental form by the schematic of Figure A-26. The circuit depicts $F_{C1}/2$, the intrinsic coercive mmf of a half-length magnet (as the full length excites two poles and this representation is on a per-pole basis) establishing magnet flux, Φ_{IM} . The drop in mmf caused by loading the magnet is $F_{MAG}/2$. Portions of Φ_{IM} stray into complex leakage paths represented as lumped permeances in the schematic so that net useful flux Φ_{I3} (contributed by one magnet to the total flux per pole Φ_{IPL}) results. It flows through the effective air gap, non-linear reluctances of the teeth and core (defined by various iron B-H data tables in storage and the geometry), and finally through the armature reaction mmf defined by load current and power factor for which a solution is sought.

Because empirical methods of estimating tooth drop fail at the high saturation densities required in high performance machines, a precise method that accounts for the varying tooth density due to tapered tooth shape and the flux diverted into the slots is used.

The scheme for solution and geometry definition is as follows:

- (a) Guess pass--An arbitrary number of stator conductors and an arbitrary stack length define an armature reaction and a flux required to obtain the specified motor performance.
- (b) Stack length is iterated until the magnetic solution is obtained or until it is determined that armature reaction is excessive for the specified magnet, in which case stator conductors are reduced and a solution is obtained from an updated guess pass.
- (c) Stator reactance is tested against required value and conductors are adjusted toward this goal, but compatible with the magnet.
- (c) Stack length is iterated until solution is obtained.
- (e) Convergence to desired (or compatible, if desired value is forbidden by magnet) reactance at specified load freezes stack length and conductors; no-load volts, short circuit current, and stability are calculated.

AFFDL-TR-78-150

***** MPFB ADC MOTOR *****

***** MPFB ADC MOTOR *****

```

***** INPUT CARD DATA *****
SCARD1
VBASE 0 .11300000+03;
APAREL 0 .12700000+02;
RPMHAB 0 .00000000+00;
RPMH 0 .00000000+00;
PHASE 0 .30000000+01;
PCLPS 0 .00000000+01;
O 0 .14000000+01;
AL 0 .00000000+00;
SEAN
SCARD2
S 0 .20000000+01;
CONDS 0 .00030000+00;
C 0 .10000000+01;
Y 0 .50000000+01;
STRNS 0 .10000000+01;
ASTG 0 .12000000+02;
SCU 0 .32000000+00;
SFE 0 .03000000+00;
SENO
SCARD3
PTSEC 0 .00000000+00;
THOMM 0 .10000000+01;
BO 0 .33000000+00;
MO 0 .10000000+01;
MT 0 .10000000+01;
MH 0 .10000000+01;
BT 0 .10000000+01;
TEPFS 0 .00000000+03;
SPAC
SCARD4
STHESP 0 .00000000+00;
STNSHQ 0 .00000000+00;
HCI 0 .00000000+00;
RECOIL 0 .00000000+00;
PYZ 0 .20000000+01;
WPOBGM 0 .00000000+00;
SCCSG 0 .00000000+00;
STATI 0 .00000000+00;
SEAN
SCARD5
NCTI 0 .00000000+00;
MAGT 0 .00000000+00;
ALPHA 0 .00000000+00;
TBI 0 .00000000+00;
Q 0 .30000000+02;
TSKEW 0 .00000000+00;
PMAGL 0 .00000000+00;
TSTRES 0 .00000000+00;
SEAN
SCARD6
TBLCT 0 .00000000+00;
VPMIL 0 .00000000+00;
RECHOO 0 .00000000+00;
KZ 0 .20000000+00;
TVID 0 .10000000+01;
BI 0 .00000000+00;
MOOP 0 .00000000+00;
DEANOO 0 .32000000+00;

```

```

SENO
SCARD7
CHOT 0 .00000000+00;
WQOR 0 .20000000+00;
MOGSC 0 .10000000+01;
SPU300 0 .00000000+00;
RHO300 0 .00000000+00;
CMOE 0 .10000000+01;
ANEM 0 .00000000+01;
NEG 0 .00000000+01;
SENO

```

Figure A-25. Motor Computer Print Out

Figure A-25. (Cont'd)

THIS PAGE IS BEST QUALITY PRACTICABLE
FROM COPY FURNISHED TO DDC

```

***** LOAD DATA *****
SLOAD
VPU      0      .10000000+01;
APU      0      .10000000+01;
BP       0      .94000000+00;
RPM      0      .40000000+00;
SAP      0      .00000000+00;
TEMPMG   0      .00000000+00;
TC=40    0      .00000000+00;
TEMPBI   0      .00000000+00;
CODE     0      .10000000+01;
VOLTS    0      .11300000+03;
APPS     0      .12700000+02;
DEAST    0      .99218750+04;
THETA    0      .31750049+00;
PSI      0      .40100147+00;
EPST     0      .40382103+00;
EO       0      .10980794+01;
PLQAD    0      .9770+07+00;
PDR      0      .9500+04+03;

```

***** MATHS GDC MOTOR *****

DATE 140776 PAGE

```

FCORE    0      .19000001+02;
PYEETHN  0      .22000381+03;
PCAP     0      .33049343+03;
PNOOP    0      .02007703+03;
PP       0      .47154152+02;
PI       0      .87703200+03;
PHADP    0      .17704400+04;
PCIP     0      .20402015+04;
PHIS     0      .41020020+02;
PHINOP   0      .09003010+00;
PHID     0      .42523079+02;
PHITS    0      .22353021+01;
PHITE    0      .40749732+01;
PHIM     0      .40732094+02;
BETAC    0      .10000000+03;
BETAT    0      .12230191+03;
BETAS    0      .30237077+02;
BP       0      .00000000+02;
BMOOP    0      .00000000+00;
BMAC     0      .40406094+02;
STRESS   0      .19370000+00;
PLEAK    0      .16302023+00;
ELCAD    0      .12503320+00;
ENERGY   0      .74500007+03;
KVA      0      .43052000+01;
KH       0      .00000349+01;
S        0      .00000000+02;
POBOP    0      .15326738+03;
ENXPGO   0      .22044070+04;
PCINAY   0      .11029100+01;
GRATIN   0      .11029100+01;
SEN      0
SLOBH
PYOTAL   0      .39747760+00;
PPRICT   0      .70742569+04;
PHINO    0      .34275062+03;
PSCI     0      .30180900+00;
PSTRAY   0      .15109073+01;
PPGLM    0      .54073022+02;
PYEETHM  0      .42978500+01;
PCORE    0      .31010704+01;
BPP      0      .00201800+00;
PIPOL    0      .39070401+02;
PULOS    0      .14700341+02;
GI       0      .19036767+01;
EMUPD    0      .20400000+03;
RMOPO    0      .10000000+02;
EMUST    0      .10000000+03;
SPOLM    0      .4305703+03;
SEN      0

```

Figure A-25. (Cont'd)

THIS PAGE IS BEST QUALITY PRACTICABLE
FROM COPY FURNISHED TO DDO

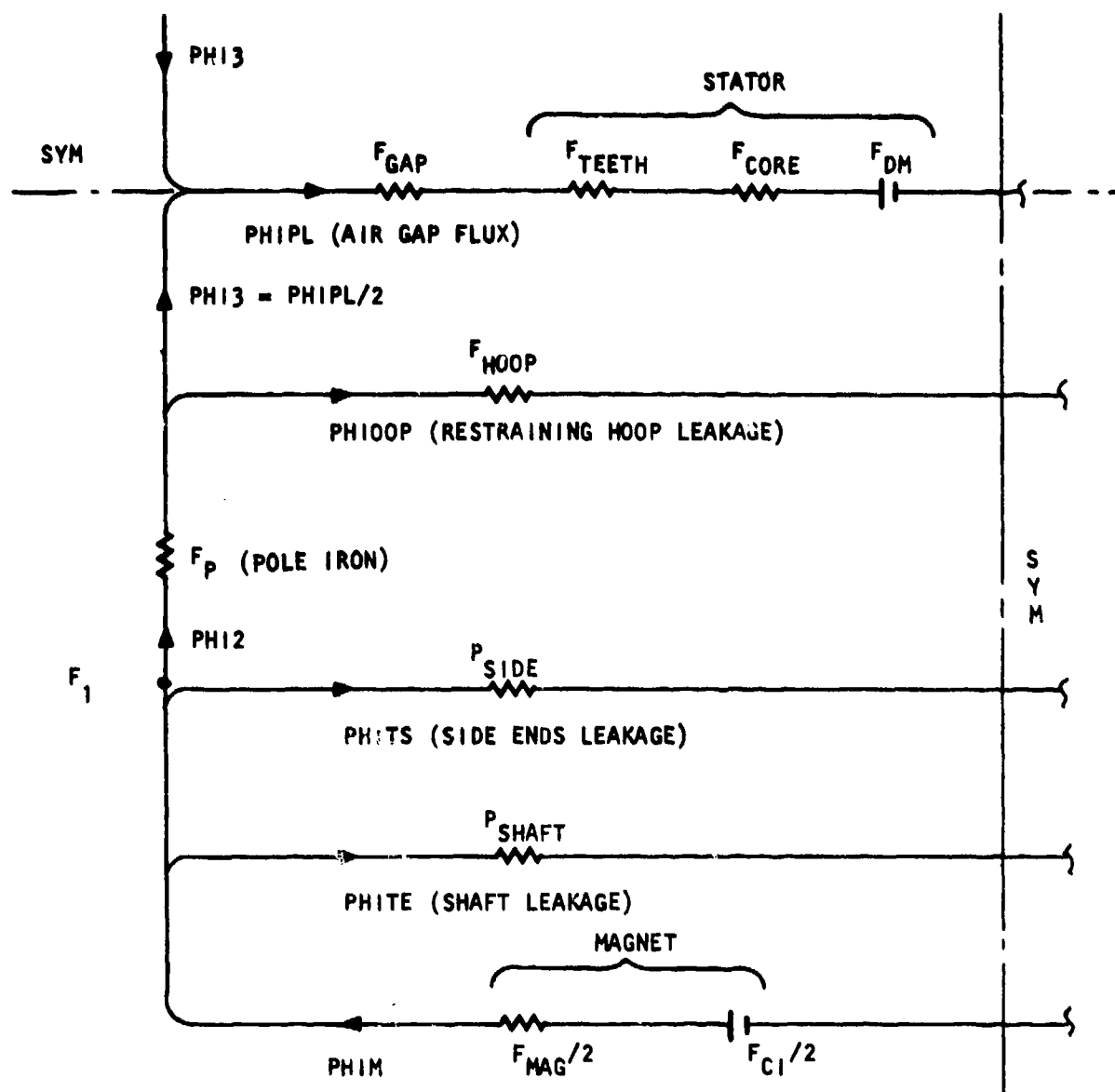
***** SUMMARY *****

SBUTCK		
POBPKW	*	.10480949+01:
POFTPD	*	.83961850+00:
EFF	*	.90281804+00:
THQOP	*	.10000000+01:
DR	*	.13832000+01:
OSTAK	*	.26527847+01:
TM	*	.31716769+01:
RPM	*	.80000000+04:

>>>>> HPAPB ADC MOTOR >>>>>

WTOT	*	.42867450+01:
KWSHAF	*	.36925573+01:
HPSHAF	*	.49498087+01:
TORGPF	*	.32496113+01:
PTOTAL	*	.39747760+00:
RECMOD	*	.00000000+00:
CMCOE	*	.10000000+01:
VOLTDC	*	.00000000+00:
AMPDC	*	.00000000+00:
DELTA1	*	.00000000+00:
ALPHA1	*	.00000000+00:
SEND		
SSCKT		
APUSC	*	.32621428+01:
HMAGSC	*	.96845870+04:
RECOIL	*	.15160000+05:
BMA6	*	.29978721+02:
VOLTS	*	.00000000+00:
SEND		

Figure A-25. (Cont'd)



BASIS: PER POLE, PER MAGNET OF HALF LENGTH
UNITS: KILOLINES AND AMPERE-TURNS

S-5219

Figure A-26. Magnetic Circuit for BIGMAG

(f) Other load points desired are calculated for the frozen design.

Particular features of BIGMAG are as follows:

- (a) Magnetic and loss data for 2 materials are stored (B-H data is 16 point curve)
- (b) Permanent magnet data (including intrinsic coercivity, recoil limit, and second-quadrant B-H data in 16 points) are stored for five materials.
- (c) Magnet characteristics are calculated for any specified temperature to account for reversible and irreversible effects.
- (d) Conductor size and number of stator slots can be program defined.
- (e) Conductors may be round or rectangular; slots or teeth may be tapered or straight.
- (f) Various magnet retention schemes can be modeled.
- (g) Rectified loads may be modeled; apparent power factor and dc volts and amps are calculated for rectified loads as a function of commutation reactance of the alternator and external reactance of a transformer.
- (h) Loss calculations include pole head, strays in stator copper, friction, and windage for any specified gas or fluid viscosity and density.
- (i) Motor or generator mode may be selected.

Rotor Position Sensor

The angular position of the rotor poles with respect to the stator conductors must be accurately sensed to provide the logic for proper commutation. A number of methods are available to accomplish this. The application dictates the selection of the most rugged and reliable of the various choices.

The position sensor choser consists of three transformers, each having a primary winding excited at a high frequency and a secondary or sense winding. The primary and secondary are wound on "C" cores and separated by an air gap. These transformers are mounted in a structure and located with respect to the stator windings. A cylindrical shutter of aluminum with precisely located milled slots is attached to the rotor shaft with the angular position of the slots established relative to the rotor poles. The shutter and transformers are axially aligned such that, on rotation, the air gap in the transformers will alternately have the aluminum shutter material or the shutter slot between the primary and the secondary circuits. The secondary output varies with the degree of coupling from the primary. When the aluminum part of the shutter is in the transformer gap, the eddy currents set up attenuate the flux linkages in the secondary thus reducing the

secondary output voltage. The position logic obtained from these three transformers and the rotating shutter thus enables the controller to direct the current to the proper stator windings to achieve optimum torque output.

Parking Brake

The parking brake is a two surface disc brake actuated by an electromagnetic coil. When the brake coil is not excited, the 50 lb brake spring clamps the brake disc between the two non-rotating brake surfaces. When the brake coil is energized the brake armature pulls in against the spring thus leaving a clearance air gap for the brake disc and the rotor assembly is free to rotate. The brake coil requires approximately 1000 ampere-turns to pull in. The excitation current this represents results in coil losses and heating beyond an acceptable level on a continuous excitation basis. Therefore, after pull-in the coil current will be modulated by the controller to approximately 25% of its pull-in value, the holding ampere turns required being significantly lower than the pull in value because there is no gap in the brake magnetic circuit after pull-in. The static brake torque will be 600 in-oz. minimum.

LONG LEAD ITEMS

The following components and items are identified for long lead procurement.

Motor

Rotor magnets	8 weeks
---------------	---------

Stator laminations	12 weeks
--------------------	----------

Actuator

Differential ring gear bearings	12 weeks
---------------------------------	----------

Motor Controller

Microprocessor	12 weeks
----------------	----------

Transistor	8 weeks
------------	---------

APPENDIX B

ACTUATION UNIT PERFORMANCE SPECIFICATION

1.0 SCOPE

The electromechanical actuation system will be designed, fabricated, and tested to show capability as a primary flight control actuation system. The system is a power-by-wire and fly-by-wire design, and the rotary actuator part of the system serves as the control surface hinge.

2.0 APPLICABLE DOCUMENTS

TBD

3.0 REQUIREMENTS**3.1 FUNCTION****3.1.1 Definition**

The rotary electromechanical actuation system comprises the following elements, as shown in Figure B-1:

Controller (2 channel, redundant)

Two motors with integral parking brakes

Rotary hinge-line type geared actuator with velocity summing differential

Position Feedback Transducers

3.1.2 Controller

The controller interfaces with control surface position commands from the aircraft automatic flight control system. The digital controller provides power to the servomotor by pulsewidth modulation of power transistor switches. Control surface position sensing is used to close the servoloop. The controller includes built-in-test provisions.

3.1.3 Motor Assembly**3.1.3.1 Motor**

Normal operation requires both electric motors to be operating. The motor is a brushless dc permanent magnet rotor design directly coupled to the control surface through stages of gearing. Either motor can operate the output of the actuator independent of the other electromechanical drive channel. Operation on a single motor results in full torque capability and one-half rate capability at rate limit. An integral motor brake locks a failed drive channel.

3.1.3.2 Parking Brake

Electromagnetic brakes are included on each drive motor shaft. The brakes are used to implement the redundancy of the high-efficiency gearing in the dual drive channels. A failed electromechanical drive is held stationary by the brake to allow the operating drive assembly to position the control surface. The brake is electrically energized for the "brake off" condition. The brake is spring actuated "on".

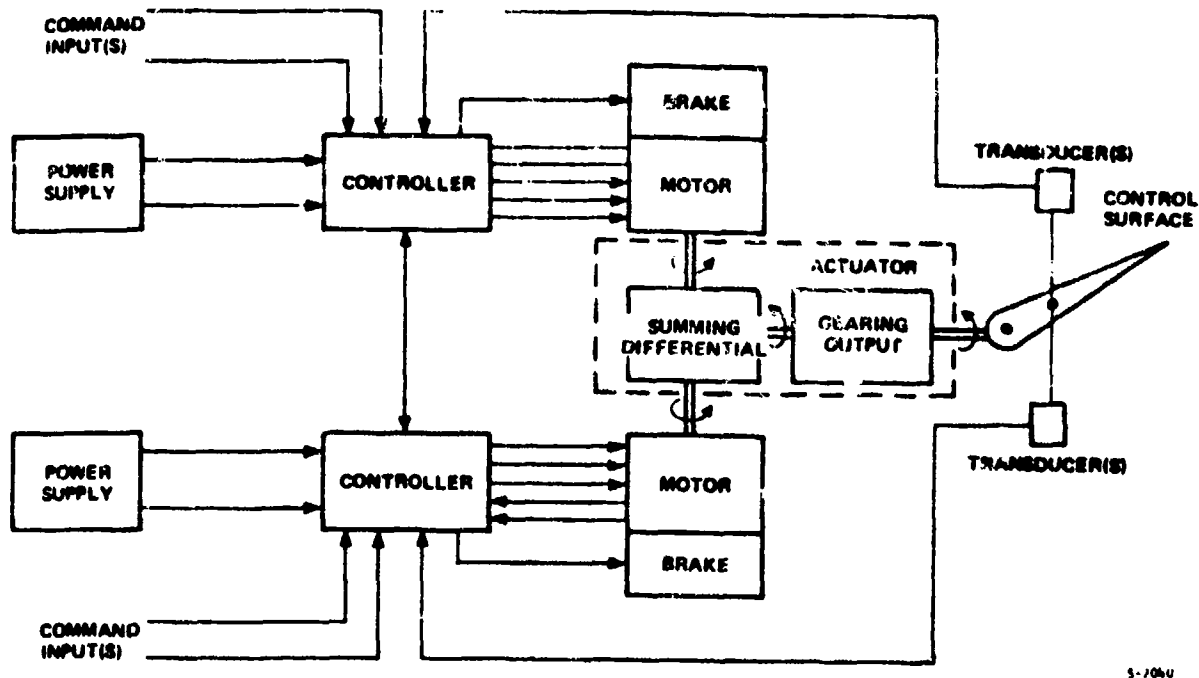


Figure 8-1. System Model

3.1.4 Actuator

The actuator consists of a velocity summing differential, and the necessary gear reduction. The actuator serves as the control surface hinge. The actuator also serves as the mounting structure for the redundant motor assemblies and the control surface position feedback transducers.

3.1.5 Position Feedback Transducers

The actuator output position will be monitored by two independent position transducers. Each transducer will be dedicated to a specific drive channel.

3.2 INTERFACE DEFINITION

3.2.1 Physical Interface

The actuator assembly will be a maximum of 4 in. in diameter. The actuator will serve as the hinge for the control surface. The controller configuration and mounting is not constrained for this evaluation program.

3.2.2 Electrical Interface

The schematic of Figure B-2 shows the electrical interfaces of the actuation system. Input power will be 270 vdc. Actuator input commands which are independent and which can be variable with time, include the following:

- a. Control surface position
- b. Rate limit
- c. Torque limit
- d. Commutation angle.

3.3 CHARACTERISTICS

3.3.1 Performance

3.3.1.1 System

3.3.1.1.1 Output Stroke

With one or two channels operating, the actuation system will be capable of positioning the output over the full stroke. For demonstration purposes, the full stroke will be ± 30 degrees.

3.3.1.1.2 Output Velocity

With two channel operating at no-load, the unit will provide a maximum open-loop velocity of 80 deg/sec.

3.3.1.1.3 Output Torque

The unit, with both channels operating together in either direction of rotation, will be capable of 8 Hz dynamic response as described in Figure B-3. The actuator stall torque will be 37,575 lbf-in. The actuator mechanical strength will have a safety factor of 1.25 stall.

3.3.1.1.4 Displacement Linearity

The displacement will be linear within 1.0 percent full stroke.

3.3.1.1.5 Threshold

The threshold will not exceed 0.1 percent of the input signal required to achieve 100 percent full stroke.

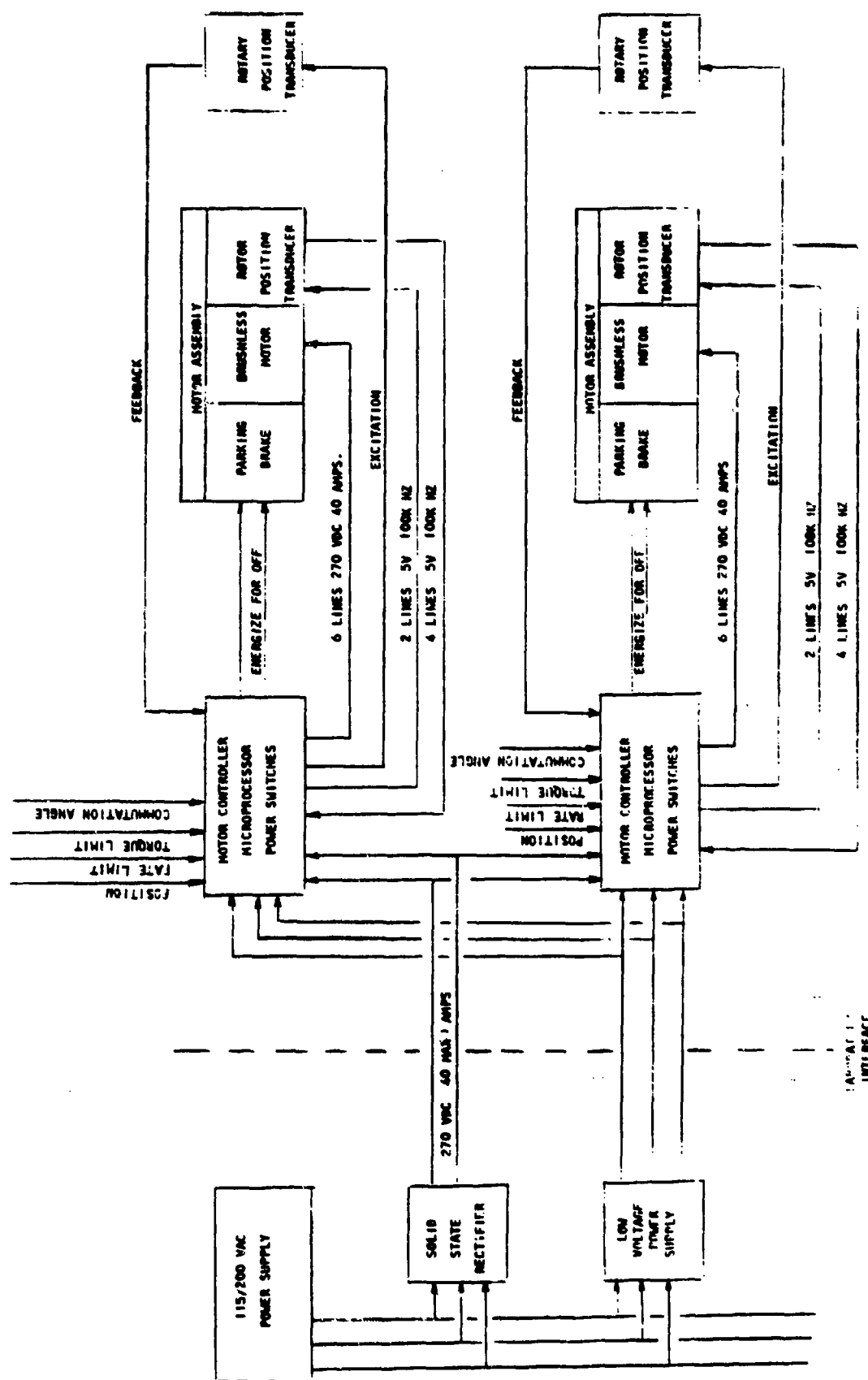
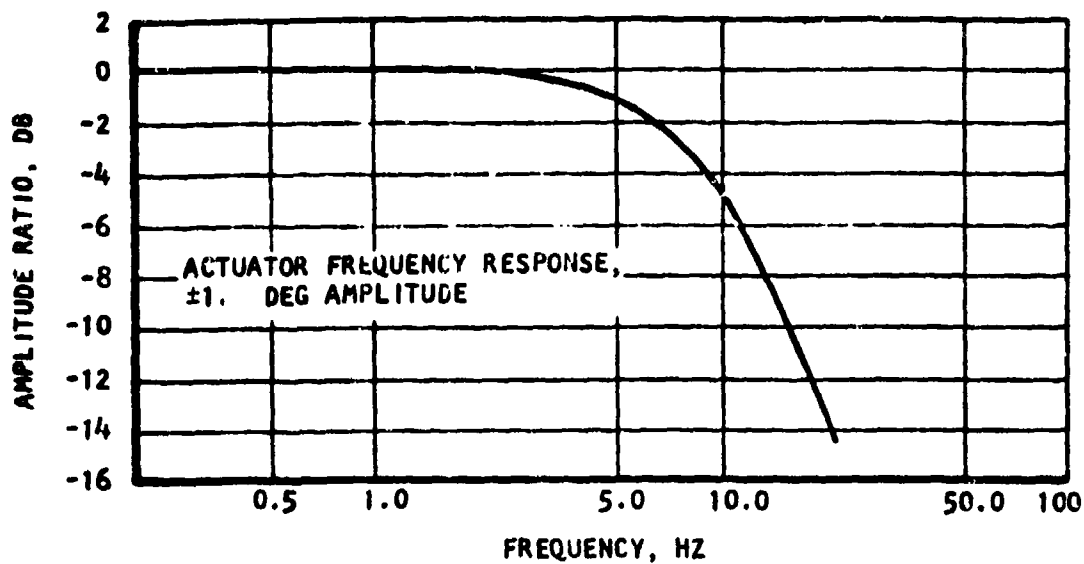
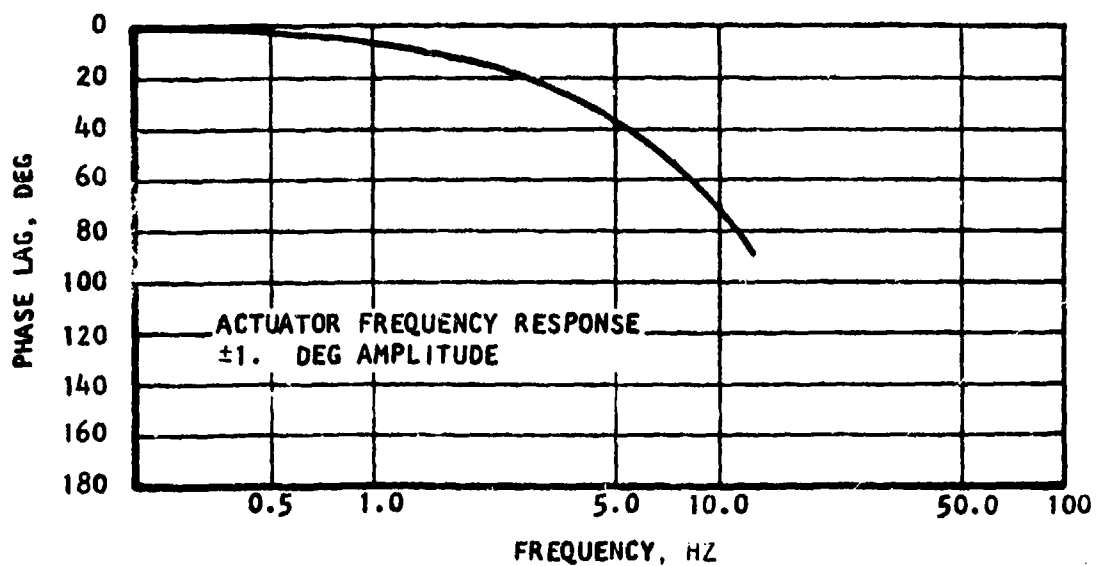


Figure B-2. Electrical Interface Schematic



Amplitude Ratio vs. Frequency



Phase Lag vs. Frequency

Figure B-3. Dynamic Response

3.3.1.1.6 Position Null

At no-load, the output position of the actuator measured from its neutral position will not exceed 0.5 deg.

3.3.1.1.7 Hysteresis

The hysteresis will not exceed 0.5 percent full stroke.

3.3.1.1.8 Motor Brake

The motor brake will brake a de-energized motor from full speed to zero speed against rated actuator torque. No electrical power will be required to engage the brake.

3.3.1.1.9 System Efficiency

Maximum efficiency is a design goal.

3.3.1.1.10 Thermal Control

3.3.1.1.10.1 Motor and Actuator

The motor actuator assembly may be cooled passively by heat rejection to the aircraft structure. The local heat rise at the mounting surface will not exceed 200°F.

3.3.1.1.10.2 Control

The thermal management of the controller is not constrained. Passive cooling is a goal.

3.3.1.1.11 Open Loop Gain

The unit will be designed for a steady state open loop gain of 45 deg/sec/deg., i.e., a position error of one degree shall generate a control surface velocity of 45 deg/sec for the no-load condition.

3.3.1.2 Controller

3.3.1.2.1 General

A digital microprocessor will be used as the central component of the controller. The control is the interface between the motor, the command input, and the electrical power bus. The controller provides a command to the commutation circuit, which provides power to the proper motor stator windings based on sensed rotor shaft position. The dc bus is connected to the windings by the electronic transistor switches. At any instant, two switches are commanded to conduct approximately every 60 deg., one switch is turned off and a new one is turned on to obtain the required current pattern in the motor armature.

The speed of rotation of the brushless dc motor is controlled by varying the average dc voltage supplied to the motor by the electronic commutator. Pulsewidth modulation techniques are used to generate the required average voltage.

The controller is programmed to provide a fixed current limit corresponding to maximum stall requirements. The current limit also may be programmed as a function of time, motor speed, or other independent properties useful in defining the performance characteristics for aircraft.

3.3.1.2.2 Input Commands

3.3.1.2.2.1 Control Surface Position

The controller will accept an analog signal corresponding to desired control surface position.

3.3.1.2.2.2 Rate and Torque Characterization

The controller will be capable of providing a maximum rate corresponding to a programmed torque. Figure B-4 shows maximum torque speed characteristics of the motor. The control will have the capability to accept any program of torque vs speed as illustrated by curves A, B or C.

3.3.1.2.2.3 Rate Limiting

The controller will have the ability to accept an adaptive command to adjust the maximum output rate in the range from 25 percent to full rate as illustrated in Figure B-5.

The command can vary from full output rate to 25 percent rate manually, or from an external signal generator.

3.3.1.2.2.4 Torque Limiting

The controller will have the ability to accept an adaptive command to adjust the maximum torque in the range from 25 percent to full stall as illustrated in Figure B-6. The command can vary from full output torque to 25 percent torque manually, or from an external signal generator.

3.3.1.2.2.5 Commutation Angle

The commutation angle will be variable from nominal by ± 15 degrees.

3.3.1.2.3 Power Switching

Pulse width modulation of power to the motor will be accomplished using transistors. Maximum average current capabilities will be 20 amps at 270 vdc for each of 2 motors.

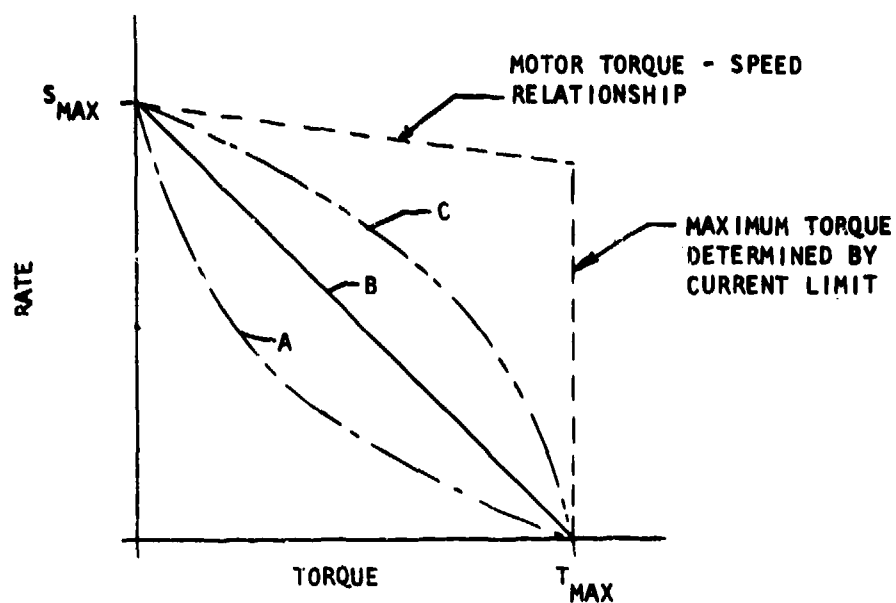


Figure D-4. Torque Speed Characterization

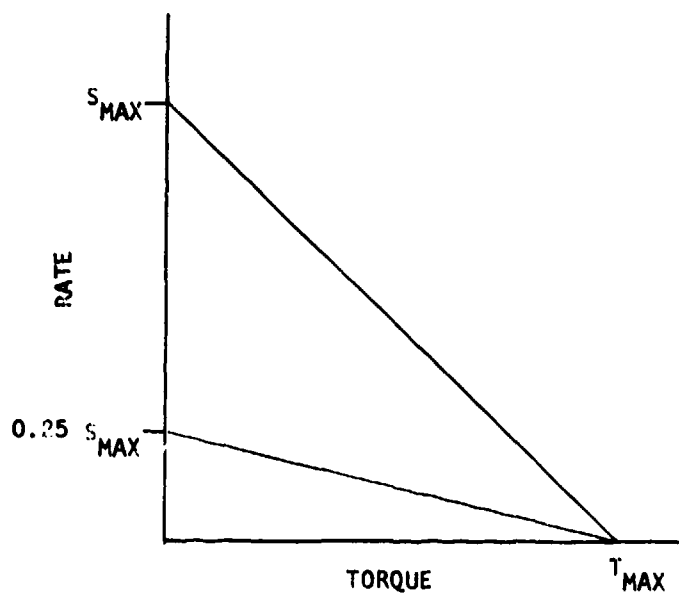


Figure B-5. Dynamic Rate Limiting

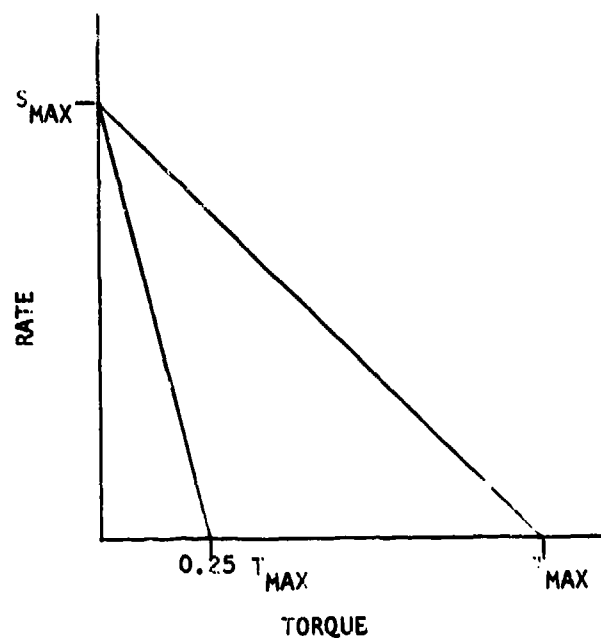


Figure B-6. Dynamic Torque Limiting

3.3.1.3 Motor

3.3.1.3.1 General

The motor is a permanent magnet, dc, brushless type comprising a wound stator and rare-earth-cobalt permanent magnet rotor. The motor assembly also will include separately excited dc brake and shaft position sensor. The position sensor detects and rotor position and activates the electronic commutator.

3.3.1.3.2 Performance

Table B-1 summarizes the significant design characteristics of the motor assembly. During normal operation, the output of two motors is combined in the differential gearing of the actuator. If a failure in one operating channel occurs, the remaining motor, in conjunction with the actuator gearing, provides full torque at one-half rated velocity at the control surface.

3.3.1.4 Actuator

3.3.1.4.1 General

The actuator is a rotary hinge-line device that serves as the structural attachment between the control surface and the wing structure. The dual-redundant electric motors are mounted on the actuator. The two input shafts operate into a velocity summing differential. The output of the differential drives through planetary gear reduction stages into the compound planetary, rotary output stage.

3.3.1.4.2 Performance

The major characteristics of the assembly are presented in Table B-2.

3.3.1.5 Position Feedback Transducer

3.3.1.5.1 General - A control surface position transducer will be used to monitor the output angular position and will be used as feedback to close the servo loop.

3.3.1.5.2 Performance - The performance of the unit will be as follows:

- | | |
|---------------|-------------------------|
| a. Stroke | 60 degrees total |
| b. Linearity | 0.5 percent full stroke |
| c. Resolution | 0.5 percent full stroke |

3.3.2 Envelope

See Drawing No. 2022194.

TABLE B-1

MOTOR CHARACTERISTICS

Rated voltage	265 vdc
No-load speed	8600 rpm
Torque per amp	39.3 ozf-in./amp
Stator resistance (68°F)	0.73 ohm
Rotor Inertia	1.077×10^{-3} lbf-in.-sec ²
Time constants	1.35 sec, electrical 15.5 sec, mechanical
Back EMF	30.8 v/1000 rpm
Brake voltage	270 vdc
Brake torque	600 ozf-in (minimum)
Envelope	Drawing no. 515018

TABLE B-2

ACTUATOR CHARACTERISTICS

Stall torque	37,500 lbf-in.
Rate	80 deg/sec
Life	100,000 cycles
Gear ratio	627:1
Gear configuration	(1) Differential: planetary (2) Intermediate: 2 stages of planetary (3) Output: compound planetary
Spring rate	3.75×10^6 lbf-in./rad
Envelope	Drawing No. 2022192

3.3.3 Weight

Designed and packaged to be lightest weight compatible with the total requirements.

3.3.4 Monitoring/Control Provisions

3.3.4.1 General

Monitoring and control of the laboratory demonstration unit may be accomplished using standard laboratory equipment. No special equipment or consoles are specifically required for this purpose, providing the data can be visually observed and/or recorded as necessary.

3.3.4.2 Control

The input control for each channel will include as a minimum the following:

- Commutation Angle
- Position Control
- Rate limit
- Torque limit
- Failure simulation
- Power/regeneration mode

3.3.4.3 Monitoring

Monitoring of each channel will include at least the following:

- Motor velocity
- Average current (power mode or regeneration mode)
- Average voltage
- Position indication
- Failed channel indication

3.3.5 Design

The design goals of the actuation system and components will consider the environmental factors listed below:

<u>Environment</u>	<u>Specification</u>	<u>Method</u>	<u>Procedures</u>
Altitude	MIL-STD-810	500.1	-
Temperature	MIL-STD-810	501.1 502.1	11 1
Humidity	MIL-STD-810	507.1	1
Saltspray	MIL-STD-810	509.1	-
Sand and Dust	MIL-STD-810	510.1	-
Vibration	MIL-STD-810	514.2	(category b.2)
Shock	MIL-STD-461	516.2	1 Fig. 516.2-1 (a) and (c)
EMC	MIL-STD-461	-	-
Explosive Atmosphere	MIL-STD-461	511.1	1
Rain	MIL-STD-461	506.1	(modified)

4.0 TEST REQUIREMENTS

Demonstration testing of a representative configuration of the electro-mechanical actuation system will be conducted.

4.1 FACILITIES

The system will be installed in a laboratory test facility with appropriate structural, loading, and electrical interfaces.

4.2 TESTS

The following tests will be conducted according to Table B-3.

TABLE B-3
TESTING

TEST	COMPONENTS REQUIRED			FULL SYSTEM
	MOTOR (ONE)	ACTUATOR	CONTROLLER (ONE)	
EMI	X		X	
Performance	X	X	X	X
Frequency Response				X
Stiffness		X		
Power Efficiency	X	X	X	X
Acceleration				X
Position Resolution				X
Velocity				X

APPENDIX C

SCREENING LOGIC DIAGRAM

1.0 INTRODUCTION

This appendix presents a summary of the screening of candidate concepts for electromechanical actuation (originally performed during the Electromechanical Actuation Feasibility Study, Reference 1). The results of the tradeoff studies were used to synthesize a selected configuration for preliminary design. The screening was performed in three parts as follows:

- Power Source--Engine-mounted electrical generation, conditioning, and distribution equipment.
- Actuator Drive--Electronic servo, electrical power switch, and servo motor.
- Gearing--Rotary hinge gearbox configuration, gear ratio, and redundancy provisions.

2.0 POWER SOURCE

The actuation power source requirements for a fighter aircraft would be in the range of 30 to 70 kw. The groundrule for the power source (from Reference 1) was to use 115/200-vac, 400-Hz power. At least three options exist, which are as follows:

- Use of the 115/200-vac power as supplied (constant frequency)
- Wild frequency 115/200-vac power, eliminating the weight and complexity of a constant-speed drive
- Convert the ac to dc, allowing use of dc electromechanical drive systems

After review of Figure C-1, it is apparent that operation of either an ac or a dc drive system requires that the primary power be conditioned by adjusting frequency, voltage, or both prior to use in the electric motor. Either ac or dc motor drive systems can function equally well from fixed-frequency ac or variable-frequency ac based upon the commonality of a dc link. Thus, the most likely power sources for operation of a drive system are (1) high-voltage dc available from rectification of a 115/200-v alternator output, (2) 400-Hz ac power, or (3) ac power provided at a frequency dependent upon operating speed.

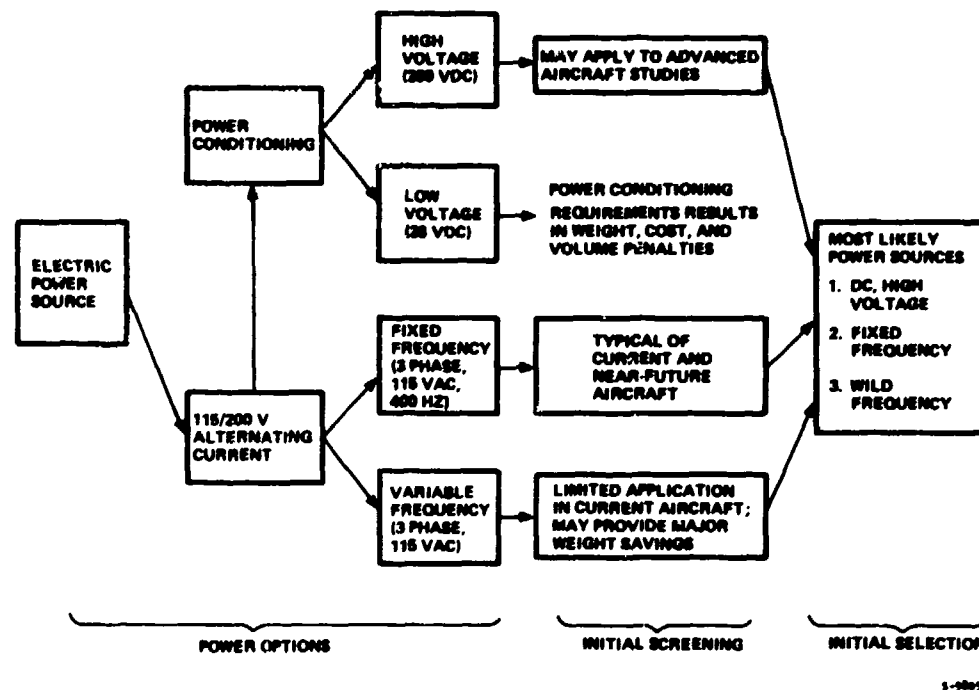


Figure C-1. Initial Screening of Power Options

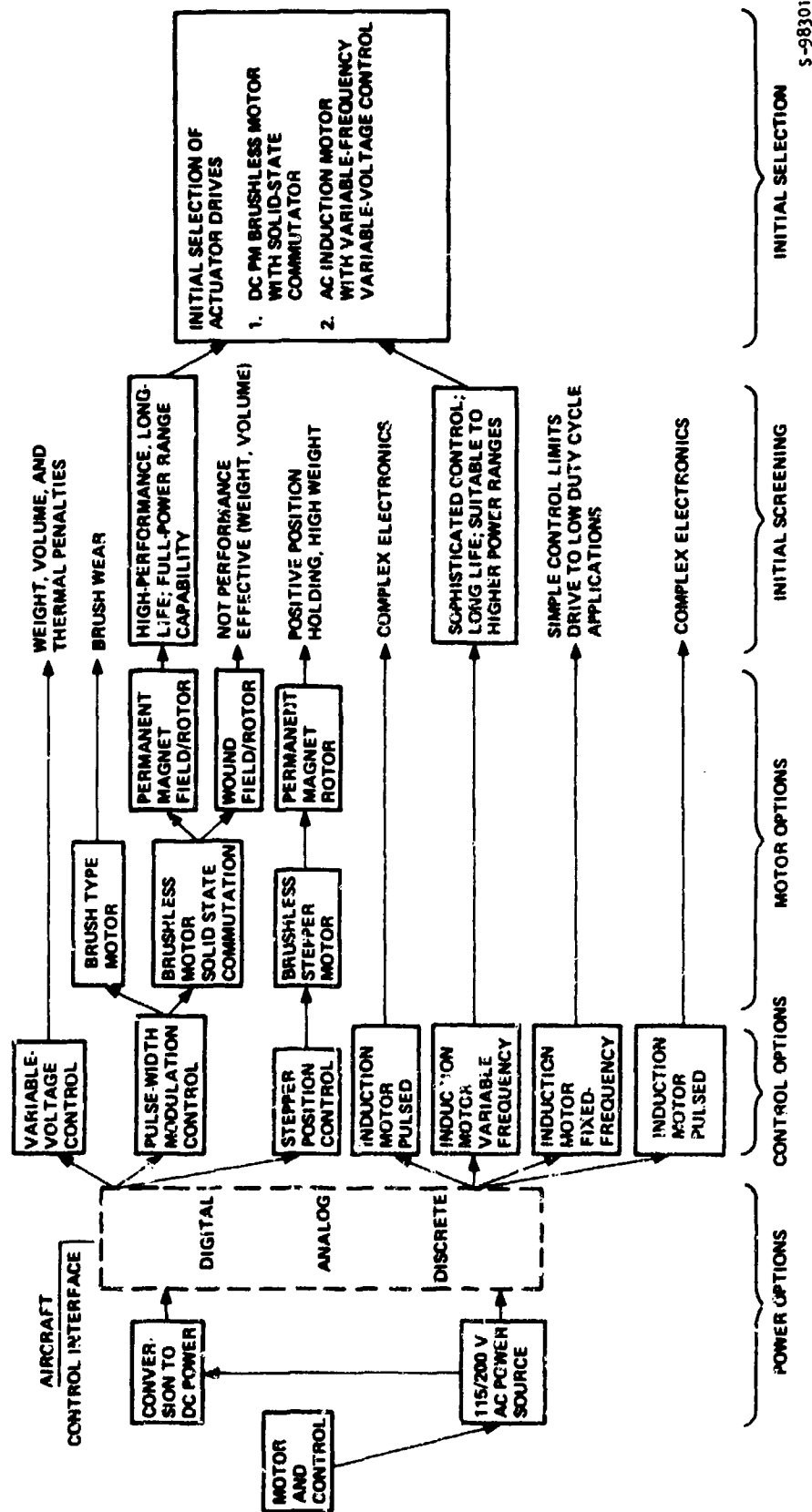
The power source tradeoff is a function of power quality required by the motor controller. Because of the dc link, a variable frequency from the electrical generator is entirely suitable for an actuation system. High quality power for airborne electronics and communications systems can be obtained from an auxiliary alternator designed for that particular application.

The selected approach for the power source is a permanent magnet generator as the electrical source, a rectifier to provide 270-vdc power, and distribution of the power through the aircraft using a dual redundant bus of aluminum conductors.

3.0 ACTUATOR DRIVE

A drive assembly comprises a motor and a controller. The controller, in turn, comprises an electronic servo, electrical power switching circuits, and any necessary feedback devices. The drive options for power-by-wire are summarized in Figure C-2, which shows that the high-voltage brushless dc motor with a permanent-magnet rotor and pulse-width modulation control provides better performance than either brush-type dc motors or stepper motors. The selection is based primarily upon consideration of the combination of lower weight and reduced thermal design problems associated with the brushless dc motor drive. Also shown is that the preferred ac motor drive is the induction motor with an inverter that provides variable frequency drive to the motor as a function of motor shaft speed. To minimize losses, the voltage also is programmed as a function of applied frequency (motor speed).

Comparison of the dc and Induction motor types was based on the following considerations.



S-98301-A

Figure C-2. Candidate Drive Options

- (a) 1 to 3 hp peak output capability in a 4.0-in.-dia maximum frame. (The typical flight control actuator problem statement requires this power output capability to drive the load at the desired rates, irrespective of frequency response requirements).
- (b) A frequency response capability of 4 to 12 Hz (8 Hz nominal).
- (c) Capable of maintaining a 50 percent duty cycle at a torque level corresponding to that produced at the peak output horsepower (one-half no-load rate and one-half stall torque.)
- (d) Capable of providing static torque in accordance with a program representing aerodynamic trim loads.

Analog and digital power servo concepts were compared for operation with the motor. A microprocessor provides the desirable operational characteristics of flexibility, versatility, and low cost. The hardware design can be fixed, while the functional characteristics can be tailored to meet modification performance requirements. By changing only software, the microprocessor motor control can operate either on an ac or dc servomotor. The processor capability to monitor and fault isolate is an additional advantage. The quantitative method of handling these requirements is accomplished by software changes for the microprocessor as opposed to hardware changes for an analog servosystem.

The selected drive approach for the hingeline actuator is a dc, brushless, permanent-magnet motor controlled by a digital microprocessor. The features of the microprocessor emphasize the versatility of the selected approach, which is the principal consideration in selection of the microprocessor for a primary flight control component.

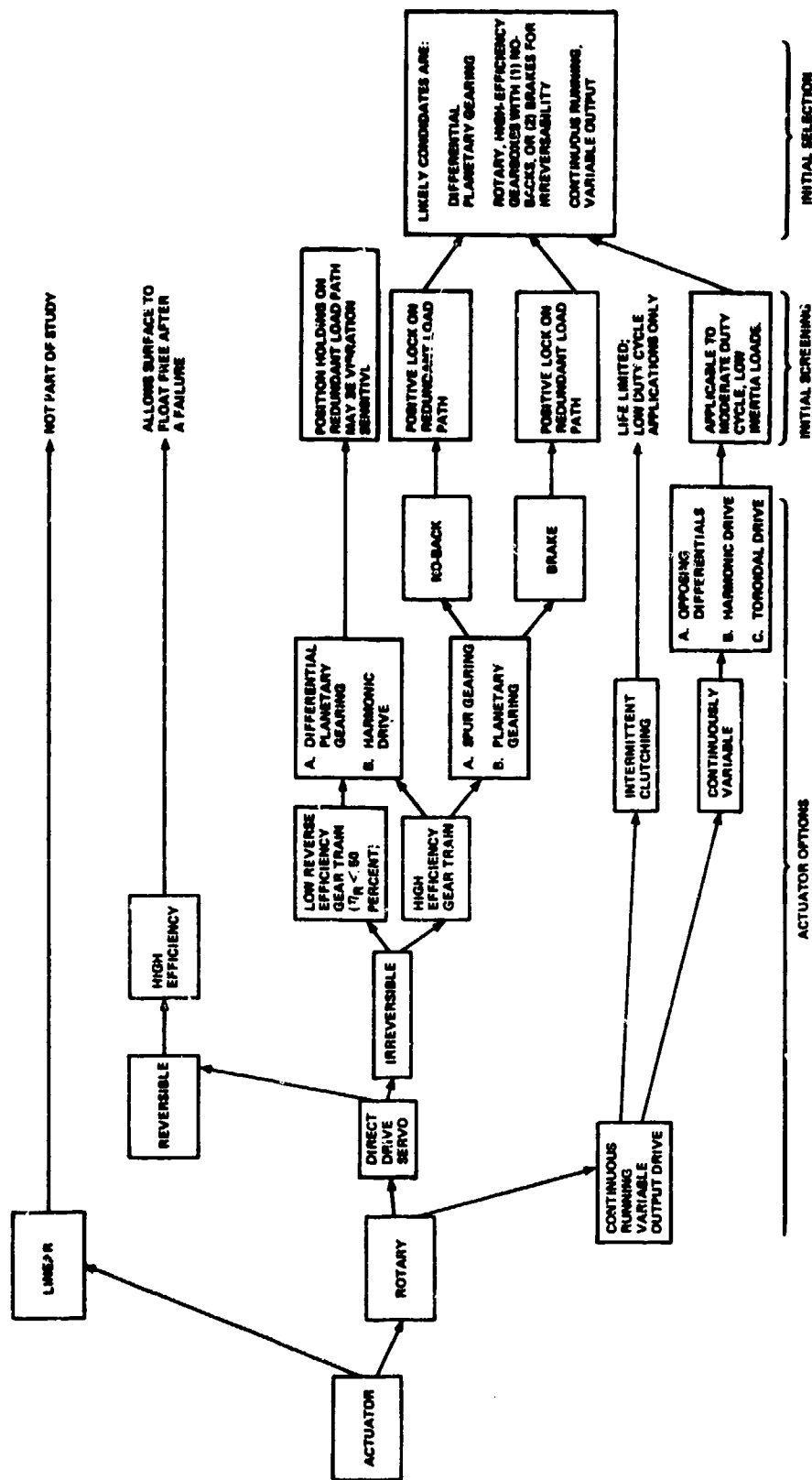
4.0 GEARING

Within the general category of actuators having a rotary output, there are many implementation techniques. A continuous-running electric drive can be mechanically controlled to provide variable rate by use of intermittent clutching (spring, electromagnetic), or by use of continuously variable toroidal transmission type drives. Intermittent clutching devices are eliminated from the study because of serious limitations of life, repeatability, and reliability. The initial screening of these approaches is presented in Figure C-3.

A direct-drive servo offers both reversible and nonreversible operation. The high-efficiency reversible approach is limited to applications where redundancy of actuation is not required. The irreversible approach using brakes or no-backs for position holding is superior to the low efficiency approach because less power is consumed in moving the surface, and the surface is positively locked even in the presence of vibration and periodically reversing loads, which can cause an irreversible geartrain to creep. The most promising actuation system elements are therefore:

Actuator Type--Rotary

Drive Type--Direct-drive servo



S-98133

Figure C-3. Initial Screening of Actuator Elements

Geartrain Efficiency--High (50 percent)Position Holding--Motor brake (used on servomotor to lock a standby)

The baseline configuration for the actuator is the differential compound hingeline geared unit. For applications requiring redundant power inputs, the actuator will include a planetary differential for velocity summing of the two motor inputs. Also required when using redundant drive inputs are separately excited dc brakes for redundancy management. The brakes are provided to hold the motor shaft stationary in the event that the drive channel is determined to be inoperative for any reason. Thus, the brake is not a part of the system dynamics.

5.0 SYSTEM INTEGRATION OF DRIVE CONCEPTS

The screening diagrams show that the power sources considered for the feasibility study each required some form of power conditioning prior to use by the actuation unit. The discussion of motor control (para. 3.3) has shown that motor torque and rate are controlled by the application of specific values of voltage and current. It is apparent that both the ac and the dc drive approaches require the primary power to be conditioned by adjusting the frequency, voltage, or both prior to use in the motor. Figure C-4 illustrates the similarity of the two drive approaches. Either concept can operate from an ac power source, because both rectify the ac power to provide a dc power link. The dc power is then conditioned to provide either pulse-width-modulated (PWM) control of a dc motor, or 3-phase ac power for the ac induction motor.

Also, if the aircraft power source is dc, rectification is unnecessary, and the dc power can be used directly by either the ac inverter or the dc PWM controller.

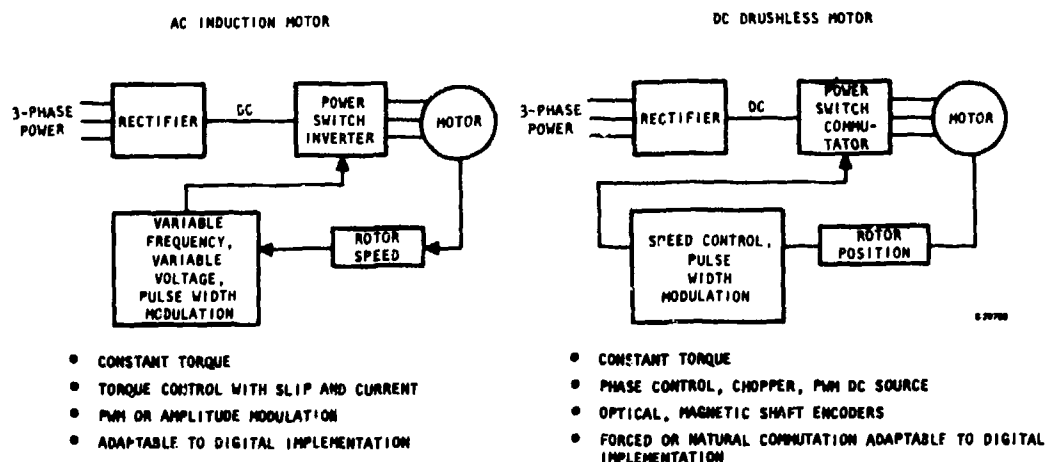


Figure C-4. Similarity of Drive Concepts

APPENDIX D

MOTOR TRADE STUDY

1.0 INTRODUCTION

This appendix presents a summary of the motor tradeoffs conducted as part of the feasibility study (Reference 1). The study included the following motor types.

Permanent-magnet and variable-reluctance steppers

Flex-spline steppers

Variable-frequency, variable-voltage induction motors

Permanent-magnet, brushless dc motors

2.0 DISCUSSION

2.1 STEPPER MOTORS

Figure D-1 shows typical torque speed and power output curves for the three-stepper types in the general size range of interest for the problem statement. The data was obtained from manufacturer's catalog literature. The stepper motors respond to programmed, pulsed, dc voltages, causing rotation of the output. The permanent-magnet (PM) stepper comprises a permanent-magnet rotor and a wound stator. The PM unit offers holding or detent torque capability. The variable-reluctance (VR) stepper design operates in the reaction between an electric field generated in the stator and a soft iron toothed rotor. The VR machine is generally capable of higher speed than the PM design.

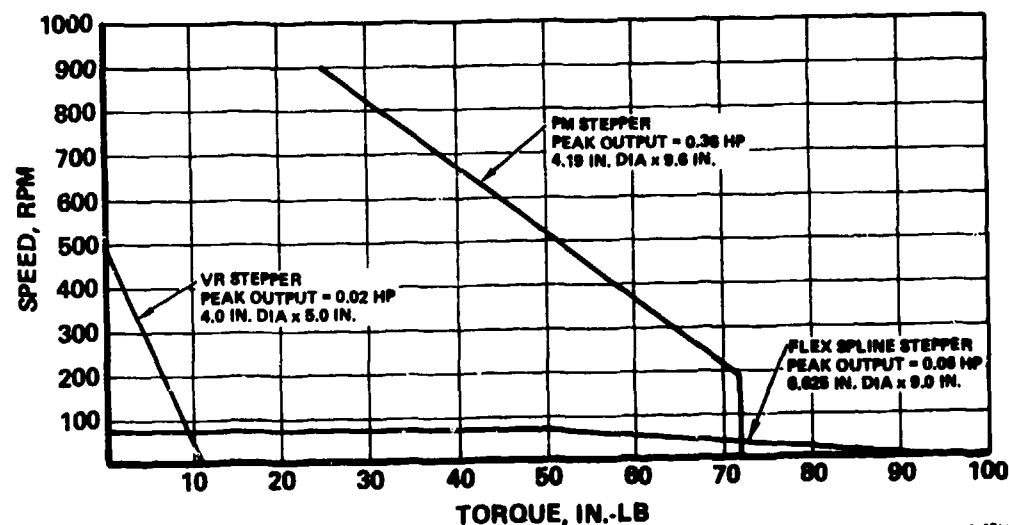


Figure D-1. Power Capability of Stepper Designs

Although the relationship of digital (pulsed) input to discrete steps at the output appears to offer advantages in the area of integration with a digital control actuation system, the basic stepper designs are not competitive with other forms of electromagnetic machines in terms of providing both the required torque and the required rate. The units are not suitable for the application because the maximum power output capability is about an order of magnitude below that required.

The flex spline stepper is a device that offers exceptionally high acceleration capability. Compared to the PM and VR steppers, the flex spline machine can provide output accelerations 100 times greater. This characteristic is not realized as an advantage, however, for the following reasons:

- (a) The acceleration requirements of a flight control system can be met with stepper or conventional servomotor components.
- (b) The mechanization of high acceleration results in excessive weight, and is not capable of substantial power, rate, or stiffness.

2.2 BRUSHLESS DC MOTOR

Figure D-2 shows a typical performance curve for a rare-earth-cobalt, permanent-magnet, brushless dc motor designed for servo applications. The motor has a peak output, corresponding to maximum speed and current limit, of 8 hp. The extremely high power output for this small unit results from two basic design features. First, the use of rare-earth-cobalt magnets, which offers high energy products, and second, the arrangement of the magnet in the rotor and using brushless commutation of the coils in the wound stator. This latter feature results in improved thermal control of the motor. The motor losses (copper losses in the stator) can be readily transferred to the motor casing, as compared to a wound-rotor configuration.

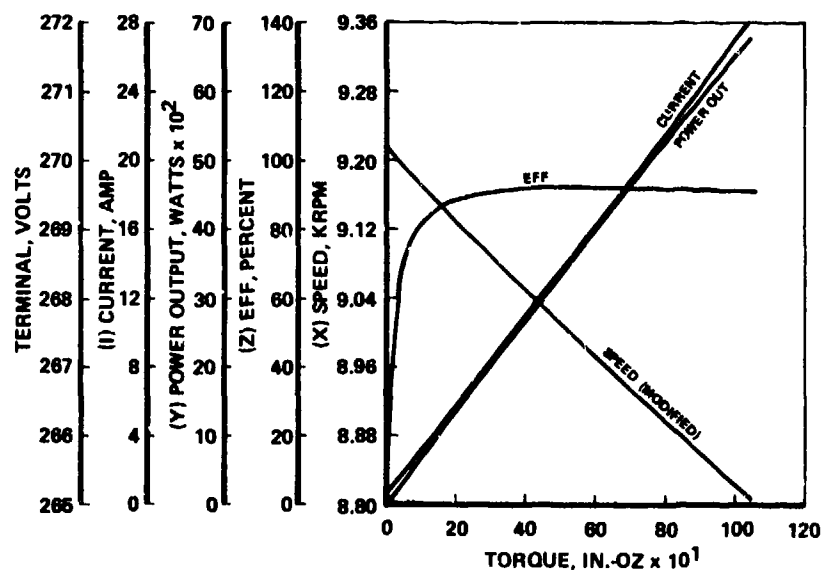


Figure D-2. Typical Motor Performance

As rare-earth-cobalt magnet materials have become commonly available for servomotor applications, they have had the following impact upon flight control servo actuators.

- (a) Smaller rotors, yielding faster response and lower weight
- (b) New construction techniques and magnet/stator arrangements that will reduce overall cost. The potential configuration changes are as follows:
 - (1) Tangential vs radial magnet arrangements
 - (2) Toothless stators, resulting in lower cost of manufacture
- (c) Improved resistance to demagnetization due to high magnetic flux fields from electrical sources, lightning, and electromagnetic pulses

2.3 AC INDUCTION MOTORS

The characterization of the ac induction motor is based upon the same set of operating characteristics as for the dc brushless machine. The power characteristics of the ac induction motor are shown in Figure D-3 for the condition of an applied frequency of 255 Hz and 100 v. This torque speed plot shows a stall torque of approximately one-half the peak torque value. To provide a more uniform torque from stall to near-synchronous speed and to limit rotor heating (which occurs at high slip), the motor is driven by a variable frequency. The generator frequency is a function of motor speed. Therefore, the motor drive frequency is continuously variable from synchronous speed at full-rated no-load speed down to approximately 10 percent of maximum synchronous speed.

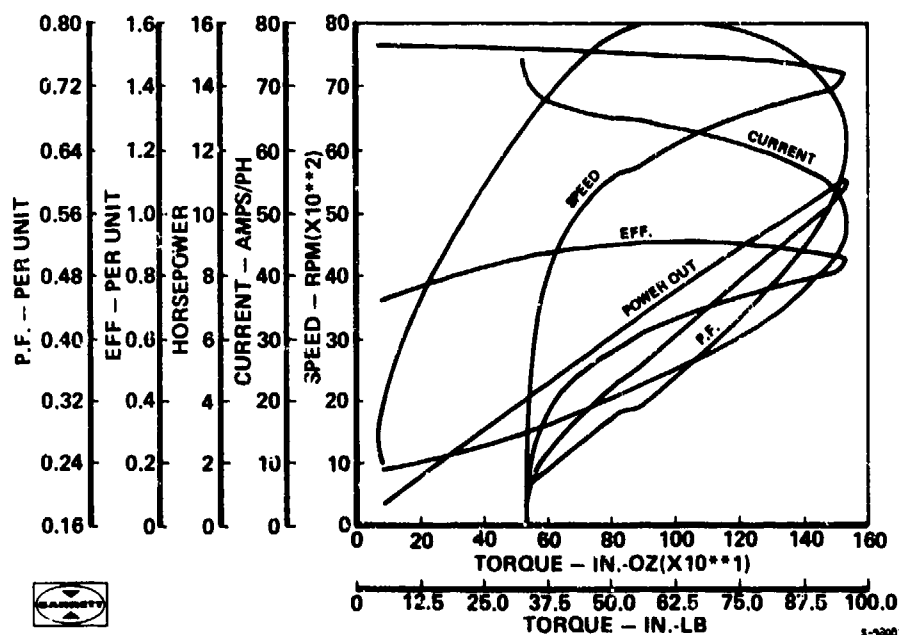


Figure D-3. Motor Power Characteristics

Five selected torque-speed curves from the continuously variable family of relationships are shown in Figure D-4. As frequency is adjusted, so is the applied voltage. Figure D-5 shows the relationship of voltage and slip to the applied drive frequency.

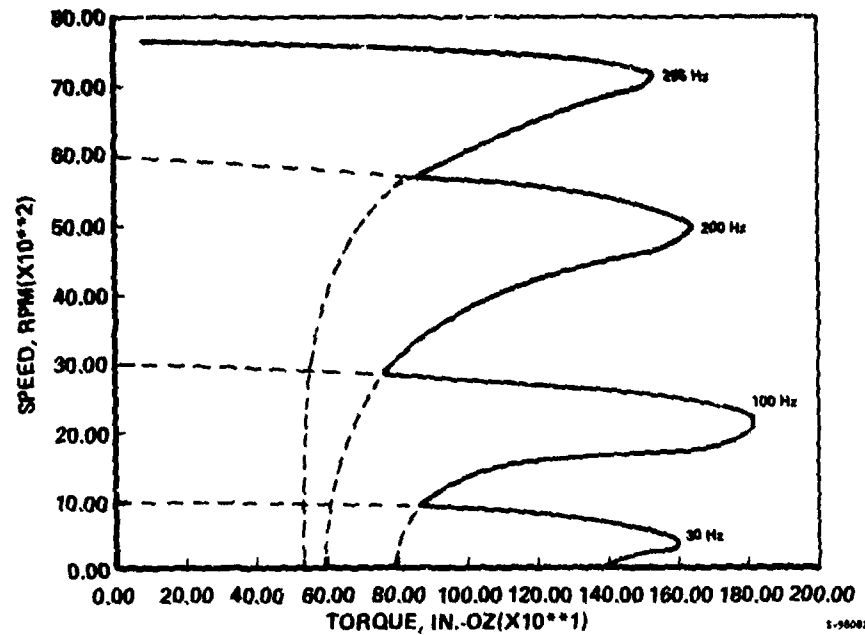


Figure D-4. Variable Frequency Motor Drive

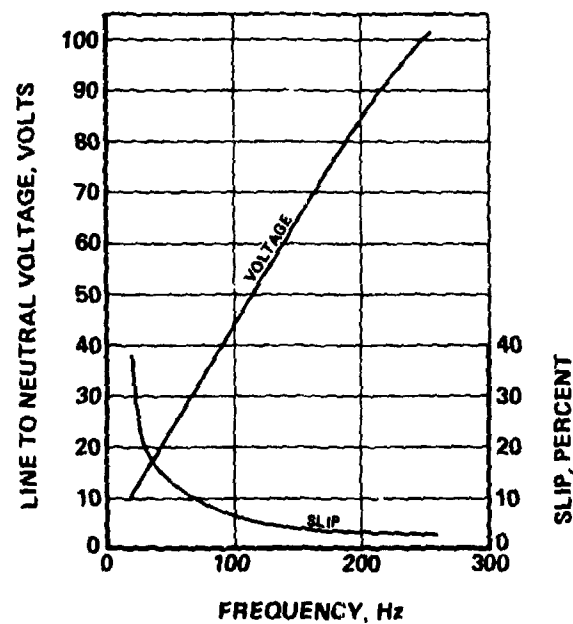


Figure D-5. Ac Inverter Voltage Schedule

3.0 COMPARISON OF MOTORS

As described above, the stepper motor does not provide the required power output for a flight control application. The remaining candidates are the brushless dc and the ac induction motors. A comparison of these two designs, based upon identical guidelines, is presented in Table D-1. Comparison of the two concepts shows similarity, except the brushless dc shows advantages in the areas of acceleration, current required, weight, and growth potential. The brushless dc is therefore selected as the candidate baseline for the flight control actuator design.

TABLE D-1
MOTOR COMPARISON

	Ac Induction	Dc Brushless
Maximum duty cycle, %	42	82
Motor acceleration, rad/sec ²	30,369	35,510
No load speed, rpm	7643	9200
Actuator gear ratio	573	67
Output acceleration, rad/sec ²	53	53
Maximum current, amp	30	29
Overall length, in.	8-3/4	7-1/2
Weight, lb	19	18
Diameter, in.	4	4
Growth potential	None	Magnets

APPENDIX E

MICROPROCESSOR CONTROLLER

1.0 INTRODUCTION

The summary of this report, Section 2.0, describes the chronology of development of the controller. Briefly, the following controller configurations were developed and tested.

- Dual microprocessors (baseline configuration)
- One microprocessor in one channel and one analog servo circuit in the other channel
- Dual analog circuits (final configuration)

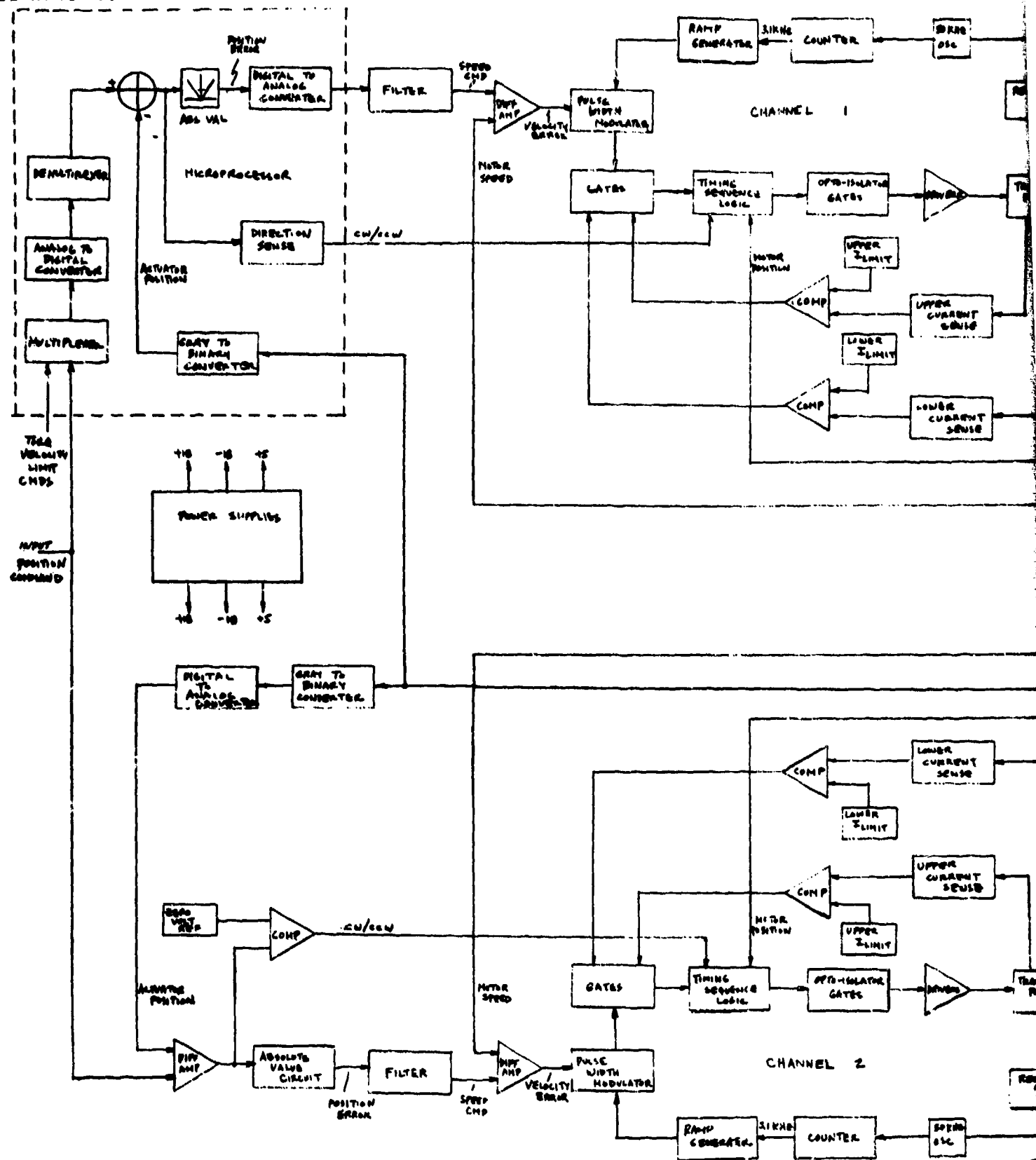
In this appendix, the results pertaining to the microprocessor development are summarized.

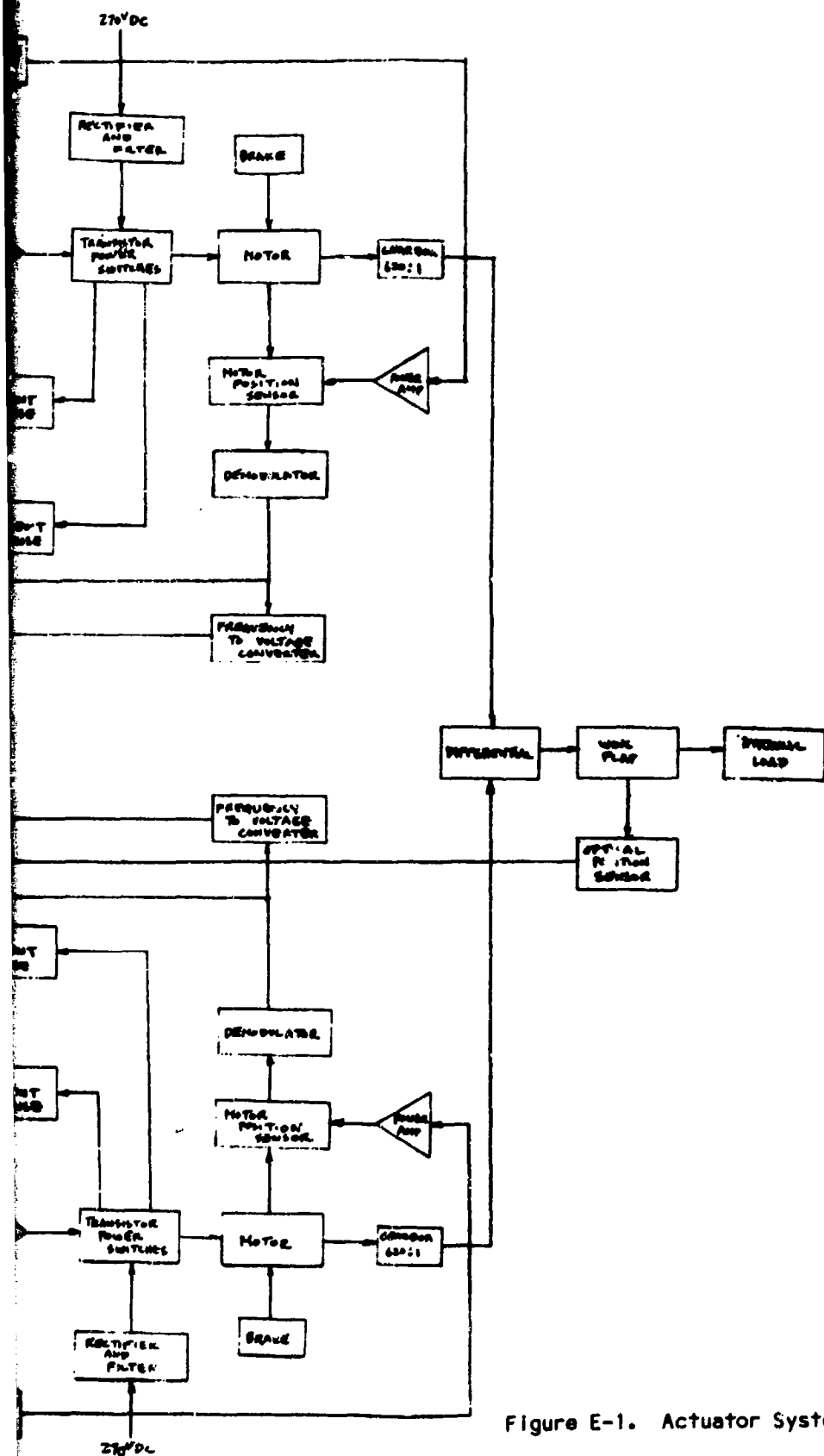
2.0 OPERATION

The microprocessor controller breadboard is composed of two independent servo-controlled channels. The servocontrollers are fabricated using Intel 8080 microprocessors manufactured by Wave Mate, Gardena, Calif. The block diagram of the breadboard is shown in Figure E-1. Each channel of the actuator consists of control and drive electronics. In the normal mode of operation, both channels are activated and both motors are operating. Each motor has independent control and drive electronics providing servocontrol and power control modes of operation, including motoring and electrical braking. If one channel fails, its motor is braked. The breadboard is powered from a rectified dc source with a nominal terminal voltage of 270 vdc.

As shown in Figure E-1, the input position command and the actuator output position feedback signals are compared by the differential amplifier. The polarity at the output of the differential amplifier is tested to determine the direction of rotation command, CW/CCW. The signal at the output of the differential amplifier is also used to develop the position error. Position error is derived by obtaining the absolute value of the signal at the output of the differential amplifier. The position error signal then is filtered by the loop compensation network to obtain the speed control signal. The speed control signal is compared with the motor velocity feedback signal to develop a pulse width modulation (PWM) signal. The PWM, current limit, and position signals are applied to the timing sequence generator. The timing sequence generator turns on the transistor power switches in synchronism with the motor position to provide current for the brushless dc motor. The motor produces a torque as required to equal the reflected hinge moment of the load.

The function of the lower of the two current signals is to protect the transistor switches against excessive currents when subjected to step input





S-20466

Figure E-1. Actuator System Block Diagram

commands. When the current exceeds this lowest current limit value, the transistor switches are turned off for a fixed time interval to allow the motor current to decay to a safe value. The upper current limit circuits, however, are used to protect the transistor switches when the actuator is subjected to plug reverse conditions. Plug reverse conditions occur when the motor is commanded to turn in one direction while it is turning in the opposite direction. When this condition occurs, the motor becomes a generator. The transistor switches then must be protected against excessive generator currents.

Both channels of the controller are functional in normal operation. Each motor is controlled essentially in the manner described above, but a motor speed correction loop also is included. The motor speed information is obtained from the motor position sensor frequency signal. The motor speed is compared with the speed command to form a velocity error signal. If the two motors are not rotating at the same angular velocity, the error signal causes the slower motor to speed up, and the faster motor to slow down. In this manner, each motor operates at the same speed, produces the same torque, and shares the load equally with the other motor.

2.1 CONTROLLER DESCRIPTION

The breadboard controller consists of a 270-vdc power source, two channels of control electronics, and an instrumentation rack. The 270-vdc power source consists of a 3-phase full-wave rectifier, a variac, an isolation transformer, and a capacitor bank. The power source is mounted on the laboratory bench. The electronics rack, which houses the two channels of electronics, consists of two inverters, power supplies, an input interface front panel, and a microprocessor development system. The functions shown in section III of the controller schematic in Figure E-2 (gray to binary conversion, digital-to-analog conversion, position error generation, CW/CCW, and voltage command generation by the absolute value circuit) are implemented both with the analog circuits and with the microprocessor. The instrumentation to monitor various system voltages, currents, and load stress is mounted in a separate rack.

2.2 DESCRIPTION OF THE ELECTRONICS SCHEMATIC

In section III of the controller schematic shown in Figure E-2, the electronics circuit for the motor position encoder consists of the 50-kHz oscillator, 19 A, and the discrete drivers Q₆ and Q₇. The 50-kHz signal from the discrete drivers is sent to the primary windings of three motor position sense transformers located around the periphery of the motor shaft.

A mechanical motor rotor position sensor connected to the motor shaft interrupts the flux linkages between the primary and secondary of the motor rotor position sensor transformers. The motor position sensor demodulator consists of ac-to-dc converters (17, 3, 15) and threshold trip circuits (16A, 18A, 18B). The demodulator circuits remove the 50-kHz carrier signals and recover the rotor position information.

Integrated circuits 33, 6, and 20 constitute the lower current limit (acceleration limit) circuit. The scale factor through the lower current sense

resistor is set to 2 amp/v. When the current through the lower current sensor resistors exceeds 14 amp, the output of the integrated circuit comparator (6) goes low to generate an inhibit command. At the same time, the delay circuit (20) is triggered and current through the lower power transistors is cut off for a fixed 140 μ sec time interval. The motor current, however, continues to flow through the upper set of flyback diodes, A40M. Integrated circuits 102, 19B, and 101 constitute the upper current limit circuit. The scale factor through the upper current sense (deceleration limit) resistors also is set to be 2 amp/v. The upper current limit threshold is set to 16 amp, 2 amp higher than the lower current limit.

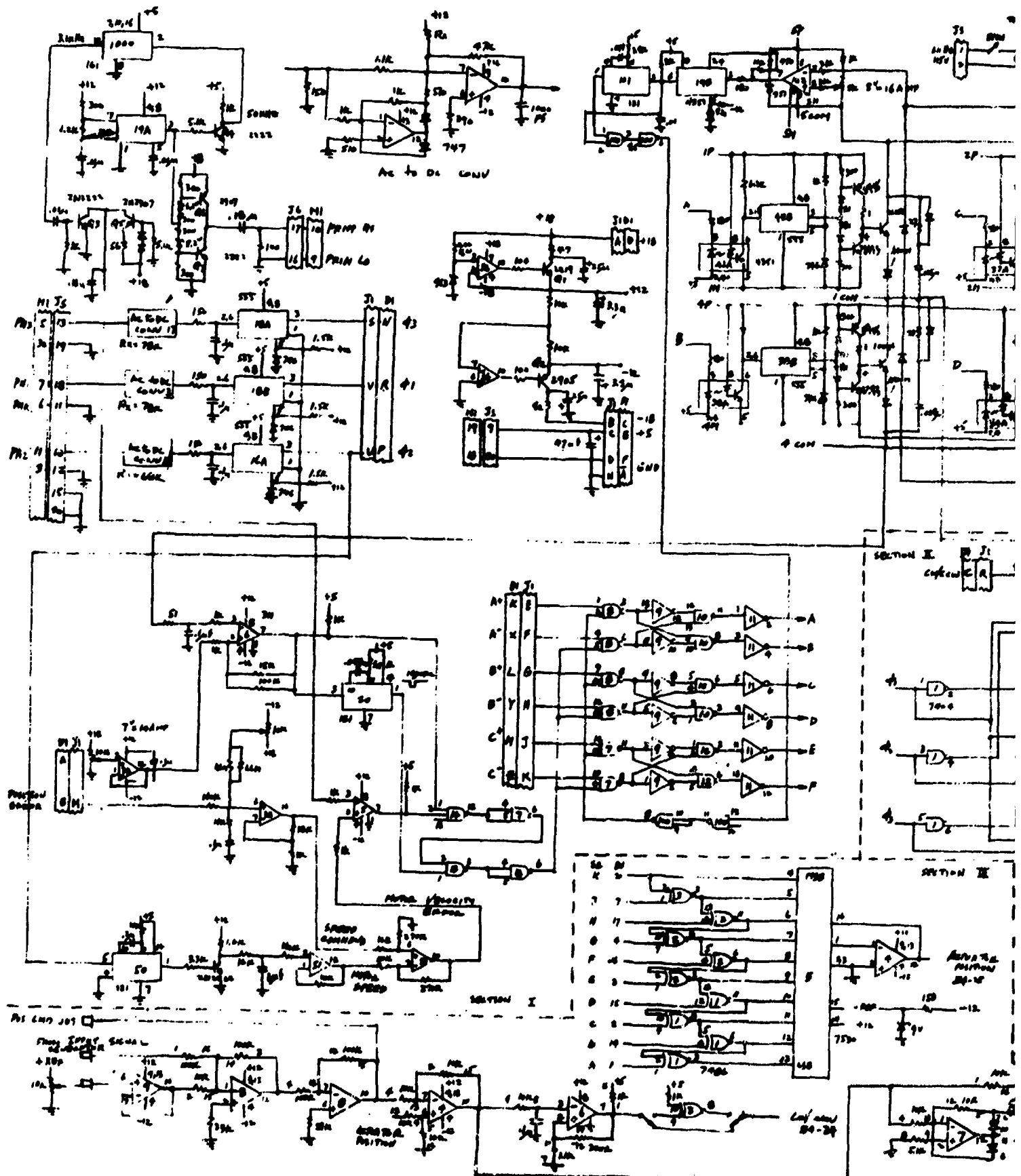
In the plug reverse condition when the motor becomes a generator, the upper switch power transistors are shut off when the current exceeds 16 amp. The generator current then flows through the upper and lower flyback diodes to regenerate into the source. Energy is returned to the source and the actuator brakes to a stop.

The timing sequence logic can be understood best by referring to the timing diagram as shown in Figure E-3. The demodulated signals from the motor position sensor are θ_1 , θ_2 , and θ_3 . The power switch drive signals A+ through C- are generated by the timing sequence generator so that the switch output relative to the back emf of the motor is as shown in Figure E-3. Torque from the brushless dc motor is maximized when the switching waveform is aligned as shown. The logic circuit shown in section I of the controller schematic, which converts A+ through C- to A through F, ensures that the upper and lower power transistor pairs are never turned on simultaneously.

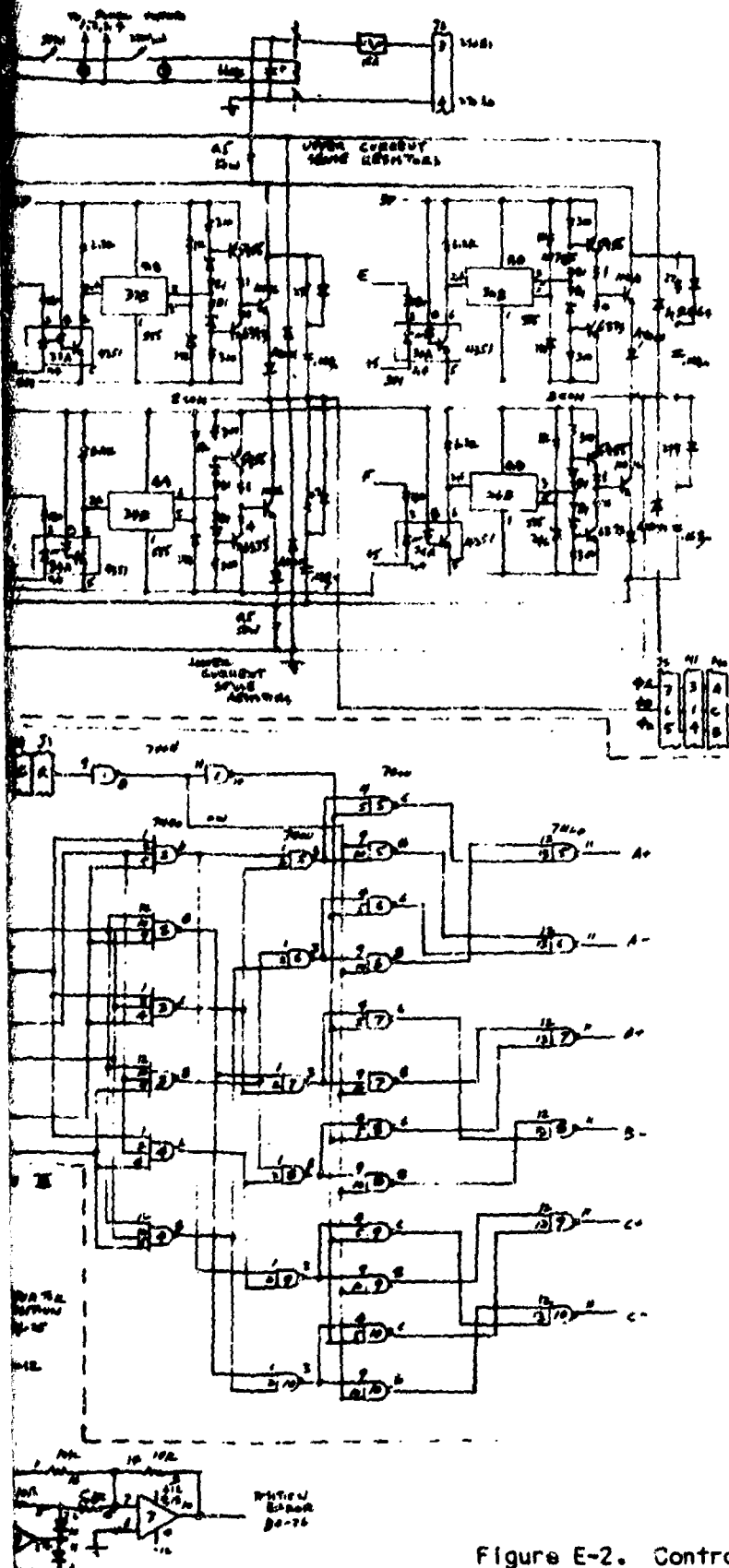
The position error detection is implemented by integrated circuits 4, 6 and 3 shown in section III and integrated circuit 33 shown in section I of the controller schematic. The input position command is compared with the actuator position feedback signal by the difference amplifier (integrated circuit 4). The comparator (integrated circuit 6) develops a CW/CCW command signal for the timing sequence generator shown in section II. The output of integrated circuit 4 also is routed to the absolute value generator (integrated circuit 7) to produce the position error signal.

The position error signal goes to the filter and gain of amplifier 18, integrated circuit 33 in section I. The output of integrated circuit 33 is the speed command. In an alternate mechanization of the position error loops, the microprocessor software development system replaces the hardware shown in section III of the controller schematic.

The velocity feedback loop is mechanized with integrated circuits 50, 51, and the PWM circuits (integrated circuits 1000, 5, and transistors Q3 and Q5). The frequency of the signal θ_2 is proportional to the speed of the motor. When the output of the fixed delay circuit (integrated circuit 50) is filtered, the resulting dc voltage represents the motor speed. The motor speed is compared with the speed command by the linear difference amplifier (integrated circuit 51). The output of the difference amplifier (the motor velocity error) is applied to the PWM comparator (integrated circuit 5). The PWM circuit consists of the counter, integrated circuit 1000, the sawtooth waveform generator, transistors Q3 and Q5, and the comparator (integrated circuit 5). The output



THIS PAGE IS BEST QUALITY PRACTICABLE
FROM COPY FURNISHED TO DDG



8-28456

Figure E-2. Controller Schematic

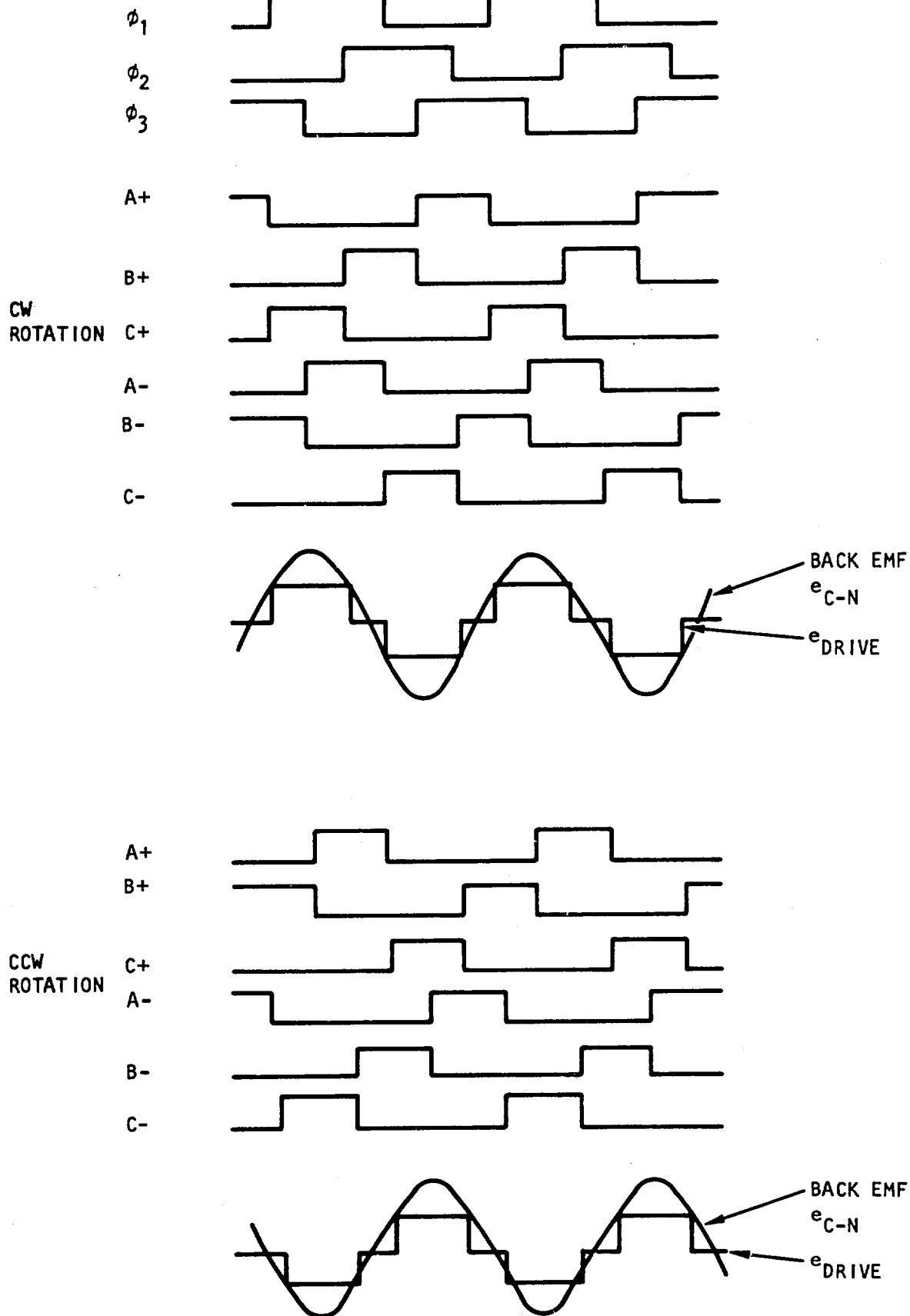


Figure E-3. Sequencer Timing Diagrams

S-25536

of the comparator is applied to the logic circuit, which in turn controls the power switch driver circuit.

The power switch driver circuits are drawn in the upper right hand section of the controller schematic. Control signals from the timing sequence generator are coupled to the power switch drivers through the 4351 optical couplers. The optical coupler outputs are connected to the 555 integrated circuit threshold trigger circuits. The 555 outputs, in turn, drive the 2N3741 and 2N3767 power switch driver transistors. One-amp base drive signals are supplied to the 10016 power transistor switches. Minus 5-v reverse bias is applied to the power switches for the turnoff conditions. The 27-ohm resistor, 0.068- μ f capacitor, and the shunt diode across the 27-ohm resistor constitute a turnoff-snubber network.

A circuit schematic of the floating power supplies 1P through 5M is shown in Figure E-4. The primary of the T1 and the input transformer for the floating power supplies for the power switch drivers are connected to the 60-Hz, 115-v line. Laboratory power supplies are used for the 18, -18, and the 5-v source.

2.3 SOLUTIONS TO PROBLEMS ENCOUNTERED DURING THE HARDWARE DEVELOPMENT PHASE

One of the first problem areas that had to be solved during the hardware development phase for the microprocessor configured controller was the design of the current limit circuits. Two functions are performed by the current limit circuits in the present design. First, the current limit circuits protect the power switch transistors from overcurrents. The overcurrent source may be either the 270-vdc power supply or the motor operating in the generator mode. Second, the current limit circuits allow the motor to stop in a minimum amount of time when subjected to plug reverse conditions. The motor is forced to stop quickly by modulating the power switch transistors with the current limit circuits and forcing the motor into a dynamic braking mode.

During dynamic braking, the energy stored in the windings is returned to the 270-vdc power source. A 13,000- μ f capacitor bank was added to the output of the 270-vdc power source to allow current to flow from the motor back to the supply. The magnitude of the voltage that the dc power source is allowed to increase from the nominal 270-vdc conditions is directly interchangeable with the size of the capacitor bank.

Another problem that had to be solved before reliable power switch transistor operation could be ensured concerned power turnon sequencing for the manual switches. The manual switches were interlocked so that the low voltage power for the controller logic power supplies were turned on before the high voltage 270-vdc power source was turned on. Capacitors were shunted directly across the power switch transistors to prevent transient voltage spikes from destroying the transistors when the 270-vdc power source was turned off. Turn-on sequencing also required that the disc brakes be released before power was turned on to prevent excessive heat of the motor.

At the beginning of the design phase, the software program was written to let the microprocessor development system perform time sequencing and speed control as well as position error loop control functions. Alignment of the

C1,5	100/35	220/16	CAPACITOR, ELECT.
C2,3	550/35	1000/16	CAPACITOR, ELECT.
C4	.001/100	.001/100	CAPACITOR, MYLAR
U1	uA723	uA723	3C VOLTAGE REGULATOR
CR1,2,3,4	AE1C	AE1C	DIODE, 1A 200V
CR5	—	1N752	DIODE, ZENER
Q1	12500-4	12500-4	TRANSISTOR, NPN
SCR1	—	50303L33	SCR 3A
R11	1K	220 Ω	RESISTOR, 1/2 W 5% CF
R12	—	47 Ω	
R2	2.2K	47 Ω	
R5	220 Ω	220 Ω	
R3	—	—	
R4	15 Ω	—	
R6	4.7K	1.6K	
R10	1.6K	3.3K	RESISTOR, 1/2 W, 5% CF
R8	1.5K	1.5K	POTENTIOMETER, 2W, WW
R9	300 Ω	6.8 Ω	RESISTOR 1/2 W 5% CF
R13	47 Ω (C.F.)	750 Ω	RESISTOR 1/2 W 5% MF
R14	—	1.10K	RESISTOR 1/2 W 5% MF
R4	—	.39 Ω	RESISTOR 2W BWH
CHASSIS	12567	12567	CHASSIS
T1	12573	12569	TRANSFORMER
P.C.B	12574	12574	P.C. BOARD

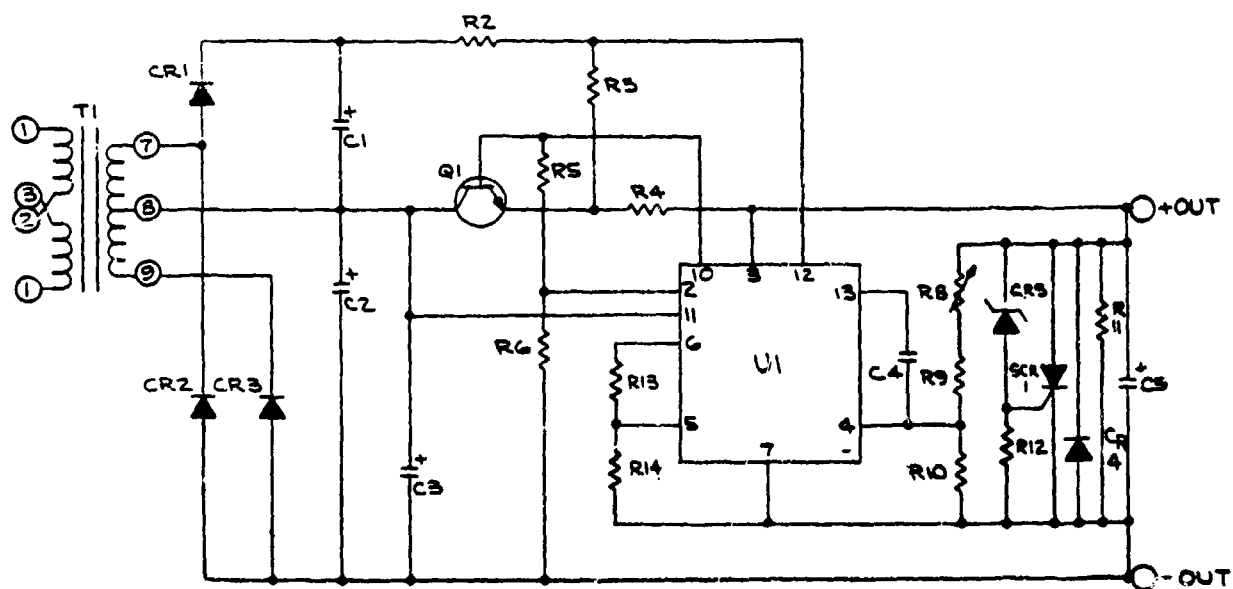


Figure E-4. Power Supply Schematic

timing sequencing commands relative to the back emf, however, was difficult due to the real time requirement of the motor switch command signals. The timing sequencing commands were implemented with discrete integrated logic chips to overcome this problem. The software interrupt mode was used initially for the speed control function. However, hardware implementation replaced the software because of noise susceptibility of the interrupt mode and use of excessive time in the program for the speed control function.

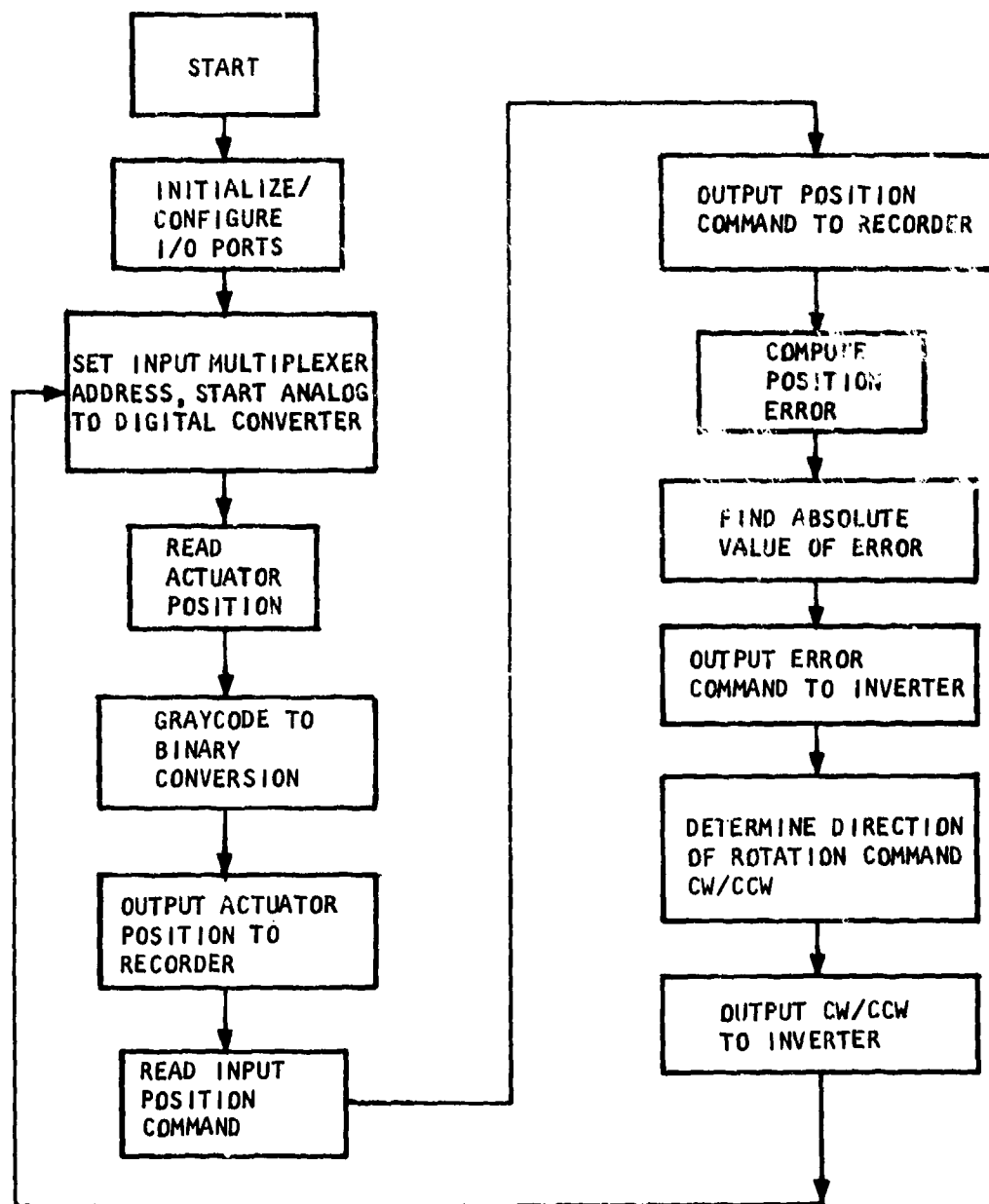
3.0 SOFTWARE DEVELOPMENT

The software was initially written to include speed torque programming and interchannel communication; however, this portion of the program was abandoned because of its complexity. The microprocessor then performed the position error loop control function, which included analog-to-digital conversion, CW or CCW command generation, and analog signal generation of input and output signals. A flow chart summarizing controller logic is shown in Figure E-5. The function of each of the subroutines in the program is summarized in Table E-1.

TABLE E-1
FUNCTIONS OF PROGRAM SUBROUTINES

<u>Subroutine</u>	<u>Function</u>
INIT	Configures and interrupts, I/O parts
START	Selects multiplex (MUX) address, starts analog-to-digital converter
FBK	Reads and stores actuator position
GRAYCO	Converts graycode to binary and outputs actuator position
READ	Reads and outputs the input position command
ERROR	Computes position error
ABS	Computes absolute value of position error and outputs error command to inverter
CWCCW	Determines CW/CCW command and outputs command to inverter

The program is written using assembly computer language.



S-29837

Figure E-5. WPAFB Actuator Controller Flow Chart

APPENDIX F

EQUIPMENT TEST PLAN
(AIRESEARCH REPORT 76-13276, Dec. 1976)

1.0 PURPOSE

1.1 INTRODUCTION

This document is submitted in accordance with the data requirements (Sequence 5) of Contract F33615-76-C-3043 issued by AFFDL of Wright-Patterson Air Force Base. This document is a test plan for the demonstration testing of an electromechanical, hingeline actuation system.

1.2 SCOPE

This plan describes the tests to be conducted on the electromechanical hingeline rotary actuation system being developed under Air Force Contract F33615-76-C-3043. The primary flight control actuation system will be tested under laboratory conditions, with installation and operating interfaces simulated to the highest extent practical.

The actuation system will be evaluated in terms of simulated interfaces with the aircraft including structural attachments, thermal provisions, and dual redundant control surface actuation. The brass board electronic controller and transistor power switches will be exercised to demonstrate maximum capability and flexibility of actuating a simulated control surface.

1.3 OBJECTIVE

The overall objective of this test program is to evaluate the components and system to determine the (1) characteristics of the electromechanical actuation system as an alternate to hydraulic actuation, and (2) satisfaction of performance goals. The following detail objectives of the test program are listed in approximate order of significance:

- a. Provide test data based upon hardware operation in known environments and controlled conditions.
- b. Demonstrate that the components are compatible as on operating actuation system.
- c. Demonstrate that the components operate in the manner predicted.

1.4 REFERENCES

- 1) Air Force Contract, F 33615-76-C-3043, Section F, Description/Specifications
- 2) AiResearch Proposal, 75, 12136, November 15, 1975, Integrated Hinge (Rotary) Electromechanical Actuation Development
- 3) Electromechanical Actuation Development Design Data Package, AiResearch Report No. 76-12943

4) Performance Specification Electromechanical Flight Control Actuation System, AiResearch Report No. 76-12942

5) AiResearch Drawings

Actuator Outline	2022194
Gearbox cross section	2022192
Motor cross section	515018
Position Decoder	2022196

2.0 TEST CONCEPTS

2.1 TEST ARTICLES

The hardware to be tested consists of components, assemblies and a system, as described below:

Component			Assembly		System Name
Name	Qty.	Part No.	Name	Part No.	
Motor	(2)	P515018	} Actuator	2022194	} Primary flight Control Hinge-Line Servo Sys.
Gearbox	(1)	2022192			
Controller	Assy.	--	--	--	
Position Encoder	(2)	2022196	--	--	

2.2 TEST PLAN

2.2.1 Flow Diagram

The overall test flow diagram is presented in Figure 1. It shows the flow of components through acceptance testing, assembly tests and full system testing. The circled numbers on the figure indicates the test brief (Section 5.0) which describes the tests to be conducted during each event.

2.2.2 Schedule

The schedule of tests is presented in Figure 2. The sequence of testing is consistent with the flow diagram of Figure 1. The major milestone of the schedule is the beginning of system tests on March 1, 1977. The total testing effort is programmed to be 7 months duration.

2.2.3 Facilities

The test program will be conducted in the existing facilities of AiResearch. Component acceptance tests will be conducted in the electronic and electromechanical laboratories. EMI evaluation will be performed in the

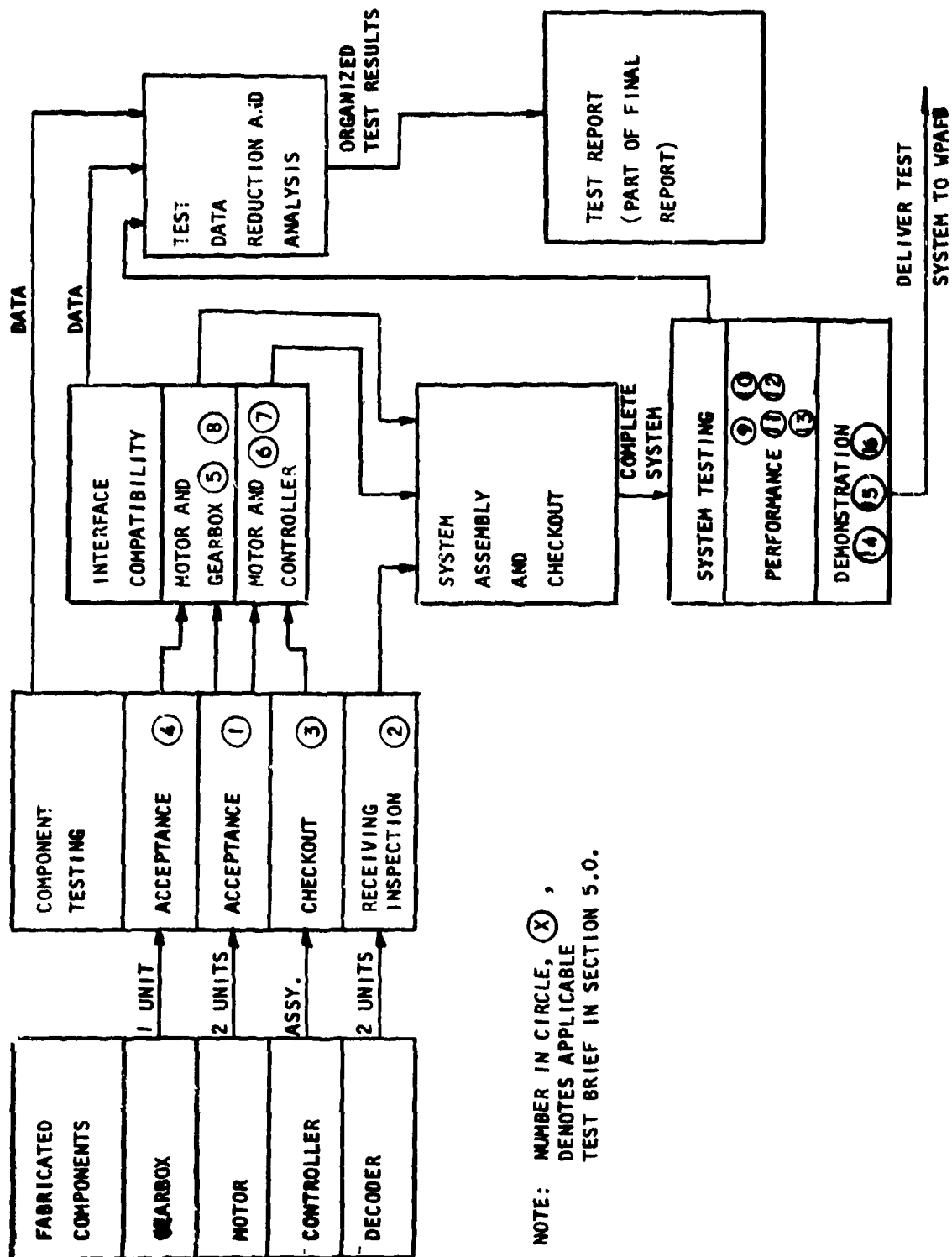


Figure 1. Test Flow Diagram

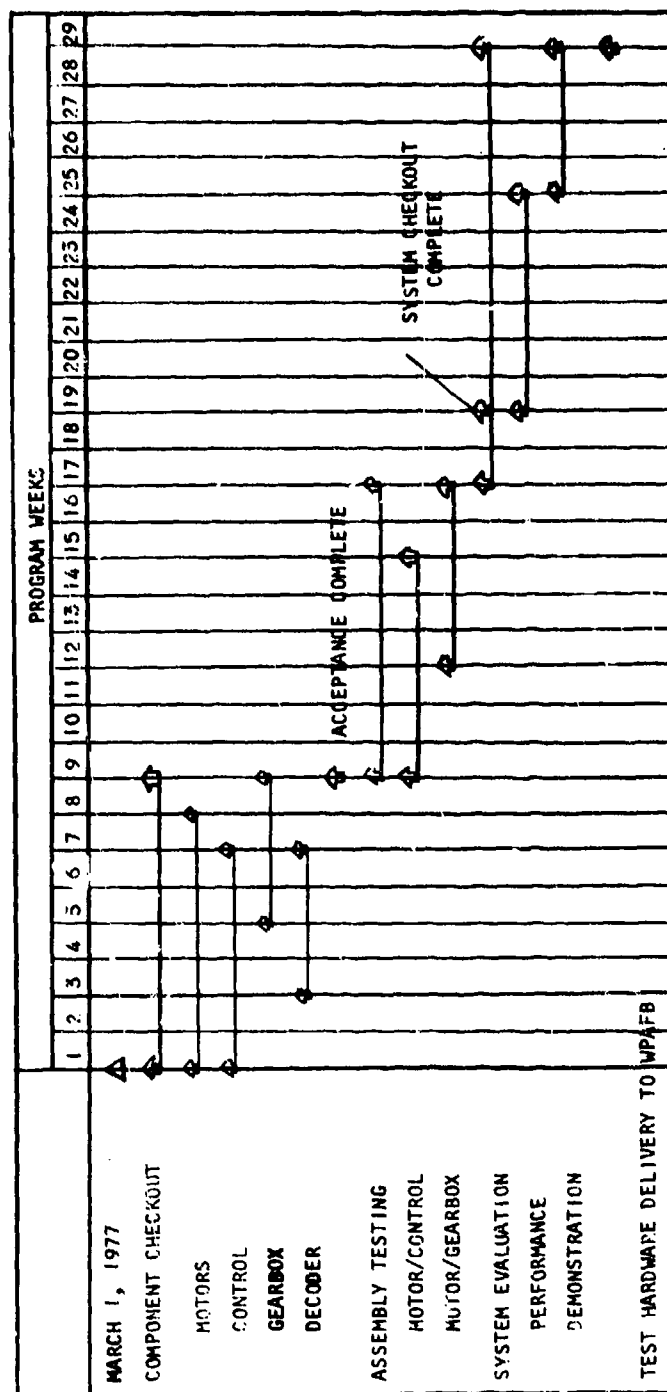


Figure 2. Test Schedule

EMI laboratory. All system testing will be conducted in the hydraulic test laboratory.

3.0 TEST REQUIREMENTS AND CRITERIA

The test requirements will be based upon the system performance defined in Reference 4. The values of performance will be used to establish the range of test conditions and results to be evaluated.

Criteria for test completion is conformance to the procedure of the test brief, and the recording of data including tolerance limits and special situations or conditions of the test. Required data and accept/reject criteria of each test is presented on the corresponding test brief.

4.0 TESTING

This paragraph describes the general approach to test of the electro-mechanical actuation system and includes discussions of the following test categories:

Functional - Component
Compatibility - System
Performance Evaluation - System
Demonstration - System

4.1 FUNCTIONAL - COMPONENT

Component testing will be conducted as shown in Figure 1, to determine performance and functional characteristics of the motor, gearbox, controller, and encoder. The component evaluation will include, for example, the acceptance test records prepared during fabrication of the motor. The controller component tests will consist of extensive operation of the equipment for evaluation and checkout of the program routines and the tabular input data. Test briefs numbered 1, 2, 3, and 4 describe these component test activities.

4.2 COMPATIBILITY - SYSTEM

The physical and function interfaces of the system elements will be evaluated. The motor, controller, and encoder will be operated to verify functional compatibility, and specifically to show that the components operate as a closed servo loop, as expected.

The motor and gearbox physical interface will be established.

Test briefs numbered 5 and 6 describe the evaluation of assemblies to be performed.

4.3 PERFORMANCE EVALUATION - SYSTEM

Certain performance evaluation tests will be conducted at the component/assembly level, and some will be conducted as a complete system.

The EMI signature evaluation, for example, will be performed using one motor and one controller channel. The purpose of the evaluation is to determine the conducted and radiated EMI, and the susceptibility to conducted EMI. The actuator will be replaced with a dynamometer to load the motor.

Static stiffness of the actuator will be evaluated by using the gearbox only. The input pinions will be locked, the output loaded, and the rotational displacement measured.

These assembly tests are described in test briefs 7 and 8.

The tests to be conducted upon the complete actuation system include the following:

<u>Test</u>	<u>Test Brief No.</u>
Frequency Response	9
Dynamic Stiffness	10
Velocity	11
Position Resolution	12
Power Efficiency	13

4.4 DEMONSTRATION-SYSTEM

This category of test provides for evaluation of the versatility and applicability of the microprocessor controlled electromechanical actuation system to various flight control problem statements.

These tests are summarized below:

<u>Test</u>	<u>Objective</u>	<u>Test Brief No.</u>
Regeneration	To evaluate the conservation of aiding load energies by the technique of electric power regeneration	14
Continuous running servo demonstration	To determine characteristics of a servo system wherein the output motion is derived from the differential action of two coordinated servo mechanisms	15
Reliability demonstration	To demonstrate the mechanism of dual channel redundancy, including operation after a single simulated fault.	16
Thermal management	To demonstrate dutycycle capability	17

5.0 TEST PROCEDURES

This section includes the test briefs describing the component, assembly, and system demonstration tests to be performed. The briefs include the following information:

- Objective
- Facility for conducting the test
- Test setup schematic
- Special instrumentation required
- Test procedure summary
- Required data to be recorded
- Criteria for acceptance or rejection of tests and any special notes.

6.0 DOCUMENTATION

Documentation of tests conducted will be included in the final report for this contract. The format of test reporting will be determined by the nature of the individual test but will include the following:

- Test results summary
- Test objective
- Test results
 - Reduced data
 - Raw data
- Discussion

THIS PAGE IS BEST QUALITY PRACTICABLE
FROM COPY FURNISHED TO DDO



TEST ①
MOTOR ACCEPTANCE

Prepared by: LUWERTE/WOOD

Part No. 5150B

Date _____

OBJECTIVE

VERIFY PERFORMANCE AND
CRITICAL DESIGN PARAMETERS.

FACILITY

ELECTROMECHANICAL
LABORATORY

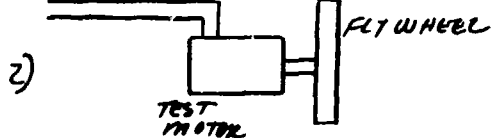
LABORATORY
DRIVE MOTOR

SCHEMATIC

TEST MOTOR



POWER FROM
CONTROLLER



EQUIPMENT AND
INSTRUMENTATION

- 1) DRIVE MOTOR
- 2) FLY WHEEL INERTIA
LOAD
- 3) SPEED SENSOR,
VOLTMETER

PROCEDURE

- a) MEASURE DIELECTRIC STRENGTH AND STATOR WINDING RESISTANCE
- b) OPERATE MOTOR AS A GENERATOR (CONFIG. 1) TO DETERMINE
FLUX LINKAGES. MAKE FINAL MECHANICAL ADJUSTMENT TO
COMMUTATOR
- c) MAKE ACCELERATION RUNS (CONFIG. 2) TO DETERMINE
TORQUE-SPEED; EFFICIENCY; AND TORQUE PER AMP.
- d) ~~WEIGH THE MOTOR~~

REQUIRED DATA

- 1) OUTPUT VOLTAGE
- 2) SPEED
- 3) NO-LOAD VOLTAGE
- 4) TIME HISTORY OF FLY WHEEL SPEED
- 5) MOTOR WEIGHT

ACCEPT/REJECT CRITERIA

GATHER PERFORMANCE
DATA.

NOTES



TEST (C)
ENCLOSURE
RECEIVING INSPECTION

Prepared by: WOOD
Part No. 2022196
Date _____

<p>OBJECTIVE</p> <p>TO VERIFY FORM AND FUNCTION OF VENDOR PART</p>	<p>FACILITY</p> <p>INSPECTION</p>
<p>SCHEMATIC</p> <p>YMF6 PART NO 25AE-12GC-7A3-C3 RENCO CORPORATION</p>	<p>EQUIPMENT AND INSTRUMENTATION</p> <p>STANDARD INSPECTION EQUIPMENT</p>
<p>PROCEDURE</p> <ol style="list-style-type: none"> 1) VERIFY PART NO'S 2) VERIFY ENVELOPE DIMENSIONS AND INTERFACE DEFINITION 3) VERIFY FUNCTION 	
<p>REQUIRED DATA</p> <p>DIMENSIONAL DATA ; CODE OUTPUT VS. SHAFT POSITION</p>	
<p>ACCEPT/REJECT CRITERIA</p> <p>MANUFACTURERS SPECIFICATION</p>	<p>NOTES</p>

1-95237

76-73876
Page 9

THIS PAGE IS BEST QUALITY PRACTICABLE
FROM COPY FURNISHED TO DDC



TEST ③
CONTROLLER
CHECK OUT

Prepared by: ASHMUE/LUDER

Part No. _____

Date _____

OBJECTIVE

VERIFY OPERATION OF INPUT-OUTPUT
CIRCUITS, SERVO LOOP, AND SWITCH MODULES.

FACILITY

ELECTRONICS
LABORATORY

SCHEMATIC

- 1) CONTROLLER CONSISTS OF 2-CHANNEL
MICROPROCESSOR BY WAVE-MATE, AND
FABRICATED 2-CHANNEL TRANSISTOR
BRIDGE FOR SWITCHING POWER TO
MOTOR WINDINGS.
- 2) BREDBOARD HARDWARE TO BE
MOUNTED IN INSTRUMENT RACK, INCLUDING
CRT DISPLAY AND KEYBOARD.

EQUIPMENT AND
INSTRUMENTATION

PROCEDURE

- BREDBOARD DEVELOPMENT TO INCLUDE
- 1) CIRCUIT DESIGN AND CHECKOUT
 - 2) PROGRAM CHECKOUT
 - 3) OPERATION OF CONTROLLER WITH SIMULATED
MOTOR LOAD.

REQUIRED DATA

ACCEPT/REJECT CRITERIA

ENGINEERING
ACCEPTANCE

NOTES

THIS PAGE IS BEST QUALITY PRACTICES
FROM COPY FURNISHED TO DDC



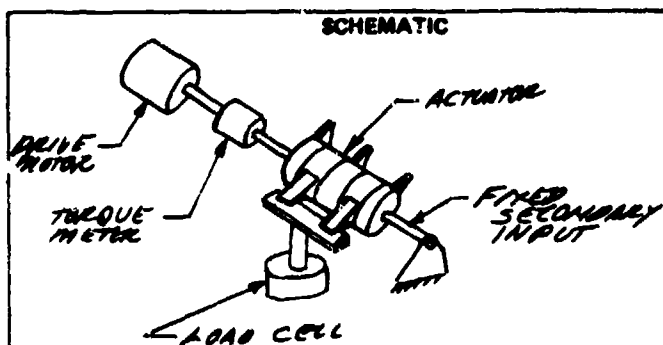
TEST ④
ROTARY GEAR BOX
ACCEPTANCE

Prepared by: STARKS/LINDPart No. 2022192

Date _____

OBJECTIVE
TO DETERMINE FUNCTIONAL
CHARACTERISTICS OF GEAR BOX

FACILITY
ELECTROMECHANICAL
LABORATORY



EQUIPMENT AND
INSTRUMENTATION
DRIVE MOTOR
TORQUE METER
SHAFT PIN
LOAD CELL

- PROCEDURE
- 1) WITH ONE INPUT LOCKED, OPERATE DRIVE MOTOR AND MEASURE INPUT TORQUE AND OUTPUT TORQUE
 - 2) REVERSE ACTUATOR AND DRIVE SECONDARY INPUT WITH PRIMARY INPUT LOCKED
 - 3) WEIGH ACTUATOR GEAR BOX.

- REQUIRED DATA
- 1) PRIMARY SHAFT INPUT TORQUE VS. OUTPUT TORQUE
 - 2) SECONDARY SHAFT INPUT TORQUE VS. OUTPUT TORQUE
 - 3) WEIGHT

ACCEPT/REJECT CRITERIA
ENGINEERING
ACCEPTANCE

NOTES
GEAR RATIO CAN BE
DETERMINED BY CHECK TO
PRINT PRIOR TO ASSEMBLY,
AND TOOTH COUNT.

S-95237

96-13176
Page 11

THIS PAGE IS BEST QUALITY PRACTICABLE
FROM COPY FURNISHED TO DDO



TEST (5)
MOTOR AND GEAR BOX
COMPATIBILITY

Prepared by: WOODPart No. 2022194

Date _____

OBJECTIVE

VERIFY INTERFACE AND FUNCTIONAL
COMPATIBILITY

FACILITY

ELECTRO MECHANICAL
LABORATORY

SCHEMATIC

EQUIPMENT AND
INSTRUMENTATION

1) STANDARD LABORATORY
EQUIPMENT AND
FIXTURES.

2) ONE MOTOR

3) GEAR BOX

PROCEDURE

- 1) ASSEMBLY MOTOR TO ONE END OF GEAR BOX
- 2) OPERATE MOTOR TO VERIFY GEAR BOX OUTPUT MOTION
- 3) REMOVE MOTOR FROM GEAR BOX
- 4) ASSEMBLY MOTOR TO OPPOSITE END OF GEAR BOX
- 5) OPERATE MOTOR TO VERIFY GEAR BOX OUTPUT MOTION

REQUIRED DATA

- 1) PHYSICAL INTERFACE COMPATIBILITY CHECK, BOTH CHANNELS
- 2) FUNCTIONAL OPERATION CHECK, BOTH CHANNELS.

ACCEPT/REJECT CRITERIA

ENGINEERING
ACCEPTANCE

NOTES

5-95237

76-13276
Page 12

THIS PAGE IS BEST QUALITY PRACTICABLE
FROM COPY FURNISHED TO DDO



TEST
MOTOR AND CONTROLLER
COMPATIBILITY

Prepared by: Ashman/Wood

Part No. _____

Date _____

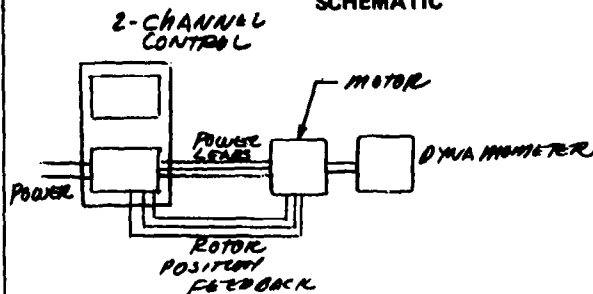
OBJECTIVE

VERIFY DRIVE CIRCUITS FOR
MOTOR CONTROL.

FACILITY

ELECTROMECHANICAL
LABORATORY

SCHEMATIC



EQUIPMENT AND
INSTRUMENTATION

- 1) 2-CHANNEL control
- 2) MOTOR
- 3) DYNAMOMETER

PROCEDURE

- 1) OPERATE CONTROLLER TO VERIFY COMPATIBILITY WITH MOTOR
- 2) EXERCISE ALL FEATURES SUCH AS CURRENT LIMIT, RATE AND TORQUE LIMIT, AND VERIFY LIMITING PROVISIONS SUCH AS MINIMUM CURRENT, VOLTAGE AND SPEED
- 3) OPERATE MOTOR AT MAXIMUM CURRENT LIMIT, (APPROXIMATELY 17 AMPS).

REQUIRED DATA

ENGINEERING VERIFICATION OF MOTOR/CONTROLLER
OPERATIONAL COMPATIBILITY.

ACCEPT/REJECT CRITERIA

ENGINEERING
EVALUATION OF
PROPER OPERATION

NOTES

S-95237

76-13276
Page 12

THIS PAGE IS BEST QUALITY PRACTICABLE
FROM COPY FURNISHED TO DDO



TEST 7
EMI SIGNATURE

Prepared by: K.N. DULLACK

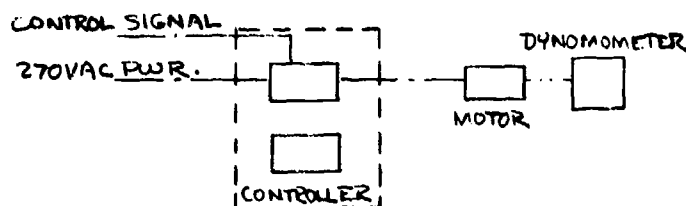
Part No. _____

Date 12-10-76**OBJECTIVE**

DEFINE SIGNATURE OF EMI CONDUCTED
AND SUSEPTABILITY TO CONDUCTED EMI

1. LITY

EMI LABORATORY
FACILITY 901

SCHEMATIC

SINGLE CHANNEL EVALUATION

**EQUIPMENT AND
INSTRUMENTATION**

1. RADIATED SIGNAL (dB)
2. OSCILLOGRAPH
3. PULSE GENERATOR
4. OSCILATOR
5. DYNOMOMETER
6. POWER SUPPLY
7. MOTOR & CONTROL
FROM COMPATIBILITY
EVALUATION.

PROCEDURE

1. PERFORM TEST IN ACCORDANCE WITH MIL-STD-461
2. PARAMETERS DEFINED PER MIL-STD-462
3. OPERATE ACTUATOR AT ZERO AND ONE HALF LOAD
AT 50% MAXIMUM RATE, AND AT ONE HALF LOAD
AND 8 HZ RATE.

REQUIRED DATA

OSCILLOSCOPE PICTURES DURING MOTOR ACCELERATION
SIGNATURE OF CONDUCTED EMI EFFECTS ON POWER LEADS
CONDUCTED SUSEPTABILITY OF EMI ON INPUT LEADS.

ACCEPT/REJECT CRITERIA

TEST
DEMONSTRATION
ONLY.

NOTES

RADIATED EMI IS NOT EVALUATED
SINCE THIS IS A FUNCTION OF THE
PACKAGE CONFIGURATION. THE
BREADBOARD CONTROLLER WILL NOT
BE OF FLIGHT CONFIGURATION.

1-95237

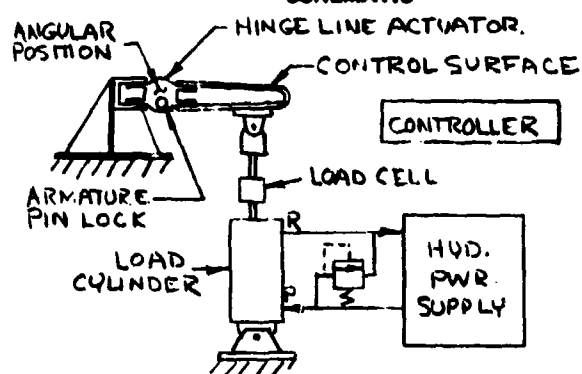
76-13876
Page 14



TEST 8 STIFFNESS

Prepared by: K.N. DULLACK

Part No. _____

Date 12-16-76**OBJECTIVE**TO DEMONSTRATE THE
SPRING RATE OF THE ACTUATOR**FACILITY**ELECTROMECHANICAL
LABORATORY
FACILITY 801**SCHEMATIC****EQUIPMENT AND
INSTRUMENTATION**

1. REACTION FIXTURE
2. HYD. LOAD SYSTEM
3. ARMATURE PIN LOCK
4. ANGULAR POSITION
5. LOAD CELL
6. X-Y PLOTTER

PROCEDURE

1. INSTALL ACTUATOR WITH ARMATURE LOCK PINS IN POSITION.
2. APPLY INCREASING LOAD TO CONTROL SURFACE: FROM 0 TO 50% RATED LOAD THEN DECREASE TO 0 LOAD.

REQUIRED DATACONTROL SURFACE POSITION (θ) VS. LOAD (LBS.)**ACCEPT/REJECT CRITERIA**TEST
DEMONSTRATION
ONLY**NOTES**

THIS PAGE IS BEST QUALITY PRACTICABLE
FROM COPY FURNISHED TO DDG



TEST 9
FREQUENCY RESPONSE

Prepared by: KINDULLACK

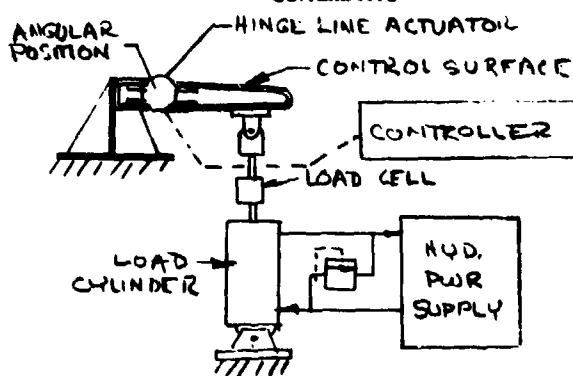
Part No. _____

Date 12-16-76**OBJECTIVE**

TO DETERMINE THE AMPLITUDE
RATIO AND THE PHASE ANGLE VS. FREQ.

FACILITY

ELECTROMECHANICAL
LABORATORY
FACILITY 801

SCHEMATIC**EQUIPMENT AND
INSTRUMENTATION**

1. OSCILLOGRAPH
2. SINE WAVE GEN.
3. POSITION INDICATOR
4. REACTION FIXTURE
5. HYD. LOAD SYSTEM
6. LOAD CELL

PROCEDURE

1. SUPERIMPOSE AN INPUT COMMAND RATE OF 1, 5, 10 AND 15 HZ AND ± 0.5 , ± 1.0 AND ± 5.0 DEGREES AMPLITUDE IN CONJUNCTION WITH ZERO AND 10% RATED LOAD

REQUIRED DATA

INPUT RATE (HZ), INPUT AMPLITUDE (MV), OUTPUT POSITION (θ)
OUTPUT LOAD (LBS)

ACCEPT/REJECT CRITERIA

TEST
DEMONSTRATION
ONLY

NOTES

1-9237

76-13776
Page 16

THIS PAGE IS BEST QUALITY PRACTICABLE
FROM COPY FURNISHED TO DDO



TEST 10 DYNAMIC STIFFNESS

Prepared by: A.N. DULLACK

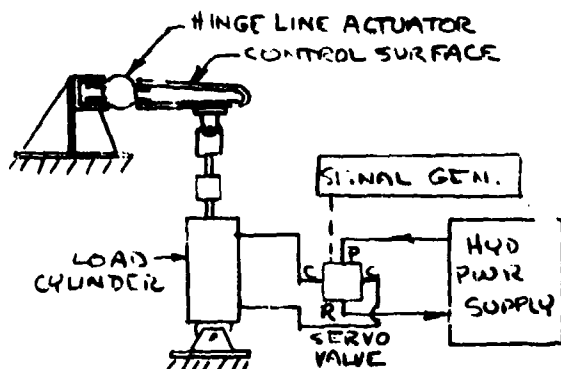
Part No. _____

Date 12-16-76**OBJECTIVE**

TO DEMONSTRATE THE DYNAMIC STABILITY
OF THE ACTUATION SYSTEM WHEN SUBJECTED
TO FLUCTUATING EXTERNAL LOADS.

FACILITY

ELECTROMECHANICAL
LABORATORY
FACILITY 801

SCHEMATIC**EQUIPMENT AND
INSTRUMENTATION**

1. SERVO CONTROLLED
LOAD SYSTEM
2. OSCILLOGRAPH
3. SIGNAL GENERATOR
4. POSITION INDICATOR
5. REACTION FIXTURE
6. LOAD CELL

PROCEDURE

1. MAINTAIN THE CONTROLLER ELECTRICALLY INACTIVE
2. APPLY 15, 25 AND 35% RATED LOAD AT
1 TO 15 Hz IN 3 Hz INCREMENTS.

REQUIRED DATA

CONTROL SURFACE POSITION (°) MOTOR CURRENT & VOLTAGE

ACCEPT/REJECT CRITERIA

TEST
DEMONSTRATION
ONLY

NOTES

1-95237

16-73276
Page 17

THIS PAGE IS BEST QUALITY PRACTICABLE
FROM COPY FURNISHED TO DDO



TEST II STEP RESPONSES

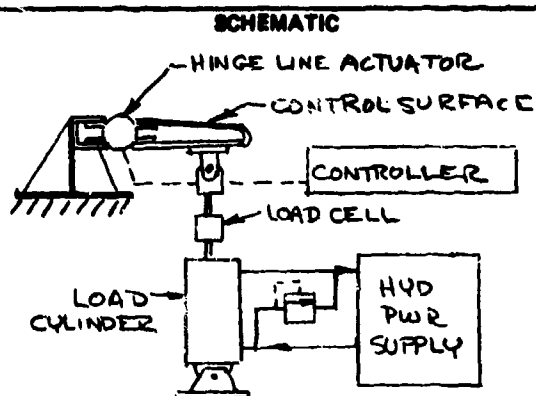
Prepared by: K.N. DULLACK

Part No. _____

Date 12-16-76

OBJECTIVE
TO DETERMINE THE QUALITY OF
TRANSIENT RESPONSE TO STEP
INPUTS

FACILITY
ELECTROMECHANICAL
LABORATORY
FACILITY 801



**EQUIPMENT AND
INSTRUMENTATION**
1. HYDRAULIC LOAD
SYSTEM
2. OSCILLOGRAPH
3. SIGNAL GENERATOR
4. POSITION INDICATOR
5. REACTION FIXTURE
6. LOAD CELL

- PROCEDURE**
1. APPLY STEP INPUT COMMANDS TO EXTEND THE ACTUATOR TO DEFLECTIONS OF 1, 5, 10 AND 20 DEG, WHILE OPERATING INTO OPPOSING LOADS OF 0, 15, 25, AND 35 PERCENT OF RATED CAPABILITY.

REQUIRED DATA
LOAD (LBS), POSITION (θ), VELOCITY ($\frac{d\theta}{dt}$), ACCELERATION ($\frac{d^2\theta}{dt^2}$)
MOTOR CURRENT AND VOLTAGE

ACCEPT/REJECT CRITERIA

TEST
DEMONSTRATION
ONLY.

NOTES

- 1) DATA TO BE RECORDED ON OSCILLOGRAPH TO OBTAIN TIME HISTORIES
- 2) RATE CAPABILITY OF ACTUATOR CORRESPONDS TO 37,500 LB-IN TORQUE

1-95237

76-13276, REV 1
Page 18



TEST 12 POSITION RESOLUTION

Prepared by: K. N. DULLACK

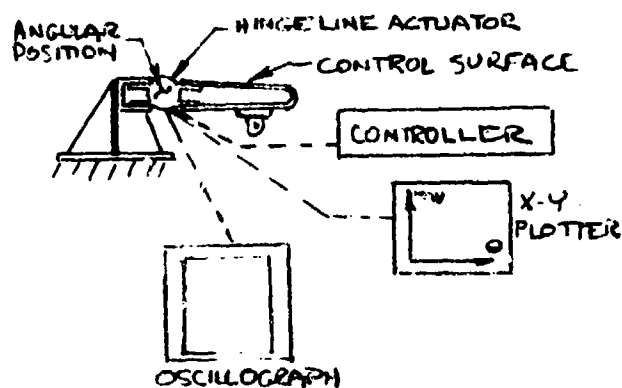
Part No. _____

Date 12-12-76**OBJECTIVE**

TO DETERMINE THE HYSTERESIS BAND BETWEEN THE INPUT COMMAND AND THE CONTROL SURFACE POSITION.

FACILITY

ELECTROMECHANICAL
LABORATORY
FACILITY 801

SCHEMATIC**EQUIPMENT AND INSTRUMENTATION**

1. REACTION FIXTURE
2. OSCILLOGRAPH
3. SIGNAL GENERATOR
4. X-Y PLOTTER
5. POSITION INDICATOR

PROCEDURE

1. DEPLOY ACTUATOR LINEARLY TO + 30 DEG, REVERSE TO -35 DEG, THEN TO 0 DEG, AT NO LOAD RECORD HYSTERESIS.
2. APPLY A TRIANGULAR WAVE INPUT AT .1 AND 5 HZ AND ± 10 DEG, ± 20 DEG, AND ± 30 DEG, PLOT DATA ON OSCILLOGRAPH.

REQUIRED DATA

INPUT COMMAND(MV)(HZ) ANGULAR POSITION(θ) PHASE(ϕ)

ACCEPT/REJECT CRITERIA

TEST
DEMONSTRATION
ONLY

NOTES

THIS TEST MAY BE
PERFORMED IN CONJUNCTION
WITH FREQUENCY RESPONSE



TEST 13 POWER EFFICIENCY

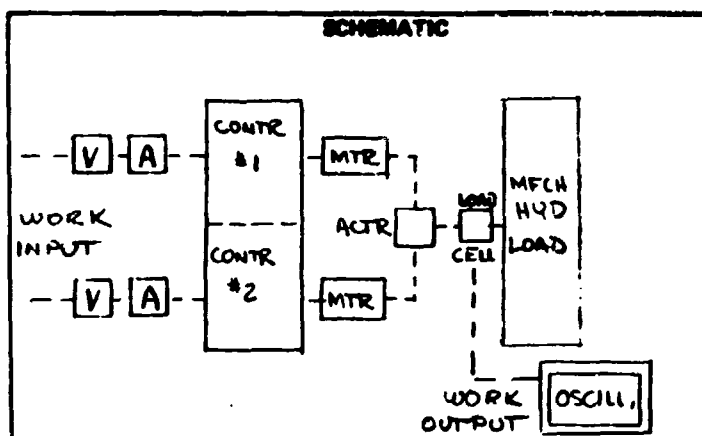
Prepared by: K. N. DULLACK

Part No. _____

Date 12-17-76

OBJECTIVE
TO DETERMINE THE ENERGY
INPUT VS. OUTPUT RELATIONSHIP

FACILITY
ELECTROMECHANICAL
LABORATORY
FACILITY 803



EQUIPMENT AND INSTRUMENTATION

1. HYD. SPRING LOAD
2. OSCILLOGRAPH
3. SIGNAL GENERATOR
4. POSITION INDICATOR
5. ELECT. INST.
6. LOAD CELL

PROCEDURE

1. VARY INPUT COMMANDS BETWEEN ± 1 DEG. AND ± 10 UFG. AND AT .1 HZ TO 10 HZ.
2. COMPARE INPUT POWER VS. OUTPUT POWER.

REQUIRED DATA

INPUT POWER (VOLTS)(AMPS), LOAD (LBS), ELAPSED TIME
POSITION (G)

ACCEPT/REJECT CRITERIA

TEST
DEMONSTRATION
ONLY

NOTES

INTEGRATE THE LOAD/TIME
TRACE WITH RESPECT TO
POSITION TO DETERMINE
OUTPUT POWER

1-55137

76-13276
Page 20



TEST 14 REGENERATION

Prepared by: K.N. DULLACK

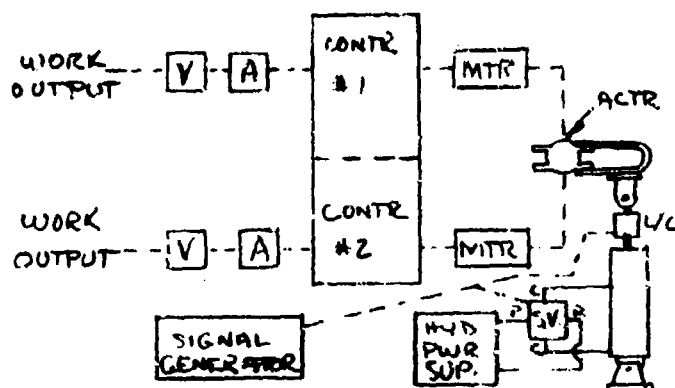
Part No. _____

Date 12-12-76**OBJECTIVE**

TO DETERMINE THE OPERATING
CHARACTERISTICS AS A GENERATOR
WHEN BACK DRIVEN.

FACILITY

ELECTROMECHANICAL
LABORATORY
FACILITY 801

SCHEMATIC**EQUIPMENT AND
INSTRUMENTATION**

1. SERVO CONTROLLED
LOAD SYSTEM
2. OSCILLOGRAPH
3. SIGNAL GENERATOR
4. POSITION INDICATOR
5. REACTION FIXTURE
6. LOAD CELL
7. ELECTRICAL INST.
8. ELECTRICAL LOAD.

PROCEDURE

1. APPLY A LOW FREQUENCY INPUT, 0.1 HZ AND 2 HZ
AT 20% RATED LOAD, TO THE CONTROL SURFACE
AT ± 5 DEGREE AMPLITUDES.
2. DETERMINE NO LOAD OUTPUT VOLTAGE AND
VARIOUS LOADED OUTPUTS.

REQUIRED DATA

POSITION (θ) LOAD (LBS) VOLTAGE, CURRENT

ACCEPT/REJECT CRITERIA

TEST
DEMONSTRATION
ONLY

NOTES

1-9237

76-13276
Page 21

THIS PAGE IS BEST QUALITY PRACTICABLE
FROM COPY FURNISHED TO DDO



TEST 15
CONTINUOUS RUNNING
SERVO DEMONSTRATION

Prepared by: K.N. DULLACK

Part No. _____

Date 12-12-76

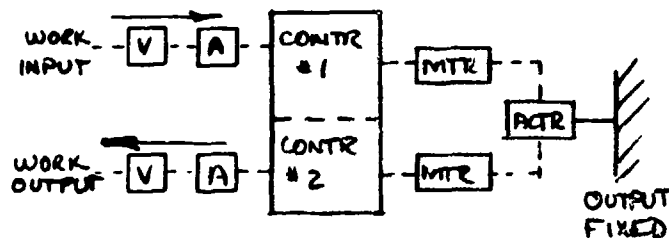
OBJECTIVE

TO DETERMINE THE REGENERATION
EFFECTIVENESS AS A SYSTEM WITH
THE CONTROL SURFACE LOCKED.

FACILITY

ELECTROMECHANICAL
LABORATORY
FACILITY 801

SCHEMATIC



**EQUIPMENT AND
INSTRUMENTATION**

1. REACTION FIXTURE
2. OSCILLOGRAPH
3. ELECTRICAL INST.

PROCEDURE

1. LOCK THE CONTROL SURFACE IN POSITION
2. COMMAND SYSTEM No.1 TO DRIVE CONTINUOUSLY
3. FEED THE GENERATED OUTPUT OF SYSTEM No.2
BACK INTO THE POWER SUPPLY.
4. COMPARE ELECTRICAL POWER ON BOTH SYSTEMS.

REQUIRED DATA

VOLTAGE, CURRENT

ACCEPT/REJECT CRITERIA

TEST
DEMONSTRATION
ONLY

NOTES

NO BACK DEVICE REMOVED
FROM SYSTEM No 2 FOR
DURATION OF THIS TEST.



TEST 16 RELIABILITY MANAGEMENT DEMONSTRATION

Prepared by: K.N. DULLACK

Part No. _____

Date 12-17-76

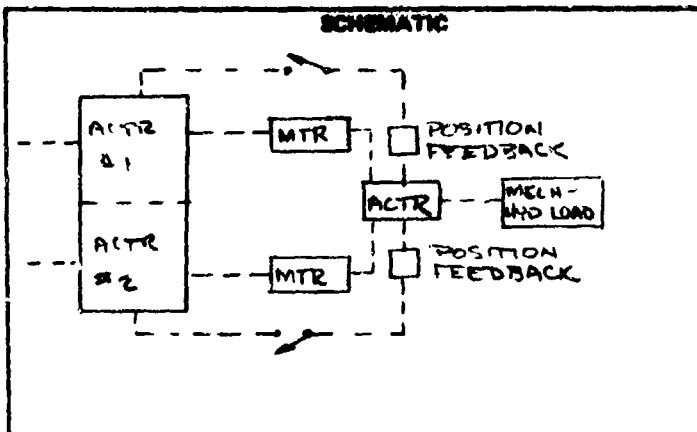
OBJECTIVE

TO DEMONSTRATE THE RESULTING
CONTROL SURFACE ACTION AS THE
FEEDBACK LOOP IS DISABLED

FACILITY

ELECTROMECHANICAL
LABORATORY
FACILITY 801

SCHEMATIC



EQUIPMENT AND INSTRUMENTATION

1. REACTION FIXTURE
2. HYD. LOAD SYSTEM
3. OSCILLOGRAPH
4. SIGNAL GENERATOR
5. POSITION INDICATOR
6. LOAD CELL
7. ELECTRICAL INST.

PROCEDURE

1. OPERATE CONTROL SYSTEM AT 1 HZ AND ± 5 DEGREES WITH 20% RATED LOAD.
2. INTERRUPT THE FEEDBACK CIRCUIT AND RECORD SYSTEM RESPONSE ON OSCILLOGRAPH.
3. REPEAT TEST WHILE OPERATING ONLY ONE SYSTEM.

REQUIRED DATA

POSITION (G) VOLTAGE, CURRENT, LOAD (LBS)
ELAPSED TIME (SEC), INTERRUPT SIGNAL

ACCEPT/REJECT CRITERIA

TEST
DEMONSTRATION
ONLY

NOTES

4-3311

76-13276
Page 23

THIS PAGE IS BEST QUALITY PRACTICABLE
FROM COPY FURNISHED TO DDQ



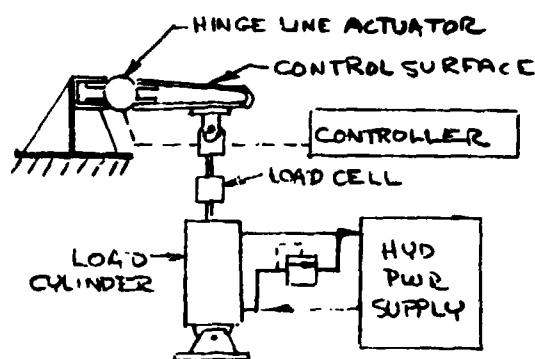
TEST 17
THERMAL MANAGEMENT

Prepared by: WOOD
Part No. 575787M
Date 1-25-77

OBJECTIVE
TO EVALUATE THERMAL CHARACTERISTICS
OF MOTOR AND GEARBOX DURING
SIMULATED DUTY CYCLE LOADS.

FACILITY
ELECTROMECHANICAL
LABORATORY
FACILITY 801

SCHEMATIC



EQUIPMENT AND
INSTRUMENTATION

1. HYDRAULIC LOAD SYSTEM
2. OSCILLOGRAPH
3. SIGNAL GENERATOR
4. POSITION INDICATOR
5. REACTION FIXTURE
6. LOAD CELL
7. TEMPERATURE SENSORS FOR MOTOR AND ACTUATOR

PROCEDURE

- 1) APPLY ± 2 deg sine wave position at 6 Hz frequency
- 2) INCREASE LOAD UNTIL 1 AMP RMS MOTOR CURRENT IS REACHED
- 3) MINUTE MOTOR R/W GEAR BOX TEMPERATURE UNTIL STEADY STATE IS REACHED
- 4) REPEAT (2) and (3) WITH LOADS INCREASED TO YIELD RMS CURRENT LEVELS OF 2, 4, 8 AND 16 AMPS.

REQUIRED DATA

- 1) LOAD CELL OUTPUT, CONTROL SURFACE POSITION, MOTOR CURRENT, MOTOR VOLTAGE

ACCEPT/REJECT CRITERIA

NO DISCREPANCY ONLY

NOTES

- 1) DATA TO BE RECORDED ON OSCILLOGRAPH
- 2) AT HIGH CURRENT LEVELS, 8 AND 16 AMPS, MONITOR TEMPERATURE CLOSELY TO PREVENT OVERHEATING OF COMPONENTS.

APPENDIX G
PREDICTED PERFORMANCE

The actuation unit digital simulation program was used to predict representative response to input commands (refer to para. 3.5). Table G-1 presents an index to the conditions used as input parameters for evaluation. The results of analysis are shown on the pages following the table.

TABLE G-1
INDEX TO PREDICTED PERFORMANCE RESULTS

Figure Number	Figure Title	Waveform	Amplitude, deg	Frequency, Hz
G-1	Single Channel Step Response, No-Load	Square	1	--
G-2	Single Channel Step Response, No-Load	Square	5	--
G-3	Single Channel Step Response, No-Load	Square	10	--
G-4	Single Channel Frequency Response, No Load	Sinusoid	± 1	0.5
G-5	Single Channel Frequency Response, No Load	Sinusoid	± 1	1
G-6	Single Channel Frequency Response, No Load	Sinusoid	± 1	2
G-7	Single Channel Frequency Response, No Load	Sinusoid	± 1	4
G-8	Single Channel Frequency Response, No Load	Sinusoid	± 1	6
G-9	Single Channel Frequency Response, No Load	Sinusoid	± 1	8
G-10	Single Channel Frequency Response, No Load	Sinusoid	± 1	10
G-11	Dual Channel Step Response, No Load	Square	1	--
G-12	Dual Channel Step Response, No Load	Square	5	--
G-13	Dual Channel Step Response, No Load	Square	10	--
G-14	Dual Channel Step Response, No Load	Square	30	--
G-15	Dual Channel Frequency Response, No Load	Sinusoid	± 1	0.5
G-16	Dual Channel Frequency Response, No Load	Sinusoid	± 1	1
G-17	Dual Channel Frequency Response, No Load	Sinusoid	± 1	2
G-18	Dual Channel Frequency Response, No Load	Sinusoid	± 1	4
G-19	Dual Channel Frequency Response, No Load	Sinusoid	± 1	6
G-20	Dual Channel Frequency Response, No Load	Sinusoid	± 1	8
G-21	Dual Channel Frequency Response, No Load	Sinusoid	± 1	10
G-22	Dual Channel Frequency Response, 50 Percent Load	Sinusoid	± 1	0.5
G-23	Dual Channel Frequency Response, 50 Percent Load	Sinusoid	± 1	1
G-24	Dual Channel Frequency Response, 50 Percent Load	Sinusoid	± 1	2
G-25	Dual Channel Frequency Response, 50 Percent Load	Sinusoid	± 1	4
G-26	Dual Channel Frequency Response, 50 Percent Load	Sinusoid	± 1	6
G-27	Dual Channel Frequency Response, 50 Percent Load	Sinusoid	± 1	8
G-28	Dual Channel Frequency Response, 50 Percent Load	Sinusoid	± 1	10
G-29	Dual Channel Dynamic Stiffness, 10 Percent Load	Sinusoid	0.05	0.5
G-30	Dual Channel Dynamic Stiffness, 10 Percent Load	Sinusoid	0.054	1
G-31	Dual Channel Dynamic Stiffness, 10 Percent Load	Sinusoid	0.074	2
G-32	Dual Channel Dynamic Stiffness, 10 Percent Load	Sinusoid	0.062	4
G-33	Dual Channel Dynamic Stiffness, 10 Percent Load	Sinusoid	0.082	8
G-34	Dual Channel Dynamic Stiffness, 10 Percent Load	Sinusoid	0.18	16
G-35	Dual Channel Dynamic Stiffness, 10 Percent Load	Sinusoid	0.19	32

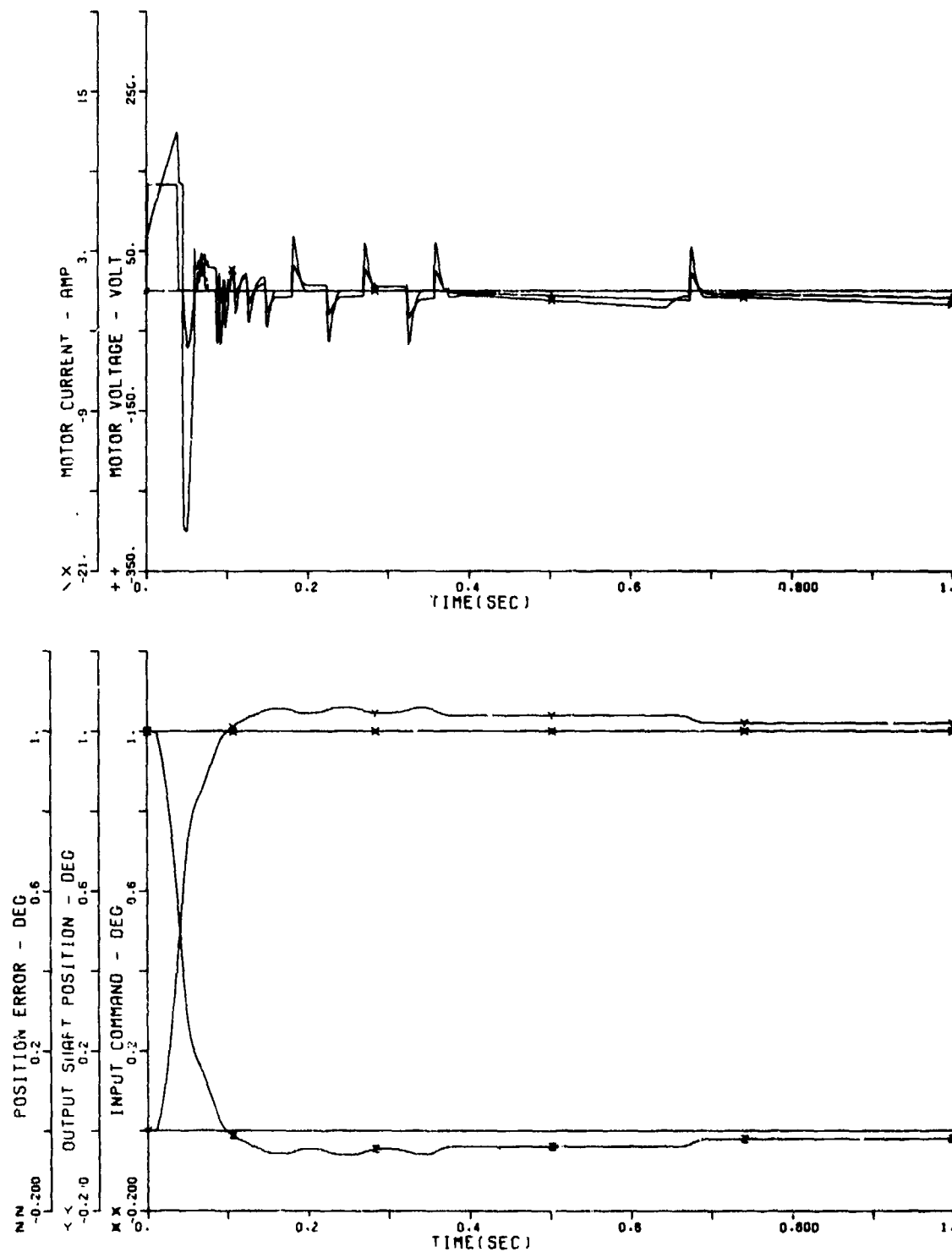


Figure G-1. Single-Channel Step Response
at No Load and 1-deg Step

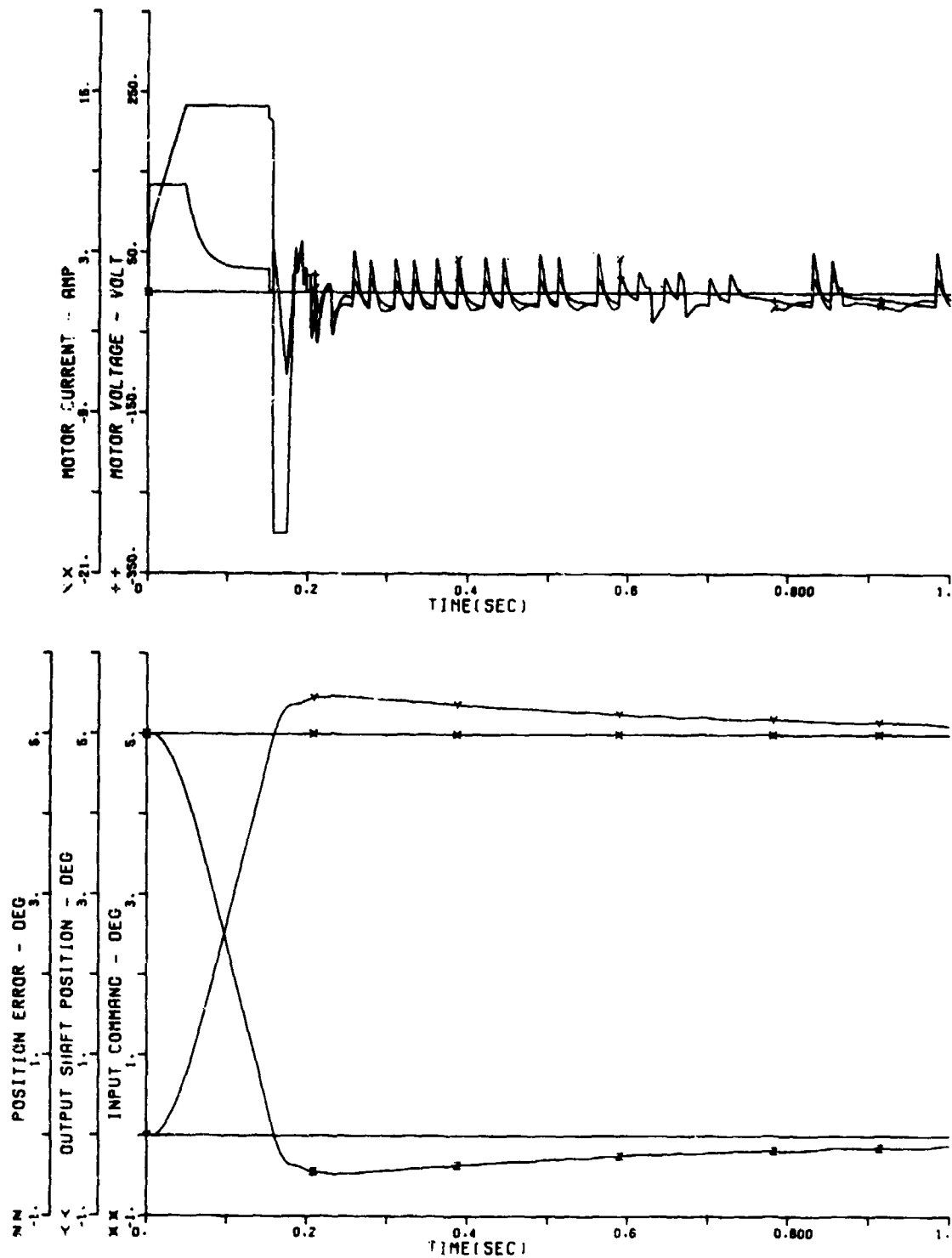


Figure G-2. Single-Channel Step Response
at No Load and 5-deg Step

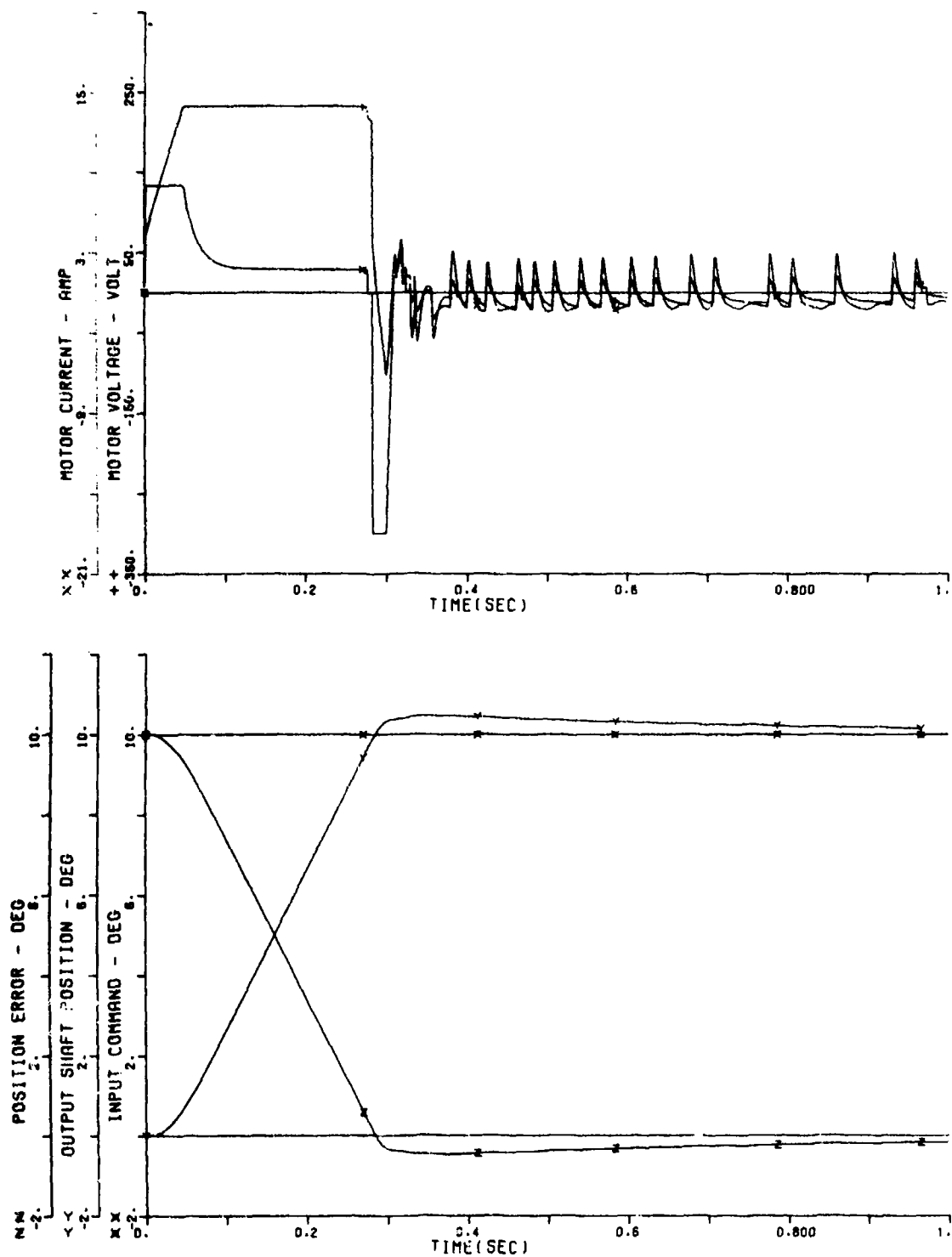


Figure G-3. Single-Channel Step Response
at No Load and 10-deg Step

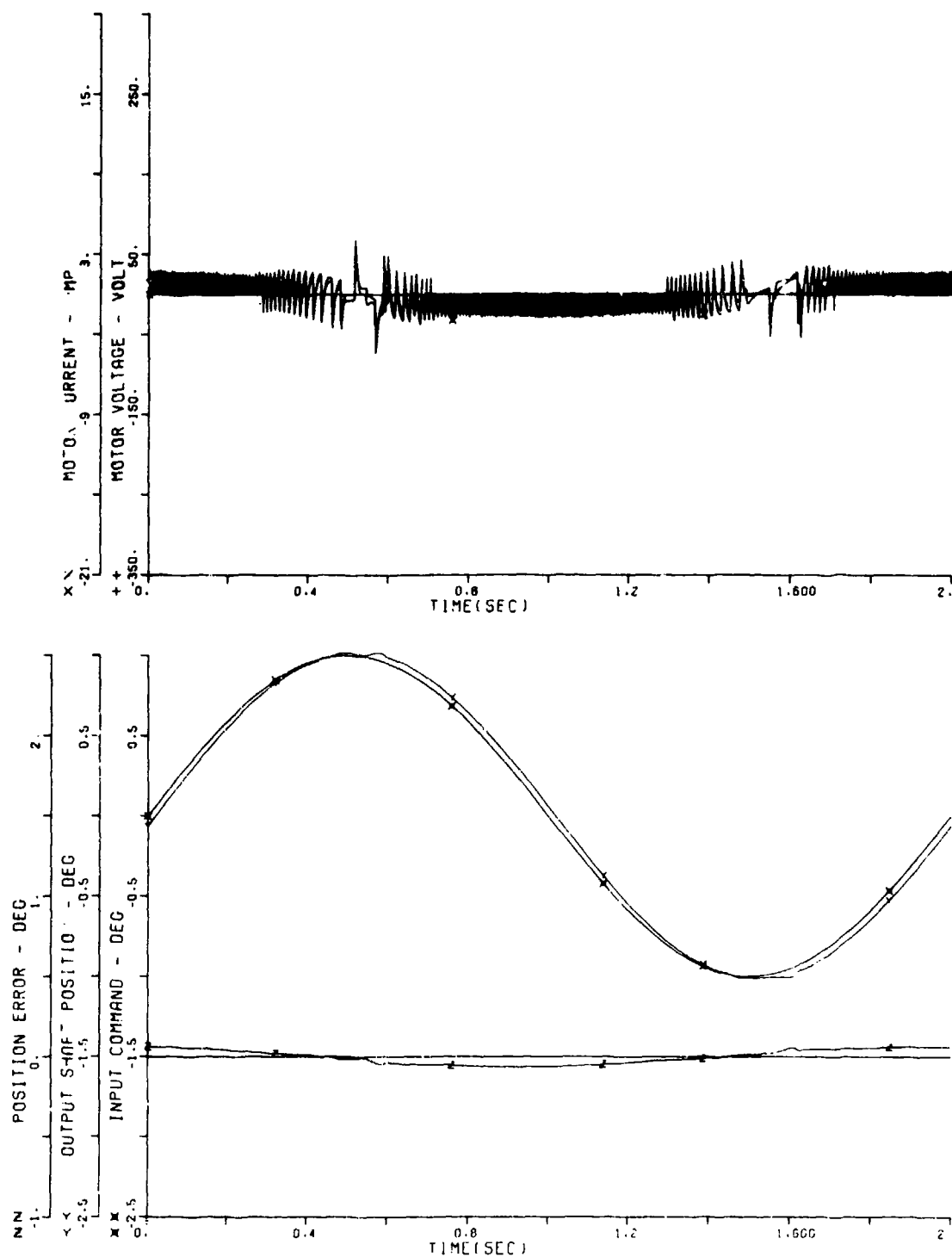


Figure G-4. Single-Channel Frequency Response, No Load

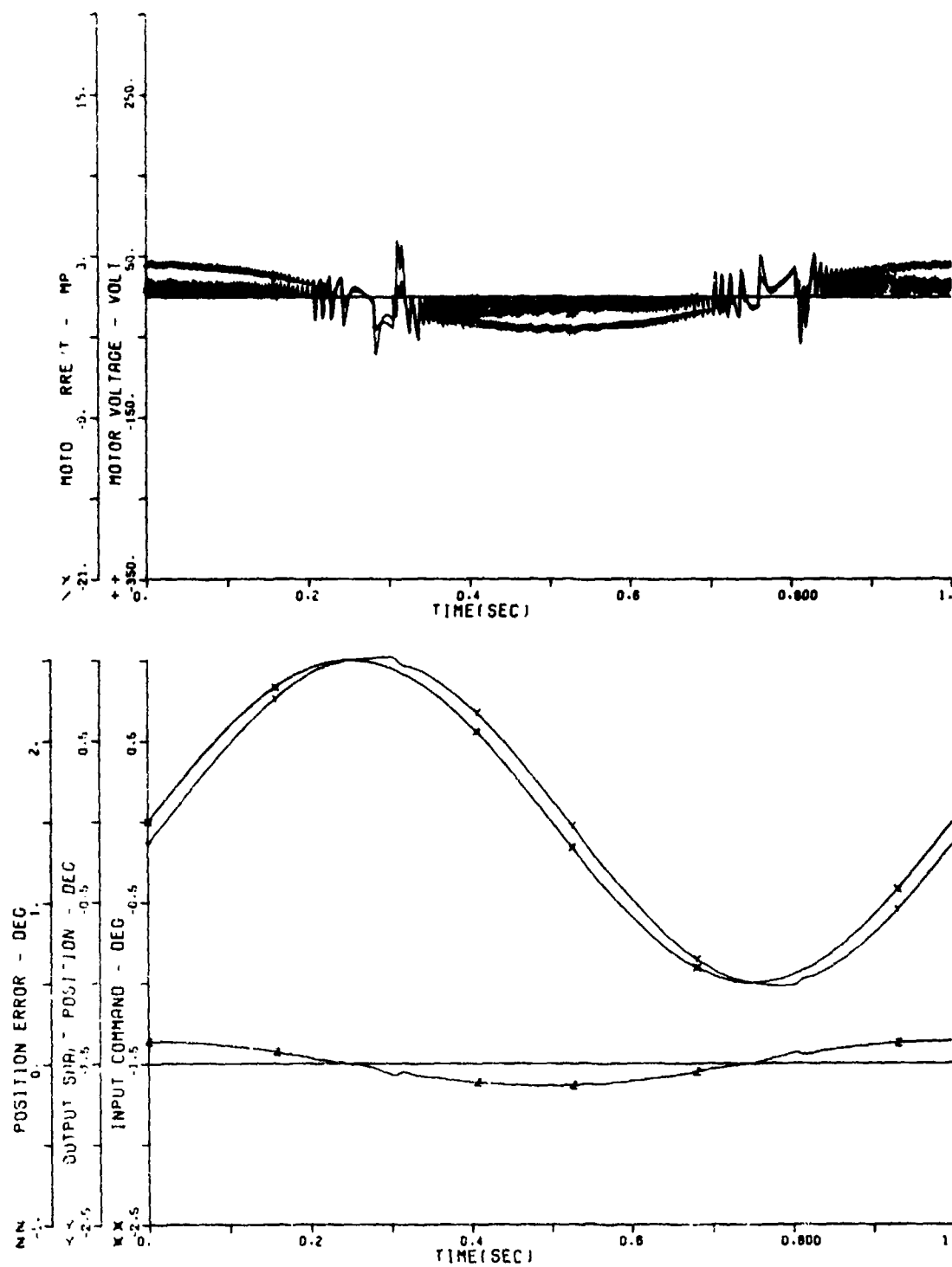


Figure G-5. Single-Channel Frequency Response, No Load

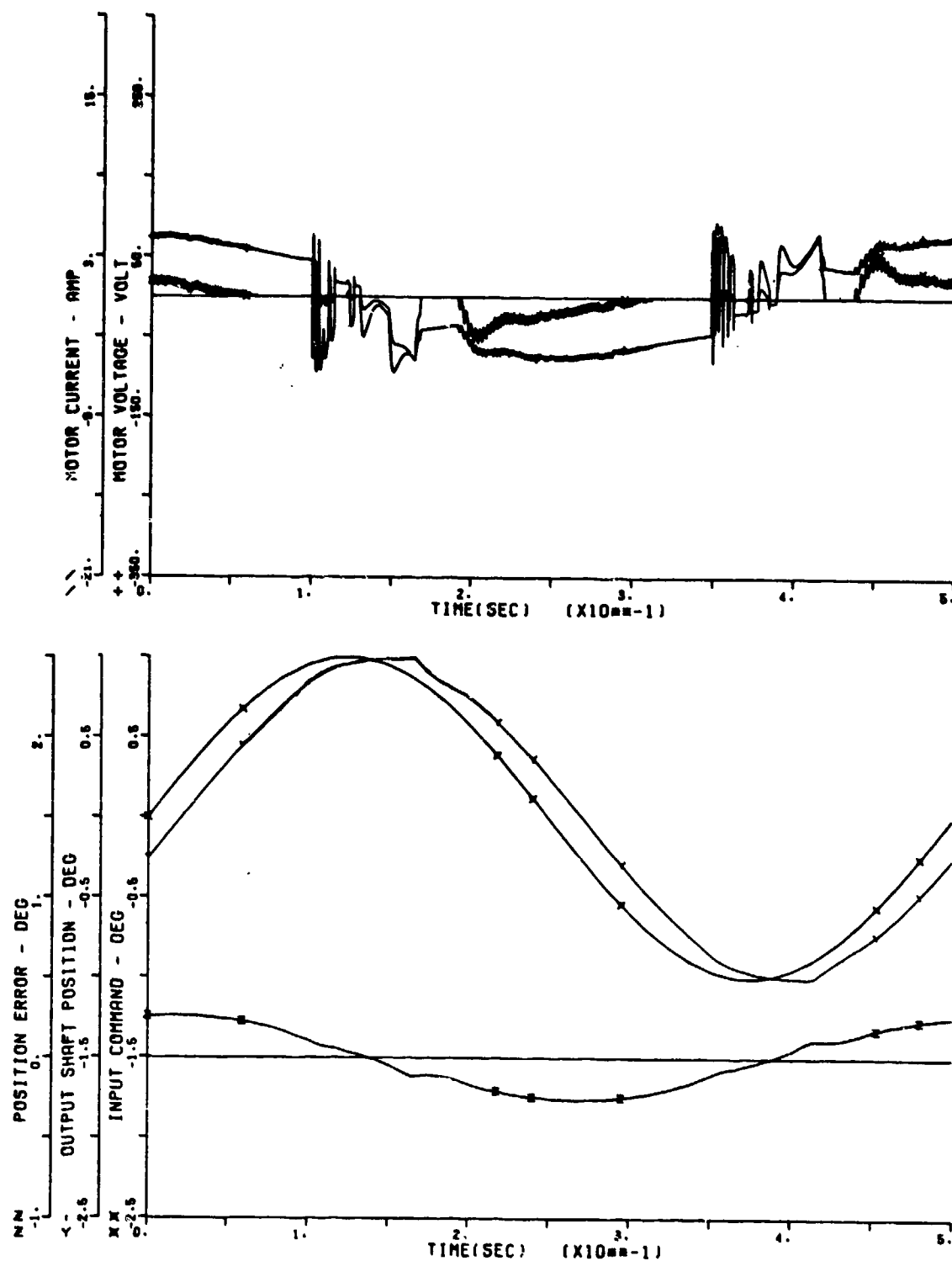


Figure G-6. Single-Channel Frequency Response, No Load

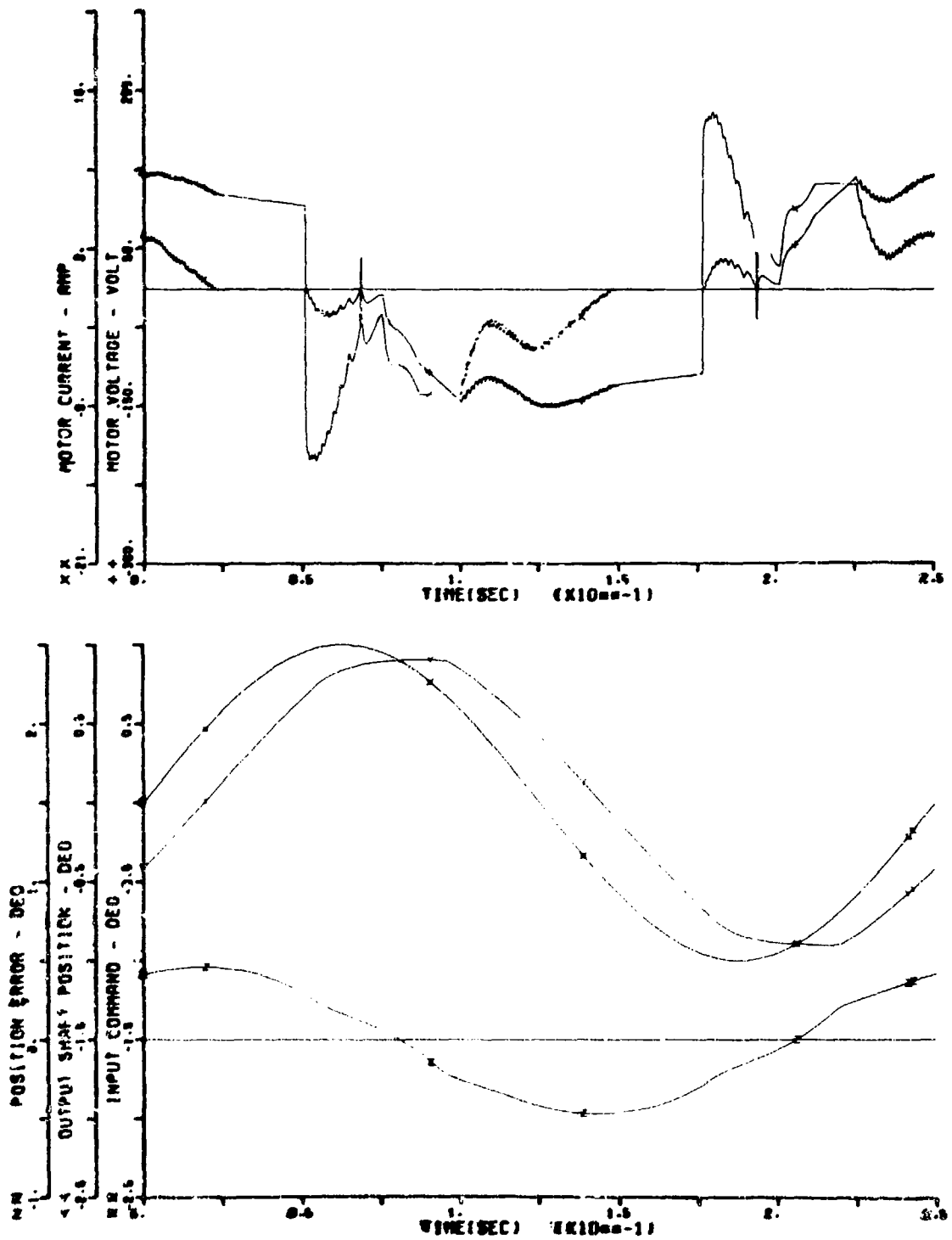


Figure G-7. Single-Channel Frequency Response, No Load

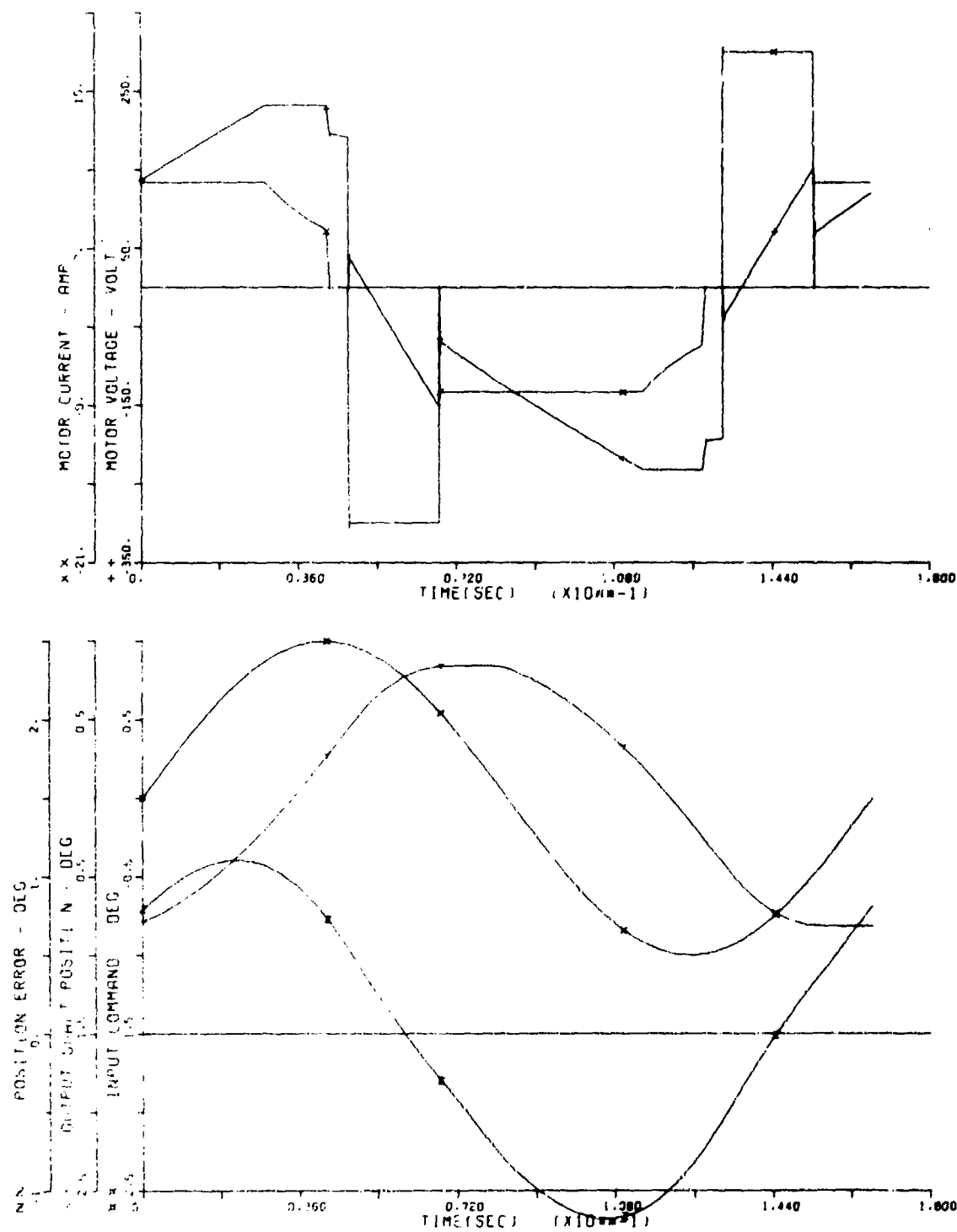


Figure G-8. Single-Channel Frequency Response, No Load

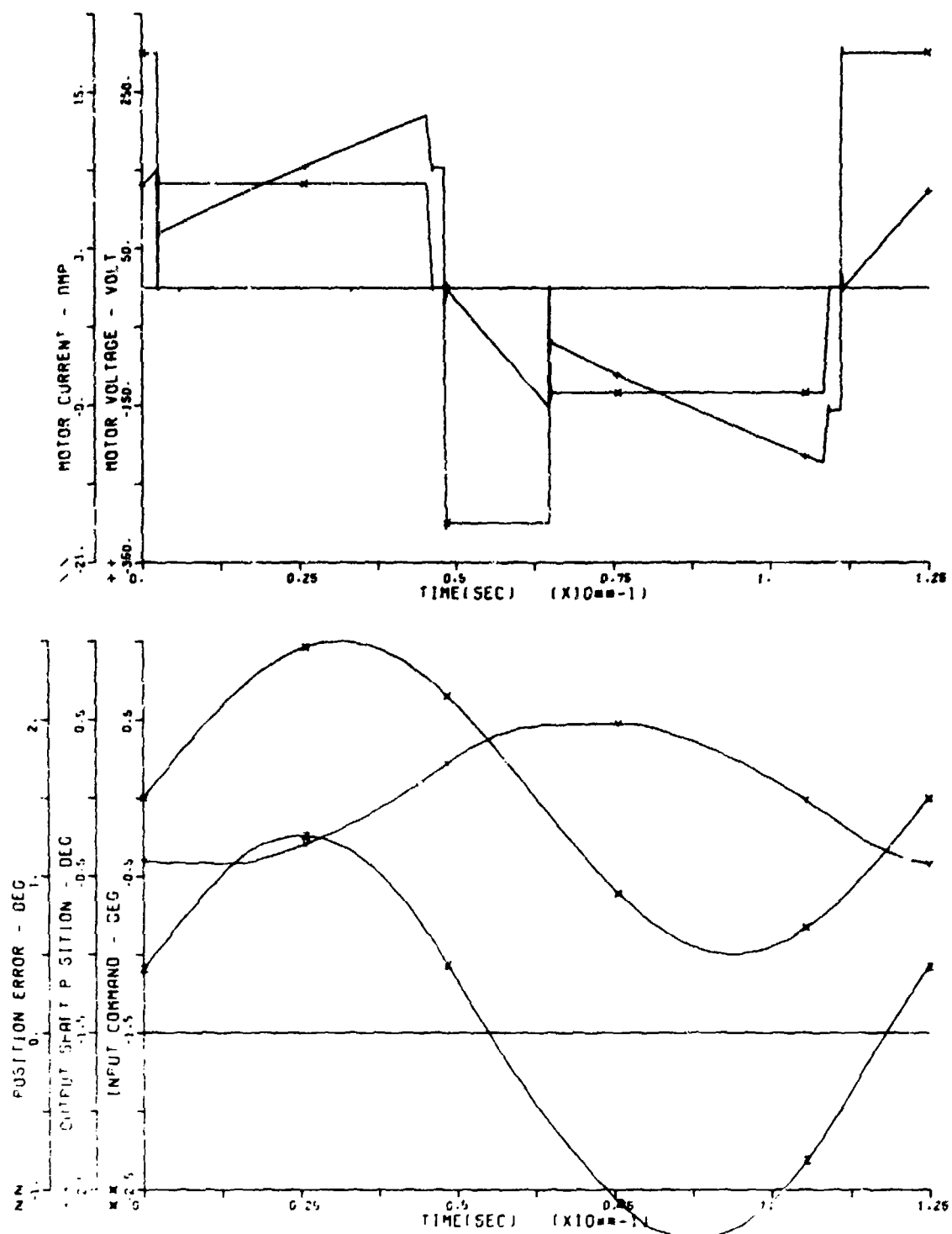


Figure G-9. Single-Channel Frequency Response, No Load

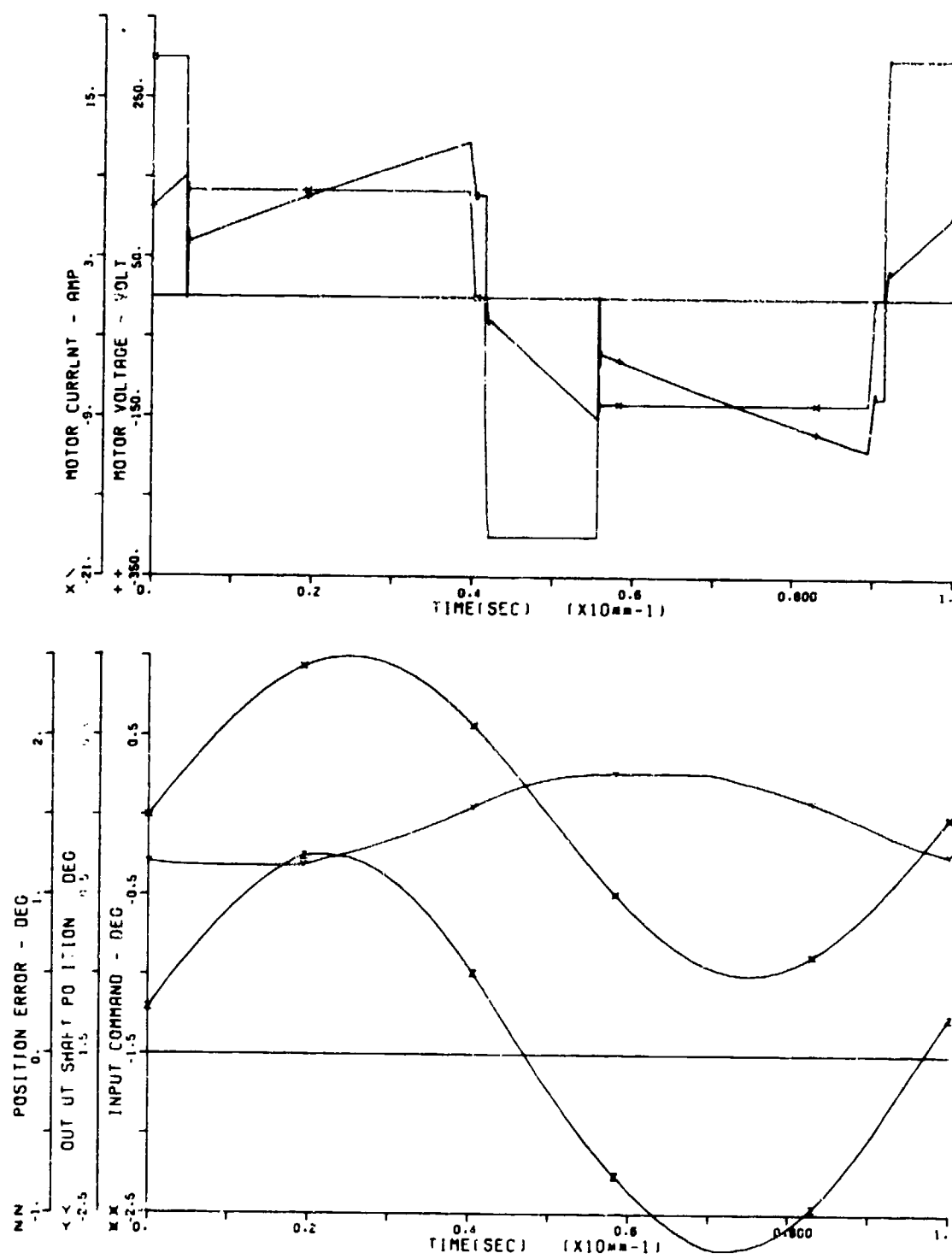


Figure G-10. Single-Channel Frequency Response, No Load

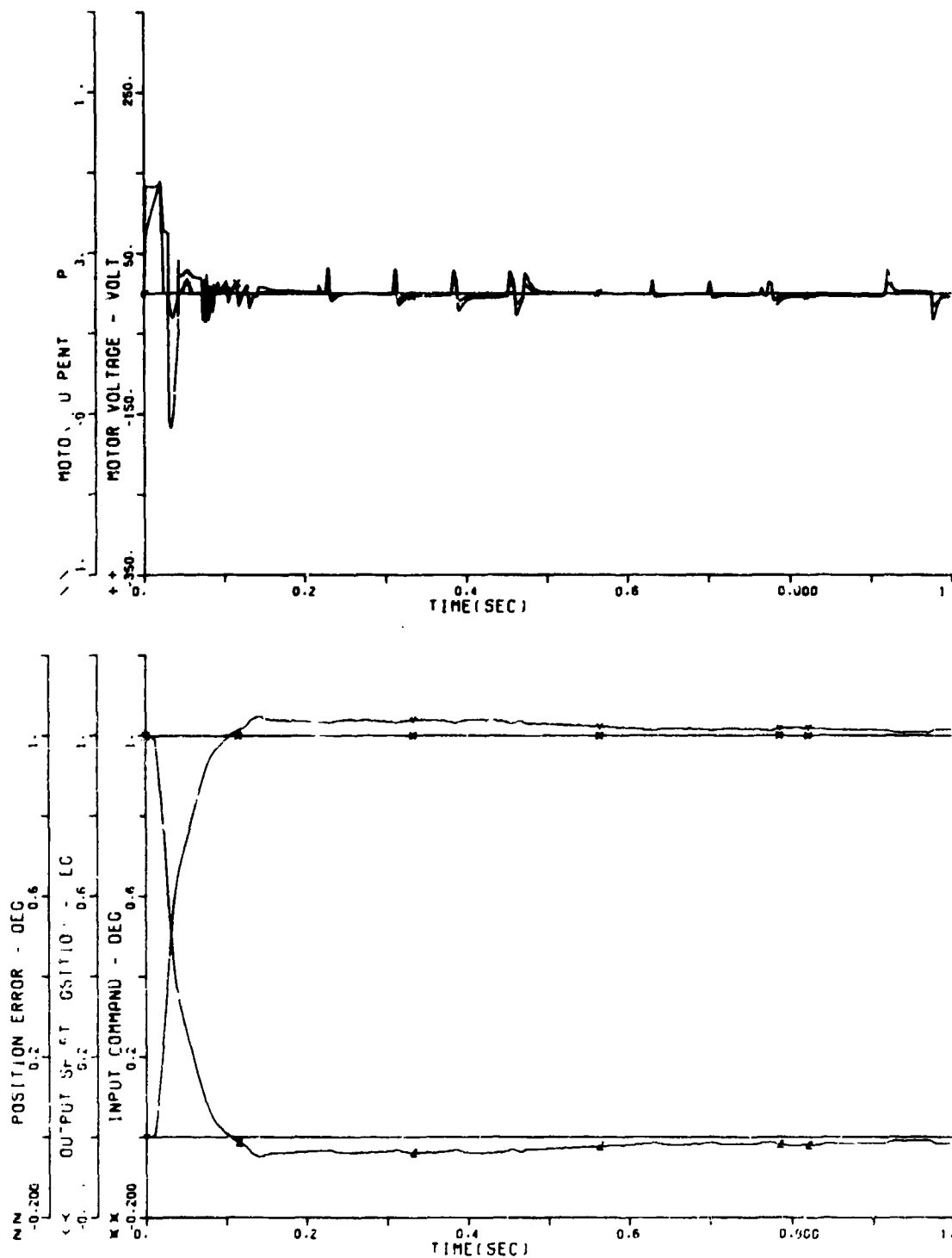


Figure G-11. Dual Channel Step Response, No Load

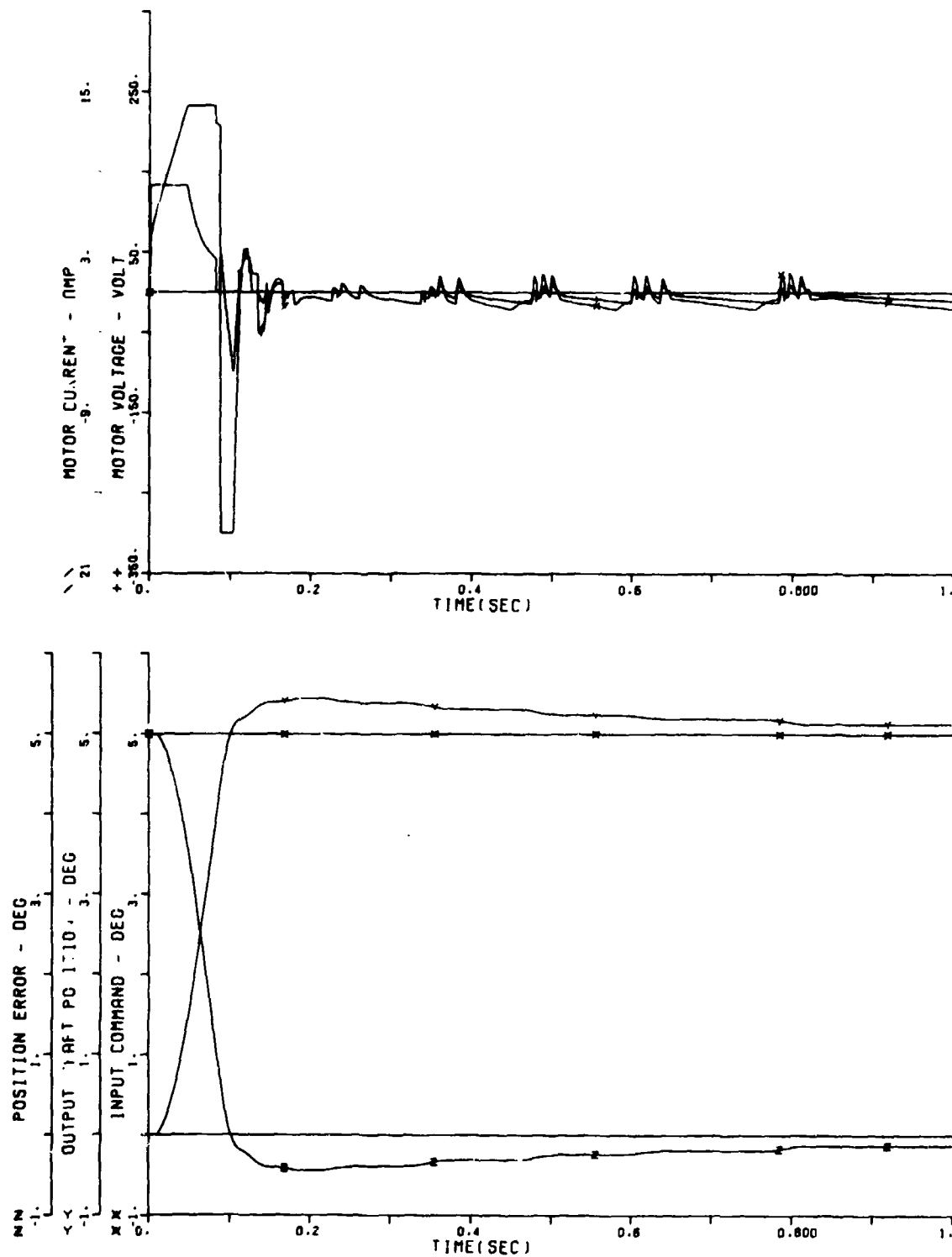


Figure G-12. Dual Channel Step Response, No Load

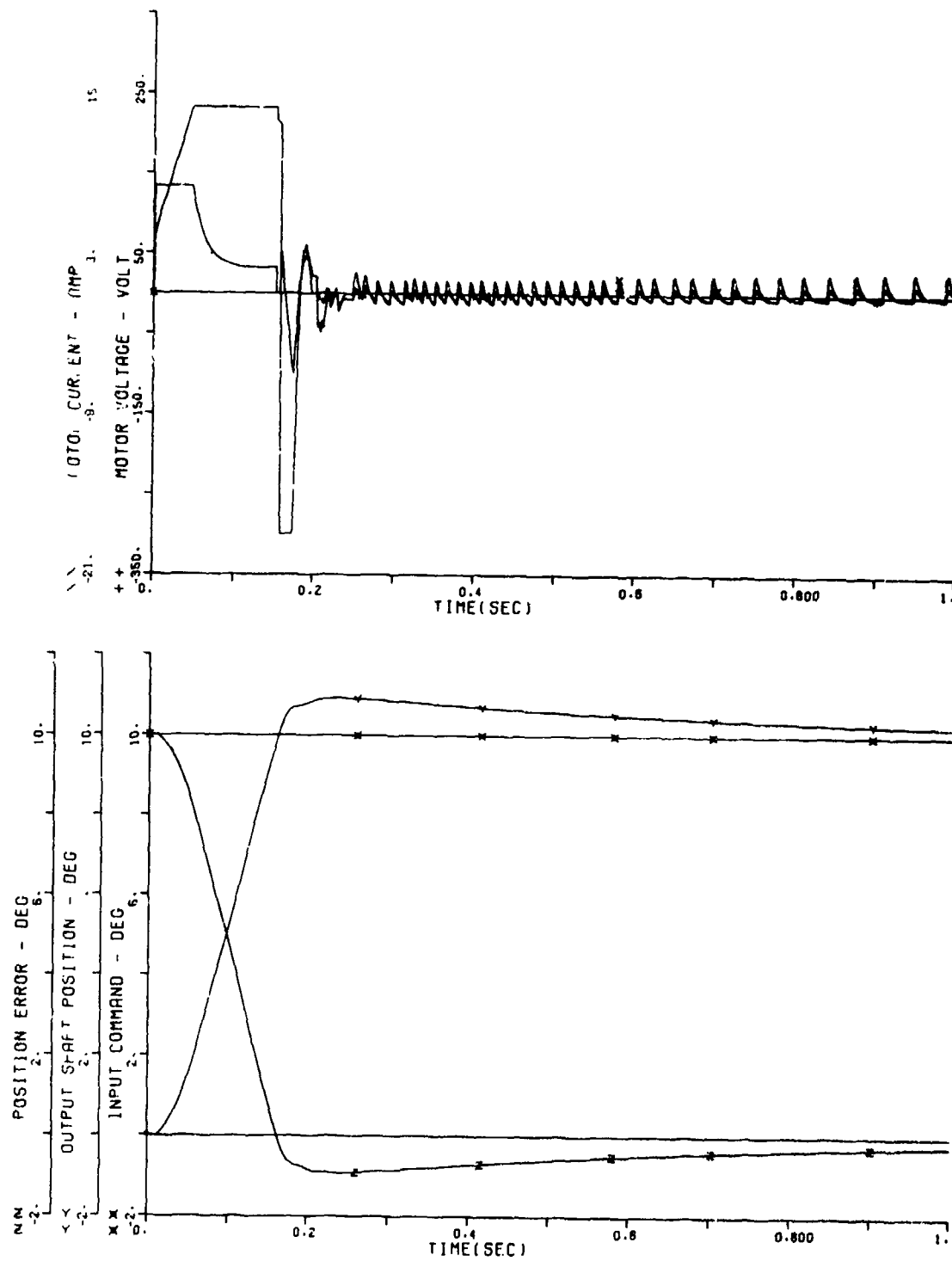


Figure G-13. Dual Channel Step Response, No Load

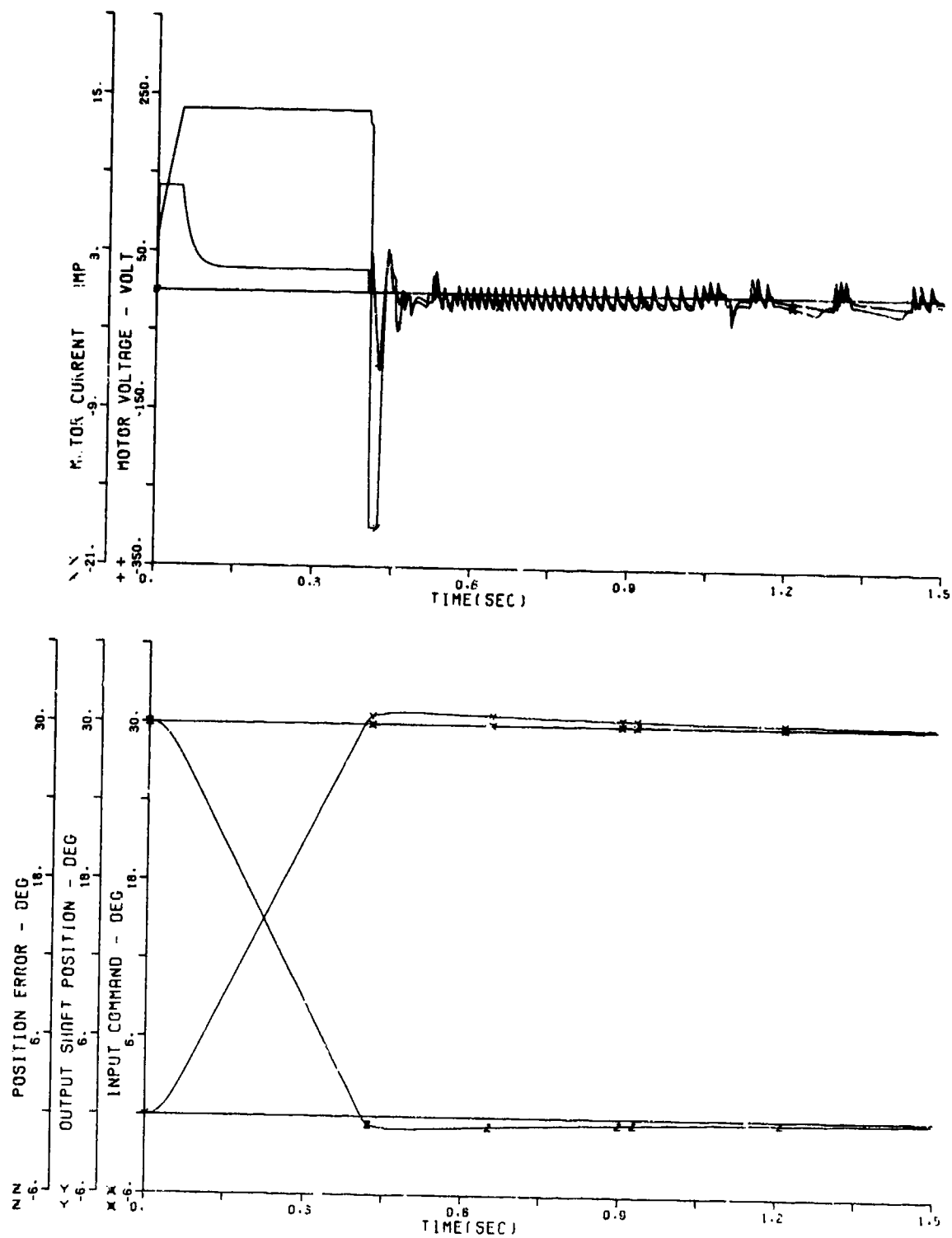


Figure G-14. Dual Channel Step Response, No Load

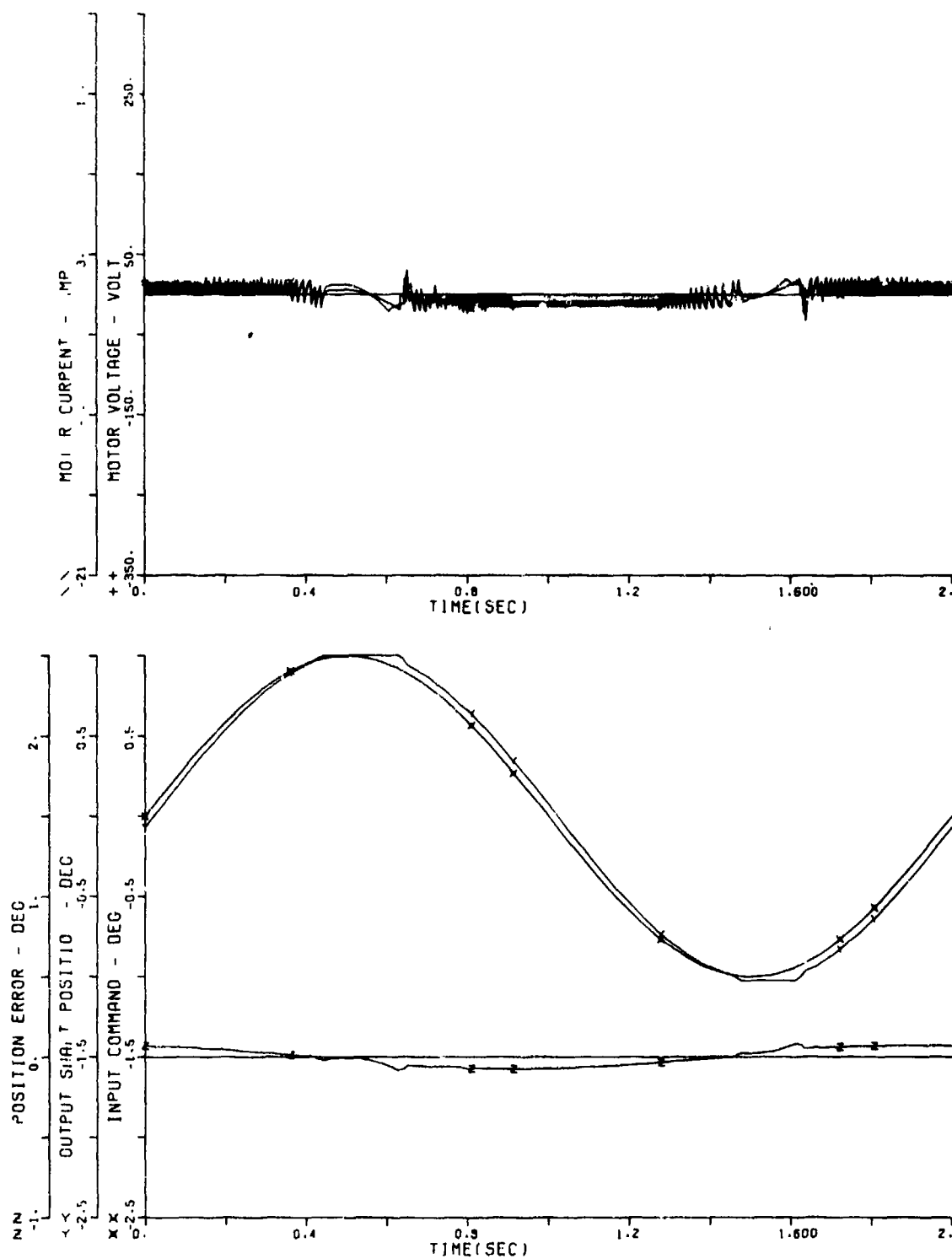


Figure G-15. Dual Channel Frequency Response, No Load

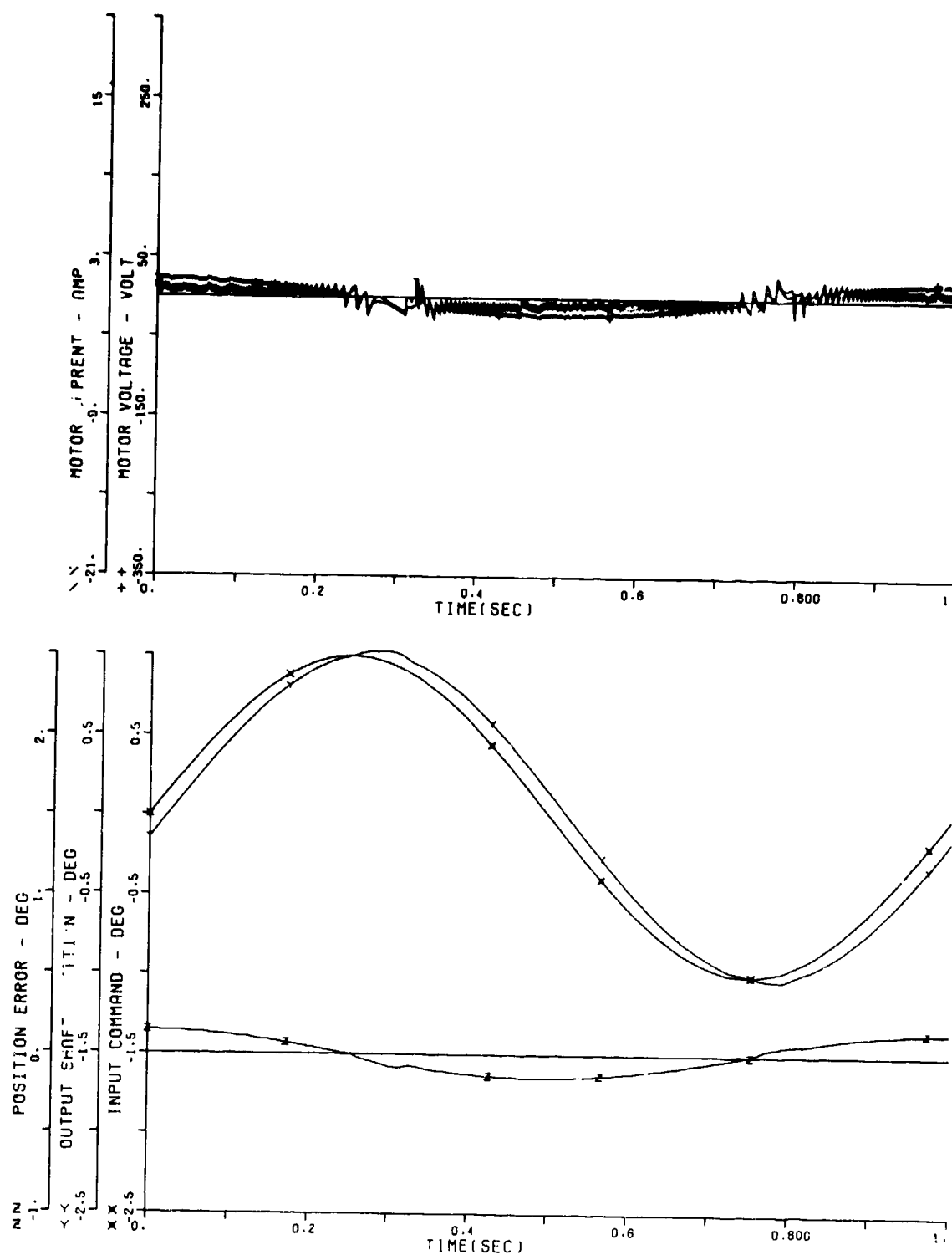


Figure G-16. Dual Channel Frequency Response, No Load

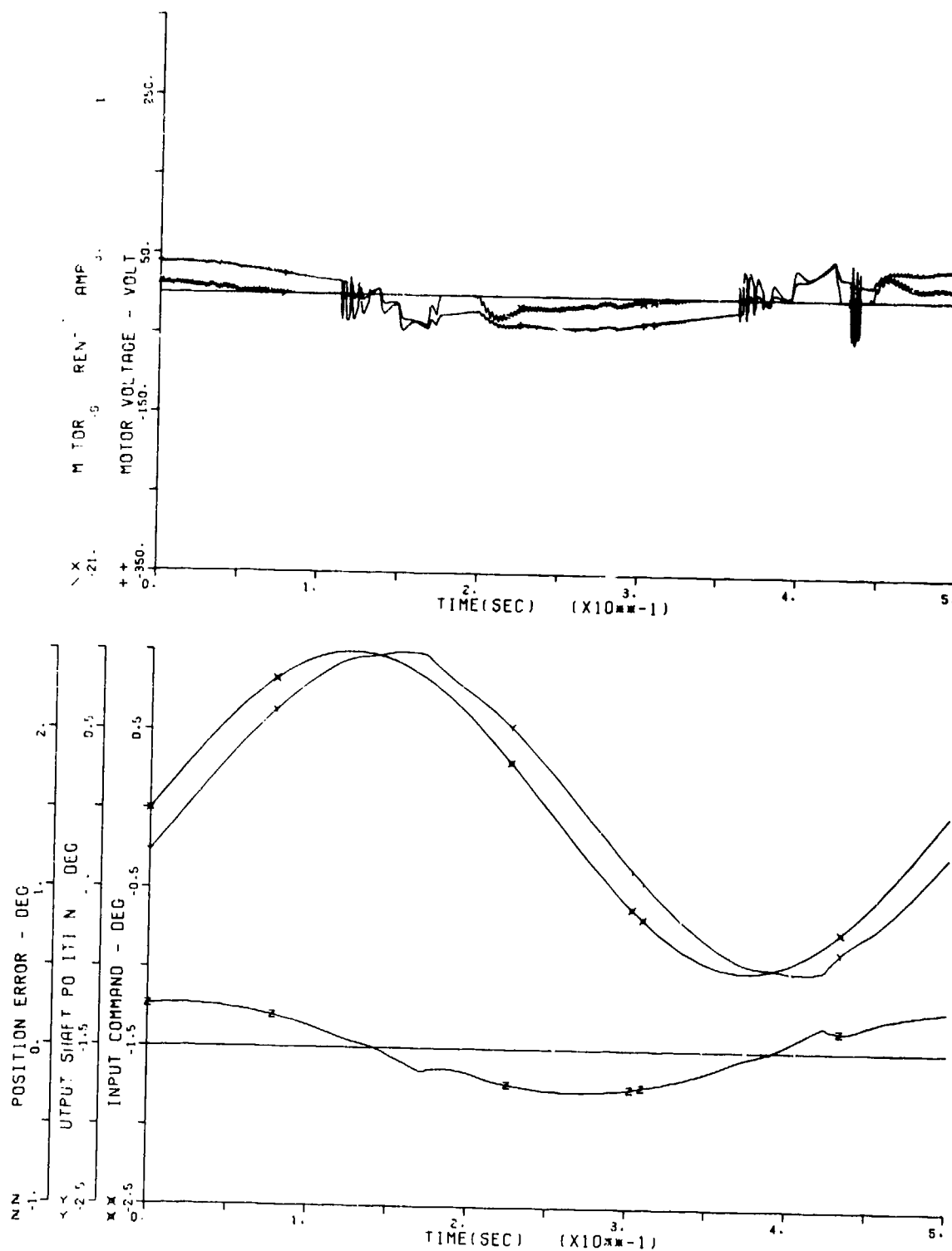


Figure G-17. Dual Channel Frequency Response, No Load

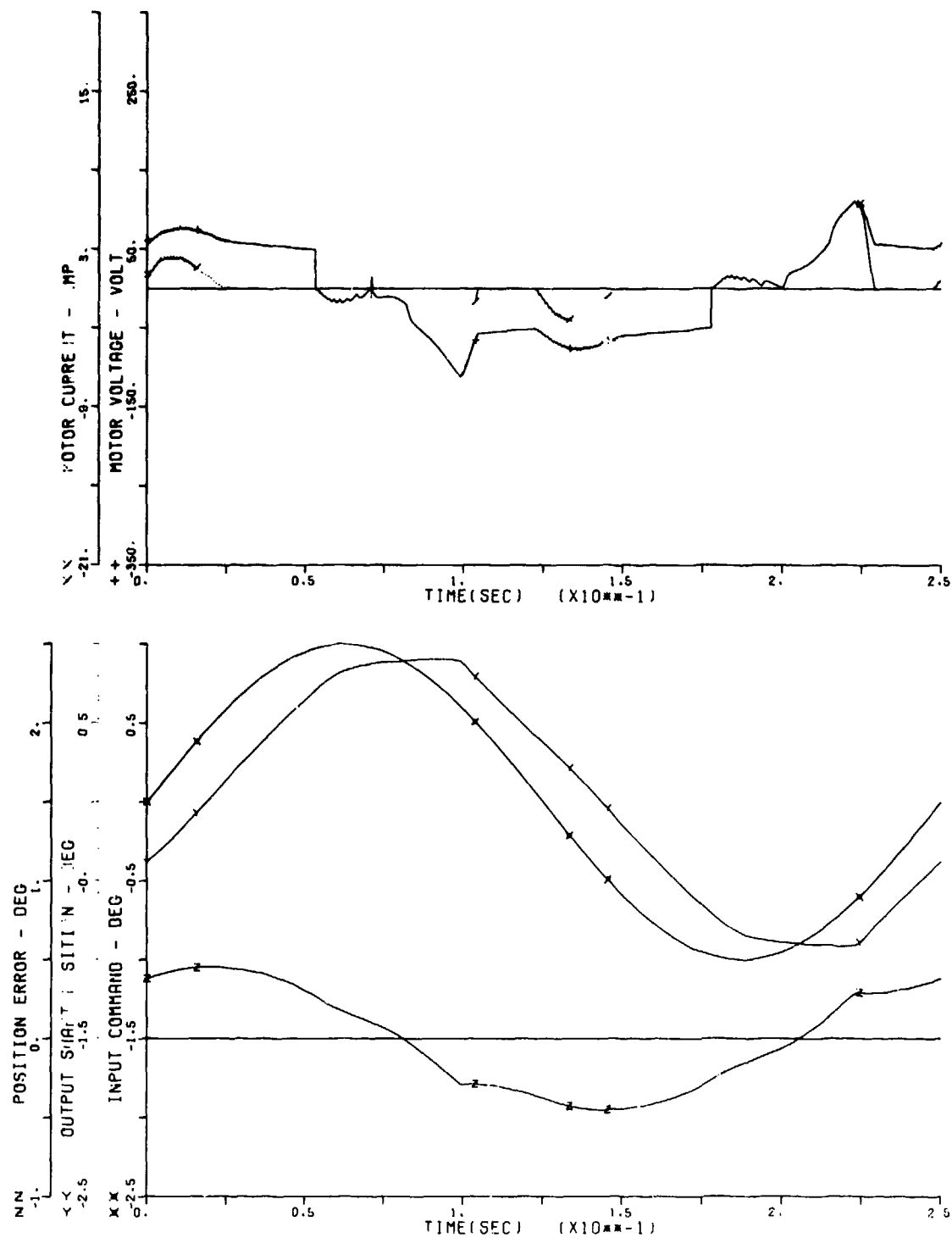


Figure G-18. Dual Channel Frequency Response, No Load

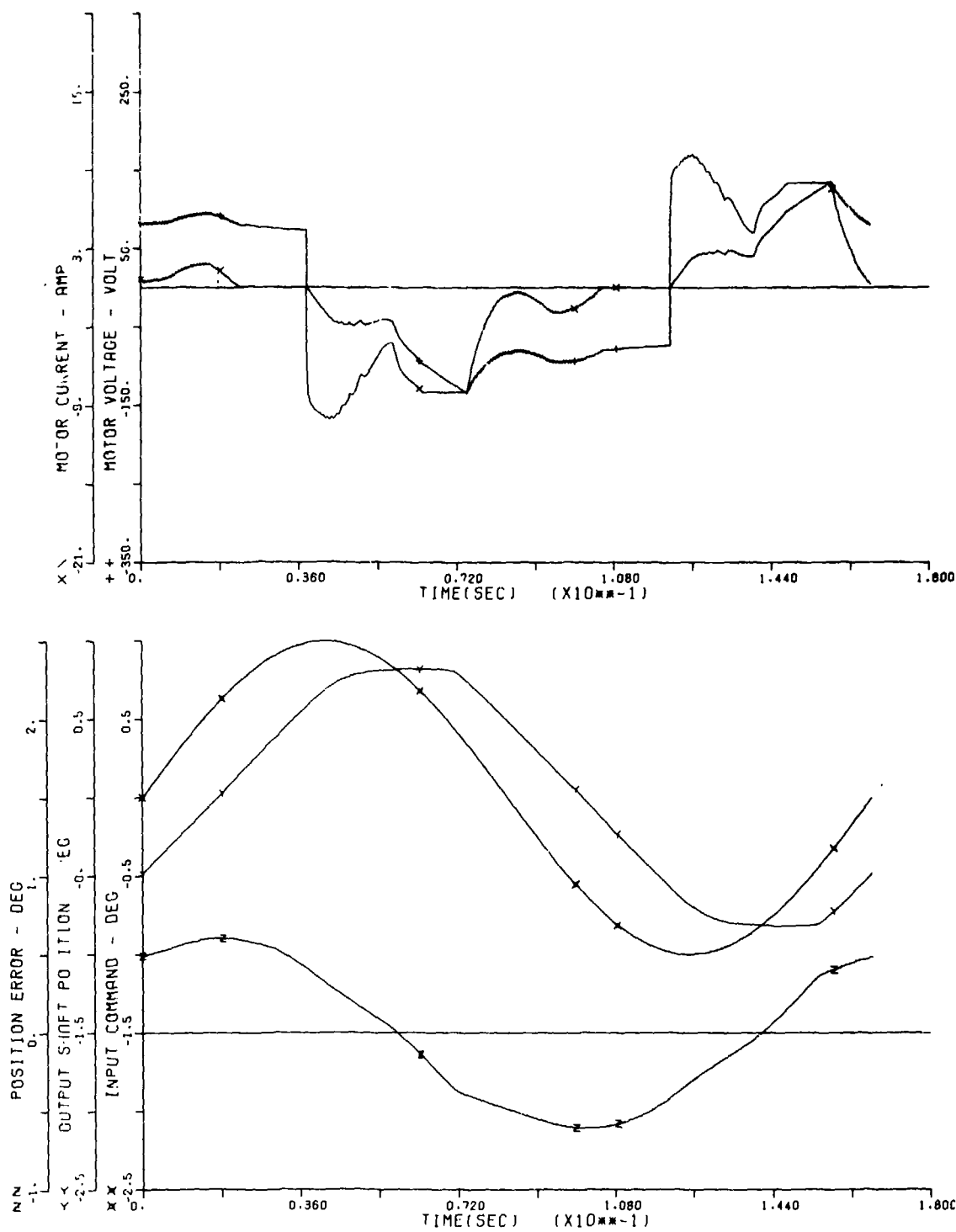


Figure G-19. Dual Channel Frequency Response, No Load

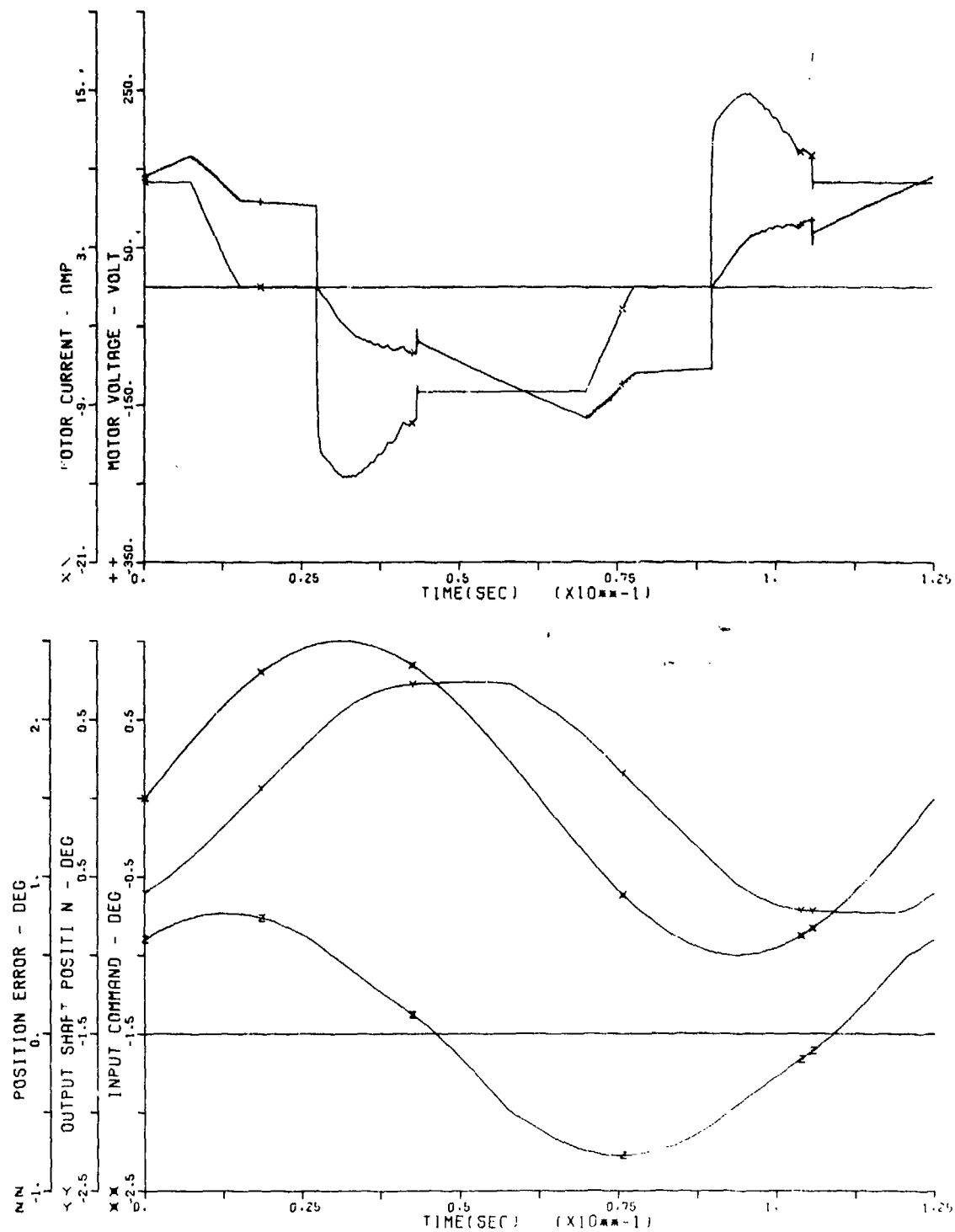


Figure G-20. Dual Channel Frequency Response, No Load

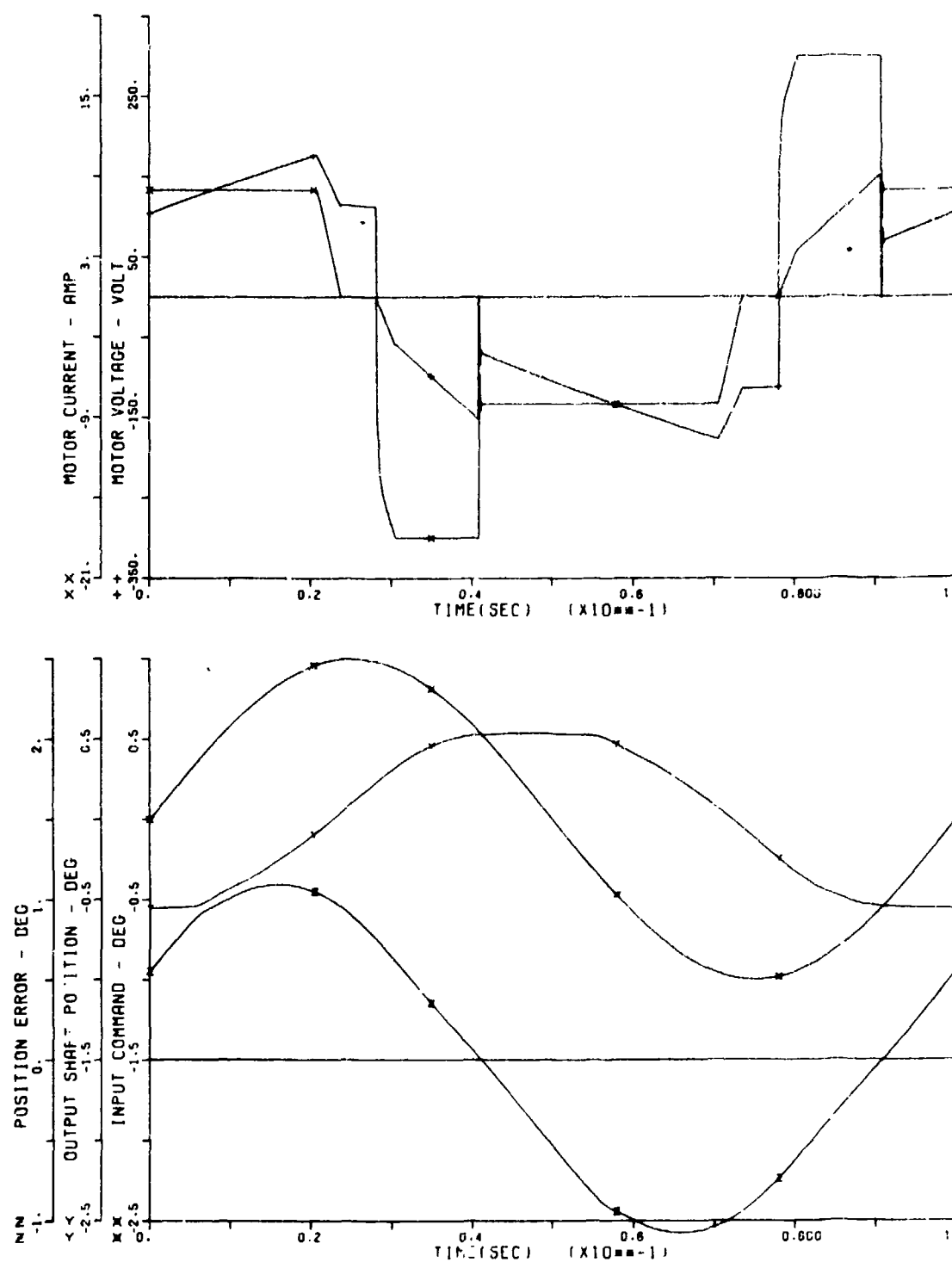


Figure G-21. Dual Channel Frequency Response, No Load

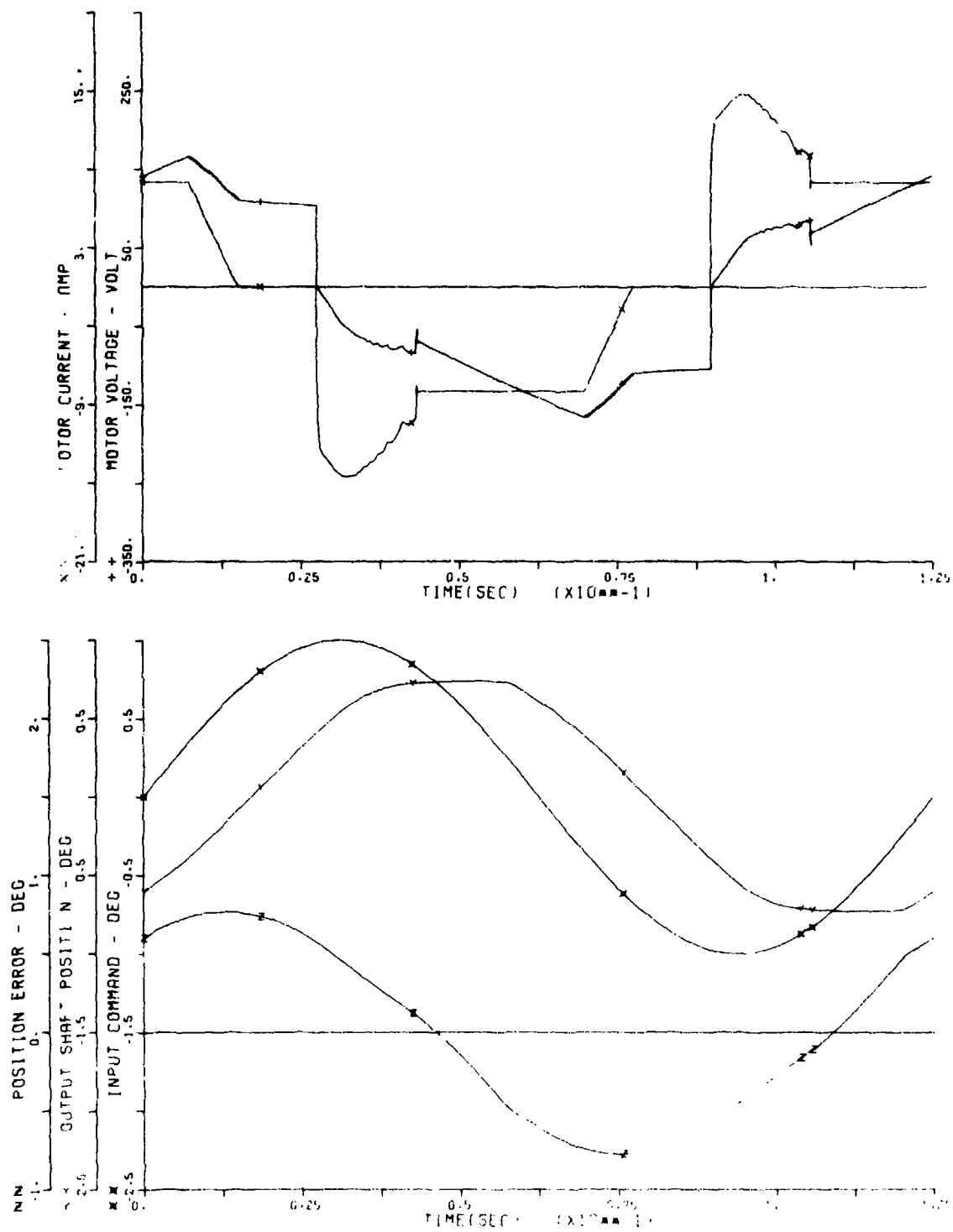


Figure G-20. Dual Channel Frequency Response, No Load

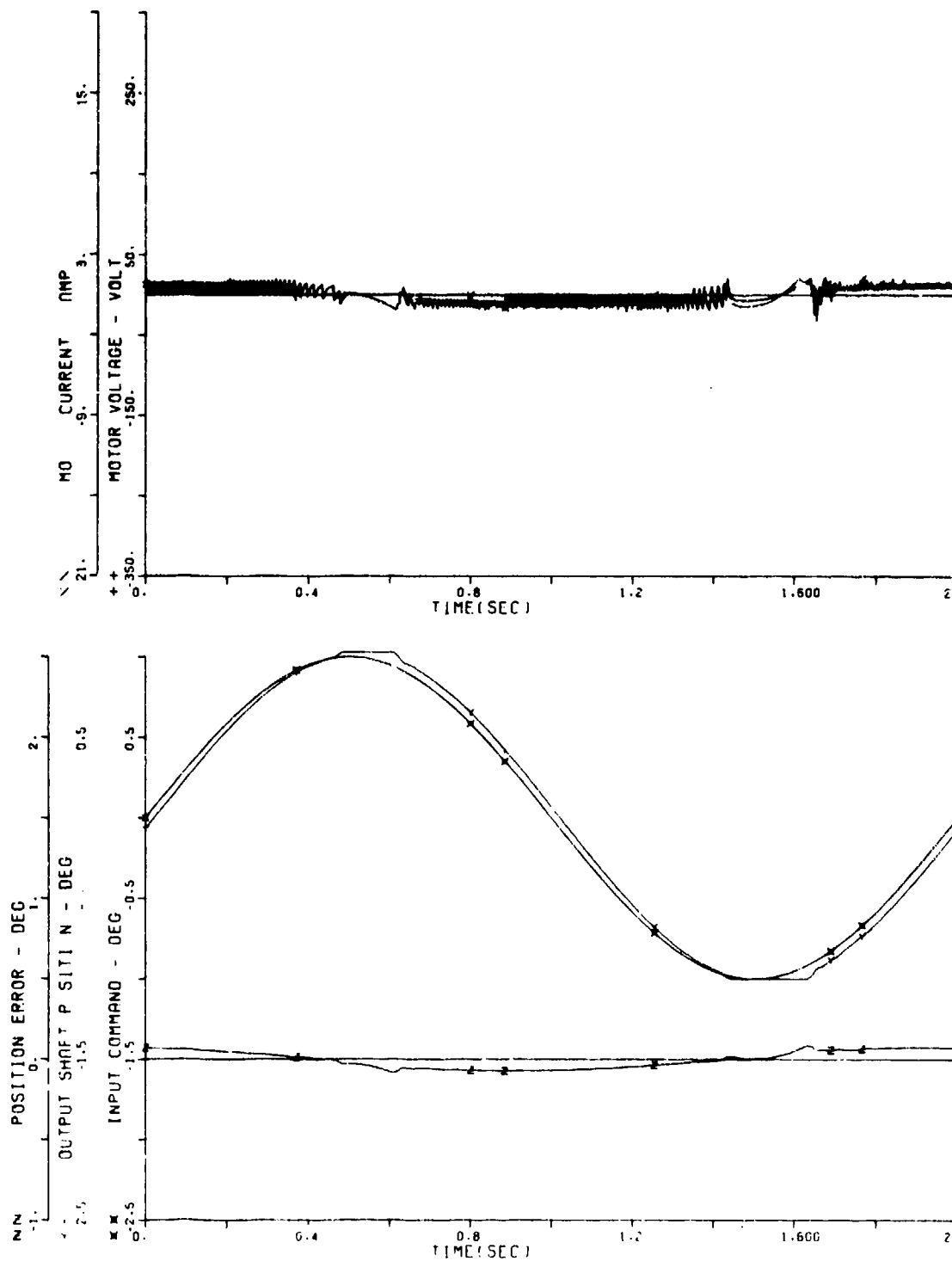


Figure G-22. Dual Channel Frequency Response, 50 Percent Load

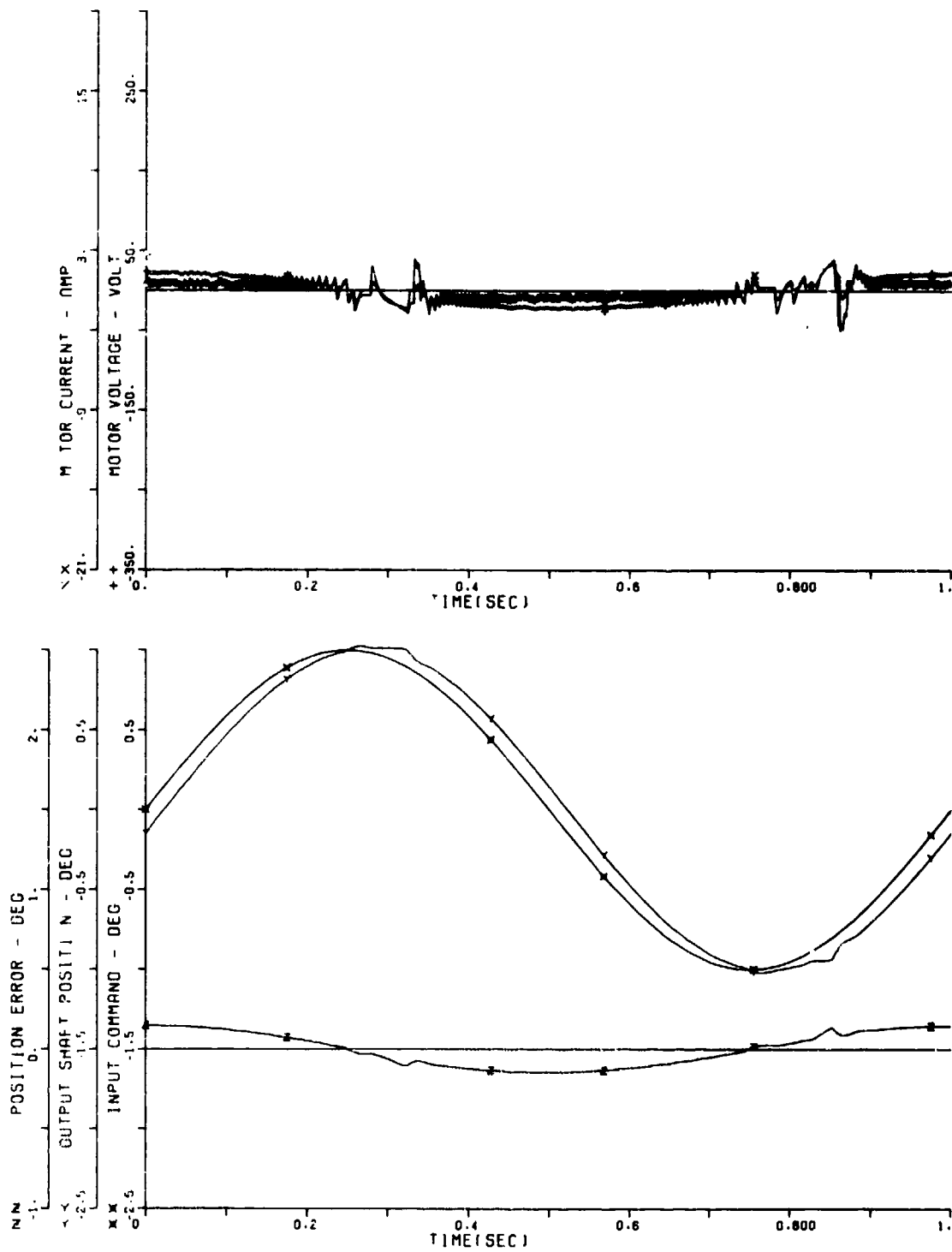


Figure G-23. Dual Channel Frequency Response, 50 Percent Load

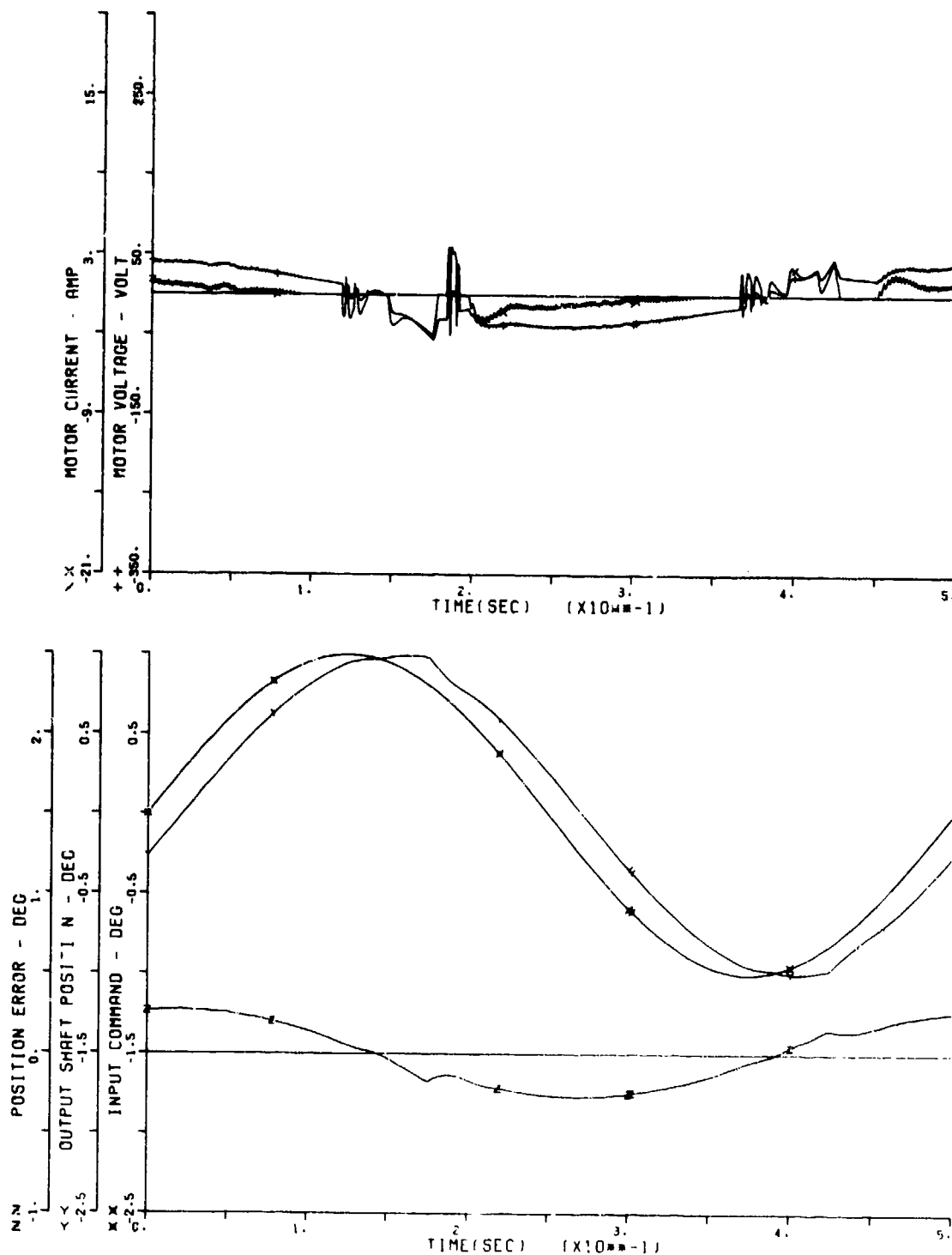


Figure G-24. Dual Channel Frequency Response, 50 Percent Load

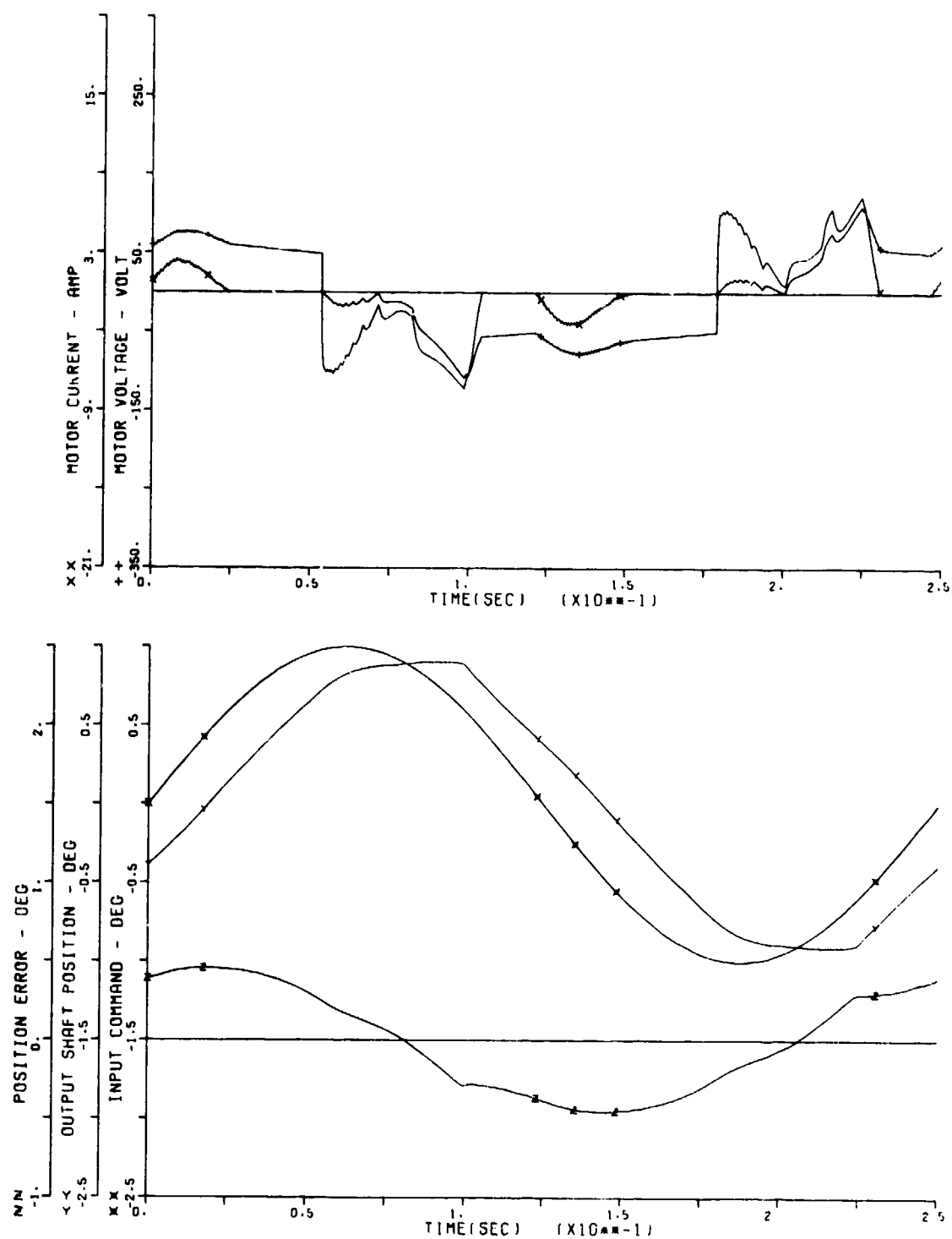


Figure G-25. Dual Channel Frequency Response, 50 Percent Load

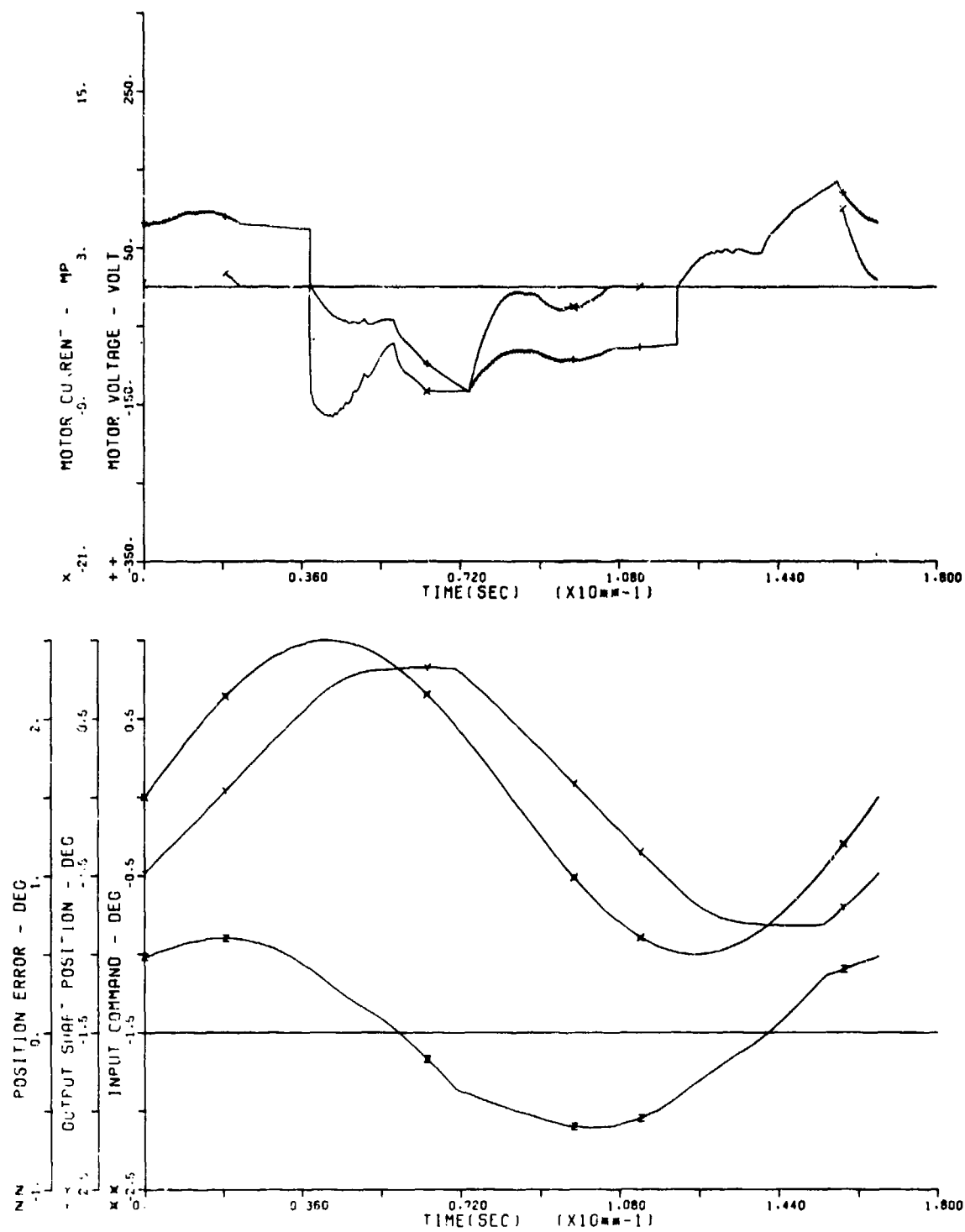


Figure G-26. Dual Channel Frequency Response, 50 Percent Load

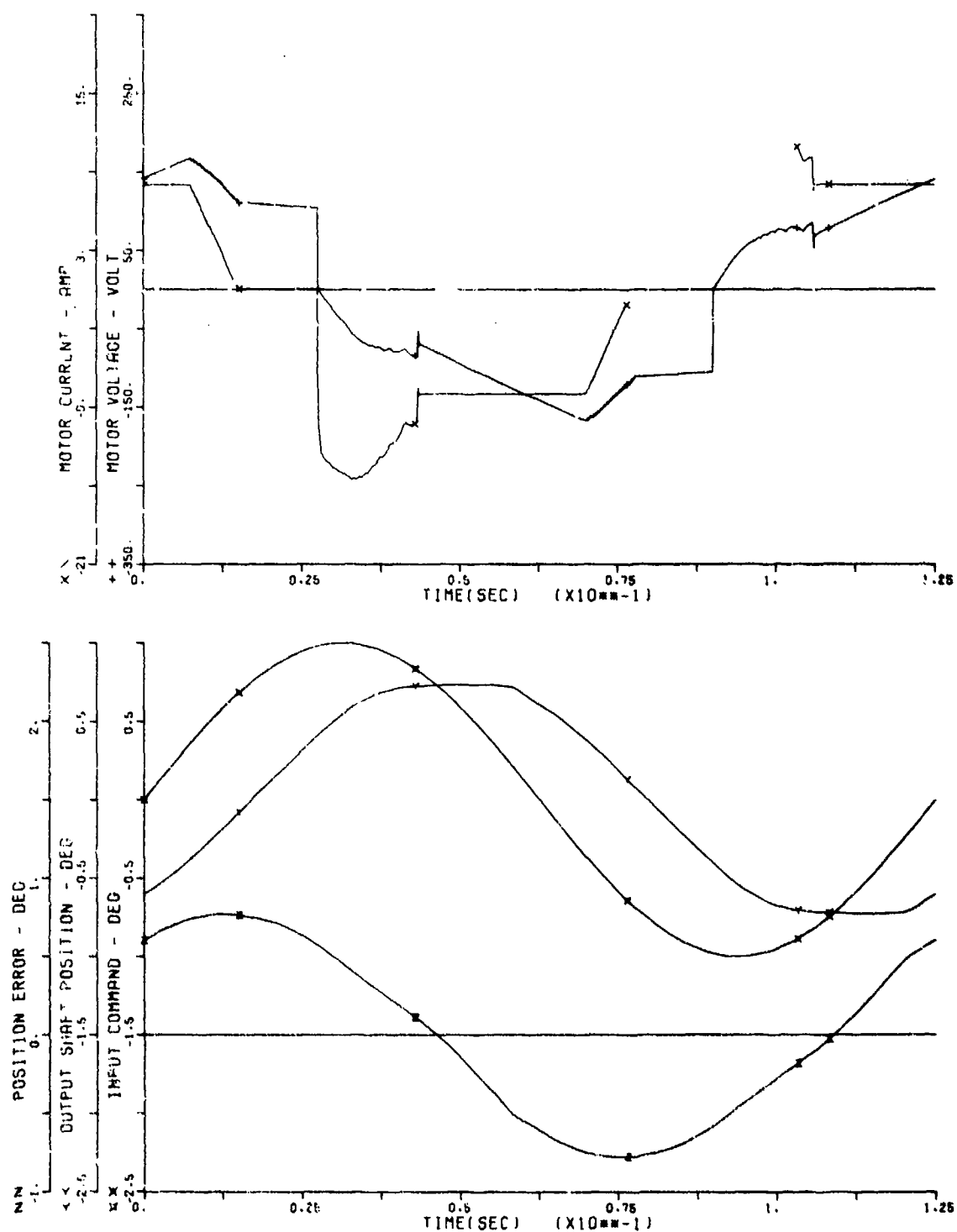


Figure G-27. Dual Channel Frequency Response, 50 Percent Load

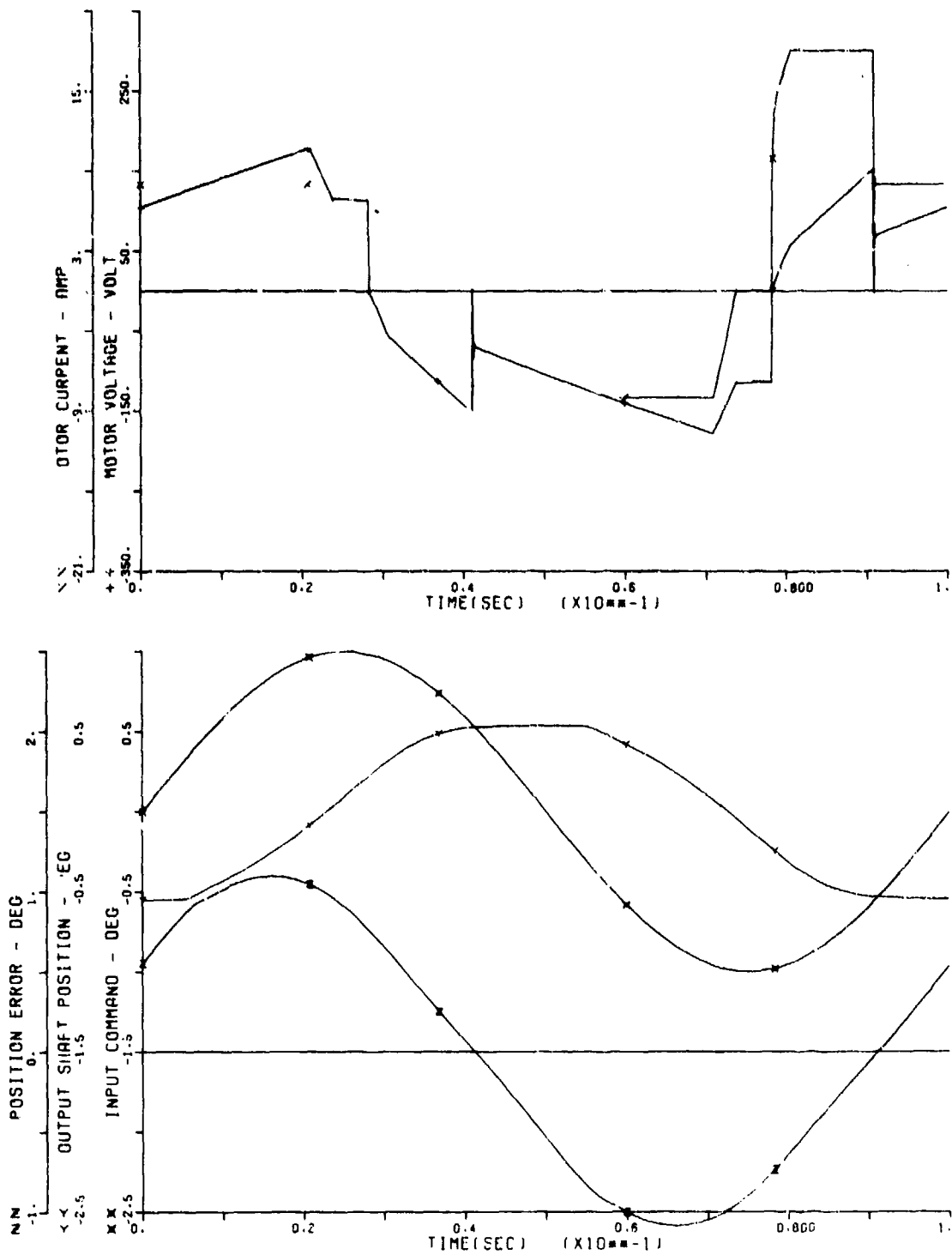


Figure G-28. Dual Channel Frequency Response, 50 Percent Load

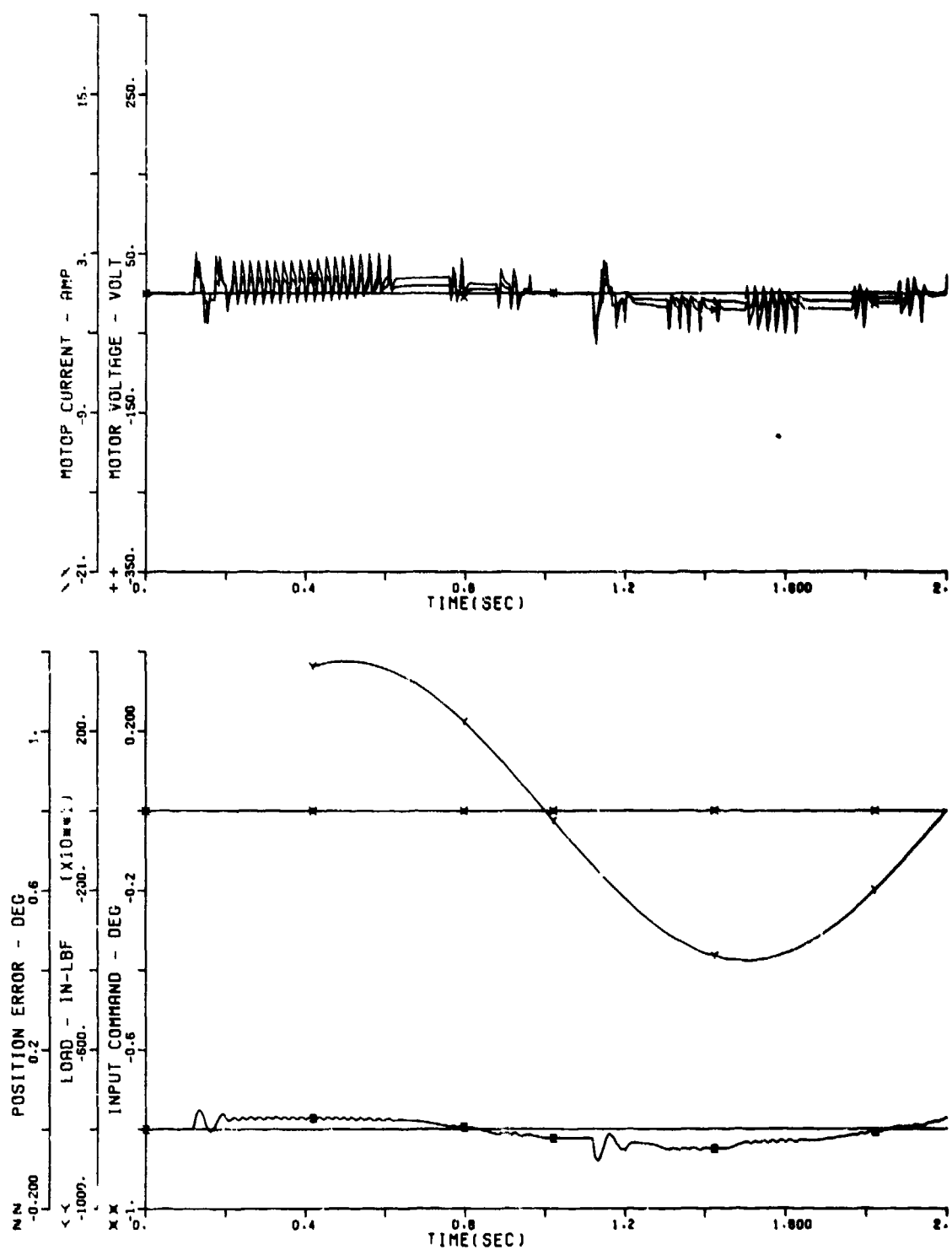


Figure G-29. Dual Channel Dynamic Stiffness, 10 Percent Load

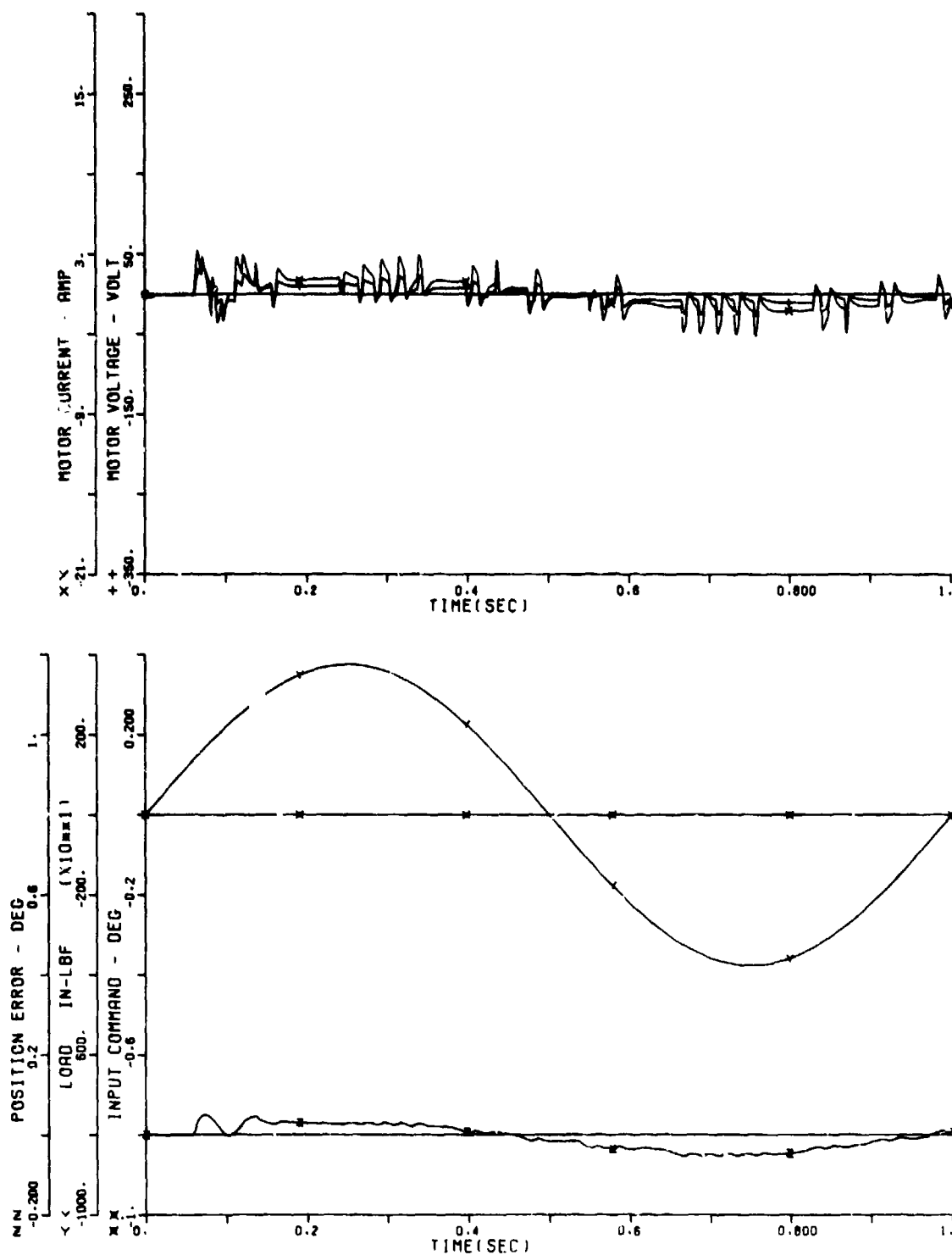


Figure G-30. Dual Channel Dynamic Stiffness, 10 Percent Load

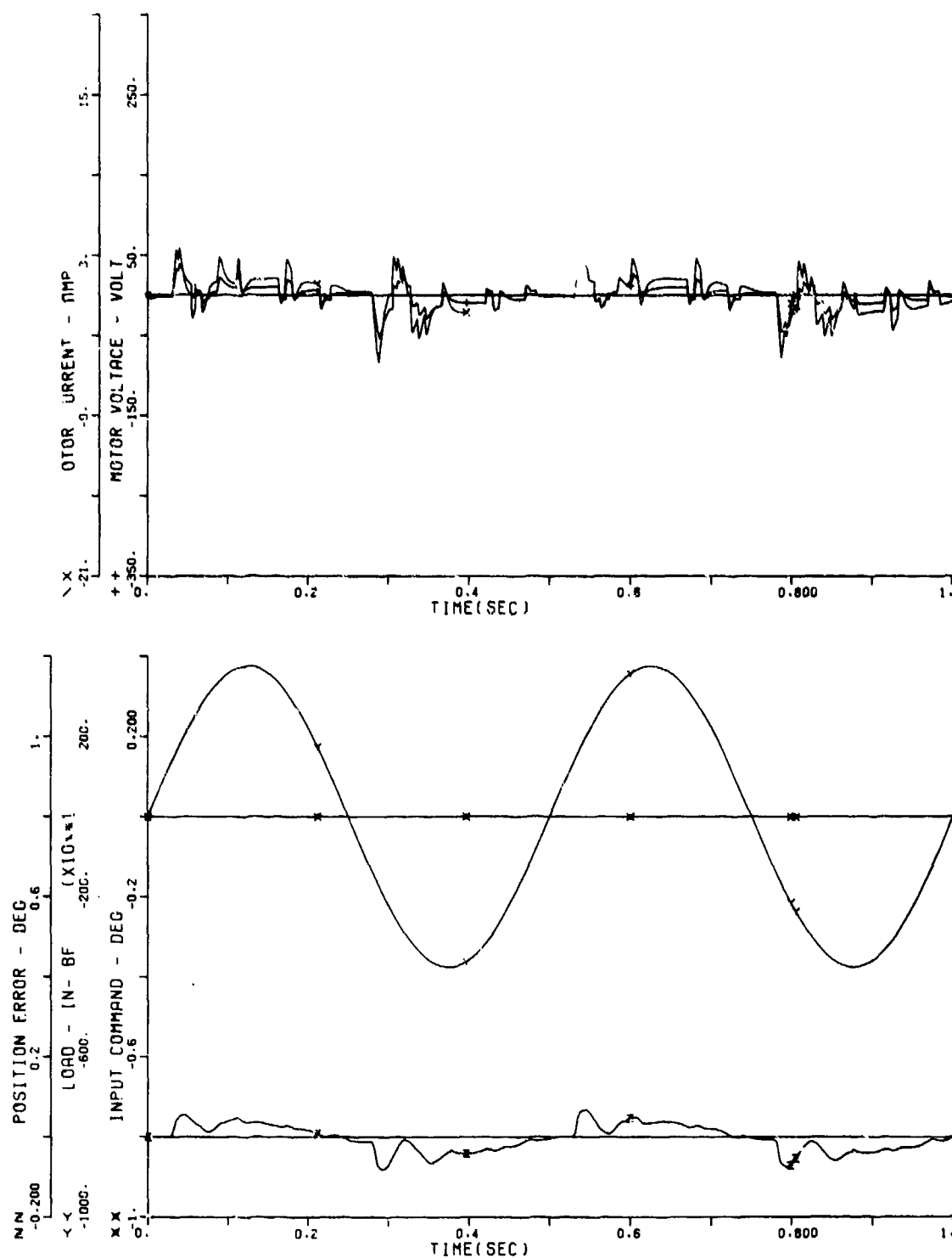


Figure G-31. Dual Channel Dynamic Stiffness, 10 Percent Load

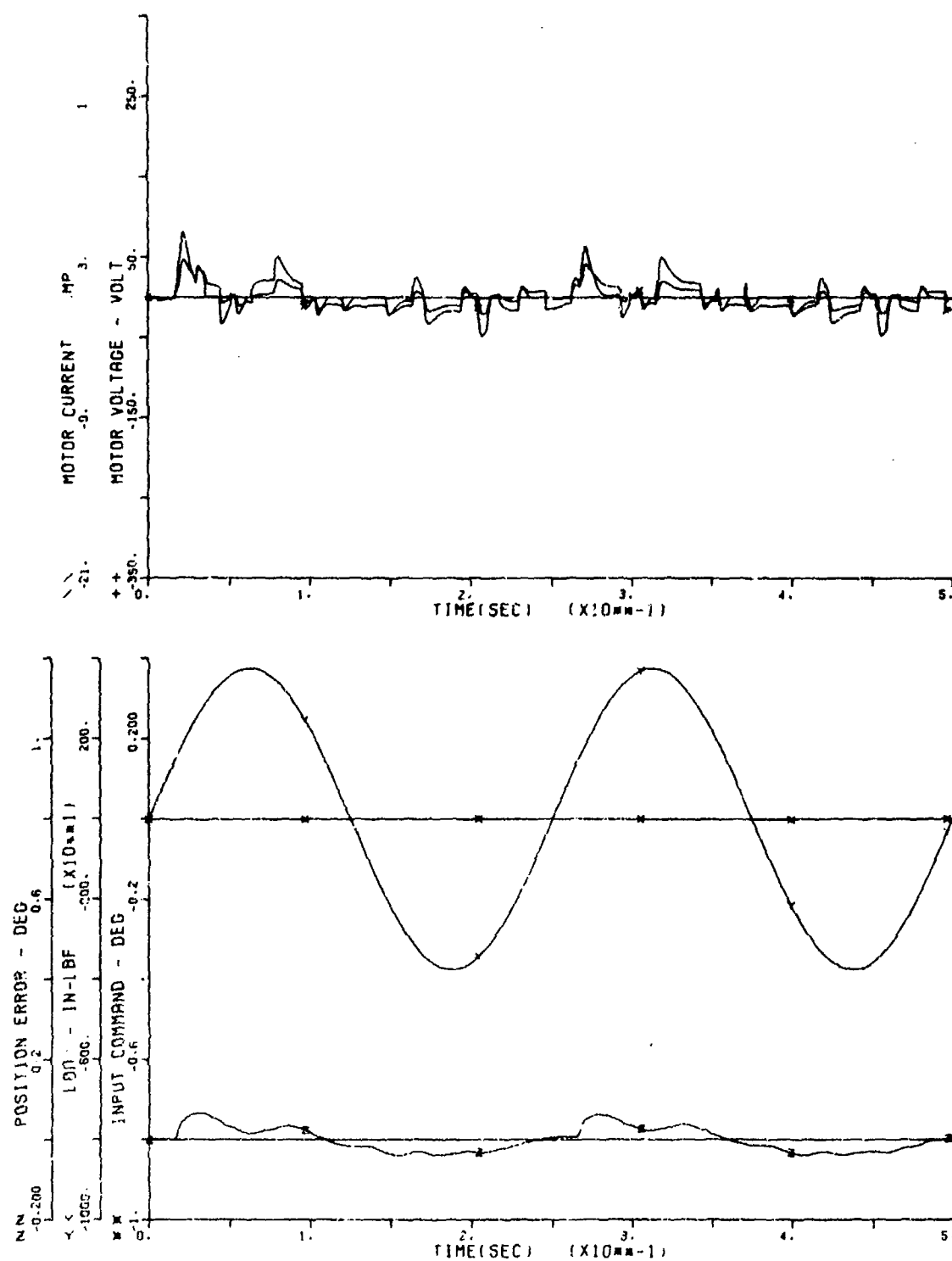


Figure G-32. Dual Channel Dynamic Stiffness, 10 Percent Load

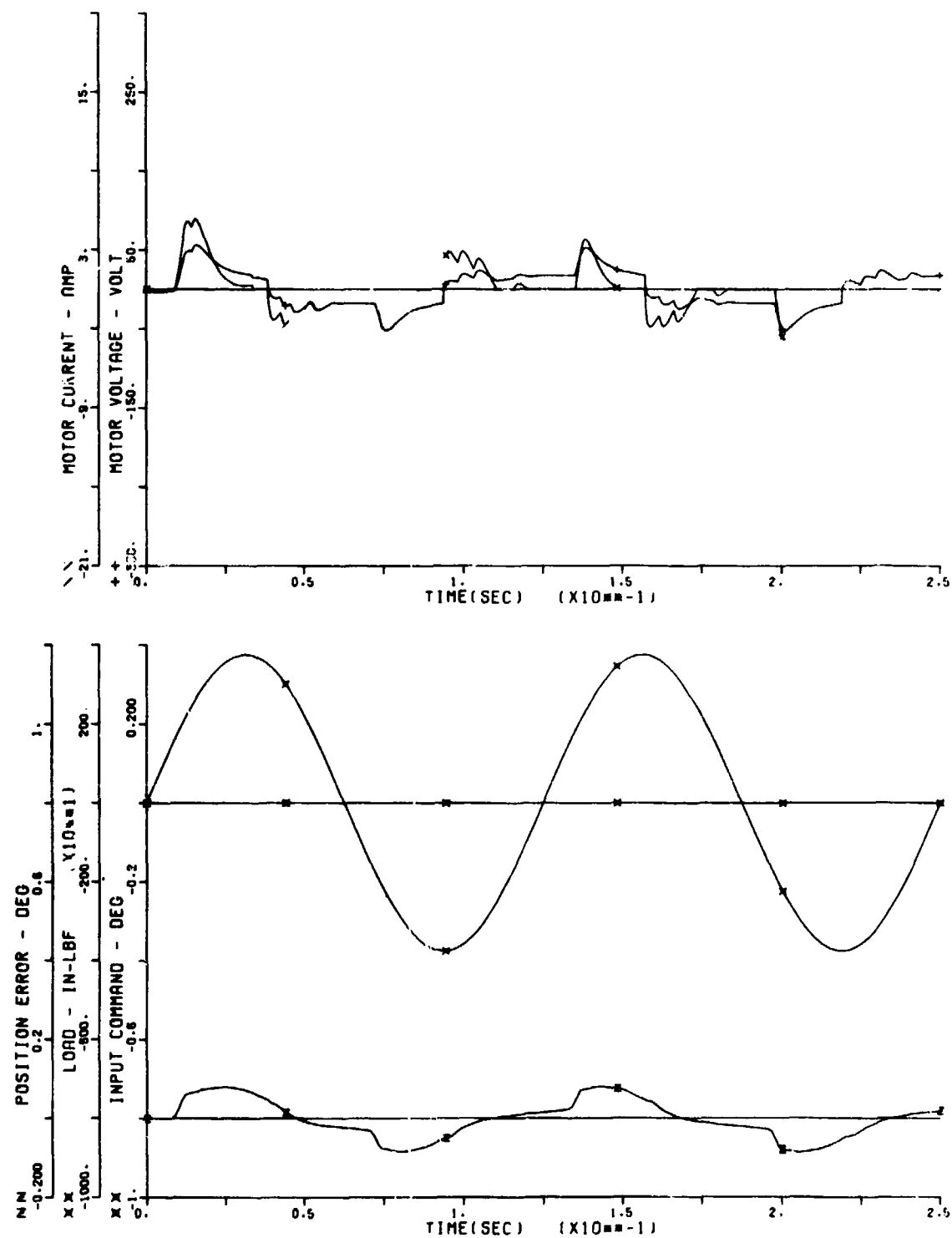


Figure G-33. Dual Channel Dynamic Stiffness, 10 Percent Load

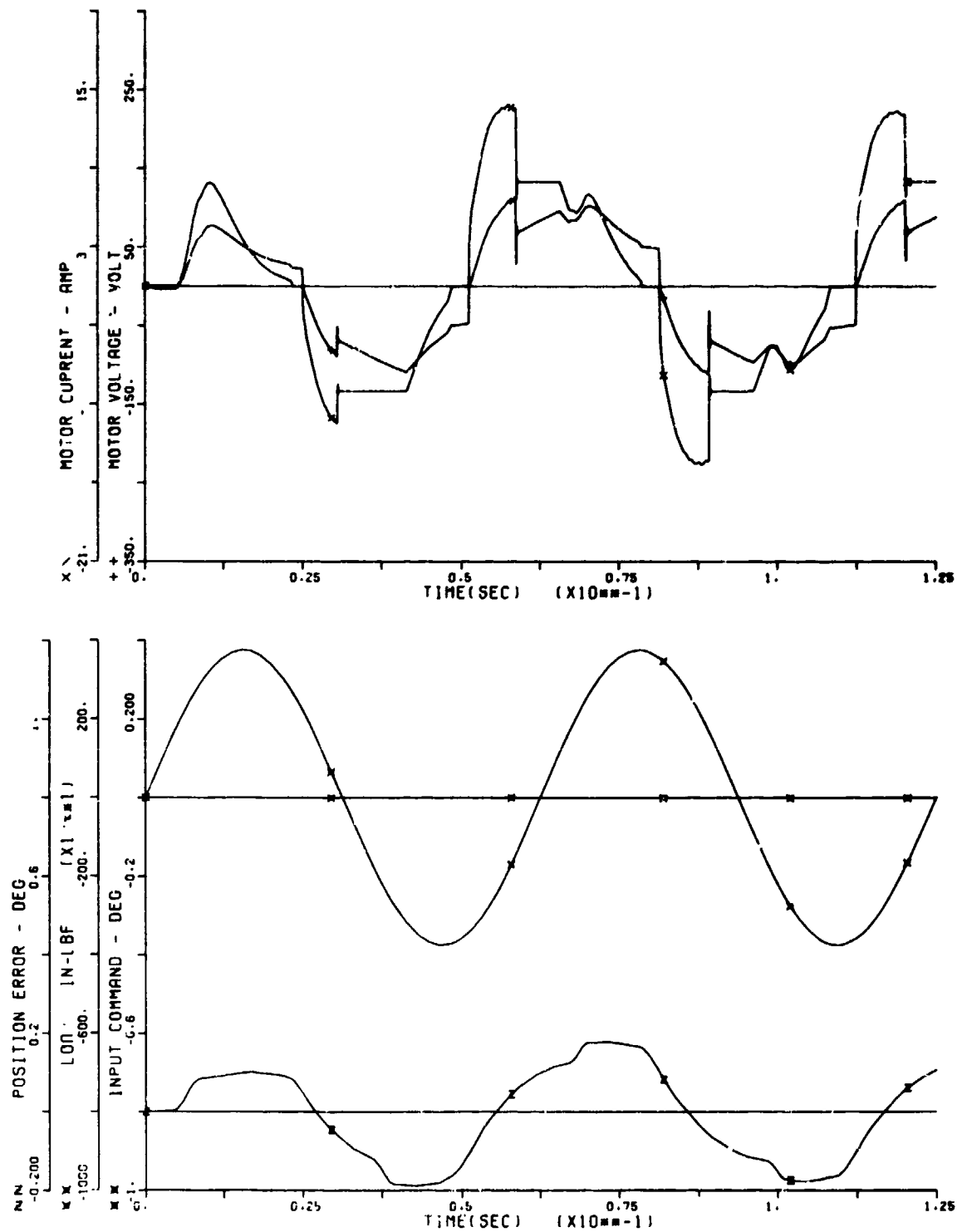


Figure G-34. Dual Channel Dynamic Stiffness, 10 Percent Load

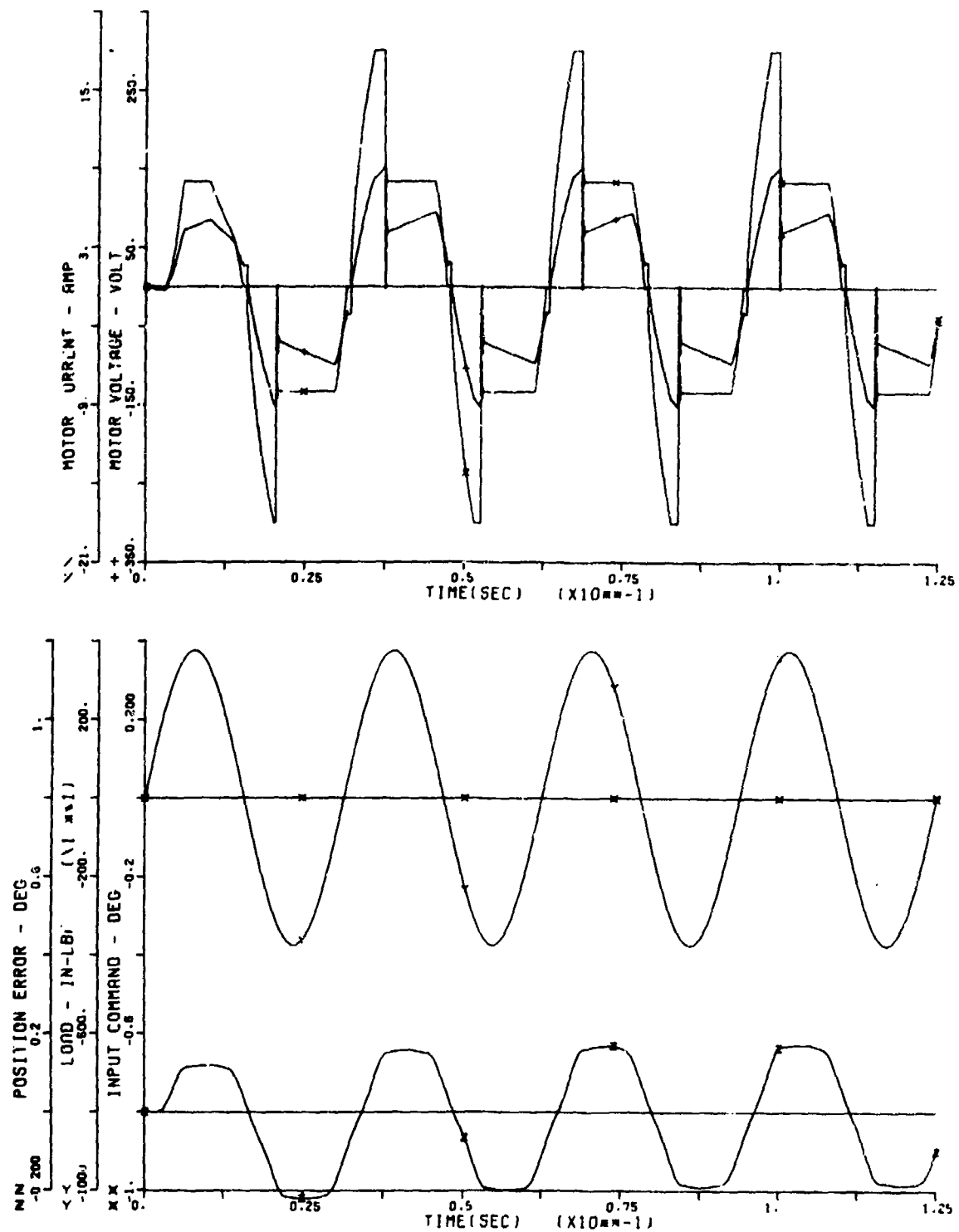


Figure G-35. Dual Channel Dynamic Stiffness, 10 Percent Load

APPENDIX H

HARDWARE TEST DATA

This appendix contains pertinent raw test data obtained from the rotary hingeline actuator unit. Table H-1 indexes the arrangement of these data, which include various input frequencies, loads, amplitudes, and waveforms. The scale factors are the same on each plot. The input command and output position signals are 5 deg/in. and the current is measured using 10 amp/in.

Loads are applied to a 10-in. arm by using a spring with a constant displacement of 750 lb/in.

TABLE H-1

INDEX TO HARDWARE TEST RESULTS

Figure No.	Type of Test	Load at Null, lb	Frequency, Hz	Amplitude, deg
H-1 through H-4	Single-Channel Frequency Response	None None None None	0.5 2 4 8	+1 +1 +1 +1
H-5	Single-Channel Step Response	None	--	10
H-6	Dual-Channel Step Response	1125 <u>+655</u>	--	10
H-7 through H-11	Dual-Channel Frequency Response	None None None None None	0.5 2 4 6.3 8	+1 +1 +1 +1 +1

CONDITIONS: FREQUENCY = 0.5 HZ
AMPLITUDE = ± 1 DEG

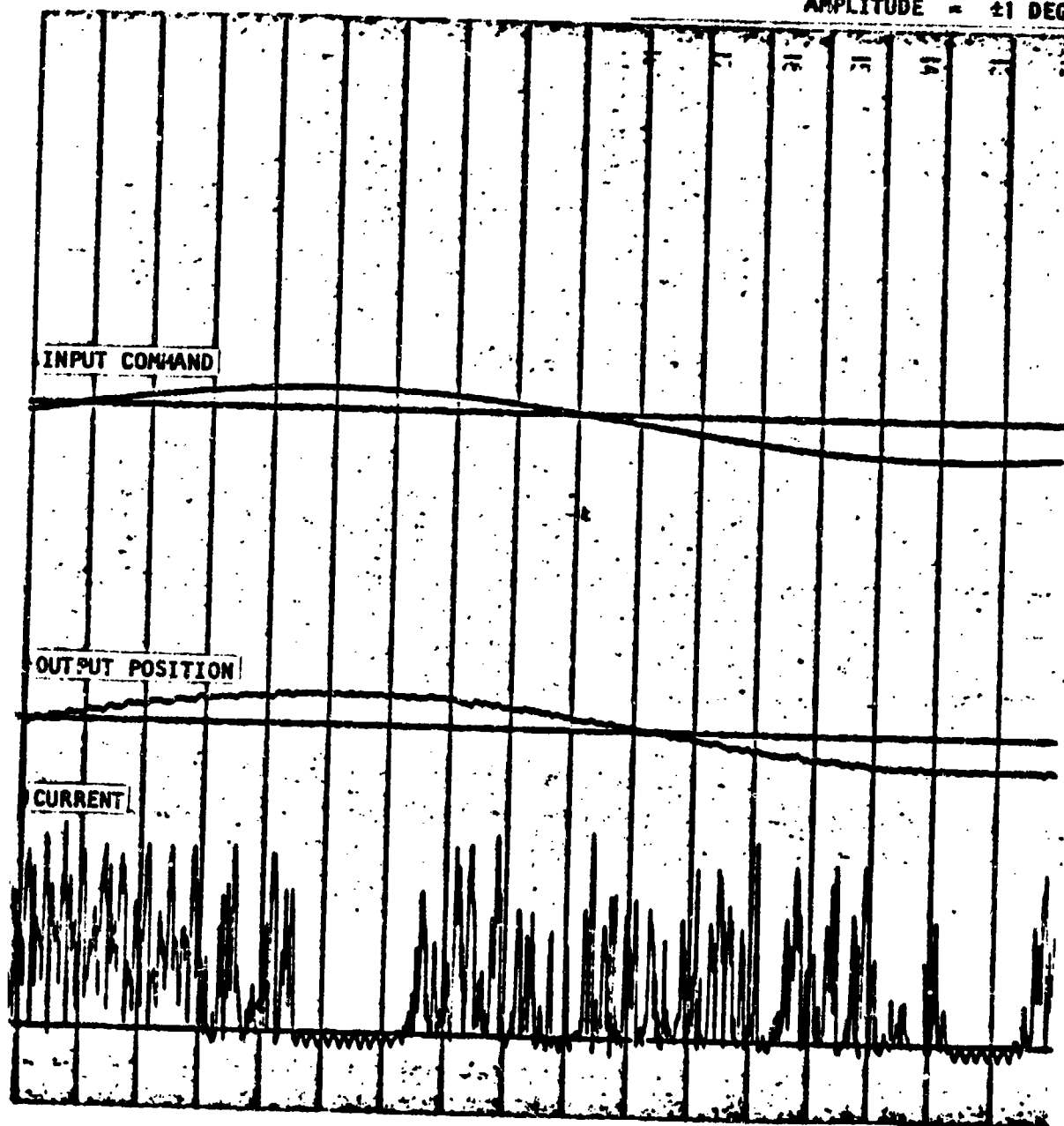


Figure H-1. Single-Channel Frequency Response, No Load

CONDITIONS: FREQUENCY = 2 HZ
 AMPLITUDE = ± 1 DEG

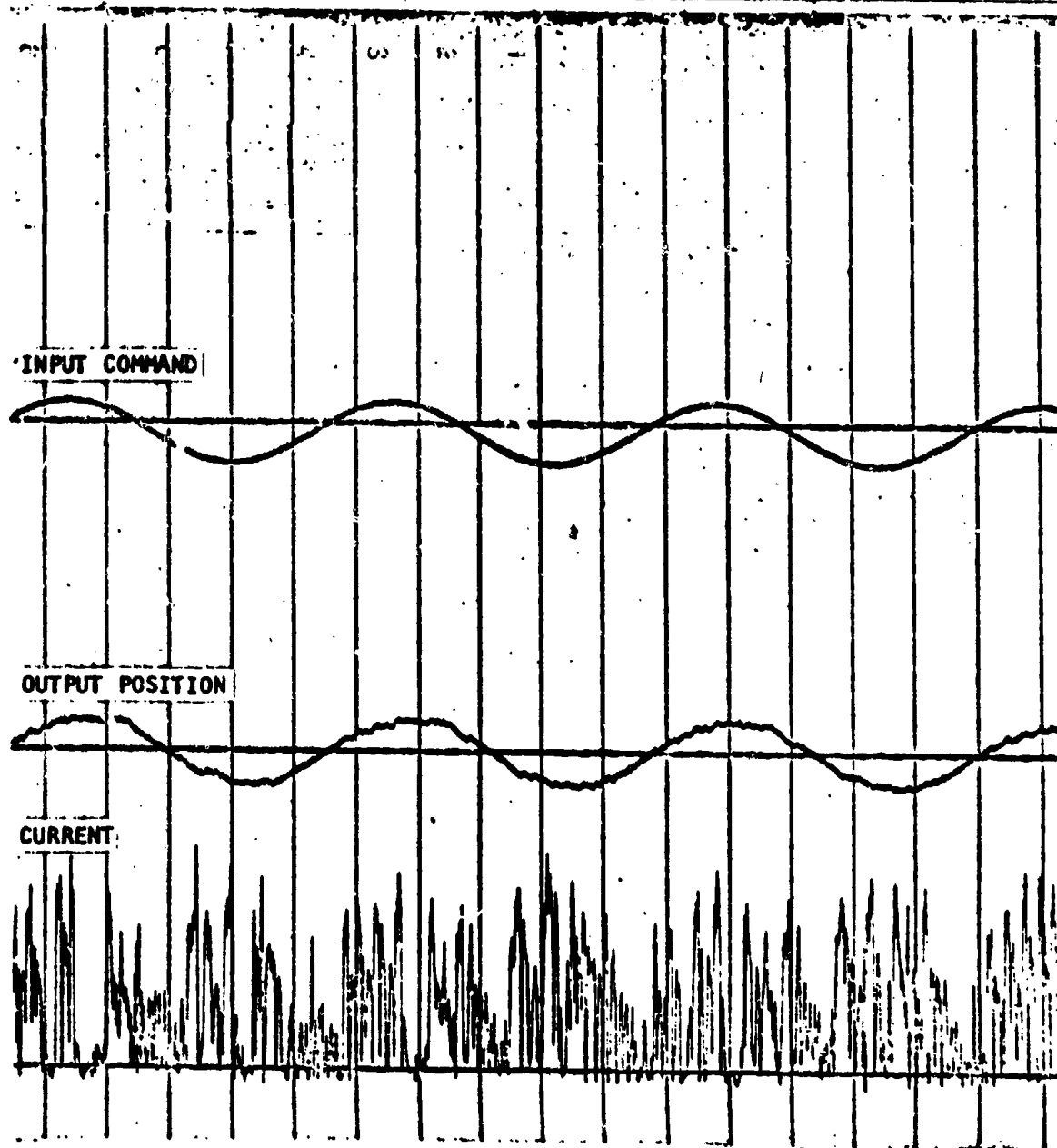


Figure H-2. Single-Channel Frequency Response, No Load

CONDITIONS: FREQUENCY = 4 HZ
AMPLITUDE = ± 1 DEG

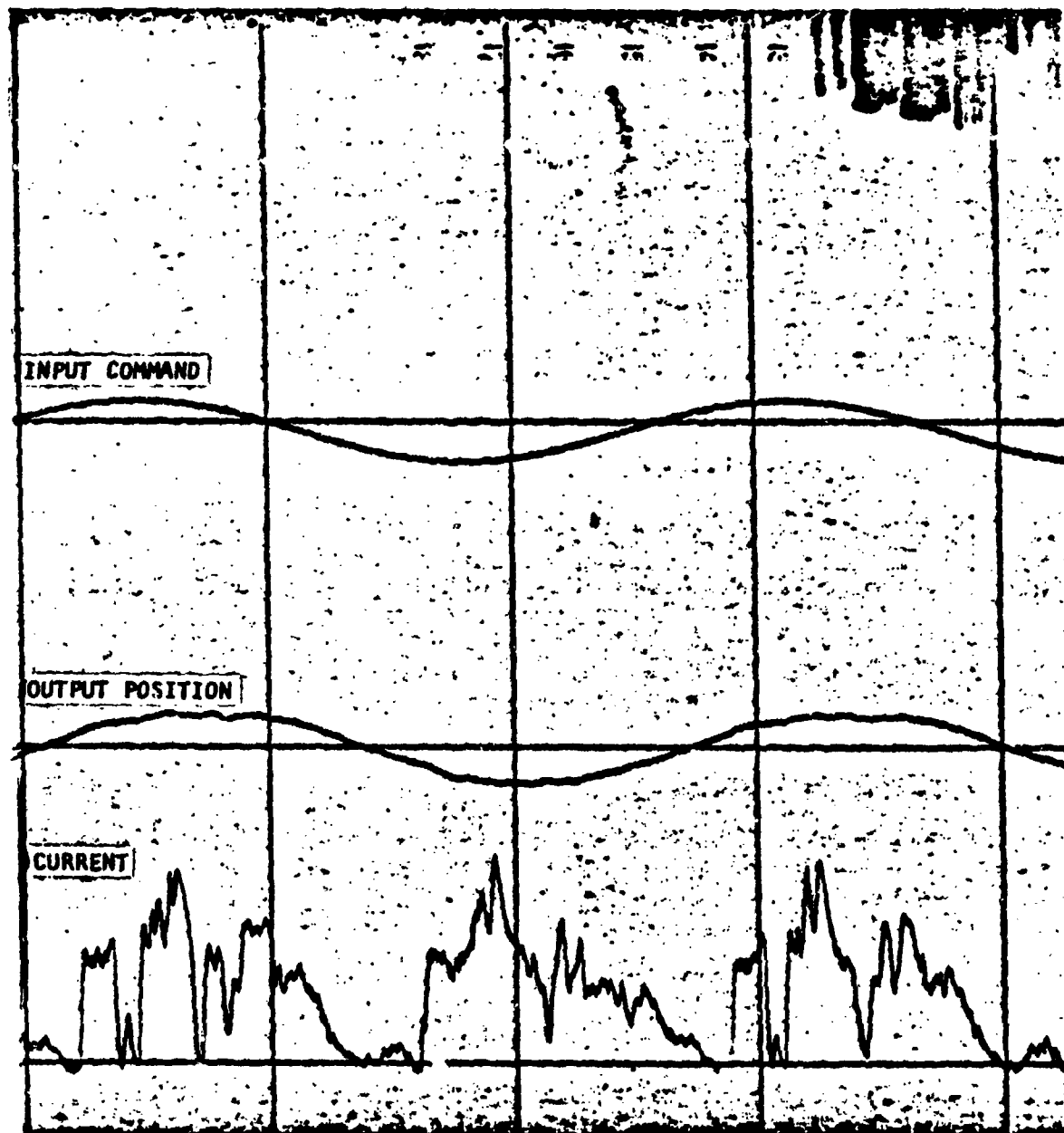


Figure H-3. Single-Channel Frequency Response, No Load

CONDITIONS: FREQUENCY = 8 HZ
 AMPLITUDE = ± 1 DEG

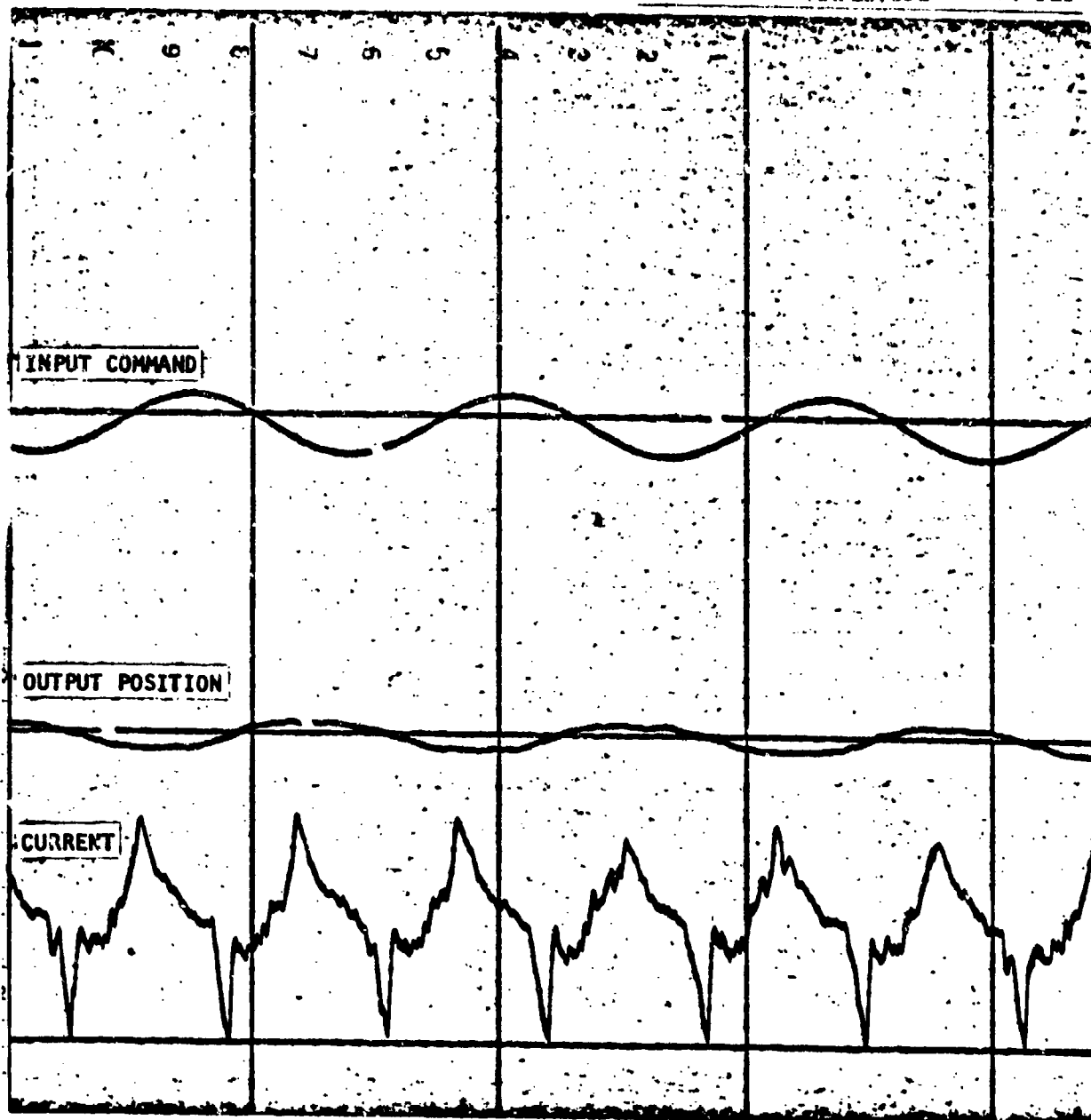


Figure H-4. Single-Channel Frequency Response, No Load

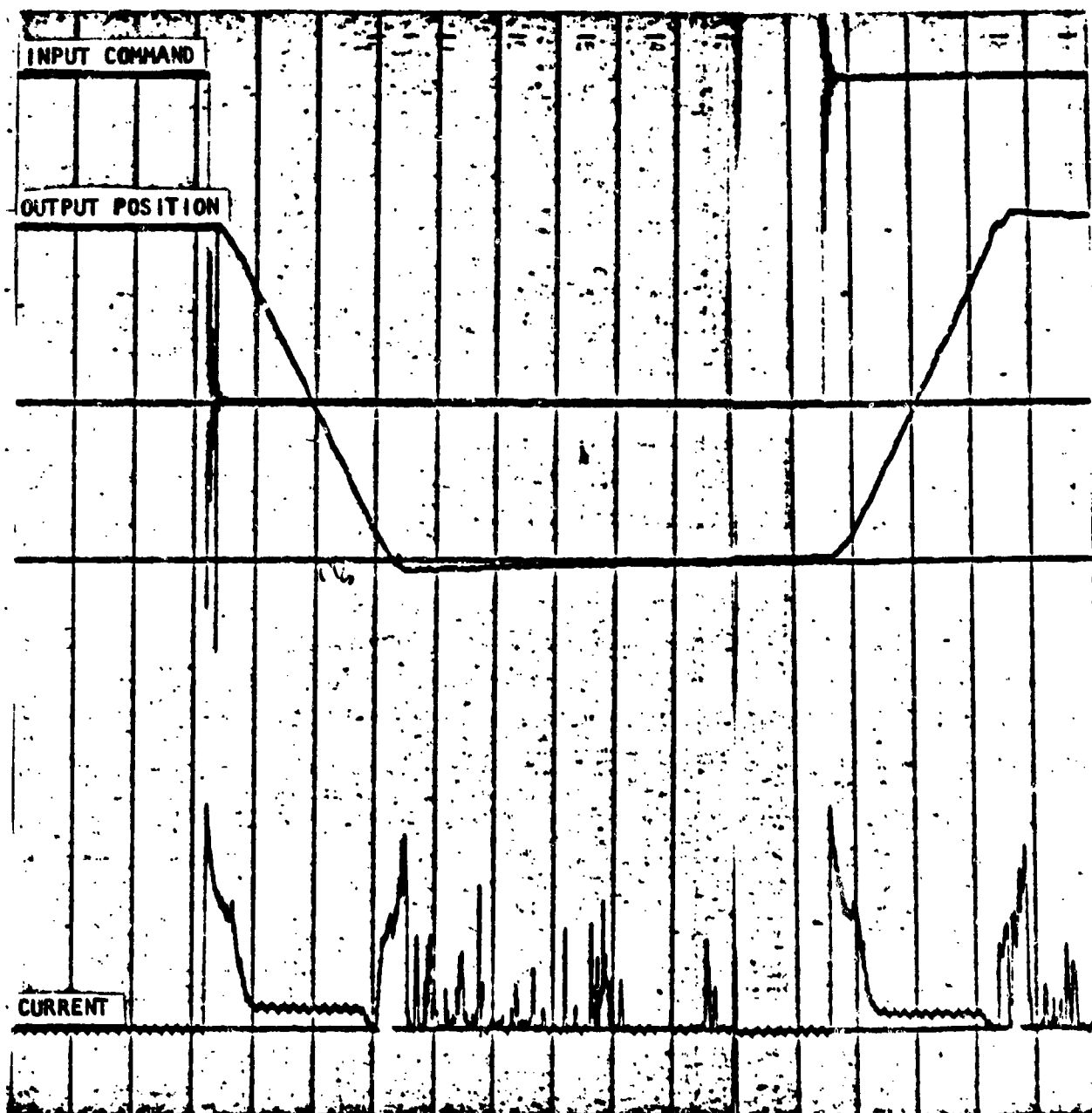


Figure H-5. Test Results for Single-Channel Step Response at No Load and 10-deg Step

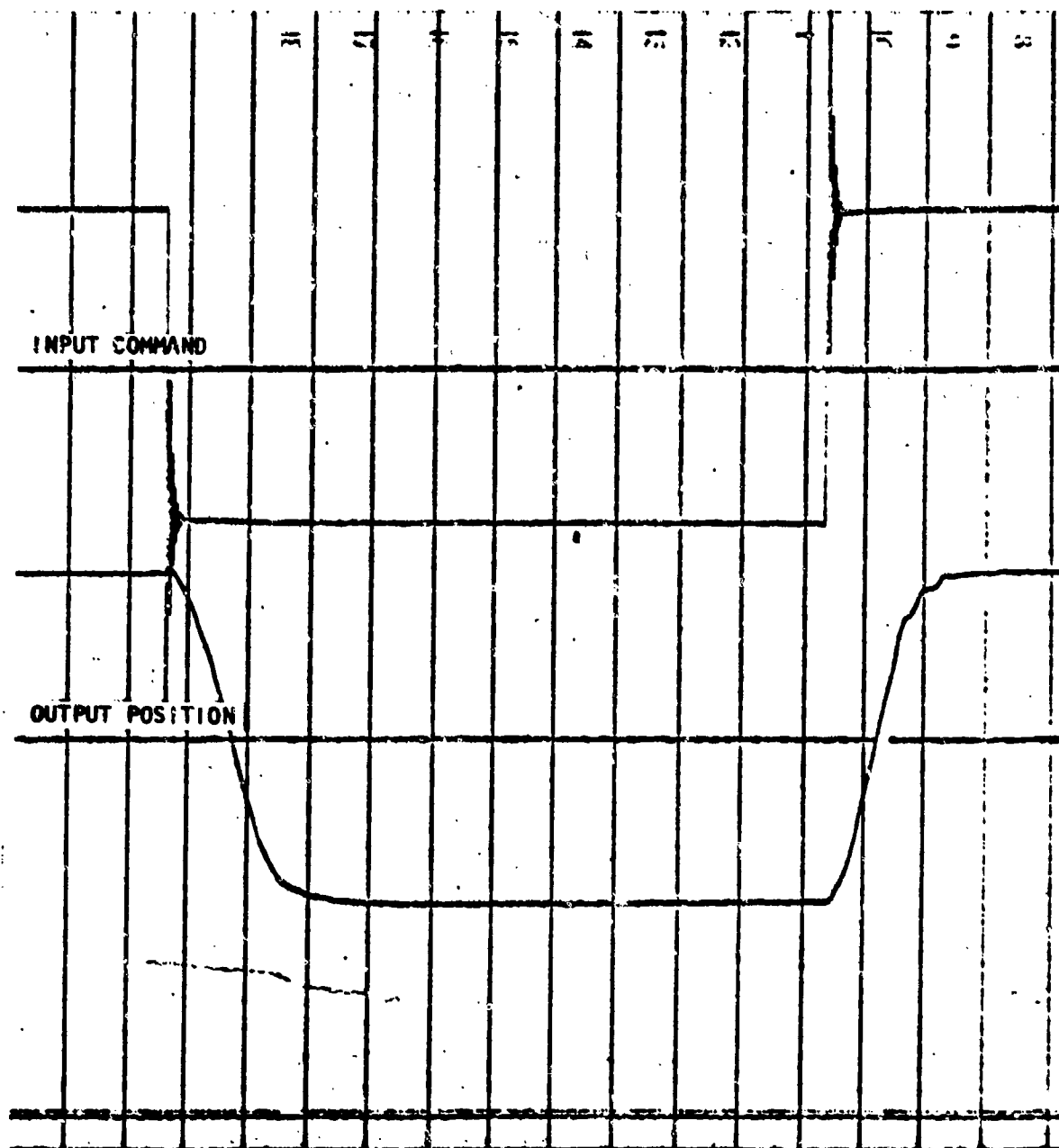


Figure H-6. Dual-Channel Step Response at 1125 \pm 655 lb Load and 10-deg Step

CONDITIONS: FREQUENCY = 0.5 HZ
AMPLITUDE = ± 1 DEG

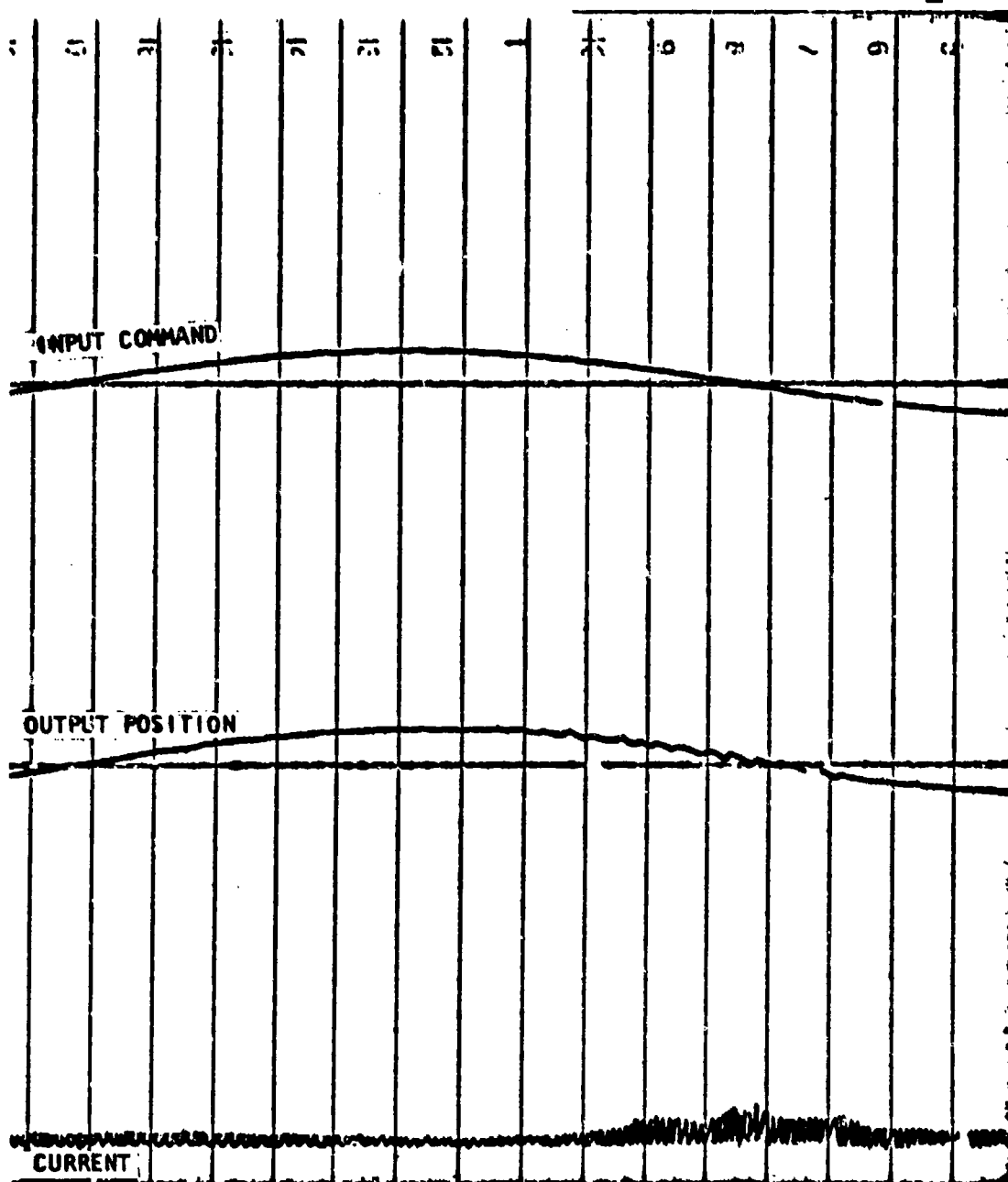


Figure H-7. Dual-Channel Frequency Response, No Load

CONDITIONS: FREQUENCY = 2 HZ
AMPLITUDE = ± 1 DEG

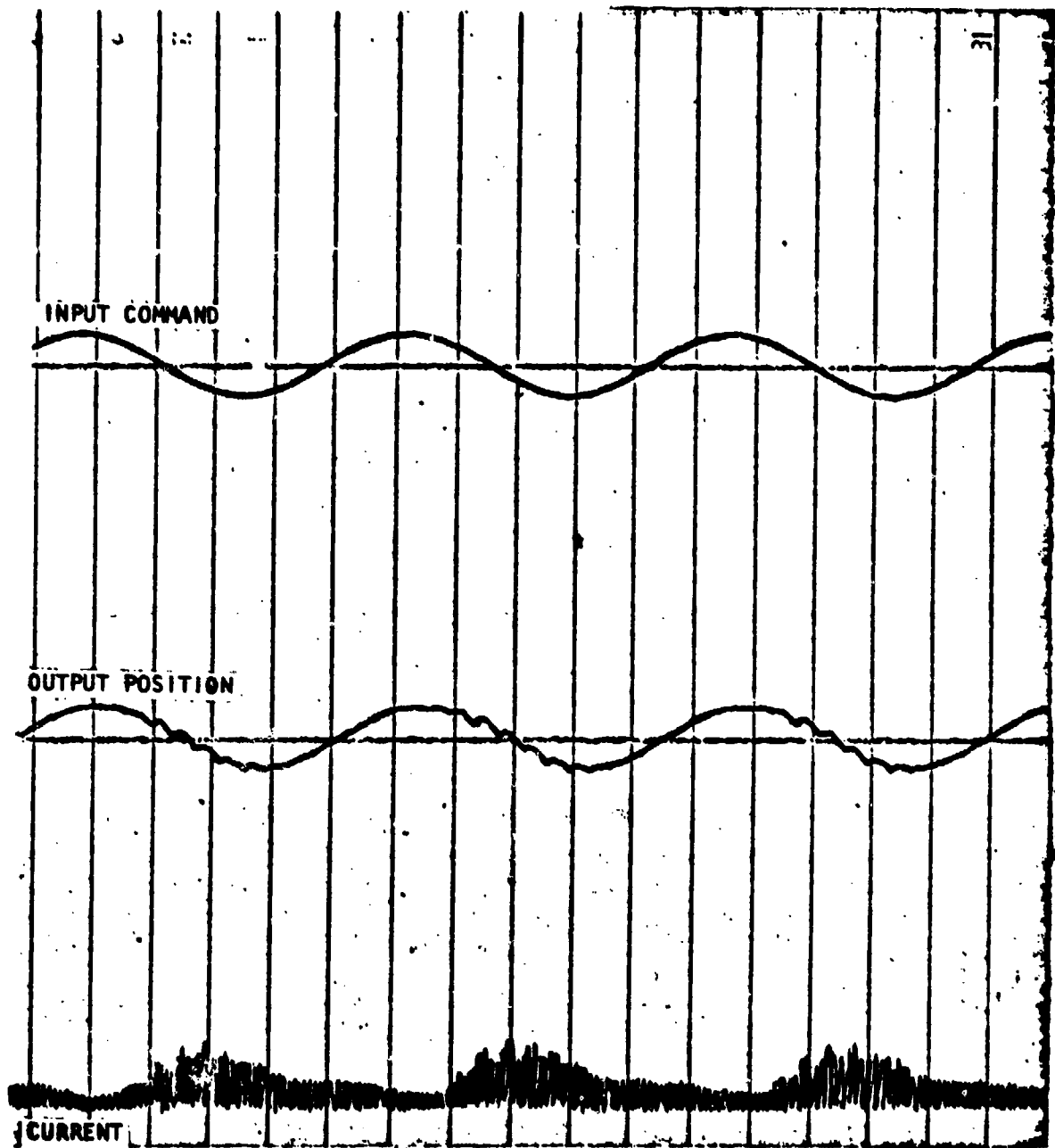


Figure H-8. Drive Channel Frequency Response, No Load

CONDITIONS: FREQUENCY = 4 HZ
AMPLITUDE = ± 1 DEG

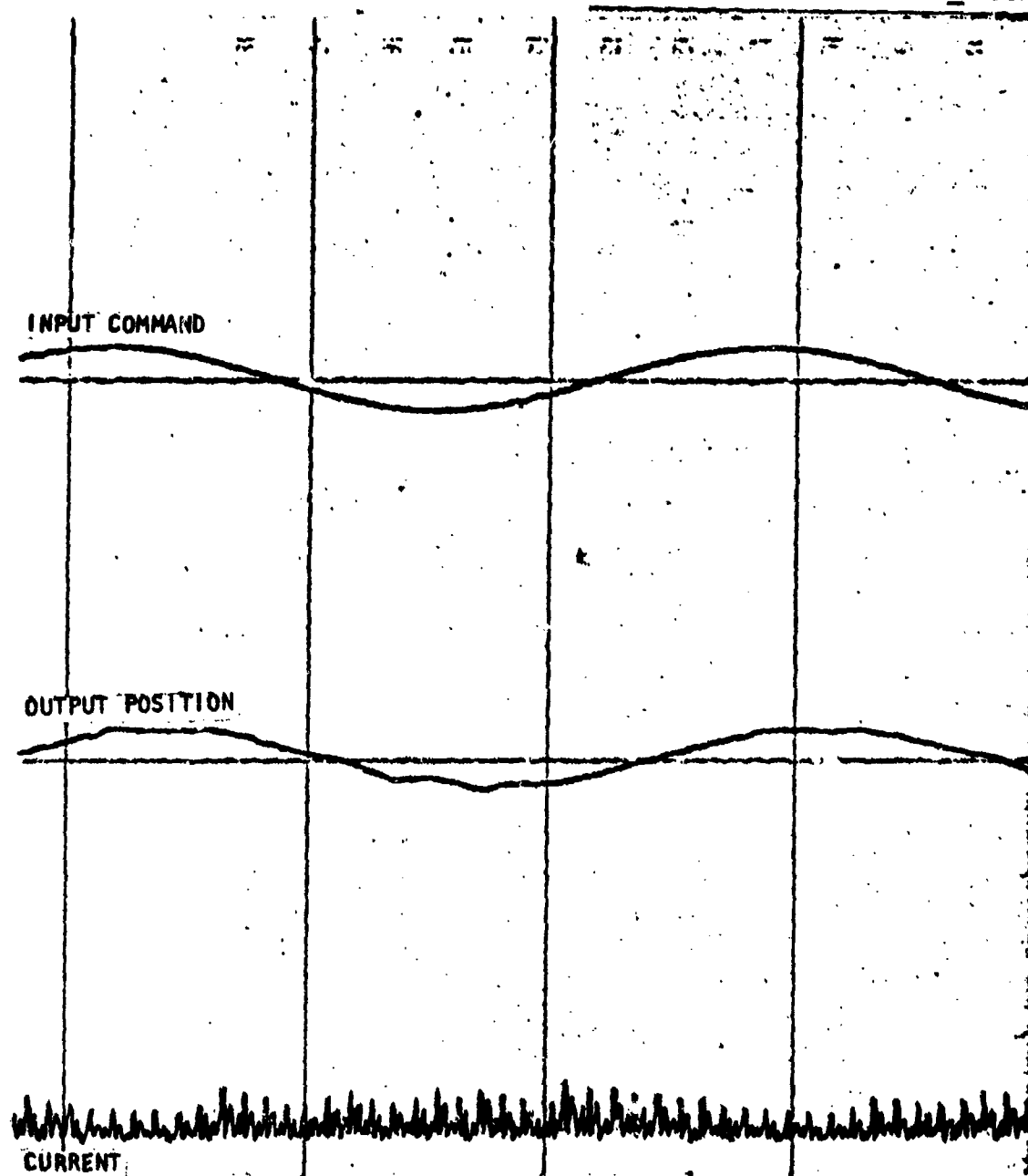


Figure H-9. Dual-Channel Frequency Response, No Load

CONDITIONS: FREQUENCY = 6.3 HZ
AMPLITUDE = ± 1 DEG

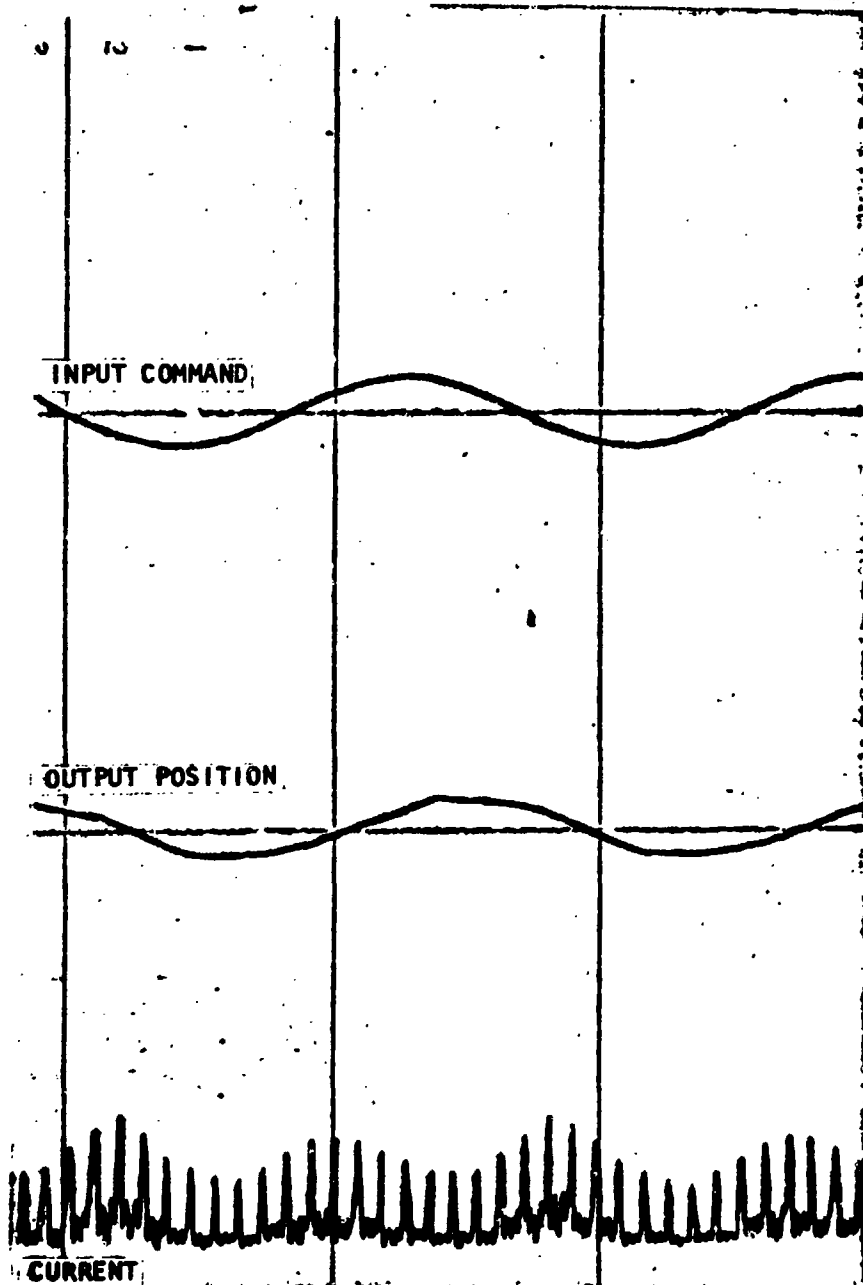


Figure H-10. Dual-Channel Frequency Response, No Load

CONDITIONS: FREQUENCY = 8 HZ
AMPLITUDE = +1 DEG

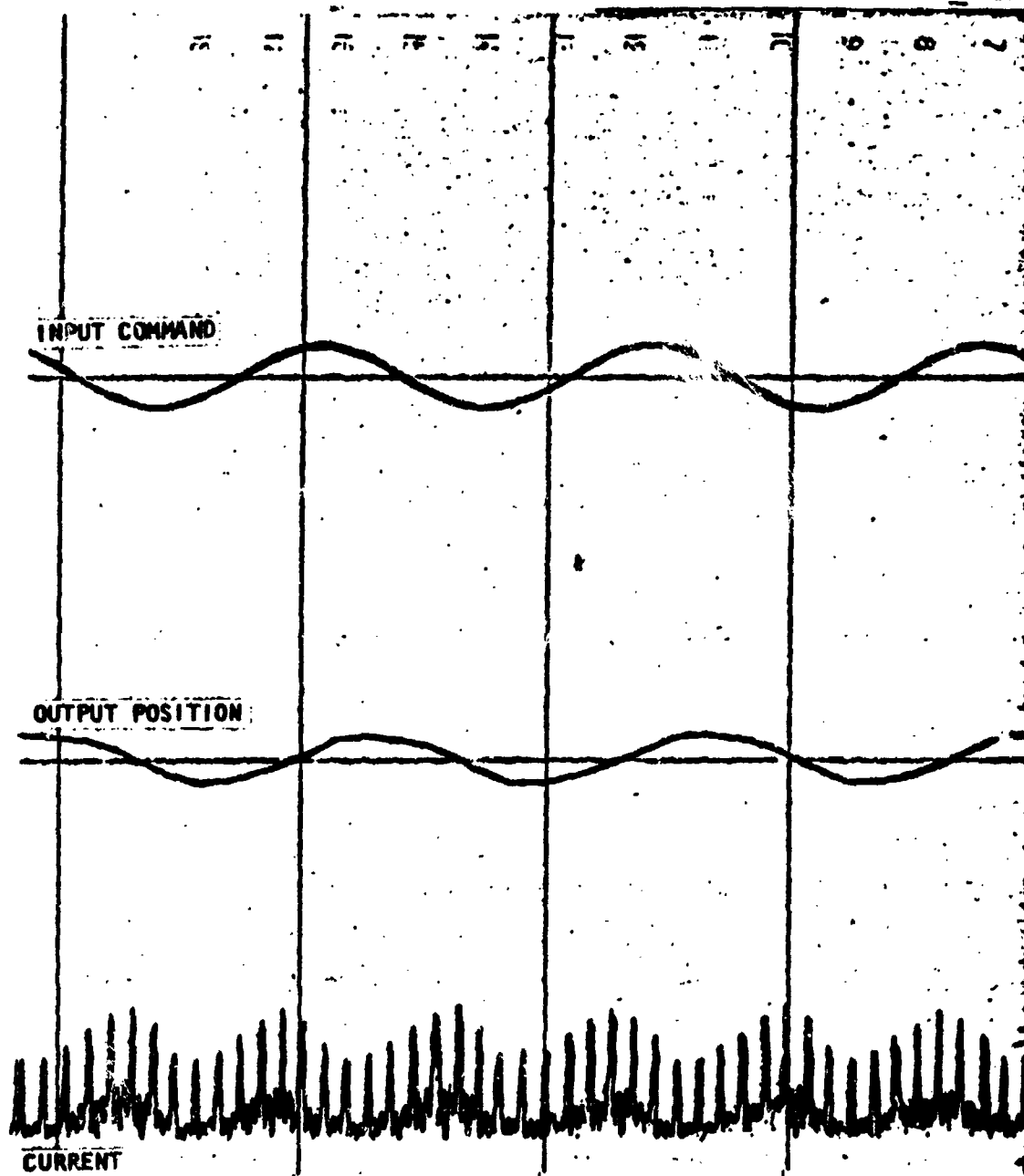


Figure H-11. Dual-Channel Frequency Response, No Load